frontiers | Research Topics

Improving crop health: Understanding the interaction mechanisms between crops and their pathogens

Edited by
Yuheng Yang, Shunyuan Xiao, Zhanhong Ma, Guotian Li, Yang Yu and Qiong Zhang

Published in
Frontiers in Plant Science

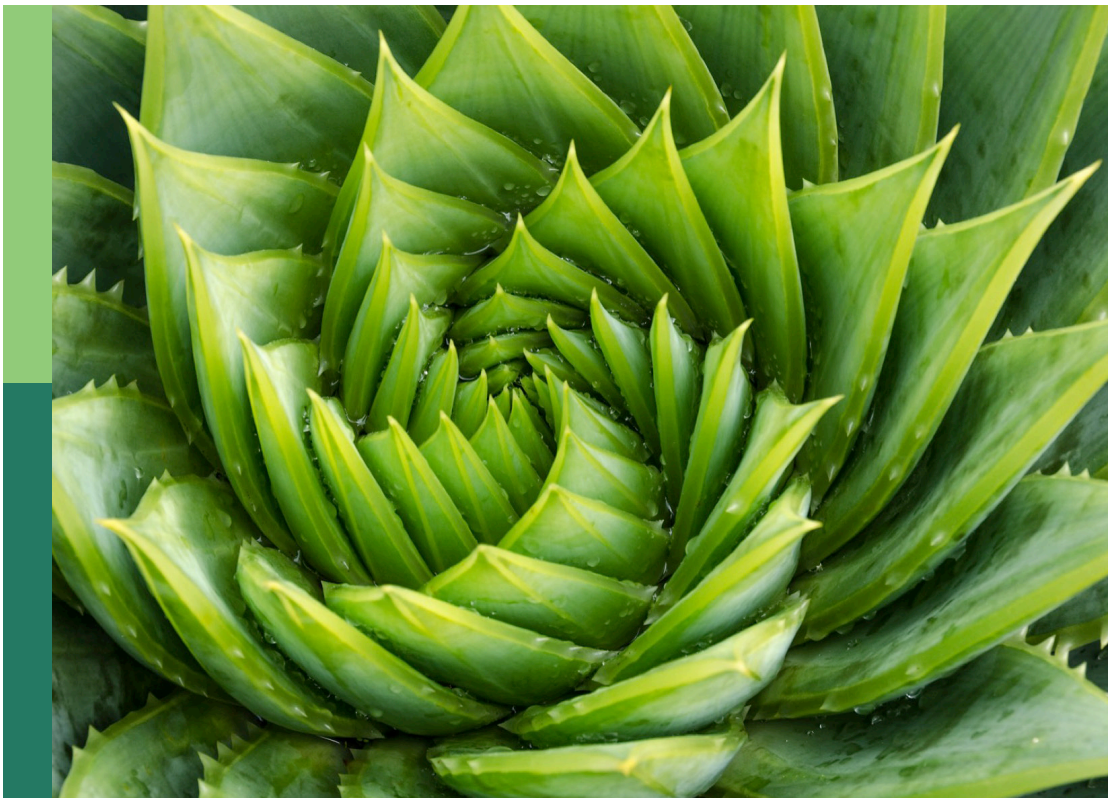

ISSN 1664-8714
ISBN 978-2-83251-846-5
DOI 10.3389/978-2-83251-846-5

About Frontiers

Frontiers is more than just an open access publisher of scholarly articles: it is a pioneering approach to the world of academia, radically improving the way scholarly research is managed. The grand vision of Frontiers is a world where all people have an equal opportunity to seek, share and generate knowledge. Frontiers provides immediate and permanent online open access to all its publications, but this alone is not enough to realize our grand goals.

Frontiers journal series

The Frontiers journal series is a multi-tier and interdisciplinary set of open-access, online journals, promising a paradigm shift from the current review, selection and dissemination processes in academic publishing. All Frontiers journals are driven by researchers for researchers; therefore, they constitute a service to the scholarly community. At the same time, the *Frontiers journal series* operates on a revolutionary invention, the tiered publishing system, initially addressing specific communities of scholars, and gradually climbing up to broader public understanding, thus serving the interests of the lay society, too.

Dedication to quality

Each Frontiers article is a landmark of the highest quality, thanks to genuinely collaborative interactions between authors and review editors, who include some of the world's best academicians. Research must be certified by peers before entering a stream of knowledge that may eventually reach the public - and shape society; therefore, Frontiers only applies the most rigorous and unbiased reviews. Frontiers revolutionizes research publishing by freely delivering the most outstanding research, evaluated with no bias from both the academic and social point of view. By applying the most advanced information technologies, Frontiers is catapulting scholarly publishing into a new generation.

What are Frontiers Research Topics?

Frontiers Research Topics are very popular trademarks of the *Frontiers journals series*: they are collections of at least ten articles, all centered on a particular subject. With their unique mix of varied contributions from Original Research to Review Articles, Frontiers Research Topics unify the most influential researchers, the latest key findings and historical advances in a hot research area.

Find out more on how to host your own Frontiers Research Topic or contribute to one as an author by contacting the Frontiers editorial office: frontiersin.org/about/contact

Improving crop health: Understanding the interaction mechanisms between crops and their pathogens

Topic editors

Yuheng Yang — Southwest University, China
Shunyuan Xiao — University of Maryland, College Park, United States
Zhanhong Ma — China Agricultural University, China
Guotian Li — Huazhong Agricultural University, China
Yang Yu — Southwest University, China
Qiong Zhang — University of California, Berkeley, United States

Citation

Yang, Y., Xiao, S., Ma, Z., Li, G., Yu, Y., Zhang, Q., eds. (2023). *Improving crop health: Understanding the interaction mechanisms between crops and their pathogens*. Lausanne: Frontiers Media SA. doi: 10.3389/978-2-83251-846-5

Table of contents

frontiers | Frontiers in Plant Science

TYPE Editorial
PUBLISHED 21 February 2023
DOI 10.3389/fpls.2023.1161154

OPEN ACCESS

EDITED AND REVIEWED BY
Leo Marcelis,
Wageningen University and Research, Netherlands

*CORRESPONDENCE
Yuheng Yang
yyh023@swu.edu.cn
Qiong Zhang
qiongzh@berkeley.edu
Yang Yu
zbyuyang@swu.edu.cn
Guotian Li
li4@mail.hzau.edu.cn
Shunyuan Xiao
xiao@umd.edu
Zhanhong Ma
mazh@cau.edu.cn

SPECIALTY SECTION
This article was submitted to Crop and Product Physiology, a section of the journal Frontiers in Plant Science

RECEIVED 08 February 2023
ACCEPTED 13 February 2023
PUBLISHED 21 February 2023

CITATION
Yang Y, Zhang Q, Yu Y, Li G, Xiao S and Ma Z (2023) Editorial: Improving crop health: Understanding the interaction mechanisms between crops and their pathogens. *Front. Plant Sci.* 14:1161154. doi: 10.3389/fpls.2023.1161154

Editorial: Improving crop health: Understanding the interaction mechanisms between crops and their pathogens

Yuheng Yang [1]*, Qiong Zhang [2,3]*, Yang Yu [1]*, Guotian Li [4]*, Shunyuan Xiao [5]* and Zhanhong Ma [6]*

[1]College of Plant Protection, Southwest University, Chongqing, China, [2]Department of Bioengineering, University of California, Berkeley, Berkeley, CA, United States, [3]Department of Plant & Microbial Biology, University of California, Berkeley, Berkeley, CA, United States, [4]State Key Laboratory of Agricultural Microbiology, Hubei Hongshan Laboratory, Hubei Key Laboratory of Plant Pathology, Huazhong Agricultural University, Wuhan, China, [5]Institute for Bioscience and Biotechnology Research, University of Maryland, Rockville, MD, United States, [6]Department of Plant Pathology, China Agricultural University, Beijing, China

KEYWORDS

crop protection, crop-pathogen interactions, immune response, secondary metabolites, synthetic chemicals

Editorial on the Research Topic

Improving crop health: Understanding the interaction mechanisms between crops and their pathogens

Crop diseases are responsible for substantial yield losses worldwide, thereby threatening global food security. In this Research Topic, a collection of high-quality articles reported recent research progress concerning genes, proteins, secondary metabolites involved in the interactions between crop plants and their pathogens as well as utilization of new synthetic chemicals in control of crop diseases. As co-editors of this research topic, we appreciate the contributions from the authors of the papers published under this topic and highlight the three themes drawn from their research findings.

Identification of key genes and proteins in immune response and evasion

The immune response of crop plants to pathogen attacks and the immune evasion of pathogens from their host plants have attracted more and more attention in the field of phytopathology research. Jiang et al. and Zhan et al. systematically analyzed the roles of TaSnRK and TaPAL members in wheat against notorious pathogens, including *Blumeria graminis*, *Fusarium graminearum* and *Puccinia striiformis*.

Ralstonia solanacearum causes devastating diseases in a variety of economically important crops. Cao et al. identified 23 differentially expressed long intergenic ncRNAs (lincRNAs) in tomato inoculated with *R. solanacearum*, and predicted 171 possible target genes of these lincRNAs. Further studies suggested that lincRNAs might be involved in hormone signaling pathways and regulation of AGO protein expression in response to *R. solanacearum*. An et al. showed that a type III effector RipTPS from the avirulent *R. solanacearum* strain specifically induced cell death in *Nicotiana tabacum* but not in *N. benthamiana*. Three amino acid residues in RipTPS have been identified to be critical for the recognition of $RipTPS_G$ in *N. tabacum*.

Huanglongbing (HLB), caused by *Candidatus* Liberibacter asiaticus (CLas), is the most devastating citrus disease. Basu et al. discovered that two CLas proteins, LasP235 and Effector 3, interact with and inhibit the functions of multiple citrus proteins involved in the production of reactive oxygen species and antibacterial metabolites as well as programed cell death.

Characterization of secondary metabolites involved in crop-pathogen interactions

Various secondary metabolites of plants are involved in the process of disease resistance. The role of the hydroxycinnamate amide (HCAA) pathway in plant immunity was reviewed by Liu et al. in three layers: biosynthesis of HCAAs from the phenylpropanoid pathway, function of HCAAs in plant disease resistance, and regulatory pathways of HCAAs accumulation. This review refines the mechanisms by which various secondary metabolites of plants are involved in immune responses and points the way to future exploration of phytochemical defense metabolites.

As one of the lipophilic secondary metabolites deposited in the plant cell wall, suberin is an essential component of the Casparian strip of the root endodermis. Chen et al.reviewed the function of plant root suberin lamella as a physical barrier in defense against biotic and abiotic stresses in four layers: establishment of suberin lamellae in the cell wall, biosynthesis of suberin, deposition of suberin in cell wall, and stress tolerance.

Secondary metabolites play important roles in plant pathogens too. Ralsolamycin, one of secondary metabolites in *R. solanacearum*, is known to be involved in crosstalk between *R. solanacearum* and fungi. Li et al. demonstrated that Ralsolamycin biosynthesis can be oppositely regulated by PhcA and PhcR in *R. solanacearum* to respond and adapt to changing environmental conditions.

Utilization of new synthetic chemicals for crop disease control

The development and utilization of novel fungicides with novel structures, high efficiency and low toxicity are of great importance for crop disease control. Yao et al. designed and synthesized a series of 1,3,4-oxadiazole derivatives from benzoyl hydrazine and aromatic aldehydes. Compared to control fungicide carbendazim, most of the oxadiazole derivatives exhibited enhanced activities against three fungal pathogens of maize, especially *Exserohilum turcicum*. Molecular docking illustrated that oxadiazole derivatives can bind to the active site of succinate dehydrogenase (SDH) through hydrophobic contacts and hydrogen bonds, indicating that 1,3,4-oxadiazole derivatives are promising candidates for fungicide development.

As an important agrochemical, nitrogen fertilizer plays a central role in plant growth and fitness, and some specific forms of nitrogen fertilizer may also improve plant resistance. Maywald et al. found that application of nitrate or cyanamide instead of ammonium to wheat plants significantly suppressed two important wheat fungal pathogens, i.e., airborne *B. graminis* and soilborne *Gaeumannomyces graminis*. They also observed relatively higher abundance of fungal pathogenic taxa in wheat plants fertilized with ammonium. These interestingly observations suggest that nitrate and cyanamide fertilization could reduce the severity of some fungal diseases in wheat.

Additionally, biocontrol of plant diseases is an alternative disease management strategy that is environmentally benign, durable, and compatible with other control measures. Xu et al. identified a new *Bacillus amyloliquefaciens* strain XY-1 that exhibits antagonistic activity against a variety of phytopathogens. For example, antagonism tests using wheat spikelet inoculation showed that strain XY-1 displayed strong antifungal activity against *F. graminearum*, indicating that strain XY-1 can be used as a biological agent in the field to control Fusarium head blight.

In conclusion, these articles on this Research Topic have collectively given readers a snapshot of the most recent advances in research towards improving crop health. We hope that the findings presented in these articles will not only provide useful new information for specific research projects, but also help attract additional researchers to this rapidly expanding field of crop protection.

Author contributions

All authors listed have made a substantial, direct, and intellectual contribution to the work and approved it for publication.

Funding

This work was supported by National Key R&D Program of China (2022YFD1901402) and Chongqing Technology Innovation

and Application Development Special Project (CSTB2022TIAD-LUX0004) to YYa, UC Berkeley Miller Basic Research Fellowship to QZ, Natural Science Foundation of Chongqing (cstc2021jcyj-msxmX0629) to YYu, Natural Science Foundation of China (32172373, 31801723) to GL, National Science Foundation (IOS-1901566) to SX, National Key R&D Program of China (2021YFD1401000) and Natural Science Foundation of China (31972211) to ZM.

Acknowledgments

The authors would like to thank all the handling editors and reviewers for their contribution to this Research Topic.

Conflict of interest

The authors declare that the research was conducted in the absence of any commercial or financial relationships that could be construed as a potential conflict of interest.

Publisher's note

frontiers | Frontiers in Plant Science

ORIGINAL RESEARCH
published: 02 May 2022
doi: 10.3389/fpls.2022.869178

Two Liberibacter Proteins Combine to Suppress Critical Innate Immune Defenses in Citrus

*Supratim Basu[1], Loan Huynh[1], Shujian Zhang[1], Roel Rabara[1], Hau Nguyen[1], Jeanette Velásquez Guzmán[1], Guixia Hao[2], Godfrey Miles[2], Qingchun Shi[2], Ed Stover[2] and Goutam Gupta[1]**

[1] Biolab, New Mexico Consortium, Los Alamos, NM, United States, [2] Horticulture and Breeding, U. S. Horticultural Research Laboratory, Fort Pierce, FL, United States

We adopted a systems-based approach to determine the role of two *Candidatus* Liberibacter asiaticus (*C*Las) proteins, $LasP_{235}$ and Effector 3, in Huanglongbing (HLB) pathogenesis. While a published work suggests the involvement of these *C*Las proteins HLB pathogenesis, the exact structure-based mechanism of their action has not been elucidated. We conducted the following experiments to determine the structure-based mechanisms of action. First, we immunoprecipitated the interacting citrus protein partners of $LasP_{235}$ and Effector 3 from the healthy and *C*Las-infected Hamlin extracts and identified them by Liquid Chromatography with tandem mass spectrometry (LC–MS/MS). Second, we performed a split green fluorescent protein (GFP) assay in tobacco to validate that the interactions observed *in vitro* are also retained *in planta*. The notable *in planta* citrus targets of $LasP_{235}$ and Effector 3 include citrus innate immune proteins. Third, *in vitro* and *in planta* studies were performed to show that $LasP_{235}$ and Effector 3 interact with and inhibit the functions of multiple citrus proteins belonging to the innate immune pathways. These inhibitory interactions led to a high level of reactive oxygen species, blocking of bactericidal lipid transfer protein (LTP), and induction of premature programed cell death (PCD), all of which are beneficial to *C*Las lifecycle and HLB pathogenesis. Finally, we performed molecular dynamics simulations to visualize the interactions of $LasP_{235}$ and Effector 3, respectively, with LTP and Kunitz protease inhibitor. This led to the design of an LTP mimic, which sequestered and blocked $LasP_{235}$and rescued the bactericidal activity of LTP thereby proving that $LasP_{235}$, indeed, participates in HLB pathogenesis.

Keywords: *C*Las protein, citrus immunity, HLB pathogenesis, ROS, PCD, bactericidal activity

OPEN ACCESS

Edited by:
Qiong Zhang,
University of California, Berkeley, United States

Reviewed by:
Mengji Cao,
Southwest University, China
Sung Un Huh,
Kunsan National University, South Korea
Xiudao Yu,
Gannan Normal University, China

***Correspondence:**
Goutam Gupta
ggupta@newmexicoconsortium.org

Specialty section:
This article was submitted to Crop and Product Physiology, a section of the journal Frontiers in Plant Science

Received: *04 February 2022*
Accepted: *04 April 2022*
Published: *02 May 2022*

Citation:
Basu S, Huynh L, Zhang S, Rabara R, Nguyen H, Velásquez Guzmán J, Hao G, Miles G, Shi Q, Stover E and Gupta G (2022) Two Liberibacter Proteins Combine to Suppress Critical Innate Immune Defenses in Citrus. Front. Plant Sci. 13:869178. doi: 10.3389/fpls.2022.869178

INTRODUCTION

Huanglongbing (HLB) is the most devastating citrus disease (Da Graça et al., 2016; Merfa et al., 2019; Gupta and Stover, 2022). The *Candidatus* Liberibacter asiaticus (*C*Las) colonizes the phloem sieve elements on getting transmitted to the plants during the sap feeding by Asian citrus psyllid (ACP). The *C*Las infection in citrus plants leads mottling of leaves and premature fruit drop. Three α-proteobacteria species

(*C*Las, *Candidatus* L. americanus (*C*Lam), and *Candidatus* L. africanus (*C*Laf) are associated with HLB (Prasad et al., 2016). Of these species, *C*Las is the most predominant and virulent species in the USA and vectored by two psyllid species, *Diaphorina citri* Kuwayama and *Trioza erytreae* (Wang and Trivedi, 2013). While endemic in Asia for over a century (Gottwald, 2010; Luo and Agnarsson, 2018), HLB was first encountered about 15 years ago in Florida. Since then, HLB has been widespread in Florida and is looming large on California and Texas, the two other citrus producing states in the USA.

The gram-negative bacteria secrete effector proteins that play an essential role in disease pathogenesis by suppressing multiple proteins belonging to the innate immune system in plants and thereby providing a niche for bacterial colonization and spread in the host (Dodds and Rathjen, 2010). Typically, these effectors are directly injected into the host by the type III secretion system (Feng and Zhou, 2012). The *C*Las is devoid of the type III secretion system (Mudgett, 2005; Feng and Zhou, 2012) but may alternately use type II secretion system to release potential virulence factors or effectors (Sugio et al., 2011; Solé et al., 2015; Cianciotto and White, 2017). These proteins can be encoded by the *C*Las genome or the prophage. The prophages have been shown to exert influence in bacterial pathogenicity as have been seen in *Staphylococcus aureus* (Bae et al., 2006; Zhang et al., 2011). Two autotransporter proteins ($LasA_I$ and $LasA_{II}$) with leucine-rich repeats (LRRs) have been identified in Las psy62 prophage regions and have been shown to target the mitochondria in plants (Hao et al., 2013). Note that *C*Las codes for a smaller number of effectors because of the small (1 Mb) genome-size (Duan et al., 2009; Lin et al., 2013). The gram-negative bacteria with 5 Mb genomes have several 100 unique effectors (Dillon et al., 2019) as opposed to about 80 effectors identified, so far, from the *C*Las genome (Pitino et al., 2016, 2018; Prasad et al., 2016). However, the interactome studies revealed the ability of a single effector to bind multiple protein from the host plant (Block et al., 2008; Büttner, 2016). Thus, the bacteria have evolved to utilize a smaller number of effectors to establish a niche for pathogenesis in the host. Therefore, it was of importance whether to determine the two *C*Las proteins, $LasP_{235}$ and Effector 3, may target multiple citrus proteins, suppress immunity, and contribute to HLB pathogenesis.

In this study, we focused first on identifying the critical steps associated with the breakdown of citrus innate immune defense in response by the *C*Las effectors. Typically, the plant innate immune defense involves multiple pathways including pathogen or microbe-associated molecular pattern (MAMP)-triggered immunity (MTI); pattern-triggered immunity (PTI), effector triggered immunity (ETI), and plant hormone, such as salicylic acid (SA), jasmonic acid (JA), and ethylene (ET), induced immunity (He et al., 2007; Wu L. et al., 2014; Brauer et al., 2018; Qi et al., 2018; Zhang et al., 2018; Alhoraibi et al., 2019). The PTI or MTI provides the first line of plant defense against pathogens or microbes through the recognition of PAMP or MAMP, such as bacterial liposaccharide (LPS), elongation factor thermal unstable (EF–Tu), flagellin. The PAMP or MAMP recognition is mediated by the plasma membrane pattern recognition receptors (PRR) that include LRR, flagellin receptor (FLS2), and EF–Tu receptor (EFR). The plasma membrane PRR recognition induces intracellular mitogen-associated protein kinase (MAPK) signaling leading to the expression of pathogen-related (PR) or defense genes (Dangl and Jones, 2001; Sels et al., 2008; Ali et al., 2018). However, the pathogen effectors can block both intracellular and extracellular steps in the PTI pathway (Cui et al., 2009; Büttner, 2016). To counter the pathogen induced blocking of the PTI pathway, the plants have evolved the ETI pathway in which the intracellular nod-like receptors (NLR) recognize the pathogen effectors and augment the MAPK signaling and PR gene expression. The ETI pathway also induces hypersensitive response through the production of reactive oxygen species (ROS), which causes cell death at the site of the infection thereby limiting the pathogen spread. The PTI and ETI pathways also couple to intracellular plant hormone SA/JA/ET pathways, which also involve ROS production and induction of PR genes. It has been demonstrated that the effectors from plant pathogenic bacteria can inhibit one or more steps in these pathways (Medina et al., 2018; Mine et al., 2018; Han and Kahmann, 2019; Lee et al., 2019). Also, the bacterial effectors are known to subvert multiple steps leading to programed cell death (PCD) in plant, which is a form of immune defense by PTI and/or ETI to control infection (Hoeberichts and Woltering, 2003; Abramovitch and Martin, 2005; Locato and De Gara, 2018). Therefore, it was of interest for us to determine which steps in the citrus innate immune defense are affected by the proteins encoded by the *C*Las genome and prophage.

First, we performed *in vitro* and *in planta* studies to identify the prominent citrus proteins targeted by $LasP_{235}$ and Effector 3. Second, we performed functional assays to determine whether $LasP_{235}$ and Effector 3 have inhibitory effects on their citrus protein targets. Third, we performed molecular dynamic simulations to analyze the details of interaction between $LasP_{235}$ (and Effector 3) and their selected citrus targets and predicted which pairwise interactions are critical for inhibition of the citrus target function. Finally, we validated our prediction of the inhibitory mechanism by site-specific mutations on the citrus protein(s) that affect the critical pairwise interactions. We discovered that each of the two effectors can directly target several citrus innate immune proteins. A clear understanding of the inhibitory mechanisms will provide guidelines for countering *C*Las effectors and developing anti-infectives to block HLB pathogenesis.

MATERIALS AND METHODS

Experimental Procedures

Plant Materials and Growth Conditions

Hamlin trees verified as being HLB-free and ACP-friendly were purchased and placed in the green house. One branch cage placed in the upper part of each tree (three replicates) was filled with 75ACP from an infected population while other trees had cages with clean 75ACPs placed serving as control. The insects were allowed to feed on the trees for a week and then the insects were killed by spraying with topical insecticide. The ACPs were tested for *C*Las and the trees were subsequently returned to the greenhouse. The leaf samples (12 for each biological replicate and

treatment) were collected from the untreated and infected plants and flash-frozen in liquid nitrogen and stored for further analysis.

Cloning and Overexpression of Effectors and Targets in *Escherichia coli*

The genes from *Liberibacter asiaticus* (non-culturable bacteria) were identified ($LasP_{235}$ and Effector 3), codon optimized and cloned in pUC57 by GenScript. The effectors were then amplified and cloned in pET28(a) vector between NdeI and BamHI sites and transformed in *E. coli* BL21 [BL21(DE3)pLysS]. The positive clones were inoculated overnight in LB with Kanamycin. The overnight culture (1%) was grown until the Optical density (OD) reached 0.6 and then induced with IPTG at 30°C for overnight. The cells were harvested next day and resuspended in protein isolation buffer (20-mM Tris-Cl, pH 7.4, 150-mM NaCl, and 10% glycerol). The cell suspension was sonicated and centrifuged at 14,000 rpm, 4°C, 30 min. The supernatant was collected and the inclusion bodies were treated with 9M urea. Following the treatment with urea, the cell suspension was centrifuged and supernatant was collected and refolded. The refolded protein from the inclusion bodies and the soluble fractions were purified using TALON metal affinity resin (Joshi and Puri, 2005).

Isolation of Total Protein From Citrus

Fresh leaf tissue, from five Hamlin trees (*Citrus sinensis* L. Osbeck) was pulverized in liquid nitrogen using a pestle and mortar and the resulting fine powder stirred with 1.5 volumes of extraction buffer [50-mM HEPES pH 7.5, 5-mM EDTA, 5-mM EGTA, 10-mM dithiothreitol (DTT), 10% glycerol, 7.5% polyvinylpolypyrolidone (PVPP), and a protease inhibitor cocktail, Complete™, Boehringer Mannheim]. The slurry was subsequently mixed on a reciprocating shaker (100 oscillations per min) for 10 min, at 4°C, followed by centrifugation 15,000 *g* for 30 min at 4°C. The supernatant was removed and immediately flash-frozen in liquid nitrogen and stored at −80°C until needed (Roy et al., 2011).

Pull Down Assay and LC–MS/MS Analysis to Identify Citrus Targets

The purified refolded effector proteins were incubated with total protein (15 μg) isolated from healthy and infected citrus leaf extract for 2 h at 4°C. The effector–protein complex was incubated with TALON metal affinity resin at 4°C overnight. The resin was washed with column buffer (50-mM Tris-Cl, pH 7.4, 150 mM, 10% glycerol) and eluted with imidazole (250 mM). The eluted protein complex was sent for LC–MS/MS analysis to identify the citrus targets (Zhang et al., 2017). The spectra were searched against the Uniprot database, and taxonomy was set to *C. sinensis*. The only peptides that were ranked 1 were selected and finally those targets were selected for further analysis that had a 95% confidence (Karpievitch et al., 2012).

Enzymatic Assays and Their Inhibitions by the *C*Las Effectors

Superoxide Dismutase Assay

The superoxide dismutase (SOD) assay was quantified based on its ability to inhibit the photochemical reduction of nitroblue tetrazolium (NBT) by superoxide radical and assayed following (SOD Kit; catalog No.: 7,500-100-K) with some modifications. The reaction mixture (3 ml) contained 13 mM methionine, 75-mM NBT, 2-mM riboflavin,100-mM EDTA, and 0.3-ml leaf extracts. The volume was made up to 3 ml using 50-mM phosphate buffer with the addition of riboflavin at the very end. Once the reaction mixture was made, they were mixed well and incubated below two 15-W fluorescent tubes with a photon flux density of around 40 mmol m^{-2} s^{-1} for 10 min. Once the reaction is completed, the tubes were covered with a black cloth and the absorbance was measured at 560 nm. The non-irradiated mixture served as control and the absorbance so measured is inversely proportional to the amount of enzyme added. The SOD activity is defined as the amount of enzyme that caused 50% inhibition of the enzymatic reaction in the absence of the enzyme (Basu et al., 2010). The presented data were an average of three biological replicates, and two of them were of technical replicates.

Aspartyl Protease Assay

The protease assay was performed using a fluorescence based (BODiPY) EnzChek protease assay kit. The analysis of aspartyl protease activity was done by incubating it with no other proteins in sodium citrate buffer (50 mM, pH 4.5). To perform the inhibitory effect of $LasP_{235}$ on the protease activity the renatured aspartyl protease was preincubated with increasing concentrations of $LasP_{235}$ at 4°C for 2 h in sodium citrate buffer. Following incubation, BODiPY-labeled casein substrate was added, and the reaction was monitored by measuring fluorescence in Tecan Infinite 200 PRO microplate reader at 485 ± 12.5 nm excitation/530 ± 15 nm emission filter. The assays were conducted in triplicates (Leippe et al., 2011; Coria et al., 2016).

Glycosyl Hydrolase Assay

The inhibitory effect of recombinant $LasP_{235}$ on recombinant glycosyl hydrolase was assayed using the β-Glucosidase Activity Assay Kit (MAK129, Sigma). The enzymatic reactions were carried out in K-Phosphate buffer (100 mM, pH 6.5) with *p*-nitrophenyl-β-D-glucopyranoside (β-NPG) for 20 min at 37°C. The final absorbance of the hydrolyzed product was measured at 405 nm (Henriques et al., 2017).

Aldehyde Dehydrogenase Assay

This assay was performed using aldehyde dehydrogenase (ALDH) Activity Abcam Assay Kit with modifications. In short, the purified ALDH was incubated with increasing concentration of substrate (acetaldehyde) for 1 h. The absorbance was measured at 450 nm and expressed in terms of NADH standard as mU/ml (Ouyang et al., 2019). The presented data were an average of three biological replicates, and two of them were of technical replicates.

Trypsin Inhibition Assay

The trypsin inhibition assay was done in triplicate and the result was expressed as a means of three replicates. In short, the residual trypsin activity was measured by monitoring the change in absorbance at 247 nm in presence of increasing concentration of recombinant purified Kunitz Trypsin inhibitor (KTI) when incubated with *p*-toluene-sulfonyl-L-Arg methyl ester (Sigma;

Nehir El et al., 2015). The presented data were an average of three biological replicates, and two of them were of technical replicates.

In planta Split GFP Assay (Agro-Infiltration)

Agrobacterium tumefaciens LBA4404 transformant cells carrying Las_{P235}, Effector 3 and the targets from citrus plants (Aspartyl protease, glycosyl hydrolase, SOD, KTI protein, lectin etc.), respectively, are cloned in pR101 vector and cultured overnight in LB medium with 50 μg ml^{-1} of rifampicin and 50 μg ml^{-1} kanamycin, and resuspended in 10-mM $MgCl_2$, 10-mM MES. The culture was diluted to an optical density of 0.5 (OD 600 nm). For each effector–target interaction, three leaves of 4 *Nicotiana benthamiana* plants overexpressing GFP1-9 were infiltrated with the *A. tumefaciens* suspension containing the effector and the target plasmids, respectively. The agro-infiltrated leaves were analyzed for protein localization at 3 dpi under a microscope (Olympus BX51-P) equipped with a UV light source. The agroinfiltrated plants were kept in a greenhouse for 24 h and the interaction was visualized using Illumatool lighting system (LT-9500; Lightools Research) with a 488-nm excitation filter (blue) and a colored glass 520-nm long pass filter. The photographs were taken by Photometric CoolSNAP HQ camera (Cabantous and Waldo, 2006; Liu et al., 2018).

Estimation of Superoxide Anion

The leaf disks from agro-infiltrated tobacco plants were incubated at 25°C on a shaker for 30 min in dark in 1 ml of K-phosphate buffer (20 mM, pH 6.0) containing 500-μM XTT. The increase in absorbance was measured at 470 nm in a spectrophotometer (Ramegowda et al., 2012). The presented data were an average of three biological replicates, and two of them were of technical replicates.

Lipid Binding and MIC Assays for Lipid Transfer Protein

The lipid binding activity of recombinant LTP-6X His protein overexpressed and purified from *E. coli* was mixed with of 2-*p*-toluidinonaphthalene-6-sulphonate (TNS) at 25°C. The results were recorded at excitation 320 nm and the emission at 437 nm. The inhibitory action of $LasP_{235}$ on lipid transfer protein (LTP) was assessed using increasing concentration of $LasP_{235}$ and the results were measured. The purified GFP was used as a control (Melnikova et al., 2020). The minimum inhibitory concentration (MIC) of the LTP was performed using broth microdilution technique. The assay was carried out using 5×10^5 colony forming units (CFU ml^{-1}) in MHB. The MIC was defined as the lowest concentration of the protein required to inhibit the visible growth of bacterial strains used (Ebbensgaard et al., 2015). The presented data were an average of three replicates, and two of them were of technical replicates.

Estimation of Ion Leakage From Leaf Disks

Agrobacterium tumefaciens LBA4404 transformant cells carrying Effector 3 and the targets from citrus plants KTI protein cloned in pR101 vector was cultured overnight in LB medium with 50 μg ml^{-1} of rifampicin and 50 μg ml^{-1} kanamycin and resuspended in 10-mM $MgCl_2$, 10-mM MES. The culture was diluted to an optical density of 0.5 (OD 600 nm). For the assay, three leaves of N. *benthamiana* plants previously treated with paraquat (PQ; 100 μM) were infiltrated with the *A. tumefaciens* suspension containing the effector alone, Kunitz alone and the mixture of effector 3 and Kunitz, respectively (Pitino et al., 2016, 2018) and incubated for 48 h. The leaf disks were prepared by punching the leaf disks with a cork puncher. The punctured leaf disks were placed in water (50 ml) for 5 min to mitigate the error of measuring ion leakage due to injury inflicted on the leaves due to puncturing. The water was removed and the leaf discs were incubated with 5 ml. the conductivity was measured after 3 h using Mi180 bench meter and this value is referred to as *A*. The leaf disks with the bathing solution were then incubated at 95°C for 25 min and then cooled to room temperature to enable complete ion leakage. The conductivity was measured again, and this value is referred to as *B*. The ion leakage is subsequently expressed as $(A/B) \times 100$. All experiments were carried out in three biological replicates with five leaf disks for each sample (Wu et al., 2017; Hatsugai et al., 2018).

Pathogen Inoculation and LTP Treatment in *N. benthamiana* Leaves

Pseudomonas syringae pv. *Tomato* DC3000 was cultured on King'S B (KB) medium containing 50 μg ml^{-1} rifampicin. Overnight, log-phase cultures were grown to an optical density at OD_{600nm} of 0.6–0.8 (OD 0.1 = 10^8 cfu ml^{-1}) and diluted with 10-mM $MgCl_2$ to the concentrations of 10^5 CFU ml^{-1} before inoculation. Control was performed with 10-mM $MgCl_2$. The bacterial suspensions were infiltrated into the abaxial surface of a leaf using a 1-ml syringe without a needle. *Agrobacterium tumefaciens* LBA4404 transformant cells carrying $LasP_{235}$ and LTP protein cloned in pR101 vector was cultured overnight in LB medium with 50 μg ml^{-1} of rifampicin and 50 μg ml^{-1} kanamycin and resuspended in 10-mM $MgCl_2$, 10-mM MES. The culture was diluted to an optical density of 0.5 (OD 600 nm). For the assay, the infected leaves of *N. benthamiana* plants were infiltrated with the *A. tumefaciens* suspension containing the LTP alone, LTP+ $LasP_{235}$, different mimics (Liu et al., 2013). The presented data were an average of three replicates, and two of them were of technical replicates.

The qPCR Analysis

The concentration, quality, and integrity of the DNA was analyzed using the Agilent 2100 bioanalyzer (Bio–Rad) and NanoDrop™ ND-1000 (Thermo Scientific). The qRT-PCR experiments were conducted using GoTaq qPCR Master Mix (Promega), *P.syringae* gene-specific primers (Psy-F ATGATCGGAGCGGACAAG; Psy-R GCT CTT GAG GCA AGC ACT), and *PR1b* (pathogenesis related protein): PR1F-CGAGAGGCCAAGCTATAACTAC and PR1R: GCAAGAAATGAACCACCATCC gene from tomato genome was used a as standard to show that the variation in Ct values was due to infection and treatment with LTP or the mimics (Guilbaud et al., 2016). The experiments were carried out with three biological replicates and each replicate divided into two technical replicates in a CFX-96 Bio–Rad thermocycler (Bio–Rad). Increasing temperature (0.5°C 10 s^{-1}) from 55 to 95°C was

used for melt curve analysis. The bacterial load corresponding to the CFU was calculated from standard curve. To determine the sensitivity of the qPCR assay, a culture of bacterial strain was diluted with sterile water to generate a 10-fold dilution series from 1×10^8 to 1×10 CFU·ml^{-1}. Each dilution (1 μl) of bacterial suspension was used as templates for quantifying bacterial load by direct qPCR without a DNA extraction step. The resulted Ct values were plotted against the corresponding CFU·ml–^{1} value to generate a standard curve for the detection limit. Each dilution was analyzed in three replicates.

Data Analysis

For each of the investigated parameters, the experiments were conducted in triplicate with two technical replicates. All experimental data values were expressed as means of three measurements [± standard error (SE)]. The significance of the differences between the mean values were statistically evaluated by two-sided *t*-test at $p \leq 0.05$ using the Windows 2004/Microsoft Excel computer package for significance. The K_m (Michaelis constant), V_{max} were calculated using Lineweaver Burk plot. The $K_{cat} = V_{max}/[E]$, where E is the total enzyme, i.e., free enzyme and enzyme bound to the substrate. IC_{50} = (Concentration of the effector protein × 50)/% inhibition.

Molecular Modeling

Prediction of Protein 3D Structures and Complexes

The 3D structures of the two *CLas* proteins (*LasP*$_{235}$ and Effector 3) and the two citrus proteins (LTP and KTI) were predicted using I-TASSER (https://zhanglab.ccmb.med.umich.edu/I-TASSER/). We then used HADDOCK version 2.2 webserver to predict interaction interfaces of *LasP*$_{235}$-LTP and Kunitz-E3 complexes (http://milou.science.uu.nl/services/HADDOCK2.2/). The selected complexes of *LasP*$_{235}$-LTP and Kunitz-E3 were further refined using molecular dynamics (MD) simulations of these complexes in the presence of water.

Protein-Water System Setup for MD Simulation

Our simulations started with single protein (i.e., LTP, *LasP*$_{235}$, Kunitz or E3) in water. These systems contained 10,000 water molecules in a box of 6.9 × 6.8 × 7.1 nm. To refine the models of *LasP*$_{235}$-LTP and Kunitz-E3 obtained from HADDOCK. We conducted MD simulations of these complexes in the presence of water. The protein–protein complex systems contain 30,000 water molecules in a box of 9.9 × 9.9 × 9.9 nm with excess NaCl at 150 mM to mimic experimental conditions. For Kunitz-E3 complexes, we focus on model with Kunitz's active loop in close contact with E3's interface that contain either aspartic acid or glutamic acid residues or a large hydrophobic surface. For *LasP*$_{235}$-LTP complexes, we focus on model with LTP's lipid entrance site B1 and B2 (see **Supplementary Figure 3**) in close contact with *LasP*$_{235}$. Following the MD simulation, the systems with stable complexes and adequate protein–protein pairwise residues interactions were then further validated by extended MD simulation.

Protein–Bilayer System Setup for MD Simulation

Our simulations started with a single LTP in the water and a mimetic of the *E. coli* inner membrane composed of a 3:1 ratio of 1-palmitoyl-2-oleoyl-*sn*-glycero-3-phosphoethanolamine (Wu et al., 2017) (POPE) and 1-palmitoyl-2-oleoyl-*sn*-glycero-3-phosphoglycerol (POPG). The lipid bilayers are constructed with the Charm–GUI membrane builder (Wu E. L. et al., 2014) followed by 40 ns of *NpT* simulation at 310 K with semi-isotropic pressure coupling. The LTP–bilayer system contained 10,000 water molecules and 128 lipid molecules in a box of 6.1 × 6.1 × 12.5 nm. We also conducted simulation of *LasP*$_{235}$-LTP complex in the bilayer POPE: POPG (3:1 ratio) to further refine the *LasP*$_{235}$-LTP models obtained from MD simulation of the *LasP*$_{235}$-LTP complexes in the water. The *LasP*$_{235}$-LTP/bilayer contained 23,600 water molecules and 256 lipid molecules in a box of 8.7 × 8.7 × 13.7 nm. The LTP, or *LasP*$_{235}$-LTP complex, was placed 3.5 nm away from the center of mass of the lipid bilayer along its normal. The protein/bilayer systems were neutralized and excess NaCl was added at 150 mM to mimic experimental conditions.

Simulation Protocol

For the MD simulations, the TIP3P water model was used with CHARMM modifications (Albaugh et al., 2016). The water molecules were rigidified with SETTLE (Miyamoto and Kollman, 1993) and the molecular bond-lengths were constrained with P-LINC Lennard–Jones interactions (Wennberg et al., 2013) were evaluated using a group-based cutoff, truncated at 1 nm without a smoothing function. The Coulomb interactions were calculated using the smooth particle–mesh Ewald method (Cerutti et al., 2009; Kratz et al., 2016; Boateng, 2020) with a Fourier grid spacing of 0.12 nm (Fischer et al., 2015). The simulation in the *NpT* ensemble was achieved by semi-isotropic coupling at 1 bar with coupling constants of 4 ps (Aoki and Yonezawa, 1992; Blumer et al., 2020) and temperature-coupling the simulation system using velocity Langevin dynamics with a coupling constant of 1 ps (Washio et al., 2018). The integration time step was 2 fs. The non-bonded pair-list was updated every 20 fs (Walser et al., 2002).

RESULTS

In vitro Protein Assay to Identify the Citrus Protein Targets of *LasP*$_{235}$ and Effector 3

The *LasP*$_{235}$ identified in the prophage region of Las genome encoded a 123 amino-acid protein has an N-terminal nuclear localization signal (NLS) with no typical signal peptide (Hao et al., 2019). Effector 3 on the contrary has a predicted chloroplast targeting signal sequence (Pitino et al., 2016, 2018). The homology modeling predicted the presence of helical bundles in the structure of *LasP*$_{235}$ as shown in **Supplementary Figure 1A**. Note that the similar helical bundles are also present in AvrRps4, a *P. syringae* effector involved in plant immunity (Sohn et al., 2012). It is suggested that the helical effectors from bacteria may interact with multiple plant helical proteins *via* intermolecular

coiled–coil interactions (Chan et al., 2010; Goritschnig et al., 2016). These proteins may be located on the plasma membrane, in the cytosolic fluid or vacuole, and in the nucleus. The homology modeling also predicted two helix bundles in the structure of Effector 3 in addition to a disordered C-terminal segment (see **Supplementary Figure 1B**). The latter may make Effector 3 a promiscuous binding partners of several citrus proteins. In addition, due to the presence of chloroplast targeting signal, Effector 3 may be a potential *CLas* effector. Note that multiple chloroplast proteins are involved in ROS production and plant hormone signaling (Sowden et al., 2018), which may mediate cell death as an innate immune defense.

The steps in our target identification scheme are shown in **Figure 1** (left). First, we expressed $LasP_{235}$ and Effector 3 in *E. coli* with C-terminal His_6-tags. The Effector 3 was expressed without the signal sequence. Both proteins were extracted from the inclusion body and re-folded. Second, the His-tagged $LasP_{235}$ and Effector 3 were bound to TALON columns and were incubated with citrus protein extracts from the uninfected and *CLas*-infected Hamlin. Third, bound citrus protein targets were eluted from the column and identified by LC–MS/MS. Finally, the spectra from LC–MS/MS were searched against the Uniprot database with taxonomy set to *C. sinensis*. The highest ranked citrus proteins, in terms of the LC–MS/MS protein score (Koenig et al., 2008), were selected as putative targets of $LasP_{235}$ and Effector 3. See **Supplementary Tables 1A,B** for all citrus targets of $LasP_{235}$ and Effector 3 with high protein scores. **Supplementary Table 1C** lists the background targets as obtained by first incubating the TALON column with the protein extraction buffer and then elution by the citrus protein extract. Note that the non-specific targets with low protein scores were obtained by buffer elution. As shown in **Figure 1** (right), the top-ranked citrus targets of $LasP_{235}$ and Effector 3 show protein scores far greater than those listed for the non-specific targets in **Supplementary Table 1C**. A subset of these targets was further analyzed. The selected $LasP_{235}$ targets are SOD (from infected citrus), LTP (from healthy citrus), Aspartyl Endopeptidase, (AP) and Glycosyl Hydrolase family 17, GH17 (from both healthy and infected citrus) whereas the Effector 3 targets are as follows: KTI and ALDH from both healthy and infected citrus, Elongation Factor Tu (Ef–Tu) from infected citrus, lectin, and 21 kDa seed protein-like (a functional homolog of KTI) from healthy citrus. As indicated, all target proteins listed in **Figure 1** (right) are involved in citrus innate immunity. Although, it allows identification of both extracellular and intracellular targets of *CLas* effectors from infected and healthy citrus, our method in **Figure 1** is likely to miss the citrus targets that are expressed at a low level.

In planta Validation of the Citrus Protein Targets of $LasP_{235}$ and Effector 3

In planta validation is based on a split triple GFP assay, which has been successfully applied to monitor protein–protein interactions in yeast, human, and plant (Cabantous et al., 2013; Pedelacq et al., 2019). The assay relies on the principle that specially enhanced 11 stranded GFP can be split into GFP1-9, GFP10, and GFP11 with none of the three split components showing fluorescence. However, the fluorescence is recovered when GFP1-9, GFP10, and GFP11 are re-assembled. We constructed stable transgenic tobacco lines that overexpress GFP1-9 as a detector of *in planta* protein–protein interactions. The two agrobacterium constructs, i.e., one overexpressing $LasP_{235}$ (or Effector 3) with a GFP11 tag and the other a putative citrus target with a GFP10 tag, were infiltrated in the GFP1-9 transgenic tobacco. As shown in the experimental design of **Figure 2A**, we expect to observe (i) green fluorescence in the presence of a target–effector interaction and (ii) no fluorescence in the absence of interaction. In our assay, for negative controls (see **Figure 2B**), we confirmed the lack of interaction between Effector 3 and the targets for $LasP_{235}$ (and the lack of interaction between $LasP_{235}$ and the targets for Effector 3). Agrobacterium carrying enhanced GFP was used as a positive control. Note that the leaves in the negative control appear red in color due to chlorophyll autofluorescence. The fluorescence coming from chlorophyll molecules is a result of emission characteristics of both individual chlorophyll molecules and the fluorescence is observed at excitation and emission maxima of 685 and 720–730 nm. **Figure 2B** (top) shows the results of the split GFP assay monitoring the interaction of $LasP_{235}$. Note the presence of green fluorescence at the infiltrated leaf sites for SOD, LTP, AP, and GH17, which were identified as putative targets of $LasP_{23}$ as identified from our *in vitro* protein assay as described **Figure 2A**. The pattern of fluorescence is comparable to the infiltration of agrobacterium carrying enhanced GFP. Thus, the split GFP assay shows specific *in planta* interactions between $LasP_{235}$ and citrus proteins (SOD, LTP, AP, and GH17). **Figure 2B** (bottom) shows the results of the split-GFP assay monitoring the interaction of Effector 3. The presence fluorescence at the filtrated sites indicates specific *in planta* interactions between Effector 3 and (KTI, ALDH2, lectin, and Ef–Tu) that were identified by the *in vitro* protein assay. Triple split GFP assay provides the following advantages (Serebriiskii et al., 2000; Rajagopala, 2015) over other commonly used assays such as yeast-two hybrid system for monitoring protein–protein interaction: (i) It can be readily adapted to *in planta* systems; (ii) It limits false positives and negatives; (iii) Small GFP10 and GFP11 tags retain native effector–target interactions; (iv) Positive and negative controls can easily be incorporated for *in planta* measurement to improve the fidelity of the assay.

The Two *C*Las Proteins Inhibit the Functions of Their Specific Citrus Targets *In vitro* Assays

Three targets of $LasP_{235}$, i.e., SOD, AP, and GH17, that are validated by *in planta* split GFP assay, are citrus PR or defense proteins with enzymatic activities. As described in the "Methods," the citrus target proteins were expressed in *E. coli*, extracted from the inclusion body, and purified by affinity purification schemes. After purification, the proteins were re-folded. The identity of the proteins was confirmed by western blot analysis (**Supplementary Figure 2**) and Mass spec analysis (data are not shown). Therefore, before conducting *in vitro* inhibition assays,

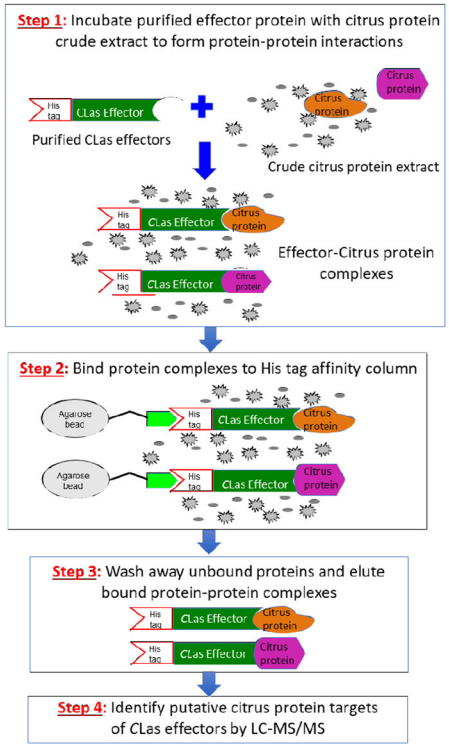

Selected Citrus Protein Targets of *CLas* P235			
	Protein Name and ID	**Protein Score**	**Function**
Healthy Citrus	Lipid Transfer Protein LTP; KDO49686	240	Involved in binding and shuttling lipids between cell membranes; acts also as antimicrobial proteins against bacteria.
Healthy and Infected Citrus	Aspartic-type Endopeptidase AP; KDO42753	1453/1143	Involved in constitutive disease resistance.
	Glycosyl Hydrolase 17 family GH17; KDO39187	811/886	Known to be involved in defense against fungal infection and also in planta cell wall metabolism.
Infected Citrus	Super Oxide Dismutase SOD; KDO57691	213	Constitutes the first line of defense against ROS produced during pathogenic infection.
Selected Citrus Protein Targets of CLas Effector 3			
Healthy Citrus	21 kDa seed protein-like; XP_015382840	143	A functional homolog of Kunitz Protease Inhibitor.
Healthy and Infected Citrus	Aldehyde Dehydrogenase ALDH; KDO69713	447/437	Primarily involved in removing toxic aldehyde but also can bind to bacterial effectors to induce host defense via programmed cell death.
	Kunitz Protease Trypsin Inhibitor KTI; KDO40321	429/288	Inhibits programmed cell death to the benefit of the host and to the detriment of the pathogen.
Infected Citrus	Elongation factor TU Ef-Tu, chloroplastic; XP_006476894	271	Affected during PTI; unknown if it is a target of bacterial effectors.

FIGURE 1 | Identification of citrus target proteins of the *CLas* effectors. (Left) Outlines of the experimental steps. Step 1. *CLas* effectors were overexpressed in *E. coli* with His_6 tag. Purified His_6-tagged effectors (colored green) were incubated with protein extracts from healthy and infected Hamlin citrus. Specific citrus target protein (colored orange and magenta) bound to the *CLas* effectors. Step 2. Effector-target complexes were TALON on Agarose beads and non-target citrus proteins were washed away. Step 3. The specific effector-target complexes were eluted. Step 4. The citrus target proteins from the eluted complexes were identified by LC–MS/MS. (Right) Selected citrus protein targets of the *CLas* effectors, $LasP_{235}$ and Effector 3. The citrus targets were chosen on the basis of their high protein scores. The target proteins were selected both from healthy and *CLas*-infected protein extracts. GenBank sequence IDs and putative functions (based on the literature data) of the citrus targets are listed.

it was necessary to determine the enzymatic activities of the recombinant enzymes to confirm that they retained the native fold and function. We then determined the inhibitory activity of $LasP_{235}$ on them by measuring IC_{50} (the concentration required for 50% reduction in enzymatic activity). The SOD, which is unique to plants, prevents damage caused by the ROS burst upon pathogen infection (Miller, 2012). While it facilitates the direct killing of the pathogen and induction of plant defense genes, excessive ROS is damaging to the plant. The SOD, produced in mitochondrion, peroxisome, and chloroplast, converts oxygen radical to molecular oxygen and hydrogen peroxide. The latter, also potentially phytotoxic, is subsequently converted by plant catalase into molecular oxygen and water. The SOD is also involved in regulating ROS signaling leading to the induction of defense genes (Wang et al., 2018). As shown in **Table 1**, $LasP_{235}$ inhibits the activity of the citrus SOD. The Citrus AP belongs to the A1 family of atypical aspartate proteases, primarily located in apoplast and chloroplast. It has been shown that an atypical aspartate protease, expressed in the apoplast, confers constitutive disease resistance 1 (CDR1) in *Arabidopsis* probably by producing a peptide ligand through cleavage and subsequent induction of SA signaling and expression of PR genes (Varghese et al., 1994; Simões et al., 2007). The results of enzyme assay show that $LasP_{235}$ inhibits the activity of the citrus AP. The GH17, a citrus (β1-3) glucanase, is another direct interactor of $LasP_{235}$. Typically, GH17 glucanases are known to provide disease resistance against fungi by hydrolyzing fungal chitins (Hrmova and Fincher, 2001). However, GH17 also has a role in immune defense in general in that it regulates the formation of callose (a β1-3 glucan polysaccharide), which is an essential component of papillae, an ultrastructure formed at the site of pathogen penetration. Apart from callose, the papillae also contain ROS and antimicrobial peptide thionin and thus provide the first line of defense against pathogen invasion. In papillae-mediated immunity, callose may be involved in two different mechanisms of plant defense against pathogens. First, the callose deposition in papillae may block pathogen spread. Second, the hydrolyzed products of callose by GH17 may serve as ligands for the PRRs and may induce SA signaling leading to plant immune defense. Thus, the GH17-mediated hydrolysis of callose may either support pathogen spread or induce SA signaling. As evident from **Table 1**, $LasP_{235}$ inhibits the glucanase activity of the citrus GH17. Therefore, it may induce SA signaling and help *CLas* to suppress citrus immune defense. The citrus

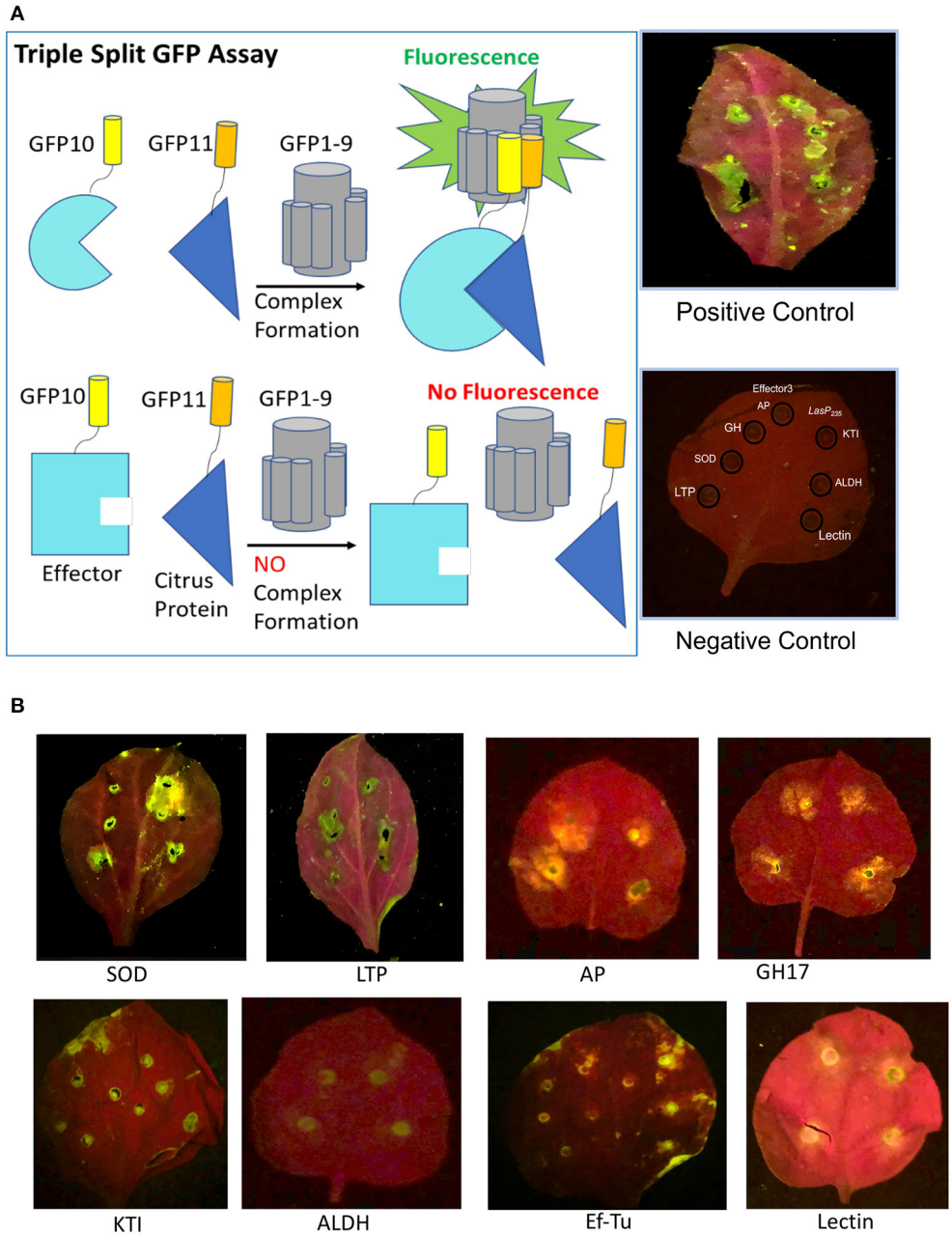

FIGURE 2 | *In planta* validation of the selected citrus protein targets of $LasP_{235}$ and Effector 3 by triple split GFP assay. [**(A)**, left] A schematic representation of the principle of the triple split GFP assay. Green fluorescence is observed when the Effector (cyan) linked to GFP10 (yellow) interacts with the target (blue) linked to GFP11 (orange) and the effector-target complex complements with GFP1-9. There is no fluorescence in the absence of an interaction. [**(A)**, right] The presence of fluorescence when agrobacterium carrying enhanced GFP is infiltrated on the leaves of transgenic tobacco expressing GFP1-9 is used as a positive control. Absence of fluorescence when the leaves of transgenic tobacco expressing GFP1-9 co-infiltrated with $LasP_{235}$ and the interactors of Effector 3 in one-half of the leaf (or Effector 3 and the interactors of $LasP_{235}$ in the other half of the leaf) served as the negative controls. Note the absence of fluorescence. Under the 488 nm excitation filter (blue) and colored glass 520 nm long pass filter, the chlorophyll background appears as red and fluorescence at the site of co-infiltration of the effector and its target appears as greenish yellow spots. **(B)** Complex formation when $LasP_{235}$ is co-infiltrated with SOD, LTP, AP, and GH17 in the leaves of GFP1-9 transgenic tobacco (top panel) and when Effector 3 is co-infiltrated with Effector 3 and KTI, ALDH, Ef–Tu, and Lectin (bottom panel).

LTP is the non-enzyme direct interactor of $LasP_{235}$. The plant LTPs possess (i) lipid binding property, which is critical to lipid homeostasis and membrane dynamics and (ii) bactericidal activity as a component of immune defense (Liu et al., 2015; Finkina et al., 2016; Salminen et al., 2016; Shenkarev et al., 2017). **Table 1** shows that $LasP_{235}$ can block both lipid-binding

TABLE 1 | The citrus AP, SOD, GH17, and ALDH were overexpressed in and purified from *E. coli* and enzymatic assays were performed on them following the protocols described in Experimental Procedures section.

	Citrus targets	K_{cat} (s^{-1})	K_m (mM)	IC50	Substrate/ligand concentration (mM)	Target concentration (mM)	MIC (μM)[b] (−P235) BL21	MIC (μM)[b] (−P235) ATCC	MIC (μM)[b] (+P235) BL21	MIC (μM)[b] (+P235) ATCC
P235	AP	277.2	315.8	6.30	10	20				
	SOD	12.45	42.3	4.37	2	4				
	GH17	0.003	0.042	1.95	1	25				
	LTP			1.43[a]	8	20	12.5	15	Growth	Growth
Effector 3	KTI			5.60[c]	4	10				
	ALDH	0.094	2.131	0.86	2	10				

K_{cat} and K_m are given for the citrus AP, SOD, GH17, and ALDH. The IC_{50} (50% reduction in catalytic activity) by the effector is provided as the ratio of the substrate concentration.
[a]Lipid binding assay was performed for LTP to demonstrate the inhibitory effect of $LasP_{235}$.
[b]Bactericidal effect of LTP was monitored using two E. coli strains: BL21 and ATCC25922; the corresponding MIC values are in μM. Addition of $LasP_{235}$ at a concentration same as the MIC completely blocks the bactericidal effect of LTP on the two E. coli strains.
[c]Effector 3 is added in the Trypsin inhibition assay by KTI to determine the IC_{50}.

and antimicrobial activities. **Table 1** shows inhibitory activities of Effector 3 on two citrus target proteins: ALDH, which converts aldehydes into carboxylic acid using NADPH/NADH as a co-factor (Jimenez-Lopez et al., 2016) and KTI, which inhibits protease activity of PCD-inducing trypsin (Li et al., 2008).

In planta Assays

In planta assays for monitoring ROS production, bacterial clearance, and PCD induction were performed in tobacco to examine the inhibitory effect $LasP_{235}$ and Effector 3 on their citrus target proteins. Paraquat was used for inducing the production of ROS in tobacco. The ROS level was monitored using a ROS/Superoxide detection assay (Zhou et al., 2018). In this experiment, the ROS level induced by agrobacterium carrying an empty vector (i.e., no gene) plus PQ was normalized to 100%. Note that, the infiltration of agrobacterium carrying citrus SOD reduced the ROS level significantly below 100%. However, as shown in **Figure 3A** (left), the simultaneous addition of agrobacteria carrying $LasP_{235}$, and citrus SOD showed the elevation in the ROS level proving *in planta* inhibition of citrus SOD by $LasP_{235}$. *In planta* bactericidal activity of citrus LTP was monitored by qPCR that showed the reduction of bacterial load in tobacco infected with *P. syringae* pv. DC3000. As shown in **Figure 3A** (right), agrobacterium carrying citrus LTP (0.4×10^8 CFU ml^{-1}) reduced the bacterial load to 37%. Increasing agrobacterium carrying citrus LTP by 10 times (i.e., 0.4×10^9 CFU ml^{-1}) led to the 75% reduction in the bacterial load. The addition of agrobacterium carrying $LasP_{235}$ (0.4×10^8 CFU ml^{-1}) or 10 times of that increased the bacterial load. This proves that $LasP_{235}$ is able to block *in planta* the bactericidal activity of the citrus LTP. **Supplementary Table 2** shows the Ct values of a *Pst* gene (a measure of bacterial load) at different $LasP_{235}$ concentrations. *In planta* studies were conducted in tobacco to examine the effect of (Effector 3–Lectin/Ef–Tu) interactions. As shown in **Figure 3B** (left), the infiltration of agrobacterium carrying Effector 3 induced ROS at a high level (85%). The ROS level due to agrobacterium carrying an empty vector plus PQ was set to 100%. Infiltration of agrobacterium carrying citrus Lectin or Ef–Tu had negligible effect on the ROS level. The co-infiltration of Effector 3 plus lectin or EF–Tu had very little effect on the ROS level induced by Effector 3 alone. However, combination of lectin and Ef–Tu was able to reduce the ROS level induced by Effector 3. In this regard, it is important to note that some bacteria, such as *Porphyromonas gingivalis*, *Mycobacterium tuberculosis*, *Helicobacter pylori*, and *Bacillus anthracis*, utilize ROS to support their growth and to establish infection (Paiva and Bozza, 2014) whereas plant lectin and Ef–Tu tend to inhibit ROS production or ROS-mediated signaling (Wang and Bouwmeester, 2017). It appears that pathogenic CLas may use Effector 3 to maintain ROS level that is beneficial to pathogen growth and infection by inhibiting anti-ROS citrus lectins and Ef–Tu. The PQ was also used to induce PCD *via* ROS in tobacco. The PCD was monitored by electrolyte leakage (Kacprzyk et al., 2016), which was set to 100% as induced by agrobacterium carrying an empty vector plus PQ. Infiltration of the agrobacterium carrying Effector 3 induced ∼50% electrolyte leakage, which, as shown in **Figure 3B** (Right), was reduced on infiltration of agrobacterium carrying citrus KTI. The co-infiltration of Agrobacteria carrying citrus KTI and Effector 3 elevated PCD thereby confirming that Effector 3 is an inhibitor of the citrus KTI.

To Predict and Validate the Molecular Mechanism of Effector–Target Inhibitory Interactions

We performed all-atom MD simulations (Li et al., 2018) to predict the interactions that stabilize the (inhibitory *CLas* effector–citrus protein target) complexes. Initially, we focused on the bactericidal effect of LTP. As described in Materials and Methods section, we first obtained an optimized homology-based model of the citrus LTP as shown in **Supplementary Figure 1C**. Then, we performed MD simulations in (water: lipid) bilayer for 10 μs. As described in the **Supplementary Figure 4A**, MD simulations revealed that the LTP helices h2, h3, h4, and the C-terminal loop were involved in interaction with the lipid bilayer defining membrane attachment, which is the first step in the

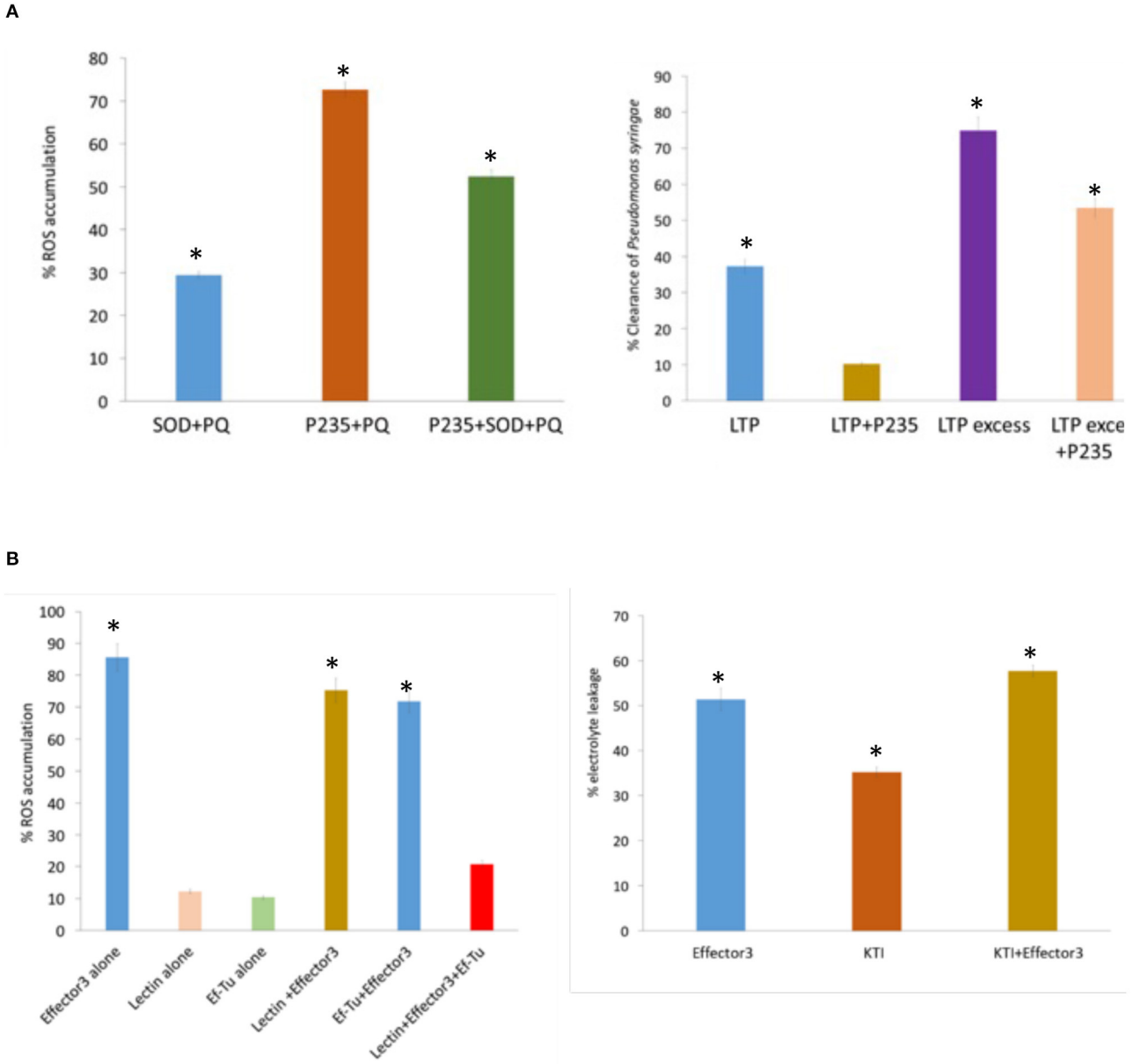

FIGURE 3 | *In vitro* and *in planta* assays to demonstrate the inhibitory activity of the CLas effectors on their citrus protein targets. First, enzymatic, binding, or bactericidal assays are performed to determine the appropriate functional properties of the citrus target proteins and subsequently, the same assays are conducted to demonstrate the inhibitory activities of the CLas effectors on their citrus targets. [**(A)**, left] The inhibitory effect of $LasP_{235}$ on SOD is monitored in tobacco by fluorescence microscopy. [**(A)**, right] Percentage reduction relative to the initial CFU of *E. coli* ATCC25922 by LTP alone and LTP plus $LasP_{235}$. [**(B)**, left] The ability of Effector 3 to induce the ROS release in tobacco. The addition of lectin or Ef–Tu is not sufficient to suppress the ROS release by Effector 3. However, the combination of lectin and Ef–Tu significantly reduces the ROS release by Effector 3. [**(B)**, right] The electrolyte leakage due to ROS-produced by PQ is set 100%. A relative electrolyte leakage due to infiltration of Effector 3, KTI, and Effector 3 + KTI in tobacco. *Indicates statistical significance at $p \leq 0.05$.

bactericidal activity. The interactions of the positively charge arginine residues R21, R32, R39, R44, R71, and R89 (shown in blue in **Figure 4B**) with the negatively charged lipid polar heads appear to be extremely critical for the LTP membrane attachment. To study the interaction of $LasP_{235}$ with LTP, we docked the homology based $LasP_{235}$ model to the optimized LTP model. We then performed MD simulations of the LTP-$LasP_{235}$ complex in aqueous environment for 6 μS to determine which mode of $LasP_{235}$ binding may block the LTP attachment to the lipid bilayer as discussed in **Supplementary Figures 4A,B**. One mode of $LasP_{235}$ (magenta) interaction, shown in **Figure 4A** (left), involves the LTP (cyan) helices h2, h3, and h4 and the C-terminal loop resulting in partial blocking of the B1 LTP site by $LasP_{235}$. The prominent pair-wise contacts between $LasP_{235}$

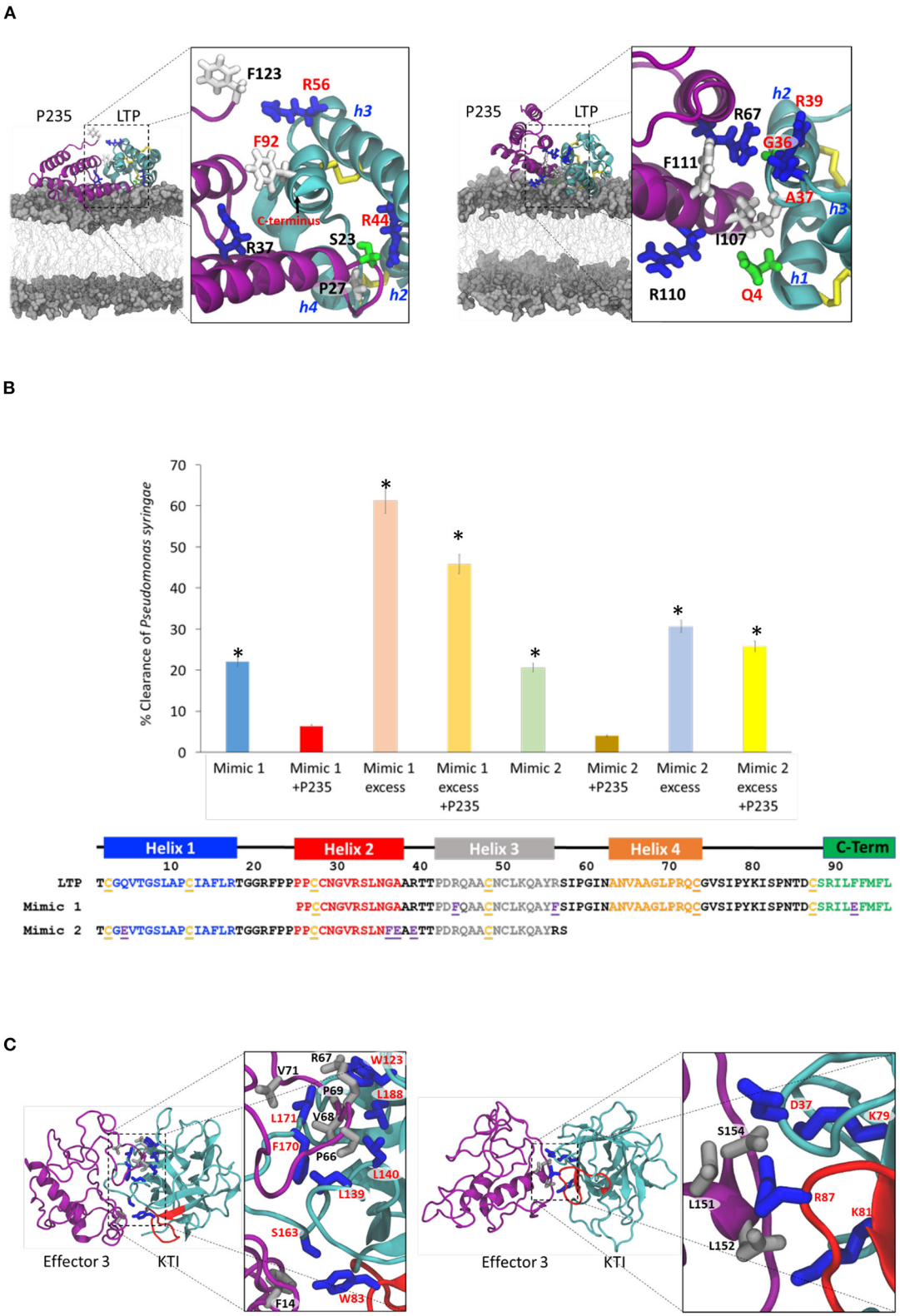

FIGURE 4 | Prediction and validation of (citrus target–*CLas* effector) interaction at the contact interface. Molecular modeling is performed to predict the pairwise interactions based on which mimics are designed to displace the effector from the (citrus target-*CLas* effector) complex. Finally, experiments are performed to determine if the mimic, indeed, displaces the effector from the complex and if so, our prediction of the pairwise interactions are validated. **(A)** Two possible modes of

(Continued)

FIGURE 4 | interactions between $LasP_{235}$ (magenta ribbon) and LTP (cyan ribbon) which block the membrane attachment of LTP thereby inhibiting the bactericidal activity. The disulfide bridges are shown as yellow sticks. The LTP helices (h2, h3, and h4) and the C-terminal segment are predicted to be involved in one mode of interaction. The LTP helices (h1, h2, and h3) are involved in the other mode of interaction. Important residues in the pairwise contacts are shown: $LasP_{235}$ residues are labeled black whereas the LTP residues are labeled red. Basic, acidic, neutral, and acidic residues are, respectively, as blue, red, green, and gray sticks. **(B)** Amino acid sequences of Mimic 1 and Mimic 2 at the bottom. Bacterial (*P. syringae* pv. tobaci) clearance in tobacco by the two mimics in the presence and absence of $LasP_{235}$. Note that an excess of the mimics is needed for significant bacterial clearance. Mimic 1 is a better bactericidal than Mimic 2. $LasP_{235}$ is an inhibitor of Mimic 1 or Mimic 2. **(C)** Two models of interactions between Effector 3 (magenta ribbon) and KTI (cyan ribbon with the reactive loop in red). Both models show interactions with the KTI reactive loop as a prominent mode of inhibition. The predicted pairwise interactions are shown. The residues from Effector 3 are shown as gray sticks and labeled black whereas the residues from KTI are shown as blue sticks and label red. *Indicates statistical significance at $p \leq 0.05$.

(magenta) and LTP (cyan) are predicted from MD simulations using the method described in **Supplementary Figure 4**. They are as follows: S23-R44, P27-R44, R37-F92, and F123-R56. Another mode of $LasP_{235}$ binding as shown in **Figure 4A** (right) involves the LTP helices h1, h2, and h3 with pairwise contacts: I107-R39, R110-A37, R110-Q4, and F111-G36. In both binding modes, the LTP attachment to the bacterial membrane is partially blocked. Based on the two modes of interactions, we designed two LTP mimics shown in **Figure 4B**, i.e., Mimic 1 containing h2, h3, h4, and the C-terminal loop and Mimic 2 containing h1, h2, and h3. We also introduced amino acid substitutions, i.e., R44F, R56F, and F92E in Mimic 1 and Q4E, G36F, A37E, R39E in Mimic 2. These amino acid substitutions are predicted to increase the strength of pairwise interactions between LTP and $LasP_{235}$ as listed above. While both mimics are predicted to partially block the inhibitory activity of $LasP_{235}$ on bactericidal LTP, Mimic 1 is supposed be a better blocker than Mimic 2. Our predictions are validated by the results of *in planta* tobacco studies shown in **Figure 4B**. Here, Mimics 1 and 2 were infiltrated to express at the same and 10 times level of $LasP_{235}$. The results show that: (i) both mimics by themselves show bactericidal effect on *P. syringae* pv. tobaci but smaller than the full-length LTP; and (ii) Mimic 1 is better $LasP_{235}$ blocker/bactericidal than Mimic 2. These experimental observations are in full agreement with our predictions. Therefore, we may conclude that interactions shown in **Figure 4B** (left) is the most prominent mode of LTP blocking by $LasP_{235}$. **Supplementary Figure 4B** shows the Ct values of a *Pst* gene (a measure of bacterial load) due to treatment of Mimics 1 and 2 at different concentrations.

We constructed two models of (Effector 3: KTI) complex with Effector 3 and Kunitz represented respectively by purple and cyan ribbons. Both complexes are chosen to block the reactive KTI loop (residues 82–94) as shown in the homology-based model of **Supplementary Figure 1D**. Blocking of the KTI reactive loop is critical in trypsin protease inhibition. We performed 2 μS MD simulations on these two complexes in aqueous environment. **Figure 4C** shows two different ways Effector 3 may block the KTI reactive loop (shown in red). The sampling of the MD trajectories reveals the following dominant pairwise interactions with C^{α}-C^{α} distance <4Å as described in **Supplementary Figure 5**. Stabilizing pairwise interactions in one model in **Figure 4C** (left) are as follows: F14-W83, P69-W123, V68-L139, V68-L140, F14-S163, V68-F170, L71-L171, and P69-L188 whereas in the other model in **Figure 4C** (right), and they are as follows: L151-D37, L151-R87, L152-K81, and S154-K79. In these pairwise interactions, Effector 3 and KTI are shown, respectively, as gray and blue ball-and-stick representations. The mutational studies are needed to discriminate the two modes of inhibition of KTI by Effector 3 described in **Figure 4C**.

DISCUSSION

Bacterial effectors are known to inhibit plant innate immune signaling networks mediated by PTI, ETI, and plant SA, JA, and ET hormones. The end products of PTI, ETI, and plant hormone signaling are the PR or immune defense proteins that either clear the invading the pathogen or block infection. Typically, each immune defense protein is induced at a low level and a single protein; therefore, can neither completely clear the pathogen nor can it totally block the infection. Interestingly, simultaneous induction of multiple immune defense proteins (albeit at low levels) can lead to effective clearance of the invading bacteria and blocking of infection caused by them. However, the multiple effectors from a pathogenic bacterium such as *C*Las can suppress multiple signaling steps to support bacterial growth and infection. Here, we report the role of two *C*Las effectors, $LasP_{235}$ and Effector 3, in HLB pathogenesis. The each of them may directly target and inhibit more than one citrus innate immune defense proteins involved in bactericidal and/or disease-blocking activity. For example, $LasP_{235}$ can inhibit the citrus targets (SOD, AP, GH17, and LTP) whereas Effector 3 can inhibit citrus targets (KTI, ALDH, Lectin, and Ef–Tu). Although, as shown here, a bacterial effector may target several plant proteins, inhibitions of all targets may not be equally important for bacterial pathogenesis. A direct evaluation of the importance of each (plant protein–bacterial effector) interaction is traditionally obtained by knockout of a specific bacterial effector. Since *C*Las is not culturable, it is not possible to conduct gene knockout experiments. However, the inhibitory activities of a *C*Las effector against different citrus targets reveal qualitatively the relative importance of different inhibitory (*C*Las effector–citrus target) interactions in HLB pathogenesis. For example, as shown in **Table 1**, $LasP_{235}$ is a potent inhibitor of LTP because at equimolar concentration it can completely block the bactericidal activity of LTP. Thus, $LasP_{235}$ may play an important role in HLB pathogenesis. Note that, relatively low IC_{50} values (within 1 to 6) in **Table 1**, argue that the corresponding inhibitory interactions may be relevant in HLB pathogenesis. **Figure 5** schematically summarizes the combined effect of the inhibitory interactions of $LasP_{235}$ and Effector 3 on their citrus targets as determined from our *in vitro* and *in*

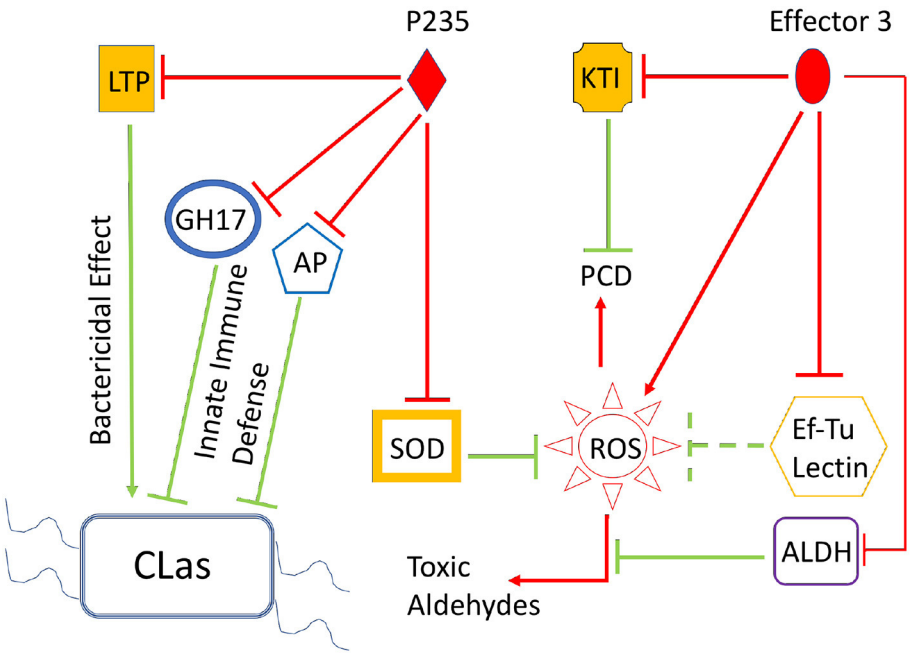

FIGURE 5 | Combined effect of the *C*Las effectors, $LasP_{235}$ and Effector 3, on the citrus innate immune due to the target proteins. The $LasP_{235}$ targets shown here are SOD, LTP, KP, and GH17 whereas the Effector 3 targets are as follows: ALDH, Lectin, KTI, and Ef–Tu. All these citrus targets participate in innate immune defense (shown as green arrows) during bacterial infection. For example, SOD controls the level of ROS such that the beneficial effects of ROS-induced immune defense can be harnessed without the level of ROS level exceeding a critical threshold over which there may cause host damage. EF–Tu and ALDH also limit the level of ROS. The GH17 and KP offer immune defense against bacterial infection. LTP can directly exert bacterial effect whereas KTI prevents premature PCD, which may help bacterial growth and infection. The effects of pathogenic *C*Las proteins, $LasP_{235}$ and Effector 3, are shown as red line arrows (promoting a process and red line blockers (as inhibiting a process). The combined effects of $LasP_{235}$ and Effector 3: elevation of ROS level, premature PCD, and inhibition of *C*Las clearance.

planta studies. The immune stimulatory defenses exerted by the identified citrus targets are marked by green lines whereas the inhibition of these targets by the two effectors $LasP_{235}$ and Effector 3 of pathogenic *C*Las are marked by red lines. Note that SOD reduces the level of ROS whereas Ef–Tu, Lectin, and ALDH tend to control the toxic damage due to ROS. The GH17 and AP provide immune defense *via* SA-signaling, which may involve ROS production whereas KTI may prevent premature ROS-induced PCD and $LasP_{235}$ may block *C*Las clearance by LTP. Thus, $LasP_{235}$ and Effector 3, target and interact with the ROS, PCD, and bactericidal pathways in a way that adversely affect citrus innate immune defense and in turn, facilitate HLB pathogenesis.

We analyzed the detailed interactions at the contact interfaces of the ($LasP_{235}$-LTP) and (Effector 3-KTI) complexes. The molecular modeling and mutational analysis revealed the predominant mechanism of LTP inhibition by $LasP_{235}$. We were able to design Mimic 1 (derived from LTP with specific amino acid substitutions) that showed intrinsic bactericidal activity and exhibited $LasP_{235}$ inhibitory activity. The Mimic 1 can be further modified to increase its $LasP_{235}$ inhibitory and bactericidal activity. We have also obtained two modes of inhibition in which Effector 3 may block the reactive loop of the citrus KTI. We have not yet completed *in plant*a experiments to determine whether one of the two modes of inhibition or both may be important. Nonetheless, the citrus KTI as the target of inhibition by a *C*Las effector is an interesting observation since such inhibition may cause premature PCD, which may be beneficial to *C*Las in causing infection (Randow et al., 2013).

DATA AVAILABILITY STATEMENT

The raw data supporting the conclusions of this article will be made available by the authors, without undue reservation.

AUTHOR CONTRIBUTIONS

GG contributed to project planning, experimental work, data analysis, and writing of the manuscript. SB performed the majority of *in vitro* and *in planta* studies, data analysis, and writing of the manuscript. LH performed the MD simulations and analyses. HN assisted in the split GFP assays. RR performed expression of some recombinant proteins. JV performed some MIC assays. ES supervised the work of GM and QS on citrus infection by *C*Las and protein extraction from healthy and infected citrus and the work of GH and SZ toward generating transgenic tobacco expressing GFP1-9. All authors contributed to the article and approved the submitted version.

FUNDING

This work was funded by the NIFA-CDRE grant (Fed Award # 2018-70016-27453 to PI: Jinhe Bai, USDA-ARS; Co-PI:

Subaward # 59-6034-8-005) on accelerating implementation of HLB hybrids as new commercial cultivars for fresh and processed citrus through a collaboration between Gupta (New Mexico Consortium) and Stover (USDA-ARS) labs.

ACKNOWLEDGMENTS

We thank Dr. Steven Buelow (Director, New Mexico Consortium) for his support and access to the resources and facilities of the Biolab. We are grateful to Dr. Geoffrey Waldo for generous gifts of plasmids and enhanced GFP used for the split GFP assay.

SUPPLEMENTARY MATERIAL

The Supplementary Material for this article can be found online at: https://www.frontiersin.org/articles/10.3389/fpls.2022.869178/full#supplementary-material

REFERENCES

Abramovitch, R. B., and Martin, G. B. (2005). AvrPtoB: a bacterial type III effector that both elicits and suppresses programmed cell death associated with plant immunity. *FEMS Microbiol. Lett.* 245, 1–8. doi: 10.1016/j.femsle.2005.02.025

Albaugh, A., Boateng, H. A., Bradshaw, R. T., Demerdash, O. N., Dziedzic, J., Mao, Y., et al. (2016). Advanced potential energy surfaces for molecular simulation. *J. Phys. Chem. B* 120, 9811–9832. doi: 10.1021/acs.jpcb.6b06414

Alhoraibi, H., Bigeard, J., Rayapuram, N., Colcombet, J., and Hirt, H. (2019). Plant immunity: the MTI-ETI model and beyond. *Curr. Issues Mol. Biol.* 30, 39–58. doi: 10.21775/cimb.030.039

Ali, S., Ganai, B. A., Kamili, A. N., Bhat, A. A., Mir, Z. A., Bhat, J. A., et al. (2018). Pathogenesis-related proteins and peptides as promising tools for engineering plants with multiple stress tolerance. *Microbiol. Res.* 212–213, 29–37. doi: 10.1016/j.micres.2018.04.008

Aoki, K. M., and Yonezawa, F. (1992). Constant-pressure molecular-dynamics simulations of the crystal-smectic transition in systems of soft parallel spherocylinders. *Phys. Rev. A* 46, 6541–6549. doi: 10.1103/PhysRevA.46.6541

Bae, T., Baba, T., Hiramatsu, K., and Schneewind, O. (2006). Prophages of *Staphylococcus aureus* Newman and their contribution to virulence. *Mol. Microbiol.* 62, 1035–1047. doi: 10.1111/j.1365-2958.2006.05441.x

Basu, S., Roychoudhury, A., Saha, P. P., and Sengupta, D. N. (2010). Differential antioxidative responses of indica rice cultivars to drought stress. *Plant Growth Regul.* 60, 50–59. doi: 10.1007/s10725-009-9418-4

Block, A., Li, G., Fu, Z. Q., and Alfano, J. R. (2008). Phytopathogen type III effector weaponry and their plant targets. *Curr. Opin. Plant Biol.* 11, 396–403. doi: 10.1016/j.pbi.2008.06.007

Blumer, M., Harris, S., Li, M., Martinez, L., Untereiner, M., Saeta, P. N., et al. (2020). Simulations of asymmetric membranes illustrate cooperative leaflet coupling and lipid adaptability. *Front. Cell Dev. Biol.* 8:575. doi: 10.3389/fcell.2020.00575

Boateng, H. A. (2020). Periodic coulomb tree method: an alternative to parallel particle Mesh Ewald. *J. Chem. Theor. Comput.* 16, 7–17. doi: 10.1021/acs.jctc.9b00648

Brauer, E. K., Popescu, G. V., Singh, D. K., Calviño, M., Gupta, K., Gupta, B., et al. (2018). Integrative network-centric approach reveals signaling pathways associated with plant resistance and susceptibility to *Pseudomonas syringae*. *PLoS Biol.* 16:e2005956. doi: 10.1371/journal.pbio.2005956

Büttner, D. (2016). Behind the lines-actions of bacterial type III effector proteins in plant cells. *FEMS Microbiol. Rev.* 40, 894–937. doi: 10.1093/femsre/fuw026

Cabantous, S., Nguyen, H. B., Pedelacq, J. D., Koraïchi, F., Chaudhary, A., Ganguly, K., et al. (2013). A new protein-protein interaction sensor based on tripartite split-GFP association. *Sci. Rep.* 3:2854. doi: 10.1038/srep02854

Cabantous, S., and Waldo, G. S. (2006). *In vivo* and *in vitro* protein solubility assays using split GFP. *Nat. Methods* 3, 845–854. doi: 10.1038/nmeth932

Cerutti, D. S., Duke, R. E., Darden, T. A., and Lybrand, T. P. (2009). Staggered Mesh Ewald: an extension of the Smooth Particle-Mesh Ewald method adding great versatility. *J. Chem. Theor. Comput.* 5:2322. doi: 10.1021/ct9001015

Chan, S. L., Mukasa, T., Santelli, E., Low, L. Y., and Pascual, J. (2010). The crystal structure of a TIR domain from *Arabidopsis thaliana* reveals a conserved helical region unique to plants. *Protein Sci.* 19, 155–161. doi: 10.1002/pro.275

Cianciotto, N. P., and White, R. C. (2017). Expanding role of type II secretion in bacterial pathogenesis and beyond. *Infect. Immun.* 85, e00014–17. doi: 10.1128/IAI.00014-17

Coria, L. M., Ibañez, A. E., Tkach, M., Sabbione, F., Bruno, L., Carabajal, M. V., et al. (2016). A *Brucella* spp. protease inhibitor limits antigen lysosomal proteolysis, increases cross-presentation, and enhances CD8+ T cell responses. *J. Immunol.* 196, 4014-4029. doi: 10.4049/jimmunol.1501188

Cui, H., Xiang, T., and Zhou, J. M. (2009). Plant immunity: a lesson from pathogenic bacterial effector proteins. *Cell Microbiol.* 11, 1453–1461. doi: 10.1111/j.1462-5822.2009.01359.x

Da Graça, J. V., Douhan, G. W., Halbert, S. E., Keremane, M. L., Lee, R. F., Vidalakis, G., et al. (2016). Huanglongbing: an overview of a complex pathosystem ravaging the world's citrus. *J. Integr. Plant Biol.* 58, 373–387. doi: 10.1111/jipb.12437

Dangl, J. L., and Jones, J. D. (2001). Plant pathogens and integrated defence responses to infection. *Nature* 411, 826–833. doi: 10.1038/35081161

Dillon, M. M., Almeida, R. N. D., Laflamme, B., Martel, A., Weir, B. S., Desveaux, D., et al. (2019). Molecular evolution of *Pseudomonas syringae* type III secreted effector proteins. *Front. Plant Sci.* 10:418. doi: 10.3389/fpls.2019.00418

Dodds, P. N., and Rathjen, J. P. (2010). Plant immunity: towards an integrated view of plant-pathogen interactions. *Nat. Rev. Genet.* 11, 539–548. doi: 10.1038/nrg2812

Duan, Y., Zhou, L., Hall, D. G., Li, W., Doddapaneni, H., Lin, H., et al. (2009). Complete genome sequence of citrus huanglongbing bacterium, "*Candidatus Liberibacter asiaticus*" obtained through metagenomics. *Mol. Plant Microbe Interact.* 22, 1011–1020. doi: 10.1094/MPMI-22-8-1011

Ebbensgaard, A., Mordhorst, H., Overgaard, M. T., Nielsen, C. G., Aarestrup, F. M., and Hansen, E. B. (2015). Comparative evaluation of the antimicrobial activity of different antimicrobial peptides against a range of pathogenic bacteria. *PLoS ONE* 10:e0144611. doi: 10.1371/journal.pone.0144611

Feng, F., and Zhou, J. M. (2012). Plant-bacterial pathogen interactions mediated by type III effectors. *Curr. Opin. Plant Biol.* 15, 469–476. doi: 10.1016/j.pbi.2012.03.004

Finkina, E. I., Melnikova, D. N., Bogdanov, I. V., and Ovchinnikova, T. V. (2016). Lipid transfer proteins as components of the plant innate immune system: structure, functions, and applications. *Acta Naturae* 8, 47–61. doi: 10.32607/20758251-2016-8-2-47-61

Fischer, N. M., Van Maaren, P. J., Ditz, J. C., Yildirim, A., and Van Der Spoel, D. (2015). Properties of organic liquids when simulated with long-range Lennard-Jones interactions. *J. Chem. Theory Comput.* 11, 2938–2944. doi: 10.1021/acs.jctc.5b00190

Goritschnig, S., Steinbrenner, A. D., Grunwald, D. J., and Staskawicz, B. J. (2016). Structurally distinct *Arabidopsis thaliana* NLR immune receptors recognize tandem WY domains of an oomycete effector. *New Phytol.* 210, 984–996. doi: 10.1111/nph.13823

Gottwald, T. R. (2010). Current epidemiological understanding of citrus Huanglongbing. *Annu. Rev. Phytopathol.* 48, 119–139. doi: 10.1146/annurev-phyto-073009-114418

Guilbaud, C., Morris, C. E., Barakat, M., Ortet, P., and Berge, O. (2016). Isolation and identification of *Pseudomonas syringae* facilitated by a PCR targeting the whole *P. syringae* group. *FEMS Microbiol. Ecol.* 92:fiv146. doi: 10.1093/femsec/fiv146

Gupta, G., and Stover, E. W. (2022). Innate Immunity LLC and US Department of Agriculture USDA. Compositions and methods for the treatment of pathogenic infections in plants. U.S. Patent Application 17/281,884.

Han, X., and Kahmann, R. (2019). Manipulation of phytohormone pathways by effectors of filamentous plant pathogens. *Front. Plant Sci.* 10:822. doi: 10.3389/fpls.2019.00822

Hao, G., Ammar, D., Duan, Y., and Stover, E. (2019). Transgenic citrus plants expressing a "*Candidatus Liberibacter asiaticus*" prophage protein LasP 235 display Huanglongbing-like symptoms. *Agri Gene* 12:100085. doi: 10.1016/j.aggene.2019.100085

Hao, G., Boyle, M., Zhou, L., and Duan, Y. (2013). The intracellular citrus huanglongbing bacterium, "*Candidatus Liberibacter asiaticus*" encodes two novel autotransporters. *PLoS ONE* 8:e68921. doi: 10.1371/journal.pone.0068921

Hatsugai, N., Nakatsuji, A., Unten, O., Ogasawara, K., Kondo, M., Nishimura, M., et al. (2018). Involvement of adapter protein complex 4 in hypersensitive cell death induced by avirulent bacteria. *Plant Physiol.* 176, 1824–1834. doi: 10.1104/pp.17.01610

He, P., Shan, L., and Sheen, J. (2007). Elicitation and suppression of microbe-associated molecular pattern-triggered immunity in plant-microbe interactions. *Cell Microbiol.* 9, 1385–1396. doi: 10.1111/j.1462-5822.2007.00944.x

Henriques, A., Huebecker, M., Blasco, H., Keime, C., Andres, C. R., Corcia, P., et al. (2017). Inhibition of β-glucocerebrosidase activity preserves motor unit integrity in a mouse model of amyotrophic lateral sclerosis. *Sci. Rep.* 7:5235. doi: 10.1038/s41598-017-05313-0

Hoeberichts, F. A., and Woltering, E. J. (2003). Multiple mediators of plant programmed cell death: interplay of conserved cell death mechanisms and plant-specific regulators. *Bioessays* 25, 47–57. doi: 10.1002/bies.10175

Hrmova, M., and Fincher, G. B. (2001). Structure-function relationships of beta-D-glucan endo- and exohydrolases from higher plants. *Plant Mol. Biol.* 47, 73–91. doi: 10.1023/A:1010619128894

Jimenez-Lopez, J. C., Lopez-Valverde, F. J., Robles-Bolivar, P., Lima-Cabello, E., Gachomo, E. W., and Kotchoni, S. O. (2016). Genome-wide identification and functional classification of tomato (*Solanum lycopersicum*) aldehyde dehydrogenase (ALDH) gene superfamily. *PLoS ONE* 11:e0164798. doi: 10.1371/journal.pone.0164798

Joshi, B. H., and Puri, R. K. (2005). Optimization of expression and purification of two biologically active chimeric fusion proteins that consist of human interleukin-13 and *Pseudomonas exotoxin* in *Escherichia coli*. *Protein Expr. Purif.* 39, 189–198. doi: 10.1016/j.pep.2004.10.012

Kacprzyk, J., Dauphinee, A. N., Gallois, P., Gunawardena, A. H., and Mccabe, P. F. (2016). Methods to study plant programmed cell death. *Methods Mol. Biol.* 1419, 145–160. doi: 10.1007/978-1-4939-3581-9_12

Karpievitch, Y. V., Dabney, A. R., and Smith, R. D. (2012). Normalization and missing value imputation for label-free LC-MS analysis. *BMC Bioinformat.* 13:S5. doi: 10.1186/1471-2105-13-S16-S5

Koenig, T., Menze, B. H., Kirchner, M., Monigatti, F., Parker, K. C., Patterson, T., et al. (2008). Robust prediction of the MASCOT score for an improved quality assessment in mass spectrometric proteomics. *J. Proteome Res.* 7, 3708–3717. doi: 10.1021/pr700859x

Kratz, E. G., Duke, R. E., and Cisneros, G. A. (2016). Long-range electrostatic corrections in multipolar/polarizable QM/MM simulations. *Theor. Chem. Acc.* 135:8. doi: 10.1007/s00214-016-1923-8

Lee, J. H., Kim, H., Chae, W. B., and Oh, M. H. (2019). Pattern recognition receptors and their interactions with bacterial type III effectors in plants. *Genes Genom.* 41, 499–506. doi: 10.1007/s13258-019-00801-1

Leippe, D. M., Nguyen, D., Zhou, M., Good, T., Kirkland, T. A., Scurria, M., et al. (2011). A bioluminescent assay for the sensitive detection of proteases. *Biotechniques* 51, 105–110. doi: 10.2144/000113716

Li, J., Brader, G., and Palva, E. T. (2008). Kunitz trypsin inhibitor: an antagonist of cell death triggered by phytopathogens and fumonisin b1 in Arabidopsis. *Mol. Plant* 1, 482–495. doi: 10.1093/mp/ssn013

Li, Z. L., Prakash, P., and Buck, M. (2018). A "Tug of War" maintains a dynamic protein-membrane complex: molecular dynamics simulations of C-Raf RBD-CRD bound to K-Ras4B at an anionic membrane. *ACS Cent. Sci.* 4, 298–305. doi: 10.1021/acscentsci.7b00593

Lin, H., Coletta-Filho, H. D., Han, C. S., Lou, B., Civerolo, E. L., Machado, M. A., et al. (2013). Draft genome sequence of "*Candidatus Liberibacter americanus*" bacterium associated with citrus huanglongbing in Brazil. *Genome Announc.* 1:13. doi: 10.1128/genomeA.00275-13

Liu, F., Zhang, X., Lu, C., Zeng, X., Li, Y., Fu, D., et al. (2015). Non-specific lipid transfer proteins in plants: presenting new advances and an integrated functional analysis. *J. Exp. Bot.* 66, 5663–5681. doi: 10.1093/jxb/erv313

Liu, T. Y., Chou, W. C., Chen, W. Y., Chu, C. Y., Dai, C. Y., and Wu, P. Y. (2018). Detection of membrane protein-protein interaction in planta based on dual-intein-coupled tripartite split-GFP association. *Plant J.* 94, 426–438. doi: 10.1111/tpj.13874

Liu, Y., Wang, L., Cai, G., Jiang, S., Sun, L., and Li, D. (2013). Response of tobacco to the *Pseudomonas syringae* pv. tomato DC3000 is mainly dependent on salicylic acid signaling pathway. *FEMS Microbiol. Lett.* 344, 77-85. doi: 10.1111/1574-6968.12157

Locato, V., and De Gara, L. (2018). Programmed cell death in plants: an overview. *Methods Mol. Biol.* 1743, 1–8. doi: 10.1007/978-1-4939-7668-3_1

Luo, Y., and Agnarsson, I. (2018). Global mtDNA genetic structure and hypothesized invasion history of a major pest of citrus. *Ecol. Evol.* 8, 257–265. doi: 10.1002/ece3.3680

Medina, C. A., Reyes, P. A., Trujillo, C. A., Gonzalez, J. L., Bejarano, D. A., Montenegro, N. A., et al. (2018). The role of type III effectors from *Xanthomonas axonopodis* pv. manihotis in virulence and suppression of plant immunity. *Mol. Plant Pathol.* 19, 593–606. doi: 10.1111/mpp.12545

Melnikova, D., Bogdanov, I., Ovchinnikova, T., and Finkina, E. (2020). Interaction between the Lentil Lipid Transfer Protein Lc-LTP2 and its novel signal ligand PI(4,5)P2. *Membranes* 10:110357. doi: 10.3390/membranes10110357

Merfa, M. V., Pérez-López, E., Naranjo, E., Jain, M., Gabriel, D. W., and De La Fuente, L. (2019). Progress and obstacles in culturing. *Phytopathology* 109, 1092–1101. doi: 10.1094/PHYTO-02-19-0051-RVW

Miller, A. F. (2012). Superoxide dismutases: ancient enzymes and new insights. *FEBS Lett.* 586, 585–595. doi: 10.1016/j.febslet.2011.10.048

Mine, A., Seyfferth, C., Kracher, B., Berens, M. L., Becker, D., and Tsuda, K. (2018). The defense phytohormone signaling network enables rapid, high-amplitude transcriptional reprogramming during effector-triggered immunity. *Plant Cell* 30, 1199–1219. doi: 10.1105/tpc.17.00970

Miyamoto, S., and Kollman, P. A. (1993). Absolute and relative binding free energy calculations of the interaction of biotin and its analogs with streptavidin using molecular dynamics/free energy perturbation approaches. *Proteins* 16, 226–245. doi: 10.1002/prot.340160303

Mudgett, M. B. (2005). New insights to the function of phytopathogenic bacterial type III effectors in plants. *Annu. Rev. Plant Biol.* 56, 509–531. doi: 10.1146/annurev.arplant.56.032604.144218

Nehir El, S., Karakaya, S., Simsek, S., Dupont, D., Menfaatli, E., and Eker, A. T. (2015). *In vitro* digestibility of goat milk and kefir with a new standardised static digestion method (INFOGEST cost action) and bioactivities of the resultant peptides. *Food Funct.* 6, 2322–2330. doi: 10.1039/C5FO00357A

Ouyang, S., Zhou, X., Chen, Z., Wang, M., Zheng, X., and Xie, M. (2019). LncRNA BCAR4, targeting to miR-665/STAT3 signaling, maintains cancer stem cells stemness and promotes tumorigenicity in colorectal cancer. *Cancer Cell Int.* 19:72. doi: 10.1186/s12935-019-0784-3

Paiva, C. N., and Bozza, M. T. (2014). Are reactive oxygen species always detrimental to pathogens? *Antioxid Redox Signal* 20, 1000–1037. doi: 10.1089/ars.2013.5447

Pedelacq, J. D., Waldo, G. S., and Cabantous, S. (2019). High-throughput protein-protein interaction assays using tripartite split-GFP complementation. *Methods Mol. Biol.* 2025, 423–437. doi: 10.1007/978-1-4939-9624-7_20

Pitino, M., Allen, V., and Duan, Y. (2018). LasΔ5315 effector induces extreme starch accumulation and chlorosis as. *Front. Plant Sci.* 9:113. doi: 10.3389/fpls.2018.00113

Pitino, M., Armstrong, C. M., Cano, L. M., and Duan, Y. (2016). Transient expression of candidatus liberibacter asiaticus effector induces cell death in *Nicotiana benthamiana*. *Front. Plant Sci.* 7:982. doi: 10.3389/fpls.2016.00982

Prasad, S., Xu, J., Zhang, Y., and Wang, N. (2016). SEC-translocon dependent extracytoplasmic proteins of. *Front. Microbiol.* 7:1989. doi: 10.3389/fmicb.2016.01989

Qi, G., Chen, J., Chang, M., Chen, H., Hall, K., Korin, J., et al. (2018). Pandemonium breaks out: disruption of salicylic acid-mediated defense by plant pathogens. *Mol. Plant* 11, 1427–1439. doi: 10.1016/j.molp.2018.10.002

Rajagopala, S. V. (2015). Mapping the protein-protein interactome networks using yeast two-hybrid screens. *Adv. Exp. Med. Biol.* 883, 187–214. doi: 10.1007/978-3-319-23603-2_11

Ramegowda, V., Senthil-Kumar, M., Nataraja, K. N., Reddy, M. K., Mysore, K. S., and Udayakumar, M. (2012). Expression of a finger millet transcription factor, EcNAC1, in tobacco confers abiotic stress-tolerance. *PLoS ONE* 7:e40397. doi: 10.1371/journal.pone.0040397

Randow, F., Macmicking, J. D., and James, L. C. (2013). Cellular self-defense: how cell-autonomous immunity protects against pathogens. *Science* 340, 701–706. doi: 10.1126/science.1233028

Roy, S., Choudhury, S. R., Singh, S. K., and Das, K. P. (2011). AtPolλ, a homolog of mammalian DNA polymerase λ in *Arabidopsis thaliana*, is involved in the repair of UV-B induced DNA damage through the dark repair pathway. *Plant Cell Physiol.* 52, 448–467. doi: 10.1093/pcp/pcr002

Salminen, T. A., Blomqvist, K., and Edqvist, J. (2016). Lipid transfer proteins: classification, nomenclature, structure, and function. *Planta* 244, 971–997. doi: 10.1007/s00425-016-2585-4

Sels, J., Mathys, J., De Coninck, B. M., Cammue, B. P., and De Bolle, M. F. (2008). Plant pathogenesis-related (PR) proteins: a focus on PR peptides. *Plant Physiol. Biochem.* 46, 941–950. doi: 10.1016/j.plaphy.2008.06.011

Serebriiskii, I., Estojak, J., Berman, M., and Golemis, E. A. (2000). Approaches to detecting false positives in yeast two-hybrid systems. *Biotechniques* 328-330, 332–326. doi: 10.2144/00282rr03

Shenkarev, Z. O., Melnikova, D. N., Finkina, E. I., Sukhanov, S. V., Boldyrev, I. A., Gizatullina, A. K., et al. (2017). Ligand binding properties of the lentil lipid transfer protein: molecular insight into the possible mechanism of lipid uptake. *Biochemistry* 56, 1785–1796. doi: 10.1021/acs.biochem.6b01079

Simões, I., Faro, R., Bur, D., and Faro, C. (2007). Characterization of recombinant CDR1, an *Arabidopsis aspartic* proteinase involved in disease resistance. *J. Biol. Chem.* 282, 31358–31365. doi: 10.1074/jbc.M702477200

Sohn, K. H., Hughes, R. K., Piquerez, S. J., Jones, J. D., and Banfield, M. J. (2012). Distinct regions of the *Pseudomonas syringae* coiled-coil effector AvrRps4 are required for activation of immunity. *Proc. Natl. Acad. Sci. U. S. A.* 109, 16371–16376. doi: 10.1073/pnas.1212332109

Solé, M., Scheibner, F., Hoffmeister, A. K., Hartmann, N., Hause, G., Rother, A., et al. (2015). *Xanthomonas campestris* pv. vesicatoria secretes proteases and xylanases *via* the Xps Type II secretion system and outer membrane vesicles. *J. Bacteriol.* 197, 2879–2893. doi: 10.1128/JB.00322-15

Sowden, R. G., Watson, S. J., and Jarvis, P. (2018). The role of chloroplasts in plant pathology. *Essays Biochem.* 62, 21–39. doi: 10.1042/EBC20170020

Sugio, A., Maclean, A. M., Kingdom, H. N., Grieve, V. M., Manimekalai, R., and Hogenhout, S. A. (2011). Diverse targets of phytoplasma effectors: from plant development to defense against insects. *Annu. Rev. Phytopathol.* 49, 175–195. doi: 10.1146/annurev-phyto-072910-095323

Varghese, J. N., Garrett, T. P., Colman, P. M., Chen, L., Høj, P. B., and Fincher, G. B. (1994). Three-dimensional structures of two plant beta-glucan endohydrolases with distinct substrate specificities. *Proc. Natl. Acad. Sci. U. S. A.* 91, 2785–2789. doi: 10.1073/pnas.91.7.2785

Walser, R., Hünenberger, P. H., and Van Gunsteren, W. F. (2002). Molecular dynamics simulations of a double unit cell in a protein crystal: volume relaxation at constant pressure and correlation of motions between the two unit cells. *Proteins* 48, 327–340. doi: 10.1002/prot.10143

Wang, N., and Trivedi, P. (2013). Citrus huanglongbing: a newly relevant disease presents unprecedented challenges. *Phytopathology* 103, 652–665. doi: 10.1094/PHYTO-12-12-0331-RVW

Wang, Y., and Bouwmeester, K. (2017). L-type lectin receptor kinases: new forces in plant immunity. *PLoS Pathog.* 13:e1006433. doi: 10.1371/journal.ppat.1006433

Wang, Y., Branicky, R., No,ë, A., and Hekimi, S. (2018). Superoxide dismutases: dual roles in controlling ROS damage and regulating ROS signaling. *J. Cell Biol.* 217, 1915–1928. doi: 10.1083/jcb.201708007

Washio, T., Sugiura, S., Kanada, R., Okada, J. I., and Hisada, T. (2018). Coupling langevin dynamics with continuum mechanics: exposing the role of sarcomere stretch activation mechanisms to cardiac function. *Front. Physiol.* 9:333. doi: 10.3389/fphys.2018.00333

Wennberg, C. L., Murtola, T., Hess, B., and Lindahl, E. (2013). Lennard-Jones Lattice summation in bilayer simulations has critical effects on surface tension and lipid properties. *J. Chem. Theor. Comput.* 9, 3527–3537. doi: 10.1021/ct400140n

Wu, E. L., Cheng, X., Jo, S., Rui, H., Song, K. C., Davila-Contreras, E. M., et al. (2014). CHARMM-GUI Membrane Builder toward realistic biological membrane simulations. *J. Comput. Chem.* 35, 1997–2004. doi: 10.1002/jcc.23702

Wu, L., Chen, H., Curtis, C., and Fu, Z. Q. (2014). Go in for the kill: how plants deploy effector-triggered immunity to combat pathogens. *Virulence* 5, 710–721. doi: 10.4161/viru.29755

Wu, L., Xie, S. S., Meng, E., Li, W. Y., Liu, L., and Zhang, D. Y. (2017). Molecular dynamics simulation reveals unique interplays between a tarantula toxin and lipid membranes. *J. Membr. Biol.* 250, 315–325. doi: 10.1007/s00232-017-9965-y

Zhang, S., Flores-Cruz, Z., Zhou, L., Kang, B. H., Fleites, L. A., Gooch, M. D., et al. (2011). "*Ca. Liberibacter asiaticus*" carries an excision plasmid prophage and a chromosomally integrated prophage that becomes lytic in plant infections. *Mol. Plant Microbe Interact.* 24, 458–468. doi: 10.1094/MPMI-11-10-0256

Zhang, W., Zhao, F., Jiang, L., Chen, C., Wu, L., and Liu, Z. (2018). Different pathogen defense strategies in. *Cells* 7:120252. doi: 10.3390/cells7120252

Zhang, X., Smits, A. H., Van Tilburg, G. B., Jansen, P. W., Makowski, M. M., Ovaa, H., et al. (2017). An interaction landscape of ubiquitin signaling. *Mol. Cell* 28, 941–955.e948. doi: 10.1016/j.molcel.2017.01.004

Zhou, Y., He, W., Sun, W., Zhou, Z., Sun, M., Xia, P., et al. (2018). Sulfotanshinone IIA sodium ameliorates glucose peritoneal dialysis solution-induced human peritoneal mesothelial cell injury *via* suppression of ASK1-P38-mediated oxidative stress. *Cell Physiol. Biochem.* 46, 2434–2444. doi: 10.1159/000489650

Conflict of Interest: The authors declare that the research was conducted in the absence of any commercial or financial relationships that could be construed as a potential conflict of interest.

Publisher's Note: All claims expressed in this article are solely those of the authors and do not necessarily represent those of their affiliated organizations, or those of the publisher, the editors and the reviewers. Any product that may be evaluated in this article, or claim that may be made by its manufacturer, is not guaranteed or endorsed by the publisher.

frontiers | Frontiers in Plant Science

ORIGINAL RESEARCH
published: 04 May 2022
doi: 10.3389/fpls.2022.912091

Development of 1,3,4-Oxadiazole Derived Antifungal Agents and Their Application in Maize Diseases Control

Lin Yao[1,2], Guanghua Zhang[1], Lili Yu[2], Shaojing Liu[2], Xiaoku Wang[2], Tao Fan[2], Hui Kang[2] and Wenzhi Feng[2]*

[1]*Shaanxi Key Laboratory of Chemical Additives for Industry, Shaanxi University of Science and Technology, Xi'an, China,* [2]*College of Pharmacy, Xi'an Medical University, Xi'an, China*

Maize is an important food crop and its fungal disease has become a limiting factor to improve the yield and quality of maize. In the control of plant pathogens, commercial fungicides have no obvious effect on corn diseases due to the emergence of drug resistance. Therefore, it is of great significance to develop new fungicides with novel structure, high efficiency, and low toxicity to control maize diseases. In this paper, a series of 1,3,4-oxadiazole derivatives were designed and synthesized from benzoyl hydrazine and aromatic aldehydes through condensation and oxidation cyclization reaction. The antifungal activity of oxadiazole derivatives against three maize disease pathogens, such as *Rhizoctonia solani* (*R. solani*), *Gibberella zeae* (*G. zeae*), and *Exserohilum turcicum* (*E. turcicum*), were evaluated by mycelium growth rate method *in vitro*. The results indicated that most of the synthesized derivatives exhibited positive antifungal activities. Especially against *E. turcicum*, several compounds demonstrated significant antifungal activities and their EC_{50} values were lower than positive control carbendazim. The EC_{50} values of compounds 4k, 5e, and 5k were 50.48, 47.56, 32.25 μg/ml, respectively, and the carbendazim was 102.83 μg/ml. The effects of active compounds on *E. turcicum* microstructure were observed by scanning electron microscopy (SEM). The results showed that compounds 4k, 5e, and 5k could induce the hyphae of *E. turcicum* to shrink and collapse obviously. In order to elucidate the preliminary mechanism of oxadiazole derivatives, the target compounds 5e and 5k were docked with the theoretical active site of succinate dehydrogenase (SDH). Compounds 5e and 5k could bind to amino acid residues through hydrophobic contact and hydrogen bonds, which explained the possible mechanism of binding between the inhibitor and target protein. In addition, the compounds with antifungal activities had almost no cytotoxicity to MCF-7. This study showed that 1,3,4-oxadiazole derivatives were worthy for further attention as potential antifungal agents for the control of maize diseases.

Keywords: oxadiazole derivatives, antifungal pesticides, maize diseases, plant fungicides, crop protection, crop health

OPEN ACCESS

Edited by:
Yuheng Yang,
Southwest University, China

Reviewed by:
Dong Fang Ma,
Yangtze University, China
Shengkun Li,
Guizhou University, China

***Correspondence:**
Guanghua Zhang
zhanggh@sust.edu.cn

Specialty section:
This article was submitted to Technical Advances in Plant Science, a section of the journal Frontiers in Plant Science

Received: *04 April 2022*
Accepted: *20 April 2022*
Published: *04 May 2022*

Citation:
Yao L, Zhang G, Yu L, Liu S, Wang X, Fan T, Kang H and Feng W (2022) Development of 1,3,4-Oxadiazole Derived Antifungal Agents and Their Application in Maize Diseases Control. Front. Plant Sci. 13:912091. doi: 10.3389/fpls.2022.912091

INTRODUCTION

Plant diseases, especially crop diseases are one of the major agricultural disasters, which cause huge losses to agricultural production every year. Around 70–80% of crop diseases are caused by plant pathogenic fungi. As the main source of crop infections, these fungi can cause a variety of plant diseases, resulting in crop yield and quality reduction (Bebber and Gurr, 2015; Fones et al., 2020; Nazarov et al., 2020). Maize (*Zea mays* L.) is one of the most important crops for food, feed, and energy throughout the world, and is grown in many countries and regions (Waheed et al., 2020; Wang et al., 2021a,b). The main diseases in maize are northern leaf blight (*Exserohilum turcicum*), southern corn rust (*Puccinia polysora*), fusarium head blight (*Gibberella zeae*), corn sheath blight (*Rhizoctonis solani*), gray leaf spot (*Cercospora zeae-maydis*), etc. (Van Rensburg et al., 2016; Hao et al., 2020; Silva et al., 2021). Among them, the northern corn leaf blight caused by *E. turcicum* is one of the most common maize diseases worldwide (Abdelsalam et al., 2022; De Rossi et al., 2022). These diseases are widespread in the world's major corn producing areas. Because of their wide impact area and great economic loss, they have attracted the attention of domestic and foreign researchers. These diseases are also the most important threat to corn production in China and seriously hinder the stable development of corn production (Hao et al., 2020; Wang et al., 2021b). The most cost-effective and environmentally sustainable way to control plant diseases is to use tolerant or resistant cultivars. However, a single cultivar usually cannot resist all diseases in practice. Chemical control is still one of the most feasible technologies to ensure production efficiency (De Rossi et al., 2022). In order to control diseases, many chemical fungicides have been selected and used for crop protection (Ma et al., 2020). With the widespread application of fungicides in the control of crop diseases, the resistance of plant pathogens to existing fungicides has increased significantly, leading to the unsatisfactory control effect of current commercial fungicides on corn diseases (Leroux and Walker, 2013; Yoon et al., 2013; Shao et al., 2021). Therefore, it is particularly important to develop new fungicides with unique structure, high activity, and low toxicity to effectively control maize diseases.

Heterocyclic compounds have been the focus of research because of their high specificity, high activity, low dose, and low toxicity (Lamberth, 2013). Among them, azole, such as pyrazole, imidazole, oxazole, and other important members of five-member heterocyclic system, exist in many products with physiological active structure, are widely used in biology, medicine, industry and other fields, and show unique properties (Küçükgüzel and Şenkardeş, 2015; Lipunova et al., 2015; Guerrero-Pepinosa et al., 2021; Rulhania et al., 2021; Parikh et al., 2022). Many azole derivatives had become important drugs, which can be used in the treatment of antifungal (Lipunova et al., 2015; Wei et al., 2018; Guerrero-Pepinosa et al., 2021; Zhang et al., 2022), antitumor (Küçükgüzel and Şenkardeş, 2015; Silva-Ortiz et al., 2016; Titi et al., 2020; Balaraju et al., 2021; Oskuei et al., 2021), antituberculosis (Xu et al., 2017; Fan et al., 2018; Negalurmath et al., 2019), hypoglycemic (Al-Harbi et al., 2013), anti-inflammatory (Selvam et al., 2014), and other diseases, especially in pesticides, often used as fungicides and herbicides (Price et al., 2015; Shevaldina et al., 2019). Among them, oxazole derivatives were often used in the structural design of active molecules due to their biological activities such as antifungal, antiparasitic (Yamamuro et al., 2015; Adeyemi et al., 2021), antitumor (Balaraju et al., 2021), antituberculosis (Negalurmath et al., 2019), antimalaria (Verma et al., 2018), hypoglycemia (Taha et al., 2015), and antioxidation (Hejazi et al., 2019).

Therefore, in order to solve the problems of maize diseases caused by plant pathogenic fungi, a series of 1,3,4-oxadiazole derivatives were prepared using oxadiazole as lead compound. The derivatives were used to control three main plant pathogenic fungi (such as *E. turcicum*, *G. zeae*, and *R. solani*) causing maize diseases, and their biological activities against pathogens were evaluated in order to screen out compounds with higher activities. This study can provide candidate compounds for the prevention and control of maize disease.

MATERIALS AND METHODS

Materials and Chemicals

All reagents and solvents required for the synthesis of compounds were analytical or chemical pure, purchased from commercial suppliers and used without further purification. The reactions were observed and monitored by thin layer chromatography (TLC) under UV light (254 nm) using silica gel precoated plate (GF_{254}, 0.25 mm). About 200 ~ 300 mesh silica gel was used for column chromatography separation and purification (Qingdao Haiyang Co., Ltd., Qingdao, Shandong, China). All compounds were eluted using a mixture of petroleum ether (PE), dichloromethane (DCM), and ethyl acetate (EA). The melting points (m.p.) were measured by JHX-4B micro-melting point apparatus (Shanghai JIAHANG Instrument Co., Ltd) and were uncorrected. ^{1}H-NMR and ^{13}C-NMR spectra were recorded on Bruker Advance III 400 MHz nuclear magnetic resonance spectrometer (Bruker Company, United States) using $CDCl_3$ or DMSO-d_6 as solvent and tetramethylsilane (TMS) as internal standard. The chemical shifts for the NMR spectra were reported in δ ppm. Peak multiplicities were expressed as singlet (s), doublet (d), triplet (t), quartet (q), and multiplet (m).

Fungi

Three plant pathogenic fungi species *R. solani*, *G. zeae*, and *E. turcicum* were provided by College of Plant Protection, Southwest University, Chongqing, China. These pathogens can cause corn sheath blight, fusarium head blight, and northern corn leaf blight. The fungi were removed from the storage tube and incubated in a petri dish with potato dextrose agar (PDA) medium at 25°C for 1 week. The activated fungal mycelia were used in antifungal experiments.

General Procedures of 1,3,4-Oxadiazole Derivatives

General Synthetic Procedure for Compounds 4a–4l

p-Methoxy benzoyl hydrazide (166 mg, 1 mmol) and *p*-methoxy benzaldehyde (136 mg, 1 mmol) were dissolved in anhydrous EtOH (20 ml), and refluxed at 80°C for 6–10 h. The progress

of reaction was monitored by TLC. The reaction was stopped until the initial material disappeared. After the reaction mixture was cooled, the solvent was concentrated under reduced pressure to obtain the first step product *N*-acylaldehyde hydrazone, which was directly used for the next reaction (Majji et al., 2014; Polkam et al., 2017).

Anhydrous K_2CO_3 (276 mg, 2 mmol) and I_2 (26 mg, 0.1 mmol) were added to *N*-acylaldehyde hydrazine and dissolved in 3 ml DMSO. The reaction mixture was refluxed at 60–70°C for 10–12 h. H_2O_2 (30% solution in water, 0.45 ml, 4 mmol) was added to the reaction solution nine times in 3 h during the reaction. After the reaction stopped, it was quenched with 5% sodium thiosulfate solution (5 ml). The reaction mixture was extracted with ethyl acetate (3 × 15 ml), the combined organic layer was washed with saturated sodium chloride (1 × 3 ml) and dried over anhydrous Na_2SO_4. The organic phase was then filtered and concentrated under reduced pressure to remove the solvent. The product was separated and purified by silica gel column chromatography with a solvent mixture of petroleum ether/dichloromethane/ethyl acetate (4:1:1, *v*/*v*) as mobile phase, and the compound 4a was obtained after vacuum drying for 12 h. Compounds 4b–4l were synthesized by the same method. The synthetic routes and structures of compounds were shown in **Scheme 1**.

General Synthetic Procedure for Compounds 5a–5l

Substitute *p*-methoxy benzoyl hydrazide with benzoyl hydrazide, and the synthetic methods and dosage were the same as general synthetic procedure for compounds 4a–4l to obtain compounds 5a–5l.

General Synthetic Procedure for Compounds 6a–6f

Substitute *p*-methoxy benzoyl hydrazide with *p*-methylbenzoyl hydrazine, and the synthetic methods and dosage were the same as general synthetic procedure for compounds 4a–4l to obtain compounds 6a–6f.

Antifungal Activity Assay *in vitro*

Antifungal Activity Assay

The antifungal activity of oxadiazole derivatives and the positive control carbendazim were evaluated against three plant pathogenic fungi by the mycelium growth rate method (Fan et al., 2020; Yang et al., 2022). Firstly, the compounds were dissolved in DMSO and mixed with sterile molten PDA to obtain medicated medium with final concentration of 50 μg/ml. The mixture was poured into disposable petri plates (6 cm), and 3 mm mycelial disks were taken from the edge of hyphae and inoculated on the medicated medium. Three mycelial disks were placed evenly in each petri dish and then were cultured at 30°C PDA containing corresponding concentration of DMSO was used as blank control. The mycelial growth diameters were measured and the data were recorded when the control fungi grew and covered 3/4 of the petri dish. The diameters (mm) of inhibition zones were measured by the cross-bracketing method. The growth inhibition rates were calculated according to the following formula:

$$\text{Mycelial growth inhibiton}(\%) = \frac{\left[(C-d)-(T-d)\right]}{C-d} \times 100$$

where d represent the diameter of the mycelial disks (3 mm), C and T represents growth diameters of fungi on untreated PDA and treated PDA, respectively.

The EC_{50} values of the compounds with high inhibitory activity were determined. The target compounds were dissolved in DMSO and prepared to obtain a series of concentrations (100.00, 50.00, 25.00, 12.50, and 6.25 μg/ml). Three parallel controls were established for each concentration, with DMSO as blank control and carbendazim as positive control (Shivamogga Nagaraju et al., 2020). The log value of drug concentration (lg*c*) was taken as the independent variable (x), and average inhibition rate was taken as the dependent variable (y). The EC_{50} values of the target compound were calculated by regression equation.

Scanning Electron Microscopy Observations

In order to investigate the effects of active compounds on *E. turcicum* microstructure, the Scanning electron microscopy (SEM) observations were performed according to the literature method (Li et al., 2019). First, *E. turcicum* at logarithmic growth stage (1.5 ml) was centrifuged at 7,000 rpm for 1–2 min to remove the supernatant, then washed with PBS (3 × 1 ml) and suspended in 1.5 ml PBS. Compounds 4k, 5e, and 5k dissolved in DMSO were added to the suspension to make the final concentrations 50.0, 50.0, and 25.0 μg/ml, respectively, and cultured at 30 ± 1°C and 180 rpm for 24–48 h. DMSO was used as blank control, and three parallel controls were established for each compound. Afterward, the hyphae in three parallel samples were combined after washing with PBS (3 × 1 ml) and treated by 1 ml 2.5% glutaraldehyde at 4°C overnight. After removing the fixative, the samples were dehydrated with 1 ml gradient ethanol series (10, 30, 50, 70, 90 and 100%) with 5 min for each time and replaced with 100% tert-butanol twice. Finally, the treated samples were observed by scanning electron microscope (TESCAN MIRA LMS, Czech Republic) after dried in cryogenic freeze-drying device and gold-sprayed.

Cytotoxicity Assay

The cytotoxic activities of oxadiazole derivatives against MCF-7 were evaluated by MTT method (Mi et al., 2021). The tumor cells were cultured to logarithmic phase and inoculated into 96-well flat-bottom culture plates with the density of 1.0×10^5 cells. The cells were incubated at 37°C under 5% CO_2 atmosphere for 24 h. The different concentrations of compounds (1.5625, 6.25, 25, and 100 μM) were added into the 96-well plates. About 1% DMSO was used as blank control, and three replicates were set for each concentration. Then, the cells were cultured for 24 h. Subsequently, MTT/PBS solution (1:9, *v*/*v*) was added to each well plate. Around 4 h later, the absorbance at 490 nm was detected by ELISA, and the cell viability was calculated by following equation:

$$\text{Cell viability}(\%) = \left(OD_{treatment} / OD_{control}\right) \times 100$$

where $OD_{\text{treatment}}$ represent the absorbance of samples and OD_{control} represent the absorbance of blank control.

SCHEME 1 | General synthetic procedure of 1,3,4-oxadiazole derivatives (4a–4l, 5a–5l, and 6a–6f).

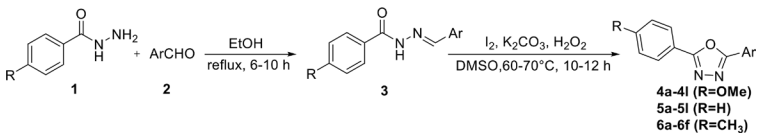

Compound	R	Ar	Compound	R	Ar
4a	OMe	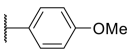	5d	H	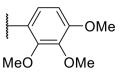
4b	OMe	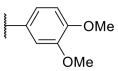	5e	H	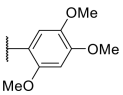
4c	OMe	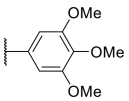	5f	H	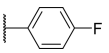
4d	OMe	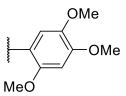	5g	H	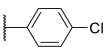
4e	OMe	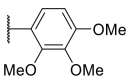	5h	H	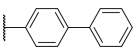
4f	OMe	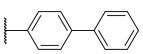	5i	H	
4g	OMe	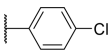	5j	H	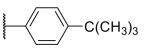
4h	OMe	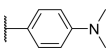	5k	H	
4i	OMe	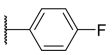	5l	H	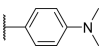
4j	OMe	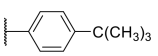	6a	Me	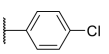
4k	OMe		6b	Me	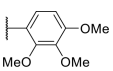
4l	OMe		6c	Me	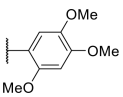
5a	H	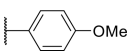	6d	Me	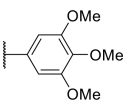
5b	H	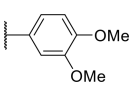	6e	Me	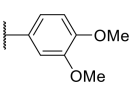
5c	H	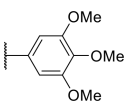	6f	Me	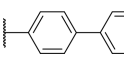

Molecular Docking

In order to evaluate the binding modes between target compounds (5e and 5k) with target enzymes succinate dehydrogenase (SDH; Yan et al., 2019; Yu et al., 2021), the molecular docking was conducted using Surflex-Dock program in the Sybyl-X software (version 2.1.1), and interaction analyzed using Ligplot+ client (version 2.2.4) and Pymol client. The crystal structure of SDH was downloaded from the Protein Data Bank (PDB code: 2FBW). Ligands and H_2O in the crystal structure of protein were deleted, and hydrogen atoms and charges were added using the AMBER7 FF99 method. The structures of compounds 5e

and 5k were optimized by adding charge (Gasteigere–Hückel) and Tripos force field.

RESULTS AND DISCUSSION

Chemical Synthesis

The synthetic routes of intermediates and oxadiazole derivatives were performed as illustrated in **Scheme 1**. Firstly, *p*-methoxy benzoyl hydrazide (1) and aromatic aldehyde (2) were condensed in EtOH by condensation reaction to obtain the intermediate *N*-acylaldehyde hydrazone (3). Then, the intermediate three were oxidized and cyclized by H_2O_2 in I_2 and K_2CO_3 to obtain 2, 5-disubstituted-1,3,4-oxadiazole derivatives (4a–4l). Similarly, compound 1 was replaced with benzoyl hydrazine or *p*-methylbenzoyl hydrazine, and oxadiazole derivatives 5a–5l and 6a–6f were obtained using the same experimental method. The yields of these compounds ranged from 47 to 90%. The purity and structure of target compounds were confirmed by TLC, melting point determination, ^{1}H-NMR and ^{13}C-NMR. The NMR Spectra of oxadiazole derivatives are shown in the supporting materials. All NMR data were consistent with the structure of the target compounds.

Antifungal Activity *in vitro* and Structure–Activity Relationship

Antifungal Activity *in vitro*

The antifungal activities of oxadiazole derivatives and the positive control carbendazim were evaluated against three plant pathogenic fungi causing maize diseases by the mycelium growth rate method, including *R. solani*, *G. zeae*, and *E. turcicum*. Firstly, the antifungal activities of 29 compounds were determined at 50 μg/ml *in vitro*. As shown in **Table 1**, the results indicated that compound 5k had superior inhibitory activities against three tested fungi. The inhibitory rates of compound 5k were 50.93, 59.23, and 70.56% against *R. solani*, *G. zeae*, and *E. turcicum*, respectively. Compounds 4k, 5c, and 5k had significant inhibitory effects against *G. zeae*, and the inhibitory rates were more than 50%, among them, 4k showed the highest activity with an inhibitory rate of 70.46%, followed by 5c with an inhibitory rate of 55.52%. Among the three pathogens, oxadiazole derivatives had the most significant activity against *E. turcicum*. The antifungal activities of compounds 4k, 5b, 5d, 5e, 5i, 5k, and 6e were all greater than 50%, and compound 5k had the highest inhibition rate of 70.56%, followed by 4k with 62.19% (**Figure 1**).

In order to further research the antifungal activities of oxadiazole derivatives, the EC_{50} values of compounds with higher inhibition rate were determined, and the results were illustrated in **Table 2**. Compound 5k showed high antifungal activities against three pathogens. In addition, oxadiazole derivatives had obvious antifungal activity against *E. turcicum*. The inhibitory activities of 4d, 4k, 5b, 5e, 5i, 5j, and 5k were better than positive control carbendazim. Especially, the EC_{50} values of 4k, 5e, 5i, and 5k were 50.48, 47.56, 47.05, and 32.25 μg/ml, respectively, and the positive control carbendazim was 102.83 μg/ml. Among them, 5k showed the strongest activity, it was about 3-fold more active than carbendazim. These results indicate that oxadiazole derivatives have potential as control drugs for maize diseases.

TABLE 1 | Antifungal activities of oxadiazole derivatives *in vitro* at 50 μg/ml.[a]

Compound	Inhibition rate[b] (%)		
	Rhizoctonia solani	*Gibberella zeae*	*Exserohilum turcicum*
4a	0.00	2.37 ± 3.35	21.02 ± 1.93
4b	5.05 ± 0.58	26.16 ± 0.98	14.50 ± 0.22
4c	3.13 ± 0.56	0.00	0.00
4d	23.13 ± 0.62	32.04 ± 3.11	44.52 ± 1.53
4e	6.31 ± 1.68	0.00	18.54 ± 1.49
4f	0.44 ± 0.98	0.00	4.65 ± 2.37
4g	0.00	5.67 ± 2.65	6.52 ± 1.08
4h	0.00	14.98 ± 1.14	14.17 ± 2.14
4i	0.44 ± 1.74	0.38 ± 5.54	14.02 ± 4.35
4j	0.00	13.01 ± 4.15	7.77 ± 3.69
4k	26.51 ± 1.25	70.46 ± 3.85	62.19 ± 2.67
4l	12.00 ± 1.94	4.23 ± 2.31	41.40 ± 2.45
5a	0.00	0.00	21.54 ± 1.86
5b	24.76 ± 1.88	15.81 ± 6.87	51.25 ± 0.18
5c	31.62 ± 2.41	55.52 ± 6.43	36.97 ± 1.20
5d	17.34 ± 1.96	17.98 ± 5.89	53.31 ± 4.17
5e	22.22 ± 1.27	35.41 ± 5.05	59.92 ± 3.84
5f	3.00 ± 0.10	20.44 ± 4.03	27.91 ± 3.45
5g	5.47 ± 2.14	23.14 ± 0.82	22.45 ± 3.87
5h	0.00	14.44 ± 6.41	4.13 ± 3.20
5i	41.22 ± 1.33	37.03 ± 2.12	55.71 ± 3.16
5j	22.67 ± 2.75	38.60 ± 0.76	44.52 ± 1.70
5k	50.93 ± 2.84	59.23 ± 2.64	70.56 ± 2.57
6a	0.00	0.00	0.52 ± 1.70
6b	3.15 ± 1.27	3.39 ± 0.42	5.73 ± 1.12
6c	2.89 ± 1.18	9.98 ± 6.11	18.03 ± 5.66
6d	0.00	0.00	14.55 ± 0.24
6e	30.38 ± 2.55	30.18 ± 4.11	53.55 ± 2.17
6f	4.70 ± 1.41	0.00	0.00

[a]*Rhizoctonia solani (R. solani), Gibberella zeae (G. zeae), and Exserohilum turcicum (E. turcicum).*

[b]*Values are the mean ± SD of three replicates.*

Structure–Activity Relationship

Based on the antifungal activity data (**Tables 1, 2**), the structure–activity relationship (SAR) of oxadiazole derivatives were analyzed. Compounds 5i and 5k had superior inhibitory effects on the three tested plant pathogenic fungi. Their structures contain aromatic five-membered heterocycles, in which 5i was furan ring and 5k was thiophene ring. It shows that the introduction of aromatic five-membered heterocycles may promote the improvement of antifungal activity. Such as compound 4k contained furan ring and exhibited higher inhibition against the other two fungi except *R. solani*.

However, not all oxadiazole derivatives containing five-membered heterocycles had significant antifungal activity. For example, compound 4l contained thiophene ring, but its inhibitory activities against *R. solani* and *G. zeae* were inferior than 5i and 5k. This was probably due to the presence of methoxide group on the other side of oxazole ring, which weakens hydrophobic force of thiophene. Among the three series of compounds, the activity of series 5 was stronger than series 4 and series 6. These results inferred that most of highly active compounds were not

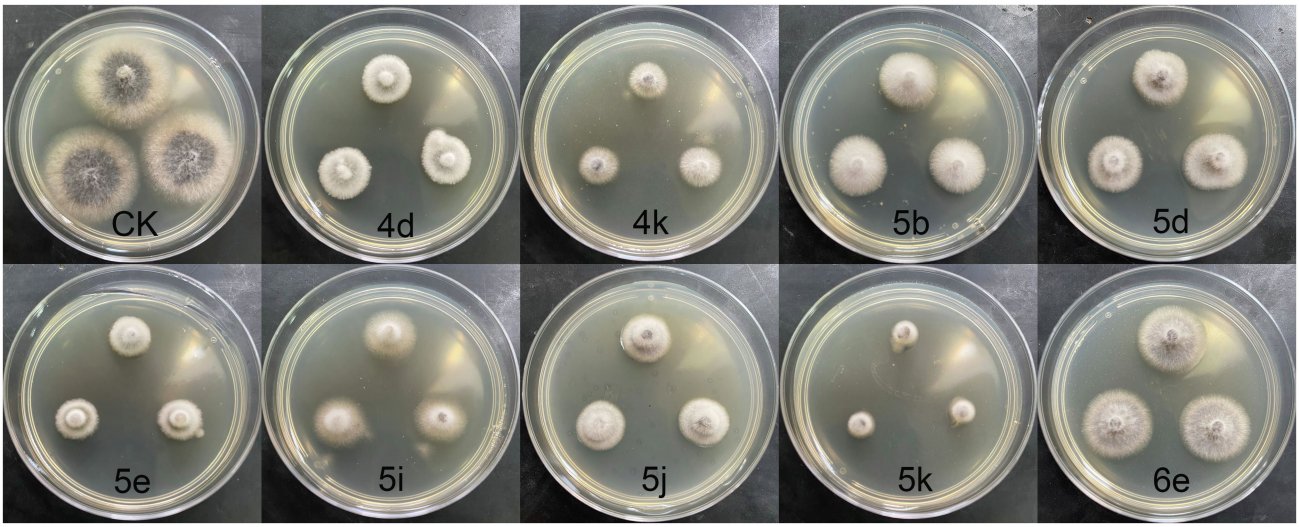

FIGURE 1 | Antifungal activities of active compounds against *Exserohilum turcicum*.

TABLE 2 | Antifungal activities with EC_{50} of the target compounds against three plant pathogenic fungi *in vitro*.

Fungal species	Compound	Regression equation[a]	EC_{50} (μg/ml)	R^2
Rhizoctonia solani	5i	$y=1.7176x+1.8239$	63.04	0.8844
	5k	$y=-0.4371x+3.2440$	47.43	0.9332
	Carbendazim[b]	$y=4.8410x+1.7872$	1.23	0.8419
Gibberella zeae	4k	$y=0.0758x+2.4399$	104.28	0.9193
	5i	$y=2.8069x-0.3231$	78.79	0.9999
	5k	$y=-0.0755x+2.8019$	64.78	0.9141
	Carbendazim	$y=3.8018x+0.9276$	19.58	0.9974
Exserohilum turcicum	4d	$y=3.3590x+0.8333$	93.15	0.9694
	4k	$y=0.7614x+2.4888$	50.48	0.9298
	5b	$y=2.2442x+1.3916$	95.57	0.8648
	5d	$y=4.0792x+0.4099$	176.45	0.8721
	5e	$y=2.9551x+1.2192$	47.56	0.9784
	5i	$y=0.7322x+2.5516$	47.05	0.9955
	5j	$y=1.0486x+2.0898$	77.77	0.9763
	5k	$y=2.0559x+1.9516$	32.25	0.9779
	6e	$y=3.8762x+0.3870$	801.73	0.9787
	Carbendazim	$y=0.0875x+2.4415$	102.83	0.9497

[a]*x represents the logarithm of molar concentration (lgc) and y represents the average inhibition rate.*

[b]*Commercial fungicide carbendazim as positive control.*

substituted or only one substituted on the oxadiazole-linked aromatic ring. The simultaneous attachment of substituents to 2, 5-position aromatic groups of oxadiazole may have an adverse effect on its antifungal activity. Other groups, such as the position and number of methoxy group and the presence of halogen, had no obvious influence on antifungal activity.

Effects on Mycelial Morphology of Plant Pathogenic Fungi

The morphological changes of *E. turcicum* mycelia treated by active compounds were observed under SEM. Three compounds 4k, 5e, and 5k were selected according to the results of their antifungal activity and structures. The results were shown in **Figure 2**. The edge of the blank control hyphae treated by DMSO (**Figure 2A**) was uniform, and the surface of hyphae was regular and relatively smooth. However, after treated by 4k, 5e, and 5k (**Figures 2B–D**), the morphology of *E. turcicum* hyphae were curved, with obvious shrinkage and collapse on the surface and roughness on the outer walls. These results conjectured that compounds 4k, 5e, and 5k may disrupt the morphology and structure of mycelium and lead to cytoplasmic outflow. The SEM results further confirmed that the inhibitory effects of oxazole derivatives against plant pathogens were consistent with the experimental results *in vitro*.

Cytotoxicity

The cytotoxic activities of several oxadiazole derivatives against MCF-7 cell line were determined by MTT assay (Gewirtz, 1999), and the results were shown in **Figure 3**. Specifically, compounds 4d, 4k, 5b, 5d, 5i, 5k, and 6e demonstrated no cytotoxicity at all tested concentrations, with survival rates greater than 80% at 100 μmol/L. Only 5e and 5j manifested weaker inhibition, the survival rates were 69 and 48%, respectively. The cell viability of two compounds decreased at the concentration of 100 μmol/L, but the toxicities were not significant. Compounds with superior antifungal activities, such as 4k, 5e, 5i, and 5k, showed no cytotoxic activities. These results can preliminarily show that most oxadiazole derivatives had no potential damage on mammalian cells. However, the cytotoxicity against human normal liver cells remains to be further verified.

Molecular Docking Results

In order to elucidate the preliminary mechanism of antifungal activities of these compounds, the target compounds were docked with the theoretical active site of SDH by SYBYL-X. SDH was one of the important molecular targets for developing

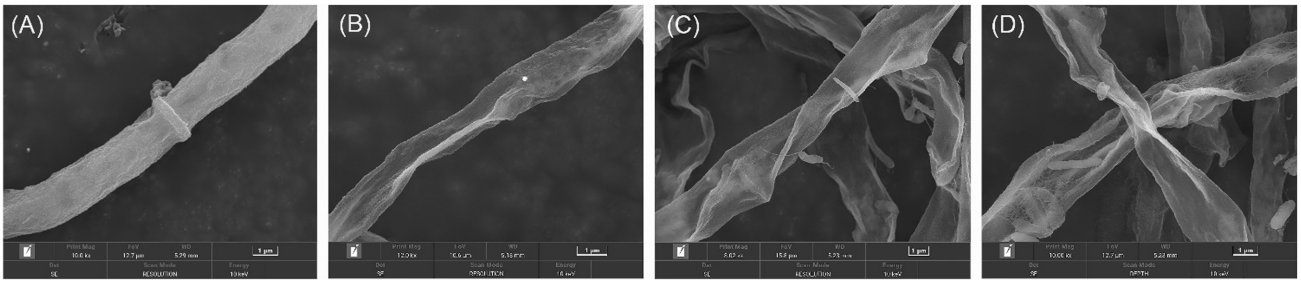

FIGURE 2 | Scanning electron microscopy (SEM) micrographs of *Exserohilum turcicum* hyphae. **(A)** Blank control, **(B)** Treated by 4k at 50 μg/ml, **(C)** Treated by 5e at 50 μg/ml, and **(D)** Treated by 5k at 25 μg/ml.

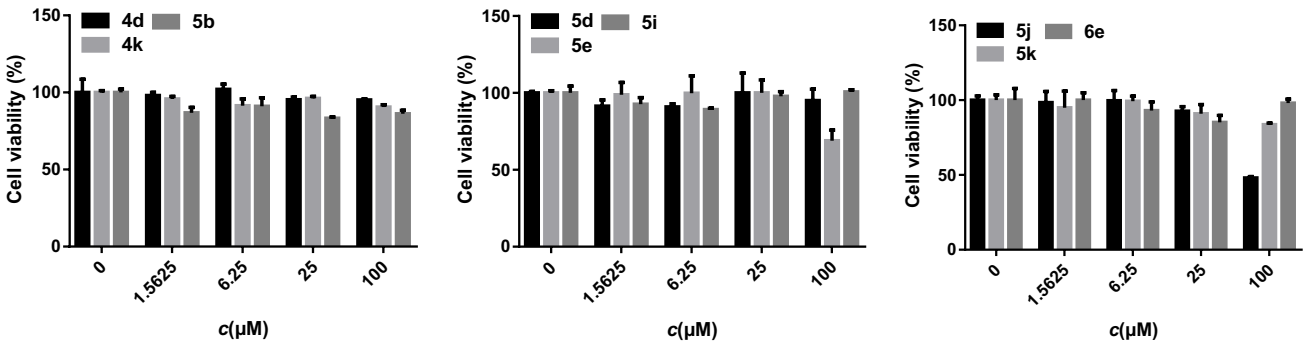

FIGURE 3 | Cytotoxic activity results of target compounds.

new fungicides. Compounds 5e and 5k were selected for molecular docking because of their high antifungal activities and different structural units. Molecular docking results were shown in **Figure 4**.

In **Figures 4A,B**, compounds 5e was bound in the active pocket of SDH, and can produce hydrophobic contact with 10 amino acid residues, including Trp173, Tyr58, His216, Arg43, Asp57, Ser39, Ile218, Ile40, Trp32, and Ile27. Meanwhile, compound 5e can form two hydrogen bonds with amino acid residues Trp173 and tyr58 through the oxygen atom on the oxadiazole ring, which was crucial for the binding between the inhibitor and SDH. The hydrogen bond lengths were 1.9 Å and 2.5 Å, respectively (**Figure 4C**). In **Figures 4D,E**, compounds 5k can produce hydrophobic contact with 11 amino acid residues, including Trp173, Trp32, Met36, Ile40, Ser39, His216, Arg43, Asp57, Tyr58, Pro169, and Ile27, and can form three hydrogen bonds with amino acid residues Trp173 and Tyr58 through nitrogen atoms on the oxadiazole ring. The hydrogen bond lengths were 2.0, 2.1, and 2.3 Å, respectively (**Figure 4F**).

It can be seen that the number of residues and hydrogen bonds between compound 5k and SDH are greater than 5e. The presence of 2,4,5-methoxyl group in the 5e structure leads to its repulsion with amino acid residues, which may be the reason for its relative weaker antifungal potency. Molecular docking results showed that hydrophobic contact and hydrogen bond formation could promote the binding between compound and SDH, and improve the antifungal activity.

CONCLUSION

Maize is an important food crop and its fungal disease has become a limiting factor to improve the yield and quality of maize. In the control of plant pathogens, commercial fungicides have no obvious effect on corn diseases due to the emergence of drug resistance. Therefore, it is of great significance to develop new fungicides with novel structure, high efficiency, and low toxicity to control maize diseases. In this paper, a series of 1,3,4-oxadiazole derivatives (4a–4l, 5a–5l, and 6a–6f) were designed and synthesized from three kinds of benzoyl hydrazine and various aromatic aldehydes. The antifungal activities of oxadiazole derivatives against *R. solani*, *G. zeae*, and *E. turcicum* which caused maize diseases were evaluated. The results indicated that compound 5k had superior inhibitory activities against three tested fungi. Especially against *E. turcicum*, the inhibitory activity of 5k exceeded carbendazim, and their EC_{50} values were 32.25 and 102.83 μg/ml, respectively. The compounds with antifungal activities had almost no cytotoxicity to MCF-7, which could provide a basis for further cytotoxicity study on normal human liver cells. The preliminary mechanism research indicated that compounds 4k, 5e, and 5k could induce the obvious shrinkage and collapse of *E. turcicum* mycelia. Molecular docking results further revealed the interaction between receptor and ligand. Compounds 5e and 5k could bind to amino acid residues through hydrophobic contact and hydrogen bonds, which explained the possible mechanism of binding between the inhibitor and target

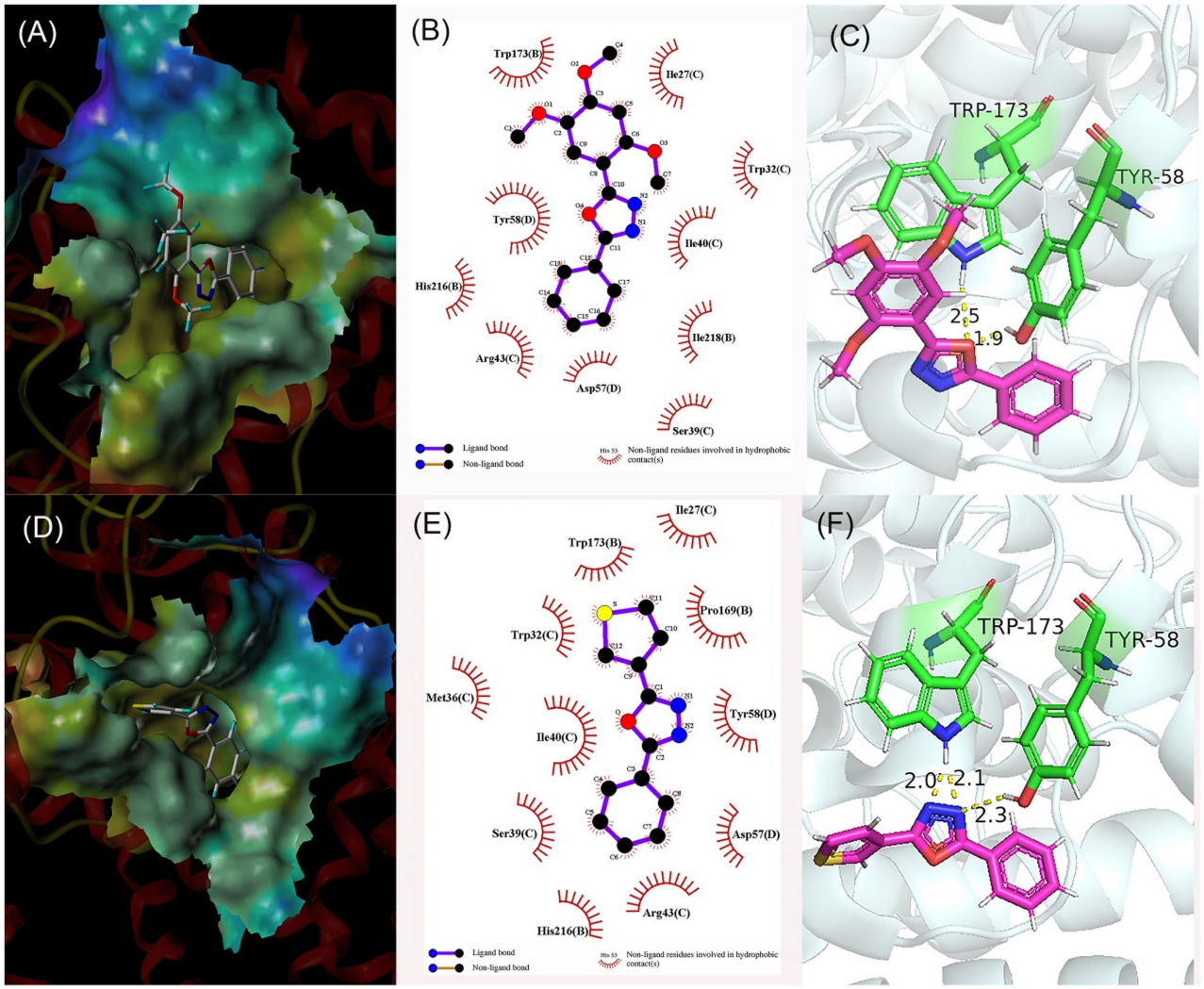

FIGURE 4 | Molecular docking results of compound 5e **(A–C)** and compound 5k **(D–F)**. **(A,D)** Predicted binding mode of compound within active pocket; **(B,E)** Predicted interactions between compound and amino acids; and **(C,F)** Binding modes of compound and amino acids.

protein. Consequently, oxadiazole derivatives have the potential as plant fungicides to control maize diseases.

DATA AVAILABILITY STATEMENT

The original contributions presented in the study are included in the article/**Supplementary Material**, further inquiries can be directed to the corresponding author.

AUTHOR CONTRIBUTIONS

LYa, GZ, and LYu contributed to the conception and design of this study. SL characterized the structure of the derivatives. XW measured the cytotoxic activity of the derivatives. TF completed the molecular docking. HK and WF completed the determination of antifungal activities and the statistics of some databases. LYa finished the first draft. All authors contributed to the article and approved the submitted version.

FUNDING

This work was supported financially by the Special Scientific Research Program of Shaanxi Education Department (No. 20JK0892), the Natural Science Basic Research Project of Shaanxi Science and Technology Department (No. 2022JM-492), and the Science and Technology Innovation Team of Xi'an Medical University (No. 2021TD07).

SUPPLEMENTARY MATERIAL

The Supplementary Material for this article can be found online at: https://www.frontiersin.org/articles/10.3389/fpls.2022.912091/full#supplementary-material

REFERENCES

Abdelsalam, N. R., Balbaa, M. G., Osman, H. T., Ghareeb, R. Y., Desoky, E.-S. M., Elshehawi, A. M., et al. (2022). Inheritance of resistance against northern leaf blight of maize using conventional breeding methods. *Saudi J. Biol. Sci.* 29, 1747–1759. doi: 10.1016/j.sjbs.2021.10.055

Adeyemi, O. S., Eseola, A. O., Plass, W., Kato, K., Otuechere, C. A., Awakan, O. J., et al. (2021). The anti-parasite action of imidazole derivatives likely involves oxidative stress but not HIF-1α signaling. *Chem. Biol. Interact.* 349:109676. doi: 10.1016/j.cbi.2021.109676

Al-Harbi, N. O., Bahashwan, S. A., Fayed, A. A., Aboonq, M. S., and Amr, A. E.-G. E. (2013). Anti-parkinsonism, hypoglycemic and anti-microbial activities of new poly fused ring heterocyclic candidates. *Int. J. Biol. Macromol.* 57, 165–173. doi: 10.1016/j.ijbiomac.2013.03.019

Balaraju, V., Kalyani, S., Sridhar, G., and Laxminarayana, E. (2021). Design, synthesis and biological assessment of 1, 3, 4-oxadiazole incorporated oxazole-triazole derivatives as anticancer agents. *Chem. Data Collect.* 33:100695. doi: 10.1016/j.cdc.2021.100695

Bebber, D. P., and Gurr, S. J. (2015). Crop-destroying fungal and oomycete pathogens challenge food security. *Fungal Genet. Biol.* 74, 62–64. doi: 10.1016/j.fgb.2014.10.012

De Rossi, R. L., Guerra, F. A., Plazas, M. C., Vuletic, E. E., Brücher, E., Guerra, G. D., et al. (2022). Crop damage, economic losses, and the economic damage threshold for northern corn leaf blight. *Crop Prot.* 154:105901. doi: 10.1016/j.cropro.2021.105901

Fan, Y.-L., Jin, X.-H., Huang, Z.-P., Yu, H.-F., Zeng, Z.-G., Gao, T., et al. (2018). Recent advances of imidazole-containing derivatives as anti-tubercular agents. *Eur. J. Med. Chem.* 150, 347–365. doi: 10.1016/j.ejmech.2018.03.016

Fan, L., Luo, Z., Li, Y., Liu, X., Fan, J., Xue, W., et al. (2020). Synthesis and antifungal activity of imidazo [1, 2-b] pyridazine derivatives against phytopathogenic fungi. *Bioorg. Med. Chem. Lett.* 30:127139. doi: 10.1016/j.bmcl.2020.127139

Fones, H. N., Bebber, D. P., Chaloner, T. M., Kay, W. T., Steinberg, G., and Gurr, S. J. (2020). Threats to global food security from emerging fungal and oomycete crop pathogens. *Nat. Food* 1, 332–342. doi: 10.1038/s43016-020-0075-0

Gewirtz, D. A. (1999). A critical evaluation of the mechanisms of action proposed for the antitumor effects of the anthracycline antibiotics adriamycin and daunorubicin. *Biochem. Pharmacol.* 57, 727–741. doi: 10.1016/S0006-2952(98)00307-4

Guerrero-Pepinosa, N. Y., Cardona-Trujillo, M. C., Garzon-Castano, S. C., Veloza, L. A., and Sepulveda-Arias, J. C. (2021). Antiproliferative activity of thiazole and oxazole derivatives: A systematic review of in vitro and in vivo studies. *Biomed. Pharmacother.* 138:111495. doi: 10.1016/j.biopha.2021.111495

Hao, J.-J., Zhu, W.-L., Li, Y.-Q., Liu, J.-Z., Xie, S.-N., Sun, J., et al. (2020). Efficacy and profitability of fungicide use to manage Curvularia leaf spot of maize. *Crop Prot.* 132:105126. doi: 10.1016/j.cropro.2020.105126

Hejazi, I. I., Shahabuddin, S., Bhat, A. R., and Athar, F. (2019). Pharmacokinetic evaluation, molecular docking and in vitro biological evaluation of 1, 3, 4-oxadiazole derivatives as potent antioxidants and STAT3 inhibitors. *J. Pharm. Anal.* 9, 133–141. doi: 10.1016/j.jpha.2018.12.002

Küçükgüzel, Ş. G., and Şenkardeş, S. (2015). Recent advances in bioactive pyrazoles. *Eur. J. Med. Chem.* 97, 786–815. doi: 10.1016/j.ejmech.2014.11.059

Lamberth, C. (2013). Heterocyclic chemistry in crop protection. *Pest Manag. Sci.* 69, 1106–1114. doi: 10.1002/ps.3615

Leroux, P., and Walker, A.-S. (2013). Activity of fungicides and modulators of membrane drug transporters in field strains of Botrytis cinerea displaying multidrug resistance. *Eur. J. Plant Pathol.* 135, 683–693. doi: 10.1007/s10658-012-0105-3

Li, J. C., Wang, R. X., Sun, Y., Zhu, J. K., Hu, G. F., Wang, Y. L., et al. (2019). Design, synthesis and antifungal activity evaluation of isocryptolepine derivatives. *Bioorg. Chem.* 92:103266. doi: 10.1016/j.bioorg.2019.103266

Lipunova, G. N., Nosova, E. V., Charushin, V. N., and Chupakhin, O. N. (2015). Fluorine-containing pyrazoles and their condensed derivatives: synthesis and biological activity. *J. Fluor. Chem.* 175, 84–109. doi: 10.1016/j.jfluchem.2015.03.011

Ma, Y., Yang, L., Liu, X., Yang, J., and Sun, X. (2020). Development of celecoxib-derived antifungals for crop protection. *Bioorg. Chem.* 97:103670. doi: 10.1016/j.bioorg.2020.103670

Majji, G., Rout, S. K., Guin, S., Gogoi, A., and Patel, B. K. (2014). Iodine-catalysed oxidative cyclisation of acylhydrazones to 2, 5-substituted 1, 3, 4-oxadiazoles. *RSC Adv.* 4, 5357–5362. doi: 10.1039/c3ra44897e

Mi, Y., Zhang, J., Han, X., Tan, W., Miao, Q., Cui, J., et al. (2021). Modification of carboxymethyl inulin with heterocyclic compounds: synthesis, characterization, antioxidant and antifungal activities. *Int. J. Biol. Macromol.* 181, 572–581. doi: 10.1016/j.ijbiomac.2021.03.109

Nagaraju, R. S., Sriram, R. H., and Achur, R. (2020). Antifungal activity of Carbendazim-conjugated silver nanoparticles against anthracnose disease caused by Colletotrichum gloeosporioides in mango. *J. Plant Pathol.* 102, 39–46. doi: 10.1007/s42161-019-00370-y

Nazarov, P. A., Baleev, D. N., Ivanova, M. I., Sokolova, L. M., and Karakozova, M. V. (2020). Infectious plant diseases: etiology, current status, problems and prospects in plant protection. *Acta Nat.* 12, 46–59. doi: 10.32607/actanaturae.11026

Negalurmath, V. S., Boda, S. K., Kotresh, O., Lakshmi, P. A., and Basanagouda, M. (2019). Benzofuran-oxadiazole hybrids: design, synthesis, antitubercular activity and molecular docking studies. *Chem. Data Collect.* 19:100178. doi: 10.1016/j.cdc.2019.100178

Oskuei, S. R., Mirzaei, S., Jafari-Nik, M. R., Hadizadeh, F., Eisvand, F., Mosaffa, F., et al. (2021). Design, synthesis and biological evaluation of novel imidazole-chalcone derivatives as potential anticancer agents and tubulin polymerization inhibitors. *Bioorg. Chem.* 112:104904. doi: 10.1016/j.bioorg.2021.104904

Parikh, P. H., Timaniya, J. B., Patel, M. J., and Patel, K. P. (2022). Microwave-assisted synthesis of pyrano [2, 3-c]-pyrazole derivatives and their anti-microbial, anti-malarial, anti-tubercular, and anti-cancer activities. *J. Mol. Struct.* 1249:131605. doi: 10.1016/j.molstruc.2021.131605

Polkam, N., Kummari, B., Rayam, P., Brahma, U., Naidu, V. G. M., Balasubramanian, S., et al. (2017). Synthesis of 2, 5-disubstituted-1, 3, 4-oxadiazole derivatives and their evaluation as anticancer and antimycobacterial agents. *ChemistrySelect* 2, 5492–5496. doi: 10.1002/slct.201701101

Price, C. L., Parker, J. E., Warrilow, A. G., Kelly, D. E., and Kelly, S. L. (2015). Azole fungicides–understanding resistance mechanisms in agricultural fungal pathogens. *Pest Manag. Sci.* 71, 1054–1058. doi: 10.1002/ps.4029

Rulhania, S., Kumar, S., Nehra, B., Gupta, G., and Monga, V. (2021). An insight into the medicinal perspective of synthetic analogs of imidazole. *J. Mol. Struct.* 1232:129982. doi: 10.1016/j.molstruc.2021.129982

Selvam, T. P., Kumar, P. V., Saravanan, G., and Prakash, C. R. (2014). Microwave-assisted synthesis, characterization and biological activity of novel pyrazole derivatives. *J. Saudi Chem. Soc.* 18, 1015–1021. doi: 10.1016/j.jscs.2011.12.006

Shao, W., Zhao, Y., and Ma, Z. (2021). Advances in understanding fungicide resistance in Botrytis cinerea in China. *Phytopathology* 111, 455–463. doi: 10.1094/PHYTO-07-20-0313-IA

Shevaldina, E. V., Opredelennova, K. A., Chichvarina, O. A., Spiridonov, Y. Y., Smol'yakov, A. F., Dorovatovskii, P. V., et al. (2019). One-pot acid-free ferrocenylalkylation of azoles with α-ferrocenyl alcohols: ferrocene-based plant growth regulators and herbicide safeners. *Appl. Organomet. Chem.* 33:e5228. doi: 10.1002/aoc.5228

Silva, T. S., Da Fonseca, L. F., Yamada, J. K., and Pontes, N. D. C. (2021). Flutriafol and azoxystrobin: an efficient combination to control fungal leaf diseases in corn crops. *Crop Prot.* 140:105394. doi: 10.1016/j.cropro.2020.105394

Silva-Ortiz, A. V., Bratoeff, E., Ramírez-Apan, M. T., García-Becerra, R., Ordaz-Rosado, D., Noyola-Martínez, N., et al. (2016). Synthesis and biological activity of two pregnane derivatives with a triazole or imidazole ring at C-21. *J. Steroid Biochem.* 159, 8–18. doi: 10.1016/j.jsbmb.2016.02.013

Taha, M., Ismail, N. H., Imran, S., Rokei, M. Q. B., Saad, S. M., and Khan, K. M. (2015). Synthesis of new oxadiazole derivatives as α-glucosidase inhibitors. *Bioorg. Med. Chem.* 23, 4155–4162. doi: 10.1016/j.bmc.2015.06.060

Titi, A., Messali, M., Alqurashy, B. A., Touzani, R., Shiga, T., Oshio, H., et al. (2020). Synthesis, characterization, X-ray crystal study and bioctivities of pyrazole derivatives: identification of antitumor, antifungal and antibacterial pharmacophore sites. *J. Mol. Struct.* 1205:127625. doi: 10.1016/j.molstruc.2019.127625

Van Rensburg, B. J., Mc Laren, N. W., Schoeman, A., and Flett, B. C. (2016). The effects of cultivar and prophylactic fungicide spray for leaf diseases on colonisation of maize ears by fumonisin producing Fusarium spp. and fumonisin synthesis in South Africa. *Crop Prot.* 79, 56–63. doi: 10.1016/j.cropro.2015.10.009

Verma, G., Chashoo, G., Ali, A., Khan, M. F., Akhtar, W., Ali, I., et al. (2018). Synthesis of pyrazole acrylic acid based oxadiazole and amide derivatives as antimalarial and anticancer agents. *Bioorg. Chem.* 77, 106–124. doi: 10.1016/j.bioorg.2018.01.007

Waheed, A., Goyal, M., Gupta, D., Khanna, A., Hassanien, A. E., and Pandey, H. M. (2020). An optimized dense convolutional neural network model for disease recognition and classification in corn leaf. *Comput. Electron. Agric.* 175:105456. doi: 10.1016/j.compag.2020.105456

Wang, H., Hou, J., Ye, P., Hu, L., Huang, J., Dai, Z., et al. (2021a). A teosinte-derived allele of a MYB transcription repressor confers multiple disease resistance in maize. *Mol. Plant* 14, 1846–1863. doi: 10.1016/j.molp.2021.07.008

Wang, S., Huang, X., Zhang, Y., Yin, C., and Richel, A. (2021b). The effect of corn straw return on corn production in Northeast China: an integrated regional evaluation with meta-analysis and system dynamics. *Resour. Conserv. Recycl.* 167:105402. doi: 10.1016/j.resconrec.2021.105402

Wei, Y., Li, S. Q., and Hao, S. H. (2018). New angular oxazole-fused coumarin derivatives: synthesis and biological activities. *Nat. Prod. Res.* 32, 1824–1831. doi: 10.1080/14786419.2017.1405408

Xu, Z., Gao, C., Ren, Q.-C., Song, X.-F., Feng, L.-S., and Lv, Z.-S. (2017). Recent advances of pyrazole-containing derivatives as anti-tubercular agents. *Eur. J. Med. Chem.* 139, 429–440. doi: 10.1016/j.ejmech.2017.07.059

Yamamuro, D., Uchida, R., Ohtawa, M., Arima, S., Futamura, Y., Katane, M., et al. (2015). Synthesis and biological activity of 5-(4-methoxyphenyl)-oxazole derivatives. *Bioorg. Med. Chem. Lett.* 25, 313–316. doi: 10.1016/j.bmcl.2014.11.042

Yan, W., Wang, X., Li, K., Li, T.-X., Wang, J.-J., Yao, K.-C., et al. (2019). Design, synthesis, and antifungal activity of carboxamide derivatives possessing 1, 2, 3-triazole as potential succinate dehydrogenase inhibitors. *Pestic. Biochem. Physiol.* 156, 160–169. doi: 10.1016/j.pestbp.2019.02.017

Yang, C. J., Li, H. X., Wang, J. R., Zhang, Z. J., Wu, T. L., Liu, Y. Q., et al. (2022). Design, synthesis and biological evaluation of novel evodiamine and rutaecarpine derivatives against phytopathogenic fungi. *Eur. J. Med. Chem.* 227:113937. doi: 10.1016/j.ejmech.2021.113937

Yoon, M. Y., Cha, B., and Kim, J. C. (2013). Recent trends in studies on botanical fungicides in agriculture. *Plant Pathol. J.* 29, 1–9. doi: 10.5423/PPJ.RW.05.2012.0072

Yu, B., Zhao, B., Hao, Z., Chen, L., Cao, L., Guo, X., et al. (2021). Design, synthesis and biological evaluation of pyrazole-aromatic containing carboxamides as potent SDH inhibitors. *Eur. J. Med. Chem.* 214:113230. doi: 10.1016/j.ejmech.2021.113230

Zhang, T., Liu, H., Lu, T., Zhang, G., Xiao, T., Cheng, W., et al. (2022). Novel 4, 5-dihydro-1H-pyrazole derivatives as potential succinate dehydrogenase inhibitors: design, synthesis, crystal structure, biological activity and molecular modeling. *J. Mol. Struct.* 1249:131537. doi: 10.1016/j.molstruc.2021.131537

Conflict of Interest: The authors declare that the research was conducted in the absence of any commercial or financial relationships that could be construed as a potential conflict of interest.

Publisher's Note: All claims expressed in this article are solely those of the authors and do not necessarily represent those of their affiliated organizations, or those of the publisher, the editors and the reviewers. Any product that may be evaluated in this article, or claim that may be made by its manufacturer, is not guaranteed or endorsed by the publisher.

frontiers | Frontiers in Plant Science

ORIGINAL RESEARCH
published: 27 May 2022
doi: 10.3389/fpls.2022.903310

PhcA and PhcR Regulate Ralsolamycin Biosynthesis Oppositely in *Ralstonia solanacearum*

Peng Li[1], Xiulan Cao[1], Liwen Zhang[2], Mingfa Lv[3] and Lian-Hui Zhang[3]**

[1]*Ministry of Education Key Laboratory for Ecology of Tropical Islands, Hainan Provincial Key Laboratory for Tropical Plant and Animal Ecology, College of Life Sciences, Hainan Normal University, Haikou, China,* [2]*Biotechnology Research Institute, The Chinese Academy of Agricultural Sciences, Beijing, China,* [3]*Guangdong Province Key Laboratory of Microbial Signals and Disease Control, Integrative Microbiology Research Centre, South China Agricultural University, Guangzhou, China*

Ralsolamycin, one of secondary metabolites in *Ralstonia solanacearum*, is known to be involved in crosstalk between *R. solanacearum* and fungi. Ralsolamycin formation is catalyzed by two-hybrid synthetases of RmyA (non-ribosomal peptide synthetase) and RmyB (polyketide synthase). A methyltransferase PhcB catalyzes formation of 3-OH MAME or 3-OH PAME, signals for the quorum sensing (QS) in *R. solanacearum*, while PhcB positively modulates ralsolamycin biosynthesis. A two-component system of PhcS and PhcR can response these QS signals and activate *phcA* expression. Here, we experimentally demonstrated that deletion of *phcA* (Δ*phcA*) substantially impaired the ralsolamycin production and expression of *rmyA* and *rmyB* in *R. solanacearum* strain EP1, and failed to induce chlamydospore formation of plant fungal pathogen *Fusarium oxysporum* f. *cubense* (stran FOC4). However, deletion of *phcR* significantly increased ralsolamycin production and expression of *rmyA* and *rmyB*, and *phcR* mutants exhibited enhanced ability to induce chlamydospore formation of FOC4. Results of the electrophoretic mobility shift assay suggested that both PhcA and PhcR bind to promoter of *rmy* operon. Taken together, these results demonstrated that both PhcA and PhcR bind to promoter of *rmy* operon, but regulate ralsolamycin biosynthesis in an opposite way. It could extend our knowledge on the sophisticated regulatory networks of ralsolamycin biosynthesis in *R. solanacearum*.

Keywords: ***Ralstonia solanacearum*, ralsolamycin, PhcA, PhcR, regulatory mechanism**

OPEN ACCESS

Edited by:
Yuheng Yang,
Southwest University, China

Reviewed by:
Meixiang Zhang,
Shaanxi Normal University, China
Yong Zhang,
Southwest University, China

****Correspondence:***
Lian-Hui Zhang
lhzhang01@scau.edu.cn
Mingfa Lv
mingfalv2010@126.com

Specialty section:
This article was submitted to Technical Advances in Plant Science, a section of the journal Frontiers in Plant Science

Received: *24 March 2022*
Accepted: *05 May 2022*
Published: *27 May 2022*

Citation:
Li P, Cao X, Zhang L, Lv M and Zhang L-H (2022) PhcA and PhcR Regulate Ralsolamycin Biosynthesis Oppositely in Ralstonia solanacearum. Front. Plant Sci. 13:903310. doi: 10.3389/fpls.2022.903310

INTRODUCTION

Ralstonia solanacearum is a causal agent of bacterial wilt disease on extremely broad range of plant species, which includes *R. solanacearum* and closely related species of *R. syzygii*, *R. picketti,* and banana blood disease (BDB) bacterium (Hayward, 1991). In addition, the *R. solanacearum* is also well known for extremely wide geographic distributions and capability to live and compete for versatile and diverse habitats (Salanoubat et al., 2002; Alvarez et al., 2010).

Interaction between *R. solanacearum* and other microorganisms in virulence or environmental competition has recently attracted much attention, and secondary metabolites (SMs) plays important roles on inter-kingdom signaling communication or provides fitness advantages in dynamic polymicrobial ecosystems (Baldeweg et al., 2017). The ralfuranone family contribute to virulence of *R. solanacearum* strain OE1-1(Kai et al., 2014; Senuma et al., 2020), while the staphyloferrin B is a siderophore associated with iron scavenge in strain AW1, which has a role in the competitiveness of phytopathogen outside its host plants (Bhatt and Denny, 2004). The yersiniabactin-like siderophore micacocidin was identified as an anti-mycoplasma agent (Kreutzer et al., 2011). Recently, ralsolamycin (synonym ralstonin A) is catalyzed by two-hybrid synthetases of RmyA (non-ribosomal peptide synthetase) and RmyB (polyketide synthase) that works as an inter-kingdom signal to communicate with fungal organisms and induces chlamydospores formation of interacted fungi. (Spraker et al., 2016; Baldeweg et al., 2017; Murai et al., 2017). As a response to ralsolamycin induction, fungi enhance bikaverin biosynthesis to antagonize *R. solanacearum* (Spraker et al., 2018). These findings indicate that *R. solanacearum* is capable of a producer of diverse SMs, which has important implications for the persistence of this phytopathogen.

It has been well known that the bacterial populations can emit and detect small diffusing compounds, whose concentration is key for coordinated behaviors. The quorum sensing (QS) is such a process that allows bacterial population to regulate specific genes at the quorum cell density (Fuqua et al., 1994). In *R. solanacearum*, either methyl 3-hydroxypalmitate (3-OH PAME) and methyl 3-hydroxymyristate (3-OH MAME), signals for phc-QS system, which are encoded by a methyltransferase PhcB (Flavier et al., 1997; Kai et al., 2015). The phc-QS signals are sensed through kinase PhcS, a sensor histidine of a two-component system (TCS), and transferred to PhcA, a TCS transcriptional regulator, which in turn activates transcriptional ability of PhcR, a LysR family transcriptional regulator to globally control many phc-QS-dependent phenotypes including virulence (Genin and Denny, 2012). Genes of *phcB*, *phcS,* and *phcR* are located together that possibly form an operon to control the phc-QS system in *R. solanacearum*, which is therefore called the phc-QS system (Clough et al., 1997).

We previously demonstrated that deletion of *phcB* drastically decreased expression of *rmyA* and *rmyB* and impaired chlamydospores formation in a *Fusarium oxysporum* f. *cubense* (FOC4), soil-borne phytopathogens that exhibits attenuated antifungal activity against *Sporisorium scitamineum* (Li et al., 2017). In addition, expression of *rmyA* and *rmyB* is downregulated with *phcA* deletion (Perrier et al., 2018). Whereas it remains to be elucidated whether *phcA* mutants affects ralsolamycin production in *R. solanacearum* and chlamydospores formation in FOC4. The *phcB*, *phcS,* and *phcR* form an operon and PhcR modulates transcriptional activity of PhcA. We therefore focused on PhcA and PhcR to elucidate whether they modulate ralsolamycin biosynthesis in *R. solanacearum* and chlamydospores formation in FOC4.

In this study, we constructed the deletion mutants of *phcA* (named Δ*phcA*) and *phcR* (named Δ*phcR*), respectively, using EP1 as a parental strain (Li et al., 2016). The expression level of *rmy* genes was compared by quantitative real-time polymerase chain reaction (qRT-PCR), and the ralsolamycin production was analyzed by using matrix-assisted laser desorption ionization time-of-flight spectrometry (MALDI-TOF). Our results demonstrated that both PhcA and PhcR were involved in the modulation of ralsolamycin biosynthesis directly but with opposite modulation patterns. The findings from this study outlined the regulatory networks that govern ralsolamycin biosynthesis, suggesting that *R. solanacearum* has evolved delicate regulatory mechanisms to respond and adapt to changing environmental conditions.

MATERIALS AND METHODS

Bacterial and Fungal Strains, Plasmids, and Culture Conditions

Plasmids, *R. solanacearum*, *Escherichia coli,* and *F. oxysporum* f. *cubense* used in this study were listed in **Table 1**. *R. solanacearum* phylotype I strain EP1 causes virulence on tomato plants but elicits hypersensitive response (HR) on tobacco plants, and it was subjected as parent strain for mutant generation in this study (Li et al., 2016). *R. solanacearum* strains were grown at 28°C in casamino acid–peptone–glucose (CPG) plate (Hendrick and Sequeira, 1984) or minimal medium (MM) plate. *E. coli* DH5*α* was grown at 37°C in LB medium and used for plasmid construction. *F. oxysporum* f. *cubense* FOC4 was grown at 30°C in PDA medium. Antibiotics were supplemented when necessary at following concentrations (μg/L):

TABLE 1 | List of the bacterial and fungal strains and plasmids used in this study.

Strain/Plasmid	Relevant characteristics	Source
R. solanacearum		
EP1	Wild type, Rif^r	Li et al. (2016); CFBP8480
Δ*phcA*	*phcA* deletion mutant of EP1 (Rif^r)	This study
Δ*phcA*(*phcA*)	Δ*phcA* + *phcA* (Km^r, Rif^r)	This study
Δ*phcR*	*phcR* deletion mutant of EP1 (Rif^r)	This study
Δ*phcR*(*phcR*)	Δ*phcR* + *phcR* (Km^r, Rif^r)	This study
Fungus		
FOC4	*F. oxysporum* f. *cubense*	Li et al. (2014)
Plasmids		
pK18mobsacB	Km^r, suicide, and narrow-broad-host vector	Schäfer et al. (1994)
pBBR1MCS2	Km^r, broad-host-range cloning vector	Kovach et al. (1995)
pRK2013	Km^r	Ditta et al. (1980)
pET-32a-*phcA*	pET-32a carries the *phcA* coding region, Amp^r	This study
pET-32a-*phcR*	pET32a carries the *phcR* coding region, Amp^r	This study

ampicillin, Amp (100); kanamycin, Km (50); and rifampicin, Rif (30).

Mutants Generation With In-frame Deletion of Genes and Complementation Assay

In the present study, mutants were generated with the pK18mobsacB based homologue recombination, by which target genes were in-frame deleted as described previously (Li et al., 2017). In brief, coding sequence of target genes was removed by the joint PCR, which conjugated both ends of flanking DNA fragments. The PCR amplified DNA fragments, in which target genes were absent, were finally sub-cloned into suicide plasmid pK18mobsacB. All primers used in this study were listed in **Supplementary Table S1**. After validating sequences, recombinant plasmids helped by the pRK2013 were introduced into EP1 by the tri-parental mating on CPG plates, followed by enrichment of integration mutants of strain EP1 on MM plates supplemented with Km and Rif as described previously (Ditta et al., 1980). As results, the *phcA* and *phcR* mutants were generated after confirmed by colony PCR and DNA sequencing.

The genetic complementation was performed with the expression vector pBBR1MCS2-based complementation assay as described previously (Kovach et al., 1995). In brief, DNA fragments containing putative promoter and coding sequence of *phcA* and *phcR* were PCR amplified and finally sub-cloned into pBBR1MCS2, respectively. Genes of *phcB*, *phcS,* and *phcR* from an operon and the putative promoter of this operon (*phcB* upstream region about 235 bp) were PCR conjugated with coding sequence of *phcR*. After validating sequences, recombinant plasmids were introduced into corresponding mutants with the above tri-parental mating system, and complementary strains were confirmed by colony PCR and DNA sequencing.

RNA Preparation and qRT-PCR Analysis

R. solanacearum strains were grown to an OD_{600} of about 1.0 and total RNA were extracted by using a RNeasy Mini Kit (QIAGEN, Hilden, Germany). Contaminated genomic DNA was digested with DNaseI (Takara, Dalian, China) and confirmed by PCR using the primer pair for 16S rDNA. The cDNA was synthesized using the FastQuant cDNA first chain synthesis Kit (TIANGEN BIOTECH CO. LTD, Beijing, China) according to the manufacturer's instructions. qRT-PCR was performed with Super Real PreMix Color SYBR Green (TIANGEN BIOTECH CO. LTD, Beijing, China) on Light Cycler480II (Applied Biosystems by Roche, Germany). The absolute value of $-\Delta\Delta Ct = -(\Delta Ct1 - \Delta Ct2)$ were calculated as described in the $2^{-\Delta\Delta Ct}$ method (Livak and Schmittgen, 2001). Each assay was repeated from RNA isolation for three independent experiments with at least three replications per trial. All the Ct data of *rmy* genes, *phcA* and *phcR* in EP1 and related mutants have been listed in **Supplementary Tables S2**-**S4**.

MALDI-TOF and LC-MS Analysis

In this study, chemical compounds in bacterial extracts were detected and quantified with matrix-assisted laser desorption ionization time-of-flight spectrometry (MALDI-TOF). Ralsolamycin could be detected at the peak of *m*/*z* 1291.7142 with the MALDI-TOF and its content could be quantified by calculating the peak areas. For the MALDI-TOF analysis, a tiny number of colonies were scratched off from agar plates and transferred to a MALDI MSP 384 anchor-chip plate, followed by application of 2 µl universal matrix (1:1 mixture of 2, 5-dihydroxybenzoic acid and α-cyano-4-hydroxy-cinnamic acid). The plate was dried at 37°C for 1 h and analyzed using a Bruker Autoflex MALDI-TOF mass spectrometer (Bruker Daltonics, Billerica, MA, United States) in positive reflectron mode, with a mass range of 500–3,500 Da. Each assay was repeated for three independent experiments with four replications per trial. The natural log of data obtained was analyzed using FlexAnalysis 3.0 software (Bruker Daltonics, Billerica, MA, United States).

Electrophoretic Mobility Shift Assay

Binding of proteins onto DNA probes was determined with the electrophoretic mobility shift assay (EMSA) as described previously (Lv et al., 2018). PhcA and PhcR proteins were purified from the pET-32a based protein expression system in *E. coli* BL21 (DE3) and subjected for the binding reaction with biotinylated DNA probes using the LightShift Chemiluminescent EMSA Kit following the manufacturer's protocol (Thermo, United States). Promoter regions of the *rmyA* operon (*rmyA* upstream region of ATG site about 375 bp) and *impH* gene (424 bp of its coding sequence) were PCR amplified and labeled by biotin using the Biotin 3′ End DNA Labeling Kit (Thermo, United States). Note that promoter DNA of *impH* gene, which encodes one of the type VI secretion proteins in *R. solanacearum*, was selected as a system control. The gels were stained by SYBR GOLD dye and subjected to screening on a phosphor screen (LAS600, GE Healthcare).

Interaction Between *Ralstonia solanacearum* and *Fusarium oxysporum* f. *cubense* FOC4

R. solanacearum strains and *F. oxysporum* f. *cubense* FOC4 were dropped onto same PDA agar plate and incubated at 28°C for about eight days. When two kinds of colonies interweaved each other, the FOC4 mycelia surrounded the interaction zones at about 1 cm were harvested and subjected for chlamydospore counting under microscope (Li et al., 2017).

Statistical Analysis

Each assay was repeated for three independent experiments with at least three replications per trial. Mean values of all experiments were averaged with SD (error bars) and statistical significance was assessed using a paired two-tailed Student's *t*-test by using the GraphPad Prism 6.0 software (GraphPad, La Jolla, CA). $^{*}p \leq 0.05$; $^{**}0.001 < p < 0.01$; $^{***}\ p \leq 0.001$.

RESULTS

PhcA Positively Regulates Ralsolamycin Production and Expression of *rmy* Genes

PhcA is a QS-dependent transcriptional regulator that is activated through the phc-QS signals and in turn regulates many QS-dependent phenotypes, including ralfuranones, exopolysaccharide (EPS), and virulence (Brumbley et al., 1993; Kai et al., 2014). We previously reported that ralsolamycin biosynthesis was modulated by the phc-QS system in *R. solanacearum* EP1 (Li et al., 2017). We therefore assessed whether PhcA regulates ralsolamycin biosynthesis in EP1. Ralsolamycin production was quantified with the MADLI-TOF analysis at the peak of *m*/*z* 1,291. Deletion of *phcA* substantially decreased ralsolamycin production, which was approximately 20% of that in EP1, and complementation of *phcA* fully restored the decreased ralsolamycin production (**Figure 1**). The *rmy* operon of *rmyA* and *rmyB* genes are responsible for ralsolamycin biosynthesis in *R. solanacearum* (Spraker et al., 2016). We further assessed whether *phcA* deletion decreased expression levels of *rmyA* and *rmyB* genes. Total RNA was isolated from the wild-type strain EP1, *phcA* mutants, and its complementary strains, and mRNA levels of *rmyA* and *rmyB* were quantified with the qRT-PCR. Deletion of *phcA* substantially decreased mRNA levels of *rmyA* and *rmyB*, and complementary *phcA* fully restored the decreased transcriptional levels (**Figure 2**). These results confirmed that PhcA positively regulates expression of *rmy* genes and in turn modulates ralsolamycin biosynthesis.

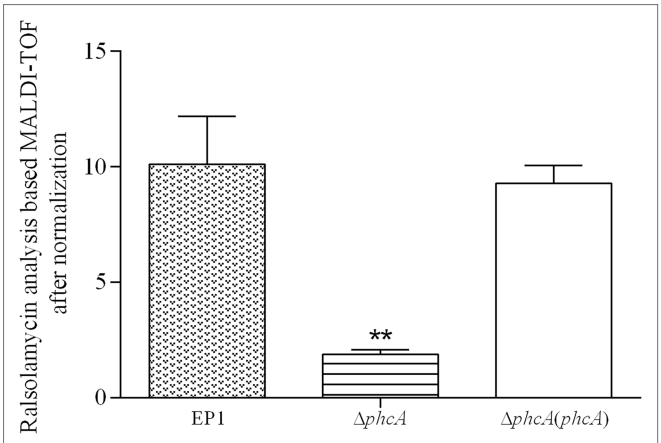

FIGURE 1 | MALDI-TOF analysis of ralsolamycin (*m*/*z* 1291.7142) production in wide type strain EP1, *phcA* deletion mutant (Δ*phcA*), and complementary strain Δ*phcA*(*phcA*). Briefly, a tiny number of colonies were scratched off from agar plates and transferred to a MALDI MSP 384 anchor-chip plate, followed by application of 2 μl universal matrix. The plate was dried at 37°C for 1 h and analyzed using a Bruker Autoflex MALDI-TOF mass spectrometer in positive reflectron mode, with a mass range of 500–3,500 Da. Each assay was repeated for three independent experiments with four replications per trial. The natural log of data obtained were analyzed using FlexAnalysis 3.0 software. Mean values of all experiments were averaged with SD (error bars) and statistical significance was assessed using a paired two-tailed Student's *t*-test by using the GraphPad Prism 6.0 software. ** means $0.001 < p \leq 0.05$.

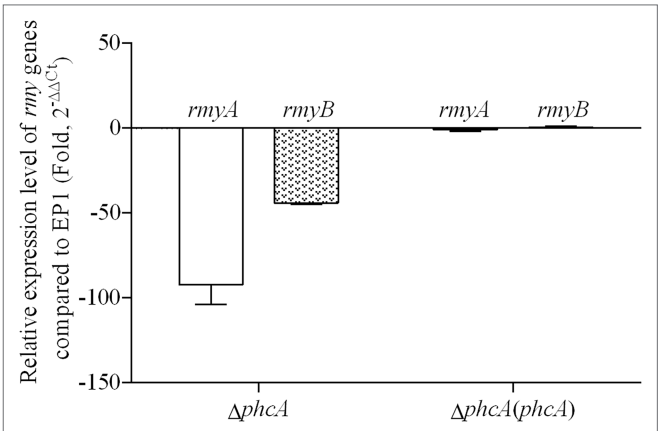

FIGURE 2 | qRT-PCR analysis of *rmyA* and *rmyB* in wide type strain EP1, *phcA* deletion mutant (Δ*phcA*), and complementary strain Δ*phcA*(*phcA*) ($OD_{600} = 1.0$). The results were calculated as $2^{-\Delta\Delta Ct}$, $-\Delta\Delta Ct = -(\Delta Ct_{mutant} - \Delta Ct_{wt})$. Three biological repeats (independent cultures) and three technical repeats were done to calculate and compare the values. Mean values of all experiments were averaged with SD (error bars) by using the GraphPad Prism 6.0 software.

PhcR Negatively Regulates Ralsolamycin Production and Expression of *rmy* Genes

The *phc* operon consists of *phcB*, *phcS,* and *phcR*, which encode the phc-QS system. The *phcB* is responsible for biosynthesis of phc-QS signals 3-OH PAME or 3-OH MAME (Flavier et al., 1997; Kai et al., 2015). The sensor histidine kinase PhcS can sense these QS signals and activate the phc-QS system *via* PhcR (Clough et al., 1997). We previously demonstrated that PhcB is involved in positive regulation on *rmy* expression and ralsolamycin production (Li et al., 2017). We thus assessed whether PhcR regulates ralsolamycin biosynthesis in EP1. Differently from that in *phcA* mutants, deletion of *phcR* significantly enhanced mRNA levels of *rmyA* and *rmyB*, and complementary *phcR* substantially decreased enhanced mRNA levels of *rmyA* and *rmyB* in *phcA* mutants (**Figure 3**), indicating that PhcR plays a negative role on *rmy* expression. Ralsolamycin production was quantified in *phcR* mutants with the MADLI-TOF analysis, and *phcR* deletion significantly increased the ralsolamycin production, which was about three folders of that in the wild-type strain (**Figure 4**). Complementary *phcA* substantially decreased the increased ralsolamycin production to levels of the wild-type strain (**Figure 4**). These results confirmed that PhcR negatively regulates expression of *rmy* genes and in turn modulates ralsolamycin biosynthesis.

PhcA and PhcR Affect Chlamydospore Formation of FOC4 in an Opposite Way

The ralsolamycin produced by *R. solanacearum* plays important roles on interaction between *R. solanacearum* and fungi that can induce chlamydospore formation in fungi (Spraker et al.,

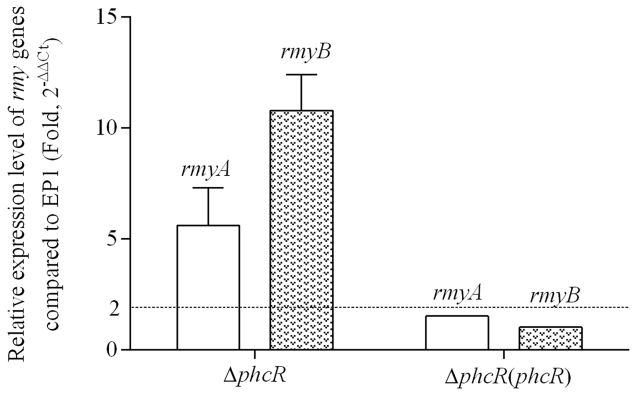

FIGURE 3 | qRT-PCR analysis of *rmyA* and *rmyB* in wide type strain EP1, *phcR* deletion mutant (Δ*phcR*) and complementary strain Δ*phcR* (*phcR;* $OD_{600} = 1.0$). The results were calculated as $2^{-\Delta\Delta Ct}$, $-\Delta\Delta Ct = -(\Delta Ct_{mutant} - \Delta Ct_{wt})$. Three biological repeats (independent cultures) and three technical repeats were done to calculate and compare the values, mean values of all experiments were averaged with SD (error bars) by using the GraphPad Prism 6.0 software.

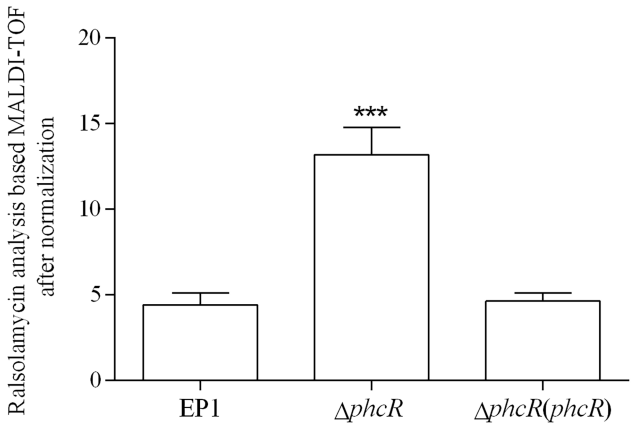

FIGURE 4 | matrix-assisted laser desorption ionization time-of-flight spectrometry analysis of ralsolamycin production in wide type strain EP1, *phcR* deletion mutant (Δ*phcR*) and complementary strain Δ*phcR* (*phcR*). Presence of the peak in the bacterial extract showing the accurate mass of ralsolamycin (*m/z* 1291.7142) was identified, and the corresponding peak areas of wild type and mutants were compared and calculated. Each assay was repeated for three independent experiments with four replications per trial. The natural log data obtained were analyzed using FlexAnalysis 3.0 software. Mean values of all experiments were averaged with SD (error bars) and statistical significance was assessed using a paired two-tailed Student's *t*-test by using the GraphPad Prism 6.0 software. *** means $p \leq 0.001$.

2016). PhcA and PhcR play opposite regulatory roles on ralsolamycin production. We further assessed whether PhcA and PhcR affect interaction between *R. solanacearum* and *F. oxysporum* f. *cubense* FOC4. *R. solanacearum* and FOC4 were dropped onto same PDA plate, and then development of mycelia and chlamydospore production of FOC4 was evaluated (Li et al., 2017). The wild-type strain EP1 and *phcR* mutants could form clear inhibition haloes against FOC4 mycelia at four to 10 days post-inoculation (dpi), while *phcA* mutants failed to form inhibition haloes even till to 10 dpi and FOC4 mycelia could cover colonies of *phcA* mutants (**Figure 5A**). Complementary *phcA* or *phcR* restored corresponding changed phenotypes in each mutant, respectively (**Figure 5A**). The chlamydospores formation of FOC4 in the interaction zones were counted under microscope at 10 dpi. Chlamydospore quantities were substantially impaired when co-cultured with *phcA* mutants, which was approximately 15% of the control with EP1 and complementation of *phcA* substantially restored the impaired chlamydospore formation (**Figure 5B**). On the contrary, chlamydospore formation was slightly increased when co-cultured with *phcR* mutants ($p = 0.035168$; **Figure 5B**). These results confirmed that PhcA and PhcR affect chlamydospore formation of FOC4 in an opposite way.

Both PhcA and PhcR Can Bind Directly to Promoter DNA of *rmy* Operon Genes

Given the fact that PhcA and PhcR regulated expression of *rmyA* an *rmyB* genes, we evaluated whether these two transcriptional regulators could bind directly to promoter DNA of *rmy* operon genes with the EMSA. Genes *rmyA* and *rmyB* are located together and form a *rmy* operon to work together for ralsolamycin biosynthesis. The spacer between *rmyA* and its prior gene is 831 bp, a sequence of 375-bp located before the ATG site of *rmyA* was amplified as the promoter DNA, which empirically harbors the native promote and indeed worked as promote to fulfill above complementation assays. In addition, 424 bp of *impH* coding region, one of the T6SS genes, was PCR amplified as a system control to assess whether PhcA and PhcR proteins could bind to any the promoter DNA. PhcA and PhcR proteins failed to bind to the coding sequence of *impH*, but bound to the promoter DNA of *rmy* operon (**Figure 6**), indicating that both PhcA and PhcR can bind directly to promoter DNA of *rmy* operon genes.

PhcA and PhcR Was Independent of Either Transcriptional Expression

We further evaluated whether PhcA or PhcR could regulate transcriptional expression of the other gene with the qRT-PCR. Total RNA was isolated and mRNA levels of *phcA* and *phcR* were quantified with the qRT-PCR. Deletion of *phcA* did not alter mRNA levels of *phcR*, and vice versa (**Figure 7**), indicating that PhcA and PhcR were independent of transcriptional expression of the other gene.

DISCUSSION

R. solanacearum can survive in various environmental conditions, partially due to its ability to produce a variety of SMs which aids to its ability in competition with other living organisms (Delaspre et al., 2007; Schneider et al., 2009; Kreutzer et al., 2011). Among them, ralsolamycin plays an important role in interspecific interaction and cross-kingdom communications, which has profound impacts on the ability of *R. solanacearum* to colonize and survive in complex biotic environments. Our

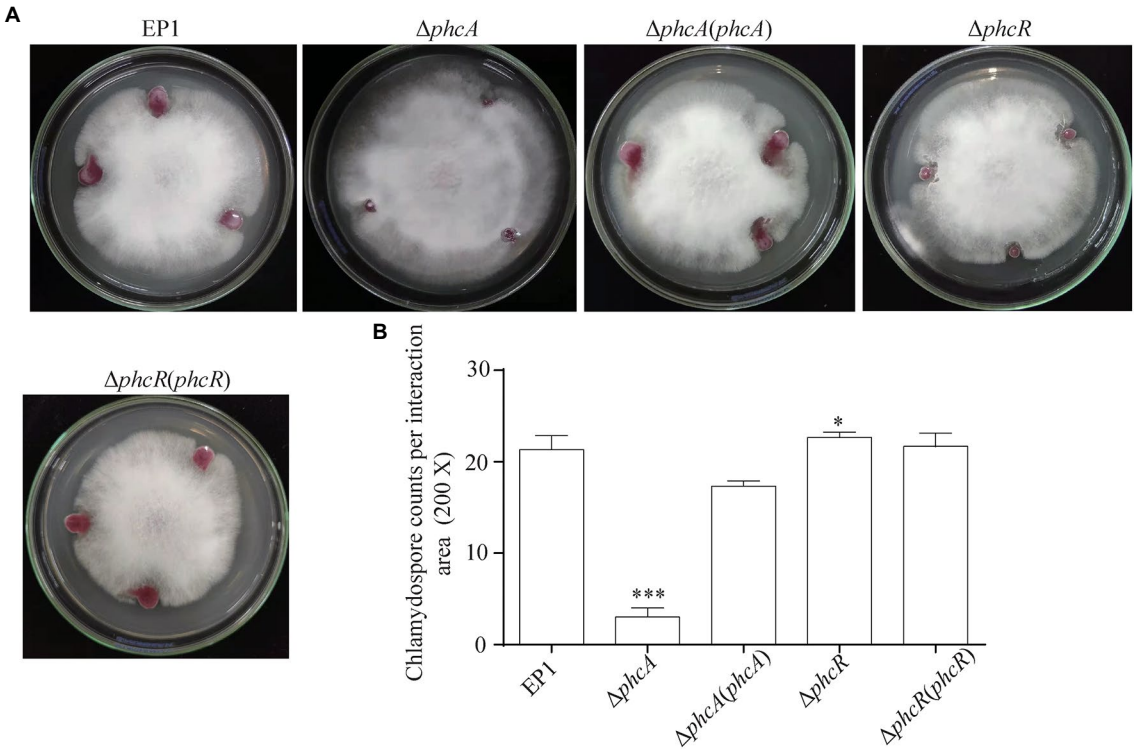

FIGURE 5 | Coculture experiment between *R. solanacearum* and FOC4 **(A)** and the chlamydospores counts (200 magnification times) in their interaction zones **(B)**. Δ*phcA* and Δ*phcR* refers to deletion of *phcA* and *phcR* from wide type strain EP1, respectively; Δ*phcA* (*phcA*) and Δ*phcR* (*phcR*) refers to the complementary strain of Δ*phcA* and Δ*phcR*, respectively. Each assay was repeated for three independent experiments with at least three replications per trial. Mean values of all experiments were averaged with SD (error bars) and statistical significance was assessed using a paired two-tailed Student's *t*-test by using the GraphPad Prism 6.0 software. * means $p < 0.05$, *** means $p < 0.001$.

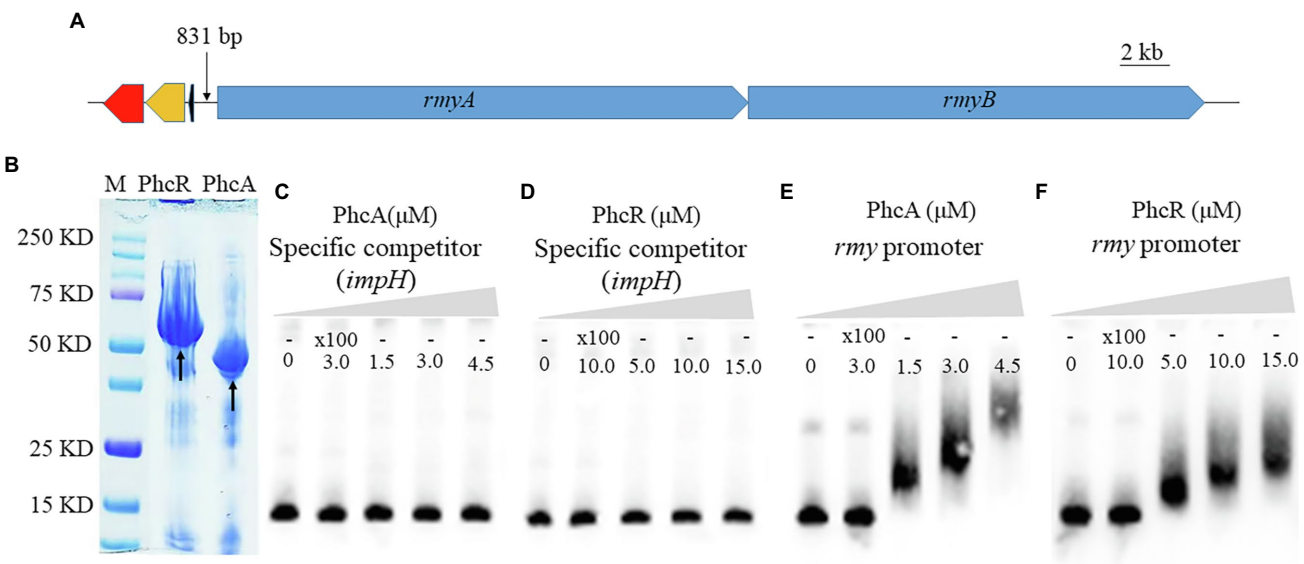

FIGURE 6 | Schematic presentation of *rmyA* and *rmyB* operons **(A)**, proteins (PhcA and PhcR) expression **(B)** and promoter binding detection by electrophoretic mobility shift assay **(E,F)**. 30 fmol of labeled DNA fragments corresponding to the promoter region of *rmyA* gene was incubation with 100 nm and 200 nm PhcA/R, respectively, using 100-fold unlabeled corresponding DNA fragments as the specific competitor. The coding sequence of *impH* (424 bp), which encodes a type VI secretion protein and is not bound by PhcA and PhcR, was used as a negative control in the EMSA experiment **(C,D)**. The positions of free DNA and of protein–DNA complexes were shown.

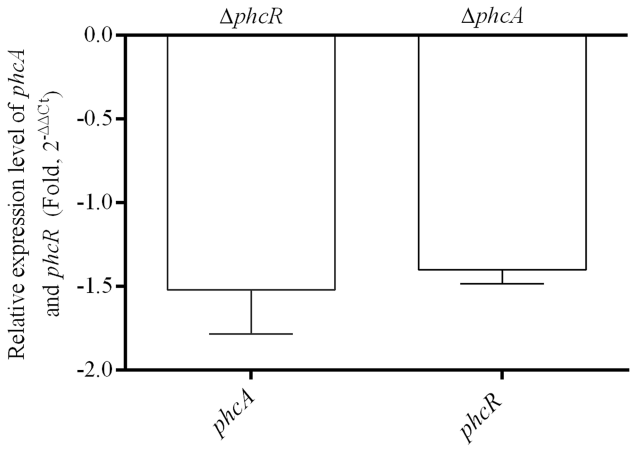

FIGURE 7 | qRT-PCR analysis of *phcA* and *phcR* gene expression in Δ*phcR* and Δ*phcA* mutant of strain EP1, respectively (OD_{600} = 1.0). The Δ*phcA* and Δ*phcR* refers to deletion of *phcA* and *phcR* from wide type strain EP1, respectively. The results were calculated as $2^{-\Delta\Delta Ct}$, $-\Delta\Delta Ct = -(\Delta Ct_{mutant} - \Delta Ct_{wt})$. Three biological repeats (independent cultures) and three technical repeats were done to calculate and compare the values, mean values of all experiments were averaged with SD (error bars) by using the GraphPad Prism 6.0 software.

previous study reported that ralsolamycin biosynthesis was decreased distinctly when the phc-QS signal coding gene *phcB* was deleted, it is not yet clear what other regulators are involved in modulation of ralsolamycin biosynthesis. In this study, we provided multiple lines of evidences to demonstrated that both PhcA and PhcR can regulate the expression of *rmy* genes and affect the ralsolamycin biosynthesis, as well as the interaction between *R. solanacearum* and the fungal pathogen FOC4. Interestingly, our results confirmed that PhcA is the positive regulator modulating the ralsolamycin biosynthesis, while PhcR is the negative regulator. Understanding the behavior and mechanisms involved in the interaction among environmental microbe that share ecological niches is fundamental in the study of microbial population adaptation and evolution (Martin et al., 2017). Thus, it is important to decipher how the ralsolamycin biosynthesis is regulated. In this work, we provide new insights into the positive and negative regulation mechanisms that conducted by PhcA and PhcR, respectively.

Extensive experiments have confirmed that PhcA is a global transcriptional regulator (Brumbley et al., 1993), which works as a molecular switch can directly or indirectly regulate the production of numerous virulence determinants, such as EPS, cell wall-degrading enzymes, chemotaxis system, and secretion systems (Denny and Ryel, 1991; Arlat et al., 1992; Huang et al., 1995; Yao and Allen, 2006; Genin and Denny, 2012). Consequently, benefited from those virulence determinants, *R. solanacearum* owns excellent ability to infect numerous plant hosts. In addition to the role in regulation of virulence, PhcA also regulates traits which help *R. solanacearum* to survive in nutrient-poor environments and to grow rapidly during early pathogenesis (Khokhani et al., 2017). Consistent with the above findings, our results showed that the *rmyA* and *rmyB* genes, which encode production of ralsolamycin, were positively regulated by PhcA. The findings that ralsolamycin production was significantly decreased in the PhcA null mutant validates that PhcA involves in the regulation of ralsolamycin biosynthesis (**Figure 1**), which was further confirmed by qRT-PCR analysis (**Figure 2**). According to the results of ralsolamycin production, deletion of *phcA* almost abolished the ralsolamycin production, it is reasonable to think that PhcA is the key regulator involved in modulation of ralsolamycin biosynthesis. In the absence of *phcA* shows a dry clone and loss the ability that inducing chlamydospore formation of fungi, as well as the competitive ability with fungi (**Figure 5**). Thus, our results identify a new regulator associated with the modulation of ralsolamycin production and the bacterium–fungus interaction and add a new list to the regulatory spectrum of the master regulator PhcA in *R. solanacearum*.

Our previous results showed that ralsolamycin production is under the regulation of the phc-QS system. Deletion of the QS signal encoding gene *phcB* caused a significant reduction in ralsolamycin production (Li et al., 2017). Toward this end, we explored the role of PhcR, which is believed to response to the phc-QS signal, in the modulation of ralsolamycin production. Results showed that the *rmy* gene expression and production of ralsolamycin were increased when the *phcR* was deleted (**Figures 3, 4**). Meanwhile, the ability to induce chlamydospore formation was also increased (**Figure 5**). Thus, PhcR showed an opposite regulatory pattern with PhcB and PhcA. Similar results were obtained with transcriptome analysis that PhcR is partially involved in the regulation of QS-dependent genes in *R. solanacearum* strain OE1-1, such as the genes *norB*, *lecM*, and *xpsR* were modulated by PhcR positively, and some flagellin biosynthesis-related genes and chemotaxis-related genes were negatively PhcR-dependent genes (Takemura et al., 2021). In addition, the similar regulatory patterns were also found in modulation of the biosynthesis of ralfuranone, which is a SM and virulence factor produced by *R. solanacearum* (Wackler et al., 2011), for the ralfuranone coding gene expression and biosynthesis is regulated positively by PhcA and negatively by PhcR (Takemura et al., 2021). However, it is not yet clear whether PhcA and PhcR regulate the ralfuranone gene expression in a direct way similar to what we have found for the regulation of ralsolamycin. Moreover, in the present study, we uncovered that the gene expression level of *phcA* and *phcR* were not affected when the *phcR* and *phcA* gene was deleted, respectively (**Figure 7**), PhcR and PhcA were thus all found to be independently involved in the control of biosynthesis of ralsolamycin. In conclusion, it is intriguing that both PhcR and PhcA bind to same promoter but display opposite regulation on the *rmy* genes expression. However, how the two regulators targeting the same promoter have opposite regulatory effects and how this regulation is carried out in a wild-type context is still needed to be studied and resolved in the further research.

Nevertheless, these findings suggest that PhcA and PhcR play key roles in modulation of SM production. A recent study showed that plant sugars d-galactose and d-glucose could activate the production of ralfuranones in *R. solanacearum* (Ishikawa et al., 2019), suggesting that both QS and cross-kingdom chemical

communications play a role in regulation of the SM. Further investigation of the response of PhcA and PhcR to various signal inputs would aid to understand their detailed regulatory mechanisms.

In conclusion, this study demonstrated that the ralsolamycin production is modulated by the global regulator PhcA and the phc-QS signal response protein PhcR directly at the transcriptional level with PhcA acting as the positive regulator and PhcR being the negative regulator. The opposite roles of PhcA and PhcR suggest complex and sophisticated regulatory networks that have been evolved in *R. solanacearum* to modulate the production of ralsolamycin and other SMs, which collectively contribute to the bacterial virulence and competitive ability against other living organisms. Taken together, this work extends our understanding on the intricacies of the regulatory networks of the phc-QS system in modulation of secondary metabolism, and highlights the possibility of cross-talking between QS and other signaling mechanisms in regulation of ralsolamycin biosynthesis in *R. solanacearum*.

DATA AVAILABILITY STATEMENT

The original contributions presented in the study are included in the article/**Supplementary Material**, further inquiries can be directed to the corresponding authors.

AUTHOR CONTRIBUTIONS

PL and L-HZ designed the experiments and wrote the paper. LZ performed the MALDI-TOF analysis. XC performed the qRT-PCR analysis. ML performed the EMSA experiment. L-HZ revised the manuscript. All authors contributed to the article and approved the submitted version.

FUNDING

This work was supported by Hainan Province key R&D Project (ZDYF2020080), the National Natural Science Foundation of China (nos. 31901846 and 31901843), Guangdong Forestry Science and Technology Innovation Project (2018KJCX009 and 2020KJCX009), and the specific research fund of the Innovation Platform for Academicians of Hainan Province (YSPTZX202130).

SUPPLEMENTARY MATERIAL

The Supplementary Material for this article can be found online at: https://www.frontiersin.org/articles/10.3389/fpls.2022.903310/full#supplementary-material

Supplementary Table S1 | Primers used in this study.

Supplementary Table S2 | Ct data of *rmyA* and *rmyB* genes in wide type strain EP1, *phcA* deletion mutant (*ΔphcA*) and complementary strain *ΔphcA(phcA)*, cell density is OD_{600} = 1.0.

Supplementary Table S3 | Ct data of *rmyA* and *rmyB* genes in EP1, *phcR* deletion mutant (*ΔphcR*) and complementary strain *ΔphcA(phcA)*, cell density is OD_{600} = 1.0.

Supplementary Table S4 | Ct data of *phcA* and *phcR* gene in EP1 and mutants (OD_{600}=1.0), cell density is OD_{600} = 1.0.

REFERENCES

Alvarez, B., Biosca, E. G., and Lopez, M. M. (2010). On the life of *Ralstonia solanacearum*, a destructive bacterial plant pathogen. *Technol. Educ. Top Appl. Microbiol. Microb. Biotechnol.* 1, 267–279.

Arlat, M., Gough, C. L., Zischek, C., Barberis, P. A., Trigalet, A., and Boucher, C. A. (1992). Transcriptional organization and expression of the large hrp gene cluster of *pseudomonas solanacearum*. *MPMI* 5, 187–193. doi: 10.1094/MPMI-5-187

Baldeweg, F., Kage, H., Schieferdecker, S., Allen, C., Hoffmeister, D., and Nett, M. (2017). Structure of ralsolamycin, the interkingdom morphogen from the crop plant pathogen *Ralstonia solanacearum*. *Org. Lett.* 19, 4868–4871. doi: 10.1021/acs.orglett.7b02329

Bhatt, G., and Denny, T. P. (2004). *Ralstonia solanacearum* iron scavenging by the siderophore staphyloferrin B is controlled by PhcA, the global virulence regulator. *J. Bacteriol.* 186, 7896–7904. doi: 10.1128/JB.186.23.7896-7904.2004

Brumbley, S. M., Carney, B. F., and Denny, T. P. (1993). Phenotype conversion in *pseudomonas solanacearum* due to spontaneous inactivation of PhcA, a putative LysR transcriptional regulator. *J. Bacteriol.* 175, 5477–5487. doi: 10.1128/jb.175.17.5477-5487.1993

Clough, S. J., Lee, K. E., Schell, M. A., and Denny, T. P. (1997). A two-component system in *Ralstonia* (*pseudomonas*) *solanacearum* modulates production of PhcA-regulated virulence factors in response to 3-hydroxypalmitic acid methyl ester. *J. Bacteriol.* 179, 3639–3648. doi: 10.1128/jb.179.11.3639-3648.1997

Delaspre, F., Nieto Penalver, C. G., Saurel, O., Kiefer, P., Gras, E., Milon, A., et al. (2007). The *Ralstonia solanacearum* pathogenicity regulator HrpB induces 3-hydroxy-oxindole synthesis. *Proc. Natl. Acad. Sci. U. S. A.* 104, 15870–15875. doi: 10.1073/pnas.0700782104

Denny, T. P., and Ryel, B. S. (1991). Genetic evidence that extracellular polysaccharide is a virulence factor of *pseudomonas solanacearum*. *Mol. Plant-Microbe Interact.* 4, 198–206. doi: 10.1094/MPMI-4-198

Ditta, G., Stanfield, S., Corbin, D., and Helinski, D. R. (1980). Broad host range DNA cloning system for gram-negative bacteria: construction of a gene bank of *rhizobium meliloti*. *Proc. Natl. Acad. Sci. U. S. A.* 77, 7347–7351. doi: 10.1073/pnas.77.12.7347

Flavier, A. B., Clough, S. J., Schell, M. A., and Denny, T. P. (1997). Identification of 3-hydroxypalmitic acid methyl ester as a novel autoregulator controlling virulence in *Ralstonia solanacearum*. *Mol. Microbiol.* 26, 251–259. doi: 10.1046/j.1365-2958.1997.5661945.x

Fuqua, W. C., Winans, S. C., and Greenberg, E. P. (1994). Quorum sensing in bacteria: The LuxR-LuxI family of cell density-responsive transcriptional regulators. *J. Bacteriol.* 176, 269–275. doi: 10.1128/jb.176.2.269-275.1994

Genin, S., and Denny, T. P. (2012). Pathogenomics of the *Ralstonia solanacearum* species complex. *Annu. Rev. Phytopathol.* 50, 67–89. doi: 10.1146/annurev-phyto-081211-173000

Hayward, A. C. (1991). Biology and epidemiology of bacterial wilt caused by *pseudomonas solanacearum*. *Annu. Rev. Phytopathol.* 29, 65–87. doi: 10.1146/annurev.py.29.090191.000433

Hendrick, C. A., and Sequeira, L. (1984). Lipopolysaccharide-defective mutants of the wilt pathogen *pseudomonas solanacearum*. *Appl. Environ. Microbiol.* 48, 94–101. doi: 10.1128/aem.48.1.94-101.1984

Huang, J., Carney, B. F., Denny, T. P., Weissinger, A. K., and Schell, M. A. (1995). A complex network regulates expression of eps and other virulence genes of *pseudomonas solanacearum*. *J. Bacteriol.* 177, 1259–1267. doi: 10.1128/jb.177.5.1259-1267.1995

Ishikawa, Y., Murai, Y., Sakata, M., Mori, S., Matsuo, S., Senuma, W., et al. (2019). Activation of ralfuranone/ralstonin production by plant sugars functions

in the virulence of *Ralstonia solanacearum*. *ACS Chem. Biol.* 14, 1546–1555. doi: 10.1021/acschembio.9b00301

Kai, K., Ohnishi, H., Mori, Y., Kiba, A., Ohnishi, K., and Hikichi, Y. (2014). Involvement of ralfuranone production in the virulence of *Ralstonia solanacearum* OE1-1. *Chembiochem* 15, 2590–2597. doi: 10.1002/cbic.201402404

Kai, K., Ohnishi, H., Shimatani, M., Ishikawa, S., Mori, Y., Kiba, A., et al. (2015). Methyl 3-hydroxymyristate, a diffusible signal mediating *phc* quorum sensing in *Ralstonia solanacearum*. *Chembiochem* 16, 2309–2318. doi: 10.1002/cbic.201500456

Khokhani, D., Lowe-Power, T. M., Tran, T. M., and Allen, C. (2017). A single regulator mediates strategic switching between attachment_spread and growth_virulence in the plant pathogen *Ralstonia solanacearum*. *mBio* 8, e00895–e00817. doi: 10.1128/mBio.00895-17

Kovach, M. E., Elzer, P. H., Steven Hill, D., Robertson, G. T., Farris, M. A., Roop Ii, R. M., et al. (1995). Four new derivatives of the broad-host-range cloning vector pBBR1MCS, carrying different antibiotic-resistance cassettes. *Gene* 166, 175–176. doi: 10.1016/0378-1119(95)00584-1

Kreutzer, M. F., Kage, H., Gebhardt, P., Wackler, B., Saluz, H. P., Hoffmeister, D., et al. (2011). Biosynthesis of a complex yersiniabactin-like natural product via the mic locus in phytopathogen *Ralstonia solanacearum*. *Appl. Environ. Microbiol.* 77, 6117–6124. doi: 10.1128/AEM.05198-11

Li, P., Wang, D. C., Yan, J. L., Zhou, J. N., Yue, D. Y., Jiang, Z. D., et al. (2016). Genomic analysis of phylotype I strain EP1 reveals substantial divergence from other strains in the *Ralstonia solanacearum* species complex. *Front. Microbiol.* 7:1719. doi: 10.3389/fmicb.2016.01719

Li, M. H., Xie, X. L., Lin, X. F., Shi, J. X., Ding, Z. J., Ling, J. F., et al. (2014). Functional characterization of the gene FoOCH1 encoding a putative alpha-1,6-mannosyltransferase in *Fusarium oxysporum* f. sp. *cubense*. *Fungal Genet. Biol.* 65, 1–13.

Li, P., Yin, W., Yan, J., Chen, Y., Fu, S., Song, S., et al. (2017). Modulation of inter-kingdom communication by PhcBSR quorum sensing system in *Ralstonia solanacearum* phylotype I strain GMI1000. *Front. Microbiol.* 8:01172. doi: 10.3389/fmicb.2017.01172

Livak, K. J., and Schmittgen, T. D. (2001). Analysis of relative gene expression data using real-time quantitative PCR and the 2-ΔΔCT method. *Methods* 25, 402–408. doi: 10.1006/meth.2001.1262

Lv, M. F., Chen, Y. F., Liao, L. S., Liang, Z. B., Shi, Z. R., Tang, Y. X., et al. (2018). Fis is a global regulator critical for modulation of virulence factor production and pathogenicity of *Dickeya zeae*. *Sci. Rep.* 8:341. doi: 10.1038/s41598-017-18578-2

Martin, M., Dragos, A., Holscher, T., Maroti, G., Balint, B., Westermann, M., et al. (2017). De novo evolved interference competition promotes the spread of biofilm defectors. *Nat. Commun.* 8:15127. doi: 10.1038/ncomms15127

Murai, Y., Mori, S., Konno, H., Hikichi, Y., and Kai, K. (2017). Ralstonins A and B, lipopeptides with chlamydospore-inducing and phytotoxic activities from the plant pathogen *Ralstonia solanacearum*. *Org. Lett.* 19, 4175–4178. doi: 10.1021/acs.orglett.7b01685

Perrier, A., Barlet, X., Peyraud, R., Rengel, D., Guidot, A., and Genin, S. (2018). Comparative transcriptomic studies identify specific expression patterns of virulence factors under the control of the master regulator PhcA in the *Ralstonia solanacearum* species complex. *Microb. Pathog.* 116, 273–278. doi: 10.1016/j.micpath.2018.01.028

Salanoubat, M., Genin, S., Artiguenave, F., Gouzy, J., Mangenot, S., Arlat, M., et al. (2002). Genome sequence of the plant pathogen *Ralstonia solanacearum*. *Nature* 415, 497–502. doi: 10.1038/415497a

Schäfer, A., Tauch, A., Jäger, W., Kalinowski, J., Thierbach, C., Pühler, A., et al. (1994). Small mobilizable multi-purpose cloning vectors derived from the *Escherichia coli* plasmids pK18 and pK19: selection of defined deletions in the chromosome of *Corynebacterium glutamicum*. *Gene* 145, 69–73.

Schneider, P., Jacobs, J. M., Neres, J., Aldrich, C. C., Allen, C., Nett, M., et al. (2009). The global virulence regulators VsrAD and PhcA control secondary metabolism in the plant pathogen *Ralstonia solanacearum*. *Chembiochem* 10, 2730–2732. doi: 10.1002/cbic.200900510

Senuma, W., Takemura, C., Hayashi, K., Ishikawa, S., Kiba, A., Ohnishi, K., et al. (2020). The putative sensor histidine kinase PhcK is required for the full expression of phcA encoding the global transcriptional regulator to drive the quorum-sensing circuit of *Ralstonia solanacearum* strain OE1-1. *Mol. Plant Pathol.* 21, 1591–1605. doi: 10.1111/mpp.12998

Spraker, J. E., Sanchez, L. M., Lowe, T. M., Dorrestein, P. C., and Keller, N. P. (2016). *Ralstonia solanacearum* lipopeptide induces chlamydospore development in fungi and facilitates bacterial entry into fungal tissues. *ISME J.* 10, 2317–2330. doi: 10.1038/ismej.2016.32

Spraker, J. E., Wiemann, P., Baccile, J. A., Venkatesh, N., Schumacher, J., Schroeder, F. C., et al. (2018). Conserved responses in a war of small molecules between a plant-pathogenic bacterium and fungi. *mBio* 9, e00820–e00818. doi: 10.1128/mBio.00820-18

Takemura, C., Senuma, W., Hayashi, K., Minami, A., Terazawa, Y., Kaneoka, C., et al. (2021). PhcQ mainly contributes to the regulation of quorum sensing-dependent genes, in which PhcR is partially involved, in *Ralstonia pseudosolanacearum* strain OE1-1. *Mol. Plant Pathol.* 22, 1538–1552. doi: 10.1111/mpp.13124

Wackler, B., Schneider, P., Jacobs, J. M., Pauly, J., Allen, C., Nett, M., et al. (2011). Ralfuranone biosynthesis in *Ralstonia solanacearum* suggests functional divergence in the quinone synthetase family of enzymes. *Chem. Biol.* 18, 354–360. doi: 10.1016/j.chembiol.2011.01.010

Yao, J., and Allen, C. (2006). Chemotaxis is required for virulence and competitive fitness of the bacterial wilt pathogen *Ralstonia solanacearum*. *J. Bacteriol.* 188, 3697–3708. doi: 10.1128/JB.188.10.3697-3708.2006

Conflict of Interest: The authors declare that the research was conducted in the absence of any commercial or financial relationships that could be construed as a potential conflict of interest.

Publisher's Note: All claims expressed in this article are solely those of the authors and do not necessarily represent those of their affiliated organizations, or those of the publisher, the editors and the reviewers. Any product that may be evaluated in this article, or claim that may be made by its manufacturer, is not guaranteed or endorsed by the publisher.

frontiers | Frontiers in Plant Science

REVIEW
published: 22 June 2022
doi: 10.3389/fpls.2022.922119

The Role of Hydroxycinnamic Acid Amide Pathway in Plant Immunity

Saifei Liu[1], Jincheng Jiang[2], Zihui Ma[1], Muye Xiao[1], Lan Yang[3], Binnian Tian[1], Yang Yu[1], Chaowei Bi[1], Anfei Fang[1] and Yuheng Yang[1]**

[1]College of Plant Protection, Southwest University, Chongqing, China, [2]Committee on Agriculture and Rural Affairs of Yongchuan District, Chongqing, China, [3]Analytical and Testing Center, Southwest University, Chongqing, China

The compounds involved in the hydroxycinnamic acid amide (HCAA) pathway are an important class of metabolites in plants. Extensive studies have reported that a variety of plant hydroxycinnamamides exhibit pivotal roles in plant–pathogen interactions, such as *p*-coumaroylagmatine and ferulic acid. The aim of this review is to discuss the emerging findings on the functions of hydroxycinnamic acid amides (HCAAs) accumulation associated with plant defenses against plant pathologies, antimicrobial activity of HCAAs, and the mechanism of HCAAs involved in plant immune responses (such as reactive oxygen species (ROS), cell wall response, plant defense hormones, and stomatal immunity). However, these advances have also revealed the complexity of HCAAs participation in plant defense reactions, and many mysteries remain to be revealed. This review provides an overview of the mechanistic and conceptual insights obtained so far and highlights areas for future exploration of phytochemical defense metabolites.

Keywords: hydroxycinnamic acid amides, plant immunity, antimicrobial activities, cell wall, *p*-coumaric acid, ferulic acid

OPEN ACCESS

Edited by:
Bourlaye Fofana, Agriculture and Agri-Food Canada (AAFC), Canada

Reviewed by:
Rajesh Chandra Misra, John Innes Center, United Kingdom
Wei Zhang, Jiangsu University, China

****Correspondence:***
Yuheng Yang
yyh023@swu.edu.cn
orcid.org/0000-0003-2613-7091
Anfei Fang
fanganfei@swu.edu.cn
orcid.org/0000-0001-9809-6255

Specialty section:
This article was submitted to Crop and Product Physiology, a section of the journal Frontiers in Plant Science

Received: *17 April 2022*
Accepted: *07 June 2022*
Published: *22 June 2022*

Citation:
Liu S, Jiang J, Ma Z, Xiao M, Yang L, Tian B, Yu Y, Bi C, Fang A and Yang Y (2022) The Role of Hydroxycinnamic Acid Amide Pathway in Plant Immunity. Front. Plant Sci. 13:922119. doi: 10.3389/fpls.2022.922119

INTRODUCTION

Plants are well stocked with chemical defense compounds that function in protection against herbivores and pathogens (Gershenzon and Ullah, 2022). The global metabolic reprogramming is a common event in plant innate immunity. A large number of compounds are involved in the process of plant disease resistance. For example, pathogens stimulated the phenylpropanoid pathway (PPP) and lead to the synthesis of secondary metabolites. These compounds can provide protection against biotic and abiotic stresses in plants. Hydroxycinnamic acid amides (HCAAs) are widely distributed in plant secondary metabolites and are often referred to as one of the major phenylpropanoid metabolites (Herrmann, 1989).

Hydroxycinnamic acid amides have been described throughout the plant kingdom and accumulated in various organs, sometimes at high concentrations, especially in injured tissues (Bassard et al., 2010). HCAAs are purported to function in several growth and developmental processes, including tuberization, flower development, pollen wall formation, pollen health effects sexual differentiation, senescence, cell division, and stress responses (Facchini et al., 2002; Luo et al., 2009). HCAAs pathway is an important offshoot pathway of the PPP (Kim et al., 2021). The PPP accessory pathway involves the biosynthesis of HCAAs, which are polymers made from hydroxycinnamic acids (HCAs) and polyamines (PA; Facchini et al., 2002). HCAAs are synthesized through the condensation of various biogenic amines with

HCAs *via* BAHD acyltransferase (Li et al., 2018). HCAAs are thought to be the final accumulation product of PA and aromatic amine metabolism, or as a form of cellular storage to regulate the metabolic pool of the two parent components (Bassard et al., 2010). HCAAs may be secreted into the apoplast space under the action of multidrug and toxin extrusion (MATE) transporters (Zeiss et al., 2021). The HCAAs tend to be present in the insoluble-bound form, as they were covalently bound to the arabinoxylans of the cell wall hemicellulose. Through dimerization and trimerization, the insoluble-bound HCAAs form an extensive network of cross-linkages that deter insect herbivory in stored grain, prevent pathogen penetration during the growing season, and impart plant tolerance to drought (Butts-Wilmsmeyer et al., 2020). Moreover, many studies have demonstrated that the biosynthesis of HCAAs and their subsequent polymerization in the plant cell play a vital role in response to pathogenic infections (Muroi et al., 2009). For instance, 24 h post *Pseudomonas syringae* pv. *tomato* (*Pst*) DC3000 and *Erwinia carotovora carotovora* infections, the content of HCAAs in *Arabidopsis thaliana* leaves was significantly increased (Macoy et al., 2022). Tyramine-derived HCAAs overproduced in plants may interfere with colonization of *Ralstonia solanacearum* by becoming incorporated into the blood vascular and perivascular cell walls, thereby restricting the movement of pathogens within the plant (Kashyap et al., 2022). Pretreatment with *p*-Coumaric acid results in an accumulation of hydroxycinnamic acid in soluble and cell wall-bound form, which protects against infection by *Xanthomonas campestris* pv. *Campestris* (Islam et al., 2018). With the development of high-throughput metabolomics technology, numerous studies have demonstrated that HCAAs are involved in plant responses to biotic stress. By using a comparative metabolomic approach, researchers identified defense-related biosynthetic pathways as affected in susceptible and resistant wheat cultivars, and HCAAs were found accumulated within 4–8 days of fungal infection in wheat (Seybold et al., 2020). In addition, experiments have demonstrated that HCAAs have antimicrobial activity (Kyselka et al., 2018).

In current knowledge, HCAAs are still a key class of secondary metabolites that were defined as biomarkers to measure plant resistance. In a previous review, the important role of HCAAs in plant defense against pathogens was also described in detail (Macoy et al., 2015). On this basis, we summarized the latest research on HCAs/HCAAs in recent years. This review paper aims to give a thorough understanding on the functions of HCAs/HCAAs accumulation during defense responses, antimicrobial activity of HCAs/HCAAs, mechanism of HCAs/HCAAs involved in plant immune responses, and the regulation of HCAAs biosynthesis in plants.

THE BIOSYNTHESIS OF HCAAs FROM THE PHENYLPROPANOID PATHWAY

Flavonoids, hydroxycinnamic acid esters, hydroxycinnamic acid amides, the precursors of lignin, lignans, and tannins are end products of PPP (Gray et al., 2012). HCAAs are the products of an important branch of the PPP, in which phenylalanine ammonia lyase (PAL), cinnamic acid 4-hydroxylase (C4H), and 4-coumaric acid-CoA ligase (4CL) are all involved (Gray et al., 2012; **Figure 1**). The PPP begins with the deamination of phenylalanine by PAL to trans-cinnamic acid or cinnamate, and then catalyzed by 4CL (Hahlbrock and Scheel, 1989). PAL directs metabolic flow from the shikimate pathway to the various branches of PPP by catalyzing phenylalanine to trans-cinnamic acid (Zhang and Liu, 2015). The second reaction is catalyzed by C4H known to catalyze the hydroxylation of trans-cinnamic acid to *p*-coumaric acid (4-hydroxycinnamic acid; Schilmiller et al., 2009). The 4CL catalyzes the third step of PPP, forms *p*-coumaroyl-CoA in an ATP-dependent manner (Gui et al., 2011). The condensation of CoA derivative of *p*-coumaric acid (thioester *p*-coumaroyl-CoA) and the amine tyramine is catalyzed by hydroxycinnamoyl-CoA:tyramineN-hydroxycinnamoyltransferase (THT), and putrescine hydroxycinnamoyl transferase (PHT) further activates the synthesis of *p*-coumaroyltyramine and *p*-coumaroylputrescine (Pushpa et al., 2014). Agmatine coumaryl transferase (ACT) catalyzes the last step in the biosynthesis of the HCAAs, where *p*-coumaroylagmatine and feruloylagmatine are generated (Muroi et al., 2009). With the action of tyrosine decarboxylase (TyDC), tyrosine is further converted into tyramine (Von Roepenack-Lahaye et al., 2003).

HCAAs PATHWAY IS INVOLVED IN PLANT DISEASE RESISTANCE

Hydroxycinnamic acid amides are conjugated PA, such as cinnamic acid, coumaric acid, caffeic acid, ferulic acid, and sinapic acid that form acylated PA (El-Seedi et al., 2012). This kind of secondary metabolites have been reported to protect plant cell against pathogen invasion by strengthening cell walls or act as antimicrobial agents directly (Campos et al., 2014). Meanwhile, the accumulation of HCAAs in plants contributes to the induction of plant hypersensitive responses (HR) in response to pathogen challenge (Walters, 2003). Since the first demonstration of *p*-coumaroyl- and feruloyl-2-hydroxyputrescine accumulation in leaves of rust-infected wheat (Samborski and Rohringer, 1970). Multiple studies have shown that HCAAs accumulated due to infection by pathogens. In wheat, untargeted metabolomic and proteomic analyses indicated that HCAAs were the major factor influencing *Fusarium graminearum* resistance (Gunnaiah et al., 2012). HCAAs synthesized as a result of *F. graminearum* infection were observed regardless of susceptibility, but occurred at different times after infection (Whitney et al., 2022). In the incompatible interaction between wheat and stripe rust, the HCAAs pathway was strongly induced, and *p*-coumaroyl agmatine was significantly increased (Liu et al., 2022). Significantly increased levels of sinapic acid and ferulic acid in wheat after infestation with stripe rust (Atta et al., 2020). In maize, HCAAs pathway was strongly induced after *Puccinia sorghi* infection (Kim et al., 2021). In cocoa-*phytophthora* spp., leaves of the tolerant genotype were found to accumulate dramatically higher levels of clovamide and

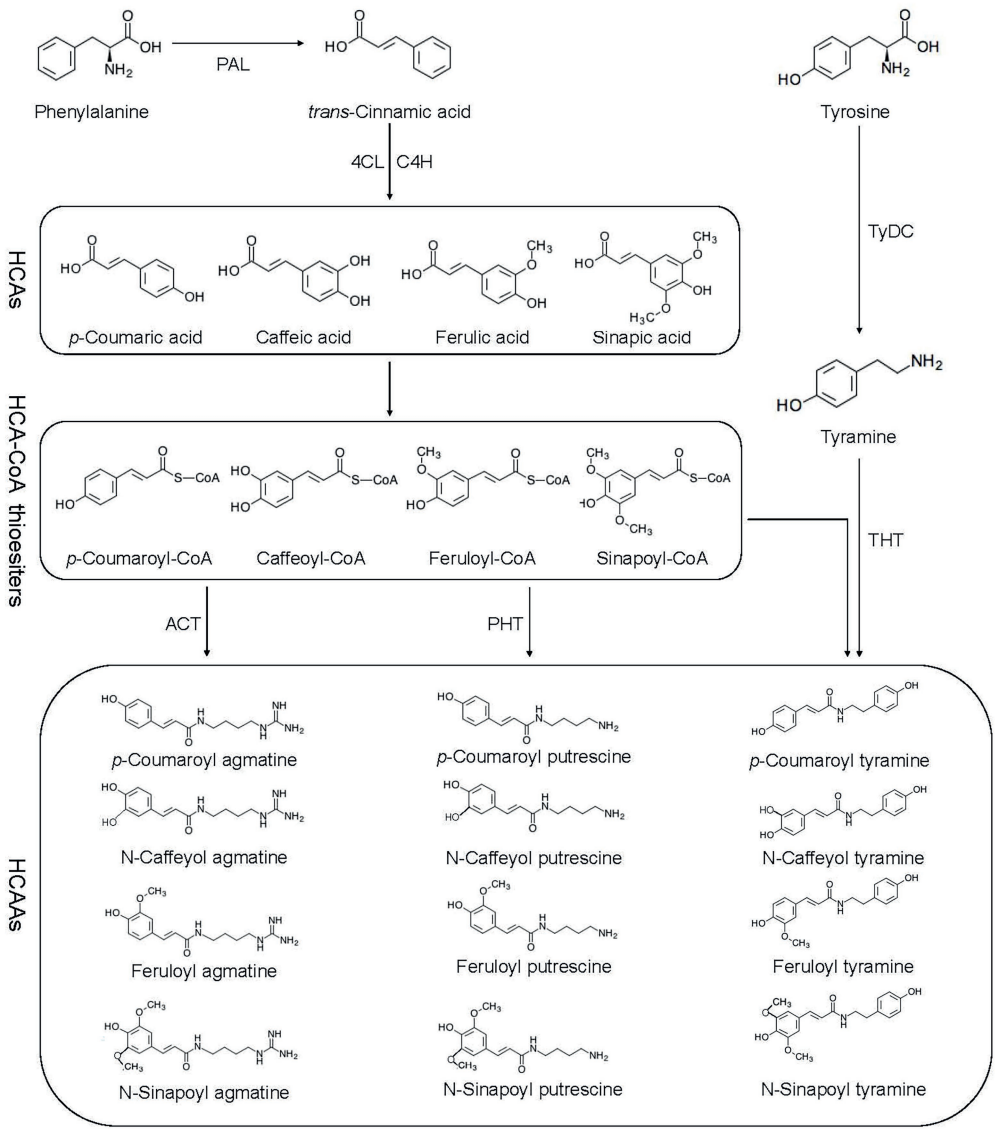

FIGURE 1 | Biosynthetic pathway of HCAAs. HCAAs, hydroxycinnamic acid amides; HCAs, hydroxycinnamic acids; PAL, phenyl alanine ammonia lyase; C4H, cinnamate 4-hydroxylase; 4-CL, 4-coumarate: CoA ligase; ACT, agmatine coumaryl transferase; TyDC, tyrosine decarboxylase; THT, tyramine hydroxycinnamoyl transferase; and PHT, putrescence hydroxycinnamoyl transferase.

several other HCAAs compared to the susceptible (Knollenberg et al., 2020). In potato, studies have suggested that HCAAs can be used as biomarker metabolites for late blight resistance and black dot (Pushpa et al., 2014). In banana, nematode-resistant varieties have very marked increases in *p*-coumaric, ferulic, and sinapic acid content compared to susceptible varieties (Vaganan et al., 2014). HCAAs were significantly increased in *Arabidopsis* after *Sclerotinia sclerotiorum* infection (Chen et al., 2021). Furthermore, plant growth-promoting rhizobacteria was shown to affect root HCAAs content in rice (Valette et al., 2020). The above reports fully demonstrated that the accumulation of HCAAs improves the resistance of plants to pathogens. Plant endogenous HCAs/HCAAs defend against infection by pathogens, and exogenous application of HCAs/HCAAs to resist the infection of pathogens by stimulating the production of plant immune responses (**Figure 2**).

Transcriptional Responses of HCAAs Pathway Related Genes in Plant Defense

Rapid transcriptional reprogramming of genes encoding biosynthetic enzymes for protective secondary metabolites (such as HCAAs) is one of the mechanisms of plant defense responses. During *Alternaria brassicicola* infection, the expression of *AtACTs* (*ATT3G03480*, *AT5G01210*, *AT5G39050*, *and AT5G61160*) in *Arabidopsis* was rapidly induced (Muroi et al., 2009). In resistant varieties of potato, relative expression of *StTyDC*, *StTHT*, *St4CL*, and *StPHT* was induced by *Solanum tuberosum* infection

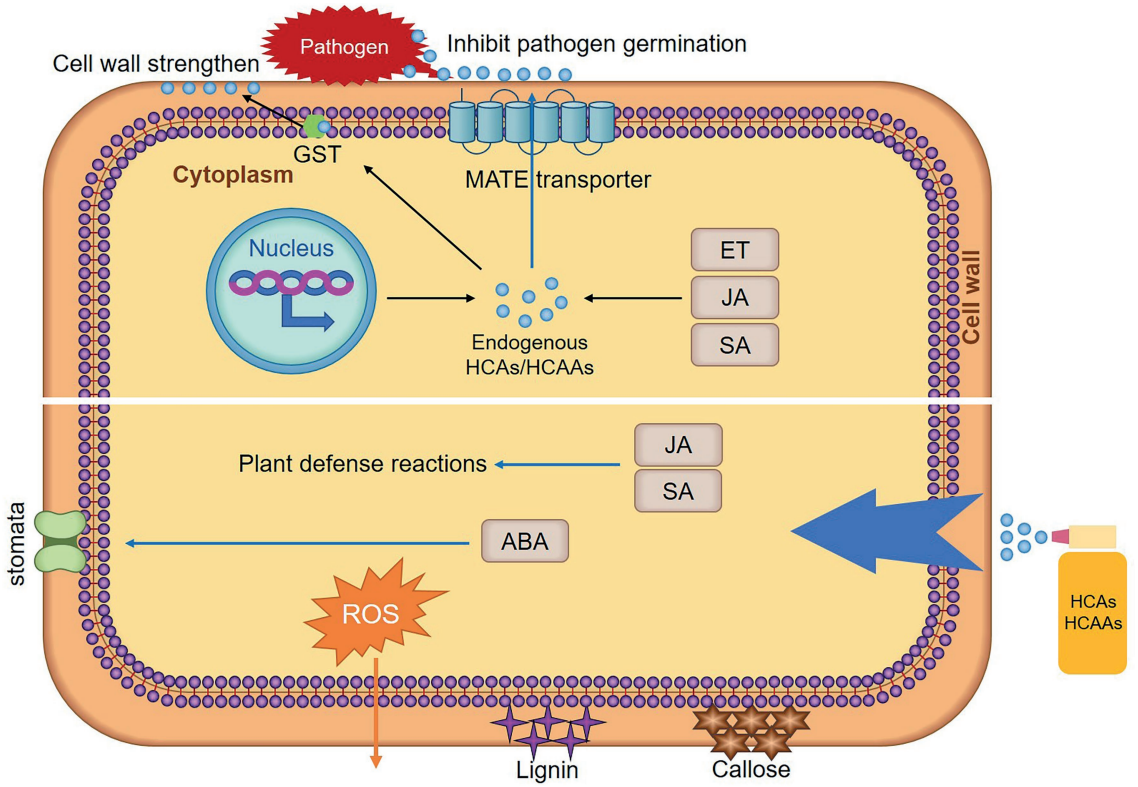

FIGURE 2 | Mechanisms of HCAs/HCAAs enhancing plant resistance. After pathogen infection, elevation of plant endogenous hormones stimulates the production of HCAs/HCAAs. Rapid transcriptional reprogramming of genes encoding biosynthetic enzymes for HCAAs is one of the mechanisms of plant defense responses. Glutathione S-transferase (GST) may act as an amide carrier protein for HCAAs translocation to the plasma membrane, then deposited on the cell wall. Under the action of MATE, HCAAs move to the leaf surface, thereby inhibiting spore germination. Exogenous HCAs/HCAAs treatment stimulated a series of plant immune responses, such as plant hormones (JA, SA, and ABA) levels are elevated, SA and JA stimulate resistance responses in plants. HCAs/HCAAs stimulated stomata opening and closing, which may be achieved by controlling the content of ABA. HCAs/HCAAs also stimulate the production of lignin, callose, and ROS. The stimulation of these immune responses increases the resistance of plants to pathogens.

(Pushpa et al., 2014). The transcriptional alterations of key genes affect HCAAs levels in pathogen-infected plants, leading to changes in plant defense responses. The *Atact* mutant was susceptible to infection by *A. brassicicola* and *p*-coumaroylagmatine content of *Atact* mutant was reduced (Muroi et al., 2009). Likewise, wheat *TaACT*-knockout plants exhibited that *p*-coumaroylagmatine content was significantly reduced and susceptibility to *F. graminearum* was increased (Kage et al., 2017a). In contrast, overexpression of *SlTHT* in tomato increased the accumulation of tyramine and octopamine derivatives and enhanced tomato resistance against *P. syringae* (Campos et al., 2014). Additionally, ectopic expression of *AtACT* increased the resistance of torenia plants to *Botrytis cinerea* (Muroi et al., 2013). In potato, simultaneous overexpression of *AtACT* and *Arabidopsis DETOOXIFICATION18* (*AtDTX18*) genes gave plants the ability to synthesize *p*-coumarin and export it to the leaf surface, so that increased the accumulation of HCAAs on plant leaf surface and reduced spore germination of *Phytophthora infestans* (Dobritzsch et al., 2016; **Figure 2**). Stable expression of N-caffeoyl-L-3,4-dihydroxyphenylalanine hydroxycinnamoyl transferase (HDT) in alfalfa resulted in foliar accumulation of p-coumaroyl- and feruloyl-L-Tyr and transient expression of HDT in *Nicotiana benthamiana* resulted in the production of caffeoyl-L-Tyr (Sullivan and Knollenberg, 2021). The above studies showed that key genes in the HCAAs pathway play a role in plant disease resistance by controlling the synthesis of HCAAs. Key genes in the HCAAs pathway have great potential for application in disease resistance breeding.

Antimicrobial Activity of HCAs/HCAAs

Hydroxycinnamic acids and their derivatives also show antimicrobial activity. As shown in **Table 1**, the inhibitory effect of HCAs/HCAAs on microorganisms involves at least two processes: direct antimicrobial activity and strengthening of secondary cell walls (Roumani et al., 2021). Natural compounds, such as caffeic acid, syringic acid, *p*-coumaric acid, and ferulic acid have strong inhibitory effect on pathogenic fungi (Hassan et al., 2021). HCAAs inhibits the growth of *Aspergillus niger*, *F. aureus*, and *Penicillium verruciformis* (Kyselka et al., 2018). Trans-cinnamic acid, ferulic acid, and *p*-coumaric acid can inhibit the growth of *Colletotrichum acutatum* (Roy et al., 2018). Ferulic acid, the most abundant HCAs in the plant kingdom, is an ester linked to arabinose (Mathew and Abraham, 2006). Ferulic acid inhibited the growth

TABLE 1 | Antimicrobial activity of various hydroxycinnamic acids (HCAs)/hydroxycinnamic acid amides (HCAAs) and their mechanisms.

Host	Pathogen	Disease name	Compounds	Mechanism	References
Solanum lycopersicum	*Pseudomonas syringae*	Bacterial speck of tomato	*p*-coumaroyltyramine, feruloyltyramine	SA, PR gene	Campos et al., 2014
Torenia fournieri Linden	*Botrytis cinerea*	_	*p*-coumaroylagmatine	Inhibit the germination and development of conidial germ tubes	Muroi et al., 2013
Solanum tuberosum	*Phytophthora infestans*	Potato late blight disease	*p*-coumaroylagmatine	Inhibit spore germination	Dobritzsch et al., 2016
Fragaria x ananassa Duch	*Colletotrichum acutatum*	Strawberry anthracnose	trans-cinnamic acid, ferulic acid, and p-coumaric acid	Inhibit fungal growth	Roy et al., 2018
Citrullus lanatus	*Fusarium oxysporum* f. sp. *niveum*	Watermelon fusarium wilt	Ferulic acid	Inhibit spore germination	Wu et al., 2010
Diospyros kaki L. var	*Alternaria*	black spot disease	Ferulic, and rho-coumaric acids	Reduce growth	Yadav et al., 2021
_	*Escherichia coli*, *Pseudomonas aeruginosa, Staphylococcus aureus*, and *Listeria monocytogenes*		Ferulic acids	Changes in membrane properties	Borges et al., 2013
Malus pumila Mill.	*Botrytis cinerea*	Apple gray mold	Caffeic acid	Activation of different branches of the phenylpropanoid metabolism pathway	Zhang et al., 2020
Nicotiana tobaccum	*Ralstonia solanacearum*	Tobacco bacterial wilt	Caffeic acid	Damaged the membrane structure and promote the accumulation of lignin	Li et al., 2021b
_	*Fusarium oxysporum* f. sp. *niveum*		Sinapic acid	Inhibit the growth and conidial germination	Wu et al., 2009
C. lanatus	*Fusarium oxysporum* f. sp. *niveum*	Watermelon fusarium wilt	*p*-coumaric acid	Increased β-1,3-glucanase activity	Ren et al., 2016
_	*Verticillium dahliae*		*p*-coumaric acid	_	Baidez et al., 2007
_	*S. aureus*, *Streptococcus pneumoniae Bacillus subtilis*, *E. coli*, *Shigella dysenteriae* and *Salmonella typhimurium*		*p*-coumaric acid	Disrupted cell membranes and binding to bacterial genomic DNA	Lou et al., 2012
_	*Botrytis cinerea*	_	*p*-coumaric acid	Retard the germination of conidia	Morales et al., 2017
_	*Dickeya dadantii*	_	*p*-coumaric acid	Manipulating the expression of the T3SS	Li et al., 2009
S. tuberosum	*P. infestans*	Potato late blight disease	N-4-coumaroyl- and N-Feruloyltyramine	Cell wall reinforcement	Schmidt et al., 1998
Arabidopsis thaliana	*Erwinia carotovora carotovora*		Coumaroyl tyramine and coumaroyl tryptamine	Increased the induction of callose deposition	Macoy et al., 2022
Brassica napus	*Xanthomonas campestris* pv. *campestris*		*p*-coumaric acid	Primed the JA-signaling-mediated induction of phenylpropanoid biosynthesis	Islam et al., 2019

of *F. oxysporum* at high concentrations and affected the activity of hydrolases associated with pathogenicity (Wu et al., 2010). Ferulic and rho-coumaric acids reduced *Alternaria* growth *in vivo* and black spot in stored fruits (Yadav et al., 2021). Ferulic acid leads to irreversible changes in cell membrane properties (charge, intracellular and extracellular permeability, and physicochemical properties) through hydrophobicity changes, reduction in negative surface charges, and local rupture of the cell membrane or pore formation, resulting in the leakage of essential intracellular components of pathogenic bacteria (Borges et al., 2013). Exogenous caffeic acid enhanced apple resistance to *B. cinerea* (Zhang et al., 2020). Caffeic acid can damage the membrane structure of *R. solanacearum* cells, resulting in thinning of the cell membrane and irregular intracellular voids. In addition, caffeic acid can also inhibit biofilm formation by inhibiting the expression of *lecM* and *epsE* genes. Exogenous caffeic acid also effectively activated peroxidase and PAL (Li et al., 2021b). Sinapic acid was chemically studied as a cinnamic acid derivative and also inhibited the growth, conidial germination of *F. oxysporum* and reduced the activity of pathogenic enzymes at high doses (Wu et al., 2009). *In vivo* test, changes in the levels of phenolic compounds in infected plants and their antifungal activity for against *Verticillium dahliae* strongly suggested that *p*-coumaric acid was involved in the natural defense or resistance mechanisms of plant (Baidez et al., 2007). Exogenously *p*-coumaric acid increased chitinase activity in leaves and β-1,3-glucanase activity in roots, thereby enhancing watermelon resistance to *F. oxysporum* (Ren et al., 2016). The antibacterial mechanism of *p*-coumaric acid includes two aspects: disrupts bacterial cell membranes and binds to bacterial genomic DNA to inhibit cell function, ultimately leading to cell death

(Lou et al., 2012). However, *p*-coumaric acid did not affect the integrity of the cell wall and plasma membrane of *B. cinerea*, nor did it produce oxidative stress (Morales et al., 2017). HCAAs have been shown against bacteria by regulating the expression of the type III secretion system (T3SS). For example, *p*-coumaric acid inhibited the expression of T3SS gene of the plant pathogen *Dickeya dadantii* (Li et al., 2009). However, ferulic acid may mimic host conditions, thereby activating T3SS expression (Zhang et al., 2017). High concentrations of HCAs can inhibit the growth of *R. solanacearum* in the medium. However, *R. solanacearum* can protect itself from HCAs toxicity by degrading low concentrations of HCA as the sole carbon source (Lowe et al., 2015). Chitosan treatment of wheat increased the content of *p*-coumaric acid, ferulic acid, and sinapic acid in leaves and enhanced resistance to *F. graminearum* (Reddy et al., 1999). The above studies have proved that HCAs can inhibit the growth of pathogenic fungi and spore germination, and HCAs can inhibit pathogenic bacteria by damaging the cell membrane and DNA of pathogenic bacteria. Pathogens have also evolved mechanisms to reduce the harm of HCAs/HCAAs, and this aspect will also be the focus of research.

HCAAs Strengthen Plant Cell Walls

Polyamines and aromatic amines bind to HCAs phenolic resins, leading to the formation of HCAAs-molecules that have the ability to confer antimicrobial activity and potentially deposit into cell walls (Zeiss et al., 2021). HCAAs in the cytosol may be transported to different vesicles and then to the plasma membrane, allowing the deposition of HCAAs into the cell wall. Glutathione S-transferase (GST) may act as an amide carrier protein for HCAAs translocation to the plasma membrane (Macoy et al., 2015; **Figure 2**). HCAAs constitute the polyaromatic domains of suberin. These polymers increased the thickness of the cell wall, limit the spread of pathogens, and act as antifungals. As a plant defense response, HCAAs require the deposition of amide conjugates in the cell wall to reduce fungal pathogen penetration and infection (Graca, 2010). HCAAs, such as coumaroylputrescine, feruloylputrescine, cinnamoyltyramine, cis-*p*-coumaroylagmatine, feruloylagmatine, coumaroylserotonin, caffeoylserotonin, and feruloylserotonin were proven to increase cell wall thickness in wheat to resist *F. graminearum* (Gunnaiah et al., 2012). Deposition of HCAAs was thought to form a barrier against pathogens by reducing cell wall digestibility (Facchini et al., 2002). In date palm-resistant cultivars, cell wall-bound phenols (*p*-coumaric acid, ferulic acid, and sinapic acid) were found to strongly reduce hyphal growth and cell wall-degrading enzymes of *F. oxysporum* production (El Modafar and El Boustani, 2001). Fungal infection of potato cell cultures and leaves has been reported to trigger the incorporation of *p*-coumaroyltyramide and feruloyltyramide into the cell wall (Schmidt et al., 1998). The two main HCAs, *p*-coumaric acid and ferulic acid, were present in the complex cell walls of oat husks and act as crosslinkers between lignin and polysaccharides or between polysaccharides. Therefore, they inhibited the biodegradation of the cell wall by microorganisms (Yu et al., 2004). HCAAs prevent the infection of pathogens by strengthen the cell wall and reduced the degradation of the cell wall.

HCAs/HCAAs Regulate Lignin and Callose Deposition

Lignin and callose deposition are two late immune responses that enhance plant cell walls. Lignin is mainly deposited in the secondary cell walls of plants (Zhao and Dixon, 2011). During pathogens infection, lignin is deposited and acts as a physical barrier to limit the spread of pathogens (Lee et al., 2019). Lignin deposition around pathogen penetration sites was found to increase potato resistance to *P. infestans* (Sorokan et al., 2018). Tobacco with lower total lignin content shows tobacco susceptibility to blackleg and bacterial wilt (Ma et al., 2018). HCAAs also affect lignin content (**Figure 2**). For example, exogenously applied *p*-coumaric acid, caffeic acid, ferulic acid, and sinapic acid were directed into the PPP, resulting in the overproduction of lignin and its main monomers (Lima et al., 2013). The perception of pathogen or microbe-associated molecular pattern molecules by plants triggers a basal defense response analogous to animal innate immunity and was defined partly by the deposition of the glucan polymer callose at the cell wall at the site of pathogen contact (Clay et al., 2009). Deposition of callose prevented powdery mildew hyphae from entering epidermal cells (Ellinger et al., 2014). Exogenous application of coumaroyltyramine and coumaroyltryptamine increased the induction of callose deposition (Macoy et al., 2022). These findings also indicate that HCAAs can resist the infection of pathogens by enhancing the synthesis of lignin and the deposition of callose.

HCAs/HCAAs Contribute to Stomatal Immunity

Stomatal is a dynamic and captivating system that opens or closes in response to external and internal cues. As part of the innate immune system, stomatal closure can limit bacterial invasion and act as a barrier against bacterial infection. Upon perception of pathogens, plants can rapidly close their stomates to restrict pathogen entry into internal tissue (Melotto et al., 2006). Stomates of silenced *NbGCN4* and *AtGCN4* were open during pathogen infection, leading to compromised disease resistance in both host and nonhost (Kaundal et al., 2017). Arabidopsis *bzip59* mutant was partially impaired in stomatal closure induced by *Pst* DC3000 and was more susceptible to *Pst* DC3000 infection (Song et al., 2022). The application of exogenous compounds also affected the opening and closing of stomatal, such as HCAAs, with sinapic acid leading to considerable closure, while ferulic acid stimulated wider openings (Plumbe and Willmer, 1986; **Figure 2**). However, recent studies have shown that low concentrations of ferulic acid significantly inhibited stomatal opening, stomatal opening rate, stomatal length and width (Fu et al., 2019). This may be due to the different concentrations of ferulic acid, resulting in different results on stomates. Plant endogenous abscisic acid (ABA) level was increased after ferulic acid treatment (Holappa and

Blum, 1991), and may regulated the opening and closing of stomatal by regulating the biosynthesis of ABA.

Role of HCAs/HCAAs in Reactive Oxygen Species

Hydroxycinnamic acid amides are formed by conjugation of amines with HCAs. Free-form PA may play two conflicting roles in regulating cellular ROS: as a source of ROS biosynthesis and a free radical scavenging compound. The catabolism of PA leads to increased intracellular and extraplasmic H_2O_2 concentrations (Zeiss et al., 2021). Production of ROS, a hallmark of successful identification of infection and activation of plant defenses, is one of the early ways in host plant defense strategies (Qi et al., 2017). It achieves plant immunity by eliminating damaged host cells, and limits further pathogen infection. ROS may be involved in signaling in plants against pathogens, enhanced resistance to stressors, and downstream cellular defense-related genes that limit infection through pathogen death (Suzuki et al., 2011). Furthermore, ROS have also been postulated as key molecules involved in the initiation of HR. Accumulation of HCAAs also plays an important role in plant HR. However, HCAAs also have antioxidant activity (Xiang et al., 2019). Studies have shown that the oxidative burst in cucumber roots occurs under the influence of ferulic acid and *p*-coumaric acid (Politycka and Bednarski, 2004; **Figure 2**). Ferulic acid concentration can lead to accumulation of ROS, and after exogenous ferulic acid stimulation, the induced genes were involved in cell wall formation, chemical detoxification, secondary metabolism, and signal transduction (Chi et al., 2013). In addition, the accumulation of ferulic acid also enhances the antioxidant capacity of plants (Zhang et al., 2022). It remains to be seen how plants are both contradictory and unified in this regard.

Accumulation of HCAs/HCAAs Is Associated With Plant Hormones

Disease resistance mediated by plant hormones, such as SA, ethylene (ET), and JA can be induced by different exogenous signals in different plants to resist different types of pathogens, which is the basic signaling pathway of plant disease resistance (Feys and Parker, 2000). These plant hormones regulated the synthesis of compounds. JA regulated the biosynthesis of many secondary metabolites, including HCAAs (Li et al., 2021a). The accumulation of *p*-coumaroylagmatine in leaves was higher at 48 h after JA treatment, and reached the highest level at 48 h after JA/ET combined treatment. These results proved that HCAAs accumulation was induced by JA and ET signals (Li et al., 2018). It has also been demonstrated that pathogen-induced ET production was essential for synthesis of HCAAs, whereas SA was also a key signal for initiating plant defense responses, not required for this response (Zacares et al., 2007). Similarly, it has also been reported that ET produced after bacterial infection was essential for the accumulation of HCAAs, and with ET as a signal to respond to pathogen attack, SA was not involved in the accumulation of HCAAs (Lopez-Gresa et al., 2011). These studies demonstrated the role of ET and JA in intracellular signaling cascades, leading to the accumulation of secondary compounds and ultimately the induction of plant resistance. However, studies have reported accumulation of HCAAs (coumaryltyramide and feruloyltyramide) accompanied by elevated SA levels and pathogenesis-related genes induction (Campos et al., 2014). The production of ferulic acid, *p*-coumaric acid, and sinapic acid was stimulated by exogenous SA (Zhang et al., 2021). In turn, exogenous HCAs can enhance these plant hormones changes and improve plant resistance (**Figure 2**). The contents of caffeic acid, ferulic acid, and *p*-coumaric acid were increased in Methyl jasmonate and SA treated plants (Napoleao et al., 2017). JA content and expression of signaling genes (*COI1* and *PDF1.2*) were increased in *p*-coumaric acid-pretreated plants, and exogenous *p*-coumaric acid triggered JA signaling-mediated induction of phenylpropanoid biosynthesis, which elicited disease resistance to black rot disease in *Brassica napus* (Islam et al., 2019). These studies demonstrated that HCAAs and plant hormones regulate each other and participate in the process of plant disease resistance together.

REGULATION OF HCAAs BIOSYNTHESIS

The spatial, temporal and induced formation of secondary metabolites and transcripts of corresponding biosynthetic genes are tightly regulated at different levels. Transcription factors (TFs) usually regulate the transcription of multiple biosynthesis genes in a pathway, which makes them attractive tools for improvement of the production of secondary metabolites (Zhou and Memelink, 2016). TFs can integrate internal and external signals to regulate genes expression, thereby controlling the specific accumulation of secondary metabolites (Yang et al., 2012). Many studies have demonstrated that TFs can regulate HCAAs pathway.

StWRKY1 can directly bind to the promoter encoding the HCAAs biosynthesis genes. After *StWRKY1* gene silencing, the abundance of HCAAs and potato resistance to late blight were reduced (Yogendra et al., 2015). Silencing of *StNACA3* and *StMYB8* altered late blight resistance in the silenced plants by significantly increasing pathogen biomass and reducing the contents of HCAAs and flavonoid glycosides (Yogendra et al., 2017). *HvWRKY23* also exhibits the same characteristics, which in turn increases barley resistance to Fusarium head blight by regulating HCAAs synthesis (Karre et al., 2019). Induced expression of the MYB caused accumulation of ferulic acid and enhanced resistance to both fungal and bacterial pathogens in plant (Kishi-Kaboshi et al., 2018). Overexpression of the petunia MYB transcript factor, *ODORANT1* (*ODO1*), combined with expression of a feedback-insensitive *E.coli* 3-deoxy-D-arabino-heptulosonate 7-phosphate synthase (AroG), altered the levels of multiple primary and secondary metabolites in tomato fruit, boosting levels of multiple secondary metabolites, including *p*-coumaric acid and ferulic acid (Xie et al., 2016). *AtMYB99*, a putative ortholog of the petunia floral scent regulator *ODO1*, controls the exclusive production of HCAAs (Battat et al., 2019). After *TaWRKY70* gene silencing, not only confirmed the weakening of resistance to *F. graminearum*, but also reduced the expression of downstream resistance genes *TaACT*, *TaDGK*

and *TaGLI1*, as well as the content of coumaroylagmatine and coumaroylputrescine (Kage et al., 2017b). Despite of numerous studies have shown that TFs regulate HCAAs biosynthesis, more studies are needed to further elucidate the relationship between TFs and HCAAs, as well as in plant–pathogen interactions.

In addition, HCAAs were also affected by UDP-glycosyltransferases (UGTs). UGTs are responsible for the glycosylation of small molecule compounds. Glycosylation can affect the homeostasis of these substances by altering chemical activity, degradation, and/or localization of compounds (Bowles et al., 2005). Glycosylation modulates the biological activity of small molecules and often results in their inactivation. *NbUGT73A24* and *NbUGT73A25* can glycosylate N-feruloyl tyramine and ferulic acid derivatives (ethyl 4-hydroxy-3-methoxy-cinnamate, trans-ferulic acid, 4-coumaric acid, caffeic acid, N-caffeoyl O-methyltyramine, N-4-trans-coumaroyl tyramine, and N-trans-feruloyl-tyramine), overexpression of both genes in *Nicotiana benthamiana* produced clear lesions on the leaves and led to a significantly reduced content of pathogen-induced plant metabolites (Sun et al., 2019). A recent study showed that *UGT73C7* can glycosylate *p*-coumaric acid and ferulic acid glycosylation activity of *UGT73C7* resulted in the redirection of phenylpropanoid metabolic flux to the biosynthesis of HCAs and coumarins, thereby affecting the immune response of plants (Huang et al., 2021). *P*-coumaric acid and ferulic acid are precursors of various metabolites, and the glycosylation of *p*-coumaric acid and ferulic acid by *UGT73C7* significantly affects the metabolism of phenylpropanes. These evidences suggested that glycosylation can simultaneously affect the abundance of HCAs/HCAAs, thereby regulating plant disease resistance.

CHALLENGES REMAINED AND FUTURE DIRECTIONS

Metabolites of HCAAs pathway were involved in various stress responses, play an important role in plants and can also directly inhibit microorganisms (**Figure 2**). It is necessary to conduct more in-depth studies on metabolites. The information from this review focuses on the induction of plant defense responses to biotic stress by HCAAs pathway, illustrating the directly inhibition of microorganisms by HCAs/HCAAs, the defense responses induced by exogenous HCAs/HCAAs in plants, and the regulation of HCAAs biosynthesis. The study helps us to understand the possible functions of HCAAs pathway during plant–pathogen interactions. HCAs/HCAAs have the potential to be developed into plant antagonists, and will also be a hotspot. Metabolomics is emerging as a new tool for understanding plant–pathogen interactions. In the future, there will be some new insights into how HCAs/HCAAs can improve the defense response of plants. Moreover, there is a rising trend in the development and application of molecular marker assays for gene mapping and discovery in field crops and trees (Rasheed et al., 2017). Resistance genes in the HCAAs pathway and genes of regulated HCAAs biosynthesis also have great application potential in molecular breeding. Varieties with high hydroxycinnamic acid concentrations can be used to produce dietary supplements or all-natural food additives, while enhancing resistance to biotic and abiotic stresses during the growing season and during grain storage.

AUTHOR CONTRIBUTIONS

All authors listed have made a substantial, direct, and intellectual contribution to the work and approved it for publication.

FUNDING

This research was financially supported by the National Natural Science Foundation of China (32001975), and the Fundamental Research Funds for the Central Universities (SWU-KT22057).

REFERENCES

Atta, B. M., Saleem, M., Ali, H., Bilal, M., and Fayyaz, M. (2020). Application of fluorescence spectroscopy in wheat crop: early disease detection and associated molecular changes. *J. Fluoresc.* 30, 801–810. doi: 10.1007/s10895-020-02561-8

Baidez, A. G., Gomez, P., Del Rio, J. A., and Ortuno, A. (2007). Dysfunctionality of the xylem in *Olea europaea* L. plants associated with the infection process by Verticillium dahliae Kleb. Role of phenolic compounds in plant defense mechanism. *J. Agric. Food Chem.* 55, 3373–3377. doi: 10.1021/jf063166d

Bassard, J. E., Ullmann, P., Bernier, F., and Werck-Reichhart, D. (2010). Phenolamides: bridging polyamines to the phenolic metabolism. *Phytochemistry* 71, 1808–1824. doi: 10.1016/j.phytochem.2010.08.003

Battat, M., Eitan, A., Rogachev, I., Hanhineva, K., Fernie, A., Tohge, T., et al. (2019). A MYB triad controls primary and Phenylpropanoid metabolites for pollen coat patterning. *Plant Physiol.* 180, 87–108. doi: 10.1104/pp.19.00009

Borges, A., Ferreira, C., Saavedra, M. J., and Simoes, M. (2013). Antibacterial activity and mode of action of Ferulic and Gallic acids against pathogenic bacteria. *Microb. Drug Resist.* 19, 256–265. doi: 10.1089/mdr.2012.0244

Bowles, D., Isayenkova, J., Lim, E. K., and Poppenberger, B. (2005). Glycosyltransferases: managers of small molecules. *Curr. Opin. Plant Biol.* 8, 254–263. doi: 10.1016/j.pbi.2005.03.007

Butts-Wilmsmeyer, C. J., Mumm, R. H., and Bohn, M. O. (2020). Quantitative genetic analysis of Hydroxycinnamic acids in maize (*Zea mays* L.) for plant improvement and production of health-promoting compounds. *J. Agric. Food Chem.* 68, 9585–9593. doi: 10.1021/acs.jafc.0c02774

Campos, L., Lison, P., Lopez-Gresa, M. P., Rodrigo, I., Zacares, L., Conejero, V., et al. (2014). Transgenic tomato plants overexpressing Tyramine N-Hydroxycinnamoyltransferase exhibit elevated Hydroxycinnamic acid amide levels and enhanced resistance to *Pseudomonas syringae*. *Mol. Plant-Microbe Interact.* 27, 1159–1169. doi: 10.1094/MPMI-04-14-0104-R

Chen, J., Ullah, C., Vassao, D. G., Reichelt, M., Gershenzon, J., and Hammerbacher, A. (2021). Sclerotinia sclerotiorum infection triggers changes in primary and secondary metabolism in *Arabidopsis thaliana*. *Phytopathology* 111, 559–569. doi: 10.1094/PHYTO-04-20-0146-R

Chi, W. C., Chen, Y. A., Hsiung, Y. C., Fu, S. F., Chou, C. H., Trinh, N. N., et al. (2013). Autotoxicity mechanism of *Oryza sativa*: transcriptome response in rice roots exposed to ferulic acid. *BMC Genomics* 14:351. doi: 10.1186/1471-2164-14-351

Clay, N. K., Adio, A. M., Denoux, C., Jander, G., and Ausubel, F. M. (2009). Glucosinolate metabolites required for an Arabidopsis innate immune response. *Science* 323, 95–101. doi: 10.1126/science.1164627

Dobritzsch, M., Lubken, T., Eschen-Lippold, L., Gorzolka, K., Blum, E., Matern, A., et al. (2016). MATE transporter-dependent export of Hydroxycinnamic acid amides. *Plant Cell* 28, 583–596. doi: 10.1105/tpc.15.00706

El Modafar, C., and El Boustani, E. (2001). Cell wall-bound phenolic acid and lignin contents in date palm as related to its resistance to Fusarium oxysporum. *Biol. Plant.* 44, 125–130. doi: 10.1023/A:1017942927058

Ellinger, D., Glockner, A., Koch, J., Naumann, M., Sturtz, V., Schutt, K., et al. (2014). Interaction of the Arabidopsis GTPase RabA4c with its effector PMR4 results in complete penetration resistance to powdery mildew. *Plant Cell* 26, 3185–3200. doi: 10.1105/tpc.114.127779

El-Seedi, H. R., El-Said, A. M. A., Khalifa, S. A. M., Goransson, U., Bohlin, L., Borg-Karlson, A. K., et al. (2012). Biosynthesis, natural sources, dietary intake, pharmacokinetic properties, and biological activities of Hydroxycinnamic acids. *J. Agric. Food Chem.* 60, 10877–10895. doi: 10.1021/jf301807g

Facchini, P. J., Hagel, J., and Zulak, K. G. (2002). Hydroxycinnamic acid amide metabolism: physiology and biochemistry. *Canad. J. Bot.* 80, 577–589. doi: 10.1139/b02-065

Feys, B. J., and Parker, J. E. (2000). Interplay of signaling pathways in plant disease resistance. *Trends Genet.* 16, 449–455. doi: 10.1016/S0168-9525(00)02107-7

Fu, Y. H., Quan, W. X., Li, C. C., Qian, C. Y., Tang, F. H., and Chen, X. J. (2019). Allelopathic effects of phenolic acids on seedling growth and photosynthesis in Rhododendron delavayi Franch. *Photosynthetica* 57, 377–387. doi: 10.32615/ps.2019.045

Gershenzon, J., and Ullah, C. (2022). Plants protect themselves from herbivores by optimizing the distribution of chemical defenses. *Proc. Natl. Acad. Sci. U. S. A.* 119:e2120277119. doi: 10.1073/pnas.2120277119

Graca, J. (2010). Hydroxycinnamates in suberin formation. *Phytochem. Rev.* 9, 85–91. doi: 10.1007/s11101-009-9138-4

Gray, J., Caparros-Ruiz, D., and Grotewold, E. (2012). Grass phenylpropanoids: regulate before using! *Plant Sci.* 184, 112–120. doi: 10.1016/j.plantsci.2011.12.008

Gui, J. S., Shen, J. H., and Li, L. G. (2011). Functional characterization of evolutionarily divergent 4-Coumarate: coenzyme A ligases in Rice. *Plant Physiol.* 157, 574–586. doi: 10.1104/pp.111.178301

Gunnaiah, R., Kushalappa, A. C., Duggavathi, R., Fox, S., and Somers, D. J. (2012). Integrated Metabolo-proteomic approach to decipher the mechanisms by which wheat QTL (Fhb1) contributes to resistance against *Fusarium graminearum*. *PLoS One* 7:e40695. doi: 10.1371/journal.pone.0040695

Hahlbrock, K., and Scheel, D. (1989). Physiology and molecular-biology of Phenylpropanoid metabolism. *Annu. Rev. Plant Physiol. Plant Mol. Biol.* 40, 347–369. doi: 10.1146/annurev.pp.40.060189.002023

Hassan, H. S., Mohamed, A. A., Feleafel, M. N., Salem, M. Z. M., Ali, H. M., Akrami, M., et al. (2021). Natural plant extracts and microbial antagonists to Control fungal pathogens and improve the productivity of zucchini (*Cucurbita pepo* L.) In vitro and in greenhouse. *Horticulturae* 7:470. doi: 10.3390/horticulturae7110470

Herrmann, K. (1989). Occurrence and content of Hydroxycinnamic and Hydroxybenzoic acid compounds in foods. *Crit. Rev. Food Sci. Nutr.* 28, 315–347. doi: 10.1080/10408398909527504

Holappa, L. D., and Blum, U. (1991). Effects of exogenously applied Ferulic acid, a potential Allelopathic compound, on leaf growth, water utilization, and endogenous Abscisic-acid levels of tomato, cucumber, and bean. *J. Chem. Ecol.* 17, 865–886. doi: 10.1007/BF01395596

Huang, X. X., Wang, Y., Lin, J. S., Chen, L., Li, Y. J., Liu, Q., et al. (2021). The novel pathogen-responsive glycosyltransferase UGT73C7 mediates the redirection of phenylpropanoid metabolism and promotes SNC1-dependent Arabidopsis immunity. *Plant J.* 107, 149–165. doi: 10.1111/tpj.15280

Islam, M. T., Lee, B. R., Das, P. R., La, V. H., Jung, H. I., and Kim, T. H. (2018). Characterization of p-Coumaric acid-induced soluble and cell wall-bound phenolic metabolites in relation to disease resistance to *Xanthomonas campestris* pv. Campestris in Chinese cabbage. *Plant Physiol. Biochem.* 125, 172–177. doi: 10.1016/j.plaphy.2018.02.012

Islam, M. T., Lee, B. R., La, V. H., Lee, H., Jung, W. J., Bae, D. W., et al. (2019). P-Coumaric acid induces jasmonic acid-mediated phenolic accumulation and resistance to black rot disease in *Brassica napus*. *Physiol. Mol. Plant Pathol.* 106, 270–275. doi: 10.1016/j.pmpp.2019.04.001

Kage, U., Karre, S., Kushalappa, A. C., and Mccartney, C. (2017a). Identification and characterization of a fusarium head blight resistance gene TaACT in wheat QTL-2DL. *Plant Biotechnol. J.* 15, 447–457. doi: 10.1111/pbi.12641

Kage, U., Yogendra, K. N., and Kushalappa, A. C. (2017b). TaWRKY70 transcription factor in wheat QTL-2DL regulates downstream metabolite biosynthetic genes to resist Fusarium graminearum infection spread within spike. *Sci. Rep.* 7:42596. doi: 10.1038/srep42596

Karre, S., Kumar, A., Yogendra, K., Kage, U., Kushalappa, A., and Charron, J. B. (2019). HvWRKY23 regulates flavonoid glycoside and hydroxycinnamic acid amide biosynthetic genes in barley to combat Fusarium head blight. *Plant Mol. Biol.* 100, 591–605. doi: 10.1007/s11103-019-00882-2

Kashyap, A., Jimenez-Jimenez, A. L., Zhang, W. Q., Capellades, M., Srinivasan, S., Laromaine, A., et al. (2022). Induced ligno-suberin vascular coating and tyramine-derived hydroxycinnamic acid amides restrict *Ralstonia solanacearum* colonization in resistant tomato. *New Phytol.* 234, 1411–1429. doi: 10.1111/nph.17982

Kaundal, A., Ramu, V. S., Oh, S., Lee, S., Pant, B., Lee, H. K., et al. (2017). GENERAL CONTROL NONREPRESSIBLE4 degrades 14-3-3 and the RIN4 complex to regulate Stomatal aperture with implications on nonhost disease resistance and drought tolerance. *Plant Cell* 29, 2233–2248. doi: 10.1105/tpc.17.00070

Kim, S. B., Van Den Broeck, L., Karre, S., Choi, H., Christensen, S. A., Wang, G. F., et al. (2021). Analysis of the transcriptomic, metabolomic, and gene regulatory responses to Puccinia sorghi in maize. *Mol. Plant Pathol.* 22, 465–479. doi: 10.1111/mpp.13040

Kishi-Kaboshi, M., Seo, S., Takahashi, A., and Hirochika, H. (2018). The MAMP-responsive MYB transcription factors MYB30, MYB55 and MYB110 activate the HCAA synthesis pathway and enhance immunity in Rice. *Plant Cell Physiol.* 59, 903–915. doi: 10.1093/pcp/pcy062

Knollenberg, B. J., Li, G. X., Lambert, J. D., Maximova, S. N., and Guiltinan, M. J. (2020). Clovamide, a Hydroxycinnamic acid amide, is a resistance factor Against *Phytophthora* spp. in *Theobroma cacao*. *Front. Plant Sci.* 11:617520. doi: 10.3389/fpls.2020.617520

Kyselka, J., Bleha, R., Dragoun, M., Bialasova, K., Horackova, S., Schatz, M., et al. (2018). Antifungal polyamides of Hydroxycinnamic acids from sunflower bee pollen. *J. Agric. Food Chem.* 66, 11018–11026. doi: 10.1021/acs.jafc.8b03976

Lee, M. H., Jeon, H. S., Kim, S. H., Chung, J. H., Roppolo, D., Lee, H. J., et al. (2019). Lignin-based barrier restricts pathogens to the infection site and confers resistance in plants. *EMBO J.* 38:e101948. doi: 10.15252/embj.2019101948

Li, J. B., Meng, Y., Zhang, K. X., Li, Q., Li, S. J., Xu, B. L., et al. (2021a). Jasmonic acid-responsive RRTF1 transcription factor controls DTX18 gene expression in hydroxycinnamic acid amide secretion. *Plant Physiol.* 185, 369–384. doi: 10.1093/plphys/kiaa043

Li, Y., Peng, Q., Selimi, D., Wang, Q., Charkowski, A. O., Chen, X., et al. (2009). The plant phenolic compound p-Coumaric acid represses gene expression in the *Dickeya dadantii* type III secretion system. *Appl. Environ. Microbiol.* 75, 1223–1228. doi: 10.1128/AEM.02015-08

Li, S. L., Pi, J., Zhu, H. J., Yang, L., Zhang, X. G., and Ding, W. (2021b). Caffeic acid in tobacco root exudate defends tobacco plants From infection by *Ralstonia solanacearum*. *Front. Plant Sci.* 12:690586. doi: 10.3389/fpls.2021.690586

Li, J. B., Zhang, K. X., Meng, Y., Hu, J. P., Ding, M. Q., Bian, J. H., et al. (2018). Jasmonic acid/ethylene signaling coordinates hydroxycinnamic acid amides biosynthesis through ORA59 transcription factor. *Plant J.* 95, 444–457. doi: 10.1111/tpj.13960

Lima, R. B., Salvador, V. H., Dos Santos, W. D., Bubna, G. A., Finger-Teixeira, A., Soares, A. R., et al. (2013). Enhanced lignin monomer production caused by Cinnamic acid and its Hydroxylated derivatives inhibits soybean root growth. *PLoS One* 8:e80542. doi: 10.1371/journal.pone.0080542

Liu, S., Xie, L., Su, J., Tian, B., Fang, A., Yu, Y., et al. (2022). Integrated metabolo-transcriptomics reveals the defense response of homogentisic acid

in wheat against *Puccinia striiformis* f. sp. tritici. *J. Agric. Food Chem.* 70, 3719–3729. doi: 10.1021/acs.jafc.2c00231

Lopez-Gresa, M. P., Torres, C., Campos, L., Lison, P., Rodrigo, I., Belles, J. M., et al. (2011). Identification of defence metabolites in tomato plants infected by the bacterial pathogen *Pseudomonas syringae*. *Environ. Exp. Bot.* 74, 216–228. doi: 10.1016/j.envexpbot.2011.06.003

Lou, Z. X., Wang, H. X., Rao, S. Q., Sun, J. T., Ma, C. Y., and Li, J. (2012). P-Coumaric acid kills bacteria through dual damage mechanisms. *Food Control* 25, 550–554. doi: 10.1016/j.foodcont.2011.11.022

Lowe, T. M., Ailloud, F., and Allen, C. (2015). Hydroxycinnamic acid degradation, a broadly conserved trait, protects *Ralstonia solanacearum* from chemical plant defenses and contributes to root colonization and virulence. *Mol. Plant-Microbe Interact.* 28, 286–297. doi: 10.1094/MPMI-09-14-0292-FI

Luo, J., Fuell, C., Parr, A., Hill, L., Bailey, P., Elliott, K., et al. (2009). A novel polyamine Acyltransferase responsible for the accumulation of Spermidine conjugates in Arabidopsis seed. *Plant Cell* 21, 318–333. doi: 10.1105/tpc.108.063511

Ma, Q. H., Zhu, H. H., and Qiao, M. Y. (2018). Contribution of both lignin content and sinapyl monomer to disease resistance in tobacco. *Plant Pathol.* 67, 642–650. doi: 10.1111/ppa.12767

Macoy, D. M., Kim, W. Y., Lee, S. Y., and Kim, M. G. (2015). Biotic stress related functions of hydroxycinnamic acid amide in plants. *J. Plant Biol.* 58, 156–163. doi: 10.1007/s12374-015-0104-y

Macoy, D. M. J., Uddin, S., Ahn, G., Peseth, S., Ryu, G. R., Cha, J. Y., et al. (2022). Effect of hydroxycinnamic acid amides, coumaroyl tyramine and coumaroyl tryptamine on biotic stress response in Arabidopsis. *J. Plant Biol.* 65, 145–155. doi: 10.1007/s12374-021-09341-2

Mathew, S., and Abraham, T. E. (2006). Bioconversions of ferulic acid, an hydroxycinnamic acid. *Crit. Rev. Microbiol.* 32, 115–125. doi: 10.1080/10408410600709628

Melotto, M., Underwood, W., Koczan, J., Nomura, K., and He, S. Y. (2006). Plant stomata function in innate immunity against bacterial invasion. *Cell* 126, 969–980. doi: 10.1016/j.cell.2006.06.054

Morales, J., Mendoza, L., and Cotoras, M. (2017). Alteration of oxidative phosphorylation as a possible mechanism of the antifungal action of p-coumaric acid against *Botrytis cinerea*. *J. Appl. Microbiol.* 123, 969–976. doi: 10.1111/jam.13540

Muroi, A., Ishihara, A., Tanaka, C., Ishizuka, A., Takabayashi, J., Miyoshi, H., et al. (2009). Accumulation of hydroxycinnamic acid amides induced by pathogen infection and identification of agmatine coumaroyltransferase in *Arabidopsis thaliana*. *Planta* 230, 517–527. doi: 10.1007/s00425-009-0960-0

Muroi, A., Matsui, K., Shimoda, T., Kihara, H., Ozawa, R., Ishihara, A., et al. (2013). Acquired immunity of transgenic torenia plants overexpressing agmatine coumaroyltransferase to pathogens and herbivore pests. *Sci. Rep.* 3:689. doi: 10.1038/srep01029

Napoleao, T. A., Soares, G., Vital, C. E., Bastos, C., Castro, R., Loureiro, M. E., et al. (2017). Methyl jasmonate and salicylic acid are able to modify cell wall but only salicylic acid alters biomass digestibility in the model grass *Brachypodium distachyon*. *Plant Sci.* 263, 46–54. doi: 10.1016/j.plantsci.2017.06.014

Plumbe, A. M., and Willmer, C. M. (1986). Phytoalexins, water-stress and Stomata.3. The effects of some phenolics, fatty-acids and Some other compounds on Stomatal responses. *New Phytol.* 103, 17–22. doi: 10.1111/j.1469-8137.1986.tb00592.x

Politycka, B., and Bednarski, W. (2004). Oxidative burst and lipoxygenase activity induced by hydroxycinnamic acids in cucumber roots. *Allelopath. J.* 14, 187–196.

Pushpa, D., Yogendra, K. N., Gunnaiah, R., Kushalappa, A. C., and Murphy, A. (2014). Identification of late blight resistance-related metabolites and genes in potato through nontargeted metabolomics. *Plant Mol. Biol. Report.* 32, 584–595. doi: 10.1007/s11105-013-0665-1

Qi, J. S., Wang, J. L., Gong, Z. Z., and Zhou, J. M. (2017). Apoplastic ROS signaling in plant immunity. *Curr. Opin. Plant Biol.* 38, 92–100. doi: 10.1016/j.pbi.2017.04.022

Rasheed, A., Hao, Y. F., Xia, X. C., Khan, A., Xu, Y. B., Varshney, R. K., et al. (2017). Crop breeding chips and genotyping platforms: Progress, challenges, and perspectives. *Mol. Plant* 10, 1047–1064. doi: 10.1016/j.molp.2017.06.008

Reddy, M. V. B., Arul, J., Angers, P., and Couture, L. (1999). Chitosan treatment of wheat seeds induces resistance to Fusarium graminearum and improves seed quality. *J. Agric. Food Chem.* 47, 1208–1216. doi: 10.1021/jf981225k

Ren, L. X., Huo, H. W., Zhang, F., Hao, W. Y., Xiao, L., Dong, C. X., et al. (2016). The components of rice and watermelon root exudates and their effects on pathogenic fungus and watermelon defense. *Plant Signal. Behav.* 11:e1187357. doi: 10.1080/15592324.2016.1187357

Roumani, M., Besseau, S., Gagneul, D., Robin, C., and Larbat, R. (2021). Phenolamides in plants: an update on their function, regulation, and origin of their biosynthetic enzymes. *J. Exp. Bot.* 72, 2334–2355. doi: 10.1093/jxb/eraa582

Roy, S., Nuckles, E., and Archbold, D. D. (2018). Effects of phenolic compounds on growth of *Colletotrichum* spp. *Curr. Microbiol.* 75, 550–556. doi: 10.1007/s00284-017-1415-7

Samborski, D. J., and Rohringer, R. (1970). Abnormal metabolites of wheat: occurrence, isolation and biogenesis of 2-Hydroxyputrescine amides. *Phytochemistry* 9, 1939–1945. doi: 10.1016/S0031-9422(00)85343-1

Schilmiller, A. L., Stout, J., Weng, J. K., Humphreys, J., Ruegger, M. O., and Chapple, C. (2009). Mutations in the cinnamate 4-hydroxylase gene impact metabolism, growth and development in Arabidopsis. *Plant J.* 60, 771–782. doi: 10.1111/j.1365-313X.2009.03996.x

Schmidt, A., Scheel, D., and Strack, D. (1998). Elicitor-stimulated biosynthesis of hydroxycinnamoyltyramines in cell suspension cultures of *Solanum tuberosum*. *Planta* 205, 51–55. doi: 10.1007/s004250050295

Seybold, H., Demetrowitsch, T. J., Hassani, M. A., Szymczak, S., Reim, E., Haueisen, J., et al. (2020). A fungal pathogen induces systemic susceptibility and systemic shifts in wheat metabolome and microbiome composition. *Nat. Commun.* 11:1910. doi: 10.1038/s41467-020-15633-x

Song, Z. Q., Zhang, C., Jin, P. Y., Tetteh, C., Dong, X. S., Luo, S., et al. (2022). The cell-type specific role of Arabidopsis bZIP59 transcription factor in plant immunity. *Plant Cell Environ.* 45, 1843–1861. doi: 10.1111/pce.14299

Sorokan, A. V., Burhanova, G. F., and Maksimov, I. V. (2018). Anionic peroxidase-mediated oxidative burst requirement for jasmonic acid-dependent *Solanum tuberosum* defence against *Phytophthora infestans*. *Plant Pathol.* 67, 349–357. doi: 10.1111/ppa.12743

Sullivan, M. L., and Knollenberg, B. J. (2021). Red clover HDT, a BAHD Hydroxycinnamoyl-coenzyme A: L-3, 4-Dihydroxyphenylalanine (L-DOPA) hydroxycinnamoyl transferase that synthesizes clovamide and other N-Hydroxycinnamoyl-aromatic amino acid amides. *Front. Plant Sci.* 12:727461. doi: 10.3389/fpls.2021.727461

Sun, G. X., Strebl, M., Merz, M., Blamberg, R., Huang, F. C., Mcgraphery, K., et al. (2019). Glucosylation of the phytoalexin N-feruloyl tyramine modulates the levels of pathogen-responsive metabolites in *Nicotiana benthamiana*. *Plant J.* 100, 20–37. doi: 10.1111/tpj.14420

Suzuki, N., Miller, G., Morales, J., Shulaev, V., Torres, M. A., and Mittler, R. (2011). Respiratory burst oxidases: the engines of ROS signaling. *Curr. Opin. Plant Biol.* 14, 691–699. doi: 10.1016/j.pbi.2011.07.014

Vaganan, M. M., Ravi, I., Nandakumar, A., Sarumathi, S., Sundararaju, P., and Mustaffa, M. M. (2014). Phenylpropanoid enzymes, phenolic polymers and metabolites as chemical defenses to infection of Pratylenchus coffeae in roots of resistant and susceptible bananas (Musa spp.). *Indian J. Exp. Biol.* 52, 252–260.

Valette, M., Rey, M., Gerin, F., Comte, G., and Wisniewski-Dyé, F. (2020). A common metabolomic signature is observed upon inoculation of rice roots with various rhizobacteria. *J. Integr. Plant Biol.* 62, 228–246. doi: 10.1111/jipb.12810

Von Roepenack-Lahaye, E., Newman, M. A., Schornack, S., Hammond-Kosack, K. E., Lahaye, T., Jones, J. D. G., et al. (2003). P-coumaroylnoradrenaline, a novel plant metabolite implicated in tomato defense against pathogens. *J. Biol. Chem.* 278, 43373–43383. doi: 10.1074/jbc.M305084200

Walters, D. R. (2003). Polyamines and plant disease. *Phytochemistry* 64, 97–107. doi: 10.1016/S0031-9422(03)00329-7

Whitney, K., Gracia-Gomez, G., Anderson, J. A., and Simsek, S. (2022). Time course metabolite profiling of Fusarium head blight-infected hard red spring wheat using ultra-high-performance liquid chromatography coupled with Quadrupole time of flight/MS br. *J. Agric. Food Chem.* 70, 4152–4163. doi: 10.1021/acs.jafc.1c08374

Wu, H. S., Luo, J., Raza, W., Liu, Y. X., Gu, M. A., Chen, G., et al. (2010). Effect of exogenously added ferulic acid on in vitro *Fusarium oxysporum*

f. sp niveum. *Sci. Hortic.* 124, 448–453. doi: 10.1016/j.scienta.2010.02.007

Wu, H. S., Wang, Y., Bao, W., Liu, D. Y., Raza, W., Huang, Q. W., et al. (2009). Responses of Fusarium oxysporum f. sp niveum to exogenously added sinapic acid in vitro. *Biol. Fertil. Soils* 45, 443–447. doi: 10.1007/s00374-009-0353-3

Xiang, J. L., Zhang, M., Apea-Bah, F. B., and Beta, T. (2019). Hydroxycinnamic acid amide (HCAA) derivatives, flavonoid C-glycosides, phenolic acids and antioxidant properties of foxtail millet. *Food Chem.* 295, 214–223. doi: 10.1016/j.foodchem.2019.05.058

Xie, Q. J., Liu, Z. Y., Meir, S., Rogachev, I., Aharoni, A., Klee, H. J., et al. (2016). Altered metabolite accumulation in tomato fruits by coexpressing a feedback-insensitive AroG and the PhODO1 MYB-type transcription factor. *Plant Biotechnol. J.* 14, 2300–2309. doi: 10.1111/pbi.12583

Yadav, A., Fennec, A., Davidovich-Rikanati, R., Meir, S., Kochanek, B., Lewinsohn, E., et al. (2021). Phenylpropanoid metabolism in astringent and nonastringent persimmon (*Diospyros kaki*) cultivars determines sensitivity to Alternaria infection. *J. Agric. Food Chem.* 69, 5628–5637. doi: 10.1021/acs.jafc.1c01312

Yang, C. Q., Fang, X., Wu, X. M., Mao, Y. B., Wang, L. J., and Chen, X. Y. (2012). Transcriptional regulation of plant secondary metabolism. *J. Integr. Plant Biol.* 54, 703–712. doi: 10.1111/j.1744-7909.2012.01161.x

Yogendra, K. N., Kumar, A., Sarkar, K., Li, Y. L., Pushpa, D., Mosa, K. A., et al. (2015). Transcription factor StWRKY1 regulates phenylpropanoid metabolites conferring late blight resistance in potato. *J. Exp. Bot.* 66, 7377–7389. doi: 10.1093/jxb/erv434

Yogendra, K. N., Sarkar, K., Kage, U., and Kushalappa, A. C. (2017). Potato NAC43 and MYB8 mediated transcriptional regulation of secondary cell wall biosynthesis to contain *Phytophthora infestans* infection. *Plant Mol. Biol. Report.* 35, 519–533. doi: 10.1007/s11105-017-1043-1

Yu, P. Q., Mckinnon, J. J., Maenz, D. D., Racz, V. J., and Christensen, D. A. (2004). The specificity and the ability of *Aspergillus* feruloyl esterase to release p-coumaric acid from complex cell walls of oat hulls. *J. Chem. Technol. Biotechnol.* 79, 729–733. doi: 10.1002/jctb.1045

Zacares, L., Lopez-Gresa, M. P., Fayos, J., Primo, J., Belles, J. M., and Conejero, V. (2007). Induction of p-coumaroyldopamine and feruloyldopamine, two novel metabolites, in tomato by the bacterial pathogen *Pseudomonas syringae*. *Mol. Plant-Microbe Interact.* 20, 1439–1448. doi: 10.1094/MPMI-20-11-1439

Zeiss, D. R., Piater, L. A., and Dubery, I. A. (2021). Hydroxycinnamate amides: intriguing conjugates of plant protective metabolites. *Trends Plant Sci.* 26, 184–195. doi: 10.1016/j.tplants.2020.09.011

Zhang, Y., Li, J., Zhang, W., Wang, R., Qiu, Q., Luo, F., et al. (2017). Ferulic acid, but not all hydroxycinnamic acids, is a novel T3SS inducer of Ralstonia solanacearum and promotes its infection process in host plants under hydroponic condition. *Front. Plant Sci.* 8:1595. doi: 10.3389/fpls.2017.01595

Zhang, X. B., and Liu, C. J. (2015). Multifaceted regulations of gateway enzyme phenylalanine ammonia-lyase in the biosynthesis of phenylpropanoids. *Mol. Plant* 8, 17–27. doi: 10.1016/j.molp.2014.11.001

Zhang, H. Y., Liu, F. R., Wang, J. J., Yang, Q. R., Wang, P., Zhao, H. J., et al. (2021). Salicylic acid inhibits the postharvest decay of goji berry (*Lycium barbarum* L.) by modulating the antioxidant system and phenylpropanoid metabolites. *Postharvest Biol. Technol.* 178:111558. doi: 10.1016/j.postharvbio.2021.111558

Zhang, M. Y., Wang, D. J., Gao, X. X., Yue, Z. Y., and Zhou, H. L. (2020). Exogenous caffeic acid and epicatechin enhance resistance against Botrytis cinerea through activation of the phenylpropanoid pathway in apples. *Sci. Hortic.* 268:109348. doi: 10.1016/j.scienta.2020.109348

Zhang, G.-L., Zhou, P.-C., Gong, Y.-L., Li, X.-M., Yan, Y., Rasheed, A., et al. (2022). Boosting the antioxidant potential of pasta by a premature stop mutation in wheat keto-acythiolase-2. *Food Chem.* 385:132634. doi: 10.1016/j.foodchem.2022.132634

Zhao, Q., and Dixon, R. A. (2011). Transcriptional networks for lignin biosynthesis: more complex than we thought? *Trends Plant Sci.* 16, 227–233. doi: 10.1016/j.tplants.2010.12.005

Zhou, M. L., and Memelink, J. (2016). Jasmonate-responsive transcription factors regulating plant secondary metabolism. *Biotechnol. Adv.* 34, 441–449. doi: 10.1016/j.biotechadv.2016.02.004

Conflict of Interest: The authors declare that the research was conducted in the absence of any commercial or financial relationships that could be construed as a potential conflict of interest.

Publisher's Note: All claims expressed in this article are solely those of the authors and do not necessarily represent those of their affiliated organizations, or those of the publisher, the editors and the reviewers. Any product that may be evaluated in this article, or claim that may be made by its manufacturer, is not guaranteed or endorsed by the publisher.

frontiers | Frontiers in Plant Science

ORIGINAL RESEARCH
published: 30 June 2022
doi: 10.3389/fpls.2022.934226

Mining the Roles of Wheat (*Triticum aestivum*) SnRK Genes in Biotic and Abiotic Responses

Baihui Jiang[1†], *Yike Liu*[2†], *Hongli Niu*[1], *Yiqin He*[1,3], *Dongfang Ma*[1,2*] *and Yan Li*[1,2*]

[1] Engineering Research Center of Ecology and Agricultural Use of Wetland, Ministry of Education/College of Agriculture, Yangtze University, Jingzhou, China, [2] Hubei Key Laboratory of Food Crop Germplasm and Genetic Improvement, Food Crops Institute, Hubei Academy of Agricultural Sciences/Wheat Disease Biology Research Station for Central China, Wuhan, China, [3] Longgan Lake National Nature Reserve Authority of Hubei, Huanggang, China

Sucrose non-fermenting-1-related protein kinases (SnRKs) play vital roles in plant growth and stress responses. However, little is known about the SnRK functions in wheat. In this study, 149 TaSnRKs (wheat SnRKs) were identified and were divided into three subfamilies. A combination of public transcriptome data and real-time reverse transcription-polymerase chain reaction (qRT-PCR) analysis revealed the distinct expression patterns of TaSnRKs under various abiotic and biotic stresses. TaSnRK2.4-B, a member of SnRK2s, has different expression patterns under polyethylene glycol (PEG), sodium chloride (NaCl) treatment, and high concentrations of abscisic acid (ABA) application. Yeast two-hybrid assay indicated that TaSnRK2.4-B could interact with the SnRK2-interacting calcium sensor (SCS) in wheat and play a role in the ABA-dependent pathway. Moreover, TaSnRK2.4-B might be a negative regulator in wheat against pathogen infection. The present study provides valuable information for understanding the functions of the TaSnRK family and provides recommendations for future genetic improvement in wheat stress resistance.

Keywords: TaSnRK, biotic and abiotic stresses, qRT-PCR, TaSnRK2.4-B, negative regulator

OPEN ACCESS

Edited by:
Yang Yu,
Southwest University, China

Reviewed by:
Furong Liu,
University of California, Davis, United States
Jianhui Wu,
Northwest A&F University, China

***Correspondence:**
Yan Li
vgly1987@sina.com
Dongfang Ma
madf@yangtzeu.edu.cn

[†] *These authors have contributed equally to this work*

Specialty section:
This article was submitted to Technical Advances in Plant Science, a section of the journal Frontiers in Plant Science

Received: *02 May 2022*
Accepted: *01 June 2022*
Published: *30 June 2022*

Citation:
Jiang B, Liu Y, Niu H, He Y, Ma D and Li Y (2022) Mining the Roles of Wheat (Triticum aestivum) SnRK Genes in Biotic and Abiotic Responses. Front. Plant Sci. 13:934226. doi: 10.3389/fpls.2022.934226

INTRODUCTION

Sucrose non-fermenting-1-related protein kinase (SnRK), a class of serine/threonine protein kinases, is widely present in the plant kingdom and strongly conserved among species. It modulates specific proteins to regulate the interrelationship of multiple signaling pathways using phosphorylation in plants and plays a vital role in their stress responses (Halford and Hey, 2009; Yan et al., 2014).

The SnRKs are subdivided into three subfamilies, SnRK1, SnRK2, and SnRK3, according to the structural characteristics of proteins (Hrabak et al., 2003; Coello et al., 2011). All plant SnRK subfamilies share a common S_TKc domain (Serine/Threonine protein kinases, PF00069). The SnRK1 subfamily specifically contains a C-terminal kinase-associated domain 1 (KA1 domain, PF02149) (Amodeo et al., 2007). The SnRK2 has an SnRK2-specific box (glutamine-303 to proline-318) (Christophe et al., 2006), and the NAF domain (Asn-Ala-Phe, PF03822) is present in the SnRK3 subfamily (Albrecht et al., 2001).

Concomitant with the diverse domains, the functions of the three subfamilies are different. In SnRK1, a heterotrimeric complex composed of α, β, and γ subunits, is homologous to the yeast SNF1 gene, which was first discovered and well-known for its role as an energy sensor in the global regulation of carbon metabolism (Hardie et al., 1998). Over-expression of MhSnRK1 in

tomatoes could regulate fruit development and increase both the carbon and nitrogen assimilation rate (Wang et al., 2012). Both SnRK2 and SnRK3 are plant-specific and are involved in signaling pathways that regulate plant responses to osmotic and adversity stresses. There are compelling pieces of evidence indicating that the divergence of SnRK2 and SnRK3 subfamilies evolved after the duplication of SnRK1, which has enabled plants to form networks connecting metabolic and genetic responses to stress, hormone, and calcium signal (Halford and Hey, 2009).

The first identified SnRK2 gene is PKABA1 (accession no. M94726), which was isolated from wheat after ABA treatment and can be induced by ABA and drought treatment (Anderberg and Walker-Simmons, 1992). Among the ten SnRK2 genes in *Arabidopsis*, nine (except for SnRK2.9) can be activated by hyperosmotic and salinity stresses. Furthermore, five (SnRK2.2, SnRK2.3, SnRK2.6, SnRK2.7, and SnRK2.8) of the nine genes can be activated by ABA (Boudsocq et al., 2007; Coello et al., 2011). SnRK3 are also known as calcineurin B-like proteins (CBL) interacting protein kinase (CIPK), which interacts with calcium sensor CBL to transfer stress signals (Sheen, 1996; Albrecht et al., 2003). The best-studied member is salt overly sensitive 2 (SOS2), which is involved in response to salt stress and ABA signaling and is required for sodium ion (Na^+) and potassium ion (K^+) homeostasis and abiotic stress tolerance (Liu et al., 2000; Guo et al., 2001).

Bread wheat (*Triticum aestivum* L.) is one of the most important food crops worldwide. Several members of the TaSnRK family genes have been identified and their functions explored. TaSnRK1α plays an important role in Fusarium head blight (FHB) resistance and is the common target of TaFROG (*Fusarium* Resistance Orphan Gene), and *Fusarium graminearum* orphan secreted protein Osp24. These two orphan proteins bind with TaSnRK1α competitively during the conflict between wheat and *F. graminearum* (Perochon et al., 2015; Jiang et al., 2020). To date, ten TaSnRK2 genes have been isolated from wheat (Zhang et al., 2016). These genes are multifunctional regulatory factors that are involved in response to various abiotic stresses (Mao et al., 2010; Zhang et al., 2010; Feng et al., 2019; Miao et al., 2021), and in thousand-kernel weight, photosynthesis, and other physiological aspects of wheat (Tian et al., 2013; Miao et al., 2017, 2021). However, the role of TaSnRK2s in biotic stresses is limited. In this study, the genes belonging to the whole SnRK family were identified through the wheat genome. The expression patterns of *TaSnRKs* under biotic and abiotic stresses were subsequently characterized. Furthermore, TaSnRK2.4-B was found to be participated in the pathway of pathogen-associated molecular patterns (PAMP) triggered immunity in *Nicotiana benthamiana*. The results of the present study provide useful information for understanding the functions of the TaSnRK family and provide recommendations for the future genetic improvement of stress resistance in wheat.

MATERIALS AND METHODS

Identification of TaSnRK Genes

The protein sequences of known 38 AtSnRKs and 47 OsSnRKs (**Supplementary Material 1**) were collected and used as a query for BLASTp (2.2.28) against the wheat reference genome IWGSC v1.1 (Hrabak et al., 2003; Saha et al., 2014; Wang et al., 2015). The samples were further screened using SMART (9.0) and NCBI CDD (v 3.18) to confirm conserved domains in the wheat SnRK family. In general, the S_TKc domain (Serine/Threonine protein kinases, catalytic domain) is present in all SnRK genes; KA1 is specifically present in SnRK1 subfamily (Amodeo et al., 2007); SnRK2-specific box (glutamine-303 to proline-318) is present in SnRK2 subfamily (Christophe et al., 2006); and, NAF (Asn-Ala-Phe) domain is specifically present in SnRK3 subfamily (Albrecht et al., 2001). According to these specific domains in different subfamilies, TaSnRKs were screened and classified. The characteristic features of TaSnRK proteins were predicted using ExPASy Server (v10). The subcellular localization of TaSnRKs was predicted using Plant-mPLoc (2.0). The information on the chromosomal location of TaSnRKs was extracted from the reference IWGSCv1.1 GFF3 file. MapInspect software was used to draw the physical map of TaSnRKs.

Phylogenetic Analysis of Wheat SnRK Gene Family

To further explore the evolutionary relationships of wheat SnRKs, multiple sequence alignments of SnRK proteins were conducted with ClustalW (2.0.10). A phylogenetic tree was constructed using the neighbor-joining (NJ) method with 1000 replicated bootstraps in MEGA X. The midpoint rooted base tree was modified via iTOL online tool (v3.2.317).

Gene Structure and Protein Motif Analysis

The gene exon-intron structures of TaSnRK genes were performed by GSDS (v2.0) (Hu et al., 2015). The conserved motifs of TaSnRK proteins were identified by MEME (v4.9.1). Finally, the motif patterns were exhibited by TBtools software (Chen et al., 2020).

Cis-Elements Analysis and Expression Pattern Analysis of TaSnRKs

Cis-acting elements in the upstream sequences (1.5 kb) of TaSnRKs were predicted using PlantCARE online tool. The result was organized and displayed by the R package "pheatmap". RNA-seq data was downloaded from expVIP (Ramírez-González et al., 2018). Morpheus was used to generate heatmaps of TaSnRKs fold change based on log2 (TPM+1) values. The TaSnRKs were classified according to their expression levels using k-means clustering (K-means = 15) (Jain, 2010).

Plant Treatment and qRT-PCR Analysis

Twenty seeds of Yangmei were surface-sterilized and germinated at 20°C for 2 days and then placed in a half-strength Hoagland nutrient solution. The seedlings were treated with 150 mM NaCl, 20% PEG 6000, and 100 μM ABA at one heart and one leaf stage. Roots were sampled at 2, 12, 24, 48, and 72 hours after treatments. Meanwhile, the plants were inoculated with *F. graminearum* (strain PH-1) (Yang et al., 2010) and powdery mildew (*Blumeria graminis f. sp. Tritici*, Bgt strain E09). The inoculated spikelets and leaves were harvested at 1, 3, and 5 days

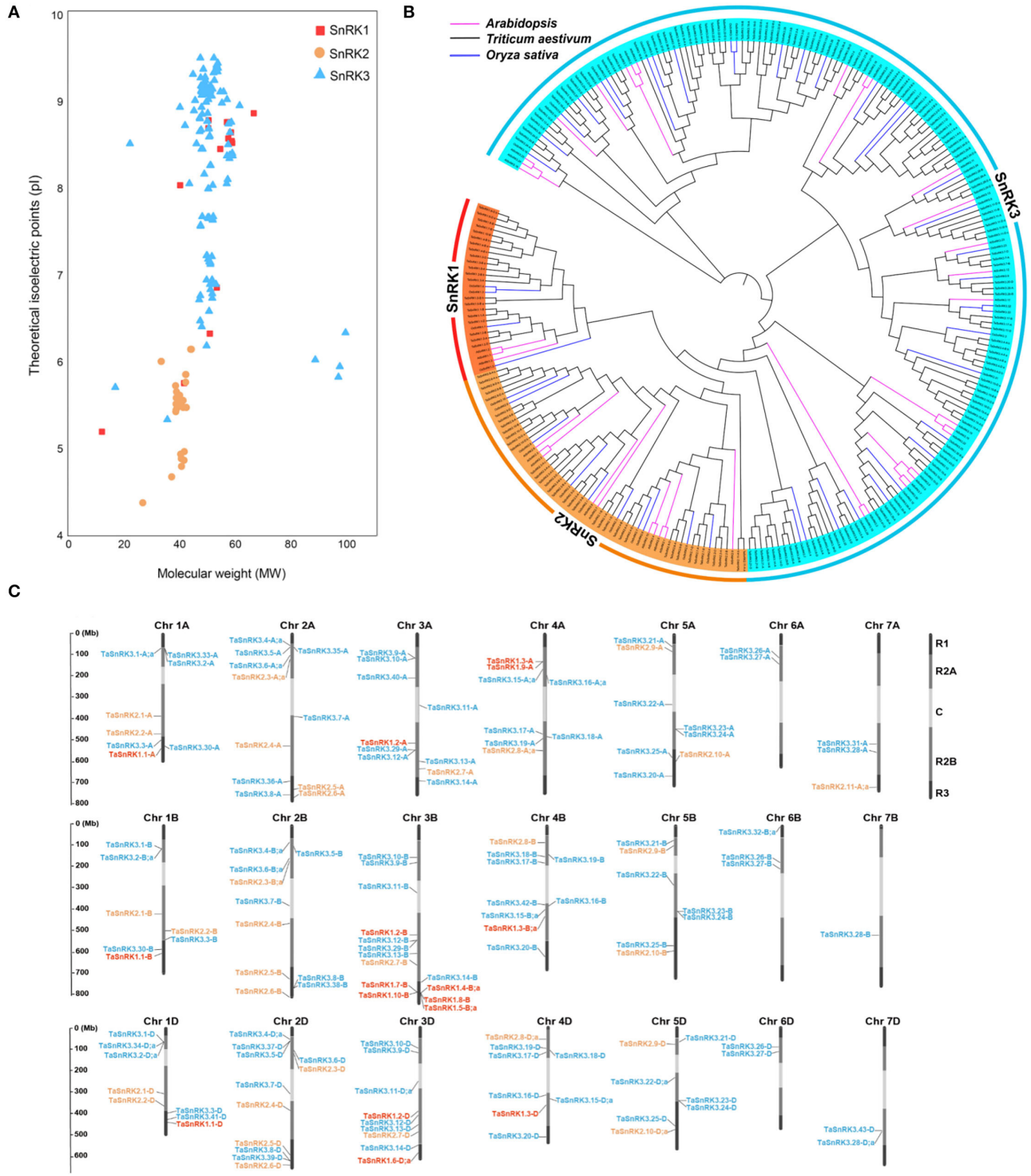

FIGURE 1 | General information of TaSnRKs. **(A)** The distribution patterns of isoelectric points (pI) and molecular weights (MW) for the three subfamilies of wheat SnRKs. **(B)** Phylogenetic tree of non-fermenting-1-related protein kinase (SnRK) predicted in wheat and those previously identified in *Arabidopsis* and *Oryza sativa*. All amino acid sequences, including 186 TaSnRKs, 47 OsSnRKs, and 38 AtSnRKs, were aligned using ClustalW2, and the phylogenetic tree was constructed using the bootstrap neighbor-joining method (NJ) tree (1,000 replicates) method and MEGA 7.0 software. Different color ribbons mark different sub-families. SnRKs from wheat, rice, and *Arabidopsis* are distinguished with different color lines. **(C)** Chromosomal locations of the 148 TaSnRK genes. The ruler line on the left indicates the physical map distance among genes (Mbp). Dark black represents R1 and R3 (distal telomeric parts of the chromosomes), light gray represents R2A and R2B (sub-central segments of the chromosomes), and white represents C (central segments of the chromosomes). Gene members of SnRK1 (red), SnRK2 (orange), and SnRK3 (blue) were mapped to corresponding chromosomes. TaSnRK3.44-U gene was not mapped in chromosomes because it was not predicted in any chromosomes. The specific location information of each gene on the chromosomes is listed in **Supplementary Material 2**.

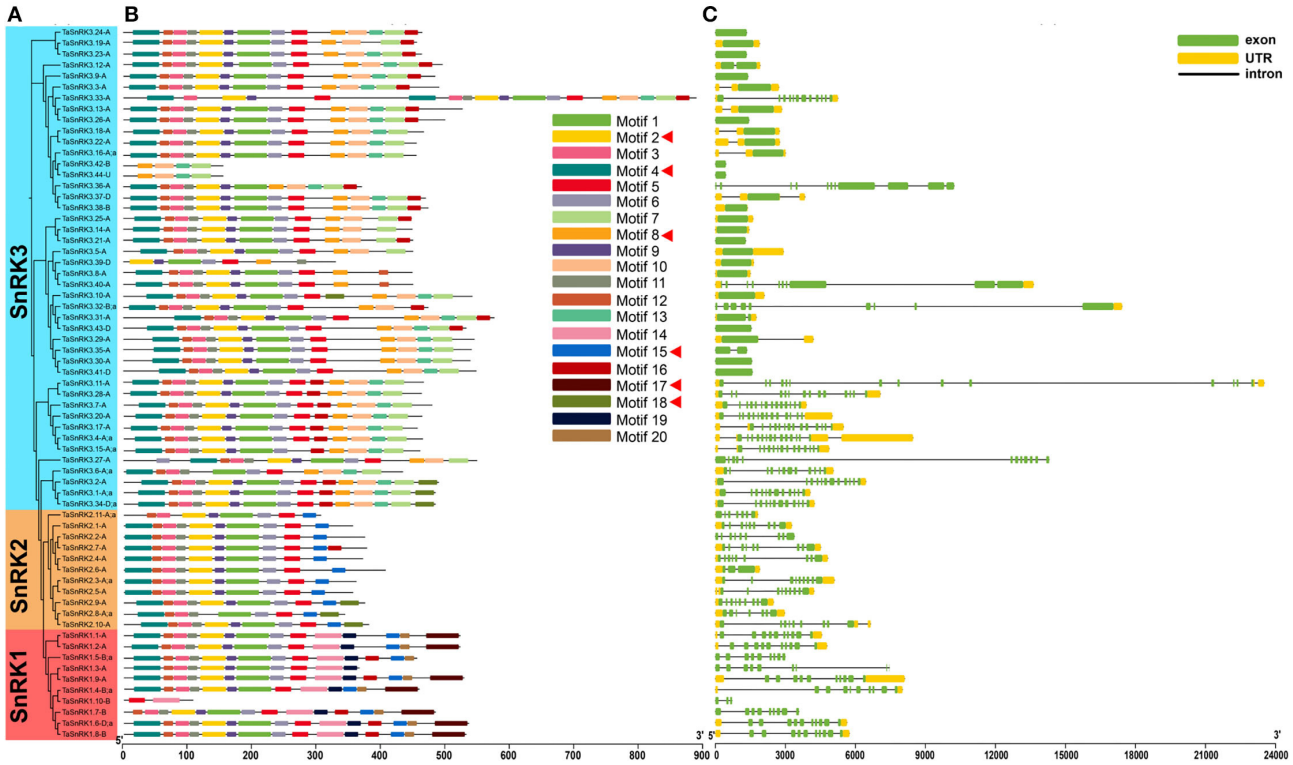

FIGURE 2 | Motif composition and exon-intron structure of 65 representative TaSnRKs. **(A)** Phylogenetic tree of TaSnRKs was created by MEGA X with the neighbor-joining (NJ) method. **(B)** Motif composition of TaSnRKs. Different motifs are indicated by a specific color. The red triangle indicates motifs related to the functional domains. **(C)** Gene structure of TaSnRKs. Gene structure and motif analyses of 186 TaSnRKs can be found in **Supplementary Material 4**.

post inoculation (dpi). All treatments were implemented with three biological replications.

Total RNA was isolated from 100 mg tissues using TRIzol reagent (Invitrogen, USA) and was digested with DNase I (TaKaRa, Beijing, China) to eliminate genome DNA. Using RevertAid Reverse Transcriptase kit (Vazyme, Nanjing, China), cDNA was synthesized. Nine genes were selected, and the primers were listed in **Supplementary Material 2**. Then, qRT-PCR was performed in a 15 μl volume containing 2× SYBR Green qPCR Master Mix (Vazyme, Nanjing, China). The relative gene expression level was calculated with the $2^{-\Delta\Delta Ct}$ method (Livak and Schmittgen, 2001).

Subcellular Localization and Transient Overexpression of TaSnRK2.4-B

The CDS region of TaSnRK2.4-B was cloned and inserted into the upstream green fluorescent protein (GFP) in the plant expression vector pART27. Then the recombinant vector was transformed into *Agrobacterium tumefaciens* strain GV3101, and the bacterial solution was injected into the leaves of 4–6-week-old *Nicotiana benthamiana*. For subcellular localization assay, 48 h post injection, the green fluorescence signal was detected and captured by laser scanning confocal microscopy (OLYMPUS, FV3000, Japan). For the luminol-based assay, 48 h post injection, 12 leaf disks were collected after washing with distilled water and were placed in the dark for 2 h. The leaf disks were then placed in an ELISA plate with 200 μl distilled water overnight in the dark. Later, the distilled water was replaced with luminol and horse radish peroxidase (HRP) solution. Finally, 50 μl 5×flg22 solution was added, and the photochemical signals were monitored immediately with a microplate reader (Hidex, SENSE 425-301, Finland).

Yeast Two-Hybrid Assay

To detect the interactions between TaSnRK2.4-B and SnRK2-interacting calcium sensor (SCS) in wheat, the coding sequence of TaSnRK2.4-B was cloned into pGBKT7, and the coding sequence of SCS in wheat was cloned into pGADT7. The primers are listed in **Supplementary Material 2**. The recombinant vectors were transformed into yeast strain AH109. Afterward, the positive clones were confirmed on SD medium without Trp, Leu, His, and Ade according to the manufacturer's instruction.

RESULTS

Identification and Phylogeny Analysis of TaSnRK Genes

After querying BLASTp with 38 AtSnRK and 47 OsSnRK proteins, 1,240 putative TaSnRK proteins were found. However, after conserved domain searching by NCBI CDD and SMART

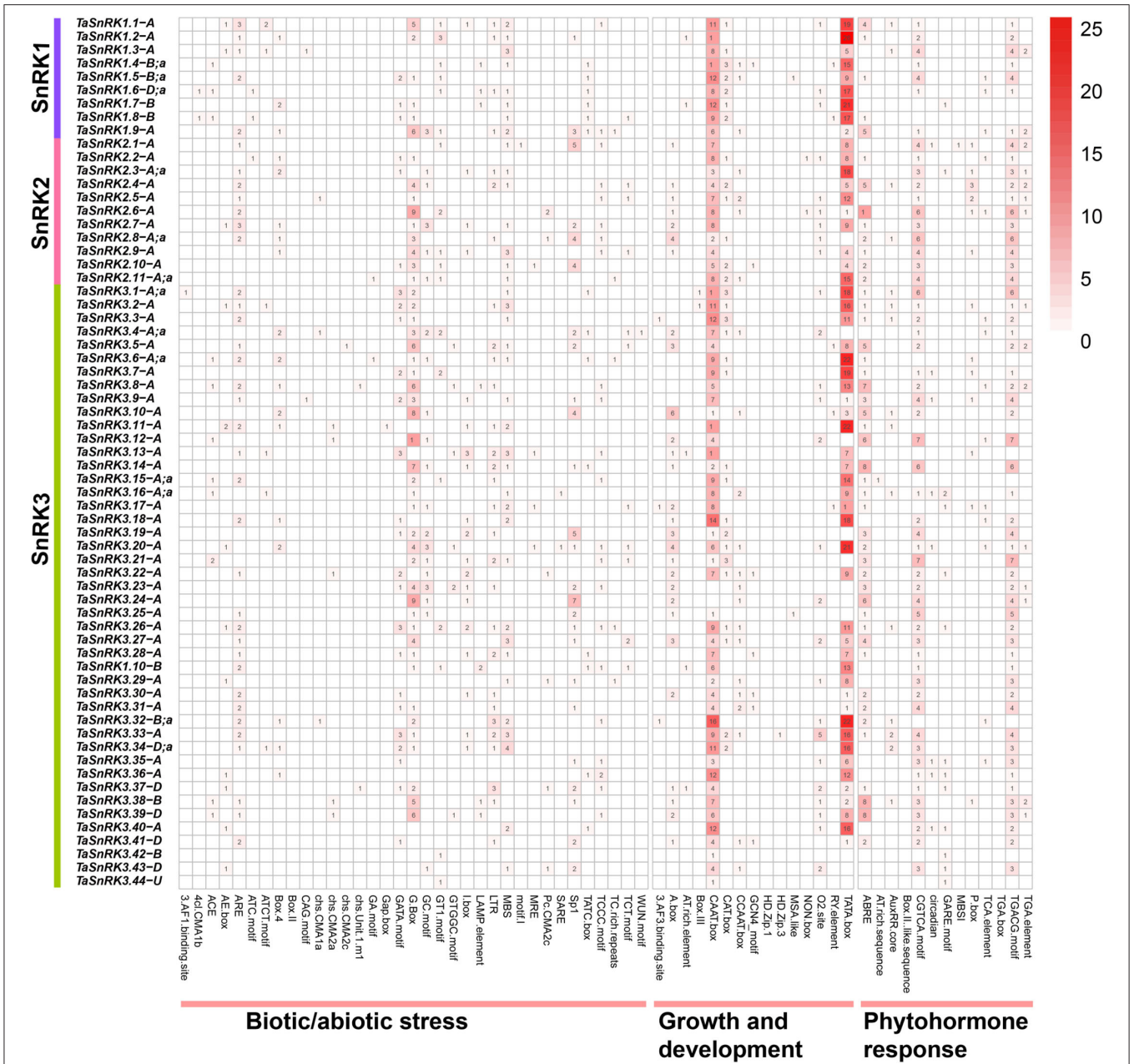

FIGURE 3 | Distribution and summarizing of predicted cis-acting elements in the 1.5 kb upstream of 65 representative TaSnRK genes. Cis-acting elements involved in biotic/abiotic stresses, growth and development, and phytohormone response in the promoter of the 65 TaSnRK genes. The different numbers and colors suggest the elements' numbers. All cis-acting elements of 186 TaSnRKs promoter are displayed in **Supplementary Material 6**.

tools, 149 genes (186 proteins due to the alternative splicing) were finally retained. It contained 21 SnRK1 proteins, 38 SnRK2 proteins, and 127 SnRK3 proteins (**Figure 1A**; **Supplementary Material 3**). The wheat SnRKs were named according to their subfamily (SnRK1, SnRK2, and SnRK3) and genome location (**Supplementary Material 3**). Triplicate genes share the same gene number but use suffixes A, B, and D to distinguish sub genome location. Consecutive lowercases were separated by a semicolon to distinguish the alternative splicing variants (e.g., TaSnRK1.3-B;a and TaSnRK1.3-B;b) (Ramírez-González et al., 2018).

To further understand the features of TaSnRKs, the protein properties of 186 TaSnRK proteins were analyzed (**Supplementary Material 3**). The length of TaSnRKs proteins ranged from 103 (TaSnRK1.10-B) to 885 (TaSnRK3.32-B;c) amino acids (aa). The average molecular weight (MW) of SnRK1, SnRK2, and SnRK3 subfamily proteins were 53, 40, and 51 kDa, respectively. And the theoretical isoelectric point

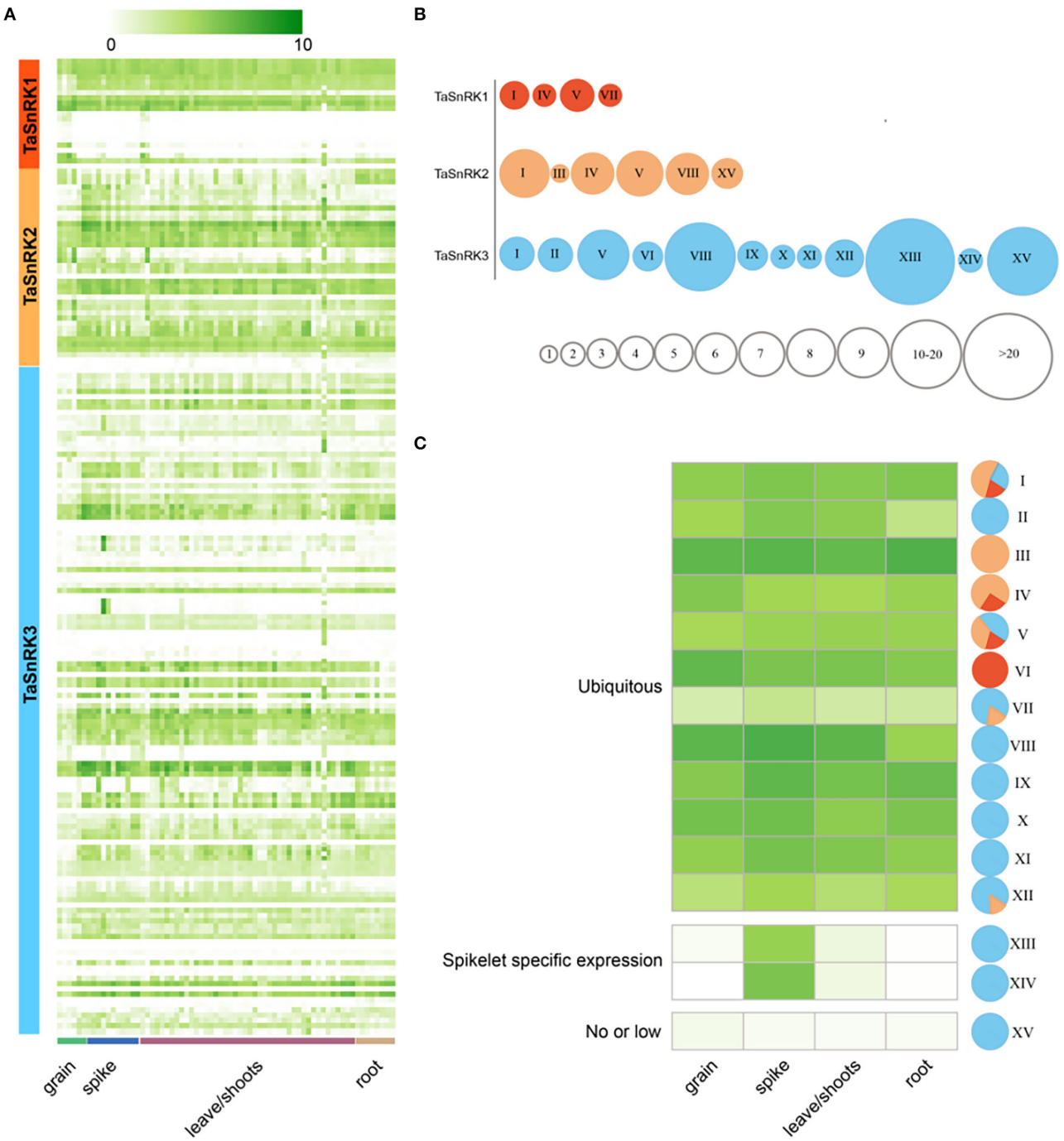

FIGURE 4 | Transcriptome analyses of 186 TaSnRKs during wheat development. **(A)** The 186 TaSnRK gene expression levels in three wheat development stages/tissues (columns) and subfamilies (rows). Different levels of gene fold change, i.e., log2 (TPM+1), are marked by colors that gradually change (Fold change > 5 suggests significant expression). Detailed information is listed in **Supplementary Material 7**. **(B)** Based on the gene expression, genes in three subfamilies were clustered into 15 types indicated by roman numerals. Smaller circles indicate fewer genes of this subfamily belong to this type (a particular circle size suggests gene numbers). **(C)** A heatmap shows average expression values for the 15 types. Colors in sectors indicate three subfamilies as **(A,B)**: SnRK1 (red), SnRK2 (orange), and SnRK3 (blue).

(pI) ranged from 4.38 (TaSnRK2.8-D;a) to 9.51 (TaSnRK3.12-B and TaSnRK3.21-B). As shown in **Figure 1A**, compared to the other two subfamilies, SnRK2 had lower MW values, and all pI values were less than 7. All the TaSnRKs belonged to hydrophilic

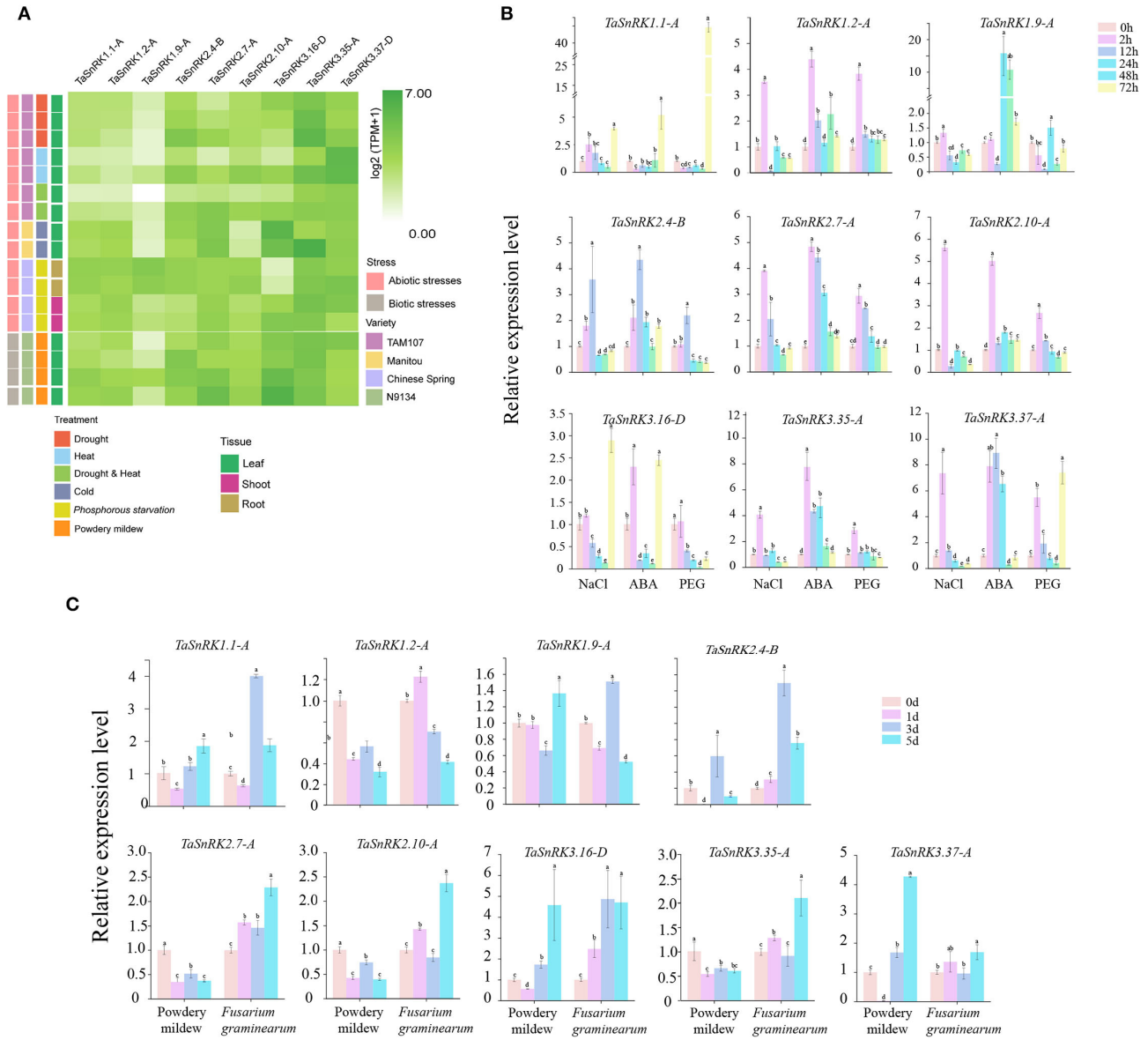

FIGURE 5 | Expression patterns of nine selected TaSnRK genes under abiotic and biotic stresses. **(A)** Expression levels of nine TaSnRK genes under multiple abiotic stresses involving PEG 6000 stress, cold stress, drought and heat combined stress, drought stress, heat stress, phosphorous starvation, and biotic stress involving powdery mildew infection. **(B)** Expression patterns of the nine TaSnRK genes under abiotic stresses including NaCl, ABA, and PEG treatment. **(C)** Expression of the nine TaSnRK genes under biotic stresses, including powdery mildew and *Fusarium graminearum* infection. The relative expression levels were determined by the $2^{-\Delta\Delta ct}$ method. Significant differences at $P < 0.05$.

proteins as their grand average of hydropathicity (GRAVY) values were negative.

The phylogenetic tree generated by SnRK protein sequences from Arabidopsis, rice, and *T. aestivum* showed that TaSnRKs belonging to the same subfamilies were clustered together (**Figure 1B**). Moreover, members of the SnRK2 subfamily had a closer relationship with those in SnRK1.

As illustrated in **Figure 1C**, TaSnRK genes were located on 21 chromosomes, except for TaSnRK3.44-U in an unanchored contig (**Supplementary Material 3**). Moreover, the chromosome distributions were uneven. Compared to gene numbers in other chromosomes, fewer genes were located in Chr 6 and Chr 7. Also, more TaSnRKs (73.3%) were located in the central segments (R2a, R2b, and C) of the chromosomes (Ramírez-González et al., 2018).

Motif Composition, Exon-Intron Structure, Protein Feature, and Structure Analysis

TaSnRKs were analyzed according to the following criteria: (1) one gene of the triplicates was retained; (2) only the first variant was kept. Consequently, 65 typical TaSnRKs were selected. As

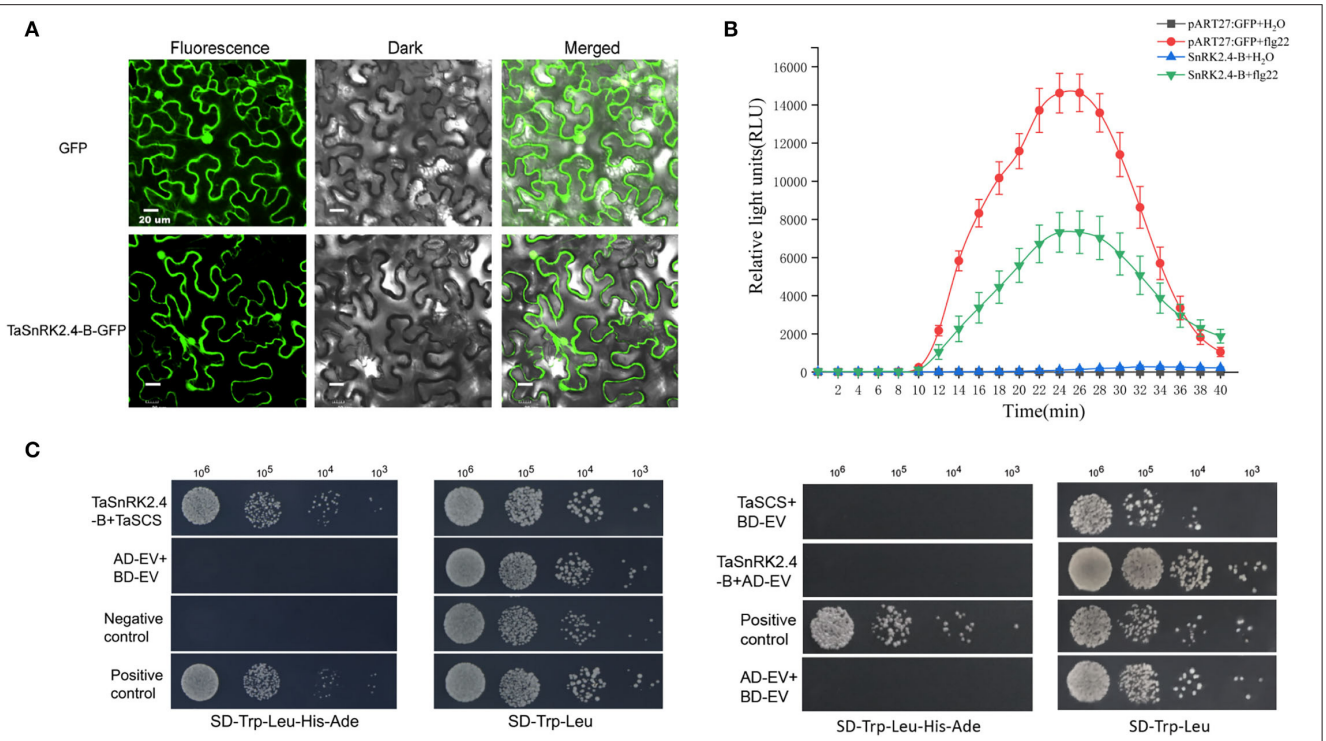

FIGURE 6 | Functional analysis of TaSnRK2.4-B. **(A)** Subcellular localization of TaSnRK2.4-B. GFP fluorescence was visualized using confocal laser scanning microscopy. Scale bar = 20 μm. **(B)** Oxidative burst triggered by 5×flg22 solution in transient overexpression of TaSnRK2.4-B leaves and vector control measured in a luminol-based assay as relative light units. Values are averages ±SE ($n = 12$). **(C)** Different concentrations (cells/ml) of yeast transformants expressing the indicated bait and prey constructs were assayed for growth on SD-Trp-Leu and SD-Trp-Leu-His-Ade plates.

illustrated in **Figures 2A,B** and **Supplementary Material 4**, the proteins with a close relationship in the phylogenetic tree shared similar motif compositions. There were six conserved motifs related to the functional domains (**Supplementary Material 5**). Motif 2 and motif 4 contained Ser/Thr active site and ATP-binding region, respectively. Motif 17 contained the specific conserved KA1 domain of SnRK1, and motif 8 contained the specific NAF domain of SnRK3. Furthermore, motif 18, present in some members of the SnRK2 and SnRK3 subfamilies, contained an ABA-specific box, which indicated that these members might play roles in response to ABA stress. As shown in **Figure 2C**, all genes in SnRK1 and SnRK2 subfamilies had introns. On the contrary, 40% of SnRK3 genes had no intron. The differences in gene and protein structure among the three subfamilies illustrate the possibility of gene subfunctionalization or neofunctionalization in the TaSnRKs family.

Promoter Analysis

The sequence analysis of 1.5 kb upstream of TaSnRK genes showed that the cis-acting elements were clustered into three categories, and most of the cis-acting elements were related to growth and development (**Figure 3**, **Supplementary Material 6**). CAAT-box, a common element in enhancer and promoter areas that plays an essential role in transcription, is predominant among these genes (98.5%). Other cis-acting elements, such as A-box, AT-rich sequence, CAT-box, CCAAT-box, GCN4_motif, and O_2-site, which participate in multiple growth regulation processes, were also found in most of the genes. Furthermore, elements related to hormone signaling pathways, like auxin (AuxRR-core and TGA-element), abscisic acid (ABRE), gibberellin (TATC-box, GARE-motif, and P-box), salicylic acid (TCA-element and SARE), and methyl jasmonate (CGTCA-motif and TGACG-motif), were present in the promoter regions of TaSnRKs.

Expression Patterns of TaSnRKs in Temporal and Spatial Variation and Different Stress Conditions

To determine the expression patterns of TaSnRKs in different tissues during different stages, 209 RNA-seq data of Azhurnaya (a hexaploid wheat variety) were analyzed (**Figure 4A**; **Supplementary Material 7**, **8**) (Ramírez-González et al., 2018). Of these, 18.81% (6 SnRK1s genes; 3 SnRK2s genes; and 26 SnRK3s genes) were not expressed due to the expression level TPM < 1. As shown in **Figure 4A**, there was no tissue-specific gene among TaSnRKs. The TaSnRKs were clustered into 15 modules according to similarity of expression patterns (**Figure 4B**). There were only four modules in SnRK1, while there were 12 modules in the SnRK3 subfamily. There were genes from all three subfamilies exhibited in modules I and V, showing the universality of these two modules. In general, the genes from

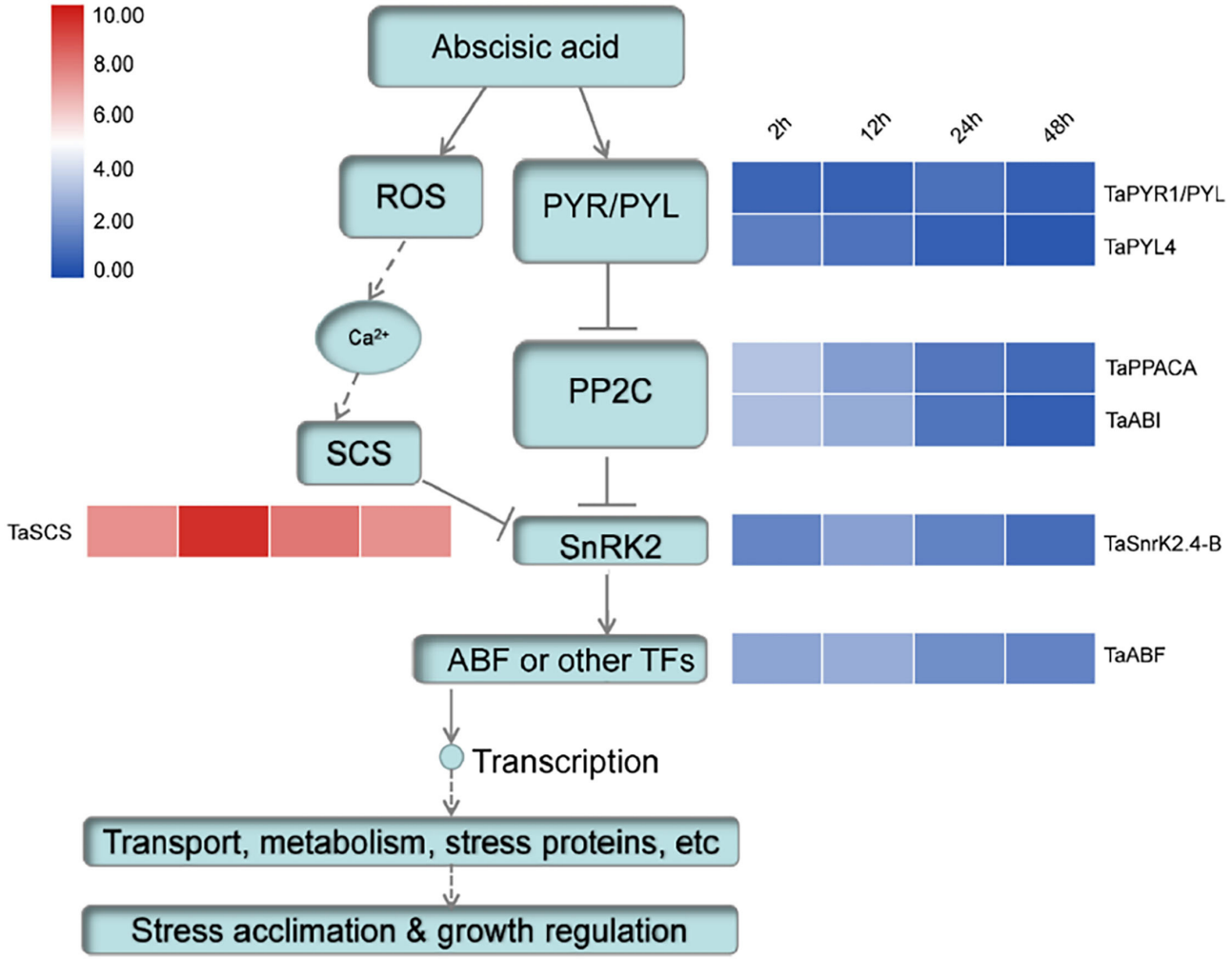

FIGURE 7 | Expression level detected by qRT-PCR of key point genes involving ABA pathway in wheat.

TaSnRK1 and TaSnRK2 subfamily were ubiquitously expressed during the whole plant life (**Figure 4C**). In addition to being generally expressed (39/127, 30.7%), the TaSnRK3 genes were also highly expressed in reproductive organ spikelets [module XIII (66/127, 60.0%) and XIV (2/127, 1.6%)], which indicated that these genes might play roles during the development of spikelet. Interestingly, most of the low or not-expressed genes (module XV) belonged to the SnRK3 subfamily (20/127, 15.7%).

To examine the responses of TaSnRKs to abiotic and biotic stresses, nine genes belonging to the three subfamilies with universal expression patterns were randomly selected (**Figure 5A**). After cold treatment for 2 weeks, the expression level of TaSnRK2.4-B was decreased. The expression pattern of TaSnRK3.16-D was similar to that of TaSnRK2.4-B. In contrast, the expression level of TaSnRK3.35-A was upregulated sharply. Under drought treatment, the expression levels of TaSnRK2.4-B, TaSnRK2.7-A, and TaSnRK3.35-A were increased significantly, which indicated that these genes might play positive roles against drought stress. The expression patterns after NaCl and ABA treatment were detected by qRT-PCR. As illustrated in **Figure 5B**, most genes were induced at 2 hours after NaCl and ABA treatment. In contrast, the expression level of TaSnRK1.1-A declined after ABA treatment.

After inoculating with powdery mildew (**Figure 5A**), the expression levels of TaSnRK2.4-B, TaSnRK2.7-A, and TaSnRK3.16-D were significantly up-regulated. In contrast, the expression level of TaSnRK3.37-D declined with infestation time. However, in qRT-PCR results (**Figure 5C**), all the genes were unexpressed on the first day after powdery mildew infection, especially TaSnRK2.4-B and TaSnRK3.37-A, of which the expression level was decreased sharply. After being inoculated with *F. graminearum*, TaSnRK1.1-A, TaSnRK2.4-B, and TaSnRK3.16-D were significantly induced on the 3rd day. Consequently, these results indicate that TaSnRKs play different roles during various treatments.

Subcellular Localization of TaSnRK2.4-B

Subcellular localization of proteins could provide clues for further functional analysis. From the previous result, TaSnRK2.4-B was predicted to be localized in the nucleus

(**Supplementary Material 2**). To validate the subcellular localization of TaSnRK2.4-B, the pART27-35S::TaSnRK2.4-B-GFP expression vector was successfully constructed and transferred into Agrobacterium GV3101. After transient expression in *N. benthamiana* leaves, the fluorescence signals of TaSnRK2.4-B-GFP was detected in the whole cell (**Figure 6A**), which was similar to the signal of blank control. This result was consistent with the localization results of its homologous genes (Zhang et al., 2016).

Transient Overexpression of TaSnRK2.4-B Reduced the ROS Level Induced by flg22

As illustrated in **Figure 6B**, the overall temporal pattern of the reactive oxygen species (ROS) burst was not affected in the transiently overexpressed leaves of TaSnRK2.4-B. Similar to vector control, the ROS level in the transiently overexpressed leaves of TaSnRK2.4-B reached its peak at 26 mins after flg22 treatment. However, the total ROS produced by transient overexpression of TaSnRK2.4-B was only 50% of that of control. This result indicates that overexpression of TaSnRK2.4-B reduced the sensitivity of *N. benthinaniana* leaves against flg22 application.

TaSnRK2.4 Can Interact With TaSCS

In Arabidopsis, AtSCS could interact with AtSnRK2 and inhibit AtSnRK2 activity (Bucholc et al., 2011; Tarnowski et al., 2019). Therefore, the interaction between TaSnRK2.4-B and TaSCS was tested by a yeast two-hybrid assay. There are 17 SCS homologous genes in wheat, and one of the closest homologs of AtSCS-A (TraesCS2D03G0940300.1) was selected (**Supplementary Material 9**). The Y2H result further confirmed that TaSnRK2.4-B could interact with TaSCS physically (**Figure 6C**).

DISCUSSION

SnRKs are highly conserved in eukaryotes and play important roles in plant development and response to various abiotic and biotic stresses (Tsai and Gazzarrini, 2012; Perochon et al., 2015; Nukarinen et al., 2016). In the present study, 149 non-redundant TaSnRK genes were identified (**Figure 1**; **Supplementary Material 2**). The number of TaSnRKs was 3.92 and 3.17 times higher than that in *Arabidopsis* and rice, respectively, which could be because of its hexaploidy and fragment replication (Mishra et al., 2021). A previous study showed that 94 proteins from 30 genes of the TaSnRK3 subfamily were identified (Sun et al., 2015). Our present study matches all these genes except TaCIPK6 because we did not retrieve its gene or CDS sequence from wheat genome data. The remaining 29 genes belonging to the SnRK3 subfamily were firstly identified in our result (**Figure 1**, **Supplementary Material 2**).

In previous studies, the SnRK2 family was sub-divided into three groups based on the expression pattern under ABA treatment. The members in Group I were not activated by ABA, and Group II SnRK2s responded weakly to ABA, whereas SnRK2s in Group III were strongly induced by ABA treatment (Zhang et al., 2016). Interestingly, we found that TaSnRK2.9-A, TaSnRK2.8-A;a, and TaSnRK2.10-A (namely TaSnRK2.9, TaSnRK2.10, and TaSnRK2.8 of Group III in Zhang's report) contained an ABA-specific box in protein (**Figure 2B**), which further proved that these three genes might play important roles in ABA signaling pathway. TaSnRK2.7 (renamed as TaSnRK2.4-D in this study), in Group I, showed no response to ABA (5 μM) (Zhang et al., 2011). However, our results showed that TaSnRK2.4-B, a triplicate gene of TaSnRK2.4-D, was significantly induced under 100 μM ABA (**Figure 6B**). Moreover, the expression level of TaSnRK2.7-A, which belonged to the same group I, was also sharply up-regulated and retained at the high level. For the inconsistent result, we speculated that it might be caused by different concentrations of ABA, and the genes in Group I could be induced by a high concentration of ABA.

Phytohormone ABA plays a significant role in plant growth and development and adaption to various stresses. SnRK2s are key positive regulators in ABA signaling (Nakashima and Yamaguchi-Shinozaki, 2013). In *Arabidopsis*, under stress conditions, ABA could activate the receptor PYR/PYL to interact with PP2Cs, which was binding with SnRK2s. Consequently, the ABA-dependent SnRK2s were released and play important regulatory roles in stomatal closure, growth, and stress response (Fujii and Zhu, 2009; Park et al., 2009). For equilibration, other proteins interact with SnRK2s to modify their activities. Previous studies showed that both AtSCS forms (AtSCS-A and AtSCS-B) could interact with SnRK2 and inhibit its activity in calcium-dependent and independent pathways (Bucholc et al., 2011; Tarnowski et al., 2019). To detect whether TaSnRK2 could interact with TaSCS, a Y2H assay was conducted. **Figure 6C** demonstrates that the TaSCS could interact with TaSnRK2.4-B. Furthermore, the expression patterns of several key genes in the ABA signaling pathway were detected. As shown in **Figure 7**, after ABA treatment, the expression level of TaPYR4 (homologous to AtPYR4) and TaPP2C (homologous to AtPP2CA and AtABI2) was continuously declined with stress time. However, expression levels of TaSnRK2.4-B and TaABF (homologous to AtABF) were increased at 12 hours. At the same time, the expression pattern of TaSCS (homologous to AtSCS-A) was consistent with that of TaSnRK2.4-B. These results indicated that the regulatory network in wheat was similar to that in *Arabidopsis*. Therefore, TaSCS probably inhibit the activity of TaSnRK2.4-B in wheat. This deduction needs further confirmation.

In contrast to the responses of TaSnRKs to abiotic stresses, the expression of all the tested genes was unexpressed on the 1st day after powdery mildew infection, especially that of TaSnRK2.4-B and TaSnRK3.37-A. This indicated that these genes may play negative roles against powdery mildew infection. To further explore the role of TaSnRK2.4-B in disease resistance, we detected the ROS burst in the *N. benthinaniana* leaves with transient overexpression of TaSnRK2.4-B after flg22 application. Flg22 is one of the typical pathogen-associated molecular patterns (PAMP) (Jones and Dangl, 2006). The plant immune system has two branches (PTI and ETI) to resist pathogen infection (Chisholm et al., 2006; Jones and Dangl, 2006). During the early stages of interaction, the plant produces a large number

of reactive oxide species (ROS) to damage and inhibit pathogen invasion (Yoshioka et al., 2009). In the present study, the total ROS produced by transient overexpression of TaSnRK2.4-B was only 50% of that of control (**Figure 6B**). This result indicated that TaSnRK2.4-B participated in the PTI pathway. Moreover, the result demonstrated that TaSnRK2.4-B might be a negative regulator in disease resistance, which can be used to improve wheat through CRISPR technology.

CONCLUSION

Wheat SnRK family genes were identified and classified into three sub-families. Transcriptomic profiling and qRT-PCR analyses indicated that the TaSnRKs played the role of multifunctional regulators responding to diversified biotic and abiotic stresses. Subcellular localization indicated that TaSnRK2.4-B existed in the whole cell. Through qRT-PCR analysis, TaSnRK2.4-B was induced after PEG, NaCl, and high concentration ABA treatment. Furthermore, it was found that TaSnRK2.4-B could interact with TaSCS and play roles in the ABA-dependent pathway. Moreover, TaSnRK2.4-B participated in the PTI pathway and might be a negative regulator in disease resistance.

DATA AVAILABILITY STATEMENT

The original contributions presented in the study are included in the article/**Supplementary Material**, further inquiries can be directed to the corresponding author/s.

AUTHOR CONTRIBUTIONS

YLi and DM designed this article. BJ, YLiu, HN, and YH directed the data analysis and manuscript writing. YLiu supervised the experiment and confirmed the manuscript. All authors contributed to the article and agreed to submit this version of the manuscript.

FUNDING

This research was supported by the Open Program of Engineering Research Center of Ecology and Agricultural Use of Wetland Ministry of Education (KFT202103), the Open Project Program of Key Laboratory of Integrated Pest Management on Crop in Central China, and Ministry of Agriculture/Hubei Province Key Laboratory for Control of Crop Diseases, Pest and Weeds (2020ZTSJJ8).

SUPPLEMENTARY MATERIAL

The Supplementary Material for this article can be found online at: https://www.frontiersin.org/articles/10.3389/fpls.2022.934226/full#supplementary-material

Supplementary Material 1 | The query SnRK protein sequences of *Arabidopsis* and rice used in this study.

Supplementary Material 2 | Primers used in this study.

Supplementary Material 3 | Information including chromosomal location, protein features, subcellular localization, and source of 186 SnRK proteins identified in wheat.

Supplementary Material 4 | Gene structure and motif patterns of all TaSnRKs.

Supplementary Material 5 | All 20 MEME motif sequences in wheat SnRK proteins.

Supplementary Material 6 | Cis-acting elements involved in stresses, growth and development, and phytohormone response in the promoter of 186 TaSnRKs.

Supplementary Material 7 | Expression profile of wheat SnRKs from RNA-seq data.

Supplementary Material 8 | The expression patterns of TaSnRKs in different tissues during different stages.

Supplementary Material 9 | Phylogenetic tree of TaSCSs.

REFERENCES

Albrecht, V., Ritz, O., Linder, S., Harter, K., and Kudla, J. T. (2001). domain defines a novel protein-protein interaction module conserved in Ca^{2+}-regulated kinases. *EMBO J.* 35, 1051–1063. doi: 10.1093/emboj/20.5.1051

Albrecht, V., Weinl, S., Blazevic, D., D'Angelo, C., Batistic, O., and Kolukisaoglu, U. (2003). The calcium sensor CBL1 integrates plant responses to abiotic stresses. *Plant J.* 36, 457–470. doi: 10.1046/j.1365-313X.2003.01892.x

Amodeo, G. A., Rudolph, M. J., and Tong, L. (2007). Crystal structure of the heterotrimer core of saccharomyces cerevisiae ampk homologue snf1. *Nature* 449, 492–495. doi: 10.1038/nature06127

Anderberg, R. J., and Walker-Simmons, M. K. (1992). Isolation of a wheat cDNA clone for an abscisic acid-inducible transcript with homology to protein kinases. *Proc. Natl. Acad. Sci. USA* 89, 10183–10187. doi: 10.1073/pnas.89.21.10183

Boudsocq, M., Droillard, M. J., Barbier-Brygoo, H., and Lauriere, C. (2007). Different phosphorylation mechanisms are involved in the activation of sucrose non-fermenting 1 related protein kinases 2 by osmotic stresses and abscisic acid. *Plant Mol. Biol.* 63, 491–503. doi: 10.1007/s11103-006-9103-1

Bucholc, M., Ciesielski, A., Goch, G., Anielska-Mazur, A., Kulik, A., Krzywi_nska, E., et al. (2011). SNF1-related protein kinases 2 are negatively regulated by a plant-specific calcium sensor. *J. Biol. Chem.* 286, 3429–3441. doi: 10.1074/jbc.M110.115535

Chen, C. J., Chen, H., Zhang, Y., Thomas, H. R., Frank, M. H., He, Y. H., et al. (2020). TBtools: an integrative toolkit developed for interactive analyses of big biological data. *Mol. Plant* 13, 1194–1202. doi: 10.1016/j.molp.2020.06.009

Chisholm, S. T., Coaker, G., and Day, B. (2006). Host-microbe interactions: shaping the evolution of the plant immune response. *Cell* 124, 803–814. doi: 10.1016/j.cell.2006.02.008

Christophe, B., Pierre-Olivier, D. F., Clara, B., Stephane, C., Jean-Marie, S., Alain, V., et al. (2006). Identification of features regulating OST1 kinase activity and OST1 function in guard cells. *Plant Physiol.* 141, 1316–1327. doi: 10.1104/pp.106.079327

Coello, P., Hey, S. J., and Halford, N. G. (2011). The sucrose non-fermenting-1-related (SnRK) family of protein kinases: potential for manipulation to improve stress tolerance and increase yield. *J. Exp. Bot.* 62, 883–893. doi: 10.1093/jxb/erq331

Feng, J., Wang, L., Wu, Y., Luo, Q., Zhang, Y., Qiu, D., et al. (2019). TaSnRK2.9, a sucrose non-fermenting 1-related protein kinase gene, positively regulates plant response to drought and salt stress in transgenic tobacco. *Front. Plant Sci.* 9, 2003. doi: 10.3389/fpls.2018.02003

Fujii, H., and Zhu, J. K. (2009). Arabidopsis mutant deficient in 3 abscisic acidactivated protein kinases reveals critical roles in growth, reproduction, and stress. *Proc. Natl. Acad. Sci. USA* 106, 8380–8385. doi: 10.1073/pnas.0903144106

Guo, Y., Halfter, U., Ishitani, M., and Zhu, J. (2001). Molecular characterization of functional domains in the protein kinase SOS2 that is required for plant salt tolerance. *Plant Cell* 13, 1383–1400. doi: 10.1105/TPC.010021

Halford, N. G., and Hey, S. J. (2009). Snf1-related protein kinases (SnRKs) act within an intricate network that links metabolic and stress signalling in plants. *Biochem J*. 419, 247–259. doi: 10.1042/BJ20082408

Hardie, D. G., Carling, D., and Carlson, M. (1998). The AMP-activated/SNF1 protein kinase subfamily: metabolic sensors of the eukaryotic cell? *Annu. Rev. Biochem*. 67, 821–855. doi: 10.1146/annurev.biochem.67.1.821

Hrabak, E. M., Catherine, W., Chan, M., Gribskov, M., Harper, J. F., Choi, J. H., et al. (2003). The Arabidopsis CDPK-SnRK superfamily of protein kinases. *Plant Physiol*. 132, 666–680. doi: 10.1104/pp.102.011999

Hu, B., Jin, J., Guo, A. Y., Zhang, H., Luo, J., and Gao, G. (2015). GSDS 2.0: an upgraded gene feature visualization server. *Bioinformatics* 31, 1296–1297. doi: 10.1093/bioinformatics/btu817

Jain, A. K. (2010). Data clustering: 50 years beyond K-means. *Pattern Recogn. Lett*. 31, 651–666. doi: 10.1016/j.patrec.2009.09.011

Jiang, C., Hei, R., Yang, Y., Zhang, S., Wang, Q., Wang, W., et al. (2020). An orphan protein of Fusarium graminearum modulates host immunity by mediating proteasomal degradation of TaSnRK1α. *Nat. Commun*. 11, 4382. doi: 10.1038/s41467-020-18240-y

Jones, J., and Dangl, J. L. (2006). The plant immune system. *Nature* 444, 323–329. doi: 10.1038/nature05286

Liu, J., Ishitani, M., Halfter, U., Kim, C. S., and Zhu, J. (2000). The Arabidopsis thaliana SOS2 gene encodes a protein kinase that is required for salt tolerance. *Proc. Natl. Acad. Sci. USA*. 97, 3730–3734. doi: 10.1073/pnas.97.7.3730

Livak, K. J., and Schmittgen, T. D. (2001). Analysis of relative gene expression data using real-time quantitative PCR and the 2(-Delta Delta C(T)) method. *Methods* 25, 402–408. doi: 10.1006/meth.2001.1262

Mao, X., Zhang, H., Tian, S., and Jing, R. (2010). TaSnRK2.4, an SNF1-type serine/threonine protein kinase of wheat (*Triticum aestivum* L.), confers enhanced multistress tolerance in Arabidopsis. *J. Exp. Bot.* 61, 683–696. doi: 10.1093/jxb/erp331

Miao, L., Mao, X., Wang, J., Liu, Z., Zhang, B., and Li, W. (2017). Elite haplotypes of a protein kinase gene TaSnRK2.3 associated with important agronomic traits in common wheat. *Front. Plant Sci*. 8, 368. doi: 10.3389/fpls.2017.00368

Miao, L. L., Zhang, L., i,. Y. Y., Zhang, H. J., Liu, H. J., and Wang, X. L. (2021). JY, et al. TaSnRK2.4 is a vital regulator in control of thousand-kernel weight and response to abiotic stress in wheat. *J. Integr. Agric*. 20, 46–54. doi: 10.1016/S2095-3119(19)62830-3

Mishra, S., Sharma, P., Singh, R., Tiwari, R., and Singh, G. P. (2021). Genome-wide identification and expression analysis of sucrose nonfermenting-1-related protein kinase (SnRK) genes in *Triticum aestivum* in response to abiotic stress. *Sci Rep*. 11, 22477. doi: 10.1038/s41598-021-99639-5

Nakashima, K., and Yamaguchi-Shinozaki, K. (2013). ABA signaling in stress-response and seed development. *Plant Cell Rep.* 32, 959–970. doi: 10.1007/s00299-013-1418-1

Nukarinen, E., Nagele, T., and Pedrotti, L. (2016). Quantitative phosphoproteomics reveals the role of the ampk plant ortholog SnRK1 as a metabolic master regulator under energy deprivation. *Sci Rep*. 6, 31697. doi: 10.1038/srep31697

Park, S. Y., Fung, P., Nishimura, N., Jensen, D. R., Fujii, H., and Zhao, Y. (2009). Abscisic acid inhibits type 2C protein phosphatases via the PYR/PYL family of START proteins. *Science* 324, 1068–1071. doi: 10.1126/science.1173041

Perochon, A., Jia, J. G., Kahla, A., Arunachalam, C., Scofield, S. R., Bowden, S., et al. (2015). TaFROG encodes a pooideae orphan protein that interacts with SnRK1 and enhances resistance to the mycotoxigenic fungus *Fusarium graminearum*. *Plant Physiol.* 169, 2895–2906. doi: 10.1104/pp.15.01056

Ramírez-González, R. H., Borrill, P., Lang, D., Harrington, S. A., and Brinton, J. (2018). The transcriptional landscape of polyploid wheat. *Science* 361, 662. doi: 10.1126/science.aar6089

Saha, J., Chatterjee, C., Sengupta, A., Gupta, K., and Gupta, B. (2014). Genome-wide analysis and evolutionary study of sucrose non-fermenting 1-related protein kinase 2 (SnRK2) gene family members in Arabidopsis and Oryza. *Comput. Biol. Chem.* 49, 59–70. doi: 10.1016/j.compbiolchem.2013.09.005

Sheen, J. (1996). Ca2+-dependent protein kinases and stress signal transduction in plants. *Science* 274, 1900–1902. doi: 10.1126/science.274.5294.1900

Sun, T., Wang, Y., Wang, M., Zhou, Li,. T. T., Wang, Y., et al. (2015). Identification and comprehensive analyses of the CBL and CIPK, gene families in wheat (*Triticum aestivum* L.). *BMC Plant Biol.* 15, 269. doi: 10.1186/s12870-015-0657-4

Tarnowski, K., Klimecka, M., Ciesielski, A., Goch, G., Kulik, A., and Fedak, H. (2019). Two SnRK2-interacting calcium sensor isoforms negatively regulate snrk2 activity by different mechanisms. *Plant Physiol.* 182, 00900. doi: 10.1104/pp.19.00900

Tian, S., Mao, X., Zhang, H., Chen, S., Zhai, C., and Yang, S. (2013). Cloning and characterization of TaSnRK2.3, a novel SnRK2 gene in common wheat. *J. Exp. Bot.* 7, 2063–2080. doi: 10.1093/jxb/ert072

Tsai, Y. L., and Gazzarrini, S. (2012). Overlapping and distinct roles of AKIN10 and FUSCA3 in ABA and sugar signaling during seed germination. *Plant Signal. Behav*. 7, 1238–1242. doi: 10.4161/psb.21549

Wang, L. Z., Hu, W., Sun, J. T., Liang, X. Y., Yang, X. Y., and Wei, S. Y. (2015). Genome-wide analysis of SnRK gene family in Brachypodium distachyon and functional characterization of BdSnRK2.9. *Plant Sci.* 237, 33–45. doi: 10.1016/j.plantsci.2015.05.008

Wang, X., Peng, F., Yang, L., i,. M., Li, L., and Expression, G. (2012). of a heterologous SnRK1 in tomato increases carbon assimilation, nitrogen uptake and modifes fruit development. *Plant Physiol*. 169, 1173–1182. doi: 10.1016/j.jplph.2012.04.013

Yan, J., Niu, F., Liu, W., Zhang, H., Wang, B., and Yang, B. (2014). Arabidopsis CIPK14 positively regulates glucose response. *Biochem. Biophys. Res.* 450, 1679–1683. doi: 10.1016/j.bbrc.2014.07.064

Yang, X. M., Ma, J., Ma, L., i,. H. B., Yao, H. X., Liu, J. B., et al. (2010). genes can be responsible for crown rot resistance at different developmental stages of wheat and barley. *Eur. J. Plant Pathol*. 128, 495–502. doi: 10.1007/s10658-010-9680-3

Yoshioka, H., Asai, S., and Kobayashi, Y. M. (2009). Molecular mechanisms of generation for nitric oxide and reactive oxygen species, and role of the radical burst in plant immunity. *Mol. Cells*. 28, 321–329. doi: 10.1007/s10059-009-0156-2

Zhang, H. Y., Mao, L., i,. W. Y., Jing, X. G., Jia, R. L., and Differential, H. F. (2016). activation of the wheat snrk2 family by abiotic stresses. *Front. Plant Sci.* 7, 420. doi: 10.3389/fpls.2016.00420

Zhang, H. Y., Mao, X., Jing, R. L., Chang, X. P., and Xie, H. M. (2011). Characterization of a common wheat (*Triticum aestivum* L.) TaSnRK2.7 gene involved in abiotic stress responses. *J. Exp. Bot.* 3, 975–988. doi: 10.1093/jxb/erq328

Zhang, H. Y., Mao, X., and Wang, C. (2010). Overexpression of a common wheat gene TaSnRK2.8 enhances tolerance to drought, salt and low temperature in *Arabidopsis*. *PLoS ONE* 5, e16041. doi: 10.1371/journal.pone.0016041

Conflict of Interest: The authors declare that the research was conducted in the absence of any commercial or financial relationships that could be construed as a potential conflict of interest.

Publisher's Note: All claims expressed in this article are solely those of the authors and do not necessarily represent those of their affiliated organizations, or those of the publisher, the editors and the reviewers. Any product that may be evaluated in this article, or claim that may be made by its manufacturer, is not guaranteed or endorsed by the publisher.

frontiers | Frontiers in Plant Science

TYPE Original Research
PUBLISHED 09 September 2022
DOI 10.3389/fpls.2022.946584

OPEN ACCESS

EDITED BY
Qiong Zhang,
University of California,
Berkeley, United States

REVIEWED BY
Claudia Martinez-Anaya,
UNAM Campus Morelos, National Autonomous University of Mexico, Mexico
Witoon Purahong,
Helmholtz Association of German Research Centres (HZ), Germany

*CORRESPONDENCE
Niels Julian Maywald
niels.maywald@uni-hohenheim.de

SPECIALTY SECTION
This article was submitted to Crop and Product Physiology, a section of the journal Frontiers in Plant Science

RECEIVED 17 May 2022
ACCEPTED 11 August 2022
PUBLISHED 09 September 2022

CITATION
Maywald NJ, Mang M, Pahls N, Neumann G, Ludewig U and Francioli D (2022) Ammonium fertilization increases the susceptibility to fungal leaf and root pathogens in winter wheat. *Front. Plant Sci.* 13:946584. doi: 10.3389/fpls.2022.946584

Ammonium fertilization increases the susceptibility to fungal leaf and root pathogens in winter wheat

Niels Julian Maywald*, Melissa Mang, Nathalie Pahls, Günter Neumann, Uwe Ludewig and Davide Francioli

Department of Nutritional Crop Physiology, Institute of Crop Science, University of Hohenheim, Stuttgart, Germany

Nitrogen (N) fertilization is indispensable for high yields in agriculture due to its central role in plant growth and fitness. Different N forms affect plant defense against foliar pathogens and may alter soil–plant-microbe interactions. To date, however, the complex relationships between N forms and host defense are poorly understood. For this purpose, nitrate, ammonium, and cyanamide were compared in greenhouse pot trials with the aim to suppress two important fungal wheat pathogens *Blumeria graminis* f. sp. *tritici* (*Bgt*) and *Gaeumannomyces graminis* f. sp. *tritici* (*Ggt*). Wheat inoculated with the foliar pathogen *Bgt* was comparatively up to 80% less infested when fertilized with nitrate or cyanamide than with ammonium. Likewise, soil inoculation with the fungal pathogen *Ggt* revealed a 38% higher percentage of take-all infected roots in ammonium-fertilized plants. The bacterial rhizosphere microbiome was little affected by the N form, whereas the fungal community composition and structure were shaped by the different N fertilization, as revealed from metabarcoding data. Importantly, we observed a higher abundance of fungal pathogenic taxa in the ammonium-fertilized treatment compared to the other N treatments. Taken together, our findings demonstrated the critical role of fertilized N forms for host–pathogen interactions and wheat rhizosphere microbiome assemblage, which are relevant for plant fitness and performance.

KEYWORDS

disease management, crop-pathogen interactions, plant-microbe interactions, nitrogen, nitrate, cyanamide, *Blumeria graminis*, *Gaeumannomyces graminis*

Introduction

The control of phytopathogenic microorganisms like *Blumeria graminis* f. sp. *tritici* (*Bgt*) and *Gaeumannomyces graminis* f. sp. *tritici* (*Ggt*) is crucial for high quality and yield stability in modern agriculture (Peng et al., 2021). Therefore, pesticides are extensively used worldwide. However, due to pesticide residues in food, in the environment, and because of threats to biodiversity, the use of synthetic chemical pesticides is increasingly criticized, and there are demands to reduce their application (Pogacean and Gavrilescu, 2009; Jacquet

et al., 2022). Organic farming represents a cultivation system that does not require synthetic chemical pesticides (Seufert et al., 2017), but the higher land use, lower product quality and reduced food supply compared to conventional farming limit its general application (Niggli et al., 2008). The development of an improved and sustainable farming system suitable to supply the growing world population with sufficient high-quality food is therefore one of the greatest challenges of this century (Giller et al., 2021; Zimmermann et al., 2021).

Mineral fertilization targeted at pathogen defense has been neglected in the recent past due to the high use of chemical pesticides. However, it has been widely shown that the addition of mineral nutrients can alter plant physiology, genetics, and plant-associated microbiota and improve plant resistance to biotic and abiotic stresses (Fernandes and Rossiello, 1995; Walters and Bingham, 2007; Geisseler and Scow, 2014; Ding et al., 2021). In this context, the focus has mostly been on the macronutrient nitrogen (N), whose uptake and utilization is the primary limiting factor for plant growth and crop yield. In most cases, nitrogen fertilization has a negative impact on plant resistance to pathogens (Sun et al., 2020). For instance, increased susceptibility to *Bgt* has been found in cereals with N fertilization (Last, 1953; Jensen and Munk, 1997).

It is known that specific forms of nitrogen can lead to different effects on plant resistance. This is attributed to many factors and is not the same for all host–parasite associations (Mur et al., 2017; Sun et al., 2020). Most of the benefits of a particular form of nitrogen have been observed in moderately susceptible or partially resistant crop varieties (Huber and Watson, 1974). The results of previous experimental studies also suggest that the source of nitrogen may be as important as the rate of application (Baker and Martinson, 1970; Huber and Watson, 1974). The infestation-influencing effect of nitrate and ammonium fertilization depends strongly on the host plant and the emerging pathogen (Sun et al., 2020). In general, it has been observed that nitrate can increase the resistance of the plant in a concentration-dependent manner. Investigations into the mechanisms behind this revealed a stronger hypersensitive response (HR) and higher pathogenesis-related (PR) gene expression (Mur et al., 2017). Elevated levels of salicylic acid (SA) were also found in nitrate fertilized plants. SA is the major pathogen defense hormone in plants against biotrophic and hemibiotrophic pathogens (Fagard et al., 2014). Nitrate also increases the production of polyamines such as spermine and spermidine, which can act as defense signals (Mur et al., 2017). Nitric oxide (NO) production and associated defense mechanisms are also nitrate-dependent. NO has been shown to be released following early basal defenses initiated by pathogen-associated microbial patterns or gene-for-gene mediated defenses (Delledonne et al., 1998; Mur et al., 2005; Chen et al., 2014). Instead, ammonium fertilization leads to reduced plant resistance to pathogens through an increase in apoplastic sugars and amino acids (Gupta et al., 2013). The availability of these N compounds could favor the spread of pathogens. Indeed, reduced HR and lower levels of NO may promote pathogen infestation (Planchet et al., 2005; Gupta et al., 2013).

Cyanamide is a classical nitrogen source that has been used mainly for its herbicidal effect, although its application can also reduce fungal diseases (Verona, 1970). Heitefuss and Brandes (1970) reported that cyanamide reduced *Bgt* infection in wheat compared to ammonium nitrate fertilization under field conditions. Despite these positive effects, cyanamide fertilization is now considered controversial, as harmful effects on humans and the environment cannot be excluded (European Chemicals Agency, 2018).

In this study, we investigated the role of nitrogen sources, including nitrate, ammonium, and cyanamide, on *Bgt* and *Ggt* infestation in winter wheat to gain insights into the plant's physical and biochemical mechanisms mediated by the interaction between nitrogen source and pathogen. To assess the impact of different N forms on the wheat root-associated microbiota, we characterized the bacterial and fungal community associated with the wheat rhizosphere using next-generation sequencing. We hypothesized that (1) mineral N fertilization in form of ammonium would increase the disease severity of foliar and soil-based fungal pathogens compared to nitrate or cyanamide fertilization, and (2) increased pathogenic susceptibility would be associated with biomass loss. In addition, we hypothesized that (3) microbial composition and structure would be affected differently by the varying forms of mineral N fertilization. The overall objective of this study was to demonstrate that the choice of nitrogen form can prophylactically suppress foliar or soil-borne pathogens, thus providing a promising alternative to chemical pesticides.

Materials and methods

Experiments with *Blumeria graminis* f. sp. *tritici*

Experimental setup

Winter wheat *Triticum aestivum* cv. Emerick (KWS Saat SE & Co. KGaA, Einbeck, Germany), which is partially resistant to *Bgt,* was maintained for 6 weeks in a greenhouse compartment at 21/18°C with a relative humidity of 70% and a photoperiod of 12 h. Per pot, two wheat plants were cultivated. Each pot contained 2 kg of a topsoil and quartz sand mixture (70:30 w:w) with the soil properties given in Supplementary Table 1. In addition, each pot was fertilized with 80 mg kg^{-1} $Ca(H_2PO_4)_2$, 150 mg kg^{-1} K_2SO_4, and 50 mg kg^{-1} $MgSO_4$. The three different nitrogen treatments, nitrate, ammonium, and cyanamide, were-fertilized with 200 mg kg^{-1} of the corresponding nitrogen source using calcium nitrate, ammonium sulfate with nitrification inhibitor (3,4-dimethylpyrazole phosphate) (NovaTec Solub 21, Compo GmbH, Münster, Germany), and calcium cyanamide (Perlka, AlzChem Group AG, Trostberg, Germany). The pots were watered by weight up to a water holding capacity (WHC) of 80% when the water holding capacity fell below 40%.

The experiment consisted of a randomized complete block design with six blocks. A block design was chosen to minimize the effect of a temperature gradient in the greenhouse. Each block contained two replicates of each treatment. After 2 weeks of cultivation, three blocks were inoculated with *Bgt*. The three uninoculated blocks were kept separated from the inoculated blocks to avoid pathogen infestation without pesticides (Supplementary Figure 1A).

Inoculum production, inoculation, and disease assessment

To produce the inoculum, 2-week-old wheat plants of the cultivar Akteur were infected by cultivating them with already heavily infected wheat plants in a growth chamber. To ensure a consistently high level of viable inoculum, old conidia were shaken off the plants 24 h before inoculation. The infected plants were then used to inoculate the experimental plants by gently dusting the *Bgt* conidia over the experimental plants. The spore density of about 400 conidia cm^{-2} was estimated by counting the number of spores per unit area on coverslips placed in the dusted area. Plants were inoculated on the 14th day after sowing. The inoculated plants were then observed daily for powdery mildew development. Visual assessment of fungal infestation was done 14, 21, and 28 days post-infection (dpi). Based on the scorings of Trommer (1989) and Bundessortenamt (2000), a scale with 10 disease severity levels ranging from 0 to 9 was established, where 0 = no infestation, 1 = 1% infestation of the leaf area, 2 = 3%, 3 = 5%, 4 = 7.5%, 5 = 10%, 6 = 17.5%, 7 = 25%, 8 = 32.5%, 9 = >40%. Then, the disease index was calculated as described in Huang et al. (2007):

$$DI = \frac{\sum_{n=0}^{n}(x \times f)}{n \times \sum_{n=0}^{n} f} \times 100,$$

where x is the disease severity degree, f the total number of leaves of each degree of disease severity and n is the highest observed degree of disease severity.

Plant analyses

The dry weight of the above-ground plant tissue was determined after 6 weeks of cultivation. The plant parts were dried at 40°C for 1 week and then weighted. Chlorophyll concentration was estimated at 21, 28, 35, and 42 days after sowing. To determine the chlorophyll concentration in the leaves, reflectometric leaf chlorophyll measurements were performed using a Minolta SPAD-502plus (Konica Minolta INC, Osaka, Japan) by measuring the last fully developed leaf three times. SPAD values were then converted into leaf chlorophyll concentration using the formula developed for wheat in Uddling et al. (2007): $[\mu g/cm^2] = 5.99 \times e^{0.0493 \times SPAD\_Value}$.

Analysis of mineral nutrients

Total nitrogen, carbon, and sulfur were determined with the Vario MAX CNS elemental analyzer (Elementar Analysensysteme GmbH, Langenselbold, Germany). For the determination of mineral nutrients, 250 mg of dried, ground shoot material was weighed in and ashed 5 h in a muffle furnace at 500°C. Afterward, the samples were dried twice on a hot plate after adding 2.5 ml HNO_3 (1:3) and then dissolved in 2.5 ml HCl (1:3). The samples were then rinsed with 12.5 ml of hot, deionized water and boiled for at least 2 min after adding 2–3 boiling stones, to convert the meta-and pyrophosphates to orthophosphates. After cooling the samples to room temperature, the solution was filled up to 12.5 ml with deionized water, shaken, and filtered through a blue ribbon filter. To measure the iron and manganese concentrations, 0.1 ml caesium chloride/lanthanum chloride buffer solution was added to 4.9 ml ash solution. For the determination of phosphate, 3 ml vanadate-molybdate reagent was added to the ash solution and filled up with HCl (1:30) to a total volume of 10 ml (Gericke and Kurmies, 1952). The potassium and calcium concentrations were measured by an ELEX 6361 flame emission photometer (Eppendorf, Hamburg, Germany). The concentrations of magnesium, iron, zinc, and manganese were determined with an ATI Unicam Solaar 939 atomic absorption spectrometer (Thermo Electron, Waltham, United States). The phosphate content was determined by measuring the absorbance at 436 nm with a U-3300 spectrophotometer (Hitachi Ltd., Tokyo, Japan).

Superoxide dismutase assay

The superoxide dismutase (SOD) assay was performed according to the method described by Beauchamp and Fridovich (1971). 100 mg of frozen plant tissue were ground in liquid nitrogen and extracted with 1.5 ml extraction buffer (25 mM HEPES (pH 7.8), 0.1 mM EDTA). After centrifugation at 10,000×*g* at 4°C for 10 min, 100 µl supernatant was added to 300 µl 62.5 mM HEPES (pH 7.8), 75 µl 1 mM EDTA, 75 µl 20 mM Na_2CO_3, 75 µl 120 mM L-methionine, 150 µl 750 µM nitro blue tetrazolium (NBT) and 225 µl 10 µM riboflavin. As a control, 100 µl extraction buffer was added to the reaction mixture instead of 100 µl supernatant. The light reaction was started by exposing the samples at 25°C with 8,000 lux. Subsequently, the absorbance was measured spectrophotometrically at 560 nm using a FLUOstar Omega microplate reader (BMG Labtech, Ortenberg, Germany). The SOD activity inhibiting the NBT reduction was calculated according to the following formula: Units of SOD = $[(A_{Control} - A_{Sample}) \sqrt{(50\%\ A_{Control})}]$. The specific SOD activity was then expressed as units of SOD per mg of total protein.

Determination of H_2O_2

The spectrophotometric determination of the hydrogen peroxide content was carried out according to Velikova et al. (2000). For this purpose, 100 mg of frozen plant tissue was ground to a powder in liquid nitrogen. The frozen powder was homogenized with 2 ml 0.1% trichloroacetic acid (w:v). After centrifugation at 12,000×*g* for 15 min, 0.5 ml of the supernatant were added to 0.5 ml 10 mM potassium phosphate buffer (pH 7.0) and 1 ml 1 M potassium iodide. The absorbance was measured spectrophotometrically at 390 nm using a FLUOstar Omega microplate reader (BMG Labtech, Ortenberg, Germany). The H_2O_2 content was calculated using a standard curve in the range of 0–120 µM H_2O_2.

Determination of total antioxidant capacity

The free radical scavenging activity of natural antioxidants was evaluated according to Brand-Williams et al. (1995). 100 mg of frozen plant tissue was ground to a powder in liquid nitrogen and extracted with 1 ml of ethanol:H_2O (1:1). After centrifugation at 4°C for 10 min at 10,000×*g*, 28 µl of the supernatant were added to 3 mM 1,1-diphenyl-2-picrylhydrazyl radical (DPPH•) ethanol solution and 944 µl ethanol. The DPPH• solution was stored at 4°C in the dark and covered with aluminum foil. Additionally, a blank was prepared containing 28 µl 3 mM DPPH• solution and 972 µl ethanol. The reaction and blank mixtures were incubated at room temperature in the dark for 10 min. Spectrophotometric determination was performed at 515 nm using a FLUOstar Omega microplate reader (BMG Labtech, Ortenberg, Germany). The decline in absorbance per sample was recorded and percentage quenching of DPPH• was calculated based on the observed decrease in absorbance using the formula: % inhibition = $[(A_0 - A_1) \div A_0] \times 100$, with A_0 the absorbance value of the DPPH• blank and A_1 the absorbance value of the sample.

Determination of total phenolics

Total phenolic content was measured according to Ainsworth and Gillespie (2007). After grinding, 20 mg frozen plant powder were added to 2 ml of ice-cold 95% methanol (v:v). Samples were incubated at room temperature for 48 h in the dark and then centrifuged at 13,000×*g* for 5 min. 100 µl of the supernatant were mixed with 200 µl 10% Folin and Ciocalteu's phenol reagent and 800 ml 700 mM Na_2CO_3. After incubation at room temperature for 2 h, the absorbance was measured spectrophotometrically at 765 nm using a FLUOstar Omega microplate reader (BMG Labtech, Ortenberg, Germany). A standard curve from 0 to 1 mM gallic acid from Sigma-Aldrich (St. Louis, United States) was conducted to determine total phenolics as gallic acid equivalents.

Determination of protein content

The total soluble protein content in the leaves was determined by the Bradford (1976) method. For this, 100 mg ground fresh leaf material were extracted with 1.5 ml of extraction buffer containing 25 mM HEPES (pH 7.8) and 0.1 mM EDTA. After centrifugation at 15,000×*g* for 15 min, 0.05 ml of the supernatant was added to 2.5 ml Bradford Reagent (Sigma-Aldrich, St. Louis, United States). After 5 min of reaction time, the absorbance was measured spectrophotometrically at 595 nm using a FLUOstar Omega microplate reader (BMG Labtech, Ortenberg, Germany). To determine the protein content, the values were calculated from a standard curve of 0 to 2 µg µl^{-1} Bovine Serum Albumin (Merck KGaA, Darmstadt, Germany).

Determination of salicylic acid by UHPLC–MS analysis

One gram of frozen leaf material per sample was ground with liquid nitrogen. For extraction, 5 ml 80% (v:v) methanol was added. The samples were treated with a Miccra D-9 homogenizer (MICCRA GmbH, Heitersheim, Germany) for 1 min and then placed into a Sonorex RK510 ultrasonic bath (BANDELIN electronic GmbH & Co. KG, Berlin, Germany) for 15 s. Subsequently, 2 ml of the suspension were centrifuged at 10,000×*g* for 5 min. 350 µl of the supernatant were added to 700 ml ultrapure water, mixed, and centrifuged again at 12,000 rpm for 5 min. The supernatant was then filtered with a Chromafil disposable filter O-20/15 MS (MACHEREY-NAGEL GmbH & Co. KG, Düren, Germany). Analytical UHPLC–MS analysis was performed on a Velos LTQ System (Thermo Fisher Scientific, Waltham, United States). Separation was achieved on a Synergi Polar 4 µm 3 × 150 mm column. The mobile phase consisted of 5% acetonitrile and 0.05% formic acid (solvent A), and acetonitrile LCMS grade (solvent B). The gradient used was: 95% A/5% B, 0–1 min; 10% A/90% B, 11–13 min; 95% A/5% B, 13.1 min; 95% A/5% B, 16 min. The flow rate was 0.5 ml min^{-1}, and the injection volume was 1 µl. The SA standard was purchased from Merck KGaA (Darmstadt, Germany). The standard was prepared in concentrations of 0.1, 0.5, 1.0 mg L^{-1} with water/acetonitrile (70:30 v:v). Phytohormone content in µg g^{-1} was calculated using the formula: Phytohormone content [µg g^{-1}] = $\frac{\left[x\frac{\mu g}{mL}\times\left(\frac{1050\,\mu L}{350\,\mu L}\right)\times 5mL\right]}{initial\ weight\,(1g)}$.

Experiments with *Gaeumannomyces graminis* f. sp. *tritici*

Experimental setup

The greenhouse experiment with *Ggt* was conducted with the same winter wheat variety and the same temperature, lighting, and humidity settings as described in the previous experiment. Here, a fully randomized design with three replicates for each treatment was chosen (Supplementary Figure 1B). The soil used was a clayey loam derived from an Ap horizon of a long-term organically cultivated field site at the Hohenheim University agricultural research station Kleinhohenheim, Germany. Soil properties are listed in Supplementary Table 2. The soil was mixed with 30% (w:w) quartz sand to improve soil texture and facilitate root collection. After sieving the soil through a 5 mm mesh, it was fertilized with 80 mg kg^{-1} $Ca(H_2PO_4)_2$, 150 mg kg^{-1} K_2SO_4, 50 mg kg^{-1} $MgSO_4$, and 200 mg kg^{-1} N of the three respective nitrogen forms calcium nitrate, ammonium sulfate, and calcium cyanamide. Additionally, non-nitrogen-fertilized soil was used as a control. The soil was then inoculated with *Ggt*, and 2 kg of soil were filled in each pot. The pots were inserted into a cooling system designed to regulate the root zone temperature of plants. The root zone temperature was set to 12°C to provide optimal conditions for *Ggt* infection.

The filled pots were kept moist at 70% WHC without plants for 2 weeks. Before planting, seeds were surface-sterilized by rinsing them in 10% H_2O_2 solution for 20 min. They were then stored overnight in an aerated 10 mM $CaSO_4$ solution at 25°C in the dark. The next day, the seeds were placed on filter paper soaked with 4 mM $CaSO_4$ solution. After 3 days of germination,

the seedlings were transferred to the soil-sand substrate. Plants were cultivated for 4 weeks at 70% WHC and irrigated every other day. The day before harvest, irrigation of the plants was stopped to facilitate the separation of rhizosphere soil (RS) from bulk soil. Roots with adhering soil were gently separated from the bulk soil by hand agitation or mechanical shaking (Gouzou et al., 1993). The RS was then collected by mechanical shaking and careful separation of sticky soil from the roots. The soil samples were immediately frozen in liquid nitrogen and stored at −80°C. The pH of the RS was measured in 0.01 M $CaCl_2$. After visual scoring of the roots, plant parts were dried separately at 40°C for 1 week and then weighted.

Inoculum production, inoculation, and disease assessment

The fungal strain *Gaeumannomyces graminis* var. *tritici* (DSM 12044) from the Leibniz Institute DSMZ (Braunschweig, Germany) was cultivated on potato dextrose agar plates for 18 days at 25°C until the plates were completely covered with the fungus. The soil was inoculated with 2 cm agar disks (10 per kg soil) by mixing them homogeneously into the soil-sand substrate. After harvesting, the roots were examined under a stereoscopic microscope (25× magnification) for intense vascular discoloration, a major characteristic of *Ggt*. The percentage of *Ggt* infected roots was estimated by counting the wheat plants' discolored and non-discolored primary roots.

DNA extraction, amplicon library preparation, and sequencing

DNA extraction from the collected rhizosphere samples was performed using the DNeasy PowerLyzer PowerSoil Kit (Qiagen). The universal primer pair 27F/536R, which targets the V1-V3 region of the bacterial 16S rRNA gene was used to characterize the entire bacterial community (Weisburg et al., 1991; Leser et al., 2002). The primer pair ITS3/ITS4 was used to amplify the fungal internal transcribed spacer (ITS) rRNA region (White et al., 1990). PCR amplifications were performed in triplicate with a total volume of 50 µl reaction mix containing 1 µl of soil DNA template, 25 µl GoTaq G2 Master Mix (Promega, Mannheim, Germany), and 1 µl of each primer (25 µM). Amplicons were sequenced on an Illumina MiSeq instrument with 2 × 300 base pair kits by Eurofins Genomics Europe Sequencing (Constanz, Germany). Demultiplexing was performed with Illumina bcl2fastq 2.17.1.14 software following clipping of barcode and sequencing adapters. Reads with quality score of <20 were removed. DADA2 pipeline was used to determine amplicon sequence variants (ASV) from the raw sequences (Callahan et al., 2016). For bacterial sequences, forward and reversed reads were truncated at 270 and 140 bp, respectively. For fungal reads, forward and reversed reads were truncated at 260 and 160 bp, respectively. Alpha diversity metrics were calculated from the normalized sequence library, which was rarefied to 20,000 reads per sample for both microbial groups (bacterial and fungal samples). Rarefaction curve for both microbial groups reached plateau, indicated the sequencing depth was adequate (Supplementary Figure 2). Only ASVs that were detected in more than two samples were included in the data analyses. Bacterial 16S ASV representative sequences were classified using the naive Bayesian classifier (Wang et al., 2007) for Silva 138. Representative sequences for fungal ITS ASVs were classified using the naive Bayesian classifier (Wang et al., 2007) against Unite 8.3 reference database (Nilsson et al., 2019). All sequences were submitted to the European Nucleotide Archive (study accession numbers PRJEB52826 for bacterial and PRJEB52827 for fungal data).

Statistics

Statistical analyses were performed using R version 4.1.1 (2021-08-10). The comparison of means was statistically analyzed with a two-factorial ANOVA followed by a Tukey's HSD *post hoc* test ($p < 0.05$ significance level). Unless otherwise stated, data are presented as means ± SE. Normal distributions and variance homogeneities were checked by the Shapiro–Wilk test and by Levene's test, as well as graphically against the predicted values by QQ-plots, histograms, and graphs of the residuals. If the normal distribution was not given, the data were transformed by taking the inverse of it. A "letter display" was used to visualize statistically significant differences in the means.

Differences in bacterial and fungal ASVs richness were compared using ANOVA followed by a Tukey's HSD *post hoc* test. To assess differences in the bacterial and fungal microbiota structure between the different fertilization treatments, we first calculated Bray–Curtis dissimilarities using square-root transformed relative abundances (Hellinger transformation; Legendre and Gallagher, 2001). Permutational multivariate analysis of variances (PERMANOVA) based on the Bray–Curtis dissimilarity index was performed to analyze the effect of different N forms applications on the bacterial and fungal community structure, using 999 permutations for each test. Principal coordinates analysis (PCoA) based on the Bray–Curtis dissimilarity index was used to visualize the distribution of microbial community patterns in relation to the fertilization treatments. Linear discriminant analysis effect size (LEfSe) was applied to identify biomarker taxa explaining differences between the microbiota in the different N fertilization treatments (Segata et al., 2011).

Results

Leaf infection with *Blumeria graminis* f. sp. *tritici* and disease symptoms of powdery mildew

Plant performance with different N-fertilizers and *Bgt* infection

To determine whether fertilization with a specific N form and *Bgt* infection affected the plant performance, the dry weight and

chlorophyll concentration of the plants were examined. *Bgt* infection led to a reduction in dry weight in ammonium-fertilized plants, but not in nitrate-and cyanamide-fertilized plants. Overall, cyanamide-fertilized plants showed a lower plant dry weight than nitrate- and ammonium-fertilized plants (Figure 1A). After about 2 weeks of *Bgt* infestation, the chlorophyll concentration of the plants in the ammonium- and cyanamide-fertilized plants started to decrease gradually after *Bgt* infection. The chlorophyll concentration of plants fertilized with nitrate was lower than with the other fertilizers, but remained unaffected by *Bgt* inoculation throughout the study period (Figure 1B).

Leaf disease symptoms by *Bgt* infection depend on nitrogen form

Bgt infestation of wheat plants fertilized with different N forms was evaluated by visual assessment of the leaves. In this context, the disease index was calculated and, together with leaf images, the disease outbreak was documented. Tremendous differences were found between the fertilizer treatments 14 days post-infection (dpi). While nitrate-fertilized wheat plants showed hardly any visual disease symptoms, ammonium-fertilized leaves were already heavily infected. Microscopic analysis showed the presence of mycelium and conidial chains on these leaves. In addition, visual inspection indicated that cyanamide-fertilized leaves were less infected than ammonium-fertilized leaves (Figure 2). The disease index varied in all three fertilizer treatments 14 days after inoculation and gradually increased in ammonium- and nitrate-fertilized plants. Ammonium-fertilized leaves were nearly entirely covered with mycelium at 28 dpi, while nitrate-fertilized leaves were, by contrast, at a very low infection level. Ammonium fertilization increased the disease severity by 80% compared to nitrate fertilization and by 77.5% compared to cyanamide fertilization at 28 dpi. In cyanamide-grown plants, the disease index barely increased over time and at 21 and 28 dpi, and no differences to nitrate-fertilized plants were observed (Table 1).

Analysis of mineral nutrients

Wheat leaves were analyzed for important macro-and micronutrients after 28 dpi to determine the nutritional status of the plants under control conditions and *Bgt* infection. Nitrate-fertilized plants had slightly lower nitrogen concentrations in comparison with cyanamide-fertilized plants, but nitrogen status was in all treatments above the critical value of 4.4% N (Justes et al., 1994), indicating no N deficiency. Regardless of *Bgt* infection, higher calcium concentrations were encountered in nitrate-fertilized plants compared to ammonium- and cyanamide-fertilized plants. Plants fertilized with ammonium had the highest P concentrations compared to the other fertilizations under non-infected conditions. With *Bgt* infection, nitrate-fertilized plants had higher magnesium and manganese concentrations, although all nutrients were at sufficiency levels (Bergmann, 1983). The fertilization regime and *Bgt* infection had no effect on the concentrations of carbon, sulfur, potassium, iron, and zinc (Supplementary Table 3).

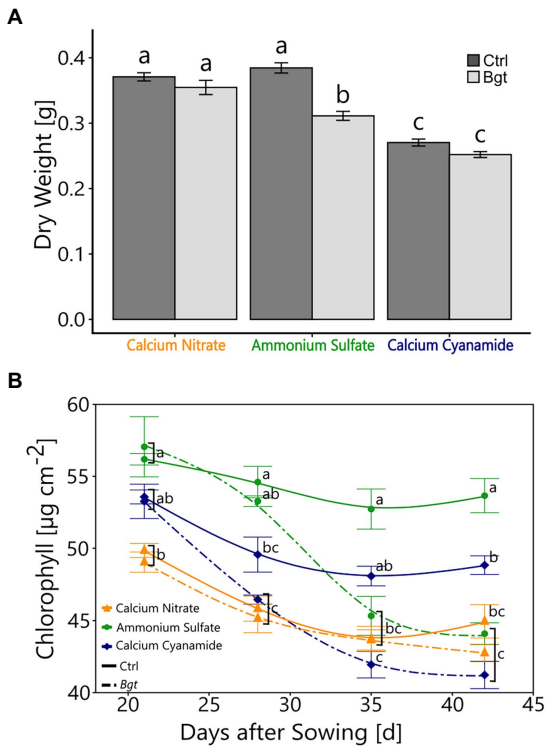

FIGURE 1
Plant performance with different N fertilizers and *Bgt* infection. **(A)** Plant dry weight (g) of winter wheat plants 28 days post-infection. **(B)** Chlorophyll content (µg cm^{-2}) of winter wheat plants 21, 28, 35, and 42 days after sowing, treated with different nitrogen forms (calcium nitrate, ammonium sulfate, calcium cyanamide) under control conditions and *Bgt* infection. Data represent mean values of three biological replicates±SE. The different lowercase letters indicate significant differences at 0.05 probability level according to Tukey multiple comparison test.

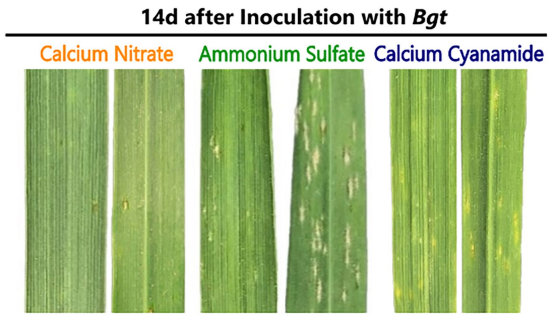

FIGURE 2
Powdery mildew infestation on the upper (left) and lower (right) surface of winter wheat leaves when fertilized with calcium nitrate, ammonium sulfate, or calcium cyanamide, 14 days (d) after *Bgt* infection.

Defense-related compounds with different N-fertilizer and *Bgt* infection

To gain insight into plant defense during pathogen infection, key defense-related compounds, including hydrogen peroxide

TABLE 1 Disease index of powdery mildew on winter wheat cultivar Emerick treated with different nitrogen forms (calcium nitrate, ammonium sulfate, calcium cyanamide) at 14, 21, 28 days post-infection (dpi).

Nitrogen fertilization	Powdery mildew (*Bgt*)		
	Disease index		
	14 dpi	21 dpi	28 dpi
Calcium nitrate	0a	4.44a	17.78a
Ammonium sulfate	44.44c	60b	88.89b
Calcium cyanamide	15.56b	15.56a	20a

Data represent mean values of three biological replicates ± SE. The different lowercase letters indicate a significant difference at 0.05 probability level according to Tukey multiple comparison test.

(H_2O_2) concentration, antioxidant potential, superoxide dismutase (SOD) activity, and salicylic acid concentration, were determined. Here, the leaf hydrogen peroxide concentration increased by 77% (nitrate) and 29% (ammonium) compared to the non-infected controls. However, no differences were measured in calcium cyanamide-fertilized plants with or without *Bgt* infection. Nevertheless, calcium cyanamide-fertilized plants tended to have higher leaf hydrogen peroxide concentrations under control conditions (Figure 3A). SOD activity was higher in *Bgt* infected, nitrate-fertilized plants, while ammonium-and cyanamide-fertilized plants infected with *Bgt* showed no differences in SOD activity compared to their respective non-infected controls (Figure 3C). For all fertilizer treatments, the antioxidant potential was consistently higher in *Bgt* infected plants (Figure 3B). Interestingly, plants infected with *Bgt* showed 42% and 162% higher salicylic acid concentrations with ammonium and cyanamide. In contrast, salicylic acid was not increased in nitrate-fertilized *Bgt* infected plants and was lower overall compared to the other fertilizer treatments (Figure 3D). Total protein and total phenolics were independent of fertilizer and *Bgt* infection (Supplementary Figure 3).

Experiments with *Gaeumannomyces graminis f.* sp. *tritici (Ggt)*

Plant performance and root disease infestation by *Ggt*

The performance of *Ggt*-infested plants fertilized with different N forms as well as without N was determined by measuring root and shoot dry weight. In line with our expectations, wheat plants without additional N fertilizer had lower shoot dry weight in comparison with the ones fertilized with different N forms at 28 days after sowing, but shoot dry weight was similar with all different N forms (Figure 4A). By contrast, the root dry weight was higher when plants were not N-fertilized, compared to nitrate-or ammonium-fertilized plants (Figure 4B).

Ggt infestation was determined by visual assessment of take-all infested roots and determination of the relative abundance of *Ggt* in the wheat rhizosphere. Plants fertilized with ammonium were found to have a high infestation of take-all, indicated by a 75% discoloration of the primary roots. A lower infestation of 46% and 37% of *Ggt* infected roots was observed in nitrate-fertilized plants and plants without N fertilization, respectively. Cyanamide-fertilized plants were the least infected, with 24% of the primary roots being discolored (Figure 4C). In addition, a higher relative abundance of *Ggt* in the rhizosphere was observed in the ammonium treatment as shown by the amplicon sequencing data. In other treatments, the relative abundance of *Ggt* in the rhizosphere was similarly low (Figure 4D).

The pH of the rhizosphere was 6.73 without N fertilization, 6.81 with nitrate and 6.13 with ammonium, while cyanamide raised pH to 7.12 (Supplementary Table 4).

Microbial composition of the wheat rhizosphere

Metabarcoding was used to obtain information on bacterial and fungal communities and their composition in the rhizosphere of wheat. A total of 606,069 16S bacterial and 557,603 ITS fungal high-quality reads were recovered from the 12 rhizosphere samples, which clustered into 1,914 bacterial and 518 fungal amplicon sequence variants (ASVs). Overall, bacterial sequences were affiliated with 22 phyla (Supplementary Figure 4), 61 classes, 131 orders, 188 families, and 301 genera. Actinobacteriota were the most abundant phylum, comprising ~36.7% of the total bacterial reads (603 ASVs), followed by Proteobacteria (24.7% of reads; 419 ASVs) and Chloroflexi (10.2%, of reads; 237 ASVs). The most abundant bacterial genera detected across all soil samples were *Nocardioides* (3.8%), KD4-96 (3.4%), *Bradyrhizobium* (2.4%), *Gemmatimonas* (2.2%) and *Flavobacterium* (2.2%). The fungal sequences were associated with 8 phyla (Supplementary Figure 5), 28 classes, 70 orders, 127 families, and 130 genera. Ascomycota (92.7% of reads; 382 ASVs) was the dominant fungal phylum, followed by Basidiomycota (3.7% of reads; 55 ASVs), and Mucoromycota (1.9% of reads; 15 ASVs). Each of the other fungal phyla represented <1%. *Fusarium*, *Blumeria,* and *Cladosporium* were the most abundant genera identified in this study, accounting for 11.8%, 5.7%, and 4.3%, of the total fungal reads, respectively.

Effect of N fertilizer form on the bacterial and fungal alpha and beta diversity

To investigate the effect of N fertilization on the bacterial and fungal communities associated with the wheat rhizosphere, we first calculated the observed richness and Bray–Curtis dissimilarity as proxies for alpha and beta diversity metrics, respectively, for both microbial groups. Bacterial richness ranged from 720 to 969 ASVs and it did not differ among the four fertilization N treatments (Figure 5A). Likewise, bacterial community structure was not affected by N application and N form (PERMANOVA; $F = 1.042$; $p = 0.263$). At a higher taxonomic level, no differences in the proportion of the main bacterial classes were observed among N treatments (Figures 5B,C). Fungal richness ranged from 161 to 312 ASVs and it was higher in soil

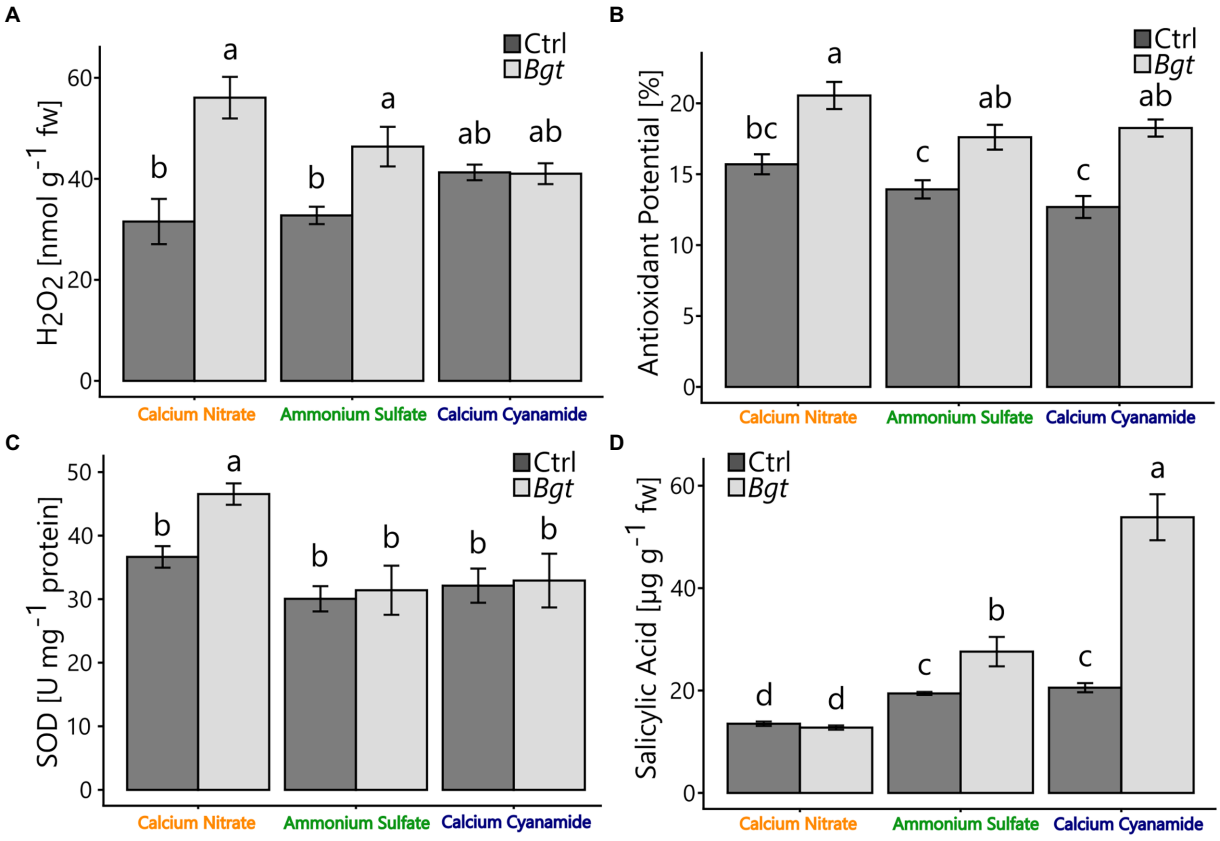

FIGURE 3
(A) Hydrogen peroxide (H_2O_2) (nmol g^{-1} fw), **(B)** antioxidant potential (%), **(C)** superoxide dismutase (U mg^{-1} protein), and **(D)** endogenous concentrations of salicylic acid (µg g^{-1} fw) of winter wheat plants after 28dpi treated with different nitrogen forms (calcium nitrate, ammonium sulfate, calcium cyanamide) under control conditions (black bars) and *Bgt* infection (gray bars). Data represent mean values of three biological replicates±SE. The different lowercase letters indicate significant differences at 0.05 probability level according to Tukey multiple comparison test.

without any fertilization and in the ammonium treatment, while the soil amended with nitrate showed the lowest value in richness (Figure 6A). Fungal community structure was affected by N fertilizer (PERMANOVA; $F = 1.977$, $p = 0.004$), which accounted for 42.6% of community variation. Principal coordinate analysis (PCoA) confirmed the notable effect of differential N forms on fungal community structure, displaying a clear separation of the different N treatments along with both coordinates, which together explained more than 40% of the variation (Figure 6B).

Compositional shifts in fungal, but not bacterial, community assembly by N fertilizer

To better understand how microbial community assembly was affected by the application of the different N forms, we sought to explore the composition and structure of the wheat rhizosphere microbiota. Looking at the bacterial community associated with the four N treatments, we observed that they were dominated by the same bacterial groups across different taxonomic ranks (Figure 5C). Indeed, the unique ASVs detected in each N treatment accounted for a marginal proportion of sequences (Supplementary Figure 6), while more than 80% of the total bacterial sequences were found in all treatments (Supplementary Figure 7). Many of these shared ASVs were affiliated with several representative families and genera (>1% abundance), most of which did not show abundance shifts across N treatments (Supplementary Figure 7). Furthermore, only a handful of low representative taxa were found as indicative biomarkers of the four fertilization treatments (Supplementary Figure 8). Overall, these findings indicated high similarities in bacterial community composition and structure among N treatments, corroborating the results obtained by beta diversity analysis.

Contrarily to the bacteria, the differences observed in fungal beta diversity between the four N treatments were reflected by substantial shifts in the abundance of several fungal taxonomic groups (Figure 6C; Supplementary Figure 9). Linear discriminant analysis (LDA) effect size (LEfSe) further confirmed these observations, identifying 26 fungal biomarker taxa associated with the different N forms applied (Figure 7; Supplementary Figure 10). For instance, enrichments within the Ascomycota groups Sordariomycetes (class) and Capnodiales (order) characterized the nitrate-fertilized samples. On the other hand, cyanamide fertilization increased the abundance of taxa affiliated with the Mucoromycota phylum and the Agaricales order (Basidiomycota). The fungal community identified in ammonium-fertilized soil was represented by a higher proportion of members within the

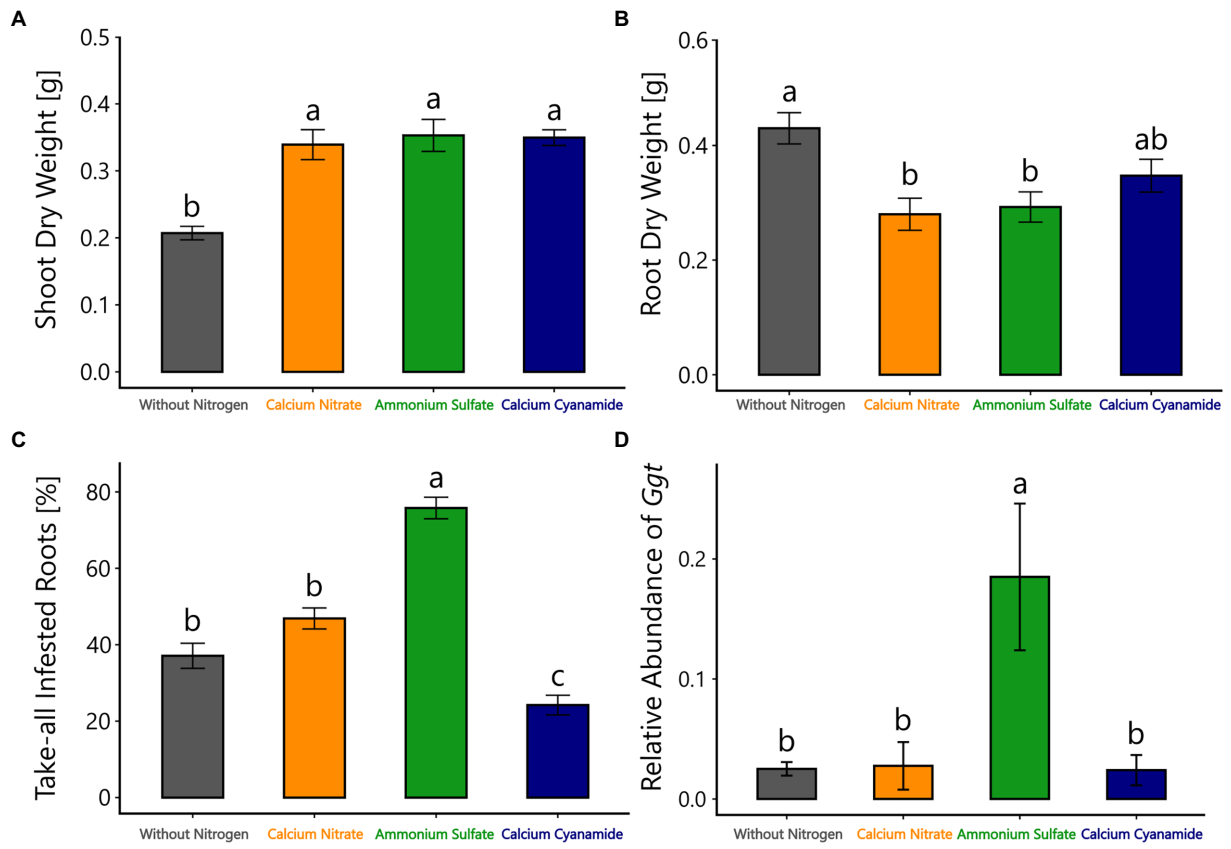

FIGURE 4
(A) Shoot and **(B)** root dry weight (g), **(C)** take-all infested roots (%), and **(D)** relative abundance of *Ggt* in the rhizosphere of winter wheat from the amplicon sequencing data, 28 days after sowing, treated with different nitrogen forms (without nitrogen, black bar; calcium nitrate, orange bar; ammonium sulfate, green bar; calcium cyanamide, blue bar) under *Ggt* infection. Data represent mean values of three biological replicates±SE. The different lowercase letters indicate significant differences at 0.05 probability level according to Tukey multiple comparison test.

Ascomycota class Leotiomycetes and Magnaporthales order. At a finer taxonomic ranking, we observed increased abundance of fungal groups associated with the Ascomycota genera *Fusarium* and *Cladosporium* in nitrate-fertilized soil. Conversely, the Ascomycota genera *Clonostachys*, *Periconia,* and *Tolypocladium*, together with the Basidiomycota genus *Hypholoma* were found as biomarkers for the cyanamide treatment. Intriguingly, we found that ammonium fertilization promoted the build-up of fungal pathogens affiliated to the genera *Blumeria* and *Gaeumannomyces*, as they were more abundant in this fertilization treatment compared to the others. Notably, the mean abundance of the genus *Gaeumannomyces* was approximately six times higher in the ammonium treatment than in the other N fertilized soils (Figure 4D), reflecting the higher root infection rate observed in this treatment (Figure 4C). Finally, fungal taxa associated with the Basidiomycota family Strophariaceae were found as a biomarker for the treatment without N fertilization.

Discussion

In this study, we investigated the interaction between N forms (nitrate, ammonium, and cyanamide) and two economically important specialist fungal pathogens: an obligate biotroph, *B. graminis* f. sp. *tritici* and a soil-borne necrotroph, *Gaeumannomyces graminis* f. sp. *tritici*. We conducted greenhouse experiments in which wheat was deliberately inoculated with these pathogens. This allowed us to examine winter wheat plants' growth and key metabolite defense reactions during pathogen interaction. Our findings highlighted that wheat leaves inoculated with the foliar pathogen *Bgt* were comparatively less infested when fertilized with nitrate or cyanamide than with ammonium. Likewise, soil inoculation with the fungal pathogen *Ggt* revealed a higher percentage of infected roots in ammonium-fertilized plants. Additionally, metabarcoding data revealed that bacterial communities were merely affected by N fertilization, whereas the fungal community assemblage was differently shaped by N fertilization type. Specifically, we observed a dramatic increase in the abundance of fungal pathogens associated with cereal crop diseases along with ammonium fertilization. Overall, our study demonstrates that particular N fertilization treatments could select, promote or reduce specific groups of beneficial or detrimental soil microorganisms, and give indications that ammonium fertilization facilitates the build-up of plant pathogens in winter wheat.

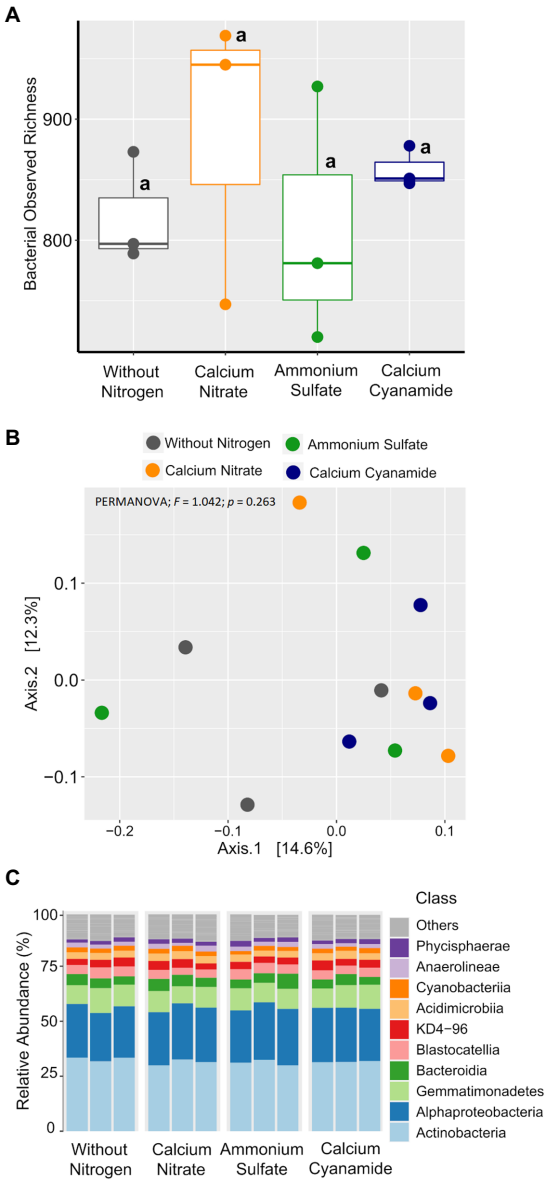

FIGURE 5
Box plots of the bacterial observed richness. **(A)** Principal coordinates analysis (PCoA) based on Bray–Curtis dissimilarity. **(B)** Colors: without nitrogen, black; calcium nitrate, orange; ammonium sulfate, green; calcium cyanamide, blue. Effects of N fertilization were tested with PERMANOVA (based on Hellinger transformed data and the Bray–Curtis distance measure). **(C)** Mean relative abundance of the main classes of the bacterial communities detected. The same lowercase letters indicate no significant differences at 0.05 probability level according to Tukey multiple comparison test.

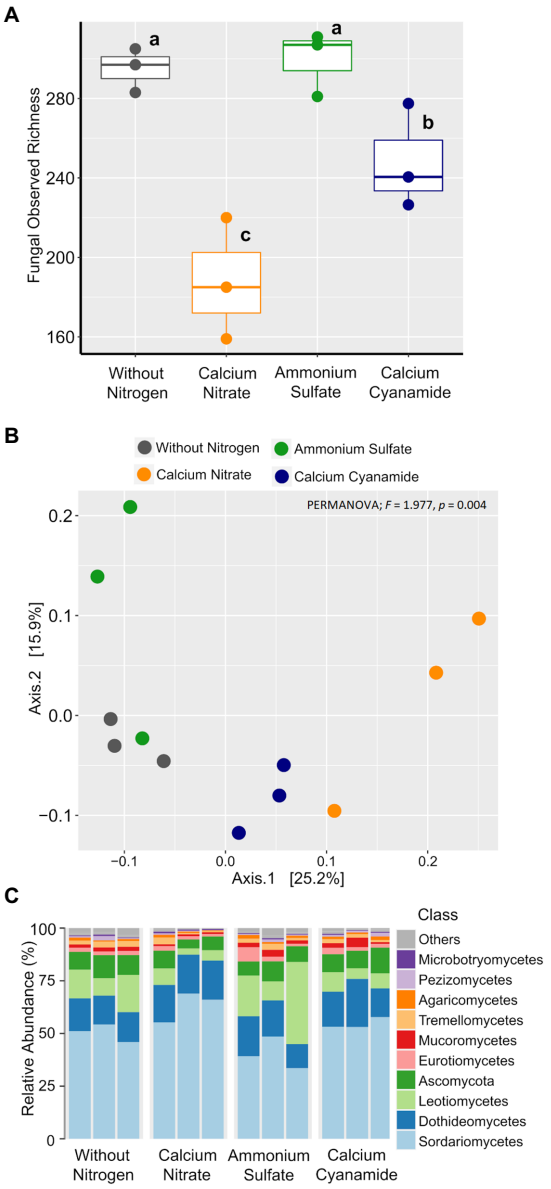

FIGURE 6
Box plots of the fungal observed richness. **(A)** Principal coordinates analysis (PCoA) based on Bray–Curtis dissimilarity. **(B)** Colors: without nitrogen, black; calcium nitrate, orange; ammonium sulfate, green; calcium cyanamide, blue. Effects of N fertilization were tested with PERMANOVA (based on Hellinger transformed data and the Bray–Curtis distance measure). **(C)** Mean relative abundance of the main classes of the fungal communities detected. The different lowercase letters indicate significant differences at 0.05 probability level according to Tukey multiple comparison test.

Ammonium fertilization increased wheat's susceptibility to *Bgt*, while nitrate and cyanamide fertilization could reduce the disease infestation

N fertilization in the form of ammonium made the plant most susceptible to *Bgt* infection (Table 1; Figure 2). Besides the visual scoring of the plant's disease severity, also leaf chlorophyll concentration, a common indicator of healthiness and plant-pathogen interactions (Rolfe and Scholes, 2010; Li et al., 2017; Yang and Luo, 2021), decreased after 3 weeks of infection (Figure 1B). Additionally, the *Bgt* infection resulted in lower dry weight (Figure 1A), confirming that ammonium-fertilized plants suffered severe pathogen infestation. The higher susceptibility of

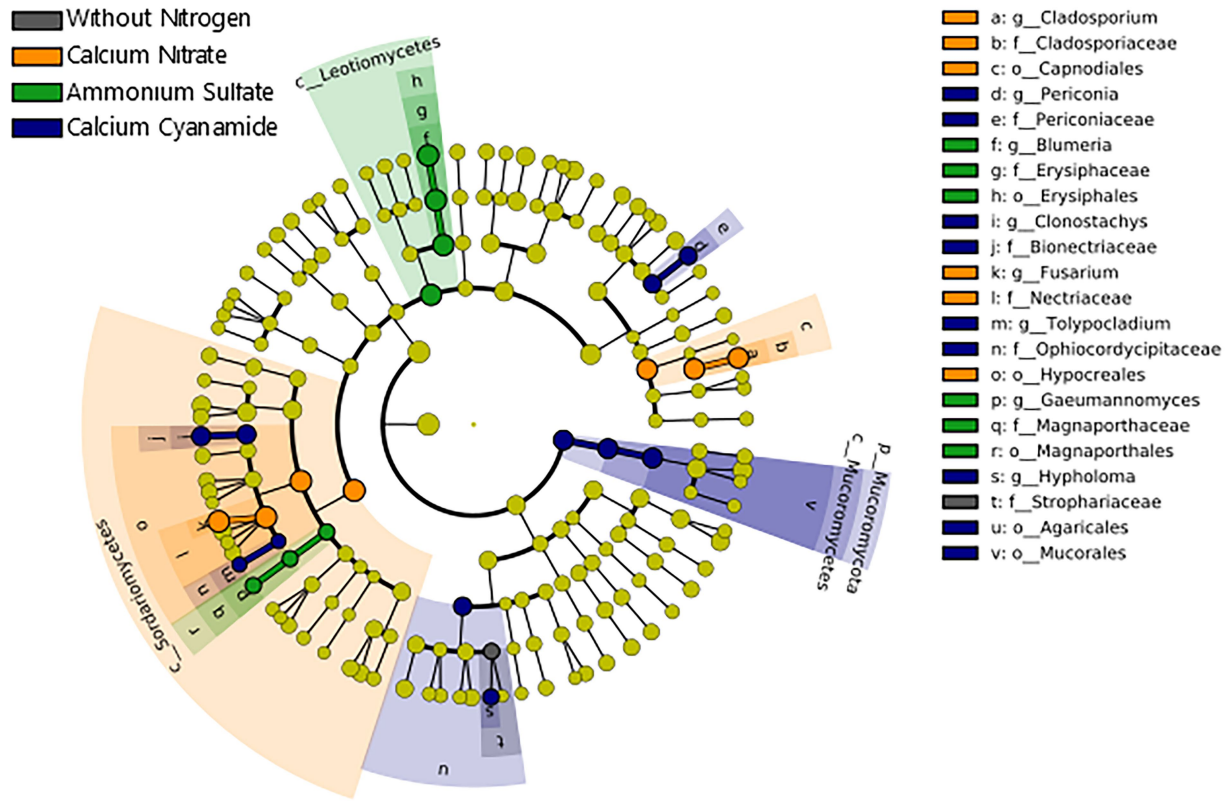

FIGURE 7
Cladogram illustrating the taxonomic groups explaining the most variation among the fungal taxa. Each ring represents a taxonomic level, with phylum (p_), class (c_), order (o_), family (f_), and genus (g_) emanating from the center to the periphery. Each circle is a taxonomic unit found in the dataset, with circles or nodes shown in colors (other than yellow) indicating where a taxon was significantly more abundant. Black: without nitrogen, orange: calcium nitrate, green: ammonium sulfate, blue: calcium cyanamide.

ammonium-fertilized shoots could result from the overall highest chlorophyll concentrations measured in ammonium-fertilized leaves in early infection stages. The resulting leaf metabolism might be more favorable for leaf pathogens. Defense-related metabolites or enzymatic activities were affected in ammonium-fertilized plants infected with *Bgt* and showed an increase in H_2O_2, antioxidant potential, and SA (Figure 3). Only SOD activity was not enhanced in infected plants. Overall, ammonium-fertilized plants apparently defended themselves against the pathogen attack, but this did not alter their susceptibility. In the literature, ammonium fertilization is often associated with increased susceptibility to various pathogens (Bolton and Thomma, 2008; Mur et al., 2017). This was attributed to reduced NO levels, as nitrate reductase (NR) is inactive without nitrate (Planchet et al., 2005). *Bgt* spread on the leaf surface could also be enhanced by higher P concentrations that we measured in ammonium-fertilized plants (Supplementary Table 3). Leaf pathogens, like *Bgt*, are known to take advantage of nutrients released into the apoplast of epidermal cell walls (Mustafa et al., 2016). The higher leaf P concentrations can be attributed to decreased rhizosphere/soil pH, resulting from nitrification and the intentional release of protons in exchange for ammonium by the root (Grunes et al., 1958; Riley and Barber, 1971).

The fertilization of nitrate resulted in the lowest *Bgt* infestation compared to the other fertilizer treatments (Figure 2). Besides the low visual scoring of the plant's disease severity, chlorophyll concentration and dry weight (Figure 1A) did not decrease between control and inoculated plants (Figure 1B). Nevertheless, leaves of nitrate-fertilized plants generally had lower chlorophyll concentrations than leaves of plants fertilized with the other N fertilizers. This can be attributed to the slightly lower percentage of N measured in the leaves of nitrate-fertilized plants (Supplementary Table 1), which is highly correlated with the chlorophyll concentration (Bojović and Marković, 2009). A lower nitrogen concentration in the plant is frequently related to a higher tolerance against leaf pathogens and could be an explanation for the lower infestation rate (Huber and Watson, 1974; Sun et al., 2020). Furthermore, nitrate-fertilized shoots exhibited an enhanced defense response after contact with the pathogen, as evidenced by elevated H_2O_2 concentration, SOD activity, and antioxidant potential (Figure 3). Especially H_2O_2 is locally needed at the infection site to promote pathogen defense *via* the oxidative burst (Bolwell, 1999; Apel and Hirt, 2004; Shetty et al., 2007). H_2O_2 is required for polysaccharide-protein cross-linking and lignification, processes involved in fungal penetration defense (Shetty et al., 2007). Also, H_2O_2 is produced during the oxidative deamination of

polyamines by a series of amine oxidases (Cona et al., 2006). Gupta et al. (2013) detected high levels of polyamides in nitrate-fertilized plants, which increased hypersensitive response-associated resistance in cereals against *B. graminis* (Cowley and Walters, 2002a,b). Additionally, various enzymatic and non-enzymatic detoxification mechanisms protect the surrounding cell areas from oxidative stress and are regulated by nitrogen nutrition (Sun et al., 2020). Though nitrate promotes the formation of protective substances in the plant in presence of the pathogen to resist the *Bgt* infestation, we observed low levels of SA in nitrate-fertilized control and infected plants (Figure 3D). This might partially be explained by the low level of *Bgt* infection with nitrate. Additionally, higher concentrations of the nutrients Mg, Mn, and Ca were found with nitrate (Supplementary Table 2), potentially due to charge balance requirements. While the role of Mg on plant diseases is mainly *via* indirect mechanisms, no direct effects on *Bgt* infection are known (Huber and Jones, 2013). In contrast, as a cofactor of the SOD, Mn participates in the plant's defense against oxidative stress and additional fertilization of Mn can reduce the infection of *Bgt* in wheat (Colquhoun, 1940). Higher Ca concentrations can be partially explained by the fertilization of nitrate in form of calcium nitrate. Nevertheless, cyanamide was also applied as calcium cyanamide and showed lower concentrations of leaf *Ca.* Higher concentrations of Ca in the shoot tissue, especially in pectin fractions of the cell wall, may also help the plant to resist against pathogens. Ca^{2+} sensors and their target proteins are part of defense-signaling pathways that interact downstream with effectors that modulate numerous biochemical and cellular functions in pathogen defense responses (Zhang et al., 2014).

N fertilization in form of cyanamide decreases the *Bgt* infection in comparison with ammonium fertilization as well (Table 1). Under field conditions, Heitefuss and Brandes (1970) already reported a reduction in *Bgt* infection in wheat when fertilizing cyanamide in comparison with other mineral fertilizers, such as ammonium nitrate. Besides the enhanced *Bgt* resistance, our results showed that cyanamide fertilization reduced plant biomass and height under control conditions (Figure 1A). This might indicate that plants were stressed by the phytotoxicity of cyanamide and its detrimental effect on plant growth, which is usually stronger in dicots (Soltys et al., 2012; European Chemicals Agency, 2018). The stress indicator H_2O_2 might confirm these assumptions, as it was higher in the cyanamide-fertilized control in comparison with the other fertilizers and remained similar in plants infected with *Bgt* (Figure 3A; Saxena et al., 2016). The phytotoxic effect of cyanamide is often observed in young plants when further degradation of this compound is not yet sufficiently advanced (Temme, 1948). A common plant response to the increased oxidative stress promoted by cyanamide application is the increase in antioxidant plant potential (Soltys et al., 2012; Sabatino et al., 2019), but SOD activity was not higher. Interestingly, SA was strongly elevated in this N treatment infected with the pathogen (Figure 3D). Collectively, these findings suggested a prompted activation of the plant defense response and the establishment of systemic acquired resistance with cyanamide applications (Grant and Lamb, 2006; Bari and Jones, 2009).

Independent from nitrogen nutrition, Jawhar et al. (2017) found that cereals infected with *Blumeria graminis* showed higher levels of total SA in the leaves. After *Bgt* inoculation, Xin et al. (2012) reported an altered expression of genes encoding key enzymes in the phenylpropanoid pathway such as cytochrome P450 monooxygenase which converts benzoic acid to SA. This indicates that SA plays a positive role in signaling events during fungal infection and is involved in an early local defense response at the primary *Blumeria graminis* infection site. Additionally, SA plays a central role in systemic resistance to pathogen infection. In this signaling pathway, NO is also known to be an integral component, which is closely related to nitrate nutrition due to the catalysis of nitrate reductase (Mur et al., 2005, 2013; Chen et al., 2014).

Ammonium fertilization promoted *Ggt* root infestation and the build-up of important soil borne pathogens compared to other N forms

In the second set of experiments that involved soil inoculation of the fungal pathogen *Ggt*, causing take-all disease in wheat, the different N fertilization treatments resulted in similar shoot and root dry weights, indicating that application of different N forms substantially did not influence plant biomass. However, the non-N fertilized control treatment led to higher root dry weight and reduced shoot dry weight (Figures 4A,B). Such change in root/shoot ratio is commonly observed in N-deficient plants, as they may attempt to increase N availability *via* investing in belowground biomass (Luo et al., 2020), a process that is disease-independent. Intriguingly, cyanamide fertilization produced the lowest *Ggt* infection rate, with no negative impact on plant performance. This is the opposite of what we observed in the first experiment with the shoot pathogen. Perhaps, cyanamide lost its possible phytotoxicity in these experiments, as the fertilized pots were incubated for 2 weeks prior to plant sowing and soil microorganisms need approximately this time window to convert cyanamide into urea, ammonium, and finally nitrate (Temme, 1948).

Notably, the highest take-all infestation was again observed in ammonium-fertilized plants (Figure 4C). *Ggt* abundance in the wheat rhizosphere was higher in this treatment compared to the other ones (Figure 4D). In contrast to our findings, it has been reported that nitrogen fertilization in form of ammonium can suppress root infections promoted by *Ggt*. This process was mainly attributed to the direct inhibition of ectotrophic hyphal growth of *Ggt* by a decrease in pH of wheat root surface by the application of ammonium fertilizer (Smiley and Cook, 1973; Smiley, 1978). The decrease in rhizosphere pH associated with ammonium could also increase the availability of micronutrients, such as Mn, which is known to influence host susceptibility to take-all, especially in cereal crops (Huber and Wilhelm, 1988; Huber, 1993; Ownley et al., 2003). However, such a suppressive pH effect was only visible after 7 weeks from the pathogen inoculation (almost twice our experiment running time), and it was removed by fumigating

the soil before *Ggt* inoculation, implying that *Ggt* suppression is highly dependent on soil microbes. Indeed, the soil and plant-associated microbiota play a crucial role in plant growth, plant health, and stress tolerance, including pathogen control (Arif et al., 2020; Song et al., 2020). There is also evidence that wheat cultivars differ in their ability to support the suppression of take-all disease promoted by *Ggt* and other microbes, suggesting that this disease likely involves a complex interaction between the take-all fungus, wheat host genotype, and soil and plant-associated microbiota (Yang et al., 2018). In this context, several studies on *Ggt*-suppressive soils, soils that prevent *Ggt* establishment or reduce disease incidence (Jara and Elizondo, 2011) even in presence of a susceptible host plant, and favorable soil or climate conditions, have shown that native soil microorganism activity can be pivotal in *Ggt* disease suppression (Durán et al., 2017). Although the mechanisms of such soil suppressiveness are not fully understood, it has been often reported that *Ggt*-suppressive soils are characterized by a decrease in rhizosphere pH together with the enrichment of populations of root-associated *Pseudomonas* spp. (Weller et al., 2002). In particular, this may target *Pseudomonas fluorescens* strains, which can produce the antifungal polyketide 2,4-diacetylphloroglucinol (2,4-DAPG; Raaijmakers and Weller, 1998; Raaijmakers et al., 1999; Ownley et al., 2003). In our experiment, ammonium fertilization decreased rhizosphere pH (Supplementary Table 4), but *Ggt* disease was not suppressed, and *Pseudomonas* spp. were not increased in abundance and accounted only for a relatively small proportion of bacterial sequences (less 1% of total reads). In this line, our results showed that N fertilization merely affected bacterial community composition and structure, which agrees with insignificant changes found with a meta-analysis on agricultural systems (Geisseler and Scow, 2014) and several other studies where minimal effect was found of mineral fertilizers on soil bacteria community assembly in the very short term (few weeks from their applications; Marschner et al., 2001; Stark et al., 2007; She et al., 2018) or even long term (Liu and Ludewig, 2019). Moreover, a very recent work highlighted that short-term nitrogen fertilization had a greater impact on fungal community composition and structure than on bacterial communities in different compartments along the soil-root continuum (bulk soil, rhizosphere, and endophytic environment) of maize (Bai et al., 2022). Our results supported these observations, as we found that the fungal community was highly responsive to N fertilization, which partially validated our hypotheses. Indeed, differences in alpha and beta diversity were evident among the different N treatments, and distinct fungal assemblages characterized each N fertilized soil. In the short-term, fungal communities may respond to nitrogen fertilization as a disturbance, with consequent profound shifts in community assembly (Paungfoo-Lonhienne et al., 2015; Treseder et al., 2018; Cai et al., 2021; Castle et al., 2021). However, the type of N form employed might play a crucial role in selectively increasing or decreasing specific fungal groups with important ecological and agricultural consequences, such as favoring pathogenic over mutualistic fungal taxa, or vice versa (Huber and Watson, 1974; Francioli et al., 2016; Gu et al., 2020; Lekberg et al., 2021). Here, we observed a pronounced effect of ammonium fertilization in the build-up of important fungal pathogens such as *Ggt* and *Blumeria graminis* (Figure 7). Surprisingly, the relative abundance of *Ggt* was almost sixfold higher in the ammonium-fertilized wheat rhizosphere than in the other N amended soils, highlighting the detrimental effect of this N form on the wheat root-associated microbiota. The increase in plant susceptibility to pathogens from NH_4^+ fertilization has been ascribed to enhanced content of apoplastic sugar, amino acids, as well as γ-amino-n-butyric acid (GABA), which may represent efficient nutritional sources for the pathogen (Gupta et al., 2013; Mur et al., 2017). Furthermore, ammonium fertilization increased asparagine concentrations, which promote the development of *Rhizoctonia solani* in beet, and *Fusarium* wilt on tomato (Huber and Watson, 1974). However, more recent studies have illustrated that the interactions between mineral nitrogen and plant disease susceptibility are highly complex, and highlighted the role of endophytes, mainly fungal, in the reduction and suppression of take-all caused by *Ggt* (Maciá-Vicente et al., 2008; Liu et al., 2009; Durán et al., 2018; Gholami et al., 2019). Overall, our findings underlined the crucial role of N form in mineral fertilizers, as it can negatively influence the outcome of plant-pathogen interactions, as observed in this study with ammonium and winter wheat. To make a recommendation on which fertilizer strategy is preferable for winter wheat considering yield, disease control, safety and environmental impact, field trials need to be conducted at multiple locations.

Data availability statement

The data presented in the study are deposited in the https://www.ebi.ac.uk/ena repository, accession numbers PRJEB52826 and PRJEB52827.

Author contributions

NM and UL conceived and designed the experiments. NM and NP conducted the experiments and collected the data. NM, DF, MM, and GN analyzed the data. NM and DF wrote the manuscript with UL. All authors contributed to the article and approved the submitted version.

Funding

This research was conducted within the projects "Agriculture 4.0 without Chemical-Synthetic Plant Protection" and the project DiControl within the program BonaRes (soil as a sustainable resource for the bio economy). Both projects are funded by the German Federal Ministry of Education and Research (BMBF), grant numbers 031B0731A and 031A560A-F, respectively.

Acknowledgments

We thank Helene Ochott and the Core Facility Hohenheim (CFH) for performing the nutrient analysis of our samples. In addition, we also thank the agricultural research station Kleinhohenheim for providing the soil that has been used in this work.

Conflict of interest

The authors declare that the research was conducted in the absence of any commercial or financial relationships that could be construed as a potential conflict of interest.

Publisher's note

Supplementary material

The Supplementary material for this article can be found online at: https://www.frontiersin.org/articless/10.3389/fpls.2022.946584/full#supplementary-material

References

Ainsworth, E. A., and Gillespie, K. M. (2007). Estimation of total phenolic content and other oxidation substrates in plant tissues using Folin-Ciocalteu reagent. *Nat. Protoc.* 2, 875–877. doi: 10.1038/nprot.2007.102

Apel, K., and Hirt, H. (2004). Reactive oxygen species: metabolism, oxidative stress, and signal transduction. *Annu. Rev. Plant Biol.* 55, 373–399. doi: 10.1146/annurev.arplant.55.031903.141701

Arif, I., Batool, M., and Schenk, P. M. (2020). Plant microbiome engineering: expected benefits for improved crop growth and resilience. *Trends Biotechnol.* 38, 1385–1396. doi: 10.1016/j.tibtech.2020.04.015

Bai, L., Zhang, X., Li, B., Sun, F., Zhao, X., Wang, Y., et al. (2022). Fungal communities are more sensitive to nitrogen fertilization than bacteria in different spatial structures of silage maize under short-term nitrogen fertilization. *Appl. Soil Ecol.* 170, 104275. doi: 10.1016/j.apsoil.2021.104275

Baker, R., and Martinson, C. A. (1970). "Epidemiology of diseases caused by *Rhizoctonia Solani*" in *Rhizoctonia Solani, Biology and Pathology*. ed. J. R. Parmeter (Oakland, California: University of California Press), 172–188. doi: 10.1525/9780520318243-014

Bari, R., and Jones, J. D. G. (2009). Role of plant hormones in plant defence responses. *Plant Mol. Biol.* 69, 473–488. doi: 10.1007/s11103-008-9435-0

Beauchamp, C., and Fridovich, I. (1971). Superoxide dismutase: improved assays and an assay applicable to acrylamide gels. *Anal. Biochem.* 44, 276–287. doi: 10.1016/0003-2697(71)90370-8

Bergmann, W. (1983). *Ernährungsstörungen bei Kulturpflanzen*. Jena: Gustav Fischer Verlag.

Bojović, B., and Marković, A. (2009). Correlation between nitrogen and chlorophyll content in wheat (*Triticum aestivum* L.). *Kragujevac J. Sci.* 31, 69–74.

Bolton, M. D., and Thomma, B. P. (2008). The complexity of nitrogen metabolism and nitrogen-regulated gene expression in plant pathogenic fungi. *Physiol. Mol. Plant Pathol.* 72, 104–110. doi: 10.1016/j.pmpp.2008.07.001

Bolwell, G. P. (1999). Role of active oxygen species and NO in plant defence responses. *Curr. Opin. Plant Biol.* 2, 287–294. doi: 10.1016/S1369-5266(99)80051-X

Bradford, M. M. (1976). A rapid and sensitive method for the quantitation of microgram quantities of protein utilizing the principle of protein-dye binding. *Anal. Biochem.* 72, 248–254. doi: 10.1016/0003-2697(76)90527-3

Brand-Williams, W., Cuvelier, M. E., and Berset, C. (1995). Use of a free radical method to evaluate antioxidant activity. *LWT-Food Sci. Technol.* 28, 25–30. doi: 10.1016/S0023-6438(95)80008-5

Bundessortenamt (2000). *Richtlinien für die Durchführung von landwirtschaftlichen Wertprüfungen und Sortenversuchen*. Hannover: Landbuch Verlagsgesellschaft GmbH.

Cai, J., Zhang, J., Ding, Y., Yu, S., Lin, H., Yuan, Z., et al. (2021). Different fertilizers applied alter fungal community structure in rhizospheric soil of cassava (*Manihot esculenta* Crantz) and increase crop yield. *Front. Microbiol.* 12:663781. doi: 10.3389/fmicb.2021.663781

Callahan, B. J., McMurdie, P. J., Rosen, M. J., Han, A. W., Johnson, A. J. A., and Holmes, S. P. (2016). DADA2: high-resolution sample inference from Illumina amplicon data. *Nat. Methods* 13, 581–583. doi: 10.1038/nmeth.3869

Castle, S. C., Samac, D. A., Gutknecht, J. L., Sadowsky, M. J., Rosen, C. J., Schlatter, D., et al. (2021). Impacts of cover crops and nitrogen fertilization on agricultural soil fungal and bacterial communities. *Plant Soil* 466, 139–150. doi: 10.1007/s11104-021-04976-z

Chen, J., Vandelle, E., Bellin, D., and Delledonne, M. (2014). Detection and function of nitric oxide during the hypersensitive response in *Arabidopsis thaliana*: where there's a will there's a way. *Nitric Oxide* 43, 81–88. doi: 10.1016/j.niox.2014.06.008

Colquhoun, T. T. (1940). Effect of manganese on powdery mildew of wheat. *J. Aust. Inst. Agric. Sci.* 61:54.

Cona, A., Rea, G., Angelini, R., Federico, R., and Tavladoraki, P. (2006). Functions of amine oxidases in plant development and defence. *Trends Plant Sci.* 11, 80–88. doi: 10.1016/j.tplants.2005.12.009

Cowley, T., and Walters, D. R. (2002a). Polyamine metabolism in an incompatible interaction between barley and the powdery mildew fungus, *Blumeria graminis* f. sp *hordei*. *Phytopathologische Zeitschrift* 150, 581–586. doi: 10.1046/j.1439-0434.2002.00816.x

Cowley, T., and Walters, D. R. (2002b). Polyamine metabolism in barley reacting hypersensitively to the powdery mildew fungus *Blumeria graminis* f. sp. *hordei*. *Plant Cell Environ.* 25, 461–468. doi: 10.1046/j.0016-8025.2001.00819.x

Delledonne, M., Xia, Y., Dixon, R. A., and Lamb, C. (1998). Nitric oxide functions as a signal in plant disease resistance. *Nature* 394, 585–588. doi: 10.1038/29087

Ding, S., Shao, X., Li, J., Ahammed, G. J., Yao, Y., Ding, J., et al. (2021). Nitrogen forms and metabolism affect plant defence to foliar and root pathogens in tomato. *Plant Cell Environ.* 44, 1596–1610. doi: 10.1111/pce.14019

Durán, P., Jorquera, M., Viscardi, S., Carrion, V. J., Mora, M. L., and Pozo, M. J. (2017). Screening and characterization of potentially suppressive soils against *Gaeumannomyces graminis* under extensive wheat cropping by chilean indigenous communities. *Front. Microbiol.* 8:1552. doi: 10.3389/fmicb.2017.01552

Durán, P., Tortella, G., Viscardi, S., Barra, P. J., Carrión, V. J., Mora, L., et al. (2018). Microbial community composition in take-all suppressive soils. *Front. Microbiol.* 9:2198. doi: 10.3389/fmicb.2018.02198

European Chemicals Agency (2018). A preliminary assessment if the use of calcium cyanamide as a fertiliser poses an unacceptable risk to human health. Version No.1. Helsinki, Finland, 1-40. Available at: https://echa.europa.eu/documents/10162/13641/calcium_cyanamide_review_report_en.pdf/e0b43a34-1a52-b6a9-8d96-bd8183c7beb4

Fagard, M., Launay, A., Clément, G., Courtial, J., Dellagi, A., Farjad, M., et al. (2014). Nitrogen metabolism meets phytopathology. *J. Exp. Bot.* 65, 5643–5656. doi: 10.1093/jxb/eru323

Fernandes, M. S., and Rossiello, R. O. P. (1995). Mineral nitrogen in plant physiology and plant nutrition. *Crit. Rev. Plant Sci.* 14, 111–148. doi: 10.1080/07352689509701924

Francioli, D., Schulz, E., Lentendu, G., Wubet, T., Buscot, F., and Reitz, T. (2016). Mineral vs. organic amendments: microbial community structure, activity and abundance of agriculturally relevant microbes are driven by long-term fertilization strategies. *Front. Microbiol.* 7:1446. doi: 10.3389/fmicb.2016.01446

Geisseler, D., and Scow, K. M. (2014). Long-term effects of mineral fertilizers on soil microorganisms – a review. *Soil Biol. Biochem.* 75, 54–63. doi: 10.1016/j.soilbio.2014.03.023

Gericke, S., and Kurmies, B. (1952). *Colorimetrische Bestimmung der Phosphorsäure mit Vanadat-Molybdat*. Berlin: Springer Berlin Heidelberg.

Gholami, M., Amini, J., Abdollahzadeh, J., and Ashengroph, M. (2019). Basidiomycetes fungi as biocontrol agents against take-all disease of wheat. *Biol. Control* 130, 34–43. doi: 10.1016/j.biocontrol.2018.12.012

Giller, K. E., Delaune, T., Silva, J. V., Descheemaeker, K., van de Ven, G., Schut, A. G., et al. (2021). The future of farming: who will produce our food? *Food Sec.* 13, 1073–1099. doi: 10.1007/s12571-021-01184-6

Gouzou, L., Burtin, G., Philippy, R., Bartoli, F., and Heulin, T. (1993). Effect of inoculation with *Bacillus polymyxa* on soil aggregation in the wheat rhizosphere: preliminary examination. *Geoderma* 56, 479–491. doi: 10.1016/0016-7061(93)90128-8

Grant, M., and Lamb, C. (2006). Systemic immunity. *Curr. Opin. Plant Biol.* 9, 414–420. doi: 10.1016/j.pbi.2006.05.013

Grunes, D. L., Viets, F. G., and Shih, S. H. (1958). Proportionate uptake of soil and fertilizer phosphorus by plants as affected by nitrogen fertilization: I. Growth chamber experiment. *Soil Sci. Soc. Am. J.* 22, 43–48. doi: 10.2136/sssaj1958.03615995002200010013x

Gu, Z., Wang, M., Wang, Y., Zhu, L., Mur, L. A. J., Hu, J., et al. (2020). Nitrate stabilizes the rhizospheric fungal community to suppress fusarium wilt disease in cucumber. *MPMI* 33, 590–599. doi: 10.1094/MPMI-07-19-0198-R

Gupta, K. J., Brotman, Y., Segu, S., Zeier, T., Zeier, J., Persijn, S. T., et al. (2013). The form of nitrogen nutrition affects resistance against *pseudomonas syringae* pv. *Phaseolicola* in tobacco. *J. Exp. Bot.* 64, 553–568. doi: 10.1093/jxb/ers348

Heitefuss, R., and Brandes, W. (1970). Nebenwirkungen von Herbiziden und Kalkstickstoff auf den Befall von Weizen mit *Erysiphe graminis*. *Nachrichtenbl. Deutsch. Pflanzenschutzd.* 22, 40–43.

Huang, W., Lamb, D. W., Niu, Z., Zhang, Y., Liu, L., and Wang, J. (2007). Identification of yellow rust in wheat using in-situ spectral reflectance measurements and airborne hyperspectral imaging. *Precision Agric.* 8, 187–197. doi: 10.1007/s11119-007-9038-9

Huber, D. M. (1993). A multiple component analysis of the take-all disease of cereals. *Plant Dis.* 77, 437. doi: 10.1094/PD-77-0437

Huber, D. M., and Jones, J. B. (2013). The role of magnesium in plant disease. *Plant Soil* 368, 73–85. doi: 10.1007/s11104-012-1476-0

Huber, D. M., and Watson, R. D. (1974). Nitrogen form and plant disease. *Annu. Rev. Phytopathol.* 12, 139–165. doi: 10.1146/annurev.py.12.090174.001035

Huber, D. M., and Wilhelm, N. S. (1988). "The role of manganese in resistance to plant diseases," in *Manganese in Soils and Plants*. eds. R. D. Graham, R. J. Hannam and N. C. Uren (Springer Netherlands: Dordrecht), 155–173. doi: 10.1007/978-94-009-2817-6_12

Jacquet, F., Jeuffroy, M.-H., Jouan, J., Le Cadre, E., Litrico, I., Malausa, T., et al. (2022). Pesticide-free agriculture as a new paradigm for research. *Agron. Sustain. Dev.* 42, 1–24. doi: 10.1007/s13593-021-00742-8

Jara, H., and Elizondo, E. (2011). Root disease suppressive soils: "take all decline (*Gaeumannomyces graminis* var. *tritici*) in wheat", a case study. *agrosur* 39, 67–78. doi: 10.4206/agrosur.2011.v39n2-01

Jawhar, M., Al-Shehadah, E., Shoaib, A., Orfi, M., and Al-Daoude, A. (2017). Changes in salicylic acid and gene expression levels during barley-*Blumeria graminis* interaction. *J. Plant Pathol.* 99, 651–656.

Jensen, B., and Munk, L. (1997). Nitrogen-induced changes in colony density and spore production of *Erysiphe graminis* f. sp. *hordei* on seedlings of six spring barley cultivars. *Plant Pathol.* 46, 191–202. doi: 10.1046/j.1365-3059.1997.d01-224.x

Justes, E., Mary, B., Meynard, J.-M., Machet, J.-M., and Thelier-Huche, L. (1994). Determination of a critical nitrogen dilution curve for winter wheat crops. *Ann. Bot.* 74, 397–407. doi: 10.1006/anbo.1994.1133

Last, F. T. (1953). Some effects of temperature and nitrogen supply on wheat powdery mildew. *Ann. Appl. Biol.* 40, 312–322. doi: 10.1111/j.1744-7348.1953.tb01085.x

Legendre, P., and Gallagher, E. D. (2001). Ecologically meaningful transformations for ordination of species data. *Oecologia* 129, 271–280. doi: 10.1007/s004420100716

Lekberg, Y., Arnillas, C. A., Borer, E. T., Bullington, L. S., Fierer, N., Kennedy, P. G., et al. (2021). Nitrogen and phosphorus fertilization consistently favor pathogenic over mutualistic fungi in grassland soils. *Nat. Commun.* 12, 3484. doi: 10.1038/s41467-021-23605-y

Leser, T. D., Amenuvor, J. Z., Jensen, T. K., Lindecrona, R. H., Boye, M., and Møller, K. (2002). Culture-independent analysis of gut bacteria: the pig gastrointestinal tract microbiota revisited. *Appl. Environ. Microbiol.* 68, 673–690. doi: 10.1128/AEM.68.2.673-690.2002

Li, J., Yang, X., Liu, X., Yu, H., Du, C., Li, M., et al. (2017). Proteomic analysis of the compatible interaction of wheat and powdery mildew (*Blumeria graminis* f. sp. *tritici*). *Plant Physiol. Biochem.* 111, 234–243. doi: 10.1016/j.plaphy.2016.12.006

Liu, Y., and Ludewig, U. (2019). Nitrogen-dependent bacterial community shifts in root, rhizome and rhizosphere of nutrient-efficient *Miscanthus* x *giganteus* from long-term field trials. *GCB Bioenergy* 11, 1334–1347. doi: 10.1111/gcbb.12634

Liu, B., Qiao, H., Huang, L., Buchenauer, H., Han, Q., Kang, Z., et al. (2009). Biological control of take-all in wheat by endophytic *Bacillus subtilis* E1R-j and potential mode of action. *Biol. Control* 49, 277–285. doi: 10.1016/j.biocontrol.2009.02.007

Luo, L., Zhang, Y., and Xu, G. (2020). How does nitrogen shape plant architecture? *J. Exp. Bot.* 71, 4415–4427. doi: 10.1093/jxb/eraa187

Maciá-Vicente, J. G., Jansson, H.-B., Mendgen, K., and Lopez-Llorca, L. V. (2008). Colonization of barley roots by endophytic fungi and their reduction of take-all caused by *Gaeumannomyces graminis* var. *tritici*. *Can. J. Microbiol.* 54, 600–609. doi: 10.1139/W08-047

Marschner, P., Yang, C.-H., Lieberei, R., and Crowley, D. (2001). Soil and plant specific effects on bacterial community composition in the rhizosphere. *Soil Biol. Biochem.* 33, 1437–1445. doi: 10.1016/S0038-0717(01)00052-9

Mur, L. A. J., Prats, E., Pierre, S., Hall, M. A., and Hebelstrup, K. H. (2013). Integrating nitric oxide into salicylic acid and jasmonic acid/ethylene plant defense pathways. *Front. Plant Sci.* 4:215. doi: 10.3389/fpls.2013.00215

Mur, L. A. J., Santosa, I. E., Laarhoven, L. J. J., Holton, N. J., Harren, F. J. M., and Smith, A. R. (2005). Laser photoacoustic detection allows in planta detection of nitric oxide in tobacco following challenge with avirulent and virulent *Pseudomonas syringae* pathovars. *Plant Physiol.* 138, 1247–1258. doi: 10.1104/pp.104.055772

Mur, L. A. J., Simpson, C., Kumari, A., Gupta, A. K., and Gupta, K. J. (2017). Moving nitrogen to the centre of plant defence against pathogens. *Ann. Bot.* 119, mcw179–mcw709. doi: 10.1093/aob/mcw179

Mustafa, G., Randoux, B., Tisserant, B., Fontaine, J., Magnin-Robert, M., Lounès-Hadj Sahraoui, A., et al. (2016). Phosphorus supply, arbuscular mycorrhizal fungal species, and plant genotype impact on the protective efficacy of mycorrhizal inoculation against wheat powdery mildew. *Mycorrhiza* 26, 685–697. doi: 10.1007/s00572-016-0698-z

Niggli, U., Schmid, H., and Fliessbach, A. (2008). *Organic Farming and Climate Change*. Geneva: International Trade Centre (ITC).

Nilsson, R. H., Larsson, K.-H., Taylor, A. F. S., Bengtsson-Palme, J., Jeppesen, T. S., Schigel, D., et al. (2019). The UNITE database for molecular identification of fungi: handling dark taxa and parallel taxonomic classifications. *Nucleic Acids Res.* 47, D259–D264. doi: 10.1093/nar/gky1022

Ownley, B. H., Duffy, B. K., and Weller, D. M. (2003). Identification and manipulation of soil properties to improve the biological control performance of phenazine-producing *Pseudomonas fluorescens*. *Appl. Environ. Microbiol.* 69, 3333–3343. doi: 10.1128/AEM.69.6.3333-3343.2003

Paungfoo-Lonhienne, C., Yeoh, Y. K., Kasinadhuni, N. R. P., Lonhienne, T. G. A., Robinson, N., Hugenholtz, P., et al. (2015). Nitrogen fertilizer dose alters fungal communities in sugarcane soil and rhizosphere. *Sci. Rep.* 5, 8678. doi: 10.1038/srep08678

Peng, Y., Li, S. J., Yan, J., Tang, Y., Cheng, J. P., Gao, A. J., et al. (2021). Research Progress on Phytopathogenic fungi and their role as biocontrol agents. *Front. Microbiol.* 12:670135. doi: 10.3389/fmicb.2021.670135

Planchet, E., Jagadis Gupta, K., Sonoda, M., and Kaiser, W. M. (2005). Nitric oxide emission from tobacco leaves and cell suspensions: rate limiting factors and evidence for the involvement of mitochondrial electron transport. *Plant J.* 41, 732–743. doi: 10.1111/j.1365-313X.2005.02335.x

Pogacean, M. O., and Gavrilescu, M. (2009). Plant protection products and their sustainable and environmentally friendly use. *Environ. Eng. Manag. J.* 8, 607–627. doi: 10.30638/eemj.2009.084

Raaijmakers, J. M., Bonsall, R. F., and Weller, D. M. (1999). Effect of population density of *Pseudomonas fluorescens* on production of 2,4-Diacetylphloroglucinol in the Rhizosphere of wheat. *Phytopathology* 89, 470–475. doi: 10.1094/Phyto.1999.89.6.470

Raaijmakers, J. M., and Weller, D. M. (1998). Natural plant protection by 2,4-diacetylphloroglucinol-producing *Pseudomonas* spp. in take-all decline soils. *MPMI* 11, 144–152. doi: 10.1094/Mpmi.1998.11.2.144

Riley, D., and Barber, S. A. (1971). Effect of ammonium and nitrate fertilization on phosphorus uptake as related to root-induced pH changes at the root-soil interface. *Soil Sci. Soc. Am. J.* 35, 301–306. doi: 10.2136/sssaj1971.03615995003500020035x

Rolfe, S. A., and Scholes, J. D. (2010). Chlorophyll fluorescence imaging of plant-pathogen interactions. *Protoplasma* 247, 163–175. doi: 10.1007/s00709-010-0203-z

Sabatino, L., D'Anna, F., Prinzivalli, C., and Iapichino, G. (2019). Soil solarization and calcium cyanamide affect plant vigor, yield, nutritional traits, and nutraceutical compounds of strawberry grown in a protected cultivation system. *Agronomy* 9:513. doi: 10.3390/agronomy9090513

Saxena, I., Srikanth, S., and Chen, Z. (2016). Cross talk between H_2O_2 and interacting signal molecules under plant stress response. *Front. Plant Sci.* 7:570. doi: 10.3389/fpls.2016.00570

Segata, N., Izard, J., Waldron, L., Gevers, D., Miropolsky, L., Garrett, W. S., et al. (2011). Metagenomic biomarker discovery and explanation. *Genome Biol.* 12:R60. doi: 10.1186/gb-2011-12-6-r60

Seufert, V., Ramankutty, N., and Mayerhofer, T. (2017). What is this thing called organic? – How organic farming is codified in regulations. *Food Policy* 68, 10–20. doi: 10.1016/j.foodpol.2016.12.009

She, W., Bai, Y., Zhang, Y., Qin, S., Feng, W., Sun, Y., et al. (2018). Resource availability drives responses of soil microbial communities to short-term precipitation and nitrogen addition in a desert Shrubland. *Front. Microbiol.* 9, 186. doi: 10.3389/fmicb.2018.00186

Shetty, N. P., Mehrabi, R., Lütken, H., Haldrup, A., Kema, G. H. J., Collinge, D. B., et al. (2007). Role of hydrogen peroxide during the interaction between the hemibiotrophic fungal pathogen Septoria tritici and wheat. *New Phytol.* 174, 637–647. doi: 10.1111/j.1469-8137.2007.02026.x

Smiley, R. W. (1978). Antagonists of *Gaeumannomyces graminis* from the rhizoplane of wheat in soils fertilized with ammonium- or nitrate- nitrogen. *Soil Biol. Biochem.* 10, 169–174. doi: 10.1016/0038-0717(78)90092-5

Smiley, R. W., and Cook, R. J. (1973). Relationship between take-all of wheat and rhizosphere pH in soils fertilized with ammonium- vs nitrate-nitrogen. *Phytopathology* 63, 882–890.

Soltys, D., Rudzińska-Langwald, A., Gniazdowska, A., Wiśniewska, A., and Bogatek, R. (2012). Inhibition of tomato (*Solanum lycopersicum* L.) root growth by cyanamide is due to altered cell division, phytohormone balance and expansin gene expression. *Planta* 236, 1629–1638. doi: 10.1007/s00425-012-1722-y

Song, C., Zhu, F., Carrión, V. J., and Cordovez, V. (2020). Beyond plant microbiome composition: exploiting microbial functions and plant traits *via* integrated approaches. *Front. Bioeng. Biotechnol.* 8:896. doi: 10.3389/fbioe.2020.00896

Stark, C., Condron, L. M., Stewart, A., Di, H. J., and O'Callaghan, M. (2007). Influence of organic and mineral amendments on microbial soil properties and processes. *Appl. Soil Ecol.* 35, 79–93. doi: 10.1016/j.apsoil.2006.05.001

Sun, Y., Wang, M., Mur, L. A. J., Shen, Q., and Guo, S. (2020). Unravelling the roles of nitrogen nutrition in plant disease defences. *Int. J. Mol. Sci.* 21:572. doi: 10.3390/ijms21020572

Temme, J. (1948). The transformation of calcium cyanamide in the soil. *Plant Soil* 1, 145–166. doi: 10.1007/BF02080923

Treseder, K. K., Berlemont, R., Allison, S. D., and Martiny, A. C. (2018). Nitrogen enrichment shifts functional genes related to nitrogen and carbon acquisition in the fungal community. *Soil Biol. Biochem.* 123, 87–96. doi: 10.1016/j.soilbio.2018.05.014

Trommer, R. (1989). Schätzung der Befallsstärke von Blattkrankheiten des Getreides mit Hilfe einer dreistufigen Bonitурskala. *Arch. Phytopathol. Plant Protect.* 25, 375–386. doi: 10.1080/03235408909438892

Uddling, J., Gelang-Alfredsson, J., Piikki, K., and Pleijel, H. (2007). Evaluating the relationship between leaf chlorophyll concentration and SPAD-502 chlorophyll meter readings. *Photosynth. Res.* 91, 37–46. doi: 10.1007/s11120-006-9077-5

Velikova, V., Yordanov, I., and Edreva, A. (2000). Oxidative stress and some antioxidant systems in acid rain-treated bean plants. *Plant Sci.* 151, 59–66. doi: 10.1016/S0168-9452(99)00197-1

Verona, O. (1970). The effect of calcium cyanamide on some groups of lower fungi. *Landwirtsch. Forsch.* 23, 36–52.

Walters, D. R., and Bingham, I. J. (2007). Influence of nutrition on disease development caused by fungal pathogens: implications for plant disease control. *Ann. Appl. Biol.* 151, 307–324. doi: 10.1111/j.1744-7348.2007.00176.x

Wang, Q., Garrity, G. M., Tiedje, J. M., and Cole, J. R. (2007). Naive Bayesian classifier for rapid assignment of rRNA sequences into the new bacterial taxonomy. *Appl. Environ. Microbiol.* 73, 5261–5267. doi: 10.1128/AEM.00062-07

Weisburg, W. G., Barns, S. M., Pelletier, D. A., and Lane, D. J. (1991). 16S ribosomal DNA amplification for phylogenetic study. *J. Bacteriol.* 173, 697–703. doi: 10.1128/jb.173.2.697-703.1991

Weller, D. M., Raaijmakers, J. M., Gardener, B. B. M., and Thomashow, L. S. (2002). Microbial populations responsible for specific soil suppressiveness to plant pathogens. *Annu. Rev. Phytopathol.* 40, 309–348. doi: 10.1146/annurev.phyto.40.030402.110010

White, T. J., Bruns, T., Lee, S., and Taylor, J. (1990). "Amplification and direct sequencing of fungal ribosomal RNA genes for phylogenetics," in *PCR Protocols: A guide to methods and applications*. eds. M. A. Innis, D. H. Gelfand, J. J. Sninsky and T. J. White (New York: Academic Press, Inc.), 315–322.

Xin, M., Wang, X., Peng, H., Yao, Y., Xie, C., Han, Y., et al. (2012). Transcriptome comparison of susceptible and resistant wheat in response to powdery mildew infection. *Genomics Proteomics Bioinformatics* 10, 94–106. doi: 10.1016/j.gpb.2012.05.002

Yang, H., and Luo, P. (2021). Changes in photosynthesis could provide important insight into the interaction between wheat and fungal pathogens. *Int. J. Mol. Sci.* 22:8865. doi: 10.3390/ijms22168865

Yang, M., Mavrodi, D. V., Thomashow, L. S., and Weller, D. M. (2018). Differential response of wheat cultivars to *Pseudomonas brassicacearum* and take-all decline soil. *Phytopathology* 108, 1363–1372. doi: 10.1094/PHYTO-01-18-0024-R

Zhang, L., Du, L., and Poovaiah, B. W. (2014). Calcium signaling and biotic defense responses in plants. *Plant Signal. Behav.* 9:e973818. doi: 10.4161/15592324.2014.973818

Zimmermann, B., Claß-Mahler, I., von Cossel, M., Lewandowski, I., Weik, J., Spiller, A., et al. (2021). Mineral-ecological cropping systems: a new approach to improve ecosystem services by farming without chemical synthetic plant protection. *Agronomy* 11:1710. doi: 10.3390/agronomy11091710

frontiers | Frontiers in Plant Science

TYPE Original Research
PUBLISHED 16 September 2022
DOI 10.3389/fpls.2022.981281

OPEN ACCESS

EDITED BY
Yang Yu,
Southwest University, China

REVIEWED BY
Yong Zhang,
Southwest University, China
Raj Kumar Joshi,
Rama Devi Women's University, India

*CORRESPONDENCE
Dongfang Ma
madf@yangtzeu.edu.cn

SPECIALTY SECTION
This article was submitted to Crop and Product Physiology, a section of the journal Frontiers in Plant Science

RECEIVED 29 June 2022
ACCEPTED 30 August 2022
PUBLISHED 16 September 2022

CITATION
Cao P, Zhan C, Yin J, Gong S, Ma D and Li Y (2022) Genome-wide identification of long intergenic non-coding RNAs for *Ralstonia solanacearum* resistance in tomato (*Solanum lycopersicum*). *Front. Plant Sci.* 13:981281. doi: 10.3389/fpls.2022.981281

Genome-wide identification of long intergenic non-coding RNAs for *Ralstonia solanacearum* resistance in tomato (*Solanum lycopersicum*)

Peina Cao[1], Chuang Zhan[1], Junliang Yin[1], Shuangjun Gong[2], Dongfang Ma[1,2]* and Yan Li[1,2]

[1]Engineering Research Center of Ecology and Agricultural Use of Wetland, Ministry of Education/College of Agriculture, Yangtze University, Jingzhou, China, [2]Key Laboratory of Integrated Pest Management on Crop in Central China, Ministry of Agriculture/Hubei Province Key Laboratory for Control of Crop Diseases, Pest and Weeds/Institute of Plant Protection and Soil Science, Hubei Academy of Agricultural Sciences, Wuhan, China

There is growing evidences indicating that long intergenic ncRNAs (lincRNAs) play key roles in plant development and stress responses. To research tomato lincRNA functions during the interaction between tomato and *Ralstonia solanacearum*, RNA-seq data of tomato plants inoculated with *R. solanacearum* was analyzed. In this study, 315 possible lincRNAs were identified from RNA-seq data. Then 23 differentially expressed lincRNAs between tomato plants inoculated with *R. solanacearum* and control were identified and a total of 171 possible target genes for these differentially expressed lincRNAs were predicted. Through GO and KEGG analysis, we found that lincRNA might be involved in jasmonic acid and ethylene signaling pathways to respond to tomato bacterial wilt infection. Furthermore, lincRNA may also be involved in regulating the expression of AGO protein. Subsequently, analysis of expression patterns between differentially expressed lincRNAs and adjacent mRNAs by qRT-PCR revealed that part of lincRNAs and their possible target genes exhibited positive correlation. Taken together, these results suggest that lincRNAs play potential roles in tomato against *R. solanacearum* infection and will provide fundamental information about the lincRNA-based plant defense mechanisms.

KEYWORDS

LincRNA, *Ralstonia solanacearum*, qRT-PCR, differentially expressed, target genes

Introduction

As a piece of the human eating routine, tomato (*Solanum lycopersicum*) has been tamed for many years (Rambla et al., 2014). Currently, tomato has been the second most consumed vegetable in the world (after potato and before onion) (Bergougnoux, 2014). In 2020, the harvested area of tomato has reached 5,051,183 hectares and tomato production has reached 186,821,216 tons worldwide (data from FAO). However, tomato bacterial wilt, which was caused by *Ralstonia solanacearum*, is the serious disease during tomato production (Baichoo and Jaufeerally-Fakim, 2016).

R. solanacearum exists in the root surface, and then it could spread across the whole plant through xylem vessel. This bacterium could degrade the cell wall by releasing cellulase and pectinase, thereby inhibits nutrient and water transport in the tomato plant (Raza et al., 2016), eventually, causes the host plant to die and wilt within a few days (Vasse et al., 1995). *R. solanacearum* could be survived in soil for a long time. Wide host range and geographical distribution make it very hard to control (Murti et al., 2021). Host resistance is eco-friendly and low cost to control tomato bacterial wilt (Nguyen et al., 2021). Different susceptible genes (*S* genes) and resistance gene (*R* genes) can be identified by the RNA-seq approach (Gao and Bradeen, 2016).

Long intergenic ncRNAs (LincRNAs) are defined as transcribed non-coding RNAs, which are longer than 200 nucleotides (nt) and are located between two protein-coding genes without overlapping with annotated coding genes (Liu et al., 2012; Sanchita Trivedi and Asif, 2019). Previous studies have shown that lincRNAs are usually co-expressed with neighboring genes to play important regulatory roles in higher eukaryotes (Cabili et al., 2011; Wang J. X. et al., 2018). For example, lincRNAs in soybean are involved in stress response, signal transduction, and developmental processes (Golicz et al., 2017). In addition, lincRNAs are associated with epigenetic markers in rice (Wang et al., 2015). Some lincRNAs have been reported to dynamically regulate auxin to drive chromatin loop formation (Ariel et al., 2014), and also to be involved in the response to low-nutrient conditions in *Arabidopsis thaliana* (Fukuda et al., 2019). LincRNAs from populus (*Populus trichocarpa*) were found in response to drought stress (Shuai et al., 2014). LincRNAs were also found to be responsive to *Pectobacterium carotovorum* infection in *Solanum tuberosum* (Kwenda et al., 2016). Furthermore, lincRNA of wheat may play roles in response to stripe rust and powdery mildew infection (Zhang et al., 2016). These results indicated that lincRNAs play indispensable roles in regulating plant growth and stress responses. However, there are few studies on lincRNAs related to tomato disease resistance.

Many studies have demonstrated that lincRNAs play active roles in the resistance to various pathogens in different plants, there has yet to be few researches on them in tomato, especially in tomato-*R. solanacearum* interaction system. The expression patterns and functions of tomato lincRNAs during the interaction with *R. solanacearum* has not been studied extensively. In this work, we identified tomato lincRNAs in a genome-wide scale and investigated the responses of tomato to *R. solanacearum* infection. Furthermore, we predicted possible target genes of differentially expressed lincRNAs within 100 kb of chromosomal locations and profiled the expression patterns of several lincRNAs using qRT-PCR. All potential target genes were then functionally annotated to pick out genes of interest in response to *R. solanacearum* infection. Our findings will provide fundamental information about the lincRNA-based plant defense mechanisms, which is useful for future molecular breeding of pathogen-resistant plants.

Materials and methods

Transcriptome data collection

High-throughput RNA-seq data were downloaded from NCBI (accession number PRJNA787007). The samples were stems at the six-leaf stage from two tomato cultivars (resistance and susceptibility to bacterial wilt) seedlings. Each cultivar was inoculated with *R. solanacearum* as treatment group, and the control group was healthy plants without inoculation. Sample R (R0, R1) represents stem tissue taken from tomato cultivar with bacterial wilt resistance, and S (S0, S1) stands for the susceptible cultivar. There were four groups of samples with three biological replicates per group.

RNA-seq reads mapping and transcriptome assembly

The SRA files were converted into fastq files using fasterq-dump (version 2.9.1). Fastqc (version 0.11.9) was used to detect the quality of the raw reads, and trim_galore software (version 0.6.7) was used to filter adapter content and low-quality reads. HISAT2 (version 2.0.1) was used to map the clean reads to the tomato reference genome which was downloaded from the Phytozome database.[1] The format of output file was sam format. Samtools software (version 1.13) was used to converted and sorted sam files to bam files. Then the bam files are used as input files for StringTie (version 2.1.7) to get merged gtf files.

1 https://phytozome-next.jgi.doe.gov/info/Slycopersicum_ITAG4_0

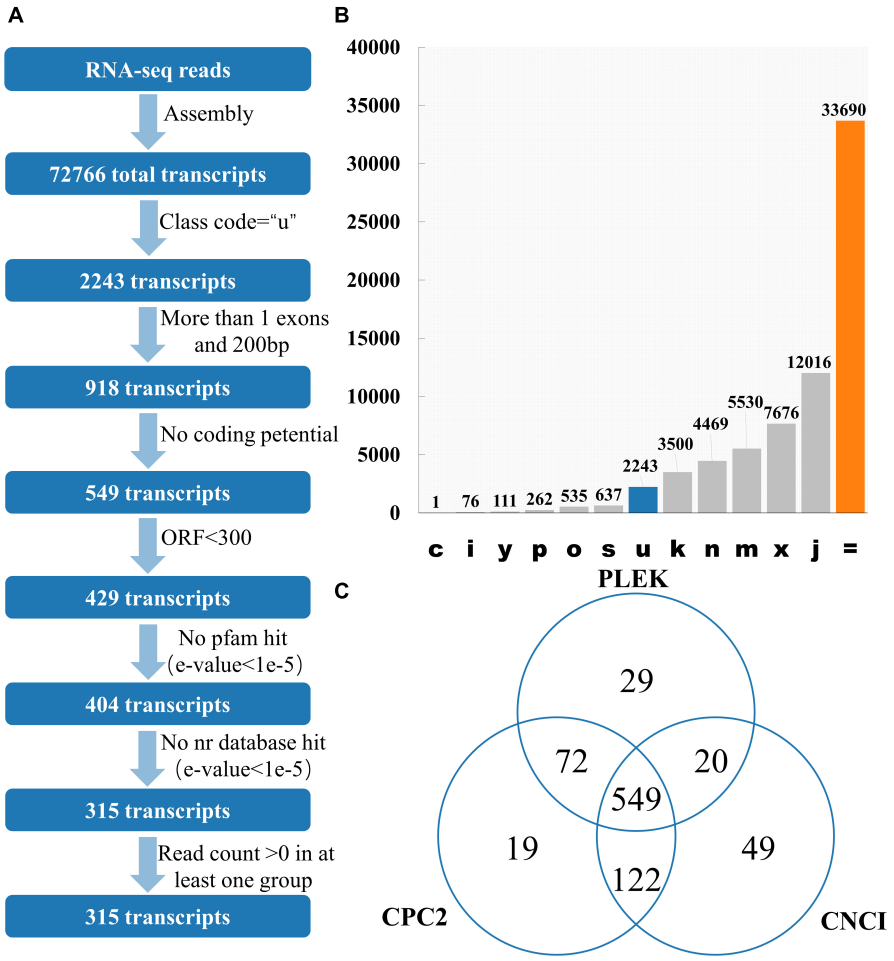

FIGURE 1
Identification of lincRNA from transcripts. **(A)** Pipeline for lincRNA Identification. **(B)** The number of each transcript. Class_code is used to indicate the position of the transcript relative to the reference genome. **(C)** Venn diagrams of transcripts without protein-coding ability evaluated by three software. Note: c represents the position of transcript relative to reference genome is contained in reference (intron compatible). i represents the position of transcript relative to reference genome is fully contained within a reference intron. y represents the position of transcript relative to reference genome is contains a reference within its intron(s). p represents the position of transcript relative to reference genome is possible polymerase run-on (no actual overlap). o represents the position of transcript relative to reference genome is other same strand overlap with reference exons. s represents the position of transcript relative to reference genome is intron match on the opposite strand (likely a mapping error). k represents the position of transcript relative to reference genome is containment of reference (reverse containment). n represents the position of transcript relative to reference genome is retained intron(s), not all introns matched/covered. m represents the position of transcript relative to reference genome is retained intron(s), all introns matched or retained. x represents the position of transcript relative to reference genome is exonic overlap on the opposite strand. j represents the position of transcript relative to reference genome is multi-exon with at least one junction match. = represents the position of transcript relative to reference genome is complete, exact match of intron chain. u represents the position of transcript relative to reference genome is none of the above (unknown, intergenetic). Class_code reference paper (Pertea and Pertea, 2020).

Pipeline for long intergenic ncRNAs identification

The main program of lincRNA recognition are as follows: (1) GffCompare can be used to classify all the transcripts (the merged gtf files obtained above) in the input samples according to the reference transcript (Genome annotation file) (Pertea and Pertea, 2020). GffCompare software (version 0.11.2) was used to compare all the transcripts with the annotated information of the genome. Transcripts without the "u" character were filtered, and intergenic transcripts with the parameter "–r" of GffCompare were retained (Pertea et al., 2016); (2) Single exon transcripts less than 200 bp in length were removed; (3) Collect the location information of exons in the remaining transcript, extract the genome sequence of corresponding exons and fuse it into a complete transcript sequence; (4) CPC2, PLEK, and CNCI tools were used to evaluate the protein-coding potential of complete transcription sequences,

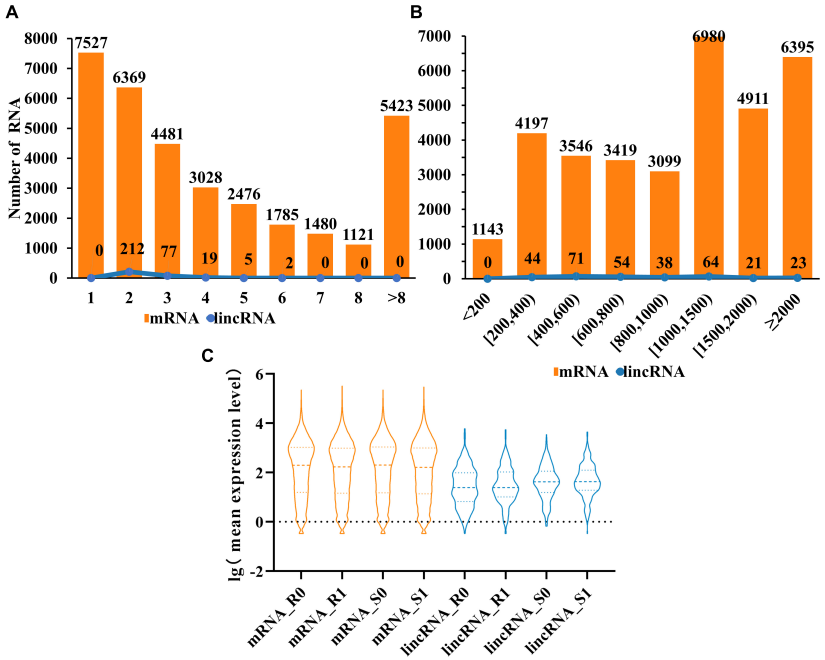

FIGURE 2
Characterization of tomato lincRNAs. **(A)** Compare the exon numbers of lincRNAs and protein-coding genes. **(B)** Compare the length of transcripts of lincRNAs and protein-coding genes. **(C)** The average expression levels of lincRNAs and protein-coding genes were compared (lincRNA in blue, mRNA in orange).

transcripts with coding capacity are discarded (Kong et al., 2007); (5) Elimination of transcripts containing any known protein-coding domain. Transdecoder (version 5.5.0) was used to identify the open reading frame of the complete transcript sequence, and transcripts with ORF greater than 300 were removed; (6) Transeq program in EMBOSS (version 6.6.0.0) was used to translate the transcript sequence into six possible amino acid sequences, these protein sequences are required to be compared with known proteins in the Pfam database for homology, and those with high homology (*E*-value < 1e-5) are discarded (Finn et al., 2015); (7) The BLASTX program was used to analyze the homology of transcription-encoded proteins with known proteins in the NR database. When the *e*-value was less than 1e-5, the corresponding transcript was discarded (Pirooznia et al., 2008); (8) The expression level of the transcript was determined using parameters "−e" and "−B" in the StringTie (Pertea et al., 2016). Transcripts with read count > 0 in at least one sample are retained as potential lincRNAs.

Characterization of tomato long intergenic ncRNAs

The exon number and transcript length of lincRNA and protein-coding genes were calculated using Excel software. GraphPad Prism 8 software was used to plot the violin plot of average gene expression.

Differential expression analysis of long intergenic ncRNAs

Differential expression analysis was performed using the OmicShare tools- DESeq2.[2] Expression abundance of lincRNA in different samples was obtained above. LincRNA whose expression levels in different treatment groups met both $|\log_2(FC)| \geq 1$ and *P*-value < 0.05 was considered to be significantly differentially expressed.

Prediction of differentially expressed long intergenic ncRNAs target genes

LincRNAs have been reported to regulate the expression of adjacent genes (Zou et al., 2018). In order to clarify the role of lincRNA of tomato after bacterial wilt infection, the potential cis-regulating target genes with differential expression of lincRNAs were predicted. Based on the tomato genome information, the mRNAs within 100 kb at 5′ upstream or 3′

2 https://www.omicshare.com/tools

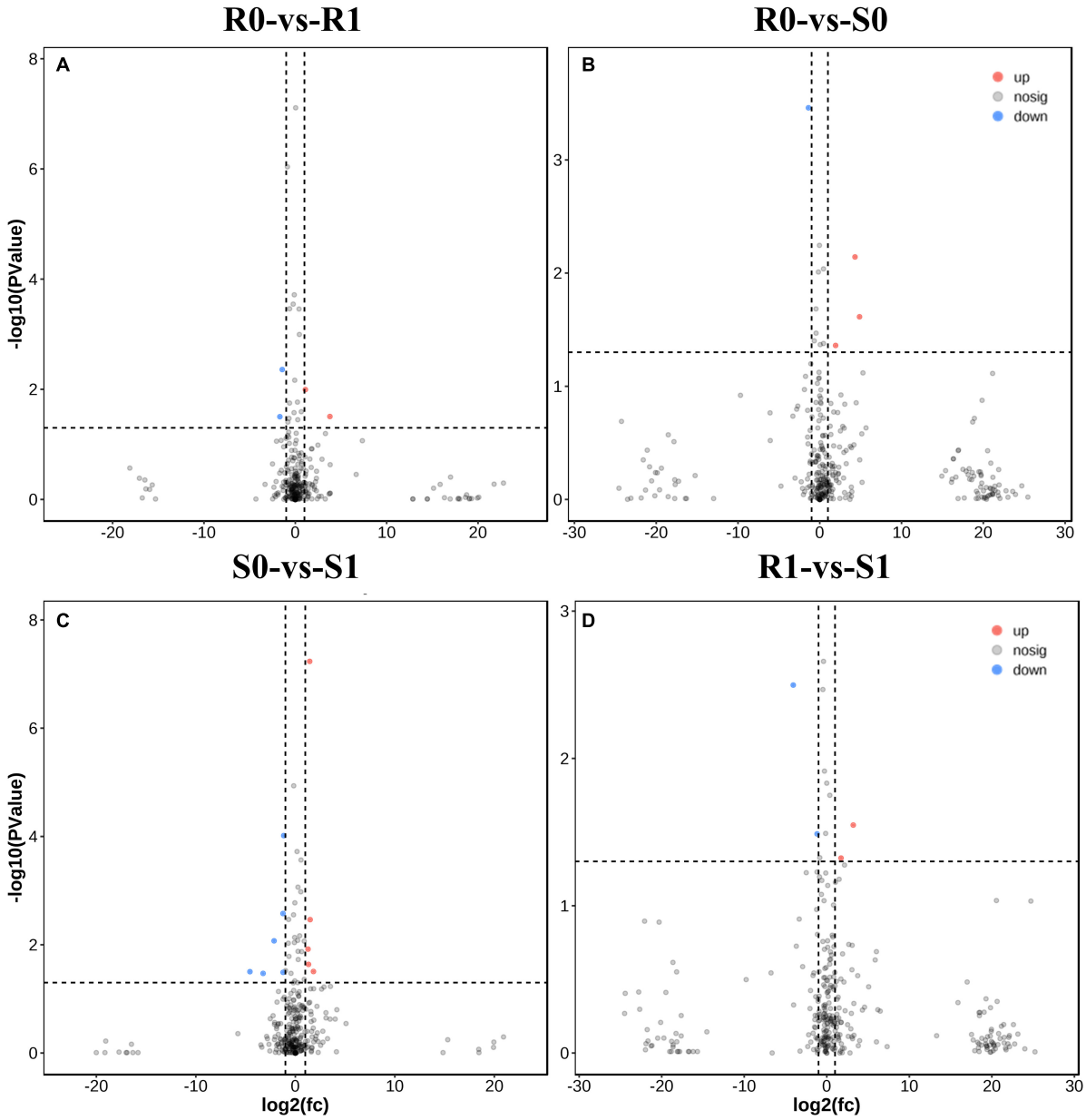

FIGURE 3
Differential expressions analysis of lincRNAs. **(A–D)** The volcano diagram of differential expression of lincRNA in different treatment groups was shown in sequence: R0 vs. R1, R0 vs. S0, S0 vs. S1, and R1 vs. S1.

downstream of each lincRNA are considered as potential cis-targets (Hou et al., 2017). Cytoscape software (version 3.9.1) was used to map the regulatory network.

Functional annotation of long intergenic ncRNAs target genes

All predicted potential target genes were functionally annotated in order to single out genes for disease resistance. GO and KEGG functional enrichment was performed using OmicShare tools. LincRNAs related to *R. solanacearum* infection were selected, and the heatmaps were drawn based on the expression level of lincRNAs.[3] Based on the annotated information of the genome, the function of adjacent target genes is obtained (**Supplementary Table 6**).

3 https://hiplot-academic.com/basic/heatmap?lang=zh_cn

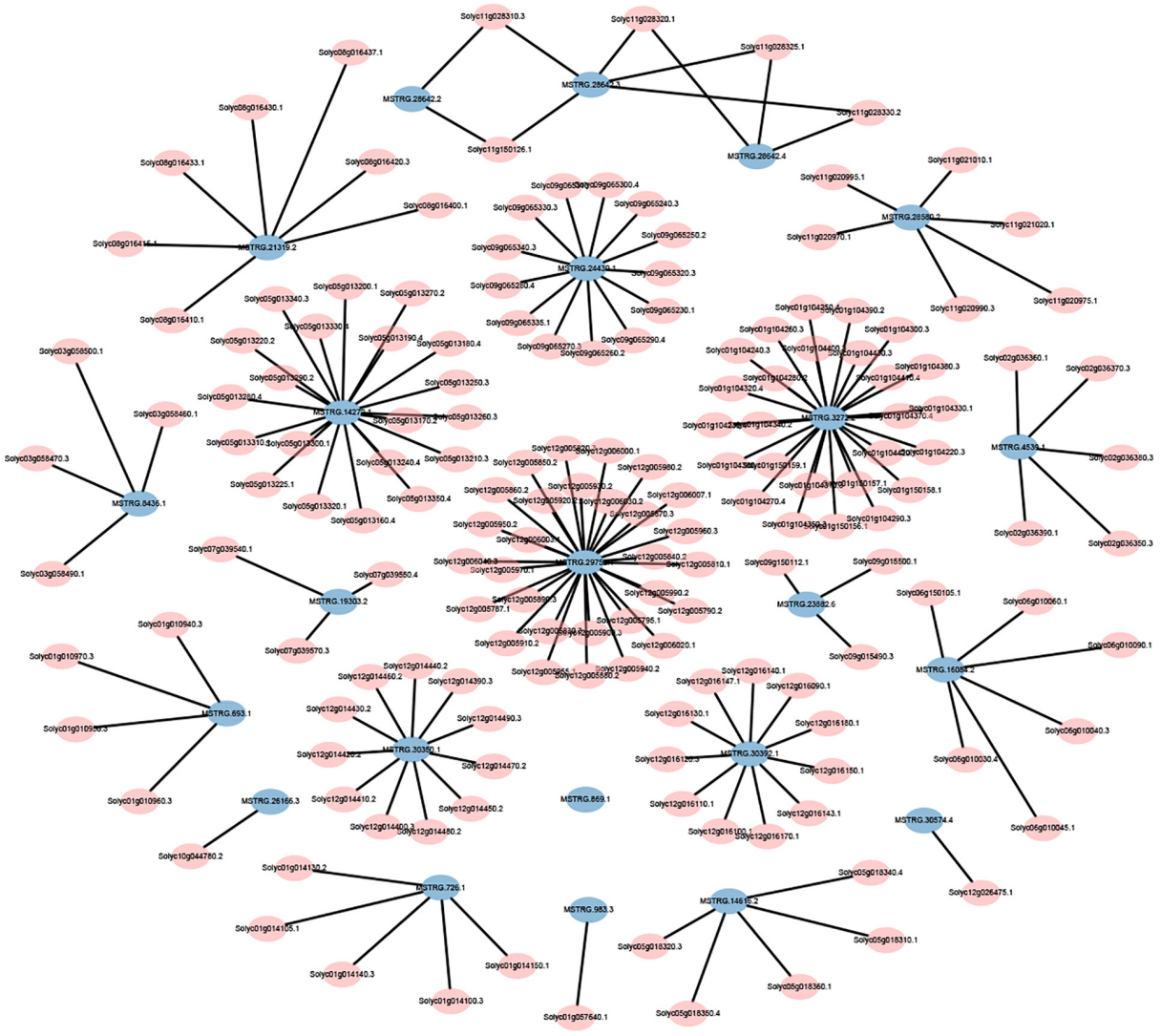

FIGURE 4
Distribution of adjacent functional genes with differential expression of lincRNAs (see **Supplementary Table 3** for details).

Plant materials and *Ralstonia solanacearum* and *Ralstonia solanacearum* inoculation

Tomato (Shouhefenguan F1 generation) seeds were germinated on wet filter papers in an incubator at 28°C for 2 days in the dark (Zhu et al., 2020). Good seedlings were selected and transferred to individual 3-inch pots. The tomato plants were cultured under 28 ± 2°C for 16 h in light and 8 h in darkness. At the six-leaf stage, the seedlings were inoculated with *R. solanacearum* strain GMI1000 which was obtained from Professor Meixiang Zhang (Shaanxi Normal University). Single colonies of *R. solanacearum* from TTC medium were transferred into NB medium for 48 h at 28°C. After centrifugation at 4,000 rpm for 10 min, the bacteria were re-suspended with sterile distilled water to give an optical density of 1.0 at 600 nm (approximately 10^8 cfu/mL). 50 mL of bacterial suspension was drenched over the soil surface for inoculation (Jaunet and Wang, 1999). The stem tissue was collected at 0, 2, 8, 12, 24, and 48 h after inoculation, then was frozen in liquid nitrogen, and was maintained in a cryogenic refrigerator. The samples at 0 h were used as control group.

RNA extraction and cDNA synthesis

Total RNA from tomato stem tissues was extracted using the TRIzol reagent (Invitrogen, USA) and digested with DNaseI (TaKaRa, Beijing, China) to remove genome DNA. The RNA was reverse transcribed using RevertAid Reverse Transcriptase

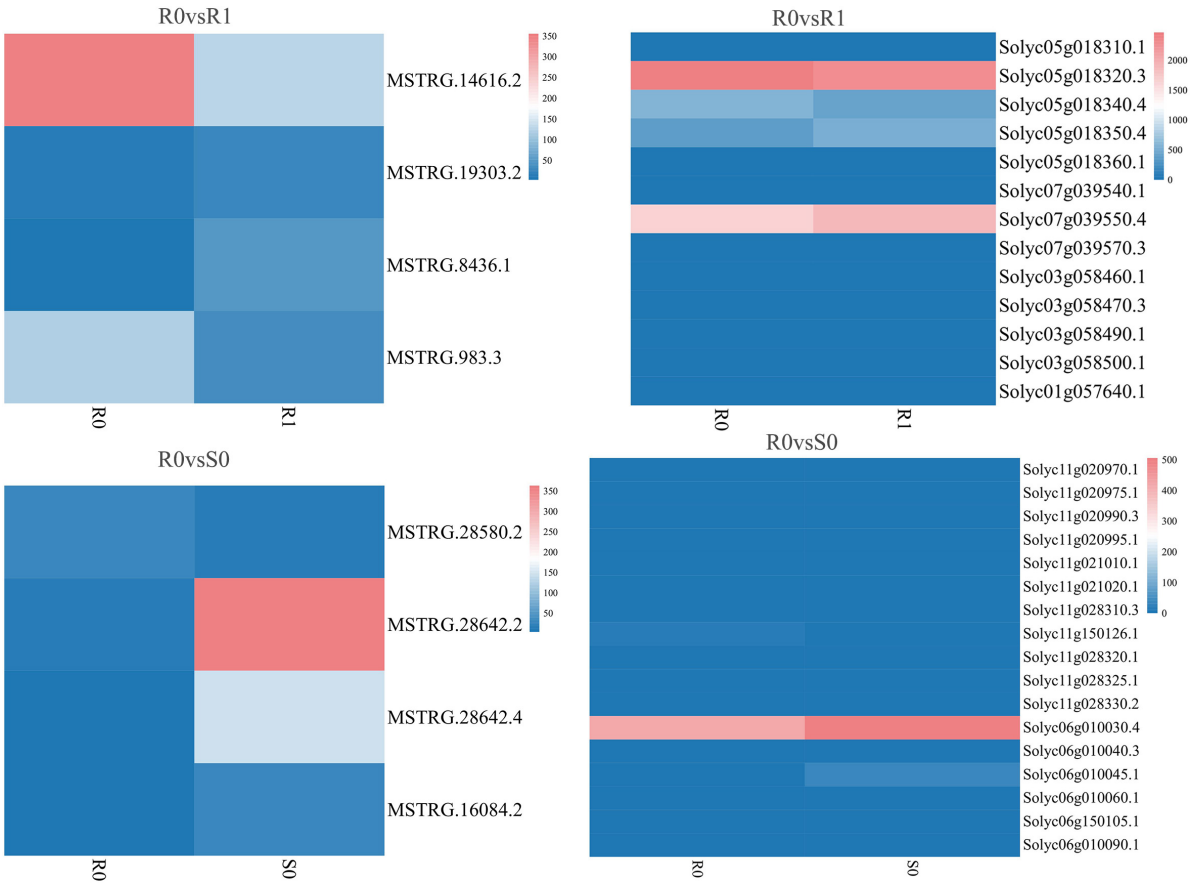

FIGURE 5
Expression of differentially expressed lincRNAs and adjacent mRNAs in R0 vs. R1, R0 vs. S0.

(Vazyme, Nanjing, China). The obtained cDNA was diluted to 100 ng/μL with enzyme-free water.

Expression pattern validation by quantitative real-time PCR

To verify whether the putative lincRNAs have cis-regulatory functions on the predicted target genes, the expression patterns of several lincRNA were verified by qRT-PCR. Nine lincRNAs were selected for qRT-PCR. They are MSTRG.4629.2-Solyc02g062230.1, MSTRG.16084.2-Solyc06g010060.1, MSTRG.14272.1-Solyc05g013220.2, MSTRG.14378.4-Solyc05g014260.3, MSTRG.3272.2-Solyc01g104370.4, MSTRG.19303.2-Solyc07g039550.4, MSTRG.30350.1-Solyc12g014390.3, MSTRG.8436-Solyc03g058460.1, MSTRG.14616.2- Solyc05g018310.3. The internal reference gene is *Actin* (GenBank No. U60480.1). Primer 5.0 software and website[4] were used to design the gene-specific primers. All the primer pairs used for PCR amplification were shown in **Supplementary Table 6**. The reactions were conducted in a 20 μL volume containing 10 μL 2 × *PerfectStart*^{TM} Green qPCR SuperMix, 0.4 μL of each primer (10 μmol/mL), 7.2 μL double distilled water, and 2 μL of the template cDNA under the following conditions: 94°C for 30 s followed by 40 two-step cycles of 94°C for 5 s and 59°C for 30 s.

Results

Genome-wide identification of long intergenic ncRNAs in tomato

12 publicly available tomato transcriptomes (**Supplementary Table 1**) were downloaded. After quality control of transcriptome data such as removal of adapter and removal of low-quality reads, 97.43% of the reads were successfully aligned with the tomato reference genome using HISAT2 (**Supplementary Table 1**). Stringtie was used to perform the assembly process, and there are 72,766 transcripts

4 https://biodb.swu.edu.cn/qprimerdb/

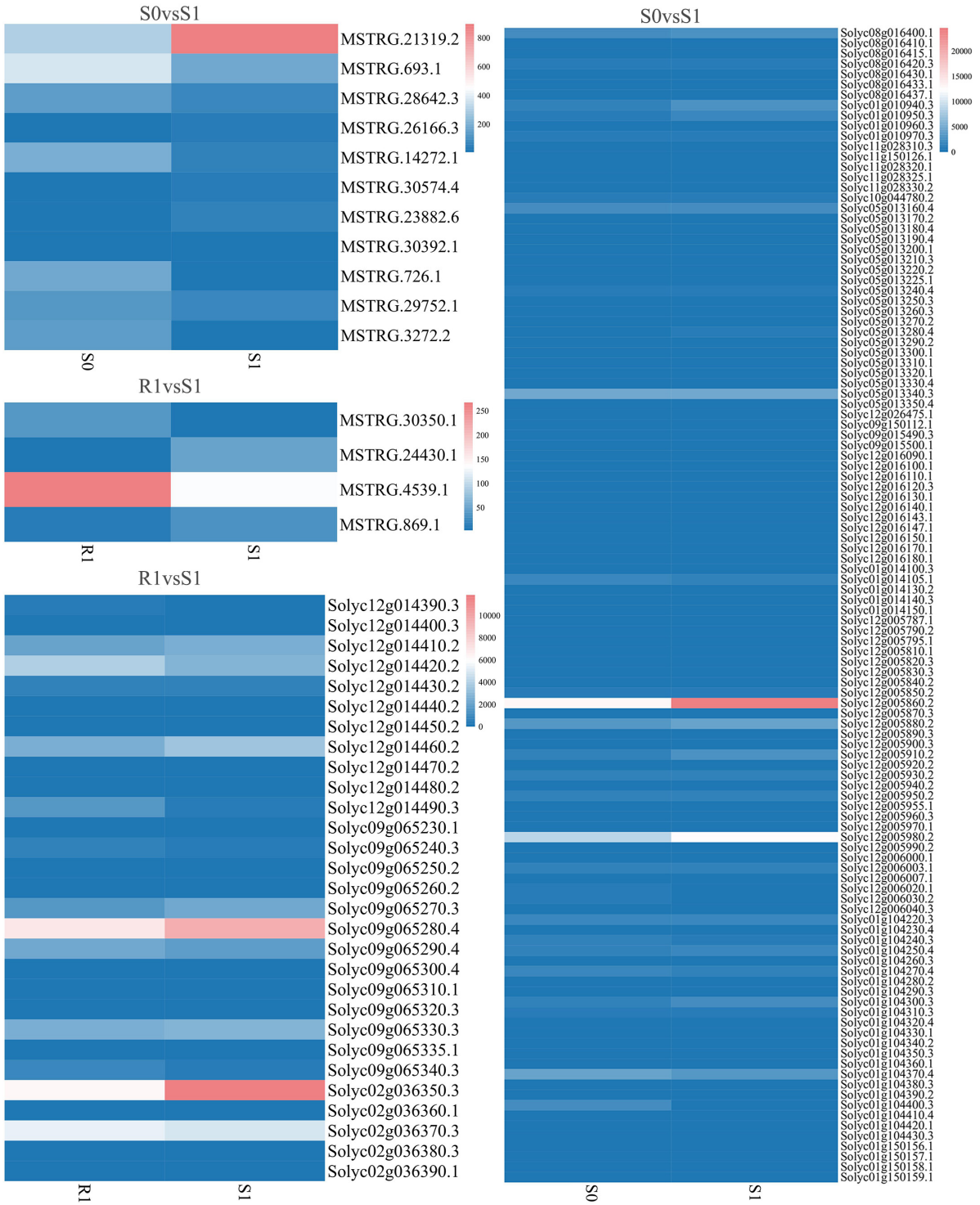

FIGURE 6
Expression of differentially expressed lincRNAs and adjacent mRNAs in S0 vs. S1, R1 vs. S1.

for lincRNA identification. GffCompare software was used to classify all the transcripts and lincRNAs are usually selected with "class_code = u" (Pertea and Pertea, 2020; **Figures 1A,B**). Among the 72,766 transcripts, 2,243 of them had a class code of u, and 918 transcripts were remained after filtering out the single exon transcripts with a length less than 200 bp. Among

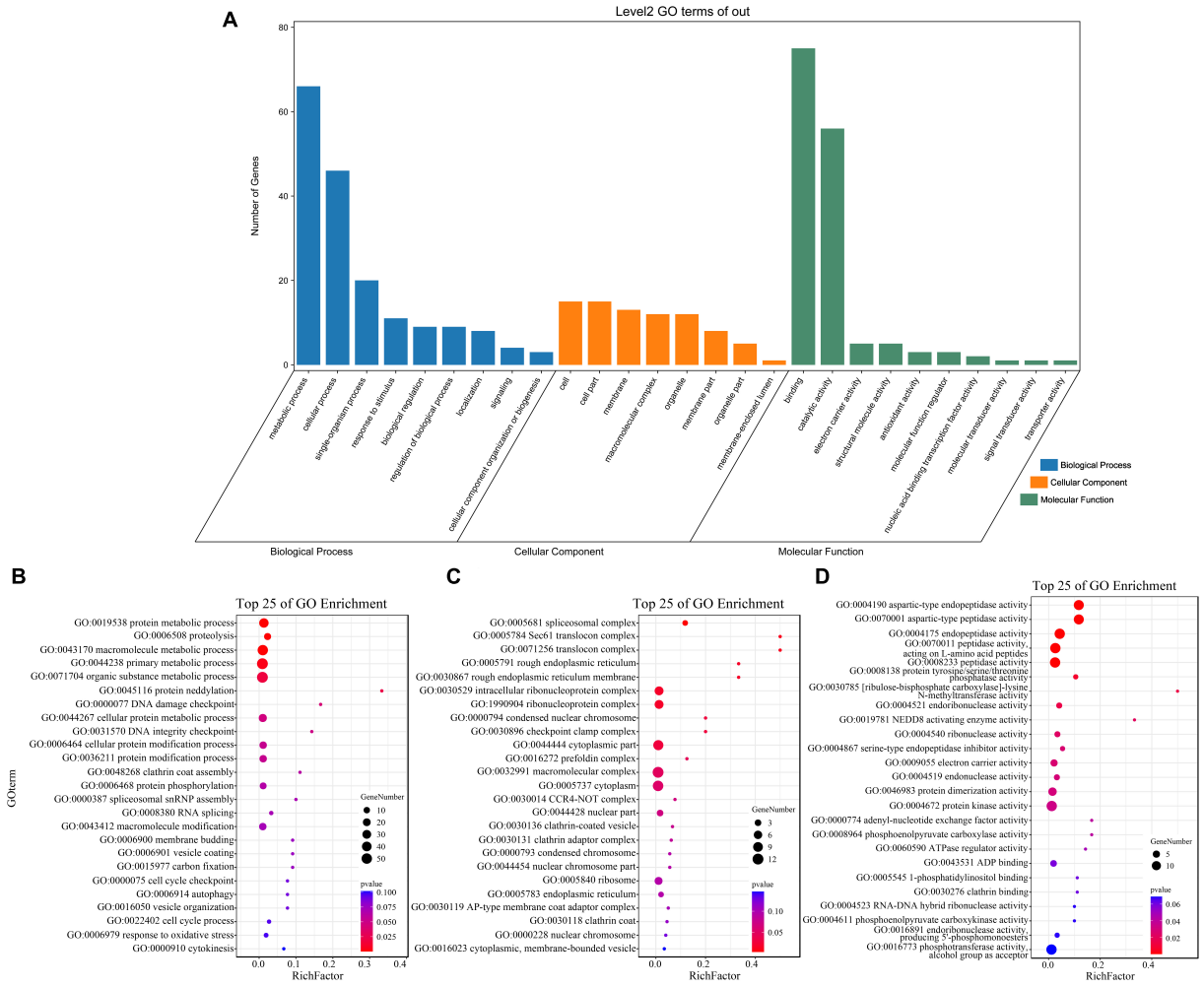

FIGURE 7
GO terms enrichment analysis of targets of 136 differentially expressed lincRNAs. **(A)** GO secondary classification statistics chart. The number of genes used for enrichment in each classification of GO was calculated. The abscissa represents the classification of GO three ontologies, namely, the secondary classification. The vertical axis represents the number of genes in each category. **(B–D)** Go enriched bubble map. Only enriched GO term (*P*-value < 0.05). The top 25 of biological process (BP), and the top 25 of molecular function (MF) and cellular component (CC) are shown. The circle size represented the gene number. Red to blue represents the low to high *P*-value.

them, CPC2 predicted results showed that 762 transcripts had no coding ability, PLEK prediction showed 670 transcripts had no coding capacity, and CNCI prediction indicated 740 transcripts had no coding capacity. The intersection of the three software results were 549 transcripts without coding capacity (**Figure 1C**). The length of the open reading frame (ORF) of the coding-capable mRNA typically greater than 300 nt. If the ORF of the RNA sequence is less than 300 nt, it is very unlikely to encode a protein. So, 429 transcripts with an ORF length less than 300 nt were finally retained. Transeq procedure was used to translate the transcript sequence into six possible protein sequences, which were compared with Pfam and Nr databases. The transcripts with high homology to the protein database were removed. Furthermore, lincRNAs with read count > 0 in at least one sample were considered to be expressed, and finally, 315 transcripts were obtained as putative tomato lincRNAs.

Characterization of tomato long intergenic ncRNAs

Compared with mRNAs, lincRNAs are smaller in length and have fewer exons has been reported (Zhu et al., 2015). To determine whether the lincRNAs in tomato have the above characteristics, we compared the transcript length and exon number of lincRNAs (315) and mRNAs (33,690) in tomato genome. The statistical data showed that the number of lincRNA and mRNA decreased gradually with the increase of the number of exons. It is noteworthy that the number of exons in the

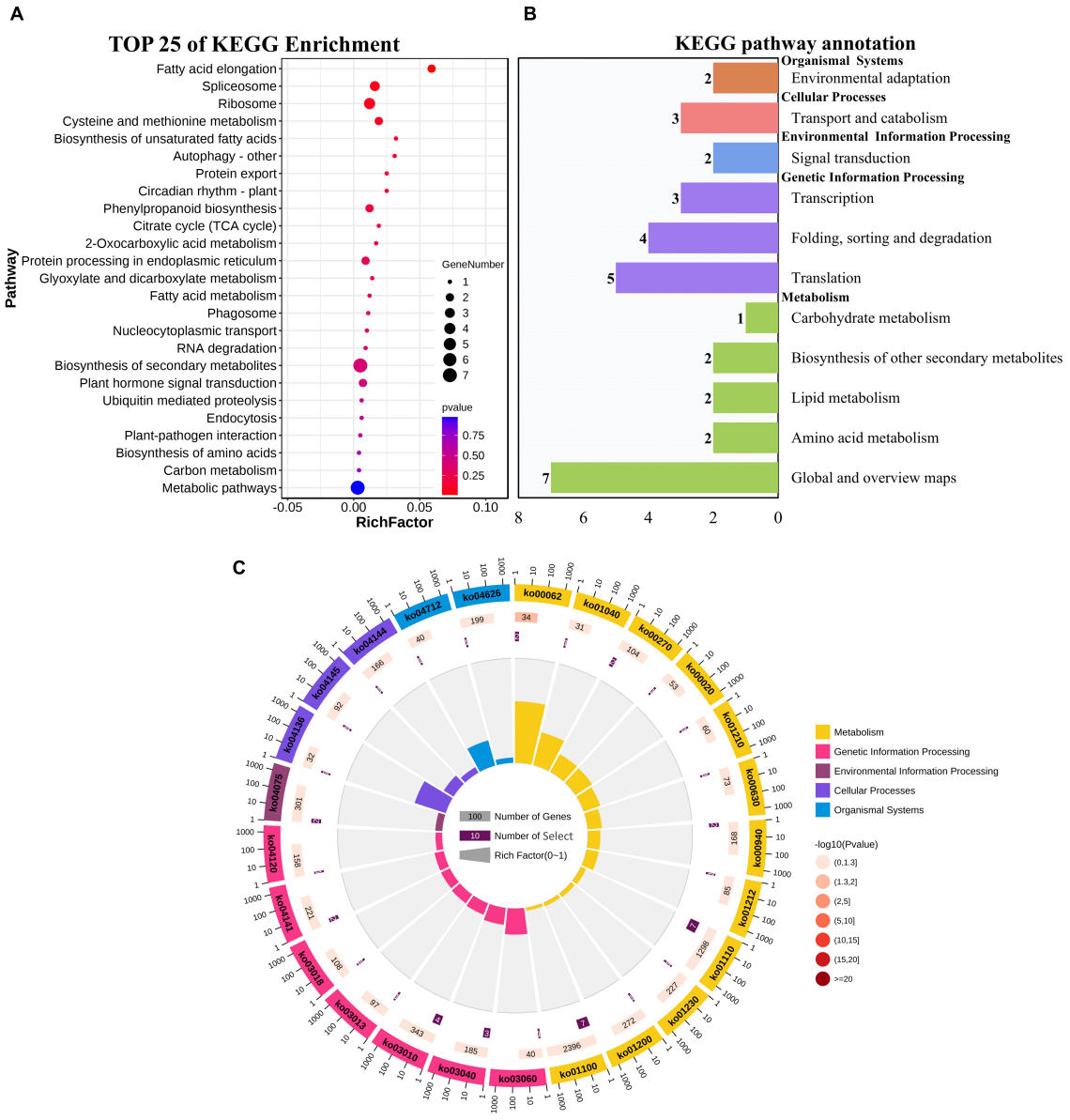

FIGURE 8
KEGG functional enrichment map of potential target genes of differentially expressed lincRNAs. **(A)** KEGG enrichment analysis of targets of 23 differentially expressed lincRNAs. The circle size represents the gene number. Red to blue represents the low to high *P*-value. **(B)** Statistical graph of number of class B gene annotations of Pathway. The names in bold black on the vertical axis are class A classification names, and the names in black are class B classification names. The horizontal axis represents the number of genes annotated to the corresponding B pathway. **(C)** Enrichment of circular graph. From the outside in, the first circle is the Pathway ID, Group colors correspond to different A class categories of KEGG, Outside the circle is the coordinate ruler of the number of genes; The bar length of the second circle corresponds to the number of background genes, the current pathway contains all genes, the color from dark to light corresponds to the *P*-value from small to large. The more genes, the longer the bar, and the smaller the *P*-value, the redder the color; the third circle corresponds to the number of target genes, the number of target genes contained in the current pathway; The polar histogram of the fourth circle is the rich factor, Represents the proportion of target gene in background genes.

lincRNAs ranges from two to six. The result revealed that although the length of lincRNAs is greater than 200 nt, the length will not be particularly long (Figure 2A). Analysis of transcript length shows that the sequence length of 66% of lincRNA is between 200 and 1,000 nt, with 34% more than 1,000 nucleotides. However, for mRNAs, 54% were greater than 1,000 nt (Figure 2B). These results indicated that, unlike mRNAs, most of the tomato lincRNAs were shorter and had fewer exons. After analyzing the mean expression level of mRNAs and lincRNAs in different treatment groups, the

results showed that the average expression levels of lincRNAs were significantly lower than mRNAs (**Figure 2C**). This may be the reason why lincRNA didn't get noticed at first. In addition, the average expression level of lincRNAs also have obvious differences between different tomato cultivars and this difference is not obvious in mRNAs. The result indicated that lincRNAs are more susceptible to cultivars factors than mRNAs.

Analysis of differentially expressed long intergenic ncRNAs and predicting the target genes

The expression levels of 315 lincRNAs in 12 samples were analyzed by differential expression analysis. The lincRNAs with at least twofold change in expression level and P-value < 0.05 were considered to be significantly differentially expressed. A total of 23 differentially expressed lincRNAs were selected from R0 vs. R1, S0 vs. S1, R0 vs. S0, and R1 vs. S1 in four comparison groups (**Figure 3**). It is worth noting that four differentially expressed lincRNAs were found between R0 and R1, while 11 differentially expressed lincRNAs were found between S0 and S1 (**Supplementary Table 2**). The results indicated that the lincRNAs response to *R. solanacearum* infection are different in different cultivars. Therefore, these lincRNAs with significantly differential expression obtained by pairwise comparison were collected together. After genome-wide comparison, 171 adjacent functional genes near 23 differentially expressed lincRNAs genes were screened (**Figure 4** and **Supplementary Table 3**). The result revealed that a single lincRNA has multiple potential adjacent target Genes. In addition, heat maps of gene expression were plotted according to their expression levels (**Figures 5**, **6**). The results of the heatmap hardly illustrate the connection between lincRNAs and mRNAs at expression levels.

Functional annotations of target genes

GO enrichment and KEGG pathway analysis were used to annotate the functions of adjacent target genes of differentially expressed lincRNAs. Functional annotation analysis was performed on 171 predicted target genes. A total of nine, eight, and ten GO terms for biological process (BP), cellular component (CC), and molecular function (MF) were obtained, respectively (**Figure 7A** and **Supplementary Table 4**). For BP, most of genes were related to protein metabolic processes (GO: 0019538; 0019538) (**Figure 7B**). For CC and MF, the most significant enrichment is spliceosomal complex (GO: 0005681) and aspartic-type endopeptidase activity (GO: 0004190), respectively (**Figures 7C,D**). The KEGG pathway result showed that the 25 pathways were enriched (**Figure 8A**). Statistical chart of level B classification of each pathway showed that the target genes belonged to 5 grade A classifications and 11 grade B classifications. Most of the annotated genes play a role in the plant metabolic processes (**Figure 8B**). KEGG enrichment circle diagram showed that ko00062 Pathway was the most significant one (P-value < 0.05). Ko00062 Pathway is fatty acid elongation pathway, the target genes involved in this pathway are Solyc05g014150.4.1 and Solyc05g013220.2.1 (**Figure 8C** and **Supplementary Table 5**). Furthermore, the possible function of 171 adjacent target genes was obtained according to the annotated information in the tomato genome (**Supplementary Table 3**). The result revealed that Solyc01g010970.3, adjacent target gene of MSTRG.693.1, was predicted to be involved in argonaute family protein. The function of Solyc05g018320.3 (adjacent target gene of MSTRG.14616.2) may be related to novel interactor of JAZ. Jasmonic acid is known to have a defense-inducing effect in plants. Solyc02g036350.3 (adjacent target gene of MSTRG.4539.1) was predicted to be related to ethylene-forming enzyme. These findings suggest that lincRNA related to tomato bacterial wilt may respond to pathogen invasion by regulating jasmonic acid, ethylene pathways, and expression of AGO protein.

The correlation between long intergenic ncRNAs and corresponding mRNAs expression patterns

Nine co-expressed lincRNAs and mRNAs were randomly selected, and the expression patterns were analyzed. A single lincRNA interacting with multiple mRNAs was detected. In this case, we selected the mRNA which is closest to lincRNA on the chromosomal for expression pattern analysis. The results show that expression patterns of randomly selected lincRNAs and corresponding mRNAs exhibited similar correlation in most of the infection time in tomato (**Figures 9A–I**). For instance, lincRNA "MSTRG.4629.2" interacting mRNA "Solyc02g062230.1" displayed positive correlation in expression trend at different times (**Figure 9A**). Moreover, a no-correlation could also be detected in several infection time, which might be either due to complex interaction network between lincRNA and mRNA or due to some unknown regions.

Discussion

LincRNAs play key roles in regulating plant growth and in response to biotic and abiotic stresses. However, lincRNAs cannot be identified directly from genome and can be only identified from RNA seq data (Shumayla et al., 2017). Some features of lincRNAs such as the temporal, spatial, inducible, and various other specific expression patterns lead most of the studies in plants to be limited scale (Shumayla et al., 2017). In this work, we performed the identification of lincRNAs in

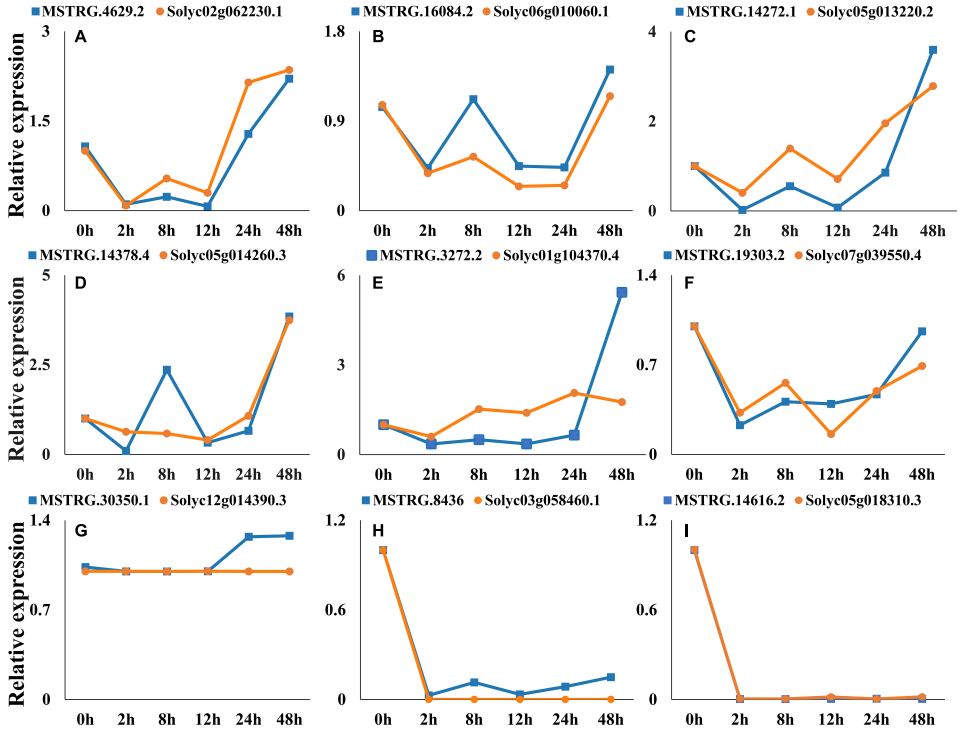

FIGURE 9
Expression pattern profiling of lincRNAs and mRNA pairs. The figure shows the expression pattern of lincRNAs. **(A)** MSTRG.4629.2-Solyc02g062230.1, **(B)** MSTRG.16084.2-Solyc06g010060.1, **(C)** MSTRG.14272.1-Solyc05g013220.2, **(D)** MSTRG.14378.4-Solyc05g014260.3, **(E)** MSTRG.3272.2-Solyc01g104370.4, **(F)** MSTRG.19303.2-Solyc07g039550.4, **(G)** MSTRG.30350.1-Solyc12g014390.3, **(H)** MSTRG.8436-Solyc03g058460.1, **(I)** MSTRG.14616.2- Solyc05g018310.3, interacting mRNAs at different times of infection.

tomato using the data from stems at the six-leaf stage from two tomato cultivars. After analyzing 12 RNA-seq data sets, and 315 possible lincRNAs were identified. These lincRNAs had fewer exons and shorter transcript length, which are markedly distinguished from mRNAs. Because of their low coding potential, their expression level is obviously lower than mRNAs. Ponjavic and Ponting (2007) found that about half of lincRNAs are transcribed near (<10 kb) to protein-coding genes, and these lincRNAs perhaps represent the best candidates for investigating the transcriptional regulation of neighboring genes. We expanded our search for neighboring genes to 100 kb of 5′ upstream and 3′ downstream of each lincRNA and 171 adjacent target genes was obtained. Furthermore, the expression patterns of lincRNAs interacting mRNAs were analyzed and part of the lincRNAs and corresponding mRNAs exhibited similar correlation in most of the infection time in tomato.

Although more and more studies have begun to focus on the identification of lincRNAs, the exploration of their functions still lags behind (Sanchita Trivedi and Asif, 2019). Because of the conservation of non-coding RNA sequences, they were initially thought to have no functions (Wang et al., 2004). In the regulation of gene expression, ncRNAs are involved in multiple mechanisms. The regulatory modality of small RNAs such as miRNAs and siRNAs has been widely reported (Pillai, 2005; Carthew and Sontheimer, 2009; Tiwari et al., 2014; Sanchita et al., 2018). These genes bind to their corresponding targets (mRNAs) to achieve gene silencing. Studies have found that lincRNAs also play critical roles in transcriptional and posttranscriptional regulation of gene expression in a wide variety of organisms (Fukuda et al., 2019). Later research found that long non-coding RNAs with potential functions in gene regulation are widespread throughout the transcriptome (Iyer et al., 2015). The non-coding region of the genome is largely composed of transposable elements, some of which are functionalized with lincRNAs (Zhao et al., 2021). How lincRNA regulates the expression of susceptibility or resistance genes in tomato to play what role needs further study. However, it has been reported that OsAGO2 negatively regulates OsHXK1 expression at the epigenetic level through DNA methylation of OsHXK1 promoter region, thus negatively regulating rice resistance to black stripe dwarf disease and some ARGONAUTE family members are required for RNAi-like phenomena (Hunter et al., 2003; Wang et al., 2021). The GO and KEGG analysis enlightened the probable function of potential target genes, however, the actual role needs to be established in future studies (Shumayla et al., 2017).

Compared to lincRNA, lncRNA is more deeply researched (lincRNA is a kind of lncRNA). Except for the length requirement, we found that lncRNAs lack a typical ORF, initiation codon, 3′ UTRs, and a termination codon. However, previous studies have shown that the formation of lncRNAs are only slightly different from protein-coding mRNAs. For example, most of the lncRNAs are transcribed by RNA polymerase II, very similar to mRNAs. Differences in lncRNAs transcription by RNA polymerase III were also found (Wu et al., 2012). Even lncRNAs is missing parts of its functional structure relative to mRNA, the lncRNAs still have all the properties like polyadenylation at 3′ end, 5′ capping and splicing (Quan et al., 2015). Similar research results indicate that lincRNAs also has methylation process, which is different from mRNAs lincRNAs had different DNA methylation profiles (Wang M. H. et al., 2018). And the researchers found that lincRNAs were obviously activated after CG DNA methylation (Zhao et al., 2021). Other studies have shown that the lincRNAs have two regulation of gene expression, cis and trans manner (Zhang et al., 2014; Quan et al., 2015). The various ways in which lincRNA functions are gradually being explored and discovered. Little by little, the mystery of lincRNA is being unraveled. Our research will focus on specific lincRNAs that play a key role in tomato infection by *R. solanacearum*. The potential lincRNAs of the tomato identified from our analysis have certain reference significance and these lincRNAs may be used for further functional genomics studies.

Data availability statement

Publicly available datasets were analyzed in this study. This data can be found here: NCBI, PRJNA787007.

Author contributions

JY and DM designed the article. PC and SG directed the data analysis and manuscript writing. CZ supervised the experiment. DM and YL confirmed the manuscript. All authors contributed to the article and agreed to submit version of the manuscript.

Funding

This research was supported by the "Open Project Program of Engineering Research Center of Ecology and Agricultural Use of Wetland, Ministry of Education" (KFT202102) and "Open Project Program of Key Laboratory of Integrated Pest Management on Crop in Central China, Ministry of Agriculture/Hubei Province Key Laboratory for Control of Crop Diseases, Pest and Weeds (2020ZTSJJ8)."

Acknowledgments

We thank Prof. Meixiang Zhang (Shaanxi Normal University, Xi'an, China) for providing *Ralstonia solanacearum* strain.

Conflict of interest

The authors declare that the research was conducted in the absence of any commercial or financial relationships that could be construed as a potential conflict of interest.

Publisher's note

Supplementary material

The Supplementary Material for this article can be found online at: https://www.frontiersin.org/articles/10.3389/fpls.2022.981281/full#supplementary-material

References

Ariel, F., Jegu, T., Latrasse, D., Romero-Barrios, N., Christ, A., Benhamed, M., et al. (2014). Noncoding transcription by alternative RNA polymerases dynamically regulates an auxin-driven chromatin loop. *Mol. Cell* 55, 383–396. doi: 10.1016/j.molcel.2014.06.011

Baichoo, Z., and Jaufeerally-Fakim, Y. (2016). *Ralstonia solanacearum* upregulates marker genes of the salicylic acid and ethylene signaling pathways but not those of the jasmonic acid pathway in leaflets of *Solanum* lines during early stage of infection. *Eur. J. Plant Pathol.* 147, 615–625. doi: 10.1007/s10658-016-1030-7

Bergougnoux, V. (2014). The history of tomato: From domestication to biopharming. *Biotechnol. Adv.* 32, 170–189. doi: 10.1016/j.biotechadv.2013.11.003

Cabili, M. N., Trapnell, C., Goff, L., Koziol, M., Tazon-Vega, B., Regev, A., et al. (2011). Integrative annotation of human large intergenic noncoding RNAs reveals global properties and specific subclasses. *Genes Dev.* 25, 1915–1927. doi: 10.1101/gad.17446611

Carthew, R. W., and Sontheimer, E. J. (2009). Origins and mechanisms of miRNAs and siRNAs. *Cell* 136, 642–655. doi: 10.1016/J.CELL.2009.01.035

Finn, R. D., Clements, J., Arndt, W., Miller, B. L., Wheeler, T. J., Schreiber, F., et al. (2015). HMMER web server: 2015 update. *Nucleic Acids Res.* 43, W30–W38. doi: 10.1093/nar/gkv397

Fukuda, M., Nishida, S., Kakei, Y., Shimada, Y., and Fujiwara, T. (2019). Genome-wide analysis of long intergenic noncoding RNAs responding to low-nutrient conditions in *Arabidopsis thaliana*: Possible involvement of trans-acting siRNA3 in response to low nitrogen. *Plant Cell Physiol.* 60, 1961–1973. doi: 10.1093/pcp/pcz048

Gao, L. L., and Bradeen, J. M. (2016). Contrasting potato foliage and tuber defense mechanisms against the late blight pathogen *Phytophthora infestans*. *PLoS One* 11:e0159969. doi: 10.1371/journal.pone.0159969

Golicz, A., Singh, M. B., and Bhalla, P. L. (2017). The long intergenic noncoding RNA (lincRNA) landscape of the soybean genome. *Plant Physiol.* 176, 2133–2147. doi: 10.1104/pp.17.01657

Hou, X. D., Du, Y. M., Liu, X. M., Zhang, H. B., Liu, Y. H., Yan, N., et al. (2017). Genome-wide analysis of long non-coding RNAs in potato and their potential role in tuber sprouting process. *Int. J. Mol. Sci.* 19:101. doi: 10.3390/ijms19010101

Hunter, C., Sun, H., and Poethig, R. S. (2003). The *Arabidopsis* heterochronic gene ZIPPY is an ARGONAUTE family member. *Curr. Biol.* 13, 1734–1739. doi: 10.1016/j.cub.2003.09.004

Iyer, M. K., Niknafs, Y. S., Rohit, M., Udit, S., Anirban, S., Yasuyuki, H., et al. (2015). The landscape of long noncoding RNAs in the human transcriptome. *Nat. Genet.* 47, 199–211. doi: 10.1038/ng.3192

Jaunet, T. X., and Wang, J. F. (1999). Variation in genotype and aggressiveness of *Ralstonia solanacearum* race 1 isolated from tomato in Taiwan. *Phytopathology* 89, 320–327. doi: 10.1094/phyto.1999.89.4.320

Kong, L., Yong, Z., Ye, Z. Q., Liu, X. Q., and Ge, G. (2007). CPC: Assess the protein-coding potential of transcripts using sequence features and support vector machine. *Nucleic Acids Res.* 35, W345–W349. doi: 10.1093/nar/gkm391

Kwenda, S., Birch, P. R. J., and Moleleki, L. N. (2016). Genome-wide identification of potato long intergenic noncoding RNAs responsive to *Pectobacterium carotovorum* subspecies *brasiliense* infection. *BMC Genomics* 17:614. doi: 10.1186/s12864-016-2967-9

Liu, J., Jung, C., Xu, J., Wang, H., Deng, S. L., Bernad, L., et al. (2012). Genome-wide analysis uncovers regulation of long intergenic noncoding RNAs in *Arabidopsis*. *Plant Cell* 24, 4333–4345. doi: 10.1105/tpc.112.102855

Murti, R. H., Afifah, E. N., and Nuringtyas, T. R. (2021). Metabolomic response of tomatoes (*Solanum lycopersicum* L.) against bacterial wilt (*Ralstonia solanacearum*) using ^{1}H-NMR spectroscopy. *Plants* 10:1143. doi: 10.3390/plants10061143

Nguyen, T. T., Le, N. T., and Sim, S. C. (2021). Genome-wide association study and marker development for bacterial wilt resistance in tomato (*Solanum lycopersicum* L.). *Sci. Hortic.* 289:110418. doi: 10.1016/j.scienta.2021.110418

Pertea, G., and Pertea, M. (2020). GFF utilities: GffRead and GffCompare. *F1000 Res.* 9:304. doi: 10.12688/f1000research.23297.1

Pertea, M., Kim, D., Pertea, G. M., Leek, J. T., and Salzberg, S. L. (2016). Transcript-level expression analysis of RNA-seq experiments with HISAT, StringTie and Ballgown. *Nat. Protoc.* 11, 1650–1667. doi: 10.1038/nprot.2016.095

Pillai, R. S. (2005). MicroRNA function: Multiple mechanisms for a tiny RNA? *RNA* 11, 1753–1761. doi: 10.1261/rna.2248605

Pirooznia, M., Perkins, E. J., and Deng, Y. (2008). Batch blast extractor: Anautomated blastx parser application. *BMC Genomics* 9(Suppl. 2):S10. doi: 10.1186/1471-2164-9-S2-S10

Ponjavic, J., and Ponting, C. P. (2007). The long and the short of RNA maps. *BioEssays* 29, 1077–1080. doi: 10.1002/bies.20669

Quan, M., Chen, J., and Zhang, D. (2015). Exploring the secrets of long noncoding RNAs. *Int. J. Mol. Sci.* 16, 5467–5496. doi: 10.3390/ijms16035467

Rambla, J. L., Tikunov, Y. M., Monforte, A. J., Bovy, A. G., and Antonio, G. (2014). The expanded tomato fruit volatile landscape. *J. Exp. Bot.* 65, 4613–4623. doi: 10.1093/jxb/eru128

Raza, W., Ling, N., Yang, L., Huang, Q., and Shen, Q. (2016). Response of tomato wilt pathogen *Ralstonia solanacearum* to the volatile organic compounds produced by a biocontrol strain *Bacillus amyloliquefaciens* SQR-9. *Sci. Rep.* 6:24856. doi: 10.1038/srep24856

Sanchita Trivedi, P. K., and Asif, M. H. (2019). Updates on plant long non-coding RNAs (lncRNAs): The regulatory components. *Plant Cell Tissue Organ Culture* 140, 259–269. doi: 10.1007/s11240-019-01726-z

Sanchita, R., Asif, M. H., and Trivedi, P. K. (2018). Dietary plant miRNAs as an augmented therapy: Cross-kingdom gene regulation. *RNA Biol.* 15, 1433–1439. doi: 10.1080/15476286.2018.1551693

Shuai, P., Liang, D., Tang, S., Zhang, Z. J., Ye, C. Y., Su, Y. Y., et al. (2014). Genome-wide identification and functional prediction of novel and drought-responsive lincRNAs in *Populus trichocarpa*. *J. Exp. Bot.* 65, 4975–4983. doi: 10.1093/jxb/eru256

Shumayla, S., Mehak, T., Shivi, T., Kashmir, S., and Upadhyay, S. K. (2017). Survey of high throughput RNA-seq data reveals potential roles for lncRNAs during development and stress response in bread wheat. *Front. Plant Sci.* 8:1019. doi: 10.3389/fpls.2017.01019

Tiwari, M., Sharma, D., and Trivedi, P. K. (2014). Artificial microRNA mediated gene silencing in plants: Progress and perspectives. *Plant Mol. Biol.* 86, 1–18. doi: 10.1007/s11103-014-0224-7

Vasse, J., Frey, P., and Trigalet, A. (1995). Microscopic studies of intercellular infection and protoxylem invasion of tomato roots by *Pseudomonas solanacearum*. *Mol. Plant Microbe Interact.* 8, 241–251. doi: 10.1556/APhyt.39.2004.1-3.10

Wang, H., Niu, Q. W., Wu, H. W., Liu, J., Ye, J., Yu, N., et al. (2015). Analysis of non-coding transcriptome in rice and maize uncovers roles of conserved lncRNAs associated with agriculture traits. *Plant J.* 84, 404–416. doi: 10.1111/tpj.13018

Wang, J., Zhang, J., Zheng, H., Li, J., Liu, D., Li, H., et al. (2004). Mouse transcriptome: Neutral evolution of 'non-coding' complementary DNAs. *Nature* 420, 563–573. doi: 10.1038/nature03016

Wang, J. X., Lin, J., Kan, J. L., Wang, H., Li, X., Yang, Q., et al. (2018). Genome-wide identification and functional prediction of novel drought-responsive lncRNAs in *Pyrus betulifolia*. *Genes* 9:311. doi: 10.3390/genes9060311

Wang, M. H., Zhao, W. H., Gao, L., and Zhao, L. X. (2018). Genome-wide profiling of long non-coding RNAs from tomato and a comparison with mRNAs associated with the regulation of fruit ripening. *BMC Plant Biol.* 18:75. doi: 10.1186/s12870-018-1300-y

Wang, Z., Chen, D., Sun, F., Guo, W., Wang, W., Li, X., et al. (2021). *ARGONAUTE 2* increases rice susceptibility to rice black-streaked dwarf virus infection by epigenetically regulating *HEXOKINASE 1* expression. *Mol. Plant Pathol.* 22, 1029–1040. doi: 10.1111/mpp.13091

Wu, J., Okada, T., Fukushima, T., Tsudzuki, T., Sugiura, M., and Yukawa, Y. (2012). A novel hypoxic stress-responsive long non-coding RNA transcribed by RNA polymerase III in *Arabidopsis*. *RNA Biol.* 9, 302–313. doi: 10.4161/rna.19101

Zhang, H., Hu, W. G., Hao, J. L., Lv, S. K., Wang, C. Y., Tong, W., et al. (2016). Genome-wide identification and functional prediction of novel and fungi-responsive lincRNAs in *Triticum aestivum*. *BMC Genomics* 17:238. doi: 10.1186/s12864-016-2570-0

Zhang, K., Shi, Z. M., Chang, Y. N., Hu, Z. M., Qi, H. X., and Hong, W. (2014). The ways of action of long non-coding RNAs in cytoplasm and nucleus. *Gene* 547, 1–9. doi: 10.1016/j.gene.2014.06.043

Zhao, T., Mei, H., Cao, Z., Wang, L., and Guan, X. (2021). Absence of CG methylation alters the long noncoding transcriptome landscape in multiple species. *FEBS Lett.* 595, 1734–1747. doi: 10.1002/1873-3468.14100

Zhu, B. Z., Yang, Y. F., Li, R., Fu, D. Q., Wen, L. W., Luo, Y. B., et al. (2015). RNA sequencing and functional analysis implicate the regulatory role of long non-coding RNAs in tomato fruit ripening. *J. Exp. Bot.* 15, 4483–4495. doi: 10.1093/jxb/erv203

Zhu, Y. X., Jiang, X. C., Zhang, J., He, Y., Zhu, X. M., Zhou, X. K., et al. (2020). Silicon confers cucumber resistance to salinity stress through regulation of proline and cytokinins. *Plant Physiol. Biochem.* 156, 209–220. doi: 10.1016/j.plaphy.2020.09.014

Zou, C., Li, L., Cheng, X. F., Li, C. C., Fu, Y. H., Fang, C. C., et al. (2018). Identification and functional analysis of long intergenic non-coding RNAs underlying intramuscular fat content in pigs. *Front. Genet.* 9:102. doi: 10.3389/fgene.2018.00102

frontiers | Frontiers in Plant Science

TYPE Original Research
PUBLISHED 30 September 2022
DOI 10.3389/fpls.2022.982457

OPEN ACCESS

EDITED BY
Guotian Li,
Huazhong Agricultural University, China

REVIEWED BY
Yachun Su,
Fujian Agriculture and Forestry University, China
Muhammad Aamir Manzoor,
Anhui Agricultural University, China

*CORRESPONDENCE
Yan Li
vgly1987@sina.com
Dongfang Ma
madf@yangtzeu.edu.cn

†These authors have contributed equally to this work

SPECIALTY SECTION
This article was submitted to Crop and Product Physiology, a section of the journal Frontiers in Plant Science

RECEIVED 30 June 2022
ACCEPTED 12 September 2022
PUBLISHED 30 September 2022

CITATION
Zhan C, Li Y, Li H, Wang M, Gong S, Ma D and Li Y (2022) Phylogenomic analysis of phenylalanine ammonia-lyase (PAL) multigene family and their differential expression analysis in wheat (*Triticum aestivum* L.) suggested their roles during different stress responses. *Front. Plant Sci.* 13:982457. doi: 10.3389/fpls.2022.982457

Phylogenomic analysis of phenylalanine ammonia-lyase (PAL) multigene family and their differential expression analysis in wheat (*Triticum aestivum* L.) suggested their roles during different stress responses

Chuang Zhan[1†], Yiting Li[1†], Han Li[1†], Mengru Wang[1], Shuangjun Gong[2], Dongfang Ma[1,2*] and Yan Li[1,2*]

[1]Engineering Research Center of Ecology and Agricultural Use of Wetland, Ministry of Education/College of Agriculture, Yangtze University, Jingzhou, China, [2]Key Laboratory of Integrated Pest Management on Crop in Central China, Ministry of Agriculture/Hubei Province Key Laboratory for Control of Crop Diseases, Pest and Weeds/Institute of Plant Protection and Soil Science, Hubei Academy of Agricultural Sciences, Wuhan, China

Phenylalanine ammonia-lyase (PAL) is a key enzyme in the phenylalanine metabolism pathway and plays an important role in plant growth and stress response. It has been widely reported in plants, but less studied in wheat. In this study, 54 *PAL* genes were identified in the wheat genome. Based on phylogenetic analysis, the 54 *TaPAL* genes were divided into four groups (I, II, III, and IV). Then, the expression levels of *TaPALs* under biotic stresses were analyzed by transcriptome data analysis. The results showed that 31 genes were up-regulated and one gene was down-regulated after inoculation with *Fusarium graminearum*, 11 genes were up-regulated and 14 genes were down-regulated after inoculation with *Puccinia striiformis*, and 32 up-regulated and three down-regulated genes after inoculation with powdery mildew. The expression patterns of the five *TaPALs* were further analyzed by qRT-PCR. After inoculation with *F. graminearum*, the expression levels of *five TaPALs* were up-regulated. However, the *TaPALs* (expect *TaPAL49*) were down-regulated when inoculated with *P. striiformis*. Finally, the functions of *TaPAL32* and *TaPAL42* in resistance of wheat to the stripe rust were further analyzed by virus induced gene silencing (VIGS) assays. The results showed that the disease severity of *TaPAL32* and *TaPAL42* silenced plants was higher than that of control plants at 14 days after inoculation. It indicated that these two genes played a positive role in wheat stripe rust resistance. This study provided new evidence support for the functional study of *PAL* genes in wheat, and provided potential application value for the breeding of wheat resistant varieties.

KEYWORDS

phenylalanine ammonia-lyase, biotic stresses, qRT-PCR, virus induced gene silencing, disease resistance

Introduction

Phenylalanine ammonia-lyase (PAL, EC: 4.3.1.5) is the first and key rate-limiting enzyme in the phenylpropane metabolism pathway, which catalyzes the deamination of L-phenylalanine (L-Phe) to produce trans-cinnamic acid (MacDonald and D'Cunha, 2007) . PAL is firstly discovered in barley (*Hordeum vulgare*) seedlings (Koukal and Conn 1966) , and now it is found in various plants and a few microorganisms (Costa et al., 2003; MacDonald and D'Cunha, 2007; Huang et al., 2010). To date, *PAL* genes have been identified in various plants such as *Arabidopsis* (Huang et al., 2010), *Populus trichocarpa* (Shi et al., 2013), banana (*Musa nana*) (Wang et al., 2016), rice (*Oryza sativa*) (Zeng et al., 2018), and walnut (*Juglans regia*) (Yan et al., 2019). The number of PAL proteins varies greatly in plants, but its molecular weight varies little, mainly ranging from 275 to 330 KDa (Rawal et al., 2013; Dong and Shang, 2013; Zhang and Liu, 2015). In plants, PAL proteins are highly conserved, and the sequence similarity of PAL among different species can even reach to 80% (Song and Wang, 2009). PAL family proteins generally contain PLN02457, Phe_AM_lyase, Lyase_aromatic and PAL-HAL domains. The active site of PAL enzyme exists in the PAL-HAL domain, most of them contain the "GTITASGDLVPLSYIAG" active center sequence, and ASG (Ala-Ser-Gly) is the most typical conserved region of PAL in plants (Song and Wang, 2009; Chen, 2019).

In plants, many secondary metabolites, such as anthocyanins, lignin, hormones and flavonoids, are synthesised by phenylpropane synthesis pathway. These secondary metabolism plays an important role in plant growth, development and environmental adaptation. (Blake et al., 2012). As the rate-limiting enzyme of phenylpropane synthesis pathway, PAL is often connected with plant resistant. Many studies have reported that PAL played positive function in plant resistant. Overexpression of a *PAL* gene from the https://www.sciencedirect.com/topics/agricultural-and-biological-sciences/tropical-pastures legume https://www.sciencedirect.com/topics/agricultural-and-biological-sciences/stylosanthes *humilis* in tobacco results in increased resistance to *Cercospora nicotianae* (Way et al., 2002). Overexpression of *Lotus japonicus PAL* (*LjPAL1*) delays the infection process and reduces the number of nodules after *Mesorhizobium loti* infection (Chen et al., 2017). Meanwhile, it has been demonstrated that PAL is involved in the biosynthesis of the signaling molecule salicylic acid, which is an organic acid necessary for the acquisition of resistance in plant systems (Lefevere et al., 2020).

Common wheat (*Triticum aestivum* L.) is the world's major cereal crop, accounting for about 30% of the world's staple food, it is also an important model tool for plant research (Zhu et al., 2015; Zhang et al., 2019). Given the resistant function of PAL, the role of PAL in wheat disease resistance was studied. The expression levels of *PAL* genes were up-regulated in wheat cultivars resistant to *Fusarium graminearum* (Golkari et al., 2009). Overexpression of *Aegilops variabilis PAL (AevPAL1)* significantly enhanced cereal cyst nematode resistance in bread wheat (Zhang et al., 2021). Although these studies further showed that the *PAL* genes played an important role in the process of stress defense, its comprehensive information and functions under biotic stress in wheat remains unclear. In this study, bioinformatics methods were used to identify and analyse *T. aestivum* PAL (TaPAL) family members and their characteristics. In addition, the expression patterns of *TaPALs* under disease stresses were also quantified. Our results provide important theoretical support for the functional study of wheat *PAL* genes, and also provide potential application value for high-yielding wheat varieties breeding against various biotic stresses.

Materials and methods

Identification of PALs protein sequences in the wheat

The wheat genome sequences IWGSC RefSeq v2.1 were downloaded from the International Wheat Genome Sequencing Association website (https://wheat-urgi.versailles.inra.fr/Seq-Repository/Assemblies) (Alaux et al., 2018). Firstly, the PAL domain sequence (Pfam accessions: PF00221) was downloaded from the Pfam database (http://pfam.xfam.org/), and were used as queries to search the PAL proteins in wheat genome by HMMER3.0 with cutoff values ≤ 1e-5 (Eddy, 2008; Finn et al., 2016). Secondly, the protein sequences of four *Arabidopsis* PALs (AtPALs), 18 maize PALs (ZmPALs), and nine rice PALs (OsPALs) were retrieved from the Arabidopsis Information Resource (TAIR10) database (http://www.arabidopsis.org/index.jsp), the Maize Genetics and Genomics Database (MaizeGDB) (https://www.maizegdb.org/), and the Rice Genome Annotation Project (RGAP) database (http://rice.plantbiology.msu.edu/), respectively (Huang et al., 2010; Zeng et al., 2018; Deng et al., 2019). Subsequently, the above mentioned 31 PAL protein sequences were used as queries to search wheat genome data through BLASTp, and the expected cutoff value was set as e ≤ 1e-5 to ensure the reliability of the protein sequence. After merging two rounds of search results and deleting redundant sequences, unique ones were further validated through SMART (http://smart.emblheidelberg.de/) and InterProScan (v71.0, http://www.ebi.ac.uk/InterProScan) to determine whether sequences contain PF00221 domain.

Characterization of predicted TaPAL proteins

The protein characteristics of the TaPALs, including protein length, isoelectric point (pI), molecular weight (MW), instability

index, atomic composition, grand average hydropathicity (GRAVY), and amino acid composition, were analyzed using ExPASy Server10 (SIB Bioinformatics Resource Portal, https://prosite.expasy.org/PS50011). The online tools TMHMM (http://www.cbs.dtu.dk/services/TMHMM/) and SignalP4.1 (http://www.cbs.dtu.dk/services/SignalP/) were used to predict the transmembrane domains and signal peptides in TaPALs (Nielsen, 2017). Subcellular localization prediction of TaPALs were performed using Plant-mPLoc online tool (http://www.csbio.sjtu.edu.cn/cgi-bin/PlantmPLoc.cgi) (Chou and Shen, 2010).

Sequence alignment and phylogenetic tree construction

After collecting the protein sequences of four AtPALs, 18 ZmPALs, nine OsPALs, and TaPALs, DNAMAN (version 6.0) was used to align all amino acid sequences. The phylogenetic tree was constructed using the Maximum Likelihood (ML) method (1000 bootstrap trials) based on an LG model in MEGA7.0 software (Kumar et al., 2016). A midpoint rooted base tree was modified using the Interactive Tree of Life (IToL, version 5.5.1, http://itol.embl.de). The TaPALs were classified basing on the phylogenetic relationships.

Gene structure, conserved motifs and cis-elements analysis of TaPALs

The *TaPAL* gene structure was exhibited using the online software GSDS V2.0 (http://gsds.cbi.pku.edu.cn/index.php) according to the wheat genome annotation information (Hu et al., 2014). Conserved motifs of TaPALs were predicted using the online program MEME V 5.1.1 (Multiple Expectation Maximization for Motif Elicitation, http://meme-suite.org/tools/meme) (Bailey et al., 2015). The parameters were as follows: each sequence could comprise any number of non-overlapping occurrences of each motif, the number of different motifs was 20, and motif length ranged from 6 to 50 amino acids (Fang et al., 2019). The conserved domains of these predicted motifs were analyzed using InterPro (http://www.ebi.ac.uk/interpro) and SMART (http://coot.embl-heidelberg.de/SMART). The PlantCARE (http://bioinformatics.psb.ugent.be/webtools/plantcare/html/) was used to predict cis-acting elements in the regions 1,500 bp upstream of the start codons of *TaPALs* (Lescot et al., 2002). TBtools software was used for combing and visualizing the above results (Chen et al., 2020).

Chromosomal location, gene duplication, and Ka/Ks analysis

The gene annotation of *TaPALs* was extracted from wheat genome GFF3 file, and the chromosomal location was drawn with MapInspect software (Jiang et al., 2019). Gene duplications were divided into tandem and segmental replications. Tandem repeated events were identified using the following assessment criteria: (1) aligned sequence length > 80% regions of each sequence; (2) identity > 80%; (3) threshold ≤ 10^{-10}; (4) only one duplication can be admitted when genes are linked closely; and (5) intergenic distance is less than 25 kb. If genes met the three conditions (1), (2) and (3) and were located on different chromosomes, they were judged as segmental duplications (He et al., 2020). The Ka (non-synonymous)/Ks (synonymous) ratio were calculated after identification of a duplicated gene, and the selection pressure and selection mode were analyzed. The CDS sequences of the duplicated gene pairs were compared using MEGA 7.0 software. After removal of gaps the alignment results were imported into DnaSP v5.10 software for Ks value and Ka/Ks ratio analyses (Librado and Rozas, 2009) . For estimation of the timing of duplication events the formula $T = Ks/2\lambda \times 10^{-6}$ Mya was used to calculate divergence time (T) in millions of years (Mya), where $\lambda = 6.5 \times 10^{-9}$ represented the rate of replacement of each locus per herb plant year (Quraishi et al., 2011; Peng et al., 2012). Duplicated gene pairs between species were identified and used to carry out an inter-species synthetic analysis using R package "circlize" (Krzywinski et al., 2009; Song et al., 2019).

Inter-species evolution analysis of TaPALs

The genome sequence data and the annotation information of *Triticum urartu* (v1.43), *Triticum dicoccoides*, and *Aegilops Tauschii* (v4.0.43) were downloaded from Ensembl Plants database (http://plant.ensembl.org/index.html) (Bai et al., 2019). In order to better understand the origin of *TaPAL* genes, The PAL family genes in *T. urartu*, *T. dicoccoides*, and *A. Tauschii* were identified by the Blastp analysis. The cutoff values (e-value < 10^{-10}, identity > 80%) were used to ensure the reliability of homologous (Li et al., 2022) . The original definition of an ortholog was two genes from two different species that were derived from a single gene of the last common ancestor of that species. Paralogs were defined as genes derived from a single gene that was repeated within the genome (Zhang et al., 2019). The synteny relationship were displayed with R package "circlize" and TBtools software (Zhu et al., 2015; Chen et al., 2020).

Expression profiling of TaPAL genes in different tissues or under various stresses

Original data sets, including different development stages and tissues from variable treatments, were downloaded from the NCBI Short Read Archive (SRA) database and mapped to the wheat reference genome using Hisat2 (Li et al., 2022). The SRA numbers of those data were listed in Supplementary file 1. Cufflinks was used to calculate the expression levels of *TaPALs* (normalized by Transcripts Per Kilobase of exon model per Million mapped reads, TPM). The R package "pheatmap" was used to produce the heatmap.

Growth and stress treatment of wheat seedlings

The hexaploid common wheat cultivars Jingshuang 16 and Yangmai 158, were moderately sensitive to *Puccinia striiformis* f. sp. *tritici* and *F. graminearum*, respectively. Full-size seeds were surface disinfected with 1% hydrogen peroxide, and thoroughly rinsed with distilled water, then germinated in 25°C saturated water on three-layer filter paper (Zhang et al., 2019). The growth conditions were 25/20°C temperature and 16 h/8 h (day/night) photoperiod. The wild type strain of *F. graminearum* (PH-1) was cultivated on PDA plate and cultured at 25°C for 3 days. And then, the actively growing mycelial agar plugs (5 mm diameter) were transferred to a 150 mL conical flask containing 50 mL of liquid mung bean medium, and was cultured at 25°C with 150rpm for 3 days to produce conidia (Cao et al., 2016). After the coleoptile reached to 0.5 cm, the seedlings of Yangmai 158 were immersed in spore suspension (5×10^5 spores/mL) for 1 minute (Yang et al., 2010). Then the seedlings were wrapped in a wet filter paper and grown at 25°C with 70% relative humidity. The uninoculated wheat seedlings were used as control. The wheat stems were sampled at 6, 12, 24, and 48 h after inoculation.

The *P. striiformis* was remained on the susceptible cultivar Jingshuang 16. At two-leaf stage, the seedings were sprayed with fresh sporangium powder of CYR23 (4 mg/mL) and kept in dark place for 24 hours with moisture. The seedlings were cultured in 10-18°C light for 16 h/8 h (day/night) photoperiod. Wheat leaves were sampled at 6, 12, 24, and 48 h after inoculation. The uninoculated wheat was used as a control. The samples were immediately frozen liquid nitrogen and stored at -80°C. Each treatment included three technical replications and three biotic replicates in each replication.

Quantitative real-time PCR and data analysis

After analyzing the transcriptome data, five *TaPAL* genes (*TaPAL10, TaPAL14, TaPAL32, TaPAL42, TaPAL49*) with high expression levels were screened out. The expression levels of these five genes under *F. graminearum* and *P. striiformis* infection were analyzed by qRT-PCR. Total RNAs were reverse transcribed into cDNAs with a 5 × All-In-One RT Master Mix (Perfect Real Time) kit (ABM, Canada). Gene-specific primers were designed using Primer Premier 5.0 and listed in Supplementary file 1. For qRT-PCR assays, the cDNA was diluted into 100 ng/μL with ddH_2O. The 20 μL reaction volume contained 10 μL of 2 × SYBR Green Mix, 1 μL of each primer (10 μM), 2 μL of template, and 6 μL of ddH_2O. All quantitative real-time PCR (qRT-PCR) amplifications were performed on the iCycler iQ instrument (Biorad, Hercules, CA, USA). The following cycling parameters were used: initial denaturation at 95°C for 2min; 50 amplification cycles consisting of denaturation at 95°C for 15s, annealing and extension at 57°C for 45 s. Single-fragment amplification was verified by dissociation curve analysis. Three biotic replicates were performed for each sample, and each replicate contained three technical replicates. ADP-ribosylation factor Ta2291 was used as internal reference gene (Paolacci et al., 2009). Relative expression levels were calculated using the $2^{-\Delta\Delta Ct}$ method (Livak and Schmittgen, 2001) . The heatmap were plotted using Origin software (Moberly et al., 2018).

Subcellular localization of TaPAL proteins

To verify the prediction results of TaPAL proteins localization, the CDS region of *TaPAL32* and *TaPAL42* were amplified using cDNA as template. The vector pART27:GFP was digested with *Xho*I (Biomarker, China) and then purified by Cycle-pure Kit (Omega, UK). The full-length gene fragments were inserted into the purified pART27:GFP vector using ClonExpress II one-step cloning kit (Vazyme, China). Then the recombinant vector pART27:TaPAL32-GFP and pART27:TaPAL42-GFP were transformed into *Agrobacterium tumefaciens* GV3101. The leaves from 6 to 8 week-old *Nicotiana benthamiana* were injected with *A. tumefaciens*. After 48 h, the GFP signals were detected and were observed under fluorescence microscope (Nikon DS-Ri2, Japan).

BSMV-mediated gene silencing

The spring wheat cultivar Fielder was used in this experiment. Approximately 120bp of gene fragments of *TaPAL32* and *TaPAL42* were amplified from wheat cDNA using the primers listed in Supplementary file 1. Then the fragments were inserted into the BSMV:γ vector. The virus was inoculated on the second leaf of the two-leaf wheat seedlings by mechanical friction method and then placed in an artificial incubator for 25°C cultured. BSMV : TaPDS (TaPDS, wheat octahydrolysin desaturase) was used as a positive

control, and 1× Fes buffer (0.1M glycine, 0.06M K2HPO4, 1% w/v tetrasodium pyrophosphate, 1% w/v bentonite, and 1% w/v celite, pH 8.5) treated plants were used as negative control (Mock) (Zhu et al., 2018). At 10 dpi, the leaves with mosaic symptoms were inoculated with fresh uredospores of *P. striiformis* (CYR23). Inoculated leaves were collected at 0, 24, and 48 h after inoculation to determine the efficiency of silencing. The experiment was repeated at least three times. Relative expression levels were determined using the $2^{-\Delta\Delta Ct}$ method (Livak and Schmittgen, 2001).

Results

Identification and characterization of PAL proteins in wheat

Firstly, 571 wheat candidate PAL proteins were obtained by Blastp analysis. Then, 65 candidate PAL proteins were screened in the wheat genome through SMART and InterProScan. Finally, the results were combined to remove redundant sequences, and 54 PAL members were identified in wheat genome. These TaPAL proteins ranged from 265-714 amino acids in length, with predicted molecular weights ranging from 29.80 kDa to 77.34 kDa (Supplementary file 2). The isoelectric points of 51 TaPAL proteins were less than 7. Only the pI values of TaPAL14, TaPAL26, and TaPAL43 had were greater than 7. The grand average of the hydrophilicity (GRAVY) of all TaPALs were less than zero, suggesting that they were almost all hydrophilic proteins. The proteins stability prediction results showed that all TaPALs were unstable proteins. Subcellular localization predicted results showed that all TaPALs were located in the cytoplasm.

Phylogenetic analyses of TaPALs

To understand the evolutionary relationships of these 54 TaPAL proteins, a maximum likelihood phylogenetic tree was built based on all PAL proteins in wheat, maize, rice, Arabidopsis (Supplementary file 3). the phylogenetic tree showed that all PAL proteins were divied into four Groups (Group I, II, III, and IV) (Figure 1), which was consistent with the previous classification (Lepelley et al., 2012; Yan et al., 2019). Overall, Group I contained the largest number of TaPALs (26) and Group III had the lowest number of TaPALs (four).

Analysis of gene structure, protein motifs and sequence conservation for TaPALs

In order to understand gene structure of TaPALs, we analyzed wheat GFF3 format annotations. The results showed that these genes contain no more than two introns, and 12 TaPAL genes were intronless. More interestingly, most of these genes were clustered into Group II and III (Figure 2). In Group I, TaPAL1 and TaPAL11 contained two introns, while the remaining members had only one intron. Compared with genes in the other three groups, the exon-intron structures of genes in Group IV were more complicated. TaPAL39 had no intron, three TaPAL genes (TaPAL37, TaPAL43, and TaPAL49) had two introns, and the remaining members had only one intron.

In order to study the conserved regions of TaPAL proteins, the motifs of 54 TaPAL proteins were analyzed by MEME online software. Twenty conservative motifs were identified (Figure 2 and Supplementary file 4). Eight of these motifs (motif1-2, 4-6, and 10-12) were found to be associated with characteristic functional domains of the typical plant PAL protein. Motif 1 was mostly present in most of TaPAL proteins. Analysis of conserved motifs showed that TaPAL protein domains were distributed in almost all of the 54 members.

Due to the high sequence homology of PAL in plants, the protein sequences of 54 TaPAL were aligned. As shown in Figure 2, most TaPAL proteins had conserved enzyme active sites in the PAL-HAL and MIO domains, except for the nine core domains of TaPAL16, TaPAL22, TaPAL28, TaPAL37 to 41, and TaPAL43. It was worth noting that TaPAL16 and TaPAL28 lacked the core domains of PAL-HAL and MIO. In the MIO region, two conserved residues, Ala and Gly, were found to be conserved in all TaPAL proteins containing this domain. Although the PAL-HAL domain was conserved among 54 TaPALs, Gly residues had been replaced by Cys and His in TaPAL22 and TaPAL43, respectively. These analyses indicated that most TaPAL proteins may have enzymatic activity, but their activities were different.

Chromosome distribution, gene duplication events, homology analysis, and Ka/Ks analysis

Chromosome mapping showed that 54 *TaPAL* genes were unevenly distributed on 16 chromosomes of common wheat (Figure 3 and Supplementary file 5). *TaPALs* were mainly distributed on chromosomes 2A, 2B and 2D, which contained eight, eight and seven genes, respectively. It was the least distributed on chromosomes 3A, 4A and 5A, and there was only one gene on each chromosome. In order to adapt to different environmental conditions, tandem replication and fragment replication were necessary for the evolution of gene families, and duplicate events of *TaPALs* need to be detected. As shown in Figure 4 and Supplementary file 6, 29 pairs of tandem duplication genes and 115 pairs of segment duplication genes were identified in 54 *TaPALs*, and most interestingly, the tandem repeat genes were only found in Group I and II.

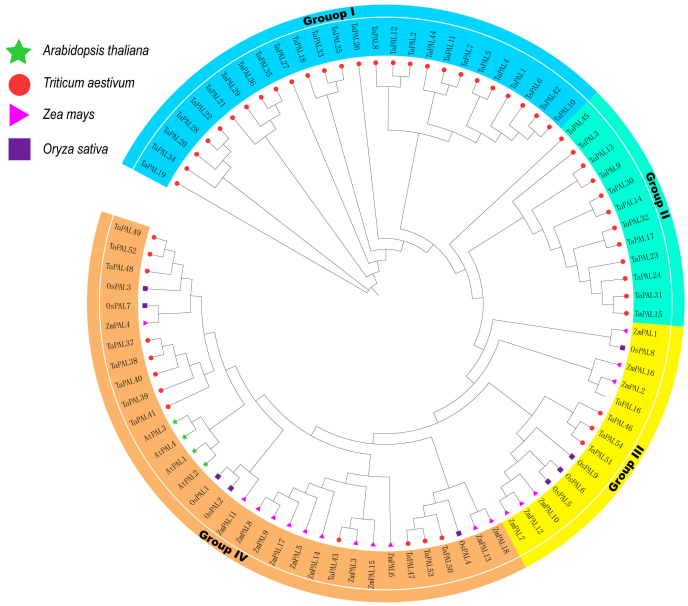

FIGURE 1
Phylogenetic relationship of TaPALs, OsPALs, AtPALs, and ZmPALs. Protein sequences were aligned using ClustalW2 sequence alignment program and the phylogenetic tree was constructed by software MEGA7 used to create Maximum Likelihood (ML) under the LG model. The tree was constructed with 1,000 bootstrap replications. Different groups were marked by different colors, and the PAL from wheat, rice, maize, and *Arabidopsis* were distinguished with different color and shape.

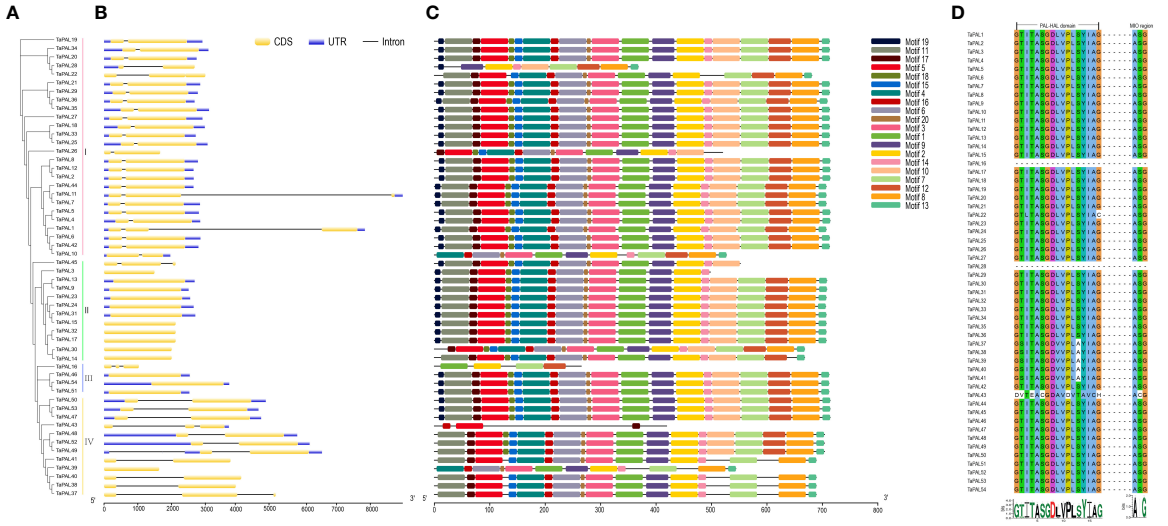

FIGURE 2
Phylogenetic analysis, gene structure, conserved motifs and sequence alignment of PAL domains of TaPALs. **(A)** The phylogenetic tree of all *PAL* genes in common wheat. The tree was created with bootstrap of 1000 by maximum likelihood (ML) method in MEGA7. **(B)** The exon-intron structure of *PAL* genes in common wheat. **(C)** The motif compositions of TaPAL were identified by MEME. Model exhibition of motif compositions in PAL amino acid sequences using MAST. **(D)** Multiple sequence alignment of PAL domains in identified wheat PAL proteins.

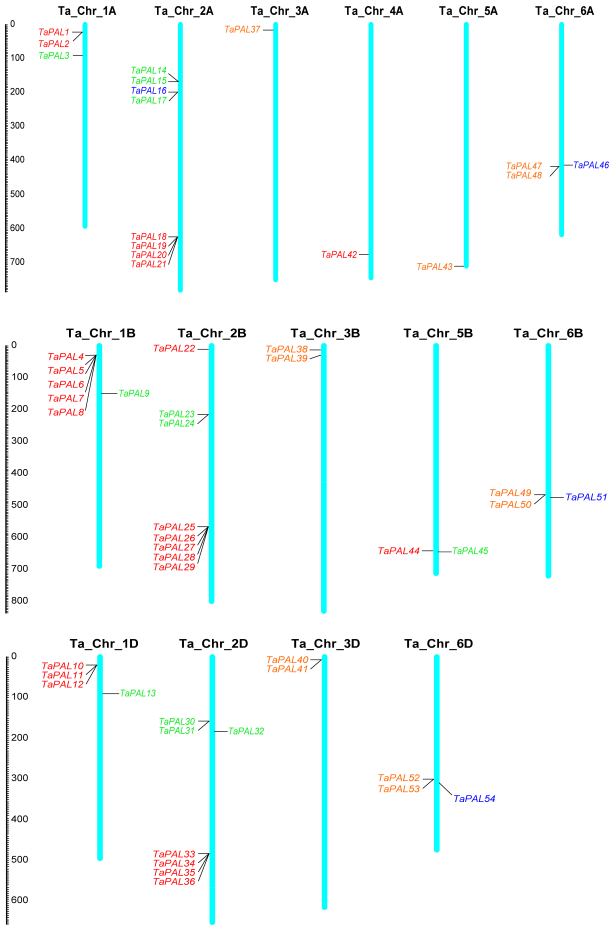

FIGURE 3
Chromosomal localization of the 54 TaPALs in wheat genome. Different classes of TaPALs are represented in different colors. Red represents TaPAL-I, green represents TaPAL-II, blue represents TaPAL-III, and orange represents TaPAL-IV. In addition, Ta represents wheat (*Triticum aestivum*), Chr represents Chromosome.

In order to further infer homology of wheat PAL family, a total of 91 PALs were identified from T. aestivum (45 TaPALs), T. urartu (9 TuPALs), T. dicoccoides (26 TdPALs) and Ae. tauschii (11 AePALs) by a computer-based method (Figure 4). After statistics, there were 393 pairs of orthologous gene pairs, 78 orthologous gene pairs were identified from T. aestivum and Ae. tauschii, 33 orthologous gene pairs were identified from T. aestivum and T. dicoccoides, and 66 orthologous gene pairs were identified from T. aestivum and T. urartu. In addition, T. aestivum, T. urartu, T. dicoccoides and Ae. tauschii had 146, 7, 25 and 6 pairs of paralogous genes respectively.

We further analyzed the Ka (nonsynonymous)/Ks (synonymous) ratio of replicated PAL genes pairs in wheat to understand the evolutionary constraints on TaPALs (Figure 4 and Supplementary file 7). In general, Ka/Ks rates can be used to evaluate the selectivity of coding sequences; the Ka/Ks ratio >1 indicates accelerated evolution with positive selection, a ratio = 1 indicates neutral selection, and a ratio < 1 indicates negative or purifying selection (Zhang et al., 2006; Peterson and Masel, 2009). The Ka/Ks ratios of 144 replicated gene pairs were calculated. The Ka/Ks ratios for all these TaPALs duplicated gene pairs were less than 1, which indicated that all repeated genes of the TaPAL family have undergone strong purifying selections which may help maintain their functional stability.

Analysis of cis-regulatory elements in the promoter region of TaPAL genes

The cis-regulatory element was specific motif that can be combined with appropriate transcription factors to further regulate the transcription of genes in plants (Wittkopp and Kalay, 2011). To identify putative cis-elements in the TaPAL gene promoter region, we analyzed the 1500 bp upstream

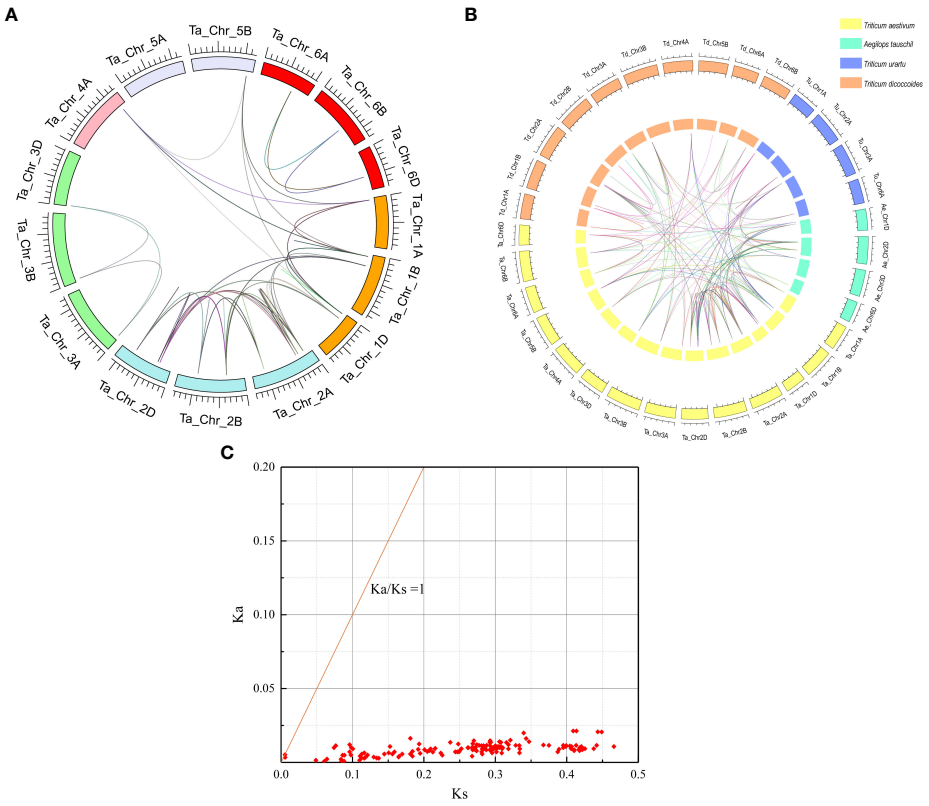

FIGURE 4
Whole genome duplication (WGD)-derived and homology relationship analysis of wheat PAL genes. **(A)** Analysis of genome-wide *PAL* genes replication events in common wheat (Ta, AABBDD). Different colors represent different chromosomes; WGD/segmentally duplicated *TaPAL* gene pairs are linked by different colored lines. **(B)** Homology relationship analysis of the *TaPAL* genes of *Triticum aestivum* and its subgenome donors *Triticum urartu*, *Triticum dicoccoides*, and *Aegilops tauschii*. The reference genomes of *T. urartu* (v. 1.43), *T. dicoccoides* (v. 1.0.43), and *A. tauschii* (v. 4.0.43) were downloaded from the Ensembl Plants database (http://plants.ensembl.org/index.html). The orange box represents *T. dicoccoides*, the blue box represents *T. urartu*, the cyan box represents *A. tauschii* and the yellow box represents *T. aestivum*. **(C)** Ka/Ks values for duplicated *TaPAL* genes pairs.

promoter region of TaPAL genes. We found that a total of 2292 cis-acting elements were predicted, of which 1422 regulatory-elements were related to growth and development, 485 regulatory elements were related to biotic and abiotic stress, and 385 active-elements were related to phytohormone (Figure 5 and Supplementary file 8). As shown in Figure 5, growth-related cis-regulatory elements include zein metabolism regulation (O2-site), seed-specific regulation (RY-element), etc. Furthermore, cis-regulatory elements related to stress included light responsive elements (ACE, GT1-motif, AE-box, ATCT-motif, and Box 4), enhancer-like element involved in anoxic specific inducibility (GC-motif), low-temperature responsiveness (LTR). The remaining cis-elements were related to phytohormone response, included cis-acting element involved in the abscisic acid responsiveness (ABRE); gibberellin-responsive element (GARE-motif and P-box). We found that CAAT box and TATA box were the most common cis-acting elements in TaPALs. Meanwhile, many cis-acting elements were related to plant abscisic acid (ABRE), which was distributed in the promoter region of most of TaPALs. Cis-element analysis showed that TaPAL family members may be play an important role in transcriptional regulation and abscisic acid metabolism pathway.

Transcriptional analysis of TaPAL genes

RNA-seq is a powerful tool to explore gene transcription patterns using high-throughput sequencing methods (Wang et al., 2010). Transcriptome data of wheat inoculated with F. graminearum, P. striiformis, and powdery mildew were used for analysis. In the expression profile (Figure 6), 15 TaPALs were not expressed and five TaPALs (TaPAL47, TaPAL48, TaPAL49, TaPAL50, TaPAL53) were generally highly expressed in various periods. The expression levels of 31 TaPALs were up-regulated and the expression level of TaPAL52 was down-regulated after

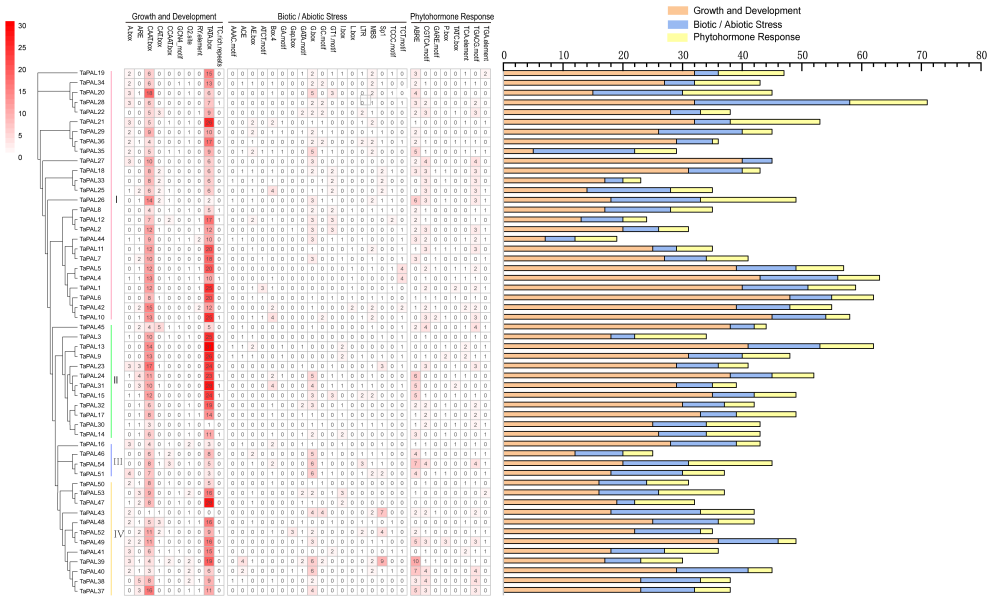

FIGURE 5
Analysis of cis-acting element numbers in TaPAL genes promoters. The different colors and numbers of the grid indicated the numbers of different promoter elements in these TaPAL genes. The different colored histogram represented the sum of the cis-acting elements in each category.

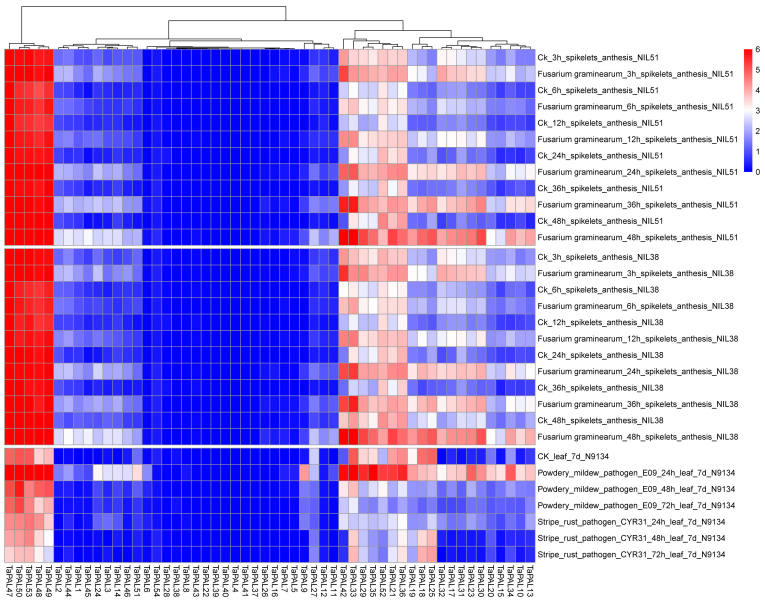

FIGURE 6
Heat map of expression profiles for TaPAL genes across different stresses under different biotic stress. Blocks with colors indicate decreased (blue) or increased (red) expression levels. The gradually change of the color indicates different level of gene log2-transformed expression (fold change > 3 is significantly expressed).

10.3389/fpls.2022.982457

inoculation with F. graminearum. The expression levels of 11 TaPALs were up-regulated and 14 TaPALs were down-regulated after inoculation with P. striiformis. Moreover, the expression levels of 32 TaPALs were higher in powdery mildew treated leaves than that in the control group, while the expression levels of TaPAL18, TaPAL25 and TaPAL27 were lower than that in the control group. These results indicated that TaPALs had different expression patterns under different disease treatments. Under the three stress conditions, the expression levels of ten TaPALs (TaPAL3, TaPAL10, TaPAL13, TaPAL14, TaPAL17, TaPAL30, TaPAL31, TaPAL32, TaPAL42, TaPAL48) were highly induced. It was inferred that these genes may be involved in the regulation of plant disease resistance.

Quantitative real-time PCR analysis of wheat PAL genes in responses to different treatments

In order to further explore the potential role of five genes (TaPAL10, TaPAL14, TaPAL32, TaPAL42, TaPAL49) under biotic stresses (F. graminearum and P. striiformis), we analyzed their expression levels by qRT-PCR. As shown in Figure 7, the expression levels of five genes were continuously up-regulated from 12 *h* to 48 *h* under F. graminearum treatment, among which only the expression levels of TaPAL32 and TaPAL42 were significantly up-regulated from 0 *h* to 6 *h*. In wheat leaves treated with P. striiformis, the expression levels of TaPAL10, TaPAL14, TaPAL32, and TaPAL42 showed a general downward trend. However, the expression level of TaPAL49 at 48 *h* was much higher than that at 24 *h*, and the expression level was gradually up-regulated during infection.

Subcellular localization of TaPALs

The predicted results from plant-MPLOC online tool showed that TaPAL proteins were located in the cytoplasm. To further confirm the predicted results, TaPAL32-GFP and TaPAL42-GFP fusion protein were transiently expressed in *N. benthamiana* leaves. As shown in Figure 8, both of TaPAL32 and TaPAL42 were expressed in the whole cell.

Silencing of TaPALs enhanced the sensitivity of wheat against Puccinia striiformis infection

We further detected the function of *TaPAL32* and *TaPAL42* in the wheat cultivar Fielder by barley stripe mosaic virus (BSMV)-mediated virus-induced gene silencing (VIGS) assay. The silenced vectors of two genes (BSMV : *TaPAL32*, BSMV : *TaPAL42*) were constructed. About 10 days after BSMV treatment, BSMV : TaPDS leaves showed symptoms of photobleaching, indicating that the virus-induced gene silencing system was working. Then, fresh urediospores of *P. striiformis* isolates CYR23 was inoculated on the fourth leaves of silenced plants. The expression levels of *TaPAL32* and *TaPAL42* at 0, 24, and 48 h after inoculation were analyzed by qRT-PCR. Compared with the control (BSMV:γ), the gene expression levels of *TAPAL32* and *TaPAL42* were significantly down-regulated, and the disease severity was photographed at 14 days after inoculation. The results showed that there were many urediospores on the leaves of silent plants compared with the control group (Figure 9). It indicated that silencing of these two genes weakened the wheat defense responses against *P. striiformis*.

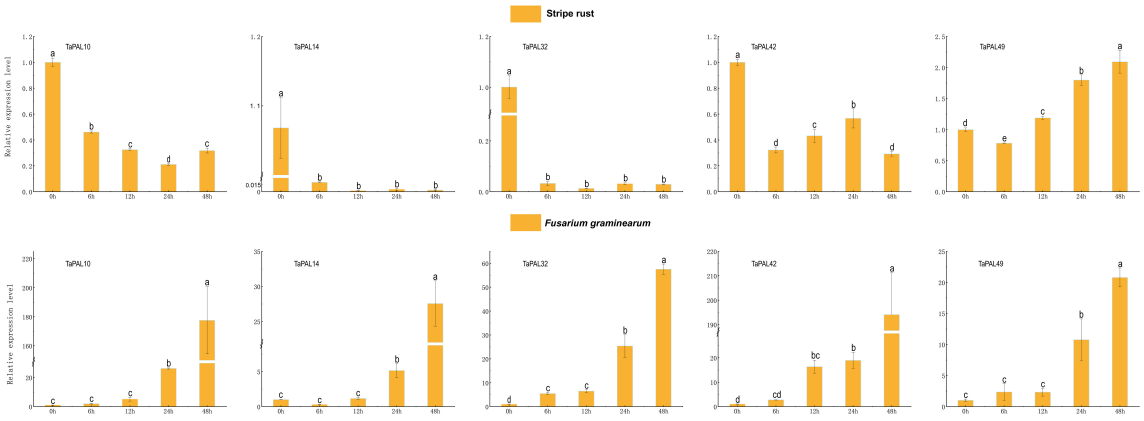

FIGURE 7
Reverse transcription quantitative PCR analysis of five TaPAL genes under, *F. graminearum*, and *P. striiformis* treatment. Each bar represents the average of three replicates, and error bar represents standard deviation (SD). Different letters in a column indicate significant differences between the treatments at $p < 0.05$ level.

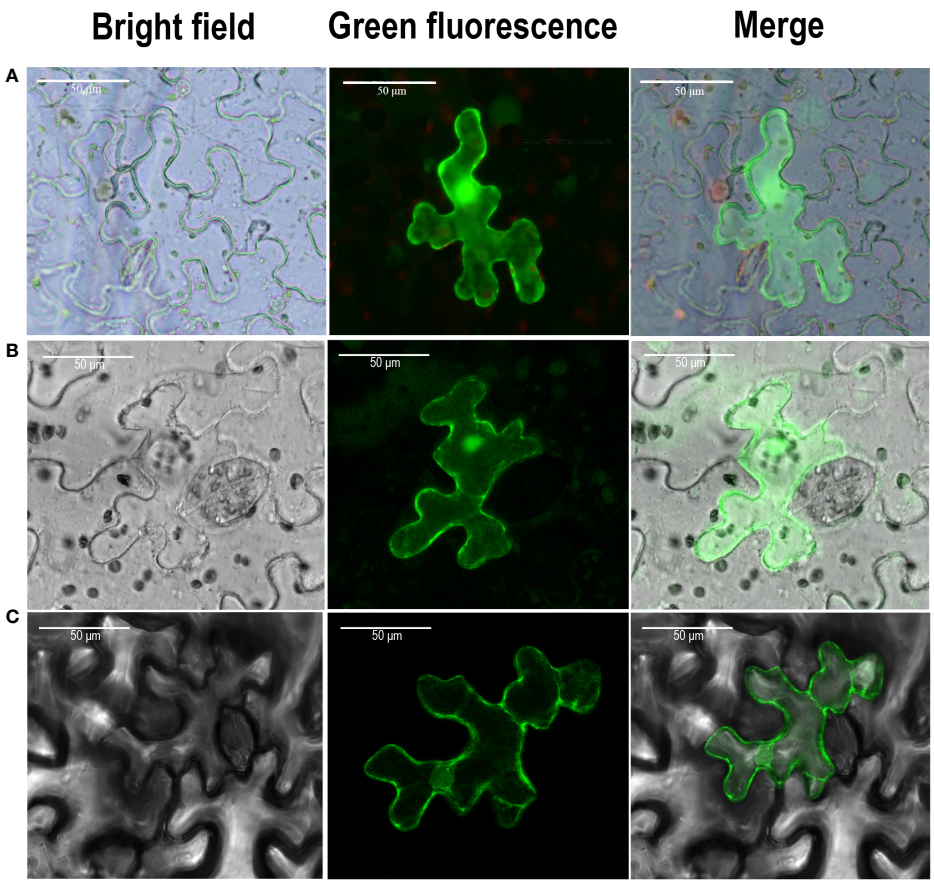

FIGURE 8
Subcellular localization of TaPAL genes. **(A)** Subcellular localization of free GFP. **(B)** Subcellular localization of TaPAL32. **(C)** Subcellular localization of TaPAL42. Subcellular localization was then observed by confocal laser scanning microscopy 48 – 72 h after infiltration. Scale bar = 50 μm.

Discussion

Phenylalanine ammonia lyase (PAL) plays an important role in the metabolic pathway of plant disease resistance substances such as lignin and phytoprotectin. When plants encounter adversity or disease, the expression of *PAL* gene can adapt to adversity or resist pathogen invasion by participating in synthesizing important secondary metabolites through phenylpropanoid metabolism (de Jong et al., 2015). At present, *PAL* genes have been isolated from many species. However, the role of PAL family in wheat has not been systematically studied. In this study, we identified 54 *TaPAL* genes in wheat genome. The result was significantly higher than the 37 *TaPALs* already reported in wheat. Because Rasool's screening conditions were more stringent, two screening conditions (sequence identity greater than 75% and value ≤ 1e-10) were set to identify the wheat PAL family members (Rasool et al., 2021) . TaPAL family can be divided into four groups based on phylogenetic analysis. In the process of plant evolution, multiplication and variation of an ancestor can produce multiple family members, which may be clustered on one chromosome or distributed on different chromosomes (Whetten and Sederoff, 1992). The *TaPAL* genes were located across 15 chromosomes, with three of them having the most genes: seven on 2A and 2D, and eight on 2B. The PAL family members are unevenly distributed on the chromosomes of wheat, which may be related to genome replication and chromosome duplication.

Phenylalanine ammonia-lyase is widely present in plants. The TaPAL proteins have different physical and chemical properties, acid base, molecular weight and coding length, indicating that *TaPALs* have a high genetic diversity. With the gradual enhancement of species evolution and environmental adaptability, the genetic variation of species has been enriched. So genetic variation is the root cause of genetic diversity (Ohta, 1980). In TaPAL family, there are differences in cis-elements among family members, which may be caused by genetic variation during evolution. The undetectable expression of *TaPAL43* in different treatments of wheat may be due to the

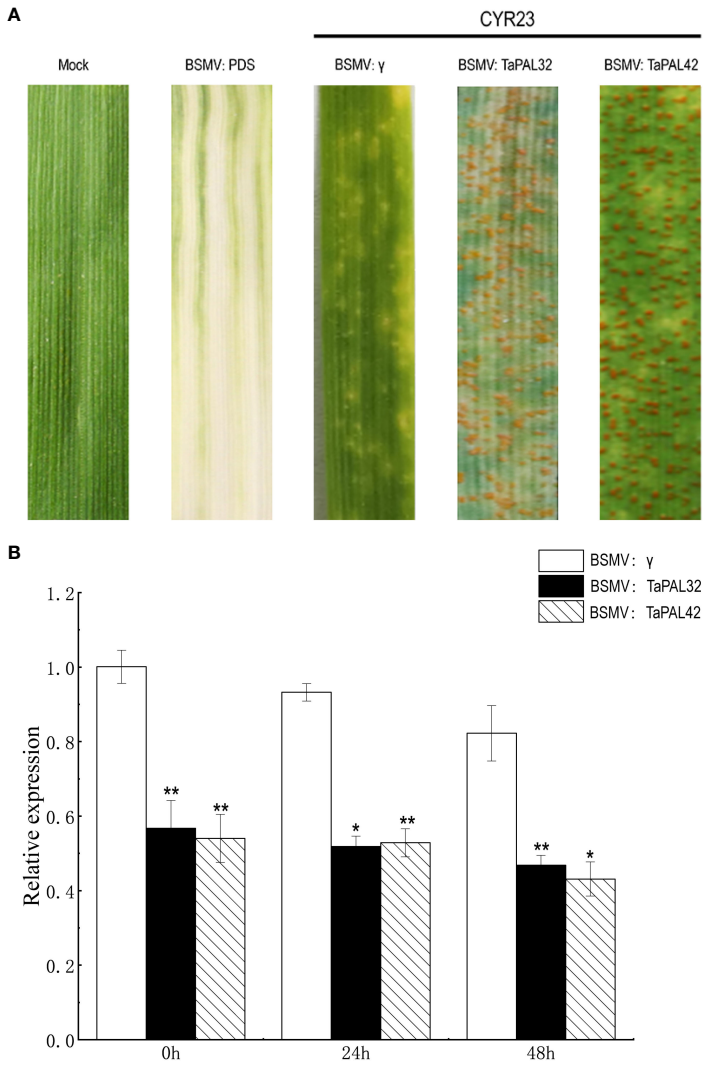

FIGURE 9
Silencing of TaPAL32 and TaPAL42 reduce the resistance of wheat to *P. striiformis*. **(A)** BSMV: TaPDS showed photobleaching at 10 dpi; Mock: wheat leaves treated with 1× Fes buffer. Disease symptoms on the leaves challenged with *Puccinia striiformis f.* sp. *tritici* race CYR23. Disease symptoms were photographed at 14 days post inoculation. **(B)** Silencing efficiency assessment of *TaPAL32* and *TaPAL42* in the 0, 24, and 48 h. *TaPAL32* and *TaPAL42* silenced plants treated with *P. striiformis* (*p < 0.05, **p < 0.01).

few CAAT boxes and TATA boxes. This result suggests that the different regulation of *TaPALs* expression may be due to the different cis-elements contained in each family member.

The products of phenylpropane metabolic pathway play a crucial role in plant growth and development and response to stress (Harakava, 2005). *PAL* genes are involved in plant response to pathogens (Alvarez et al., 2013). In *Arabidopsis thaliana*, the 4 knockout mutant of pal1/pal2/pal3/pal4 shows the phenotype of dysplasia and sterility, and is susceptible to *Pseudomonas syringae* (Huang et al., 2010). Transcriptome data showed that many *TaPAL* genes were up-regulated in *F. graminearum* and *P. striiformis* infection. Five *TaPALs* (*TaPAL10*, *TaPAL14*, *TaPAL32*, *TaPAL42*, *TaPAL49*) were screened by qRT-PCR analysis. The expression levels were significantly up-regulated under the stress of *F. graminearum*, which was consistent with the expression analyzed by transcriptome. However, except for *TaPAL49*, all *TaPALs* were down regulated under *P. striiformis* infection. This may be related to our selection of different wheat varieties for real-time PCR experiment. Transcriptome data showed that the wheat line N9134 was used as experimental material for *P. striiformis* infection. But, the susceptible wheat cultivar Jingshuang 16 was used for qRT-PCR. The expression of disease-resistant genes may also down-regulated during the process of disease infection. It had been confirmed that *GhERF5-4D* in cotton was up-regulated in resistant varieties

and down-regulated in susceptible cultivars, the silenced lines were more susceptible after gene silencing (Zhao et al., 2022). Subsequently, we silenced two genes (*TaPAL32* and *TaPAL42*) using VIGS to further verify the role of *TaPALs* in wheat stripe rust resistance. The silencing efficiency results showed that the expression levels of *TaPAL32* and *TaPAL42* decreased by about 45% compared with the control group at 0, 24 and 48 h after inoculation. At 14 days after inoculation, the symptoms of silent plants were more severe than those of control plants, indicating that silencing of these two genes resulted in decreased disease resistance of wheat. These results strongly proved that members of TaPAL family were involved in the infection of wheat stripe rust, but the mechanism of *TaPAL32* and *TaPAL42* may be complex and needs further study.

Conclusion

In this study, 54 *PAL* genes were identified from the whole genome of wheat, and their phylogenesis, chromosome distribution, conserved cis-acting elements and gene expression profile under biotic stress were characterized. More importantly, gene silencing results showed that PAL family members play an important role in wheat resistance to *P. striiformis* infection. In conclusion, our findings provide new clues for improving disease resistance in wheat. This study provides a reference for subsequent studies on the function of TaPAL family.

Data availability statement

The original contributions presented in the study are included in the article/Supplementary Material. Further inquiries can be directed to the corresponding authors.

Author contributions

YaL and DM designed this article; CZ and YaL directed the data analysis and manuscript writing. YiL, MW and HL supervised the experiment. SG confirmed the manuscript. All authors contributed to the article and agreed to submit version of the manuscript.

Funding

This research was supported by "Open Program of Engineering Research Center of Ecology and Agricultural Use of Wetland Ministry of Education" (KFT202103)", and "Open Project Program of Key Laboratory of Integrated Pest Management on Crop in Central China, Ministry of Agriculture/Hubei Province Key Laboratory for Control of Crop Diseases, Pest and Weeds (2021ZTSJJ8).

Conflict of interest

The authors declare that the research was conducted in the absence of any commercial or financial relationships that could be construed as a potential conflict of interest.

Publisher's note

Supplementary material

The Supplementary Material for this article can be found online at: https://www.frontiersin.org/articles/10.3389/fpls.2022.982457/full#supplementary-material

References

Alaux, M., Rogers, J., Letellier, T., Flores, R., Alfama, F., Pommier, C., et al. (2018). Linking the international wheat genome sequencing consortium bread wheat reference genome sequence to wheat genetic and phenomic data. *Genome Biol.* 19, 1–10. doi: 10.1186/s13059-018-1491-4

Alvarez, J. C., Rodriguez, H. A., Rodriguez-Arango, E., Monsalve, Z. I., Morales, J. G., and Arango, R. E. (2013). Characterization of a differentially expressed phenylalanine ammonia-lyase gene from banana induced during *Mycosphaerella fijiensis* infection. *J. Plant Stud.* 2, 35. doi: 10.5539/jps.v2n2p35

Bailey, T. L., Johnson, J., Grant, C. E., and Noble, W. S. (2015). The MEME suite. *Nucleic Acids Res.* 43, W39–W49. doi: 10.1093/nar/gkv416

Bai, J., Wang, Y., Guo, L., Guo, X., Guo, H., Yuan, S., et al. (2019). Genomic identification and characterization of. *MYC. Family Genes wheat. (Triticum. aestivum. L.). BMC Genomics* 20, 1–15. doi: 10.1186/s12864-019-6373-y

Blake, V. C., Kling, J. G., Hayes, P. M., Jannink, J. L., Jillella, S. R., Lee, J., et al. (2012). The hordeum toolbox: the barley coordinated agricultural project genotype and phenotype resource. *Plant Genome* 5, 81–91. doi: 10.3835/plantgenome2012.03.0002

Cao, S., Zhang, S., Hao, C., Liu, H., Xu, J. R., and Jin, Q. (2016). FgSsn3 kinase, a component of the mediator complex, is important for sexual reproduction and pathogenesis in *Fusarium graminearum*. *Sci. Rep.* 6, 1–12. doi: 10.1038/srep22333

Chen, X. (2019). Cloning and expression analysis of phenylalanine ammonia-lyase gene in lonicera macranthoides. *Chin. Tradit. Herb. Drugs* 24, 178–187. doi: 10.7501/j.issn.0253-2670.2019.01.027

Chen, C., Chen, H., Zhang, Y., Thomas, H. R., Frank, M. H., He, Y., et al. (2020). TBtools: an integrative toolkit developed for interactive analyses of big biological data. *Mol. Plant* 13, 1194–1202. doi: 10.1016/j.molp.2020.06.009

Chen, Y., Li, F., Tian, L., Huang, M., Deng, R., Li, X., et al. (2017). The phenylalanine ammonia- lyase gene *LjPAL1* is involved in plant defense responses to pathogens and plays diverse roles in *lotus japonicus*-rhizobium symbioses. *Mol. Plant-Microbe Interact.* 30, 739–753. doi: 10.1094/mpmi-04-17-0080-r

Chou, K. C., and Shen, H. B. (2010). Plant-mPLoc: A top-down strategy to augment the power for predicting plant protein subcellular localization. *PloS One* 5, e11335. doi: 10.1371/journal.pone.0011335

Costa, M. A., Collins, R. E., Anterola, A. M., Cochrane, F. C., Davin, L. B., and Lewis, N. G. (2003). An in silico assessment of gene function and organization of the phenylpropanoid pathway metabolic networks in *Arabidopsis thaliana* and limitations thereof. *Phytochemistry* 64, 1097–1112. doi: 10.1016/s0031-9422(03)00517-x

de Jong, F., Hanley, S. J., Beale, M. H., and Karp, A. (2015). Characterisation of the willow phenylalanine ammonia-lyase (PAL) gene family reveals expression differences compared with poplar. *Phytochemistry* 117, 90–97. doi: 10.1016/j.phytochem.2015.06.005

Deng, L. C., Cui, L., Yang, L., Chen, J., He, W. Z., Li, X., et al. (2019). Identification of gene family of phenylalanine ammonia-lyase and analysis of resistance to maize sheath blight in corn. *Mol. Plant Breed.* 17, 891–897. doi: 10.13271/j.mpb.017.000891

Dong, C. J., and Shang, Q. M. (2013). Genome-wide characterization of phenylalanine ammonia-lyase gene family in watermelon (*Citrullus lanatus*). *Planta* 238, 35–49. doi: 10.1007/s00425-013-1869-1

Eddy, S. R. (2008). A probabilistic model of local sequence alignment that simplifies statistical significance estimation. *PloS Comput. Biol.* 4, e1000069. doi: 10.1371/journal.pcbi.1000069

Fang, Z. W., He, Y. Q., Liu, Y. K., Jiang, W. Q., Song, J. H., Wang, S. P., et al. (2019). Bioinformatic identifcation and analyses of the non-specifc lipid transfer proteins in wheat. *J. Integr. Agric.* 19, 11770–11185. doi: 10.1016/S2095-3119(19)62776-0

Finn, R. D., Coggill, P., Eberhardt, R. Y., Eddy, S. R., Mistry, J., Mitchell, A. L., et al. (2016). The pfam protein families database: towards a more sustainable future. *Nucleic Acids Res.* 44, 279–285. doi: 10.1093/nar/gkv1344

Golkari, S., Gilbert, J., Ban, T., and Procunier, J. D. (2009). QTL-specific microarray gene expression analysis of wheat resistanceto fusarium head blight in sumai-3 and two susceptible NILs. *Genome* 52, 409–418. doi: 10.1139/G09-018

Harakava, R. (2005). Genes encoding enzymes of the lignin biosynthesis pathway in *Eucalyptus*. *Genet. Mol. Biol.* 28, 601–607. doi: 10.1590/S1415-47572005000400015

He, Y. Q., Huang, W. D., Yang, L., Li, Y. T., Lu, C., Zhu, Y. X., et al. (2020). Genome-wide analysis of ethylene-insensitive3 (EIN3/EIL) in *Triticum aestivum*. *Crop Sci.* 60, 2019–2037. doi: 10.1002/csc2.20115

Huang, J., Gu, M., Lai, Z., Fan, B., Shi, K., Zhou, Y. H., et al. (2010). Functional analysis of the arabidopsis PAL gene family in plant growth, development, and response to environmental stress. *Plant Physiol.* 153, 1526–1538. doi: 10.1104/pp.110.157370

Hu, B., Jin, J., Guo, A. Y., Zhang, H., Luo, J., and Gao, G. (2014). GSDS 2.0: an upgraded gene feature visualization server. *Bioinformatics* 31, 1296–1297. doi: 10.1093/bioinformatics/btu817

Jiang, W. Q., Yang, L., He, Y. Q., Zhang, H. T., Li, W., Chen, H. G., et al. (2019). Genome-wide identification and transcriptional expression analysis of superoxide dismutase (SOD) family in wheat (*Triticum aestivum*). *PeerJ* 7, e8062. doi: 10.7717/peerj.8062

Koukol, J., and Conn, E. E.. (1966). The metabolism of aromatic compounds in higher plants. IV. Purification and properties of the phenylalanine deaminase of Hordeum vulgare. *J. Biol. Chem.* 236, 2692–2698. doi: 10.1016/S0021-9258(18)96962-0.

Krzywinski, M., Schein, J., Birol, I., Connors, J., Gascoyne, R., Horsman, D., et al. (2009). Circos: An information aesthetic for comparative genomics. *Genome Res.* 19, 1639–1645. doi: 10.1101/gr.092759.109

Kumar, S., Stecher, G., and Tamura, K. (2016). MEGA7: Molecular evolutionary genetics analysis version 7.0 for bigger datasets. *Mol. Biol. Evol.* 33, 1870–1874. doi: 10.1093/molbev/msw054

Lefevere, H., Bauters, L., and Gheysen, G. (2020). Salicylic acid biosynthesis in plants. *Front. Plant Sci.* 11. doi: 10.3389/fpls.2020.00338

Lepelley, M., Mahesh, V., McCarthy, J., Rigoreau, M., Crouzillat, D., Chabrillange, N., et al (2012). Characterization, high-resolution mapping and differential expression of three homologous PAL genes in Coffea canephora Pierre (Rubiaceae). *Planta* 236, 313–326. doi: 10.1007/s00425-012-1613-2

Lescot, M., Déhais, P., Thijs, G., Marchal, K., Moreau, Y., Peer, Y., et al. (2002). PlantCARE, a database of plant cis-acting regulatory elements and a portal to tools for in silico analysis of promoter sequences. *Nucleic Acids Res.* 30, 325–327. doi: 10.1093/nar/30.1.325

Librado, P., and Rozas, J. (2009). DnaSP v5: a software for comprehensive analysis of DNA polymorphism data. *Bioinformatics* 25, 1451–1452. doi: 10.1093/bioinformatics/btp187

Li, Y., Liu, X., Xiao, Y., Wen, Y., Li, K., Ma, Z., et al. (2022). Genome-wide characterization and function analysis uncovered roles of wheat LIMs in responding to adverse stresses and TaLIM8-4D function as a susceptible gene. *Plant Genome* 16, e20246. doi: 10.1002/tpg2.20246

Livak, K. J., and Schmittgen, T. D. (2001). Analysis of relative gene expression data using real-time quantitative PCR and the $2^{-\Delta\Delta CT}$ method. *Methods* 25, 402–408. doi: 10.1006/meth.2001.1262

MacDonald, M. J., and D'Cunha, G. B. (2007). A modern view of phenylalanine ammonia lyase. *Biochem. Cell Biol.* 85, 273–282. doi: 10.1139/O07-018

Moberly, J. G., Bernards, M. T., and Waynant, K. V. (2018). Key features and updates for origin 2018. *J. Cheminf.* 10, 1–2. doi: 10.1186/s13321-018-0259-x

Nielsen, H. (2017). Predicting secretory proteins with SignalP. *Methods Mol. Biol.* 1611, 59–73. doi: 10.1007/978-1-4939-7015-5_6

Ohta, T. (1980). *Evolution and variation of multigene families* Vol. 37 (Berlin-New York: Springer-Verlag). doi: 10.1007/978-3-642-93138-3

Paolacci, A. R., Tanzarella, O. A., Porceddu, E., and Ciaffi, M. (2009). Identification and validation of reference genes for quantitative RT-PCR normalization in wheat. *BMC Mol. Biol.* 10, 1–27. doi: 10.1186/1471-2199-10-11

Peng, X., Zhao, Y., Cao, J., Zhang, W., Jiang, H., Li, X., et al. (2012). CCCH-type zinc finger family in maize: genome-wide identification, classification and expression profiling under abscisic acid and drought treatments. *PloS One* 7, e40120. doi: 10.1371/journal.pone.0040120

Peterson, G. I., and Masel, J. (2009). Quantitative prediction of molecular clock and Ka/Ks at short timescales. *Mol. Biol. Evol.* 26, 2595–2603. doi: 10.1093/molbev/msp175

Quraishi, U. M., Abrouk, M., Murat, F., Pont, C., Foucrier, S., Desmaizieres, G., et al. (2011). Cross-genome map based dissection of a nitrogen use efficiency ortho-metaQTL in bread wheat unravels concerted cereal genome evolution. *Plant J.* 65, 745–756. doi: 10.1111/j.1365-313X.2010.04461.x

Rasool, F., Uzair, M., Naeem, M. K., Rehman, N., Afroz, A., Shah, H., et al (2021). Phenylalanine ammonia-lyase (PAL) genes family in wheat (Triticum aestivum L.): genome-wide characterization and expression profiling. *Agronomy* 11, 2511. doi: 10.3390/agronomy11122511

Rawal, H. C., Singh, N. K., and Sharma, T. R. (2013). Conservation, divergence, and genome-wide distribution of PAL and POX a gene families in plants. *Int. J. Genomics* 2013, 1–10. doi: 10.1155/2013/678969

Shi, R., Shuford, C. M., Wang, J. P., Sun, Y. H., Yang, Z., Chen, H. C., et al. (2013). Regulation of phenylalanine ammonia-lyase (PAL) gene family in wood forming tissue of. *Populus. trichocarpa. Planta* 238, 487–497. doi: 10.1007/s00425-013-1905-1

Song, J., Ma, D., Yin, J., Yang, L., He, Y., Zhu, Z., et al. (2019). Genome-wide characterization and expression profiling of squamosa promoter binding protein-like (SBP) transcription factors in wheat (*Triticum aestivum* l.). *Agron. J.* 9, 527–570. doi: 10.3390/agronomy9090527

Song, J., and Wang, Z. (2009). Molecular cloning, expression and characterization of a phenylalanine ammonia-lyase gene (*SmPAL1*) from *Salvia miltiorrhiza*. *Mol. Biol. Rep.* 36, 939–952. doi: 10.1007/s11033-008-9266-8

Wang, Z., Gerstein, M., and Snyder, M. (2010). RNA-Seq: a revolutionary tool for transcriptomics. *Nat. Rev. Genet.* 10, 57–63. doi: 10.1038/nrg2484

Wang, Z., Li, J. Y., Jia, C. H., Li, J. P., Xu, B. Y., and Jin, Z. Q. (2016). Molecular cloning and expression of four phenylalanine ammonia lyase genes from banana interacting with *Fusarium oxysporum*. *Biol. Plant* 60, 459–468. doi: 10.1007/s10535-016-0619-1

Way, H. M., Kazan, K., Mitter, N., Goulter, K. C., Birch, R. G., and Manners, J. M. (2002). Constitutive expression of a phenylalanine ammonia-lyase gene from *Stylosanthes humilis* in transgenic tobacco leads to enhanced disease resistance but impaired plant growth. *Physiol. Mol. Plant Pathol.* 60, 275–282. doi: 10.1006/pmpp.2002.0407

Whetten, R. W., and Sederoff, R. R. (1992). Phenylalanine ammonia-lyase from loblolly pine: purification of the enzyme and isolation of complementary DNA clones. *Plant Physiol.* 98, 380–386. doi: 10.1104/pp.98.1.380

Wittkopp, P. J., and Kalay, G. (2011). Cis-regulatory elements: molecular mechanisms and evolutionary processes underlying divergence. *Nat. Rev. Genet.* 13, 59–69. doi: 10.1038/nrg3095

Yang, X., Ma, J., Li, H., Ma, H., Yao, J., and Liu, C. (2010). Different genes can be responsible for crown rot resistance at different developmental stages of wheat and barley. *Eur. J. Plant Pathol.* 128, 495–502. doi: 10.1007/s10658-010-9680-3

Yan, F., Li, H., and Zhao, P. (2019). Genome-wide identification and transcriptional expression of the PAL gene family in common walnut (*Juglans regia l.*). *Genes* 10, 46. doi: 10.3390/genes10010046

Zeng, J. L., Ouyang, L. J., Liu, J. L., He, H. H., Zhu, C. L., Peng, X. S., et al. (2018). Whole genome analysis and stress expression research of pal gene in rice. *Genomics Appl. Biol.* 9, 3881-–3888. doi: 10.13417/j.gab.037.003881

Zhang, H., Huang, Q., Yi, L., Song, X., Li, L., and Deng, G. (2021). Pal-mediated SA biosynthesis pathway contributes to nematode resistance in wheat. *Plant J.* 107, 698–712. doi: 10.1111/tpj.15316

Zhang, X., and Liu, C. J. (2015). Multifaceted regulations of gateway enzyme phenylalanine ammonia-lyase in the biosynthesis of phenylpropanoids. *Mol. Plant* 8, 17–27. doi: 10.1016/j.molp.2014.11.001

Zhang, Z., Li, J., Zhao, X. Q., Wang, J., Wong, G. K., and Yu, J. (2006). KaKs_Calculator: calculating ka and ks through model selection and model averaging. *Genomics. Proteomics Bioinf.* 4, 259–263. doi: 10.1016/S1672-0229(07)60007-2

Zhang, P., Zhu, Y., Ma, D., Xu, W., Zhou, J., Yan, H., et al. (2019). Screening, identification, and optimization of fermentation conditions of an antagonistic endophyte to wheat head blight. *Agron. J.* 9, 476. doi: 10.3390/agronomy9090476

Zhao, Z. Q., Guo, W. T., Zhang, X., Li, X. L., and Zhang, W. (2022). Cloning and functional analysis of GhERF5-4D gene related to *Fusarium oxysporum* resistance in cotton. *Biotechnol. Bull.* 38, 193. doi: 10.13560/j.cnki.biotech.bull.1985.2021-1065

Zhu, X., Liu, W., Chu, X., Sun, Q., Tan, C., Yang, Q., et al. (2018). The transcription factor *PstSTE12* is required for virulence of *Puccinia striiformis* f. sp. *tritici*. *Mol. Plant Pathol.* 19, 961–974. doi: 10.1111/mpp.12582

Zhu, Y. X., Xu, X. B., Hu, Y. H., Han, W. H., Yin, J. L., Li, H. L., et al. (2015). Silicon improves salt tolerance by increasing root water uptake in *Cucumis sativus* l. *Plant Cell Rep.* 34, 1629–1646. doi: 10.1007/s00299-015-1814-9

frontiers | Frontiers in Plant Science

TYPE Original Research
PUBLISHED 05 October 2022
DOI 10.3389/fpls.2022.1006835

OPEN ACCESS

EDITED BY
Yuheng Yang,
Southwest University, China

REVIEWED BY
Gianfranco Romanazzi,
Marche Polytechnic University, Italy
Dong Fang Ma,
Yangtze University, China

*CORRESPONDENCE
Enrico Battiston
enrico.battiston@unifi.it
Sara Falsini
sara.falsini@unifi.it

†These authors have contributed equally to this work and share first authorship

SPECIALTY SECTION
This article was submitted to Crop and Product Physiology, a section of the journal Frontiers in Plant Science

RECEIVED 29 July 2022
ACCEPTED 29 August 2022
PUBLISHED 05 October 2022

CITATION
Battiston E, Falsini S, Giovannelli A, Schiff S, Tani C, Panaiia R, Papini A, Di Marco S and Mugnai L (2022) Xylem anatomy and hydraulic traits in *Vitis* grafted cuttings in view of their impact on the young grapevine decline.
Front. Plant Sci. 13:1006835.
doi: 10.3389/fpls.2022.1006835

Xylem anatomy and hydraulic traits in *Vitis* grafted cuttings in view of their impact on the young grapevine decline

Enrico Battiston[1*†], Sara Falsini[2*†], Alessio Giovannelli[3], Silvia Schiff[2], Corrado Tani[2], Roberta Panaiia[2], Alessio Papini[2], Stefano Di Marco[4] and Laura Mugnai[1]

[1]Sezione Patologia Vegetale ed Entomologia, Dipartimento di Scienze e Tecnologie Agrarie, Alimentari, Ambientali e Forestali, Università degli Studi di Firenze, Florence, Italy, [2]Laboratorio di Biomorfologie, Dipartimento di Biologia, Università degli Studi di Firenze, Florence, Italy, [3]Istituto di Ricerca Sugli Ecosistemi Terrestri, Consiglio Nazionale delle Ricerche, Sesto Fiorentino, Italy, [4]Istituto per la Bioeconomia, Consiglio Nazionale delle Ricerche, Bologna, Italy

Grapevine grafting is an essential practice in viticulture and over the years, various bench grafting techniques have been developed to mechanize the nursery process and to increase the yield in number of viable cuttings. Bench grafting is a fundamental nursery practice that can potentially affect the quality of propagation material also in young decline associated to grapevine trunk diseases and has been recently reported to influence leaf symptoms development associated with diseases of Esca complex. The study aimed to investigate how three bench grafting methods [i.e., (i) Omega graft as mechanical technique, (ii) Whip and Tongue graft as manual technique and (iii) Full Cleft graft as semi-mechanical technique] can influence these phenomena. Specifically, the different methods were compared for their effect on the anatomical development of the grafting point and the functionality of the xylem, also considering two factors: the grapevine cultivar (Cabernet Sauvignon, Glera and Teroldego) and the scion/rootstock diameter (thin and large). Observations by light microscopy on the anatomical evolution and measurements on the xylem morphology and hydraulic traits were correlated with the grafting methods and the investigated varieties. The anatomical observations revealed that the mechanical (Omega) and semi-mechanical (Full Cleft) grafting methods have a faster callusing response while the manual technique (Whip and Tongue) has a slower but greater vascularization of the differentiated callus. Significant differences between cultivars and/or grafting types were also detected in necrotic area on the grafted tissues. Statistical analysis of the grapevine vessels suggested differences in xylem parameters between cultivars, while grafting type had no significant effects. On the other hand, the grafting type significantly affected

the intrinsic growth rate. The study confirms the potential incidence of lesions and dysfunctionalities correlated with the grafting method applied, which can potentially induce grafted vine declines in vineyards due to the necrotic area detected on the grafted tissues.

KEYWORDS

grapevine nursery, propagation material, grafting, wounds, wood diseases

Introduction

Grafting has been used for millennia as proved by ancient literature (Mudge et al., 2009) and it is still widely exploited in horticulture and arboriculture. Since the need to counteract phylloxera damages on grapevine at the end of 19th century, grafting *Vitis vinifera* scion and American *Vitis* spp. or interspecific hybrids of *Vitis* spp. rootstock, to form one composite organism (Gautier et al., 2019) became an essential practice to establish new vineyards (Granett et al., 2001).

Over the years, several bench grafting techniques on dormant propagation material have evolved to mechanize the nursery process and to increase the yield in numbers of viable cuttings (Grohs et al., 2017), such as the Full Cleft (FC) grafting, the Whip and Tongue (W&T) grafting, and the Omega grafting. FC grafting is the easiest form of bench grafting between dormant scion and dormant rootstock and especially in the past, it was also applied in the field to graft a cutting scion on an older rooted rootstock. W&T grafting was a successful evolution of the previous method. Nowadays, among the bench grafting methods, Omega grafting is the most applied grafting technique by grapevine nurseries (Gramaje and Di Marco, 2015), combining a strong union between scion and rootstock with a high number of grafts per unit of time, and mechanizing the process with a significant reduction of the grafting cost.

Whichever grafting method is applied, a successful graft union must initially repair the mechanical damage caused by the grafting wounds. In this stage, the physical and antimicrobial barrier at the injured site consists of the accumulation of polymerized phenolic compounds such as suberin and lignin (Falsini et al., 2022). On the metabolic level, defense responses such as the production of pathogenesis-related proteins are induced and expressed by the combination of an oxidative stress and a wound-related hormone signaling (Loupit and Cookson, 2020).

Combining the tissues of two different individuals implies that their somatic tissues get involved in a process during which new vascular structures are formed and differentiated (Pina et al., 2017). The differentiation of cambial cells originates the vascular tissue, beginning with the formation of phloem vessels and then xylem vessels (Trinchera et al., 2013; Melnyk et al., 2015), and allows the connection between scion and rootstock. The mechanism responsible for such integration remains poorly understood, however, it must be significantly different for the living cells of phloem and the dead cells of xylem vessels (Melnyk, 2016).

For some scion/rootstock combinations, the relationship between the two genotypes does not always form a successful graft union and the graft interface is associated with necrosis that impact the quality of the plant, even several years after grafting (Pina and Errea, 2005). Even graft incompatibilities have been described in grapevine (Sarooshi et al., 1982). In such cases, it is still not possible to predict the longevity of the grafted plant. Moreover, at the early stage of plant development, only few visible signs can indicate a successful union (Tedesco et al., 2020).

Bench grafting is one of the fundamental nursery practices that affect the quality of the initial grapevine plant material and the global nursery yield (Waite et al., 2015). Next to the graft incompatibilities, also mechanical wounds occurring during grafting can potentially affect the functionality of the new tissues (Bavaresco and Lovisolo, 2000). Through grafting, cells are inevitably disrupted, the protective periderm layers are damaged and a rapid cicatrisation of the tissues is required to prevent water loss and especially pathogen penetration.

Viable propagules of pathogens associated with grapevine trunk diseases (GTD) have been detected on grafting machines and during the grapevine propagation process (Retief et al., 2006; Aroca et al., 2010; Gramaje and Armengol, 2011; Gramaje et al., 2011; Agustí-Brisach et al., 2013; Cardoso et al., 2013). For this reason, among the grapevine nursery operations, grafting is a critical stage as the graft wounds are inherently vulnerable to contamination with trunk pathogens (Gramaje et al., 2018). Contaminated wounds and poorly matched graft unions fail to heal properly, remain open to fungal infection, and create structural weaknesses in the finished vines (Stamp, 2001).

The occurrence of grapevine trunk pathogens in bench grafted vines has been reported by several authors (Zanzotto et al., 2001). In commercial grapevine nurseries, Fourie and Halleen (2006) found that machine grafted unions had lower GTD pathogens incidence compared to hand-grafted unions, correlating the results to the large grafting wounds created by the hand grafting method and by unsterilized hands.

The impact of the grafting practice in the grapevine decline associated to GTD was considered by some authors not only because favoring infections but also because of the influence of the physiology of the vine. Among such trunk diseases, Esca, a complex of diseases linked to fungal infections (Del Frari et al., 2019, 2022), has increased greatly over the past 20 years in Europe (Claverie et al., 2020), when also the extensive use of the mechanical grafting system, performed mainly by the omega machine, spread. Some of the diseases of the Esca complex are well known for being strongly influenced in symptoms development by the physiological reaction of the plant. Andreini et al. (2014) reported a higher percentage of leaf stripe foliar symptoms on grafted vines compared to own rooted vines. More recently, Mary et al. (2017) have investigated in depth the putative influence of grafting type on the expression of Esca leaf symptoms in mature grafted vines. The study suggests that mechanical bench grafting could be one of the factors explaining the increasing incidence of the disease in vineyard. So far, little information exists on the impact of different bench grafting methods in the physiological reaction of the vine tissues up to affecting the development of GTD symptoms.

Therefore, the purpose of the present study was to investigate (i) Omega grafting as mechanical technique, (ii) Whip and Tongue grafting as manual technique, and (iii) FC grafting as semi-mechanical technique, comparing their impact on the anatomical development of the grafting point and comparing the functional integrity of the xylem following different grafting techniques by assessing hydraulic traits in the xylem vessels of the scion. To this aim also the incidence in necrotic tissue at the grafting point and the related potential risk of the young grapevine decline in vineyard were evaluated.

Materials and methods

Bench grafting types

Three methods of bench grafting were studied in the present investigation (**Figure 1**).

Full Cleft grafting

A semi-mechanical V-shaped cut was made with the Fieldcraft Topgrafter® instrument (Florsilva Ansaloni Srl, Bologna, Italy) fixed on a grafting table (**Figure 1A**); the rootstock cutting was positioned on one side of the instrument and cut, then the scion was positioned on the other side and cut by making a reverse V-shaped cut; finally rootstock and scion were manually joined and fixed in place by taping the grafting point with a generic polyethylene cling film.

Whip and Tongue grafting

A manual knife cut was made by a specialized nursery operator (**Figure 1B**), who cut carefully the rootstock and scion, that were manually joined to form finally a strong and elongated Z-shaped junction; no taping was needed on the grafting point.

Omega grafting

A mechanical cut, which takes its name from the shape of the Greek letter omega, was performed by the Omega Star® machine (Fornasier Cesare & C. Snc, Pordenone, Italy) fixed on a grafting table (**Figure 1C**); the grafting took place in two steps by first making a cut in the scion and then by inserting the rootstock cutting; no taping was needed on the grafting point.

Plant material and growing conditions

Two types of plant material were used in the present investigation according to two different bench grafting trials (**Figure 2**) performed in grapevine nursery standard conditions (Vitis Rauscedo Sca, Pordenone, Italy).

Grafting trial 1 – Cultivar influence

The scions of three *V. vinifera* cultivars were compared according to their different susceptibility to Esca diseases (Borgo et al., 2008, 2016; Michelon et al., 2010). Glera (FEDIT 8 C.S.G. clone), Cabernet Sauvignon (169 ENTAV-INRA clone) and Teroldego (SMA 138 clone) were grafted on the rootstock *V. berlandieri* × *V. riparia* cv. Kober 5BB (FEDIT 101 C.S.G. clone) with similar caliber, variable between 7 and 10 mm. Two hundred and fifty grafts per cultivar were obtained through each bench grafting method.

Grafting trial 2 – Caliber influence

The scions of the *V. vinifera* cv. Glera (FEDIT 8 C.S.G. clone) were grafted on the rootstock *V. berlandieri* × *V. riparia* cv. Kober 5BB (FEDIT 101 C.S.G. clone), comparing two caliber ranges of propagation material: "thin grafted vines" obtained from scions and rootstock cuttings with caliber variable between 6 and 8 mm were compared to "thick grafted vines" obtained from scions and rootstock cuttings with caliber variable between 9 and 11 mm. Two hundred and fifty grafts per caliber range were obtained through each bench grafting method.

In both trials, the propagation material was certified according to European Directive 2005/43/EC. After harvest from the mother fields, scion and rootstock canes were cut in scion buds (5 cm) and rootstock cuttings (30 cm) and during this operation no signs of tracheomycotic infections were detected on the base and on the top of rootstock cuttings and scion buds. Prior to grafting, propagation material was hydrated by soaking in water for 12 h, and disinfected by soaking the plant material in water containing 1 mL/L of thiophanate-methyl (Enovit Metil®, Sipcam Italia Spa, Italy) for 30 min.

After being grafted according to each condition, grafted cuttings were waxed (Stähler Rebwachs Pro®, Chauvin Agro-Distribution, Sarrians, France) and placed in callusing wood

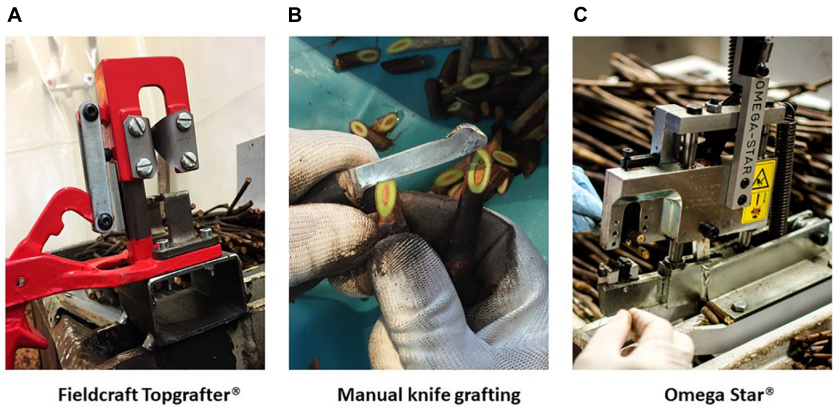

FIGURE 1
Bench grafting methods applied in nursery conditions (Vitis Rauscedo Sca, Pordenone, Italy): Fieldcraft Topgrafter® instrument (Florsilva Ansaloni Srl, Bologna, Italy) fixed on a grafting table, applied as semi-mechanical method **(A)**; manual knife grafting performed by a specialized nursery operator **(B)**, applied as manual method; Omega Star® machine (Fornasier Cesare & C. Snc, Pordenone, Italy) fixed on a grafting table, applied as mechanical method **(C)**.

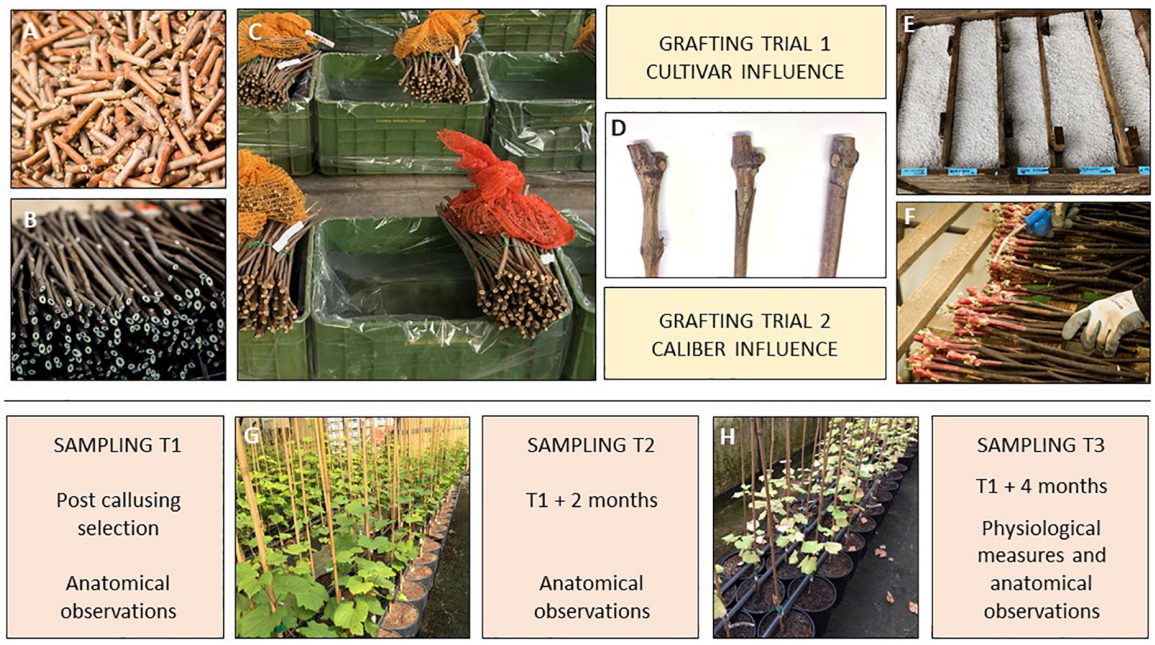

FIGURE 2
Experimental design of the bench grafting trials performed in nursery conditions (Vitis Rauscedo Sca, Pordenone, Italy): scion **(A)** and rootstock cuttings **(B)** were hydrated and disinfected prior grafting **(C)**. Propagation material was grafted according to two grafting trials **(D)**. Then callusing took place for 15 days **(E)** and finally the callused grafted cuttings were selected by discarding the non-compliant material **(F)**. Sampling T1 was performed after the post callusing selection. Sampling T2 was performed at the mid growing period **(G)** and sampling T3 was completed after the end of the growing period **(H)**.

box covered with sawdust and agriperlite on the top of the box. Callusing took place for 15 days at 28°C and 85% relative humidity, during which a solution containing 2.5 mL/L of thiophanate-methyl (Enovit Metil®, Sipcam Italia Spa, Pero (Milan), Italy) was applied as preventive treatment to control *Botrytis cinerea*. Callusing boxes were then left at environmental conditions for 10 days for the acclimatization of the callused grafted cuttings. Finally, callused plant material was removed from the boxes and selected by nursery operators in order to control: (i) the complete union between rootstock and scion and (ii) the callus uniformity. Grafted cuttings with incomplete junctions and non-uniform or hypertrophic callus

were discarded. Selected grafted cuttings were planted in 6 L plastic pots with peat-rich standard soil (Huminsubstrat N17®, Neuhaus Italia Srl, Italy). Potted grafted vines were grown under greenhouse conditions for 4 months (mid-June to mid-October): 2 L of water per pot were supplied weekly by drip irrigation and diseases controlled by spraying the foliage with a mix of 1.5 mL/L of copper hydroxide (Kocide 2000®, Spiess-Urania Chemicals GmbH, Germany) and 40 mL/L of sulfur (Thiopron®, Upl Italia Srl, Italy) every 15 days. Three additional treatments to control grapevine pests were performed during the growing stage by applying 2 mL/L of Acetamiprid (Epik SL®, Sipcam Italia Spa, Pero (Milan), Italy).

Anatomical study

Grafted samples were collected in trials 1 and 2 where the cultivar influence and the caliber effect were studied through histological observations. The sampling was carried out after callusing (T1) and 4 months after T1 (T3). Three biological repetitions (n = 3) for each of the three types of grafts (Omega, W&T and FC) per cultivar were selected randomly in Grafting trial 1. The same protocol was used for each of the six grafts (Omega, W&T and FC for the two calibers thin and thick) only per Glera cv. (Grafting trial 2). Graft longitudinal sections (approximately 100 µm in thickness) were cut with a Sledge G.L.S.-1 microtome (Gärtner et al., 2014).

Zeiss stereomicroscopic microscope equipped with an Optika microscope digital camera and a Leitz D.M.-R.B. Fluo Optic microscope (Wetzler, Germany) equipped with a Nikon DS-Fi3 digital camera were used for qualitative and quantitative analysis. Lugol was used for starch staining (Beccari and Mazzi, 1966).

To evaluate the most successful grafting techniques to get an efficient connection between the two bionts in the Grafting trials 1 and 2, the following qualitative and quantitative parameters were used (Tedesco et al., 2020; **Table 1**):

- Quality of the connection-level between scion (S) and rootstock (R) was evaluated on four categories of callogenesis. Category 4 shows a perfect connection between bionts, where callus covered the space between S and R and the graft line is practically unrecognizable. Category 3 shows a few structural imperfections in the graft border where the connection between the two bionts is almost complete. Category 2 is characterized by many discontinuities (wood or bark) in the border and in category 1 S and R are unattached and an intermediate space is clearly observed.
- Anatomical part of bionts involved in grafting connection which means parenchymal tissue or cambium of S and R, respectively.
- Internal callus (between bionts) differentiation grade.

TABLE 1 Quantitative parameters used for grafting techniques evaluation.

Callogenesis	
1	Broken/unattached union
2	Lots of discontinuities
3	Few structural imperfections
4	Perfect union
Bionts involved in graft connection	
a	Scion parenchymatic rays
b	Scion cambium
c	Rootstock parenchymatic rays
d	Rootstock cambium
Callus type	
0	Non-vascular
1	Differentiated without meristemoids
2	Differentiated with meristemoids
−1	Necrotized
External callus	
0	Non-vascular
1	Differentiated
Necrosis	
S	Scion
R	Rootstock
np	Not present
Space between bionts	
Yes	Presence
No	Absence

- External callus differentiation grade or the callus formed around the graft union (outside bionts).
- Occurrence of necrosis areas in S or R, or in both of them.
- Space between bionts.

Necrosis area measurements

Necrosis areas were considered as degenerated tissues that appeared dark colored compared to the healthy tissue. These regions were measured by analyzing the callus growth at a quarter of the sample diameter, where the parenchymatic rays and cambium of the two bionts were observed. The necrosis areas were measured with Image J software 1.47v.

Xylem morphology and hydraulic traits

In both trials, sections 2–3 cm long were cut from 1-year-old stems during dormancy. In trial 1, the 10th internode was selected for each combination of cultivars and grafting type while in trial 2, the 6th internode was sampled from Glera grafted cuttings. All the stem samples were placed in

a 50:50 (v/v) mixture of ethanol and water and stored at 5°C. The stem sections were then fixed through ice on a Peltier plate, and transverse sections of 10–12 μm thickness cut using a rotary microtome (Haworth et al., 2017). The sections were stained with a solution of 0.04% safranin, 0.15% astrablue and 2% acetic acid in distilled water, and permanently fixed with a histological mounting medium (Eukitt, Bioptica, Milan, Italy). Anatomical observations were made with a Nikon Eclipse 800E light microscope and images recorded with a Nikon DS-Fi2 camera attached to the microscope (Nikon Corporation, Tokyo, Japan). Each section was divided into lateral (L) and dorso/ventral (DV) sectors as proposed by Pouzoulet et al. (2020) and four orthogonal subsectors were defined (two L and DV sectors for each stem cross-section respectively). The subsectors contained from four to six xylem areas (Xy) each one delimited by two consecutive parenchymatic bands (lateral), phloem (outer) and pith (inner). Thus, Xy was exclusively composed of xylem elements (fibers and vessels). Digital images of each Xy were then analyzed using the computer program Nikon Nis-Elements® software and the following parameters measured: Xy area (μm^2); lumen vessels area (VA, μm^2); vessel density (Vd, mm^{-2}). The diameter of each vessel (d_v, μm) was calculated as the diameter of a circle with an area equivalent to VA.

The hydraulic weighted vessel diameter *Dh* (μm) was calculated following Sperry and Saliendra (1994) as:

$$Dh = \frac{\Sigma d_v^5}{\Sigma d_v^4} \quad (1)$$

Calculation of *Dh* incorporates the disproportionate contribution of large vessels to total flow and gives the average diameter needed for a given vessel density to result in the theoretical hydraulic conductivity for that stem Tyree et al. (2002).

The theoretical specific xylem hydraulic conductivity (K_{st}) was calculated following Santiago et al. (2004) using the Hagen–Poiseuille equation for ideal capillaries assuming laminar flow:

$$k_{st} = \left(\frac{\pi\rho}{1.28\eta A_i}\right)\Sigma d_v^4 \quad (2)$$

where ρ is the density of water (998.2 Kg m^{-3} at 20°C); η is the viscosity of water (1.002 × 10^{-9} MPa s at 20°C), and A_i is the area of the image analyzed (m^2).

Plant growth

In the trial 1, 15 grafting were randomly selected for each cultivar and grafting type combination and biweekly measured (height and number of internodes) from day of the year (DOY) 182 to 281 (July 1st to October 8th). The relative growth rate (RGR) was calculated for internode number and plant height fitting biweekly measurements by Logistic functions at three parameters as follow:

$$y = \frac{k \cdot y_0}{y_0 + (k - y_0)e^{-rt}} \quad (3)$$

where y corresponds to actual value of the measure, y_0, initial value of measure (t_0), r, intrinsic growth rate (1/time), k, carrying capacity (maximum value of the measure), t, time. The parametrization of RGR were determined using *growth rates* R statistical packages software R 0.8.2 (Petzoldt, 2020).

Statistical analysis

Hydraulic traits were analyzed on five biological replicates (n = 5) while necrosis percentage was analyzed on three biological replicates (n = 3). For growth parametrization there were fifteen biological replicates per cultivar and grafting type (n = 15). Data were checked for normal distribution (D'Agostino–Pearson's χ^2 test) and homogeneity of variance (Levene tests). Percentages were transformed by arcsin function and normal distribution verified before analyses. In both trials, the effects of the cultivars and grafting type were assessed with two-way ANOVA. *Post hoc* analysis was conducted using Bonferroni test. Correlation was evaluated by performing Pearson's test. All analyses were executed using dplyr, multcomp and car R statistical packages software R 4.0.2 (R Core Team, 2020).

Results

Grafting trial 1 – Cultivar influence

Anatomical observations

Glera (FEDIT 8 C.S.G. clone) scion on the rootstock *Vitis berlandieri* × *Vitis riparia* cv. Kober 5BB (FEDIT 101 C.S.G clone)

At T1, Omega grafting (**Figure 3A**) showed the highest callus formation (callogenesis = 3) in comparison to W&T (**Figure 3C**) and FC (**Figure 3E**) grafting (callogenesis = 2) (**Table 2**). In all three grafted cuttings the different tissues of bionts such as parenchymatic rays and cambium either of S or R, were almost equally involved since the beginning. Moreover, the callus between bionts appeared not structured and without necrosis (**Supplementary Figures S1A,C,E**) as well as the external one, as shown in **Supplementary Figure S2A**. As shown in **Figure 3A**, the space between S and R was evident and filled by callus, which ensured the continuity between the two bionts.

At T3 Omega grafting (**Figure 3B**) still showed the highest callus formation (callogenesis = 4) in comparison to W&T (**Figure 3D** and **Supplementary Figure S1D**) and FC

TABLE 2 Quantitative evaluation (see Table 1) of Glera, Cabernet Sauvignon, Teroldego scion onto K5BB rootstock comparing three different techniques (Omega, WT, and FC) at T1 and T3.

Cultivar	Survey time	Grafting techniques	Callogenesis	Bionts involved in the connections	Type of callus	External callus	Necrosis	Space between S and R	Ranking
Glera		Omega	3	3a, 3b, 3c, 3d	0	0	np	Yes	1
	T1	W&T	2	3a, 3b, 3c, 3d	0	0	np	Yes	2
		FC	2	3a, 2b, 3c, 3d	0	0	np	Yes	3
		Omega	4	3a, 3b, 3c, 3d	1	1	S, R	Yes	1
	T3	W&T	3	2a, 3b, 2c, 3d	1	1	S, R	Yes	2
		FC	3	3a, 3b, 3c, 3d	1; –1	1	S, R	Yes	3
Cabernet Sauvignon	**T1**	Omega	3	3a, 3b, 3c, 3d	0	0	np	Yes	1
		W&T	2	3a, 3b, 3c, 3d	0	0	np	Yes	2
		FC	3	3a, 3b, 3c, 3d	0	0	np	Yes	1
	T3	Omega	4	3a, 3b, 3c, 3d	1	1	S, R	No	2
		W&T	4	3a, 3b, 3c, 3d	1	1	S, R	No	1
		FC	2	3a, 3b, 3c, 3d	1; –1	1	S, R	Yes	3
Teroldego	**T1**	Omega	2	1a, 1b, 3c, 3d	0	0	np	Yes	2
		W&T	3	1a, 3b, 3c, 3d	0	0	np	Yes	1
		FC	2	2a, 2b, 3c, 3d	0	0	np	Yes	2
	T3	Omega	3	3a, 3b, 3c, 3d	2; –1	1	S	Yes	2
		W&T	4	3a, 3b, 3c, 3d	2; –1	1	S	Yes	1
		FC	2	3a, 3b, 3c, 3d	2; –1	1	S, R	Yes	3

(Figure 3F) grafting (callogenesis = 3) (Table 2). As in T1, in all three grafted cuttings the different tissues of bionts such as parenchymatic ray and cambium of either S or R continued to be involved. Moreover, at T3 the callus derived from the parenchymal and cambial cells, differentiated into wood vessels in all the three grafted cuttings. Newly formed xylem vessels were documented in Supplementary Figure S2B. All the three grafted cuttings were characterized by necrosis of the S and R, respectively, which was not observed at T1. Furthermore, at this stage the FC grafting showed the external callus more necrotized (Supplementary Figure S1F) than the other grafted cuttings. The space between S and R was evident mainly in the W&T and FC grafting where it was filled by callus but some discontinuities were evident and delimited by necrotic tissues.

Cabernet Sauvignon (169 ENTAV-INRA clone) scion on the rootstock *Vitis berlandieri* × *Vitis riparia* cv. Kober 5BB (FEDIT 101 C.S.G clone)

At T1, concerning callus proliferation, Omega and FC grafting showed a higher score (callogenesis = 3) than W&T grafting (callogenesis = 2) (Table 2). In all three grafted cuttings the different tissues of bionts such as parenchymatous ray and cambium either of S or R were almost equally involved in the callus generation since the beginning. Moreover, the callus between bionts appeared not structured and without necrosis (Figures 4A,C,E) as did the external one. The space between S and R was evident in all three grafting and was filled by callus, which ensured the tissue continuity between bionts. At T1 the highest production of external callus around the grafting samples (Supplementary Figure S3A) was observed in the FC grafting compared to Omega and W&T grafting (Supplementary Figures S3C,E). As well as in Glera (Grafting trial 1), the callus filling the space between R and S was pearly white, hyperhydric and rich in calcium oxalate crystals (Supplementary Figure S4A).

At T3, both Omega (Figure 4B) and W&T (Figure 4D) grafting showed successful connections between bionts. Only some discontinuities by the bark tissue were still observed. In particular, Omega grafting showed necrosis in both S and R (Supplementary Figure S3B) as well as in W&T (Supplementary Figure S3D). FC grafting (Figure 4F and Supplementary Figures S3F,S5A–F) appeared the worst in terms of graft union because necrotized areas were frequently found in both bionts and in the internal callus. In general, at T3 the callus was well structured and xylem vessels were recognizable among parenchymatous tissue rich in starch (Supplementary Figure S4B).

Teroldego (SMA 138 clone) scion on the rootstock *Vitis berlandieri* × *Vitis riparia* cv. Kober 5BB (FEDIT 101 C.S.G clone)

At T1, W&T showed the best callogenesis which was mostly produced by both rootstock's cambium and parenchymatic rays and only in part by scion cambium (Figure 5C). In FC grafting, both S and R were involved in the initial callogenesis (Figure 5E) although the highest level of callus production was due to

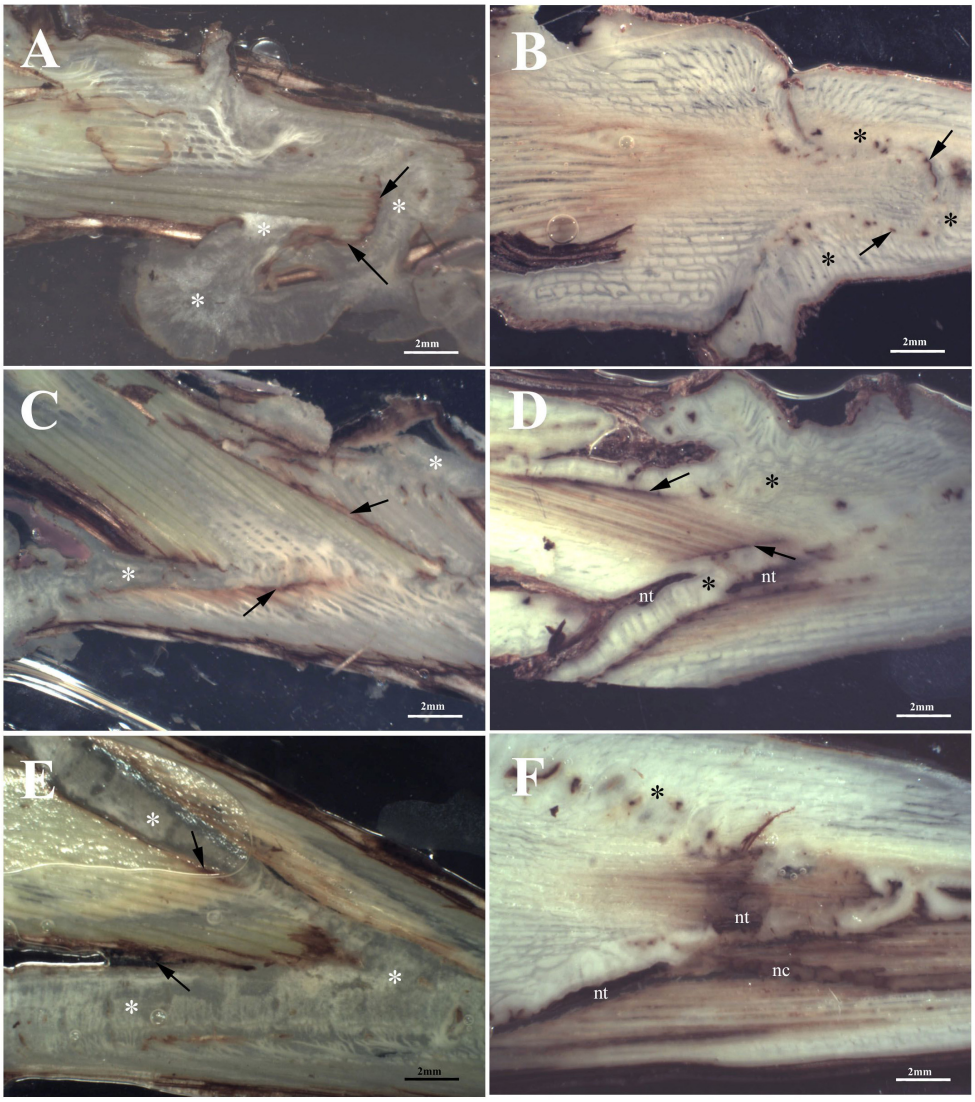

FIGURE 3
Stereoscopic images of graft longitudinal sections of Glera scion onto K5BB rootstock, at T1 **(A,C,E)** and T3 **(B,D,F)**. Callus formation in different graft union shapes: Omega **(A,B)**, W&T **(C,D)**, and FC **(E,F)**. *, Non differentiated callus; *Differentiated callus; nt, necrotic tissue; nc, necrotic callus; black arrow, discontinuity.

rootstock (Table 2). Omega grafting showed a callogenesis level similar to FC grafting (lower than W&T grafting) where the R contribution was the most significant in graft union formation (Table 2). Moreover, in all three grafting methods, the callus between bionts was not differentiated and no necrotic areas in the internal callus as well as in the external one was observed (Figures 5A,C,E). As in Glera and Cabernet Sauvignon grafted cuttings, the callus filling the space between R and S was pearly white and hyperhydric. In particular, Supplementary Figure S6A showed an example of the callus formed by parenchymatous tissue completely filling the spaces between the two components connecting the S and the R.

At T3, W&T still showed the highest callus production (callogenesis = 4) (Figure 5D), followed by Omega (callogenesis = 3) (Figure 5B) and FC (callogenesis = 2) (Figure 5F) with some bark discontinuities between S and R. At T3, in all three grafted cuttings, the different tissues of the bionts, such as parenchymatic ray and cambium of both S and R were involved in callus generation (Table 2), in comparison with T1. Moreover, in all three grafted cuttings the callus was characterized by meristemoids with xylem vessels in differentiation (Supplementary Figure S6B). This feature seems to belong exclusively to Teroldego cv. In both Omega and W&T grafting, necrotic areas were observed especially in the S, whereas FC grafting showed necrosis in both S and

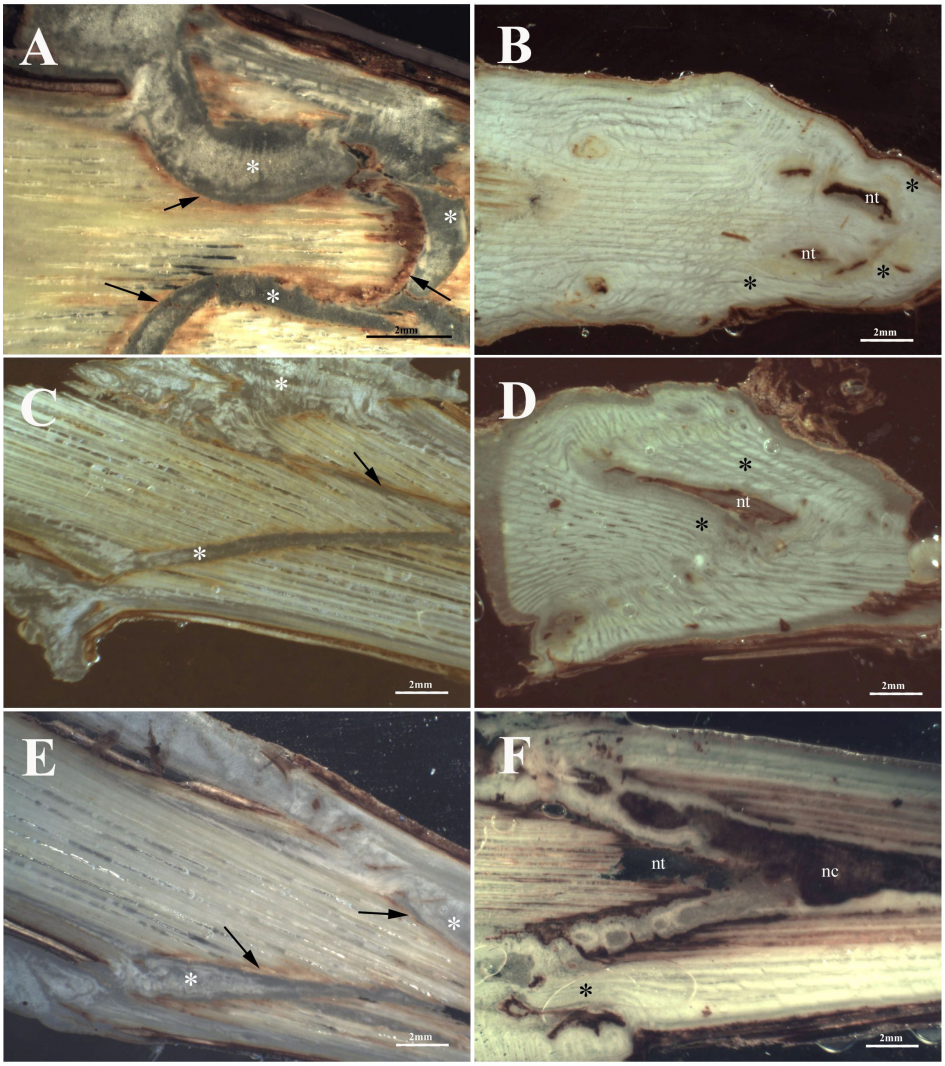

FIGURE 4
Graft longitudinal sections of Cabernet Sauvignon scion onto K5BB rootstock, at T1 **(A,C,E)** and T3 **(B,D,F)**. Callus formation in different graft union shapes: Omega **(A,B)**, W&T **(C,D),** and FC **(E,F)**. *, Non differentiated callus; *Differentiated callus; nt, necrotic tissue; nc, necrotic callus; black arrow, discontinuity.

R. The space between S and R was mainly evident in Omega and FC grafting where space was filled by callus but some discontinuities were still observed especially in the scion border, which was characterized by necrotic tissue.

Necrosis area statistical analysis

Statistical analysis on the necrosis percentage area indicated that significant differences were observed between cvs and/or grafting type (Table 3). In particular, regarding Cabernet Sauvignon, W&T grafting showed an amount of necrotic tissue (20.2 ± 3.1%) similar to Omega grafting (21.7 ± 4.2%). FC grafting necrosis value was significantly higher (43.8 ± 1%). A similar trend was evidenced in cv. Teroldego where the values of necrosis between W&T and Omega grafted cuttings (30.9 ± 7.6% and 37.3 ± 4.2%, respectively) were similar but significantly different from FC (63 ± 0.9%). On the contrary, considering cv. Glera, FC and Omega grafted cuttings (31.1 ± 1.4% and 36.1 ± 3%, respectively) showed the lowest necrosis value in comparison to W&T grafting (56.6 ± 1.8%).

Physiological measurements

Results are presented according to each cultivar (Glera, Cabernet Sauvignon, Teroldego) grafted on the common rootstock Kober 5BB and the applied bench grafting method (Omega, FC, W&T). No plant material was discarded by this operation; however, the callus feature was clearly different according to each bench grafting type, especially on cv. Glera: homogeneous callus in Omega grafted cuttings, homogeneous

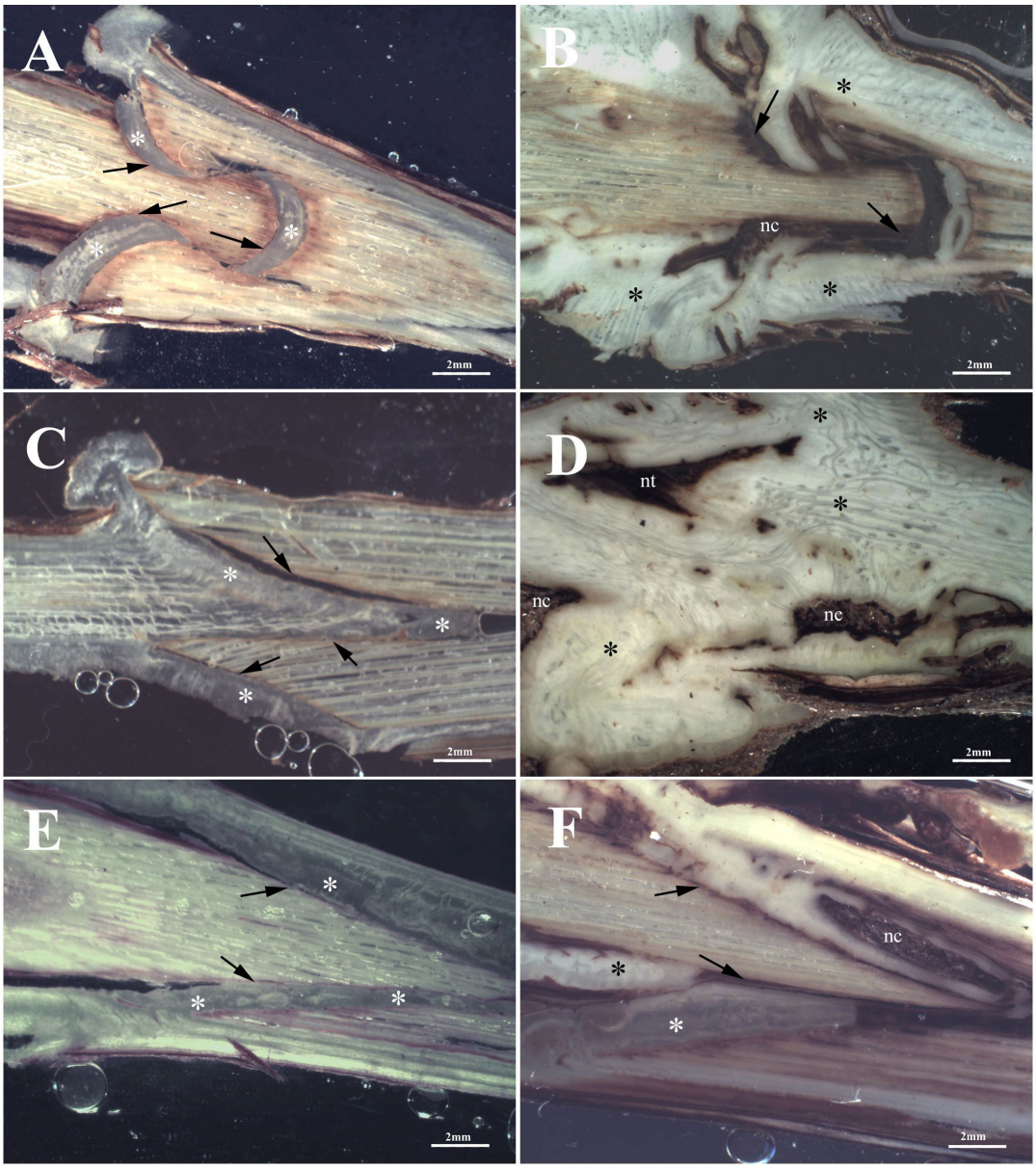

FIGURE 5
Graft longitudinal sections of Teroldego scion onto K5BB rootstock, at T1 **(A,C,E)** and T3 **(B,D,F)**. Callus formation in different graft union shapes: Omega **(A,B)**, W&T **(C,D)**, and FC **(E,F)**. *, Non differentiated callus; *Differentiated callus; nt, necrotic tissue; nc, necrotic callus; black arrow, discontinuity.

and hypertrophic callus in W&T grafted cuttings and less complete and hypertrophic callus in FC grafted cuttings.

Xylem morphology and hydraulic traits

Analysis of the grapevine vessels suggest differences in xylem traits between the three cultivars whilst grafting type did not have significant effects for all the considered traits (Table 3). The cultivar Cabernet Sauvignon exhibited significant lower xylem vessel density than Glera and Teroldego (in average 98.5 mm^{-2} vs. 120 and 121 mm^{-2} respectively). However, the significant interaction ($P < 0.01$) indicates that the Vd was affected by grafting type in relation to cultivars. Thus, Vd was significantly higher in the combination Glera-Omega than Cabernet Sauvignon-FC (137 $\pm$ 30.3 mm^{-2} and 85.2 $\pm$ 6.5 mm^{-2} respectively). Like Vd, the ratio vessel area: xylem area was significantly affected by cultivars. Glera had significant higher VA_f than Teroldego and Cabernet Sauvignon (in average 22.4% vs. 19.7 and 18.6% respectively). On the contrary, hydraulic traits (Dh and Kst) were not affected by

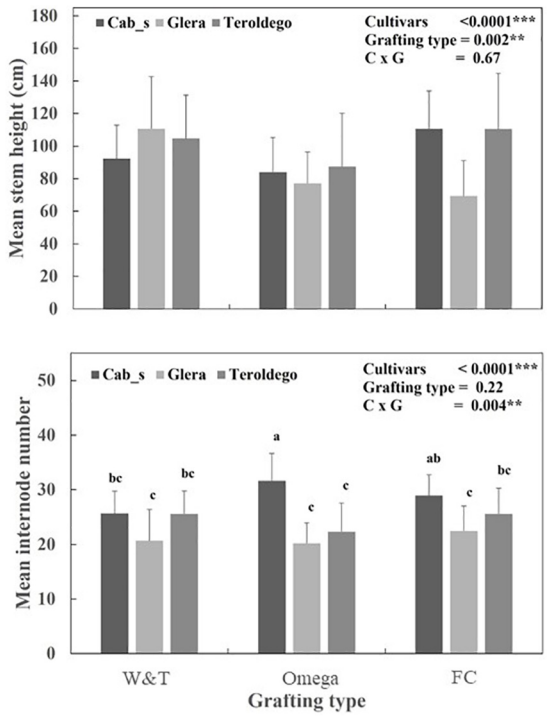

FIGURE 6
Mean value and standard deviation for mean stem height and internode numbers measured in Teroldego, Glera and Cabernet Sauvignon cultivars scion onto K5BB rootstock with Whip & Tongue (W&T), Omega, and Full Cleft (FC). Two-way ANOVA was used to assess any significant differences between treatment and/or cvs. Different letters indicate significant differences between datasets based upon a one-way ANOVA with Bonferroni *post hoc* test. $^{**}P < 0.01$,$^{***}P < 0.001$.

cultivar and grafting type. Dh ranged from 31.6 ± 3.1 and 25.7 ± 2.6 μm and Kst from 41.1 ± 12.7 and 26 ± 7.2 Kg Mpa^{-1} s^{-1} m^{-1}. At the whole, a high vessel density determined a reduction of Dh (Table 4). Correlation analyses evidenced a positive and significant relationship between VD and Dh ($P = 0.02$).

Plant growth

Comparison of the parameters of the Logistic function revealed different patterns of stem growth dynamics relatively to cultivars for internode number and cultivar/grafting type for plant height measurements (Figure 6, Supplementary Table S1 and Table 5). R^2 were higher than 0.98 for all fitted curves.

As shown in Figure 6, the three cultivars significantly differed for K ($P < 0.0001$). Cabernet Sauvignon showed a higher K and r coefficients than Teroldego and Glera (30.2 vs. 25.8 and 22.7 number of internodes respectively). However, the significant interaction ($P < 0.01$) for K coefficient indicates that the final number of internodes per plants was affected by grafting type within each cultivar. The Omega and FC grafting induced the higher number of internodes in Cabernet Sauvignon (in average more than 30 internodes each) and the lower in Glera (in average 23 internodes). Teroldego and Cabernet Sauvignon had significantly higher intrinsic growth rate than Glera (0.062–0.063 DOY^{-1} vs. 0.056 DOY^{-1} respectively, $P < 0.0001$).

As shown in Table 5, the K coefficient was significantly affected by cultivars ($P < 0.0001$) and grafting type ($P = 0.0001$). Teroldego and Cabernet Sauvignon showed the higher K than Glera (in average 102.6, 97.6, and 77.3 cm) whilst FC determined significant high K coefficients than Omega (102.6 vs. 81.2 cm respectively). The intrinsic growth rate, r, was significantly affected by grafting type ($P = 0.001$). Omega grafting determined a higher r for plant height than FC and W&T.

Grafting trial 2 – caliber influence

Anatomical observations

Vitis vinifera L. cv. Glera (FEDIT 8 C.S.G. clone) was grafted on the rootstock *V. berlandieri* × *V. riparia* cv. Kober 5BB (FEDIT 101 C.S.G. clone).

At T1, FC-thin showed the highest connection between bionts (Figure 7I) in comparison to other grafting techniques (Figures 7A,C,E,G,K) even though several discontinuities were observed. Omega thin and thick (Figures 7A,C) and W&T thick (Figure 7G) grafted cuttings showed unattached unions with evident empty spaces. In particular, the callus production in FC-thin grafting was almost due to parenchymatic rays of both R and S and only in part by R's cambium (Table 6). In all techniques, a characteristic found common was the parenchymatic rays contribution of both bionts in grafting connection (Table 6). A peculiarity was observed in the callus of FC thin which was already differentiated at T1, as shown in Supplementary Figure S8A. Necrotic areas were found only in S and R in W&T thin and thick (Supplementary Figures S7E,G) compared to the other grafted cuttings (Supplementary Figures S7A,C,K).

At T3, Omega thin showed the best connection between bionts (Figure 7B) where the callus completely filled the space and the graft border was unrecognizable. The connection was not only external (Supplementary Figure S7D) but also involved parenchymatic rays and cambium activation excluding the pith. The proliferation of parenchymatic rays and cambium to form callus is a characteristic found in all grafting techniques (Figures 7D,F,H,J,L and Supplementary Figures S7F,H–J,L) not only in Grafting trial 2 but also in the trial 1 (Supplementary Figure S7B).

Necrosis area statistical analysis

Regarding necrosis area % in Glera, Omega thin grafting showed the lowest value (9.7 ± 1.3) compared to the W&T and FC of the same caliber. Considering the thick caliber, the necrosis areas were not significantly different with value

TABLE 3 Different a two-way ANOVA was used to assess any significant differences between cvs and/or grafting type.

Cultivar	Grafting type	Necrosis (%)	Vd (mm^{-2})	VA_f (%)	Dh (μ m)	*K*st (Kg MPa^{-1} s^{-1} m^{-1})
	W&T	56.6 ± 1.8e	101 ± 15.1ab	23.7 ± 3.7	31.6 ± 3.1	34.5 ± 7.4
Glera	Omega	36.1 ± 3cd	137 ± 30.3a	22.1 ± 1.6	25.7 ± 2.6	32.1 ± 14.5
	FC	31.1 ± 1.4bc	125 ± 18.3ab	21.5 ± 2.8	27.4 ± 2.2	39.9 ± 11.1
	W&T	30.9 ± 7.6bc	130 ± 24.9ab	21 ± 3.7	26.3 ± 4.1	41.1 ± 12.7
Teroldego	Omega	37.3 ± 4.2cd	110 ± 21.2ab	17.8 ± 1.4	26.4 ± 2.7	31 ± 6.8
	FC	63 ± 0.9e	125 ± 29.2ab	20.2 ± 2.2	25.7 ± 4.1	31.5 ± 7.5
	W&T	20.2 ± 3.1a	97.9 ± 4.7ab	18.6 ± 1.3	27.8 ± 2.8	28.9 ± 9.2
Cabernet Sauvignon	Omega	21.7 ± 4.2ab	112 ± 23.7ab	18.7 ± 2.9	27 ± 3.6	26 ± 7.2
	FC	43.8 ± 1d	85.2 ± 6.5b	18.6 ± 3.2	30.9 ± 3	33.8 ± 14.6
Two-way ANOVA	**Df**	***F*-value**				
Cultivars	2	45.72***	5.813**	8.156**	2.591^{ns}	1.38^{ns}
Grafting type	2	36.88***	0.99^{ns}	1.33^{ns}	1.928^{ns}	1.236^{ns}
Cultivars × Grafting type	4	55.39***	3.036*	0.793^{ns}	2.349^{ns}	0.821^{ns}
Residuals	36					

Different letters indicate significant differences between datasets based upon a one-way ANOVA with Bonferroni *post hoc* test. Necrosis percentages were transformed by arcosin function and normal distribution verified before two-way ANOVA.
*$P < 0.05$, **$P < 0.01$, and ***$P < 0.001$.

comparable to those observed in both W&T and FC thin (Table 7).

Physiological measurements

Results are presented according to the applied bench grafting method (FC, W&T, O) and both caliber ranges (thin and thick) of Glera grafted on Kober 5BB. Few grafted cuttings were discarded after callusing: two Omega grafted cuttings for both caliber ranges did not present complete callus; one thin W&T grafted cutting with uncomplete and hypertrophic callus; as well as four thin FC grafted cuttings. In general, thick grafted cuttings showed a more homogeneous callus although more hypertrophic than thin grafted cuttings. The callus of FC grafted cuttings was less complete and hypertrophic in both caliber ranges than in the other conditions.

Hydraulic traits

The effects of the caliber ranges (thin and thick) on hydraulic traits of Glera grafted cuttings were reported in Table 8. The VD as well as Dh and *K*st calculated on the 6th internode was similar between grafting types showing a negligible effect of the size of scion on the xylem morphology and hydraulic efficiency at the end of growing season.

TABLE 4 Correlation between the cultivars evaluated by the Pearson's test.

	Vd	VA_f	Dh	*K*st
Vd	1.00			
VA_f	0.25	1.00		
Dh	−0.74*	0.37	1.00	
*K*st	−0.03	0.12	0.07	1.00

*$P < 0.05$.

Discussion

The experiments here reported aimed to investigate on possible changes induced on anatomical and hydraulic traits of just grafted vines by applying three different grafting methods on three different cvs. Field observations by Mary et al. (2017) suggest a direct relationship between foliar symptoms incidence in Esca complex over the years and the grafting method applied. It is also well known that the GTDs can not only be due to colonization and necrosis of wood tissue, but can also have strong implications of physiological disfunctions leading to the development of characteristic foliar symptoms as in diseases of the Esca complex (Lecomte et al., 2012, 2018; Claverie et al., 2020) or in declines in young vineyards.

Anatomical observations

It is well known that after intimate contact between bionts, a new parenchymatous tissue occurs as a common response to wounding (Moore and Walker, 1981a,b; Hartmann et al., 2002; Pina and Errea, 2005). One of the most relevant aims of this study was to evaluate which bionts tissue, i.e., parenchymatic rays and cambium, contributed to the callogenesis. Failure in establishing the connection is highlighted by the presence of necrotic tissue. The ongoing of necrosis indicates that an

10.3389/fpls.2022.1006835

TABLE 5 Parametrization of plant height by Logistic model.

Cultivar	Grafting type	Logistic model		
		K	y_0	*r*
Glera	Omega	70.5 ± 19.3	$4.9*10^{-9}$	0.13 ± 0.02
	FC	81.8 ± 21.8	$1.7*10^{-6}$	0.12 ± 0.04
	W&T	79.6 ± 32.3	$8.3*10^{-6}$	0.11 ± 0.03
Teroldego	Omega	87.7 ± 32.7	$7.5*10^{-7}$	0.13 ± 0.03
	FC	112 ± 34.9	$3.6*10^{-6}$	0.12 ± 0.03
	W&T	108 ± 27.4	$2.3*10^{-6}$	0.1 ± 0.03
Cabernet Sauvignon	Omega	85.3 ± 20.9	$8*10^{-9}$	0.14 ± 0.03
	FC	114 ± 23.2	$1.1*10^{-7}$	0.11 ± 0.02
	W&T	93.9 ± 20.4	$1*10^{-7}$	0.13 ± 0.02
Two-way ANOVA	**Df**		***F*-value**	
Cultivars	2	11.434***	0.948^{ns}	0.955^{ns}
Grafting type	2	7.405***	0.95^{ns}	7.153**
Cultivars × Grafting type	4	0.737^{ns}	0.754^{ns}	1.149^{ns}

*$P < 0.05$, **$P < 0.01$, and ***$P < 0.001$. ns, not significant.

insufficient amount of nutrients is able to reach the area where the necrotic area forms (Balbi et al., 2019), or that stress signaling originates in the area inducing the formation of necrotic cells. Necrotic cells are characterized by shrunken nucleus and cytoplasm, so producing a more stained protoplast that can be recognized in healthier tissue due to its darker appearance (Papini, 2018). This investigation was conducted studying grafting connection moving forward slide-by-slide from the rhytidome to the inner part to have a consistent evaluation of callogenesis similar to 3D x-ray tomography but with the added value of classical histology (Fernandez et al., 2022). Classical histology allows to obtain more detailed information on the composition of the tissue by differential staining. In this way, comparing the three cvs at T1, we were able to observe interesting differences in either R or S tissues, involved in the meristematic activity. In our opinion, such differences in tissue reaction could be attributed only to the cv. effect since the rootstock was the same. In particular, it is the first time, to our knowledge that Teroldego cv. has been reported to exhibit a slow process of wounding repairing. Nevertheless, Teroldego cv. grafted on Kober 5BB has showed a successful union as previously described by Prodorutti et al. (2009).

Considering the impact of the three grafting techniques on the successful connection between bionts at T3, Omega grafting still showed high distance (about 2 mm) between bionts and the connection was guaranteed by a differentiated callus filling this space, confirming the essential role of this tissue during the grafting union formation (Gautier et al., 2019). This was not considered as a critical parameter by Milien et al. (2012) since spaces between S and R were evident in both "bad" and "good graft."

Furthermore, the results agreed with the histological observations on autografts of *Prunus domestica* as well as heterografts of *Prunus cerasus* cvs where cell differentiation and xylogenesis led to the formation of vascular connections (Gebhardt and Goldbach, 1988). At T3, the delayed response in callus differentiation was confirmed in Teroldego, which still showed meristemoids.

To date, another important parameter obtained from our histological observations was the % of necrosis areas on the graft union. From these results, it has to be noted that Omega grafting in all cvs showed the lowest % of necrotized area, revealing the best capability of connection between the two bionts at T3 (Milien et al., 2012). Furthermore, this phenomenon was confirmed by anatomical observations, where Omega grafting, independently of the cvs showed the most homogeneous and equilibrated callus production.

Regarding caliber influence, at T1 the callogenesis was scarce and unattached unions were observed in most of the grafting while at T3, Omega thin (**Supplementary Figure S8C**) grafting showed the best connection compared to the other grafting where no necrotized callus was observed. Furthermore, in this case, the % of the necrotized area in S and R was significantly lower than in the other samples. Omega thick grafting compared to the thin grafting showed a delayed response since the callus still exhibited meristemoids (**Supplementary Figure S8B**). For these reasons, only for Omega grafting we can assume that caliber of the bionts influenced callus formation.

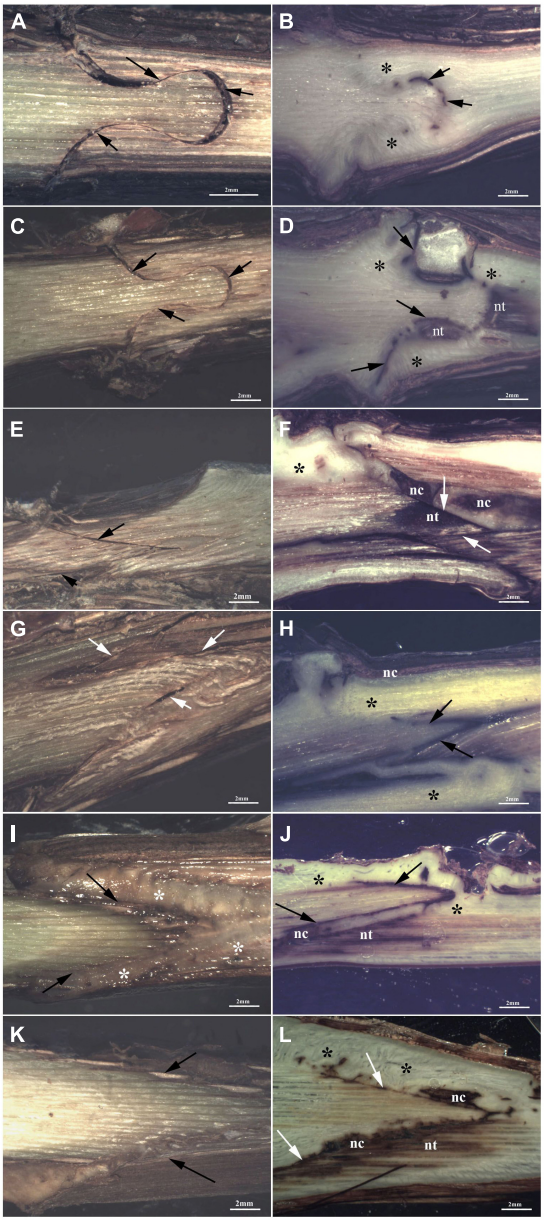

FIGURE 7
Graft longitudinal sections of Glera scion onto K5BB rootstock, at T1 **(A,C,E,G,I,K)** and T3 **(B,D,F,H,J,L)**. Callus formation in different graft union shapes: Omega-thin **(A,B)**, Omega-thick **(C,D)**, W&T-thin **(E,F)**, W&T-thick **(G,H)**, FC-thin **(I,J)**, FC-thick (**K**,**L**). *, Non differentiated callus; *Differentiated callus; nt, necrotic tissue; nc, necrotic callus; black arrow, discontinuity.

Hydraulic traits and vessel density

Hydraulic transport efficiency of the xylem is one of the most important traits determining the growth performance of a species as well as its capacity to respond to environmental constrains. The results of trial 1 showed that the vessel density (VD) expressed as number of vessels: xylem area ratio (excluding phloem and ray parenchyma) as well as the total vessel area: xylem area ratio (VA_f) were significantly influenced by cultivar ($P < 0.0001$). However, the significant interaction cultivars x grafting type ($P = 0.03$) demonstrated that the grafting type had different effect within each cultivar. The *post hoc* analyses showed that combination of Glera-Omega and Cabernet Sauvignon-Full Cleft determined significant changes in VD (137 vs. 85.2 number of vessels per mm^{-2} of xylem area, $P = 0.007$). The effect of cultivars on the xylem morphology was already reported in grapevine (Pouzoulet et al., 2014). On the whole, Cabernet Sauvignon showed the lowest VD and VA_f in comparison to Teroldego and Glera cvs, whilst no differences were detected for Dh and Kst. These results highlighted the main effect of the genotype over the grafting type on the xylem morphology and the negligible effects of these factors on the hydraulic traits. The mean VD ranged between 87 and 140 vessels mm^{-2} and these values were higher than those reported for the same cvs in other works (Pouzoulet et al., 2013). However, two considerations have to be considered: first, we excluded the phloem and ray parenchyma areas in the calculation of xylem area; second, we sampled the internodes in the distal part of the stem and a general increase of VD from the base to the apex was reported in 8-year-old *V. vinifera* cv. Chardonnay plants (Sun et al., 2006) and cv. Nebbiolo (Schubert et al., 1999). Thus, our results were similar to those reported by Lovisolo et al. (2002), who found 100 vessels per mm^{-2} in apical stem of 2-year-old plants of *V. vinifera* L. cv. Pinot noir, grafted on *V. riparia* × *berlandieri* 'Kober 5BB'. The higher VA_f recorded in Glera was determined by a higher vessels area rather than a low xylem surface (data not shown). With the same xylem area, the high vessel surface could determine a reduction of wood basal density as already reported in other woody species (Giovannelli et al., 2019). These results confirmed that VA_f is strongly dependent on genotype (Haworth et al., 2017). The significant effects of the cultivar on VD and VA_f were not found when Dh and Kst values were calculated. At a glance, this result appears somewhat counterintuitive, as, with the same xylem area, cultivar with low VD (Cabernet Sauvignon) should have wider Dh than cvs with high VD (Teroldego and Glera). It is well known that larger vessels assure higher hydraulic efficiency (lower resistance to water flow) than smaller ones (Tyree and Sperry, 1988). Conversely, the similarity of Dh values recorded in different cultivars could be due to different distribution of vessel elements in diameter classes as already reported in *V. vinifera* cvs (Pouzoulet et al., 2019). This statement can be partially supported by the significant negative correlation between VD and Dh (–0.74, $P = 0.02$) considering the three cvs pooled.

Our results showed that grafting type did not induce significant changes in vessel density and hydraulic traits. In this experiment, Glera plants had lower VD than what recorded in the first trial (in average 115 vs. 78 vessels per mm^{-2}). This discrepancy in the results can be explained by the sampling

TABLE 6 Quantitative evaluation of Glera.

	Grafting type	Callogenesis	Bionts involved in the connections	Type of callus	External callus	Necrosis	Space between S and R	Ranking
T1	Omega–Thin	1	2a, 1b, 1d, 1c	0	0	np	Yes	3
	Omega–Thick	1	3a, 2c, 2d	0	0	np	Yes	2
	W&T–Thin	1	1a, 2b, 3c	0	0	S e R	No	5
	W&T–Thick	1	3a, 1b, 2c	0	0	S e R	Yes	5
	FC–Thin	2	3a, 3c, 2d	1	0	np	No	1
	FC–Thick	1	3a, 2c, 2d	0	0	np	No	2
T3	Omega–Thin	4	3a, 3b, 3c, 3d	1	1	S	No	1
	Omega–Thick	3	3a, 3b, 3c, 3d	2	1	S and R	Yes	2
	W&T–Thin	2	3a, 3b, 3c,3d	1; –1	1	S and R	Yes	4
	W&T–Thick	3	3a, 3b, 3c, 3d	1;–1	1	R	Yes	3
	FC–Thin	3	3a, 3b, 3c, 3d	1; –1	1	R	Yes	3
	FC–Thick	3	3a, 3b, 3c, 3d	1; –1	1	R	No	3

See Table 1 of Glera scion onto K5BB rootstock comparing six different techniques (Omega, W&T, FC per two calibers) after callusing (T1) and 4 months after T1 (T3).

of internode position along the stem. In fact, in this trial we sampled the 6th internode, while in the first trial we sampled the 10th internode in the apical part of the stem.

Plant growth

The estimation of the parameters of the Logistic curves related to the number of internodes and plant height allowed to compare the growth trend for all the cultivars × grafting type combinations during the trial 1. Our results showed that the intrinsic growth rate (*r*, i.e., maximum growth rate) was affected by cultivars type for internode numbers and by grafting type for plant height. Intrinsic growth rate is an important parameter for many ecological applications, such as population risk assessment and harvest management (Dillingham et al., 2016) and represents the maximum potential exponential growth rate that a population can achieve under optimal resource conditions availability in its environment (Sibly and Hone, 2002). Thus, Cabernet Sauvignon and Teroldego showed higher *K* (maximum final plant height) as consequences of their high *r*. The significant effect of grafting type on *r*, supported the hypothesis that grafting type was able to modulate stem growth in grapevine. In particular, Omega type grafting determined a significant higher *r* than W&T and FC for the plant height. Contrary to our expectations, the high *r* did not correspond to final taller plants. This discrepancy could be explained by the

TABLE 7 Percentage of necrosis was estimated by comparing two caliber ranges of propagation material: "thin grafted vines" and "thick grafted vines."

Caliber	Grafting type	Necrosis (%)
Thin	Omega	9.7 ± 1.3a
	W&T	31.4 ± 4.8b
	FC	30.9 ± 12.6b
Thick	Omega	31.8 ± 5.4b
	W&T	27.5 ± 2.1b
	FC	15.1 ± 4.1ab
Two-way ANOVA	**Df**	***F*-value**
Cultivars	2	11.434***
Grafting type	2	7.405***
Cultivars x Grafting type	4	0.737^{ns}

Percentages were transformed by arcosin function and normal distribution verified before two-way ANOVA. Different letters indicate significant differences in the necrosis by the Bonferroni test at $P < 0.05$. Asterisks indicate significant differences in the two way Anova: ***$P < 0.001$. ns, non significant.

TABLE 8 Mean value and standard deviation for morphological traits comparing two caliber ranges of propagation material: "thin grafted vines" and "thick grafted vines."

Caliber	Grafting type	Vd (mm^{-2})	Dh (μ m)	*K*st (Kg Mpa^{-1} s^{-1} m^{-1})
Thin	W&T	74.5 ± 12.3	73.1 ± 2.2	30.7 ± 8.5
	Omega	78.8 ± 14.5	74.4 ± 1.2	47.7 ± 15.9
	FC	81.2 ± 7.4	76 ± 1.9	44.4 ± 9.6
Thick	W&T	76.5 ± 13.2	74.6 ± 1.2	46.1 ± 7.1
	Omega	81.1 ± 19.1	83.2 ± 2	42.2 ± 9.9
	FC	78.4 ± 20	75.5 ± 1.7	48.4 ± 19.9
Two-way ANOVA	**Df**		***F*-value**	
Cultivars	2	0.803^{ns}	0.756^{ns}	0.448^{ns}
Grafting type	2	0.967^{ns}	0.741^{ns}	0.385^{ns}
Cultivars × Grafting type	4	0.914^{ns}	0.909^{ns}	0.271^{ns}

ns, not significant.

presence of time lag in growth in Omega grafted plants that we were not able to detect for the longer timing range between measurements. These results emphasized the possible effect of the grafting type on the plant phenology.

Conclusion

This study confirms that all the investigated grafting techniques potentially expose the conductive elements to the development of less functional tissues. The data obtained during the first vegetative season in the nursery are not enough to justify strong differences in the development of foliar symptoms in vines that had been grafted with different methods, as suggested by Mary et al. (2017). Nevertheless, we see that grafting methods induce different changes in the formation of the vascular tissue and its hydraulic traits. Grafting showed to have an impact on anatomical and functional disorders leading to necrotic tissues in the graft union. These tissues can become weak points favoring wood pathogens colonization or latent infections.

This study confirms that all the investigated grafting techniques expose potentially the conductive elements to the development of a less functional or even necrotic area which could be related to the anatomical disorders or even to the colonization by the pathogens associated to GTDs. On the other hand, the influence of the vine training and pruning on sap flow (Lecomte et al., 2012) was already suggested to strongly influence the development of the GLSD foliar symptoms (Lecomte et al., 2018).

Furthermore, by understanding the impact of three grafting techniques on the vascularisation of the grafted tissues, the present research has highlighted the timing of callus differentiation in vascular elements as the key factor to evaluate the grafting quality. The anatomical observations have revealed that the mechanical (Omega) and semi-mechanical (Full Cleft) grafting methods have a faster callusing response while the manual technique (Whip and Tongue) has a slower but greater vascularisation of the differentiated callus, especially in the first growing time, immediately after callusing, which was found to be the most critical stage.

The grafting methods and the grapevine cultivars studied were confirmed to impact the scion hydraulic traits and growth during the first vegetative season, independently from the anatomical differences initially detected after callusing. Considering that a stem expressing extensive hydraulic failure could be more prone to express GTDs related symptoms in vineyard or, in the worst cases, to die (Bortolami et al., 2021), the detected hydraulic traits in stem scion, might have a role in expressing Esca complex leaf stripe symptoms in the mature vines, potentially contributing to vine death.

In this view, the results suggest to extend the study on the same propagation material planted in vineyard, throw mid-term observations in the mature and productive vines, in order to verify the relationship between the anatomical characters and the hydraulic traits with the young grapevine decline and GTDs incidence.

Data availability statement

The raw data supporting the conclusions of this article will be made available by the authors, without undue reservation.

Author contributions

EB and SF: conceptualization, methodology, formal analysis, investigation, data curation, and writing – review and editing. AG and SS: conceptualization, resources, methodology, formal analysis, investigation, data curation, and writing – review and editing. CT: methodology, formal analysis, investigation, and data curation. RP: investigation and data curation. AP: data curation, resources, and writing – review and editing. SD: conceptualization, methodology, and supervision. LM: conceptualization, methodology, resources, and writing – original draft, review and editing, supervision, project administration, and funding acquisition. All authors contributed to the article and approved the submitted version.

Funding

This study was funded by the Rural Development Plan 2014–2020 of the Region Friuli Venezia Giulia (Italy) – Step 16.1.1 Support to the constitution and the management of the EIP operating group on the agricultural productivity and sustainability (Regional Decrees nos. 5592/AGFOR agreed on Oct. 27th 2017 and 402/AGFOR agreed on Jan. 21st 2020) – and supported by a research fellowship of the International Organization of Vine and Wine (OIV Research Grant Program 2018).

Acknowledgments

The authors would like to acknowledge Vitis Rauscedo Sca (Pordenone, Italy) and Angelo Vittorino Divittini (Agronomi Sata, Brescia, Italy) for the technical and logistical support in performing the nursery trials. Further thanks to Alan Phillips for providing a careful review of this manuscript.

Conflict of interest

The authors declare that the research was conducted in the absence of any commercial or financial relationships that could be construed as a potential conflict of interest.

Publisher's note

All claims expressed in this article are solely those of the authors and do not necessarily represent those of their affiliated organizations, or those of the publisher, the editors and the reviewers. Any product that may be evaluated in this article, or claim that may be made by its manufacturer, is not guaranteed or endorsed by the publisher.

Supplementary material

The Supplementary Material for this article can be found online at: https://www.frontiersin.org/articles/10.3389/fpls.2022.1006835/full#supplementary-material

References

Agustí-Brisach, C., Gramaje, D., García-Jiménez, J., and Armengol, J. (2013). Detection of black-foot disease pathogens in the grapevine nursery propagation process in Spain. *Eur. J. Plant Pathol.* 137, 103–112. doi: 10.1007/s10658-013-0221-8

Andreini, L., Cardelli, R., Bartolini, S., Scalabrelli, G., and Viti, R. (2014). Esca symptoms appearance in *Vitis vinifera* L.: Influence of climate, pedo-climatic conditions and rootstock/cultivar combination. *Vitis* 53, 33–38. doi: 10.5073/vitis.2014.53.33-38

Aroca, A., Gramaje, D., Armengol, J., García-Jiménez, J., and Raposo, R. (2010). Evaluation of grapevine nursery process as a source of *Phaeoacremonium* spp. and *Phaeomoniella chlamydospora* and occurrence of trunk disease pathogens in rootstock mother vines in Spain. *Eur. J. Plant Pathol.* 126, 165–174. doi: 10.1007/s10658-009-9530-3

Balbi, R. V., Pio, R., Farias, D. H., Melo, E. T., Pereira, M. P., and Pereira, F. J. (2019). The cell regeneration and connection of grafting between pear and quince trees are defined by the cortex and phloem. *Sci. Hortic.* 257:108662. doi: 10.1016/j.scienta.2019.108662

Bavaresco, L., and Lovisolo, C. (2000). Effect of grafting on grapevine chlorosis and hydraulic conductivity. *Vitis* 39, 89–92. doi: 10.5073/vitis.2000.39.89-92

Beccari, N., and Mazzi, V. (1966). *Manuale di tecnica microscopica. Guida pratica alla ricerca istologica e istochimica*. Milano: Società Editrice Libraria.

Borgo, M., Bellotto, D., Dal Cortivo, G. L., Zanzotto, A., Tosi, L., and Marchesini, E. (2008). *Varietal susceptibility to esca disease in the Veneto region*. Bologna: Atti Giornate Fitopatologiche, 223–230.

Borgo, M., Pegoraro, G., and Sartori, E. (2016). Susceptibility of grape varieties to esca disease. *BIO Web Conf.* 7:01041. doi: 10.1051/bioconf/20160701041

Bortolami, G., Farolfi, E., Badel, E., Burlett, R., Cochard, H., and Ferrer, N. (2021). Seasonal and long-term consequences of esca grapevine disease on stem xylem integrity. *J. Exp. Bot.* 72, 3914–3928. doi: 10.1093/jxb/erab117

Cardoso, M., Inês, D., Cabral, A., Rego, C., and Oliveira, H. (2013). Unrevealing inoculum sources of black foot pathogens in a commercial grapevine nursery. *Phytopathol. Mediterr.* 52, 298–312. doi: 10.14601/Phytopathol_Mediterr-11593

Claverie, M., Notaro, M., Fontaine, F., and Wery, J. (2020). Current knowledge on grapevine trunk diseases with complex etiology: A systemic approach. *Phytopathol. Mediterr.* 59, 29–53. doi: 10.14601/Phyto-11150

Del Frari, G., Calzarano, F., and Ferreira, R. B. (2022). Understanding the control strategies effective against the esca leaf stripe symptom: The edge hypothesis. *Phytopathol. Mediterr.* 61, 153–164. doi: 10.36253/phyto-13295

Del Frari, G., Gobbi, A., Aggerbeck, M. R., Oliveira, H., Hansen, L. H., and Boavida Ferreira, R. (2019). Characterization of the wood mycobiome of *Vitis vinifera* in a vineyard affected by esca. Spatial distribution of fungal communities and their putative relation with leaf symptoms. *Front. Plant Sci.* 10:910. doi: 10.3389/fpls.2019.00910

Dillingham, P. W., Moore, J. E., Fletcher, D., Cortés, E., Curtis, K. A., James, K. C., et al. (2016). Improved estimation of intrinsic growth rmax for long-lived species: Integrating matrix models and allometry. *Ecol. Appl.* 26, 322–333. doi: 10.1890/14-1990

Falsini, S., Tani, C., Sambuco, G., Papini, A., Faraoni, P., Campigli, S., et al. (2022). Anatomical and biochemical studies of *Spartium junceum* infected by *Xylella fastidiosa* subsp. Multiplex ST 87. *Protoplasma* 259, 103–115. doi: 10.1007/s00709-021-01640-2

Fernandez, R., Le Cunff, L., Mérigeaud, S., Verdeil, J.-L., Perry, J., Larignon, P., et al. (2022). An end-to-end workflow based on multimodal 3D imaging and machine learning for nondestructive diagnosis of grapevine trunk diseases. *bioRxiv* [Preprint] doi: 10.1101/2022.06.09.495457

Fourie, P. H., and Halleen, F. (2006). Chemical and biological protection of grapevine propagation material from trunk disease pathogens. *Eur. J. Plant Pathol.* 116, 255–265. doi: 10.1007/s10658-006-9057-9

Gärtner, H., Lucchinetti, S., and Schweingruber, F. H. (2014). New perspectives for wood anatomical analysis in dendrosciences: The GSL1-microtome. *Dendrochronologia* 32, 47–51.

Gautier, A. T., Chambaud, C., Brocard, L., Ollat, N., Gambetta, G. A., Delrot, S., et al. (2019). Merging genotypes: Graft union formation and scion-rootstock interactions. *J. Exp. Bot.* 70, 747–755. doi: 10.1093/jxb/ery422

Gebhardt, K., and Goldbach, H. (1988). Establishment, graft union characteristics and growth of *Prunus* micrografts. *Physiol. Plant.* 72, 153–159.

Giovannelli, A., Traversi, M. L., Anichini, M., Hoshika, Y., Fares, S., and Paoletti, E. (2019). Effect of long-term vs. Short term ambient ozone exposure on radial stem growth, sap flux and xylem morphology of O3-sensitive poplar trees. *Forests* 10:396. doi: 10.3390/f10050396

Gramaje, D., and Armengol, J. (2011). Fungal trunk pathogens in the grapevine propagation process: Potential inoculum sources, detection, identification, and management strategies. *Plant Dis.* 95, 1040–1055. doi: 10.1094/PDIS-01-11-0025

Gramaje, D., and Di Marco, S. (2015). Identifying practices likely to have impacts on grapevine trunk disease infections: A European nursery survey. *Phytopathol. Mediterr.* 54, 313–324. doi: 10.14601/Phytopathol_Mediterr-16317

Gramaje, D., Mostert, L., and Armengol, J. (2011). Characterization of *Cadophora luteo-olivacea* and C. Melinii isolates obtained from grapevines and environmental samples from grapevine nurseries in Spain. *Phytopathol. Mediterr.* 50, S112–S126. doi: 10.14601/Phytopathol_Mediterr-8723

Gramaje, D., Úrbez-Torres, J. R., and Sosnowski, M. R. (2018). Managing grapevine trunk diseases with respect to etiology and epidemiology: Current strategies and future prospects. *Plant Dis.* 102, 12–39. doi: 10.1094/PDIS-04-17-0512-FE

Granett, J., Walker, A. M., Kocsis, L., and Omer, A. D. (2001). Biology and management of grape phylloxera. *Annu. Rev. Entomol.* 46, 387–412. doi: 10.1146/annurev.ento.46.1.387

Grohs, D. S., Kurtz Almança, M. A., Martins Fajardo, T. V., Halleen, F., and Miele, A. (2017). Advances in propagation of grapevine in the world. *Rev. Bras. Frutic.* 39:760. doi: 10.1590/0100-29452017760

Hartmann, H. T., Kester, D. E., Davies, F. T., and Geneve, R. L. (2002). *Plant propagation: Principles and practices*. Upper Saddle River, NJ: Prentice-Hall.

Haworth, M., Centritto, M., Giovannelli, A., Marino, G., Proietti, N., Capitani, D., et al. (2017). Xylem morphology determines the drought response of two *Arundo donax* ecotypes from contrasting habitats. *GCB Bioenergy* 9, 119–131. doi: 10.1111/gcbb.12322

Lecomte, P., Darrieutort, G., Limiñana, J. M., Comont, G., Muruamendiaraz, A., and Legorburu, F. J. (2012). New insights into Esca of grapevine: The development of foliar symptoms and their association with xylem discoloration. *Plant Dis.* 96, 924–934. doi: 10.1094/PDIS-09-11-0776-RE

Lecomte, P., Diarra, B., Carbonneau, A., Patrice, R., and Chevrier, C. (2018). Esca of grapevine and training practices in France: Results of a 10-year survey. *Phytopathol. Mediterr.* 57, 472–487. doi: 10.14601/Phytopathol_Mediterr-22025

Loupit, G., and Cookson, S. J. (2020). Identifying molecular markers of successful graft union formation and compatibility. *Front. Plant Sci.* 11:610352. doi: 10.3389/fpls.2020.610352

Lovisolo, C., Schubert, A., and Sorce, C. (2002). Are xylem radial development and hydraulic conductivity in downwardly-growing grapevine shoots influenced by perturbed auxin metabolism? *New Phytol.* 156, 65–74. doi: 10.1046/j.1469-8137.2002.00492.x

Mary, S., Laveau, C., Lecomte, P., Birebent, M., and Roby, J. P. (2017). Impact of grafting type on Esca foliar symptoms. *Oeno One* 51, 221–230. doi: 10.20870/oeno-one.2016.50.4.1408

Melnyk, C. W. (2016). Plant grafting: Insights into tissue regeneration. *Regeneration* 4, 3–14. doi: 10.1002/reg2.71

Melnyk, C. W., Schuster, C., Leyser, O., and Meyerowitz, E. M. (2015). A developmental framework for graft formation and vascular reconnection in *Arabidopsis thaliana*. *Curr. Biol.* 25, 1306–1318. doi: 10.1016/j.cub.2015.03.032

Michelon, L., Pellegrini, C., and Pertot, I. (2010). *Il mal dell'esca della vite in trentino. Progetto MESVIT*. Firenze: Eds Arsia Regione Toscana, 182–183.

Milien, M., Renault-Spilmont, A. S., Cookson, S. J., Sarrazin, A., and Verdeil, J.-L. (2012). Visualization of the 3D structure of the graft union of grapevine using X-ray tomography. *Sci. Hortic.* 144, 130–140.

Moore, R., and Walker, D. B. (1981a). Studies on vegetative compatibility-incompatibility in higher plants. I. Astructural study of a compatible autograph in *Sedum telephoides* (Crassulaceae). *Am. J. Bot.* 68, 820–830.

Moore, R., and Walker, D. B. (1981b). Studies on vegetative compatibility-incompatibility in higher plants. II. Astructural study of an incompatible heterograft between *Sedum telephoides* (Crassulaceae) and *Solanum pennelli* (Solanaceae). *Am. J. Bot.* 68, 831–842.

Mudge, K., Janick, J., Scofield, S., and Goldschmidt, E. E. (2009). A history of grafting. *Hortic. Rev.* 35, 437–493. doi: 10.1002/9780470593776.ch9

Papini, A. (2018). "The investigation of morphological features of autophagy during plant programmed cell death (PCD)," in *Plant programmed cell death: Methods and protocols*, eds L. De Gara and V. Locato (Totowa, NJ: Humana Press).

Petzoldt, T. (2020). *Growthrates: Estimate growth rates from experimental data, R package version 0.8.2*. Available online at: https://CRAN.R-project.org/package=growthrates

Pina, A., and Errea, P. (2005). A review of new advances in mechanism of graft compatibility–incompatibility. *Sci. Hortic.* 106, 1–11. doi: 10.1016/j.scienta.2005.04.003

Pina, A., Cookson, S. J., Calatayud, A., Trinchera, A., and Errea, P. (2017). "Physiological and molecular mechanisms underlying graft compatibility," in *Vegetable grafting principles and practices*, eds G. Colla, F. Perez Alfocea, and D. Schwarz (Wallingford: CABI), 132–154. doi: 10.1079/9781780648972.0000

Pouzoulet, J., Jacques, A., Besson, X., Dayde, J., and Mailhac, N. (2013). Histopathological study of response of *Vitis vinifera* cv. Cabernet Sauvignon to bark and wood injury with and without inoculation by *Phaeomoniella chlamydospora*. *Phytopathol. Mediterr.* 52, 313–323. doi: 10.14601/Phytopathol_Mediterr-12581

Pouzoulet, J., Pivovaroff, A. L., Santiago, L. S., and Rolshausen, P. E. (2014). Can vessel dimension explain tolerance toward fungal vascular wilt diseases in woody plants? Lessons from Dutch elm disease and esca disease in grapevine. *Front. Plant Sci.* 5:253. doi: 10.3389/fpls.2014.00253

Pouzoulet, J., Rolshausen, P. E., Charbois, R., Chen, J., Guillaumie, S., Ollat, N., et al. (2020). Behind the curtain of the compartmentalization process: Exploring how xylem vessel diameter impacts vascular pathogen resistance. *Plant Cell Environ.* 43, 2782–2796.

Pouzoulet, J., Scudiero, E., Schiavon, M., Santiago, L. S., and Rolshausen, P. E. (2019). Modeling of xylem vessel occlusion in grapevine. *Tree Physiol.* 39, 1438–1445. doi: 10.1093/treephys/tpz036

Prodorutti, D., De Luca, F., Michelon, L., and Pertot, I. (2009). Susceptibility to *Armillaria mellea* root rot in grapevine rootstocks commonly grafted onto Teroldego Rotaliano. *Phytopathol. Mediterr.* 48, 285–290. doi: 10.14601/Phytopathol_Mediterr-2738

R Core Team (2020). *R Software: Version 4.0. 2*. Vienna: RC Team R Foundation for Statistical Computing.

Retief, E., McLeod, A., and Fourie, P. H. (2006). Potential inoculum sources of *Phaeomoniella chlamydospora* in South African grapevine nurseries. *Eur. J. Plant Pathol.* 115, 331–339. doi: 10.1007/s10658-006-9025-4

Santiago, L. S., Goldstein, G., Meinzer, F. C., Fisher, J. B., Machado K., Woodruff, D., et al. (2004). Leaf photosynthetic traits scale with hydraulic conductivity and wood density in Panamanian forest canopy trees. *Oecologia* 140, 543–550. doi: 10.1007/s00442-004-1624-1

Sarooshi, R. A., Bevington, K. B., and Coote, B. G. (1982). Performance and compatibility of 'muscat gordo blanco' grape on eight rootstocks. *Sci. Hortic.* 16, 367–374. doi: 10.1016/0304-4238(82)90035-8

Schubert, A., Lovisolo, C., and Peterlunger, E. (1999). Shoot orientation affects vessel size, shoot hydraulic conductivity and shoot growth rate in *Vitis vinifera* L. *Plant Cell Environ.* 22, 197–204. doi: 10.1046/j.1365-3040.1999.00384.x

Sibly, M. R., and Hone, J. (2002). Population growth rate and its determinants: An overview. *Philos. Trans. R. Soc. B* 357, 1153–1170. doi: 10.1098/rstb.2002.1117

Sperry, J. S., and Saliendra, N. Z. (1994). Intra- and inter-plant variation in xylem cavitation in *Betula occidentalis*. *Plant Cell Environ.* 17, 1233–1241.

Stamp, J. A. (2001). The contribution of imperfections in nursery stock to the decline of young vines in California. *Phytopathol. Mediterr.* 40, 369–375. doi: 10.14601/Phytopathol_Mediterr-1640

Sun, Q., Rost, T. L., and Matthews, M. A. (2006). Pruning-induced tylose development in stem of current-year shoots of *Vitis vinifera* (Vitaceae). *Am. J. Bot.* 93, 1567–1576. doi: 10.3732/ajb.93.11.1567

Tedesco, S., Pina, A., Fevereiro, P., and Kragler, F. (2020). A phenotypic search on graft compatibility in grapevine. *Agronomy* 10:706. doi: 10.3390/agronomy10050706

Trinchera, A., Pandozy, G., Rinaldi, S., Crinò, P., Temperini, O., and Rea, E. (2013). Graft union formation in artichoke grafting onto wild and cultivated cardoon: An anatomical study. *J. Plant Physiol.* 170, 1569–1578. doi: 10.1016/j.jplph.2013.06.018

Tyree, M. T., and Sperry, J. S. (1988). Do woody plants operate near the point of catastrophic xylem dysfunction caused by dynamic water stress?: Answers from a model. *Plant Physiol.* 88, 574–580. doi: 10.1104/pp.88.3.574

Tyree, M. T., Vargas, G., Engelbrecht, B. M. J., and Kursar, T. A. (2002). Drought until death do us part: A case study of the desiccation-tolerance of a tropical moist forest seedling-tree, *Licania platypus* (Hemsl.) Fritsch. *J. Exp. Bot.* 53, 2239–2247. doi: 10.1093/jxb/erf078

Waite, H., Whitelaw-Weckert, M., and Torley, P. (2015). Grapevine propagation: Principles and methods for the production of high-quality grapevine planting material. *N. Z. J. Crop Hortic. Sci.* 43, 144–161. doi: 10.1080/01140671.2014.978340

Zanzotto, A., Borgo, M., Serra, S., and Viel, W. (2001). Investigation into the occurrence of Esca-associated fungi in cuttings and bench-grafted vines. *Phytopathol. Mediterr.* 40, 311–316. doi: 10.14601/Phytopathol_Mediterr-1627

frontiers | Frontiers in Plant Science

TYPE Original Research
PUBLISHED 13 October 2022
DOI 10.3389/fpls.2022.1040826

OPEN ACCESS

EDITED BY
Yuheng Yang,
Southwest University, China

REVIEWED BY
Yuee Tian,
Henan University of Science and Technology, China
Qiong Zhang,
University of California, Berkeley, United States
Furong Liu,
University of California, Berkeley, United States

*CORRESPONDENCE
Meixiang Zhang
meixiangzhang@snnu.edu.cn

†These authors have contributed equally to this work

SPECIALTY SECTION
This article was submitted to Crop and Product Physiology, a section of the journal Frontiers in Plant Science

RECEIVED 09 September 2022
ACCEPTED 27 September 2022
PUBLISHED 13 October 2022

CITATION
An Y, Chen J, Xu Z, Ouyang X, Cao P, Wang R, Liu P and Zhang M (2022) Three amino acid residues are required for the recognition of *Ralstonia solanacearum* RipTPS in *Nicotiana tabacum*. *Front. Plant Sci.* 13:1040826. doi: 10.3389/fpls.2022.1040826

Three amino acid residues are required for the recognition of *Ralstonia solanacearum* RipTPS in *Nicotiana tabacum*

Yuyan An[1†], Jialan Chen[2†], Zhangyan Xu[2], Xue Ouyang[2], Peng Cao[1], Rongbo Wang[3], Peiqing Liu[3] and Meixiang Zhang[1*]

[1]National Engineering Laboratory for Endangered Medicinal Resource Development in Northwest China, Key Laboratory of Medicinal Resources and Natural Pharmaceutical Chemistry of Ministry of Education, College of Life Sciences, Shaanxi Normal University, Xi'an, China, [2]Department of Plant Pathology, Nanjing Agricultural University, Nanjing, China, [3]Fujian Key Laboratory for Monitoring and Integrated Management of Crop Pests, Institute of Plant Protection, Fujian Academy of Agricultural Sciences, Fuzhou, China

Ralstonia solanacearum causes devastating diseases in a wide range of economically important crops. It secretes a large number of virulence factors, also known as effectors, to promote its infection, and some of them are recognized when the host plant contains corresponding resistance genes. In this study we showed that a type III effector RipTPS from the avirulent *R. solanacearum* strain GMI1000 ($RipTPS_G$) specifically induced cell death in *Nicotiana tabacum*, but not in *Nicotiana benthamiana*, whereas the RipTPS homolog in the virulent strain CQPS-1 ($RipTPS_C$) induced cell death in neither *N. tabacum* nor *N. benthamiana*. These results indicated that $RipTPS_G$ is recognized in *N. tabacum*. Expression of $RipTPS_G$ induced upregulation of hypersensitive response (HR) -related genes in *N. tabacum*. The virulence of CQPS-1 was reduced when $RipTPS_G$ was genetically introduced into CQPS-1, further confirming that $RipTPS_G$ functions as an avirulence determinant. Protein sequence alignment indicated that there are only three amino acid polymorphisms between $RipTPS_G$ and $RipTPS_C$. Site-directed mutagenesis analyses confirmed that the three amino acid residues are jointly required for the recognition of $RipTPS_G$ in *N. tabacum*. Expression of either $RipTPS_G$ or $RipTPS_C$ suppressed flg22-triggered reactive oxygen species (ROS) burst in *N. benthamiana*, suggesting that RipTPS contributes to pathogen virulence. Mutating the conserved residues in RipTPS's trehalose-phosphate synthase (TPS) domain did not block its HR induction and defense suppression activity, indicating that the TPS activity is not required for RipTPS's avirulence and virulence function.

KEYWORDS

RipTPS, avirulence, virulence, *Ralstonia solanacearum*, plant immunity

Introduction

The bacterial pathogen *Ralstonia solanacearum* is a destructive phytopathogen that attacks many plants over a broad geographical range (Genin and Denny, 2012). It is a soil-borne bacterium which can infect more than 200 plant species, including many important crops such as potato, tobacco, tomato, and some ornamental plants (Niu et al., 2022). The extensive genetic diversity of strains causes various bacterial wilt diseases, leading to great economic losses worldwide every year (Qi et al., 2022). In-depth study of the molecular mechanism underlying the interaction between *R. solanacearum* and plants has important theoretical significance for formulating new disease control strategies.

Plant immunity relies on two levels of pathogen perception that trigger defense mechanisms, pattern-triggered immunity (PTI) and effector-triggered immunity (ETI) (Jones and Dangl, 2006). PTI is the first layer of plant immunity, which involves the recognition of conserved microbial elicitors termed pathogen-associated molecular patterns (PAMPs), such as flagellin, cold shock protein, and elongation factor Tu, by specific plasma membrane receptors (Jones and Dangl, 2006). The receptors then activate signaling cascades in the host cell to restrict pathogen growth (Segonzac et al., 2011). Reactive oxygen species (ROS) burst is a hallmark event of PTI signaling (Segonzac et al., 2011). For example, flg22, a conserved 22-amino-acid peptide from bacterial flagellin, is a PAMP which often triggers ROS burst in host plants (Nakano and Mukaihara, 2019b; Mittler et al., 2022). However, to overcome host PTI for successful infection, adapted pathogens have evolved the ability to inject effectors inside the host cell. In turn, to counter effector-mediated suppression of PTI, plant further evolves a second layer of immunity, ETI, which is based on internal recognition of effector proteins by cytoplasmic receptors. Compared with PTI, ETI initiates stronger and more prolonged defense responses (Jones and Dangl, 2006), which often results in programmed cell death called hypersensitive response (HR) to restrict bacterial multiplication at the infection site (Mukaihara et al., 2016). Although PTI and ETI are initiated by distinct activation mechanisms, they share similar contents of defense responses (Tsuda and Katagiri, 2010). PTI and ETI are mutually linked, and potentiate each other (Ngou et al., 2021; Yuan et al., 2021).

As one of the most destructive plant pathogens, *R. solanacearum* has gained increasing attention. Genome sequencing of several representative strains of *R. solanacearum*, such as GMI1000, has broadened our knowledge of the evolution and speciation of this pathogen and led to the increasing identification of molecular determinants involved in pathogenicity and host-range specificity. *R. solanacearum* employs a type III secretion system (T3SS) which secretes more than 70 type III effectors (T3Es) into plant cells to promote infection (Genin and Denny, 2012). These effectors are powerful weapons for bacterial pathogens, but may also lead to potential recognition of the pathogens by plant immune system (Sang et al., 2020). The T3Es recognized by plant resistance proteins to activate ETI are called avirulence determinants. They restrict pathogen virulence to specific plants and often determine the host-range specificity of a pathogen (Nakano and Mukaihara, 2019b).

GMI1000 is the first genome sequenced *R. solanacearum* strain and has been used as a model strain for *R. solanacearum*-related study (Poueymiro et al., 2009). To date, many T3Es of GMI1000 have been studied to analyze their avirulence or virulence functions (Sun et al., 2017; Morel et al., 2018; Sang et al., 2020; Xian et al., 2020; Yu et al., 2020; Cheng et al., 2021; Wang et al., 2021; Niu et al., 2022; Qi et al., 2022), although very few of them have been functionally characterized thoroughly in planta. Several of the reported effectors have been shown to elicit HR and act as avirulence factors in certain plants. For example, PopP1 and PopP2, two members of the YopJ/AvrRxv family, confer avirulence in *Petunia* as well as *Nicotiana gultinosa* (Lavie et al., 2002; Poueymiro et al., 2009) and Arabidopsis (Deslandes et al., 2003), respectively. AvrA is an avirulence determinant recognized by both *Nicotiana tabacum* and *Nicotiana benthamiana* (Poueymiro et al., 2009). RipAX2 triggers specific resistance and hence is specifically recognized by eggplant AG91-25 (Morel et al., 2018). In addition, it was indicated that RipE1 is an avirulence determinant recognized by *N. benthamiana* (Sang et al., 2020) and RipAW is recognized by both *N. benthamiana* and *N. tabacum* (Niu et al., 2022). Except for GMI1000, Rip36 and RipB from another *R. solanacearum* strain RS1000 have also been suggested as avirulent factors in *S. torvum* and *N. benthamiana*, respectively (Nahar et al., 2014; Nakano and Mukaihara, 2019b). Identification of the above virulent and avirulent factors provide extraordinary insights into the interaction between *R. solanacearum* and its host/nonhost plants. However, among the extensive repertoire of T3Es, only a small fraction has been studied in depth. Therefore, there is still a long way for us to unravel the story of the non-stop battle between *R. solanacearum* and plants.

Trehalose-6-Phosphate synthesized by trehalose-phosphate synthase (TPS) is a signaling metabolite and plays important roles in plant growth and flowering regulation (Schluepmann et al., 2012; Wahl et al., 2013). Interestingly, a role for trehalose metabolism is merging in pathogen-plant interaction (Tournu et al., 2013). For example, synthesis of the disaccharide trehalose by *Pseudomonas aeruginosa* strain PA14 is required for pathogenesis in Arabidopsis (Djonovic et al., 2013). In *R. solanacearum* species complex, RipTPS is a conserved T3E which has been reported to endow with a TPS enzymatic activity (Poueymiro et al., 2014). In that report, it was demonstrated that RipTPS could specifically elicit a hypersensitive-like response on *N. tabacum*, suggesting its role as a potential avirulent factor in tobacco. Unexpectedly, the TPS activity was not involved in RipTPS-elicited hypersensitive-like

response (Poueymiro et al., 2014). It will be interesting to further characterize the function of RipTPS and the role of its TPS activity.

CQPS-1 is a *R. solanacearum* strain newly isolated from a highland and its genome has been sequenced (Liu et al., 2017). Most genes coding core T3Es were conserved in CQPS-1 compared with the model strain GMI1000. However, CQPS-1 can infect *N. tabacum* but GMI1000 cannot. Here, we found that only three amino acid polymorphisms existed between RipTPS in GMI1000 ($RipTPS_G$) and CQPS-1 ($RipTPS_C$) strains. The natural variation between these two RipTPS alleles will undoubtedly facilitate the function characterization of RipTPS. Therefore, using these materials, we provided strong evidence for the confirmation of $RipTPS_G$ as an avirulence determinant in *N. tabacum*, and proved that the three amino acid polymorphisms jointly determine the recognition of $RipTPS_G$ in *N. tabacum*. We also investigated whether RipTPS retained its ability to suppress plant immune responses by analyzing its effect on flg22-triggered ROS burst. Finally, roles of TPS activity in both $RipTPS_G$-elicited HR in nonhost *N. tabacum* and $RipTPS_G$-inhibited ROS burst induced by flg22 were evaluated through site mutagenesis analyses.

Materials and methods

Plant growth conditions and bacterial strains

Nicotiana benthamiana and *Nicotiana tabacum* plants were grown at 24°C in a walk-in chamber under long-day conditions (16 h light/8 h dark). *Agrobacterium tumefaciens* strain GV3101 was used to transiently express effectors in tobacco leaves. *Escherichia coli* strain DH5α was used for vector construction. They were cultured on Luria-Bertani (LB) agar plates or in LB liquid medium with proper antibiotics at 28°C and 37°C, respectively. *Ralstonia solanacearum* GMI1000 and CQPS-1 were grown on Bacto-agar and glucose (BG) medium at 28°C.

Sequence analysis

The sequence alignment was performed using SeqHunter software (Ye et al., 2010).

Agrobacterium-mediated transient expression

The agrobacterial cells with corresponding constructs were suspended in an infiltration buffer containing 150 μM acetosyringone, 10 mM $MgCl_2$ and 10 mM MES (pH 5.6), and were incubated at 28°C for 2 hours after being adjusted to an OD_{600} of 0.5. Then the bacterial suspensions were infiltrated into the fully expanded leaves of 5-week-old tobacco with a needless syringe.

RNA extraction and quantitative PCR

Total RNA was extracted using the RNAsimple Total RNA Extraction Kit (TIANGEN). The RNA sample was then reverse transcribed in a 20-μL volume using the HiScript II Q Select RT SuperMix for qPCR kit (Vazyme). SYBR Green quantitative PCR was performed to determine the relative expression levels of HR-related genes *NtHIN1* and *NtHsr203J*, and *NtEF1α* was selected as an internal control. Quantification of the relative changes in gene transcript levels was performed using the $2^{-\Delta\Delta Ct}$ method (Livak and Schmittgen, 2001). The primers used for amplification were listed in Table S1.

Measurement of ROS burst

The ROS production level was measured as previously described (Segonzac et al., 2011) with slight modifications. Briefly, leaf disks were taken from 5-week-old *N. benthamiana* plants, and then floated overnight in 200 μL sterile distilled water. Before measurement, water was replaced with 100 μL reaction solution containing 17 μg/mL luminol, 10 μg/mL horseradish peroxidase and 100 nM flg22. The ROS production level was monitored using a Glomax-96 Microplate Luminometer (Promega).

Generation of transgenic CQPS-1 expressing *RipTPS*$_G$

R. solanacearum *RipTPS*$_G$ was cloned into pHM1 vector with *Eco*RI/*Hind*III. The recombinant plasmid was introduced into CQPS-1 by electroporation.

Site-directed mutagenesis of $RipTPS_G$ and generation of *RipTPS*$_G$ knockout mutants

R. solanacearum *RipTPS*$_G$ was cloned into pENTR vector. PCR-based site-directed mutagenesis was performed to mutate the aspartic 23 of $RipTPS_G$ into glycine, serine 290 into arginine, alanine 483 into valine, tyrosine 154 into valine, tryptophan 163 into serine, and aspartic 208 into glycine, respectively. The LR reaction was conducted to clone $RipTPS_G^{D23G}$, $RipTPS_G^{S290R}$, $RipTPS_G^{A438V}$, $RipTPS_G^{Y154V}$, $RipTPS_G^{W163S}$, and $RipTPS_G^{D208G}$ into pGWB505, respectively. All the primers used for this experiment were listed in Table S1.

The upstream and downstream fragments of *RipTPS*$_G$ were separately amplified from GMI1000 genomic DNA and fused using overlap PCR, and the resulting fragment was inserted into the *Xba*I/*Bam*HI sites of pK18mobsacB (Schafer et al., 1994). Then the recombinant pK18mobsacB vector was transformed into *R. solanacearum* GMI1000, and the *RipTPS* deletion mutants were generated by homologous recombination-based procedures. Primers used for generation and identification of *RipTPS*$_G$ knockout mutants were listed in Table S1.

R. solanacearum infection assay

For leaf inoculation, *R. solanacearum* strains were grown in liquid BG medium at 28°C overnight. Bacterial cells were collected by centrifugation and washed with sterile water and adjusted to a final OD_{600} of 0.001. *N. tabacum* leaves were infiltrated with the bacterial solution. The bacterial titers were measured three days after inoculation.

For *R. solanacearum* soil drenching inoculation, 30-day-old *N. tabacum* plants were used. *R. solanacearum* was grown overnight at 28°C in BG liquid medium till OD_{600} to 2.0, then centrifuged and suspended in distilled water. Plants grown in pots were inoculated *via* soil drenching with a bacterial suspension (OD_{600} = 0.1). Scoring of visual disease symptoms on the basis of a scale ranging from '0' (no symptoms) to '4' (complete wilting) was performed as previously described (Vailleau et al., 2007).

Statistical analysis

All experiments were performed with at least three biological replicates, and data were analyzed using SPSS 20.0 software. Student's *t*-test was performed along with analysis of variance to compare the differences between treatments.

Results

RipTPS$_G$ induces HR on *N. tabacum*, but RipTPS$_C$ cannot

R. solanacearum strain GMI1000 cannot infect *N. tabacum*, indicating GMI1000 is recognized in *N. tabacum*. To identify the potential avirulence determinants in GMI1000 that are specifically recognized in *N. tabacum*, we screened thirteen type III effectors from GMI1000 by observing their ability to induce HR in *N. tabacum*. This assay led to the identification of an effector RipTPS, which only induced HR in *N. tabacum*, but not in *N. benthamiana* (Figure 1A). This result is consistent with a previous report (Poueymiro et al., 2014), indicating that RipTPS in GMI1000 (RipTPS$_G$) may be recognized in *N. tabacum*.

CQPS-1 is another *R. solanacearum* strain whose type III secretion system cluster is conserved compared with GMI1000 (Liu et al., 2017). In contrast to GMI1000, CQPS-1 can infect *N. tabacum* (Liu et al., 2017, Figure 1B). Here, pairwise sequence alignment of RipTPS derived from avirulent GMI1000 and virulent CQPS-1 strains showed that there are only three amino acid polymorphisms between them (Figure 1C). Interestingly, the RipTPS from CQPS-1 (RipTPS$_C$) cannot induce HR in *N. tabacum* (Figure 1D), further suggesting that RipTPS$_G$ is recognized in *N. tabacum*.

To determine whether RipTPS$_G$ triggers ETI-like response, expression of two HR-related genes *NtHIN1* and *NtHsr203J* was measured. The result showed that RipTPS$_G$ dramatically enhanced relative expression of *NtHIN1* and *NtHsr203J* in *N. tabacum* compared with LTI6b control which is a membrane-localized protein unrelated to plant immunity, whereas their induction was significantly compromised in RipTPS$_C$ (Figure 2). Together, these results indicate that RipTPS$_G$ is an avirulence protein recognized in *N. tabacum*.

Expression of *RipTPS*$_G$ in CQPS-1 reduces its virulence on *N. tabacum*

To genetically investigate the function of RipTPS$_G$ as an avirulence determinant, we expressed *RipTPS*$_G$ in CQPS-1 and investigated whether it can affect virulence of CQPS-1 on *N. tabacum*. Results showed that, compared to the empty vector control, expressing *RipTPS*$_G$ significantly decreased CQPS-1's population in the inoculated *N. tabacum* leaves (Figure 3A). In addition, expressing *RipTPS*$_G$ in CQPS-1 largely reduced the disease index (Figure 3B) and consequently enhanced the survival percent (Figure 3C) of *N. tabacum*. These results indicate that expression of *RipTPS*$_G$ significantly reduced virulence of CQPS-1 on *N. tabacum*, confirming RipTPS$_G$ as an avirulence determinant in *N. tabacum*.

The three amino acid residues jointly determine the recognition of RipTPS$_G$ in *N. tabacum*

Since RipTPS$_G$ and RipTPS$_C$ differs in only three amino acid residues, it's reasonable to speculate that these three residues are important for the recognition of RipTPS$_G$ in *N. tabacum*. The three residues are D^{23}, S^{290} and A^{483} in RipTPS$_G$. The corresponding three residues in RipTPS$_C$ are G^{23}, R^{290} and

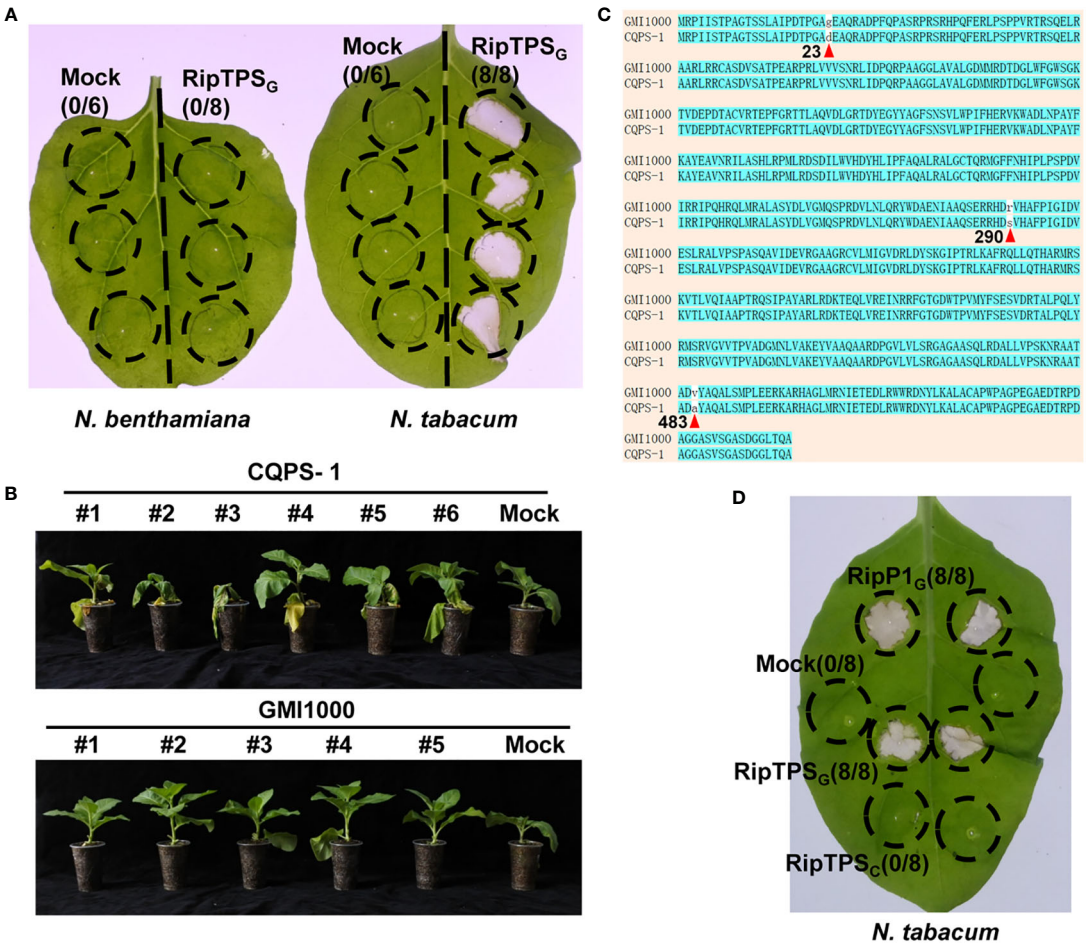

FIGURE 1
RipTPS$_G$ (RipTPS from GMI1000), but not RipTPS$_C$ (RipTPS from CQPS-1), elicits hypersensitive response (HR)-like phenotype in *Nicotiana tabacum*. **(A)** RipTPS$_G$ elicits an HR-like phenotype in *N. tabacum*, but not in *Nicotiana benthamiana*. **(B)** Phenotypes of *N. tabacum* infected with *R. solanacearum* strain GMI1000 or CQPS-1 11 days after root inoculation. **(C)** Pairwise sequence alignment of RipTPS proteins derived from avirulent GMI1000 and virulent CQPS-1. Positions of the three amino acid polymorphisms are indicated by red triangles and the corresponding numbers below the amino acids. **(D)** RipTPS$_G$ elicits an HR-like phenotype in *N. tabacum*, but RipTPS$_C$ cannot. For A and D, leaves of *N. benthamiana* or *N. tabacum* were infiltrated with *Agrobacterium tumefaciens* GV3101 carrying LTI6b (Mock, a negative control), RipP1$_G$ (RipP1 from GMI1000, a positive control), RipTPS$_G$ or RipTPS$_C$. Photographs were taken 24 hours after infiltration. Circles indicate the infiltrated area on the leaf panels. The fraction in brackets represents the number of HR over the total number of the infiltrated leaves.

V^{483}, respectively (Figure 1C). To evaluate the involvement of the three polymorphic amino acid sites in RipTPS$_G$ avirulence activity, we generated a series of RipTPS$_G$ mutants, including all three single-residue mutants and all three double-residue mutants. In these mutants, we mutated the residues in RipTPS$_G$ to the corresponding ones in RipTPS$_C$. RipTPS$_C$ can be considered as the three-residue mutant of RipTPS$_G$. After transiently expressing these mutated genes, we found that all the single-residue and double-residue mutants still elicited strong HR (Figure 4). Only when all three residues were mutated (RipTPS$_C$), RipTPS$_G$-elicited HR was abolished. These results indicate that the three amino acid polymorphisms jointly determine the recognition of RipTPS$_G$ in *N. tabacum*.

Both RipTPS$_G$ and RipTPS$_C$ suppress flg22-induced ROS burst in *N. benthamiana*

R. solanacearum usually secretes effectors to interfere with host immunity and promote its infection. To investigate whether RipTPS$_G$ affects plant basal defense, we expressed *RipTPS$_G$* in *N. benthamiana* and measured ROS production induced by the bacterial PAMP flg22, which is a major epitope peptide of bacterial flagellin. We found that a peak value greater than 3.3×10^4 relative luminescence units (RLU) was reached in control plants (Mock, Figure 5A). However, in *RipTPS$_G$*-expressing plants, the peak value was

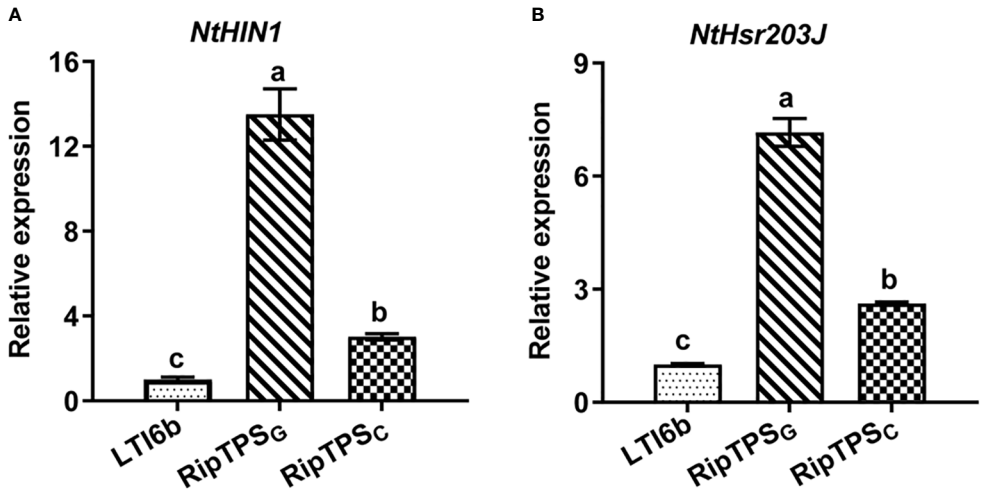

FIGURE 2
RipTPS$_G$ upregulates expression of HR-related genes in *N. tabacum*. Leaves of *N. tabacum* were infiltrated with *A tumefaciens* GV3101 carrying LTI6b (Control), RipTPS$_G$ or RipTPS$_C$. The expression of *NtHIN1* **(A)** and *NtHsr203J* **(B)** was quantified by qRT-PCR at 19 hpi. Data are means ± standard errors (SE, n = 9). The different letters indicate significant differences at $p \leq 0.01$.

less than 2.0×10^4 RLU. Compared with the LTI6b control, *RipTPS$_G$* expression significantly inhibited the total ROS accumulation during a 30 min period (Figure 5B). These results suggest that RipTPS$_G$ interferes with PAMP-triggered ROS accumulation. Similar effect was also observed for RipTPS$_C$ (Figures 5C, D), indicating that the three amino acid polymorphisms do not affect its function in suppression of basal defense response.

RipTPS's role of suppressing flg22-induced ROS burst in *N. benthamiana* is independent of its TPS enzymatic activity

Poueymiro et al. (2014) revealed that RipTPS$_G$ directs the production of plant signal metabolite trehalose-6-phosphate. They identified three residues essential for its trehalose-6-synthase enzymatic activity and showed that enzymatic activity

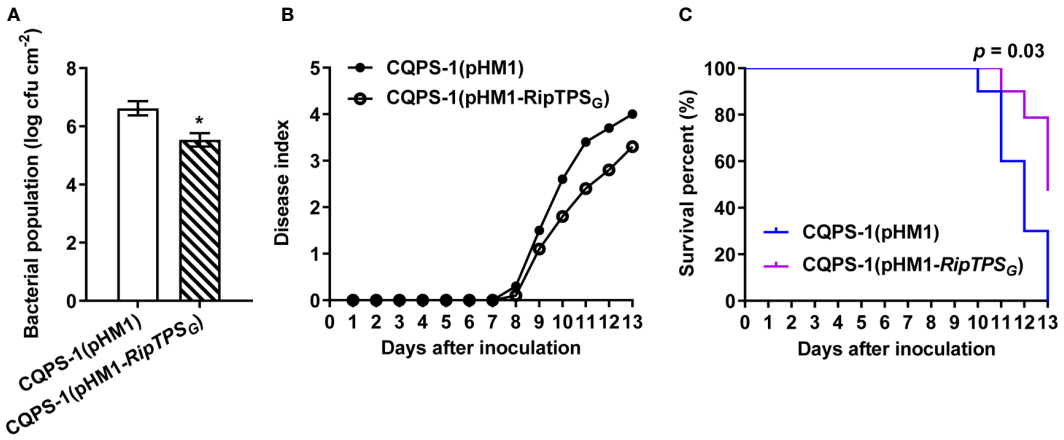

FIGURE 3
Expression of *RipTPS$_G$* in CQPS-1 reduces pathogen virulence in *N. tabacum*. **(A)** Titers of *R. solanacearum* strain CQPS-1. CQPS-1 cells expressing the empty vector (pHM1) and *RipTPS$_G$* (pHM1-RipTPS$_G$) were separately inoculated on 30-day-old *N. tabacum* leaves and bacterial population was quantified 2 days after inoculation. * indicates significant difference at $p \leq 0.05$. **(B)** Disease index of 30-day-old *N. tabacum* after soil drenching inoculation of CQPS-1(pHM1) or CQPS-1(pHM1-RipTPS$_G$). Fifteen plants were observed per genotype per biological replicate. **(C)** Survival analysis of the data in **(B)**. Statistical analysis was performed using a Log-rank (Mantel-Cox) test (n = 45), and the corresponding *p* value is shown in the graph.

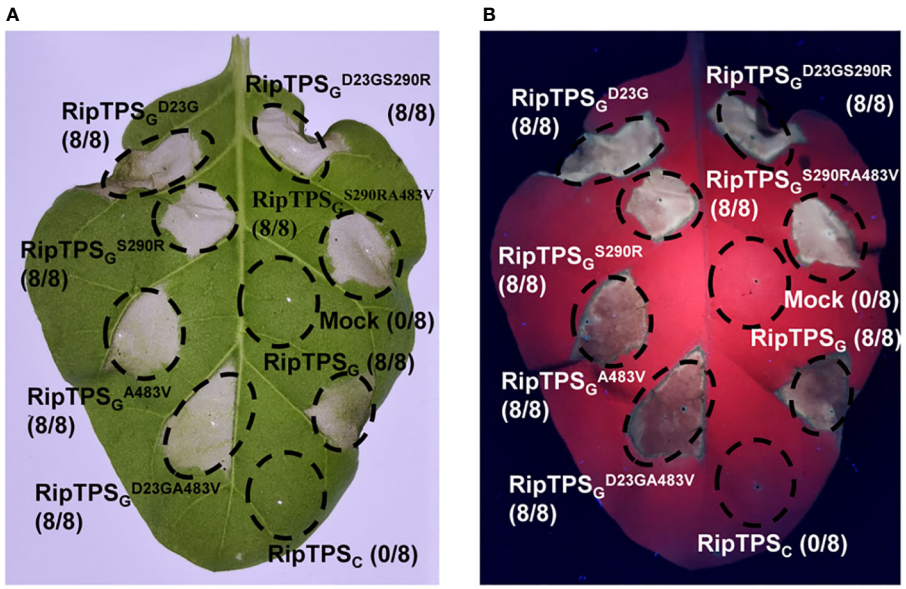

FIGURE 4
Three amino acid residues are jointly required for RipTPS$_G$-induced HR in *N. tabacum*. Leaves of *N. tabacum* were infiltrated with GV3101 carrying LTI6b (Mock, Control), RipTPS$_G$, RipTPS$_C$, or RipTPS$_G$ mutants. Photographs were taken 36 hours after infiltration under white light **(A)** or ultraviolet light **(B)**. Circles indicate the infiltrated area on the leaf panels. The fraction in brackets represents the number of HR over the total number of infiltrated leaves.

is not required for RipTPS-elicited HR in *N. tabacum*. Here, we also showed that the three catalytic mutants of RipTPS$_G$ (RipTPS$_G^{Y154V}$, RipTPS$_G^{W163S}$ and RipTPS$_G^{D208G}$) elicited HR in *N. tabacum* as well as RipTPS$_G$ (Figure 6A), confirming the finding of Poueymiro et al. (2014). Since trehalose-6-phosphate is an essential signal molecule in plants, we wonder whether RipTPS's TPS activity plays a role in its suppression of plant basal defense. We compared the effect of RipTPS$_G$ and its three catalytic mutants on flg22-induced ROS burst in *N. benthamiana* and found that all three mutants showed the similar activity to RipTPS$_G$ (Figures 6B–E). This result indicates that the trehalose-6-synthase enzymatic activity is not required for RipTPS's function in suppression of PAMP-triggered ROS production.

Deletion of *RipTPS*$_G$ does not affect GMI1000-induced HR in *N. tabacum*

To further reveal the role of RipTPS in GMI1000-induced HR in *N. tabacum*, we deleted RipTPS in GMI1000 (Figure 7A). The RipTPS deletion mutants were infiltrated into *N. tabacum* leaves, and the HR induction was observed. The result demonstrated that two independent *RipTPS* deletion mutants still induced strong HR, which is similar to the wild-type GMI1000 (Figure 7B), indicating deletion of RipTPS alone is not sufficient to abolish GMI1000-induced HR in *N. tabacum*.

Discussion

RipTPS$_G$ acts as a host-specificity avirulence factor

R. solanacearum is an aggressive pathogen with a large repertoire of T3Es (Genin and Denny, 2012). Functional characterization of these effectors is critical for understanding the mechanisms of host specificity and pathogenicity in these economically important pathogens (Kim et al., 2021; Yang et al., 2022). However, to date, only few *R. solanacearum* T3Es were characterized for their roles in interaction between *R. solanacearum* and its host/nonhost plants. The model *R. solanacearum* strain GMI1000 cannot infect either *N. benthamiana* or *N. tabacum*, but its close relative CQPS-1 infects both *N. benthamiana* and *N. tabacum*. This feature makes these two *R. solanacearun* strains good models to study host-*R. solanacearum* recognition. We analyzed HR induced by *R. solanacearum* T3Es in *N. tabacum* and *N. benthamiana*, and identified RipTPS$_G$ which induced HR in *N. tabacum* but not in *N. benthamiana*, indicating that RipTPS$_G$ is recognized in *N. tabacum*. This result was supported by a previous report (Poueymiro et al., 2014).

To further demonstrate whether RipTPS$_G$ is an avirulence determinant, we took advantage of the *R. solanacearum* CQPS-1 whose genome has also been sequenced. In contrast to GMI1000, CQPS-1 contains conserved T3SS gene clusters, but is a virulent

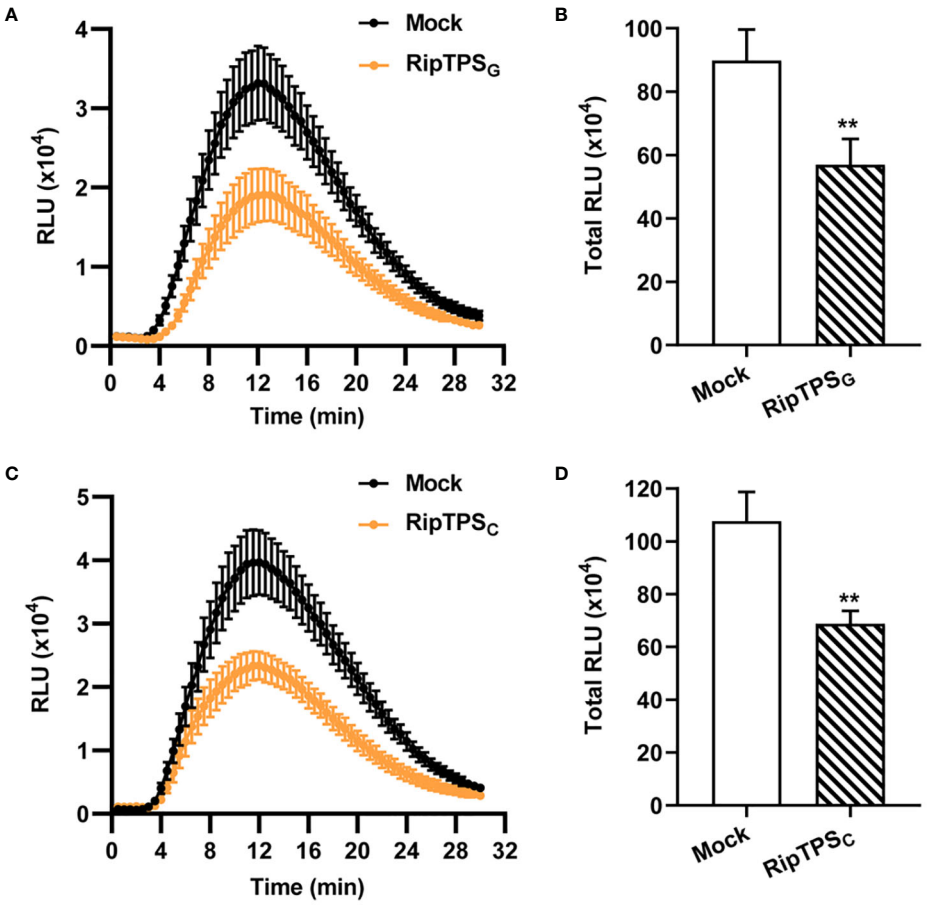

FIGURE 5
Expression of *RipTPS*$_G$ or *RipTPS*$_C$ suppresses flg22-induced reactive oxygen species (ROS) burst in *N. benthamiana*. **(A, C)** Time course curve of ROS production in leaves of *N. benthamiana* transiently expressing *LTI6b* (Mock, Control), *RipTPS*$_G$ **(A)** or *RipTPS*$_C$ **(C)**. Two days after infiltration, leaf discs were treated with 100 nM flg22 elicitor, and ROS production was measured as photon counts for 30 min. **(B, D)** Total ROS accumulation during 30 min in *N. benthamiana* leaves of **(A, C)**, respectively. RLU: relative luminescence units. Data are means ± SE from 14 independent leaf discs. ** indicates significant difference at $p \leq 0.01$.

R. solanacearum strain on tobacco (Liu et al., 2017). In the present study, we found that there are only three amino acid polymorphisms between RipTPS proteins of the two strains (Figure 1). We then took advantage of this natural variation and obtained the following evidence: (1) RipTPS$_G$ elicited HR on *N. tabacum*, but RipTPS$_C$ cannot (Figure 1); (2) RipTPS$_G$ dramatically enhanced expression of HR-related genes *NtHIN1* and *NtHsr203J* in *N. tabacum* (Takahashi et al., 2004), which was significantly compromised when RipTPS$_G$ was replaced by RipTPS$_C$ (Figure 2); (3) The *RipTPS*$_G$ expression reduced virulence of CQPS-1 on *N. tabacum* (Figure 3). These results demonstrate that RipTPS$_G$ is an avirulence determinant that triggers defense in *N. tabacum*, while RipTPS$_C$ acts as a virulence T3E. However, expression of *RipTPS*$_C$ still slightly enhanced expression of the HR marker genes (Figure 2). Similar weak responses of *N. benthamiana* to the virulent alleles has also been reported previously, especially in the overexpression assays (Westerink et al., 2004; Bos et al., 2006).

Compared with other bacterial plant pathogens, *R. solanacearum* has a large repertoire of secreted effectors (Yu et al., 2020), and some of these effectors are functionally redundant (Cunnac et al., 2004; Macho et al., 2010) and balanced for a successful infection (Sang et al., 2020). Deleting RipTPS alone in GMI1000 did not significantly affect *R. solanacearum*-induced HR in *N. tatacum* (Figure 7), indicating other avirulence genes exist in GMI1000. Indeed, AvrA (Poueymiro et al., 2009) and RipAW (Niu et al., 2022) from GMI1000 have been reported to act as avirulence factors in *N. tabacum*. Differently, AvrA and RipAW are recognized by both *N. benthamiana* and *N. tabacum* (Poueymiro et al., 2009; Niu et al., 2022). Therefore, RipTPS acts as an avirulence determinant specifically recognized in *N. tabacum*.

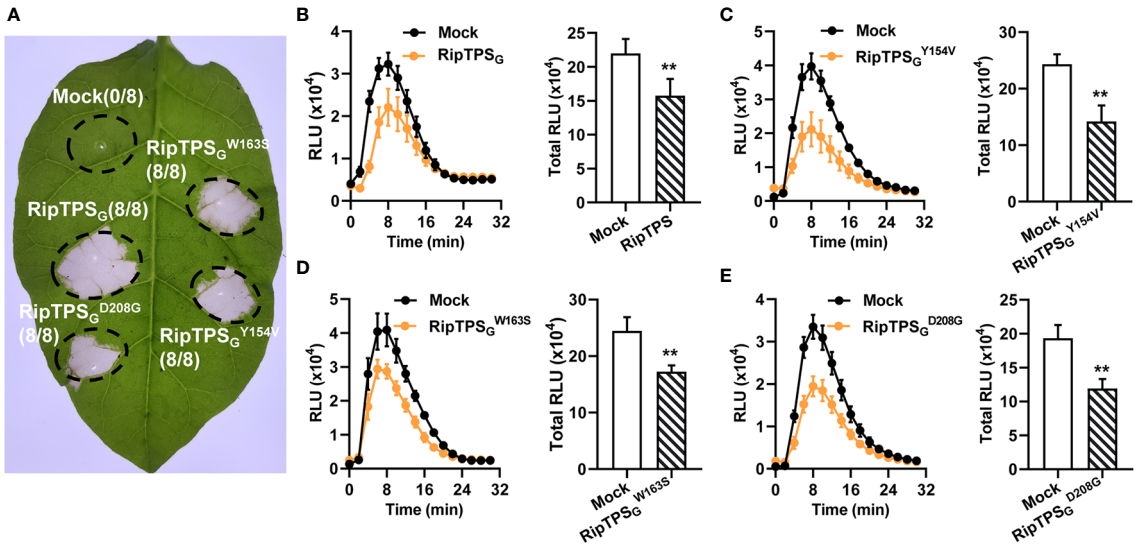

FIGURE 6
TPS activity is required for neither RipTPS$_G$-elicited HR in *N. tabacum* nor suppression of flg22-induced ROS burst in *N. benthamiana*. **(A)** RipTPS$_G$-elicited HR in *N. tabacum* is independent of its TPS activity. Leaves of *N. tabacum* were infiltrated with GV3101 carrying *LTI6b* (Mock), *RipTPS$_G$*, or *RipTPS$_G$* mutants compromised in its enzymatic activity (RipTPS$_G^{Y154V}$, RipTPS$_G^{W163s}$ and RipTPS$_G^{D208G}$). Photographs were taken 24 hours after infiltration. Circles indicate the infiltrated area on the leaf panels. The fraction in brackets represents the number of HR over the total number of infiltrated leaves. **(B–E)** Suppression of flg22-induced ROS burst by RipTPS$_G$ in *N. benthamiana* is independent of TPS activity. Both of time course curve of ROS production and total ROS accumulation in leaves of *N. benthamiana* transiently expressing *LTI6b* (Mock, Control), RipTPS$_G$, or RipTPS$_G$ mutants were showed. Two days after infiltration, leaf discs were treated with 100 nM flg22, and ROS production was measured as photon counts for 30 min. RLU: relative luminescence units. Data are means ± SE from 14 independent leaf discs. ** indicates significant difference at $p \leq 0.01$.

The three amino acid polymorphisms determine the recognition of RipTPS$_G$ in *N. tabacum*

During the coevolution of phytopathogens and plants, pathogens must overcome ETI for further infection through evolution of pathogen effectors that escape or suppress ETI (Jones and Dangl, 2006). Sang et al. (2020) showed that *R. solanacearum* effector RipAY directly inhibited another effector RipE1-triggered ETI in *N. benthamiana* to counteract its perception by plant immune system. Many plant pathogens have also developed strategies to escape host recognition by point mutations, gene deletions, transposon insertions or deliberate mistranslation (Westerink et al., 2004; Vargas-Rodriguez et al., 2021). Escaping recognition by the strategy of point mutations of avirulence factor has been reported in several phytopathogens such as *Cladosporium fulvum* (Westerink et al., 2004) and *Phytophthora infestans* (Bos et al., 2006). Here, only three polymorphic amino acid residues are present in RipTPS between avirulent strain GMI1000 and virulent strain CQPS-1. Site-directed mutagenesis analyses showed that neither the single nor the double amino acid substitution abolished RipTPS$_G$-elicted HR. RipTPS$_G$-triggered HR was abolished only when all its three polymorphic residues were substituted into the corresponding residues in RipTPS$_C$ (Figure 4). This finding suggests that all three amino acid residues are required for the recognition of RipTPS$_G$ in *N. tabacum*, and RipTPS$_C$ evades the recognition through simultaneously mutating these three residues. Poueymiro et al. (2014) pointed out that the C-terminal half (amino acid 336-557) of RipTPS$_G$ alone could trigger the HR-like response. Our result indicated that the N-terminal region of RipTPS also contributes to its recognition in *N. tabacum*, since both D23 and S290 residues are required for RipTPS$_G$-induced HR in our result (Figure 4). These three residues may affect three-dimensional structure of RipTPS protein or interactions between RipTPS and other plant proteins.

RipTPS exhibited defense suppression activity in *N. benthamiana*

ROS play a crucial role in biotic stress sensing and activation of stress-response networks (Mittler et al., 2022). ROS burst is a hallmark event for plant basal defense (Segonzac et al., 2011; Nakano and Mukaihara, 2019a). Here, we showed that expression of *RipTPS$_G$* suppressed flg22-induced ROS burst in *N. benthamiana* (Figure 5), indicating that RipTPS$_G$ interferes

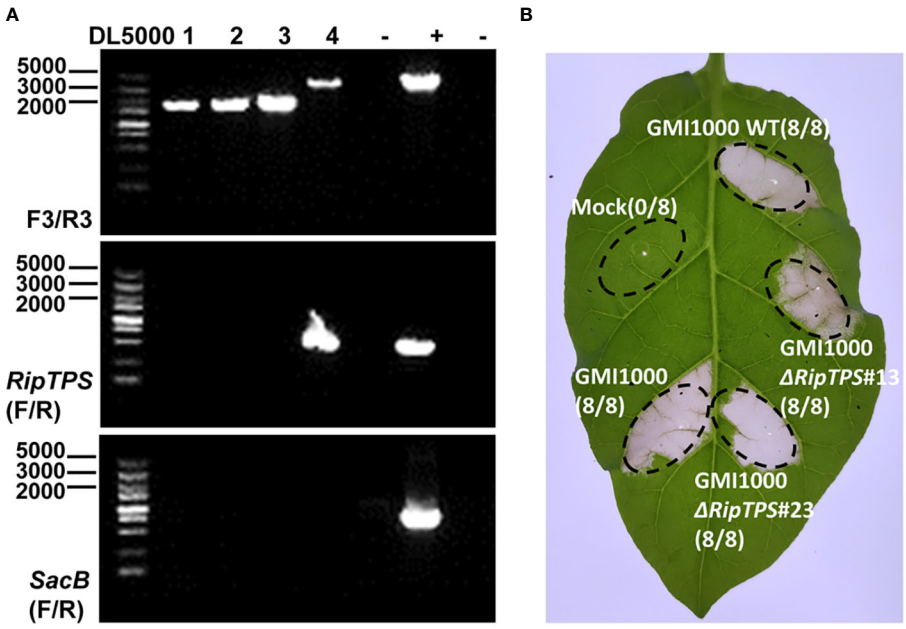

FIGURE 7
Deletion of *RipTPS* in GMI1000 does not affect its HR induction phenotype in *N. tabacum*. **(A)** Identification of *RipTPS* deletion mutants. The primer pairs F3/R3, RipTPS(F/R) and SacB(F/R) were used for confirmation of double exchange. After double exchange, the *RipTPS* gene was deleted. DL5000: DNA ladder. **(B)** HR induced by wild-type GMI1000 and *RipTPS* deletion mutants. Wild-type GMI1000 or *RipTPS* deletion mutant cells with an OD_{600} of 0.1 were infiltrated into 40-day-old *N. tabacum* leaves, respectively. Photographs were taken 48 hours after inoculation. Water was used as mock. Circles indicate the infiltrated area on the leaf panels. The fraction in brackets represents the number of HR over the total number of infiltrated leaves. GMI1000Δ*RipTPS*#13 and GMI1000Δ*RipTPS*#23 are two independent *RipTPS* deletion mutants.

with plant immune response in *N. benthamaina*. Similar phenomenon was also observed in other T3Es, such as PopP2 and AvrA which are known as avirulence determinants but contribute to pathogen virulence in susceptible host (Macho et al., 2010). Interestingly, expression of $RipTPS_C$ also suppressed flg22-induced ROS burst in *N. benthamiana* (Figure 5), indicating that $RipTPS_C$ retains its ability to suppress plant defense response and the three amino acid polymorphisms do not affect RipTPS's virulence activity.

TPS activity is involved in neither $RipTPS_G$'s avirulence nor virulence functions

The most striking feature of RipTPS is its inherently trehalose-6-synthase enzymatic activity as its name suggests (Poueymiro et al., 2014). Trehalose, a non-reducing sugar, has been found in multiple microbes ranging from bacteria to yeast and in plants. In plants, trehalose not only serves as a reserve carbohydrate and structural components of cells but also acts as a signaling molecule, and it plays important physiological roles in plant growth and stress resistance (Wahl et al., 2013; Sarkar and Sadhukhan, 2022; Shao et al., 2022). Interestingly, in some phytopathogens, trehalose metabolism has emerged as an essential player in virulence-associated phenotypes and proficient initial plant infection (Tournu et al., 2013). For instance, trehalose biosynthesis promotes *Pseudomonas aeruginosa* virulence in plants by promoting the acquisition of nitrogen-containing nutrients (Djonovic et al., 2013). However, we demonstrated that the TPS enzymatic activity was not required for its avirulence function, which is consistent with the result of Poueymiro et al. (2014). We also showed that the TPS enzymatic activity was not required for its function in suppression of PAMP-induced ROS production (Figure 6). Further studies are needed to elucidate the role of the TPS activity of RipTPS in *R. solanacearum*-plant interactions.

In summary, in this study we demonstrated that RipTPS from *R. solanacearum* strain GMI1000 is an avirulence determinant recognized in *N. tabacum*, whereas the RipTPS homolog from another strain CQPS-1 can escape this recognition. The three amino acid residues of RipTPS are jointly required for the recognition of $RipTPS_G$ in *N. tabacum*. Both $RipTPS_G$ and $RipTPS_C$ retain their ability to suppress plant defense responses. The TPS activity of RipTPS is not required for its avirulence function and also virulence activity of suppressing PAMP-induced ROS burst. It will be a promising direction to identify the corresponding resistance gene recognizing $RipTPS_G$

in *N. tabacum* and also to elucidate the role of TPS activity of RipTPS in *R. solanacearum*-plant interactions in the future.

Data availability statement

The original contributions presented in the study are included in the article/Supplementary Material. Further inquiries can be directed to the corresponding author.

Author contributions

YA and MZ conceived and designed the experiments. JC, ZX, XO, and PC performed the experiments. YA, RW, PL and MZ analyzed the data. YA, JC and MZ drafted and modified the manuscript. All authors contributed to the article and approved the submitted version.

Funding

This research was supported by the National Natural Science Foundation of China (32072399, 32272641), the Fundamental Research Funds for the Central Universities (GK202201017), the Program of Fujian Key Laboratory for Monitoring and Integrated Management of Crop Pests (MIMCP-202203), and the Joint Research Project of FAAS (DWHZ2021-13).

Conflict of interest

The authors declare that the research was conducted in the absence of any commercial or financial relationships that could be construed as a potential conflict of interest.

Publisher's note

All claims expressed in this article are solely those of the authors and do not necessarily represent those of their affiliated organizations, or those of the publisher, the editors and the reviewers. Any product that may be evaluated in this article, or claim that may be made by its manufacturer, is not guaranteed or endorsed by the publisher.

Supplementary material

The Supplementary Material for this article can be found online at: https://www.frontiersin.org/articles/10.3389/fpls.2022.1040826/full#supplementary-material

References

Bos, J. I. B., Kanneganti, T. D., Young, C., Cakir, C., Huitema, E., Win, J., et al. (2006). The c-terminal half of *Phytophthora infestans* RXLR effector AVR3a is sufficient to trigger R3a-mediated hypersensitivity and suppress INF1-induced cell death in *Nicotiana benthamiana*. *Plant J.* 48, 165–176. doi: 10.1111/j.1365-313X.2006.02866.x

Cheng, D., Zhou, D., Wang, Y. D., Wang, B. S., He, Q., Song, B. T., et al. (2021). *Ralstonia solanacearum* type III effector RipV2 encoding a novel E3 ubiquitin ligase (NEL) is required for full virulence by suppressing plant PAMP-triggered immunity. *Biochem. Bioph. Res. Co.* 550, 120–126. doi: 10.1016/j.bbrc.2021.02.082

Cunnac, S., Occhialini, A., Barberis, P., Boucher, C., and Genin, S. (2004). Inventory and functional analysis of the large hrp regulon in *Ralstonia solanacearum*: identification of novel effector proteins translocated to plant host cells through the type III secretion system. *Mol. Microbiol.* 53, 115–128. doi: 10.1111/j.1365-2958.2004.04118.x

Deslandes, L., Olivier, J., Peeters, N., Feng, D. X., Khounlotham, M., Boucher, C., et al. (2003). Physical interaction between RRS1-r, a protein conferring resistance to bacterial wilt, and PopP2, a type III effector targeted to the plant nucleus. *Proc. Natl. Acad. Sci. U.S.A.* 100, 8024–8029. doi: 10.1073/pnas.1230660100

Djonovic, S., Urbach, J. M., Drenkard, E., Bush, J., Feinbaum, R., Ausubel, J. L., et al. (2013). Trehalose biosynthesis promotes *Pseudomonas aeruginosa* pathogenicity in plants. *PloS Pathog.* 9, e1003217. doi: 10.1371/journal.ppat.1003217

Genin, S., and Denny, T. P. (2012). Pathogenomics of the *Ralstonia solanacearum* species complex. *Annu. Rev. Phytopathol.* 50, 67–89. doi: 10.1146/annurev-phyto-081211-173000

Jones, J. D. G., and Dangl, J. L. (2006). The plant immune system. *Nature* 444, 323–329. doi: 10.1146/annurev-phyto-081211-173000

Kim, B., You, H., and Cecile, S. (2021). The c-terminal domain of the *Ralstonia solanacearum* type III effector RipY is required for recognition in *Nicotiana benthamiana*. *Mol. Plant Microbe Interact.* 34, S.

Lavie, M., Shillington, E., Eguiluz, C., Grimsley, N., and Boucher, C. (2002). PopP1, a new member of the YopJ/AvrRxv family of type III effector proteins, acts as a host-specificity factor and modulates aggressiveness of *Ralstonia solanacearum*. *Mol. Plant Microbe Interact.* 15, 1058–1068. doi: 10.1094/Mpmi.2002.15.10.1058

Liu, Y., Tang, Y. M., Qin, X. Y., Yang, L., Jiang, G. F., Li, S. L., et al. (2017). Genome sequencing of *Ralstonia solanacearum* CQPS-1, a phylotype I strain collected from a highland area with continuous cropping of tobacco. *Front. Microbiol.* 8. doi: 10.3389/Fmicb.2017.00974

Livak, K. J., and Schmittgen, T. D. (2001). Analysis of relative gene expression data using real-time quantitative PCR and the $2^{-\Delta\Delta Ct}$ method. *Methods* 25, 402–408. doi: 10.1006/meth.2001.1262

Macho, A. P., Guidot, A., Barberis, P., Beuzon, C. R., and Genin, S. (2010). A competitive index assay identifies several *Ralstonia solanacearum* type III effector mutant strains with reduced fitness in host plants. *Mol. Plant Microbe Interact.* 23, 1197–1205. doi: 10.1094/Mpmi-23-9-1197

Mittler, R., Zandalinas, S. I., Fichman, Y., and Van Breusegem, F. (2022). Reactive oxygen species signalling in plant stress responses. *Nat. Rev. Mol. Cell Biol* 23, 663–669. doi: 10.1038/s41580-022-00499-2

Morel, A., Guinard, J., Lonjon, F., Sujeeun, L., Barberis, P., Genin, S., et al. (2018). The eggplant AG91-25 recognizes the type III-secreted effector RipAX2 to trigger resistance to bacterial wilt (*Ralstonia solanacearum* species complex). *Mol. Plant Pathol.* 19, 2459–2472. doi: 10.1111/mpp.12724

Mukaihara, T., Hatanaka, T., Nakano, M., and Oda, K. (2016). *Ralstonia solanacearum* type III effector RipAY is a glutathione-degrading enzyme that is activated by plant cytosolic thioredoxins and suppresses plant immunity. *mBio* 7, e00359-16. doi: 10.1128/mBio.00359-16

Nahar, K., Matsumoto, I., Taguchi, F., Inagaki, Y., Yamamoto, M., Toyoda, K., et al. (2014). *Ralstonia solanacearum* type III secretion system effector Rip36 induces a hypersensitive response in the nonhost wild eggplant *Solanum torvum*. *Mol. Plant Pathol.* 15, 297–303. doi: 10.1111/mpp.12079

Nakano, M., and Mukaihara, T. (2019a). Comprehensive identification of PTI suppressors in type III effector repertoire reveals that *Ralstonia solanacearum* activates jasmonate signaling at two different steps. *Int. J. Mol. Sci.* 20, 5992. doi: 10.3390/Ijms20235992

Nakano, M., and Mukaihara, T. (2019b). The type III effector RipB from *Ralstonia solanacearum* RS1000 acts as a major avirulence factor in *Nicotiana benthamiana* and other *Nicotiana* species. *Mol. Plant Pathol.* 20, 1237–1251. doi: 10.1111/mpp.12824

Ngou, B. P. M., Ahn, H., Ding, P. T., and Jones, J. D. G. (2021). Mutual potentiation of plant immunity by cell-surface and intracellular receptors. *Nature* 592, 110–115. doi: 10.1038/s41586-021-03315-7

Niu, Y., Fu, S. Y., Chen, G., Wang, H. J., Wang, Y. S., Hu, J. X., et al. (2022). Different epitopes of *Ralstonia solanacearum* effector RipAW are recognized by two *Nicotiana* species and trigger immune responses. *Mol. Plant Pathol.* 23, 188–203. doi: 10.1111/mpp.13153

Poueymiro, M., Cazale, A. C., Francois, J. M., Parrou, J. L., Peeters, N., and Genin, S. (2014). A *Ralstonia solanacearum* type III effector directs the production of the plant signal metabolite trehalose-6-phosphate. *mBio* 5, e02065-14. doi: 10.1128/mBio.02065-14

Poueymiro, M., Cunnac, S., Barberis, P., Deslandes, L., Peeters, N., Cazale-Noel, A. C., et al. (2009). Two type III secretion system effectors from *Ralstonia solanacearum* GMI1000 determine host-range specificity on tobacco. *Mol. Plant Microbe Interact.* 22, 538–550. doi: 10.1094/Mpmi-22-5-0538

Qi, P. P., Huang, M. L., Hu, X. H., Zhang, Y., Wang, Y., Li, P. Y., et al. (2022). A *Ralstonia solanacearum* effector targets TGA transcription factors to subvert salicylic acid signaling. *Plant Cell* 34, 1666–1683. doi: 10.1093/plcell/koac015

Sang, Y. Y., Yu, W. J., Zhuang, H. Y., Wei, Y. L., Derevnina, L., Yu, G., et al. (2020). Intra-strain elicitation and suppression of plant immunity by *Ralstonia solanacearum* type-III effectors in *Nicotiana benthamiana*. *Plant Commun.* 1, 100025. doi: 10.1016/J.Xplc.2020.100025

Sarkar, A. K., and Sadhukhan, S. (2022). Imperative role of trehalose metabolism and trehalose-6-phosphate signaling on salt stress responses in plants. *Physiol. Plant* 174, e13647. doi: 10.1111/ppl.13647

Schafer, A., Tauch, A., Jager, W., Kalinowski, J., Thierbach, G., and Puhler, A. (1994). Small mobilizable multi-purpose cloning vectors derived from the *Escherichia coli* plasmids pK18 and pK19: selection of defined deletions in the chromosome of *Corynebacterium glutamicum*. *Gene* 145, 69–73. doi: 10.1016/0378-1119(94)90324-7

Schluepmann, H., Berke, L., and Sanchez-Perez, G. F. (2012). Metabolism control over growth: a case for trehalose-6-phosphate in plants. *J. Exp. Bot.* 63, 3379–3390. doi: 10.1093/jxb/err311

Segonzac, C., Feike, D., Gimenez-Ibanez, S., Hann, D. R., Zipfel, C., and Rathjen, J. P. (2011). Hierarchy and roles of pathogen-associated molecular pattern-induced responses in *Nicotiana benthamiana*. *Plant Physiol.* 156, 687–699. doi: 10.1104/pp.110.171249

Shao, J. H., Wu, W. X., Rasul, F., Munir, H., Huang, K., Awan, M. I., et al. (2022). Trehalose induced drought tolerance in plants: physiological and molecular responses. *Not. Bot. Horti Agrobo.* 50, 12584. doi: 10.15835/Nbha50112584

Sun, Y. H., Li, P., Deng, M. Y., Shen, D., Dai, G. Y., Yao, N., et al. (2017). The *Ralstonia solanacearum* effector RipAK suppresses plant hypersensitive response by inhibiting the activity of host catalases. *Cell. Microbiol* 19, e12736. doi: 10.1111/cmi.12736

Takahashi, Y., Uehara, Y., Berberich, T., Ito, A., Saitoh, H., Miyazaki, A., et al. (2004). A subset of hypersensitive response marker genes, including HSR203J, is the downstream target of a spermine signal transduction pathway in tobacco. *Plant J.* 40, 586–595. doi: 10.1111/j.1365-313X. 2004.02234.x

Tournu, H., Fiori, A., and Van Dijck, P. (2013). Relevance of trehalose in pathogenicity: some general rules, yet many exceptions. *PloS Pathog.* 9, e1003447. doi: 10.1371/journal

Tsuda, K., and Katagiri, F. (2010). Comparing signaling mechanisms engaged in pattern-triggered and effector-triggered immunity. *Curr. Opin. Plant Biol.* 13, 459–465. doi: 10.1016/j.pbi.2010.04.006

Vailleau, F., Sartorel, E., Jardinaud, M.F., Chardon, F., Genin, S., Huguet, T., et al. (2007). Characterization of the interaction between the bacterial wilt pathogen Ralstonia solanacearum and the model legume plant Medicago truncatula. *Mol. Plant Microbe Interact.* 20, 159–167. doi: 10.1094/Mpmi-20-2-0159

Vargas-Rodriguez, O., Badran, A. H., Hoffman, K. S., Chen, M. Y., Crnkovi, A., Ding, Y. S., et al. (2021). Bacterial translation machinery for deliberate mistranslation of the genetic code. *Proc. Natl. Acad. Sci. U.S.A.* 118, e2110797118. doi: 10.1073/pnas.2110797118

Wahl, V., Ponnu, J., Schlereth, A., Arrivault, S., Langenecker, T., Franke, A., et al. (2013). Regulation of flowering by trehalose-6-phosphate signaling in *Arabidopsis thaliana*. *Science* 339, 704–707. doi: 10.1126/science.1230406

Wang, Y. R., Zhao, A. C., Morcillo, R. J. L., Yu, G., Xue, H., Rufian, J. S., et al. (2021). A bacterial effector protein uncovers a plant metabolic pathway involved in tolerance to bacterial wilt disease. *Mol. Plant* 14, 1281–1296. doi: 10.1016/j.molp.2021.04.014

Westerink, N., Brandwagt, B. F., De Wit, P. J. G. M., and Joosten, M. (2004). Cladosporium fulvum circumvents the second functional resistance gene homologue at the cf-4 locus (Hcr9-4E) by secretion of a stable avr4E isoform. *Mol. Microbiol.* 54, 533–545. doi: 10.1111/j.1365-2958.2004.04288.x

Xian, L., Yu, G., Wei, Y. L., Rufian, J. S., Li, Y. S., Zhuang, H. Y., et al. (2020). A bacterial effector protein hijacks plant metabolism to support pathogen nutrition. *Cell Host Microbe* 28, 548–557. doi: 10.1016/j.chom.2020.07.003

Yang, L., Wei, Z. L., Valls, M., and Ding, W. (2022). Metabolic profiling of resistant and susceptible tobaccos response incited by *Ralstonia pseudosolanacearum* causing bacterial wilt. *Front. Plant Sci.* 12. doi: 10.3389/Fpls.2021.780429

Ye, W. W., Wang, Y. C., and Dou, D. L. (2010). SeqHunter: a bioinformatics toolbox for local blast and sequence analysis. *China J. Bioinform.* 8, 364–367, 377.

Yuan, M. H., Jiang, Z. Y., Bi, G. Z., Nomura, K. Y., Liu, M. H., Wang, Y. P., et al. (2021). Pattern-recognition receptors are required for NLR-mediated plant immunity. *Nature* 592, 105–109. doi: 10.1038/s41586-021-03316-6

Yu, G., Xian, L., Xue, H., Yu, W. J., Rufian, J. S., Sang, Y. Y., et al. (2020). A bacterial effector protein prevents MAPK-mediated phosphorylation of SGT1 to suppress plant immunity. *PloS Pathog.* 16, e1008933. doi: 10.1371/journal.ppat.1008933

frontiers | Frontiers in Plant Science

TYPE Mini Review
PUBLISHED 25 November 2022
DOI 10.3389/fpls.2022.1056008

OPEN ACCESS

EDITED BY
Qiong Zhang,
University of California, Berkeley,
United States

REVIEWED BY
Changhai Liu,
Northwest A&F University, China
Junli Wang,
Max Planck Institute for Plant Breeding
Research, Germany

*CORRESPONDENCE
Xinping Chen
chenxp2017@swu.edu.cn

SPECIALTY SECTION
This article was submitted to
Crop and Product Physiology,
a section of the journal
Frontiers in Plant Science

RECEIVED 28 September 2022
ACCEPTED 11 November 2022
PUBLISHED 25 November 2022

CITATION
Chen A, Liu T, Wang Z and Chen X
(2022) Plant root suberin: A layer
of defence against biotic and
abiotic stresses.
Front. Plant Sci. 13:1056008.
doi: 10.3389/fpls.2022.1056008

Plant root suberin: A layer of defence against biotic and abiotic stresses

Anle Chen[1], Tong Liu[1], Zhou Wang[2] and Xinping Chen[1]*

[1]Interdisciplinary Research Center for Agriculture Green Development in Yangtze River Basin, and College of Resources and Environment, Southwest University, Chongqing, China, [2]College of Plant Protection, Southwest University, Chongqing, China

Plant roots have important functions, such as acquiring nutrients and water from the surrounding soil and transporting them upwards to the shoots. Simultaneously, they must be able to exclude potentially harmful substances and prevent the entry of pathogens into the roots. The endodermis surrounds the vascular tissues and forms hydrophobic diffusion barriers including Casparian strips and suberin lamella. Suberin in cell walls can be induced by a range of environmental factors and contribute to against biotic and abiotic threats. Tremendous progress has been made in biosynthesis of suberin and its function, little is known about the effect of its plasticity and distribution on stress tolerance. In field conditions, biotic and abiotic stress can exist at the same time, and little is known about the change of suberization under that condition. This paper update the progress of research related to suberin biosynthesis and its function, and also discuss the change of suberization in plant roots and its role on biotic and abiotic stresses tolerance.

KEYWORDS

endodermis, suberization, plant lipophilic barriers, plasticity, stress tolerance

Introduction

Plant roots acquire nutrients and water from soil and transport them to the shoots, while toxic compounds must be restricted from entering the plant. To reach the central vasculature of the root, water and nutrients must cross the major tissue types of the root: the epidermis, the cortex and the endodermis. The epidermis is the outermost cell layer of young roots. The endodermis surrounds the vascular tissue. All vascular plants normally develop an endodermis in their roots, and the majority of angiosperm roots also have an exodermis which is a cell layer beneath the epidermis. The exodermis is absent in *Arabidopsis*, soybean, oats, barley and wheat (Perumalla et al., 1990; Thomas et al., 2007; Ranathunge et al., 2008; Kreszies et al., 2018).

The differentiation of the endodermis starts by the formation of the Casparian strip, as root development progresses, another type of barrier is formed, called suberin lamellae. This

waxy, lipophilic layer is deposited all around the cellular surface of endodermal cells, impregnating the space between the cell wall and the plasma membrane (Nawrath et al., 2013; Vishwanath et al., 2015). The suberin layer appears to act as a transcellular barrier controlling the uptake or passive diffusion of ions from the apoplast into the symplastic environment of the endodermal cells (Barberon, 2017; Doblas et al., 2017). Plants have a variety of physiological response mechanisms when they are subjected to various stresses from the environment, and the deposition of suberin lamellae in the endodermis is one of them. This response can control the transport efficiency of various ions in plants, for reaching the ions balance in plants and reducing the toxic effect on plant growth and development. Suberin in cell walls can be induced by biotic and abiotic stresses (Hose et al., 2001; Enstone et al., 2003; Krishnamurthy et al., 2011; Tylova et al., 2017). It was also shown that suberin biosynthesis in Arabidopsis is affected by nutrient deficiencies such as iron (Fe), manganese (Mn), Zinc (Zn), potassium (K) and sulphur (S) (Barberon et al., 2016). It was suggested that plants can adapt to a sub-optimal nutrient supply in a highly dynamic and ion specific matter, either by an increasing or by a decreasing endodermal suberization (Barberon et al., 2016; Doblas et al., 2017). The suberized endodermis isolates the stele from the rest of the root, and function as a barrier to nematode entrance and against pathogen invasion into the xylem and spread throughout the plant (Holbein et al., 2019; Kashyap et al., 2021).

Establishment of suberin lamellae in the cell wall

The endodermal differentiation is marked by the deposition of suberin lamellae, which cover the cellular surface of endodermal cells (Nawrath et al., 2013; Vishwanath et al., 2015). From the root tip to the base, the suberized endodermal cells first form a patchy zone, then a continuous zone (Geldner, 2013; Barberon et al., 2016). The fully suberized zone has some non-suberized cells, called passage cells, which are always located close to xylem poles. The establishment of passage cells is governed by repression of cytokinin signalling in the root meristem, which ultimately results in non-suberized endodermal cells (Andersen et al., 2018).

Suberin is a chemically complex heteropolymer, which is a glycerol-based polymer consisting of a polyaliphatic polyester linked with phenolic components (Kolattukudy, 1981; Franke and Schreiber, 2007; Pollard et al., 2008). Transmission electron microscopy (TEM) shows that the suberin lamellae contain electron-lucent and electron-dense contrasts, suggested to consist of polyaliphatics and polyaromatics, respectively (Graca and Santos, 2007). Suberin is chemically similar to cutin which is an insoluble lipid polyester deposited outside of the primary cell wall and which covers the outer face of the epidermal wall. However, suberin contains an aromatic domain which is not present in cutin (Schreiber, 2010).

The chemical composition of suberin in Arabidopsis roots was analysed by gas chromatography coupled to mass spectrometry (GC-MS), monounsaturated ω-hydroxyacids, α,ω-dicarboxylic acids and glycerol are the major monomers of suberin, followed by alcohols and unsubstituted fatty acids (Franke et al., 2005). Suberin consists of polyaliphatic domains and polyaromatic domains. It was suggested that the aliphatic domain primarily made suberin a transport barrier for water due to its high hydrophobicity (Zimmermann et al., 2000; Kreszies et al., 2018). In barley, the amount of aliphatic suberin in the primary root was increased in response to osmotic stress, and the osmotic stress-induced aliphatic suberin markedly reduced the water flow through the apoplast (Kreszies et al., 2019). In potato, the aromatic domain of suberin was reported to provide resistance to pathogen penetration (Lulai and Corsini, 1998), and it was suggested that the aromatic domains primarily make suberin as a transport barrier for nutrients (Kreszies et al., 2018). The composition of suberin between species is similar, however the content of suberin is strongly species dependent and can be induced by a range of environmental factors, which affect the efficiency of suberin as a barrier.

Biosynthesis of suberin

The biosynthetic machinery responsible for suberin productions is complex due to the chemical diversity of the suberin polymers. Chemical analysis and biochemical studies three decades ago were the initial steps to elucidate the biosynthesis pathways and structure of suberin (Kolattukudy, 1981). After that, approaches of reverse genetics on bark, potato periderm, cotton fibres, Arabidopsis root endodermis and seed coats made further progress on suberin biosynthesis (Molina et al., 2009; Ranathunge et al., 2011; Beisson et al., 2012; Li-Beisson et al., 2013; Graca, 2015). However, the sequence of biosynthetic reactions, transport mechanism of monomers and the site of polymerization of the precursors remain to be elucidated.

Biosynthesis of suberin monomers involves fatty acid and phenylpropanoid pathways. In plants, fatty acid synthesis occurs in the plastid stroma. However, the relationship between regulation of diffusion or transport of fatty acids through the lipid membrane of plastid with suberin biosynthesis is not clear (Figure 1). The core reactions of the suberin biosynthetic pathway were believed to take place at the endoplasmic reticulum (ER) (Figure 1) (Li-Beisson et al., 2013). A large number of genes encoding enzymes involved in the synthesis of suberin have been identified (Vishwanath et al., 2015). However, many aspects of suberin biosynthesis remain undetermined. Whether suberin precursors are exported as monomers or building blocks is unclear (Beisson et al., 2012).

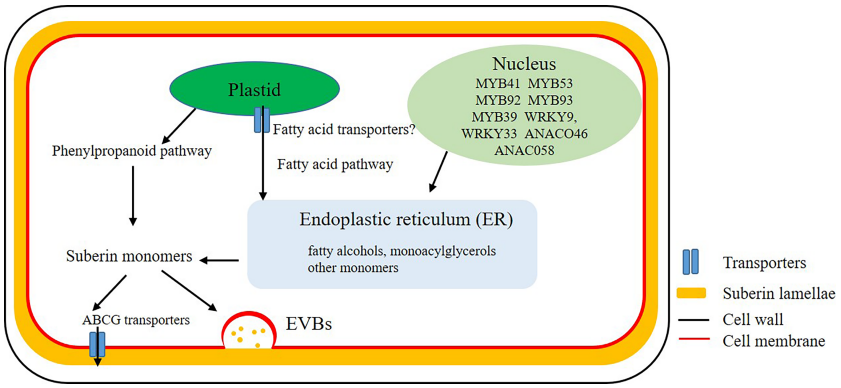

FIGURE 1
Biosynthesis and transport of suberin. Mostly biosynthesis of suberin monomers take place at the endoplasmic reticulum (ER). After a series of complex enzyme-induced reactions, fatty acids and other lipids in plastid are transported to the ER to synthesize fatty alcohols, monoacylglycerols and other monomers. Monomers, oligomers or polymers are probably transported cross the plasma membrane by ATP-binding cassette (ABC) transporters or Extracellular Vesiculo-tubular containing Bodies (EVBs).

The ATP-binding cassette (ABC) transporters, lipid transport proteins and secretion through vesicles are thought to be involved in the export of these monomers or building blocks out of plasma membrane to the site of polymerization (Figure 1) (De Bellis et al., 2022). The transporters that transport aliphatic monomers out of the plasma membrane have recently been identified, and all of them belong to the ABCG subfamily (Do et al., 2018). In Arabidopsis root, proteins of AtABCG2, AtABCG6 and AtABCG20 make contribution for the formation of suberin lamellae in endodermis (Yadav et al., 2014). Other ABC transporters, like OsABCG5 in rice root and StABCG1 in potato root and tuber periderm were also identified and described as suberin monomer transporters (Landgraf et al., 2014; Shiono et al., 2014).

Recently some regulatory genes of suberin synthesis have been described. In Arabidopsis, the transcription factorAtMYB41, AtMYB53, AtMYB92 and AtMYB93 are positive regulators of suberin biosynthesis in roots (Shukla et al., 2021). AtMYB107, AtMYB9 are required for suberin assembly in the Arabidopsis seed coat which were revealed highly conserved in angiosperms (Lashbrooke et al., 2016; Gou et al., 2017) and MdMYB93 was also described as a regulator of suberin deposition in apple fruit skins (Legay et al., 2016).

Deposition of suberin in cell wall

Suberin separates the cell wall from the plasma membrane and it can be found in root endodermis/hypodermis, seed coats, bark, and potato tuber skin (Schreiber, 2010). Suberin also deposits at the wound edges of potato periderm (Lulai et al., 2008) and at the site of lateral root emergence, where the CSs are disrupted (Li et al., 2017). The distribution of suberin in different plant tissues suggests that plants can synthesise and deposit suberin whenever and wherever they need to form a barrier (Kolattukudy, 2001; Franke and Schreiber, 2007). Recently, it is report that GELPs (GDSL-type Esterase/Lipase Protein family) play a key role in suberin polymerization and degradation both in the context of lateral root emergence and endodermal layer (Ursache et al., 2021). However, the mechanisms that regulate the onset of suberization are unclear.

The deposition of suberin in Arabidopsis roots starts in a patchy manner, then more and more endodermal cells are suberized until the whole endodermis is suberized except for some passage cells located close to xylem poles (Geldner, 2013). Suberization patterns in other plant species were also reported, there is variation between plant species due to the difference of root anatomy (Thomas et al., 2007; Waduwara et al., 2008; Ranathunge et al., 2017). In barley from root tip to root base, the deposition of suberin in endodermis was described as four different zones including non-suberized zone, patchy zone, continuous zone and fully suberized zone, and fully suberized zone was always the longest zone, accounting for about 50% of the root length, followed (in length) by the continuous, non-suberized and lastly the patchy zone (Chen, et al., 2019).

Abiotic and biotic stress tolerance

Besides the function as a barrier for water and nutrients, suberin lamellae in plant roots also contribute to abiotic and biotic stress tolerance. It has been found that suberization is induced during salt stress, cadmium (Cd) toxicity and ammonium stress, which suggest that the function of suberin

is to block the entry of toxic elements into the cytoplasm (Krishnamurthy et al., 2009; Liska et al., 2016; Ranathunge et al., 2016). Suberization is also induced under drought and waterlogged conditions, suggesting a role for suberin in preventing water and oxygen loss (Kotula et al., 2009; Shiono et al., 2014; Liska et al., 2016). In rice, suberization is enhanced during salt stress and the extent of suberin deposition in the primary roots is negatively correlated with Na uptake into the shoots as is also the case for hydraulic (Krishnamurthy et al., 2009; Krishnamurthy et al., 2011). In Arabidopsis, *horst* and *gpat5* mutants with reduced suberization show increased water transport and higher sensitivity to salt stress (Beisson et al., 2007; Ranathunge and Schreiber, 2011). In Arabidopsis, it was shown that suberization was reduced under Fe, Mn and Zn deficiencies, whereas S and K deficiencies lead to enhanced suberin (Barberon et al., 2016). The decrease in suberin was shown to be mediated by ethylene, whereas the increased suberization was controlled by abscisic acid (ABA). This endodermal suberin plasticity may reflect an adaptation of plant roots to cope with fluctuating nutrient availability by modulating the uptake of Fe, Mn and Zn and retain K and S in the stele (Barberon, 2017; Doblas et al., 2017). In the primary axis of barley roots, it was found that the suberization also responds to Mn deficiency, thus confirming the results from Arabidopsis. However, this response is not a linear process, as suberization was first reduced during mild Mn deficiency and then enhanced during strong Mn deficiency. Since the reduced suberin has secondary effects on the uptake of other nutrient elements, such as promoting K leakage from the stele, the enhanced suberization during strong Mn deficiency might favour retainment of K in the stele, thus maintaining nutrient homeostasis (Chen, et al., 2019).

Moreover, suberin might act as a barrier to prevent penetration by pathogens and nematode (Figure 2). The suberized endodermis serves as a line of defense preventing pathogens from invading the vascular tissues and spread throughout the plant (Ranathunge et al., 2008; Holbein et al., 2019; Kashyap et al., 2022). In soybean, it has been shown that there is a strong correlation between the exent of suberin and resistance to the fungus (Thomas et al., 2007). To colonize the root vasculature, the fungal hyphae have to penetrate the suberized layers and it was found that it took more time for hyphae growth in cultivars with high content of suberin (Ranathunge et al., 2008). Suberin also play important role in beneficial biotic interactions and the coordination between root suberin and the microbiome leads to a balancing of the plant ionome, which make plants adapt to abiotic stress condition (Salas-Gonzalez et al., 2020).

Perspectives

The growth of the human population will increase the demand for food in the future. However, the change of climate will intensify extreme weather conditions, for example drought, which might lead to decreased crop production. It is important to develop crops with increased yield and these crops should also be adapted to the specific soil conditions and climatic environment. The CSs and suberin lamellae in the endodermis of plant roots seem to play pivotal roles in controlling the uptake of water and nutrients and protect plants against biotic and abiotic threats (Barberon, 2017; Doblas et al., 2017; Kreszies et al., 2018). Understanding of the mechanisms underlying the

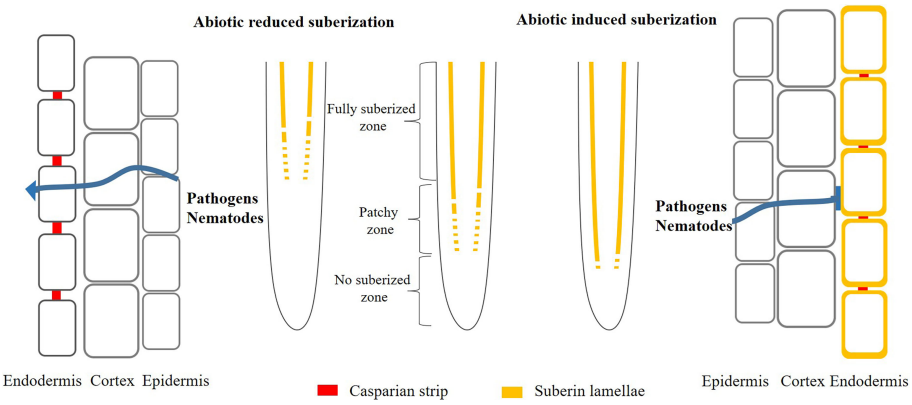

FIGURE 2
Model of abiotic induced/reduced suberization and its effect on pathogens and nematodes infection plants. Under normal conditions, plant roots deposit suberin in the endodermis. However, once the plant is stimulated by extern environment (nutrient deficiency or toxicity), it will deposit more or less suberin in the endodermis, thus protecting the plant from extern damage. Simultaneously, the change of suberization probably promote (decreased suberin) or prevent (enhanced suberin) the entry of pathogens and nematodes into the roots.

functions of these root barriers is important, as this knowledge might help to develop crop varieties with improved nutrient use efficiency and better tolerance towards e.g. nutrient deficiencies, drought, salt stress and pathogens.

Suberin is not only deposited in the endodermis of plant roots but also in the bundle sheath of plant leaves, the vascular tissues in roots and leaves are thus surrounded by suberized cells. As a transcellular barrier, suberin has a similar function both in root and leaves, which affects the fluxes of solutes and pathogen penetration. Since the vascular tissues are continuous in the whole plant, it is necessary to analyse the function of suberin as a barrier in leaves and roots at the same time. Thereby, better understanding of the function of suberin as a barrier can be obtained. Finally, the biotic and abiotic (nutrient deficiency or toxic) stress can exist at the same time in the field condition. It is necessary to analysis the effect of suberization on pathogen penetration under abiotic condition.

Author contributions

AC drafted and revised the manuscript. TL, ZW and XC revised the manuscript. All authors contributed to the article and approved the submitted version.

Funding

This work was supported by the China Agriculture Research System (CARS-02), the natural Science Foundation of Chongqing (4312100205), China Postdoctoral Science Foundation (2020M673105) and Innovation and Entrepreneurship Program for College Students (Southwest University, X202210635025).

Conflict of interest

The authors declare that the research was conducted in the absence of any commercial or financial relationships that could be construed as a potential conflict of interest.

Publisher's note

References

Andersen, T. G., Naseer, S., Ursache, R., Wybouw, B., Smet, W., De Rybel, B., et al. (2018). Diffusible repression of cytokinin signalling produces endodermal symmetry and passage cells. *Nature* 555 (7697), 529–533. doi: 10.1038/nature25976;

Barberon, M. (2017). The endodermis as a checkpoint for nutrients. *New Phytol.* 213 (4), 1604–1610. doi: 10.1111/nph.14140

Barberon, M., Vermeer, J. E., De Bellis, D., Wang, P., Naseer, S., Andersen, T. G., et al. (2016). Adaptation of root function by nutrient-induced plasticity of endodermal differentiation. *Cell* 164 (3), 447–459. doi: 10.1016/j.cell.2015.12.021

Beisson, F., Li-Beisson, Y., and Pollard, M. (2012). Solving the puzzles of cutin and suberin polymer biosynthesis. *Curr. Opin. Plant Biol.* 15 (3), 329–337. doi: 10.1016/j.pbi.2012.03.003

Beisson, F., Li, Y., Bonaventure, G., Pollard, M., and Ohlrogge, J. B. (2007). The acyltransferase GPAT5 is required for the synthesis of suberin in seed coat and root of arabidopsis. *Plant Cell* 19 (1), 351–368. doi: 10.1105/tpc.106.048033

Chen, A., Husted, S., Salt, D. E., Schjoerring, J. K., Persson, D. P., et al. (2019). The intensity of manganese deficiency strongly affects root endodermal suberization and ion homeostasis. *Plant Physiol.* 181 (2), 729–742. doi: 10.1104/pp.19.00507

De Bellis, D., Kalmbach, L., Marhavy, P., Daraspe, J., Geldner, N., and Barberon, M. (2022). Extracellular vesiculo-tubular structures associated with suberin deposition in plant cell walls. *Nat. Commun.* 13 (1), 1–11. doi: 10.1038/s41467-022-29110-0

Doblas, V. G., Geldner, N., and Barberon, M. (2017). The endodermis, a tightly controlled barrier for nutrients. *Curr. Opin. Plant Biol.* 39, 136–143. doi: 10.1016/j.pbi.2017.06.010

Do, T. H. T., Martinoia, E., and Lee, Y. (2018). Functions of ABC transporters in plant growth and development. *Curr. Opin. Plant Biol.* 41, 32–38. doi: 10.1016/j.pbi.2017.08.003

Enstone, D. E., Peterson, C. A., and Ma, F. (2003). Root endodermis and exodermis: Structure, function, and responses to the environment. *J. Plant Growth Regul.* 21 (4), 335–351. doi: 10.1007/s00344-003-0002-2

Franke, R., Briesen, I., Wojciechowski, T., Faust, A., Yephremov, A., Nawrath, C., et al. (2005). Apoplastic polyesters in arabidopsis surface tissues-a typical suberin and a particular cutin. *Phytochemistry* 66 (22), 2643–2658. doi: 10.1016/j.phytochem.2005.09.027

Franke, R., and Schreiber, L. (2007). Suberin-a biopolyester forming apoplastic plant interfaces. *Curr. Opin. Plant Biol.* 10 (3), 252–259. doi: 10.1016/j.pbi.2007.04.004

Geldner, N. (2013). The endodermis. *Annu. Rev. Plant Biol.* 64, 531–558. doi: 10.1146/annurev-arplant-050312-120050

Gou, M., Hou, G., Yang, H., Zhang, X., Cai, Y., Kai, G., et al. (2017). The MYB107 transcription factor positively regulates suberin biosynthesis. *Plant Physiol.* 173 (2), 1045–1058. doi: 10.1104/pp.16.01614

Graca, J. (2015). Suberin: the biopolyester at the frontier of plants. *Front. Chem.* 3, 62. doi: 10.3389/fchem.2015.00062

Graca, J., and Santos, S. (2007). Suberin: a biopolyester of plants' skin. *Macromol Biosci.* 7 (2), 128–135. doi: 10.1002/mabi.200600218

Holbein, J., Franke, R. B., Marhavy, P., Fujita, S., Gorecka, M., Sobczak, M., et al. (2019). Root endodermal barrier system contributes to defence against plant-parasitic cyst and root-knot nematodes. *Plant J.* 100 (2), 221–236. doi: 10.1111/tpj.14459

Hose, E., Clarkson, D. T., Steudle, E., Schreiber, L., and Hartung, W. (2001). The exodermis: A variable apoplastic barrier. *J. Exp. Bot.* 52, 2245–2264. doi: 10.1093/jexbot/52.365.2245

Kashyap, A., Jimenez-Jimenez, A. L., Zhang, W., Capellades, M., Srinivasan, S., Laromaine, A., et al. (2022). Induced ligno-suberin vascular coating and tyramine-derived hydroxycinnamic acid amides restrict ralstonia solanacearum colonization in resistant tomato. *New Phytol.* 234 (4), 1411–1429. doi: 10.1111/nph.17982

Kashyap, A., Planas-Marques, M., Capellades, M., Valls, M., and Coll, N. S. (2021). Blocking intruders: inducible physico-chemical barriers against plant vascular wilt pathogens. *J. Exp. Bot.* 72 (2), 184–198. doi: 10.1093/jxb/eraa444

Kolattukudy, P. E. (1981). Structure, biosynthesis, and biodegradation of cutin and suberin. *Ann. Rev. Plant Physiol.* 32, 539–567. doi: 10.1146/annurev.pp.32.060181.002543

Kolattukudy, P. E. (2001). Polyesters in higher plants. *Adv. Biochem. Eng. Biotechnol.* 71, 1–49. doi: 10.1007/3-540-40021-4_1

Kotula, L., Ranathunge, K., and Steudle, E. (2009). Apoplastic barriers effectively block oxygen permeability across outer cell layers of rice roots under deoxygenated conditions: roles of apoplastic pores and of respiration. *New Phytol.* 184 (4), 909–917. doi: 10.1111/j.1469-8137.2009.03021.x

Kreszies, T., Schreiber, L., and Ranathunge, K. (2018). Suberized transport barriers in arabidopsis, barley and rice roots: From the model plant to crop species. *J. Plant Physiol.* 227, 75–83. doi: 10.1016/j.jplph.2018.02.002

Kreszies, T., Shellakkutti, N., Osthoff, A., Yu, P., Baldauf, J. A., Zeisler-Diehl, V. V., et al. (2019). Osmotic stress enhances suberization of apoplastic barriers in barley seminal roots: analysis of chemical, transcriptomic and physiological responses. *New Phytol.* 221 (1), 180–194. doi: 10.1111/nph.15351

Krishnamurthy, P., Ranathunge, K., Franke, R., Prakash, H. S., Schreiber, L., and Mathew, M. K. (2009). The role of root apoplastic transport barriers in salt tolerance of rice (Oryza sativa l.). *Planta* 230 (1), 119–134. doi: 10.1007/s00425-009-0930-6

Krishnamurthy, P., Ranathunge, K., Nayak, S., Schreiber, L., and Mathew, M. K. (2011). Root apoplastic barriers block na+ transport to shoots in rice (Oryza sativa l.). *J. Exp. Bot.* 62 (12), 4215–4228. doi: 10.1093/jxb/err135

Landgraf, R., Smolka, U., Altmann, S., Eschen-Lippold, L., Senning, M., Sonnewald, S., et al. (2014). The ABC transporter ABCG1 is required for suberin formation in potato tuber periderm. *Plant Cell* 26 (8), 3403–3415. doi: 10.1105/tpc.114.124776

Lashbrooke, J., Cohen, H., Levy-Samocha, D., Tzfadia, O., Panizel, I., Zeisler, V., et al. (2016). MYB107 and MYB9 homologs regulate suberin deposition in angiosperms. *Plant Cell* 28 (9), 2097–2116. doi: 10.1105/tpc.16.00490

Legay, S., Guerriero, G., Andre, C., Guignard, C., Cocco, E., Charton, S., et al. (2016). MdMyb93 is a regulator of suberin deposition in russeted apple fruit skins. *New Phytol.* 212 (4), 977–991. doi: 10.1111/nph.14170

Li-Beisson, Y., Shorrosh, B., Beisson, F., Andersson, M. X., Arondel, V., Bates, P. D., et al. (2013). Acyl-lipid metabolism. *Arabidopsis Book* 11, e0161. doi: 10.1199/tab.0161

Li, B., Kamiya, T., Kalmbach, L., Yamagami, M., Yamaguchi, K., Shigenobu, S., et al. (2017). Role of LOTR1 in nutrient transport through organization of spatial distribution of root endodermal barriers. *Curr. Biol.* 27 (5), 758–765. doi: 10.1016/j.cub.2017.01.030

Liska, D., Martinka, M., Kohanova, J., and Lux, A. (2016). Asymmetrical development of root endodermis and exodermis in reaction to abiotic stresses. *Ann. Bot.* 118 (4), 667–674. doi: 10.1093/aob/mcw047

Lulai, E. C., and Corsini, D. L. (1998). Differential deposition of suberin phenolic and aliphatic domains and their roles in resistance to infection during potato tuber (Solanum tuberosum l.) wound-healing. *Physiol. Mol. Plant Pathol.* 53 (4), 209–222. doi: 10.1006/pmpp.1998.0179

Lulai, E. C., Suttle, J. C., and Pederson, S. M. (2008). Regulatory involvement of abscisic acid in potato tuber wound-healing. *J. Exp. Bot.* 59 (6), 1175–1186. doi: 10.1093/jxb/ern019

Molina, I., Li-Beisson, Y., Beisson, F., Ohlrogge, J. B., and Pollard, M. (2009). Identification of an arabidopsis feruloyl-coenzyme a transferase required for suberin synthesis. *Plant Physiol.* 151 (3), 1317–1328. doi: 10.1104/pp.109.144907

Nawrath, C., Schreiber, L., Franke, R. B., Geldner, N., Reina-Pinto, J. J., and Kunst, L. (2013). Apoplastic diffusion barriers in arabidopsis. *Arabidopsis Book* 11, e0167. doi: 10.1199/tab.0167

Perumalla, C. J., Peterson, C. A., and Enstone, D. E. (1990). A survey of angiosperm species to detect hypodermal casparian bands .1. roots with a uniseriate hypodermis and epidermis. *Botanical J. Linn. Soc.* 103 (2), 93–112. doi: 10.1111/j.1095-8339.1990.tb00176.x;

Pollard, M., Beisson, F., Li, Y., and Ohlrogge, J. B. (2008). Building lipid barriers: biosynthesis of cutin and suberin. *Trends Plant Sci.* 13 (5), 236–246. doi: 10.1016/j.tplants.2008.03.003

Ranathunge, K., Kim, Y. X., Wassmann, F., Kreszies, T., Zeisler, V., and Schreiber, L. (2017). The composite water and solute transport of barley (Hordeum vulgare) roots: effect of suberized barriers. *Ann. Bot.* 119 (4), 629–643. doi: 10.1093/aob/mcw252

Ranathunge, K., and Schreiber, L. (2011). Water and solute permeabilities of arabidopsis roots in relation to the amount and composition of aliphatic suberin. *J. Exp. Bot.* 62 (6), 1961–1974. doi: 10.1093/jxb/erq389

Ranathunge, K., Schreiber, L., Bi, Y. M., and Rothstein, S. J. (2016). Ammonium-induced architectural and anatomical changes with altered suberin and lignin levels significantly change water and solute permeabilities of rice (Oryza sativa l.) roots. *Planta* 243 (1), 231–249. doi: 10.1007/s00425-015-2406-1

Ranathunge, K., Schreiber, L., and Frank, R. (2011). Suberin research in the genomics era–new interest for an old polymer. *Plant Sci.* 180 (3), 399–413. doi: 10.1016/j.plantsci.2010.11.003

Ranathunge, K., Thomas, R. H., Fang, X. X., Peterson, C. A., Gijzen, M., and Bernards, M. A. (2008). Soybean root suberin and partial resistance to root rot caused by phytophthora sojae. *Phytopathology* 98 (11), 1179–1189. doi: 10.1094/PHYTO-98-11-1179

Salas-Gonzalez, I., Reyt, G., Flis, P., Custodio, V., Gopaulchan, D., Bakhoum, N., et al. (2020). Coordination between microbiota and root endodermis supports plant mineral nutrient homeostasis. *Science*. 371(6525). doi: 10.1126/science.abd0695

Schreiber, L. (2010). Transport barriers made of cutin, suberin and associated waxes. *Trends Plant Sci.* 15 (10), 546–553. doi: 10.1016/j.tplants.2010.06.004

Shiono, K., Ando, M., Nishiuchi, S., Takahashi, H., Watanabe, K., Nakamura, M., et al. (2014). RCN1/OsABCG5, an ATP-binding cassette (ABC) transporter, is required for hypodermal suberization of roots in rice (Oryza sativa). *Plant J.* 80 (1), 40–51. doi: 10.1111/tpj.12614

Shukla, V., Han, J. P., Cleard, F., Lefebvre-Legendre, L., Gully, K., Flis, P., et al. (2021). Suberin plasticity to developmental and exogenous cues is regulated by a set of MYB transcription factors. *Proc. Natl. Acad. Sci. U.S.A.* 118 (39). doi: 10.1073/pnas.2101730118

Thomas, R., Fang, X., Ranathunge, K., Anderson, T. R., Peterson, C. A., and Bernards, M. A. (2007). Soybean root suberin: anatomical distribution, chemical composition, and relationship to partial resistance to phytophthora sojae. *Plant Physiol.* 144 (1), 299–311. doi: 10.1104/pp.106.091090

Tylova, E., Peckova, E., Blascheova, Z., and Soukup, A. (2017). Casparian bands and suberin lamellae in exodermis of lateral roots: an important trait of roots system response to abiotic stress factors. *Ann. Bot.* 120 (1), 71–85. doi: 10.1093/aob/mcx047

Ursache, R., De Jesus Vieira Teixeira, C., Dénervaud Tendon, V., Gully, K., De Bellis, D., Schmid-Siegert, E., et al. (2021). GDSL-domain proteins have key roles in suberin polymerization and degradation. *Nature Plants* 7 (3), 353–364. doi: 10.1038/s41477-021-00862-9

Vishwanath, S. J., Delude, C., Domergue, F., and Rowland, O. (2015). Suberin: biosynthesis, regulation, and polymer assembly of a protective extracellular barrier. *Plant Cell Rep.* 34 (4), 573–586. doi: 10.1007/s00299-014-1727-z

Waduwara, C. I., Walcott, S. E., and Peterson, C. A. (2008). Suberin lamellae of the onion root endodermis: their pattern of development and continuity. *Botany* 86 (6), 623–632. doi: 10.1139/B08-038

Yadav, V., Molina, I., Ranathunge, K., Castillo, I. Q., Rothstein, S. J., and Reed, J. W. (2014). ABCG transporters are required for suberin and pollen wall extracellular barriers in arabidopsis. *Plant Cell* 26 (9), 3569–3588. doi: 10.1105/tpc.114.129049

Zimmermann, M., Hartmann, K., Schreiber, L., and Steudle, E. (2000). Chemical composition of apoplastic transport barriers in relation to radial hydraulic conductivity of corn roots (*Zea mays l.*). *Planta* 210, 302–311. doi: 10.1007/PL00008138

frontiers | Frontiers in Plant Science

TYPE Original Research
PUBLISHED 30 November 2022
DOI 10.3389/fpls.2022.1055213

OPEN ACCESS

EDITED BY
Qiong Zhang,
University of California, Berkeley,
United States

REVIEWED BY
Xiaodong Wang,
Agricultural University of Hebei, China
Zeguang Liu,
Université de Genève, Switzerland
Huan Luo,
Chungnam National University,
South Korea

*CORRESPONDENCE
Dongfang Ma
madf@yangtzeu.edu.cn
Huiquan Shen
jsycshq@163.com

SPECIALTY SECTION
This article was submitted to Technical Advances in Plant Science, a section of the journal Frontiers in Plant Science

RECEIVED 27 September 2022
ACCEPTED 14 November 2022
PUBLISHED 30 November 2022

CITATION
Xu X, Cheng Y, Fang Z, Yin J, Shen H and Ma D (2022) Identification and utilization of a new *Bacillus amyloliquefaciens* XY-1 against Fusarium head blight.
Front. Plant Sci. 13:1055213.
doi: 10.3389/fpls.2022.1055213

Identification and utilization of a new *Bacillus amyloliquefaciens* XY-1 against Fusarium head blight

Xiao Xu[1,2], Yifan Cheng[2], Zhengwu Fang[1], Junliang Yin[1], Huiquan Shen[2]* and Dongfang Ma[1]*

[1]Key Laboratory of Sustainable Crop Production in the Middle Reaches of the Yangtze River (Co-construction by Ministry and Province), College of Agriculture, Yangtze University, Jingzhou, China, [2]Jiangsu Academy of Agricultural Sciences, Jiangsu Coastal Area Institute of Agricultural Sciences, Yancheng, China

Fusarium head blight (FHB) is a global wheat grain disease caused by *Fusarium graminearum*. Biological control of FHB is considered to be an alternative disease management strategy that is environmentally benign, durable, and compatible with other control measures. In this study, to screen antagonistic bacteria with the potential to against FHB, 45 strains were isolated from different tissues of wheat. Among them, seven strains appeared to effectively inhibit *F. graminearum* growth, the antagonistic bacterium named XY-1 showed a highly antagonistic effect against FHB using dual culture assays. The strain XY-1 was identified as Bacillus amyloliquefaciens by 16S rDNA sequence. Antibiotic tolerance of antagonistic bacteria showed that XY-1 had antagonistic activity against Colletotrichum gloeosporioides, Rhizoctonia solani, Sclerotium rolfsii, and Alternaria alternata. Nutrition tests showed that the most suitable carbon and nitrogen sources were glucose and beef extract, respectively. The optimum growth temperature and pH value were 28 ℃ and 7.4. Antibiotics tolerance cultivation showed that XY-1 had strong resistance to Chloramphenicol and Ampicillin. Wheat spikes inoculation antagonism tests showed that strain XY-1 displayed strong antifungal activity against *F. graminearum*. Our study laid a theoretical foundation for the application of strain XY-1 as a biological agent in the field to control FHB.

KEYWORDS

***Bacillus amyloliquefaciens*, Biological control, Fusarium head blight, *Antagonistic bacterium*, XY-1**

Introduction

Fusarium head blight (FHB) is a global wheat grain disease caused by *Fusarium graminearum* (Senatore et al., 2021). The incidence of FHB increases with the increase in the area under wheat cultivation (Liu et al., 2016; Li et al., 2017). Moreover, the byproduct (deoxynivalenol (DON)) of wheat infected by *F. graminearum* can cause human and livestock poisoning (Li et al., 2022). As a consequence, wheat grains with severe head blight infection cannot be processed into flour or feed, resulting in significant economic losses (Miedaner et al., 2003; William et al., 2004; Ma et al., 2015). FHB is prevalent in the winter wheat area of the Yangtze River Basin and in areas with relatively high humidity, yield loss can reach up to 80% in some wheat fields (Zhang et al., 2014). Chemical control is still the best control method against *F. graminearum*. However, there is growing concern about the negative effects of chemical pesticides, particularly about their potentially toxic effects on humans and animals (Crane et al., 2013). Thus, alternative disease management strategies are needed to fulfill the consumer demand for pesticide-free food while maintaining environmental safety (Lamichhane et al., 2016). The use of biological control is being considered as a good alternative in the prevention and control of plant diseases (Rahman et al., 2018).

Plants provide good habitats for endophytes, and they have a wide range of beneficial biological control functions for host plants. Existing studies had shown that endophytes affect host plants through their own metabolites and signal transduction. Endophytic bacteria could secrete peptide (lipopeptide), fat gambogic pyocyanin (pyoluterin), pyrrole cephalosporins (pyrolnit rin), as well as chitinase and glucanase such as antibacterial materials (Sun et al., 2006). These antibacterial substances could degrade bacterial mycelia or pathogenic factors and had good antibacterial effect on plant pathogens. *Trichoderma afroharzianum*, evaluated for the first time in Algeria as biocontrol agent, is a promising biocontrol approach against FCR and FHB (Bouanaka et al., 2021).

Bacillus amyloliquefaciens has been widely identified as a biological control microbe against *F. graminearum*. *Bacillus amyloliquefaciens* FZB42 is a Gram-positive plant growth-promoting bacterium with an impressive capacity to synthesize nonribosomal secondary metabolites with fungal activity (Hanif et al., 2019). The commercially available strain *B. amyloliquefaciens* FZB42 showed strong activity against *F. graminearum* and the lipopeptide *bacillomycin* D, produced by FZB42, was shown to contribute to the antifungal activity (Gu et al., 2017). A bacterial strain (S76-3, identified as *Bacillus amyloliquefaciens*) that was isolated from diseased wheat spikes in the field displayed strong antifungal activity against *F. graminearum* (Gong et al., 2015). *B. amyloliquefaciens* JCK-12 could be used as an available biocontrol agent or as a chemosensitizer to chemical fungicides for controlling FHB disease and as a strategy for preventing the contamination of harvested crops with mycotoxins (Kim et al., 2017). The lower iturin levels on wheat spikes in the field could be a major factor limiting disease control in field settings (Crane et al., 2013). In this study, endophytic bacterium named XY-1 was isolated from healthy wheat plants collected from areas with severe wheat head blight. After the optimization of culture conditions, physiological and biochemical identification, resistance examination and 16S rDNA sequence analysis were carried out to determine their antibiotic tolerance and biological species. The resulting data provided a theoretical basis for an alternative method of biological control of FHB.

Materials and methods

Pathogenic fungal strains

Fusarium graminearum was provided by the Institute of Plant Protection, Jiangsu Academy of Agricultural Sciences. *Colletotrichum gloeosporioides* (an apple fruit pathogen), *Rhizoctonia solani* (a cotton pathogen), *Sclerotium rolfsii* (a rice pathogen), and *Alternaria alternata* (a pear fruit pathogen) were acquired from the lab of Pathogenic Fungi and Genomics in College of Agriculture, Yangtze University, Jingzhou, China.

Isolation and purification of endophytic bacteria

The samples were collected by five-point sampling method in Jingzhou, Hubei Province from plants grown in a field with severe wheat scab outbreak (N30°21′32.53″ E112°08′22.05″). The roots, stems, leaves, and spikelets of wheat were cut into small segments of about 5 cm and washed with water for 30 min. The following operations were carried out on a clean bench: samples were washed 4 times with sterile water, soaked in 75% ethanol for 5 min, washed with sterile water two times, soaked in 1% mercuric chloride for 3 min, and finally rinsed three times with sterile water. The sterilized plant material was placed in a sterile mortar containing an appropriate amount of quartz sand. The sample was grinded with 10 ml of sterile water, 100 µL of the solution was plated on Potato Dextrose Agar (PDA: potato 20 g/L, glucose 20 g/L, agar 15 g/L) and Nutrient Agar (NA: peptone 10 g/L, beef extract 3 g/L, glucose 2.5 g/L, agar 18 g/L) kept at a constant temperature of 28°C After three days of culture, colonies were separated and cultured on PDA and NA media, respectively. Pure strains were obtained after three times' sub-culturing.

Dual culture assays of antagonistic strain

Adopting dual culture assays tested the antagonistic effects of isolations on *Fusarium graminearum* (Su et al., 2010). In each repetition, a 5 mm mycelium pellet of *F. graminearum* was inoculated in the central portion of the PDA medium with a diameter of 90 mm, and the endophyte was attached to the periphery. Plates grown with *F. graminearum* alone served as controls, and three repetitions were set for each treatment. These were cultured at 28°C in the dark for 3 to 4 days until control dishes were covered with the *F. graminearum.* The inhibition zone was measured and statistically analyzed. The diameter of the zone of inhibition was the growth width of the antagonistic colonies, measured in a criss-cross method. Diameter of inhibition zone is calculated using the following formula: (A1 +A2)/2, where A1 and A2 are respectively the diameter of inhibition zone measured by the criss-cross method. Two independent experimental replicates were performed for each strain. Dual culture assays were used to detect the inhibitory effect of antagonistic endophyte on the previous pathogenic fungi. Three replicates were performed for each treatment.

Classification of endophyte isolates

DNA of the antagonize endophytes were extracted by using CTAB method (Liu et al., 2019). The extracted DNA was used as a template for polymerase chain reaction (PCR) to amplify with the 16S rDNA universal primers (27F: 5'-CAGAGTTT GATCCTGGCT-3', 1492R: 5'-AGGAGGTGATCCAGCCGCA-3') (Redburn and Patel, 1993). Amplification process order for: 94°C 3 min, 94°C 40 s, 65°C 40 s, 72°C 1 min, a total of 30 cycles; then 72°C 8 min. The amplified product was sequenced by Sangon Biotech. The sequencing results were used to perform BLAST searching on the NCBI website (http://www.ncbi.nlm.nih.gov/) to determine the species level. Phylogenetic tree was completed by the phylogenetic software MEGA 7.0 (Yin et al., 2017).

Antibiotic tolerance of antagonistic bacteria

Five common antibiotics, *chloramphenicol* (Ch1), *ampicillin* (Amp), *tetracycline* (Tet), *streptomycin* (Str) and *kanamycin* (Kan), were used to test the tolerance of strain XY-1. Bacterial suspensions from the colonies developed in NB were standardized to 108 CFU/mL and transferred (10 µL) to NA plates containing different concentrations of antibiotics (25 µg/mL CH1, 100 µg/mL Amp, 25 µg/mL Tet, 50 µg/mL Str, 10 µg/mL Kan).The plates were incubated at 28°C for 48 hand evaluated for the presence of bacterial growth. The colony diameter of 0-8 mm indicated that the strain had no drug resistance to antibiotics, the colony diameter of 9-17 mm had weak drug resistance, and the colony diameter larger than 17 mm had drug resistance (Xia et al., 2019).

Optimization of culture conditions of antagonistic bacteria

The antagonistic bacteria was cultured in NA liquid medium and incubated in the dark at 28°C and pH 7.0 with shaking at 180 rpm. The OD_{600} value was measured every 4 h until 36 h, and then measured every 12 h until 84 h, NA liquid medium alone was used as a control. At each time point, OD_{600} was measured by a spectrophotometer at an absorbance wavelength of 600 nm (Zhang et al., 2019).

The pH was adjusted to 3.0, 5.0, 6.0, 7.0, 7.4, 8.0, 10.0, and 12.0 with NaOH and HCl, respectively, and 0.1 mL of bacterial suspensions was cultured in 100 mL of NA liquid medium with different pH values, shaken at 28°C, 180 r/min, and the OD_{600} value was measured at 600 nm after 48 h. NA liquid medium alone was used as a control, and three independent biological replicates were set for each treatment.

The optimum growth temperature curve was drawn with 0.1 mL of bacterial suspensions in 100 mL of NA culture medium (pH 7.4). The endophyte bacterial suspensions was cultured at different temperatures (4°C,10°C, 16°C, 22°C, 28°C, 34°C, 40°C, 46°C, and 52°C). The OD_{600} value was measured at 600 nm after 48 h. NA liquid medium alone was used as a control, and three independent biological replicates were set for each treatment.

A liquid medium with glucose (2.5 g/L) and peptone (10 g/L) as carbon source and nitrogen source, respectively, was used as the basic medium. Then, the carbon source of glucose was replaced by sucrose and lactose, and the nitrogen source of peptone was replaced by beef extract or ammonium nitrate to explore the best combination of carbon and nitrogen sources for endophyte fermentation.

Effect of culture supernatant on mycelial morphology

0.5 mL of bacterial suspensions was inoculated into 50 mL of the optimized liquid medium and incubated for 2 days at 28°C with shaking at 180 r/min. The culture supernatant was collected from the culture broth by centrifugation at 8,000 rpm for 30 min at 4°C. The bacteria XY-1 in the culture supernatant was filtered out through a 0.22 µm microfiltration membrane. One group was poured 5 mL of the culture broth into a petri dish containing 10 mL of PDA medium, and inoculated the center of the dish with *F. graminearum* mycelia plug. The other group was inoculated with *F.*

graminearum mycelia plug alone. Then they were cultured in a constant temperature incubator at 28°C for 3 to 5 days. The medium at the junction of the inhibition ring was observed under a microscope, and the morphological characteristics of the mycelium of the treatment group and the control group were compared. Each treatment contains 3 replicates.

Wheat spikes inoculation antagonism tests

Testing for the antagonistic effect of endophyte against *F. graminearum* was performed on detached spikelets from wheat cultivar "Emai 170". Detached spikelets were soaked in a suspension of endophyte or control water for 2 min, before being placed on plates filled with water agar medium (3 g/L). Five days later, a conidia suspension of *Fusarium graminearum* (10^5 conidia/mL) was sprayed on spikelets. Under conditions of 20/15°C day/night temperature, 16/8 h light/dark photoperiod, and 65% of relative humidity. Two weeks later, morbidity, disease index and 1000-grain weight was recorded. Each treatment consisted of two independent experimental replicates with at least 30 spikelets per replicate.

Statistical analysis

Data were subjected to analysis of variance using SPSS 19.0, where F tests were significant at $p < 0.05$, and the means were separated by Duncan's Multiple Range test at $p < 0.05$.

Results

Selection of endophytic bacteria

According to the differences of colony morphology and color, a total of 45 bacterial strains were isolated from different tissues of wheat. Seven strains antagonistic to *Fusarium graminearum* were screened by dual culture assays. Among them, the stain XY-1 isolated from root, exhibited the best antagonistic effect. The average diameter of the inhibition zone was larger than other strains, which was 29.7 mm (Figure 1). Therefore, XY-1 was selected for further study.

Anti-fungal activity of strain XY-1

Strain XY-1 was tested for antagonism against several common crops and fruit tree pathogens by using dual culturing assays. The results showed that XY-1 displayed an inhibitory effect on the growth of four tested pathogens, namely *Colletotrichum gloeosporioides*, *Rhizoctonia solani*, *Sclerotium rolfsii*, and *Alternaria alternate*. The zone of inhibition ranged from 17.7 to 32 mm. In addition, XY-1 exhibited the best inhibitory effect on *Alternaria alternata*, followed by *Sclerotium rolfsii* (Table 1).

The optimal fermentation conditions of strain XY-1

In order to observe the growth of strain XY-1, the bacterial solution was inoculated into the NA liquid medium, incubated at 28°C with shaking (160 r/min), and its OD_{600} value was measured at a wavelength of 600 nm. As shown in Figure 2A, XY-1 was in the exponential phase within 24 h after inoculation into the NA culture medium; it was in the stable phase within 24-60 h of inoculation; it entered the recession phase after 60 h (Figure 2A).

Figure 2B showed that XY-1 could grow at pH 4.0-10.0, but not at pH 3.0. The pH range for growth was 5.0 to 9.0, with an optimum pH of 7.4 (Figure 2B). Strain XY-1 was placed in NA broth at pH 7.4 and placed at different temperatures. The results showed that strain XY-1 could grow at 10–50°C with an optimum temperature of 28°C (Figure 2C).

In this experiment, sucrose, glucose and lactose were used as carbon sources, and peptone, beef extract and ammonium nitrate were used as nitrogen sources. The results showed that XY-1 could utilize all carbon and nitrogen sources tested in this study. Among them, glucose was the most suitable carbon source, and beef extract was the most suitable nitrogen source (Figure 2D).

Antibiotics tolerance cultivation

In order to test the resistance of the strain XY-1 to common antibiotics, *chloramphenicol* (Ch1), *streptomycin* (Str), *tetracycline* (Tet), *kanamycin* (Kan), and *ampicillin* (Amp) was placed in NA liquid medium, respectively. The plaque diameters were counted after culturing in a constant temperature incubator at 28°C for 2 days. The results showed that the resistance of XY-1 to the five antibiotics was different, that XY-1 had better resistance to *chloramphenicol* and *ampicillin* (Table 2).

Identification of strain XY-1

The sequencing data showed that the length of the 16S rDNA sequence of the strain XY-1 was 1207 bp. The sequence was blast aligned in the NCBI database (http://www.ncbi.nlm.

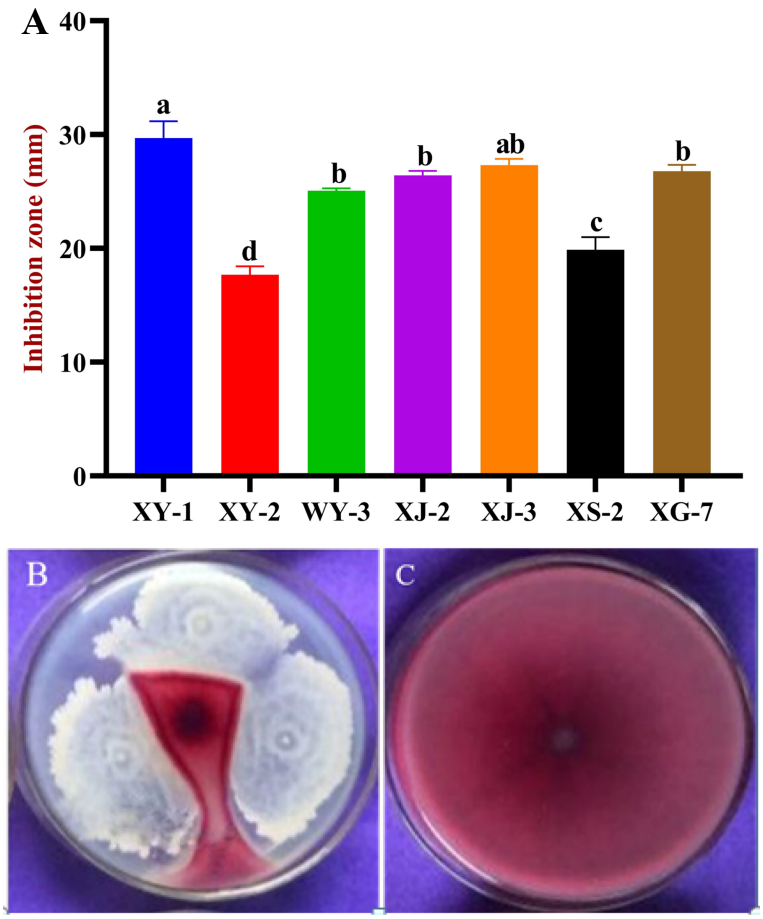

FIGURE 1
Antagonistic effects of endophytic bacteria on *Fusarium graminearum*. **(A)** Inhibition effects of six endophyte bacteria against *F. graminearum*. **(B)** The antagonistic effect of XY-1 against *F. graminearum*. **(C)** *F. graminearum* growth alone. Values are means ± SD (n = 10). Different letters above the bars indicate a significant difference at $p < 0.05$.

nih.gov/), and the phylogenetic tree was constructed using Mega7.0 software (Figure 3). The analysis showed that XY-1 belonged to *Bacillus*, and the sequence similarity with *Bacillus amyloliquefaciens* (EU855184.1) was 95%. Based on its physiological and biochemical characteristics, the strain XY-1 was preliminarily classified as *Bacillus amyloliquefaciens*.

TABLE 1 Antagonistic activities of strain XY-1 against other four plant fungal pathogens.

Pathogens	Average inhibition zone diameter (mm)
Colletotrichum gloeosporioides	22.10 ± 3.11a
Sclerotium rolfsii	29.91 ± 0.90b
Rhizoctonia solani	19.80 ± 0.70c
Alternaria alternata	30.00 ± 1.39d

Data are means ± SD (n = 3). Different letters indicate a significant difference among treatments at p < 0.05 level. The data were subjected to one-way ANOVA with Duncan's multiple range test using SPSS 19.0 software.

Culture supernatant affects *F. graminearum* growth

The medium at the junction of the inhibition ring was observed under a microscope, and the morphological characteristics of the mycelium of the treatment group and the control group were compared. The results showed that the hyphae of *F. graminearum* grew alone normally (Figure 4A), and the hyphae of the pathogenic fungi with culture supernatant of XY-1 were obviously inhibited (Figure 4B). As shown in Figure 4C, the mycelium morphology of *F. graminearum* grown alone was normal, slender and long (Figure 4C). By comparison, the mycelium morphology of *F. graminearum* with culture supernatant was malformation, thick and short (Figure 4D).

10.3389/fpls.2022.1055213

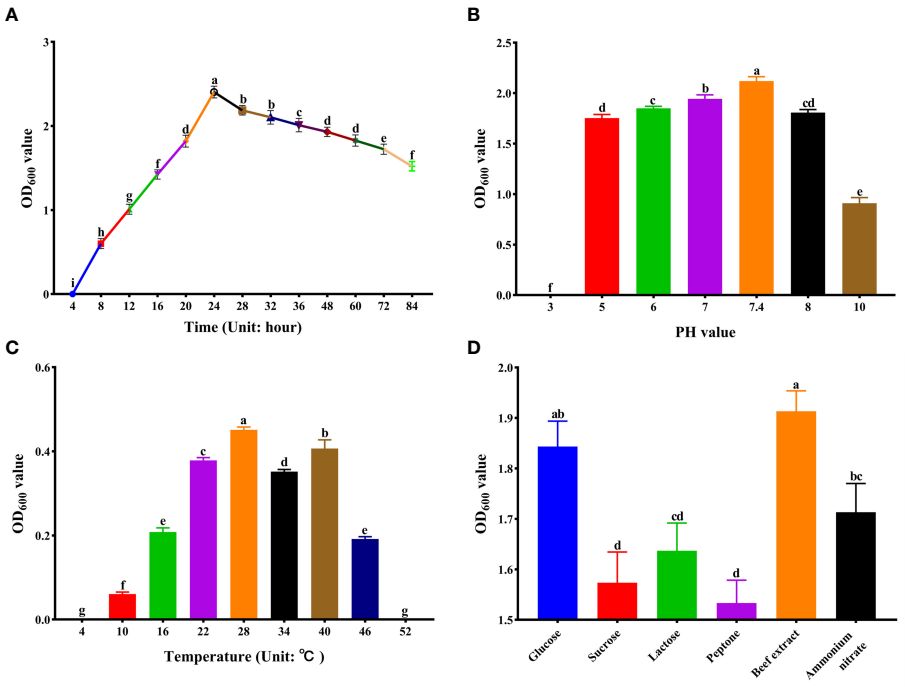

FIGURE 2
Optimization of Culture Conditions for strain XY-1. **(A)** Growth curve. **(B)** Growth in different pH. **(C)** Growth in different temperatures. **(D)** Growth in different carbon and nitrogen sources. Values are means ± SD (n = 6). Different letters above the bars indicate a significant difference at $p < 0.05$.

The antagonistic effect of endophyte on *F. graminearum*

The antagonistic effect of XY-1 against *F. graminearum* was further tested in isolated wheat spikelets. Spikes inoculated with alone developed typical wheat head blight symptoms within two weeks, and inoculated with distilled water alone did not cause any visible disease symptom (Figure 5A). As shown in Figure 5B, CK were the isolated spikelets that were not inoculated with *Fusarium graminearum*, and they were symptomless. The incidence rate of isolated spikelets that were immersed in the filtered culture supernatant and then inoculated with PH-1 was 13.5%, and the incidence rate of the isolated spikelets that were inoculated with *F. graminearum* alone was 100%. The results showed that the culture supernatant of strain XY-1 reduced the incidence of *F. graminearum* by 86.5% (Figure 5B). The study showed that bacteria XY-1 reduced the disease index by 56.7% (Figure 5C). The 1000-grain weight measurement data for each group of wheat showed that the group inoculated with *F. graminearum* alone was 15 g, the treatment group with culture supernatant of XY-1 just reduced by 3g compared with CK (Figure 5D). The application of XY-1 greatly reduced the yield decline caused by FHB.

TABLE 2 Antagonistic bacteria XY-1 drug resistance experimental results.

Antibiotic	Concentration (mg/mL)	Average colony diameter(mm)	Tolerance
Chloramphenicol (Ch1)	25	25.00	Strong effect
Ampicillin (Amp)	100	25.30	Strong effect
Tetracycline (Tet)	25	16.80	weak effect
Streptomycin (Str)	50	8.00	no effect
Kanamycin (Kan)	10	8.00	no effect
CK	—	43.00	———

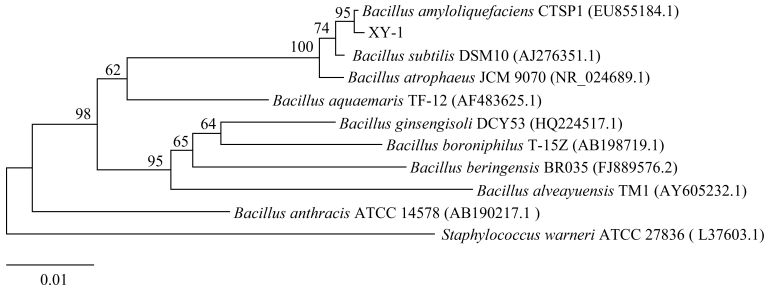

FIGURE 3
Phylogenetic trees of strain XY-1 based on 16S rDNA sequence. The phylogenetic tree was constructed using MEGA7.0 software with the maximum likelihood method. Bar indicates the numbers of nucleotide substitutions per site.

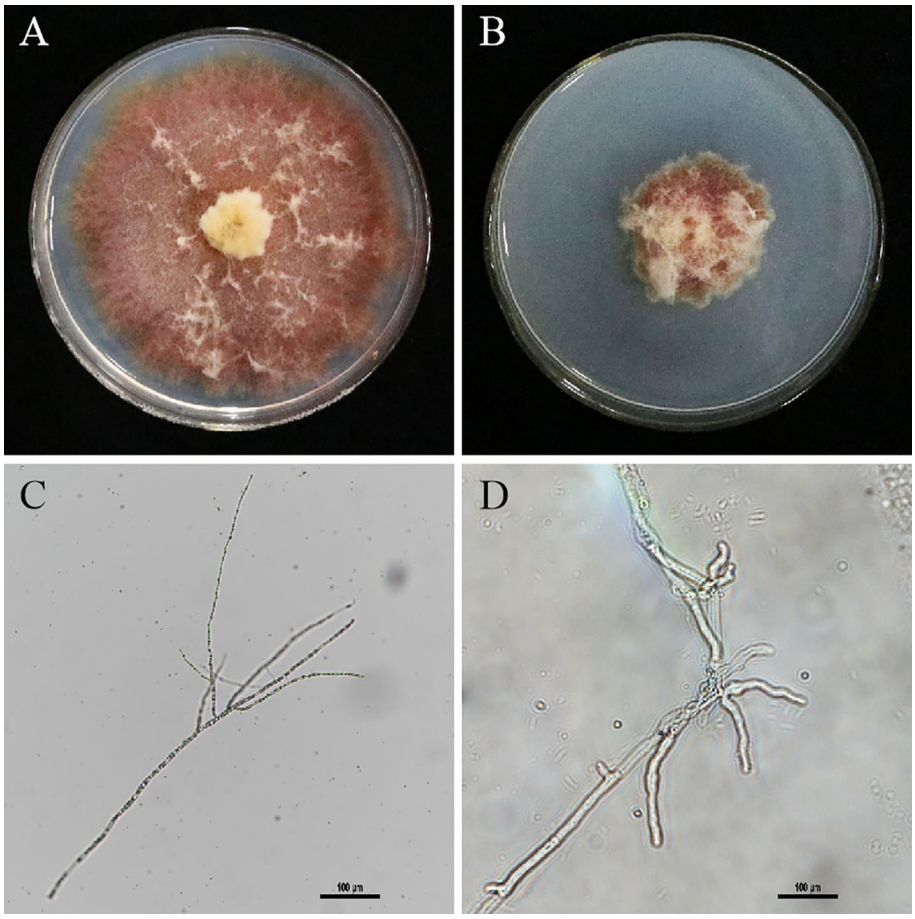

FIGURE 4
Effect of culture broth on mycelium morphology. **(A)** *F. graminearum* growth alone. **(B)** The antagonistic effect culture supernatant against *F. graminearum*. **(C)** The mycelium morphology of *F. graminearum* grown alone under microscope. **(D)** The mycelium morphology of Figure B with culture supernatant under microscope.

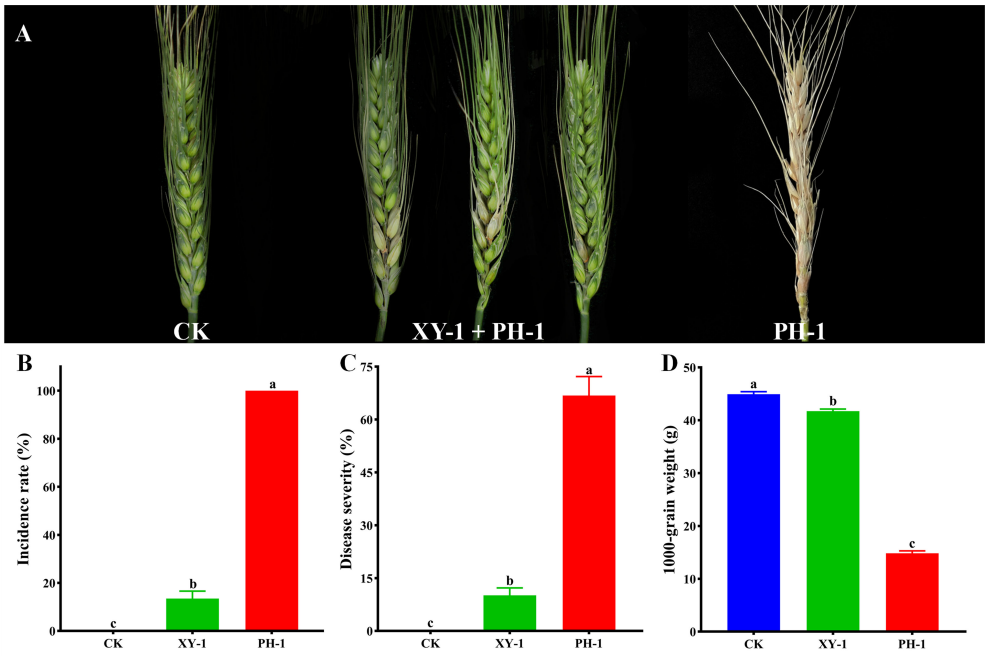

FIGURE 5
Antagonistic of XY-1 against *F. graminearum* on spikes. **(A)** Distilled water was used as a CK, symptoms of wheat heads inoculated with XY-1 plus PH-1 and FHB alone; **(B)** Incidence of wheat scab of CK, XY-1 plus PH-1 and PH-1 alone; **(C)** Disease index of CK, XY-1 plus PH-1 and PH-1 alone; **(D)** 1000-grain weight of CK, XY-1 plus PH-1 and PH-1 alone. Incidence is calculated using the following formula: n/N × 100%, where n represents the number of diseased wheat spikes, respectively, and N represents the total number of wheat spikes used. Disease index is calculated using the following formula: (n0 × 0 + n1 × 1 + n2 × 2 + n3 × 3)/3N × 100%, where n0, n1, n2, and n3 represent the number of wheat heads exhibiting disease levels 0, 1, 2, and 3, respectively, and N represents the total number of wheat spikes used. Values are means ± SD (n = 6). Different letters above the bars indicate a significant difference at $p < 0.05$.

Discussion

The rapid occurrence and prevalence of FHB in warm and humid environments not only causes serious economic losses, but also causes food safety problems. Therefore, FHB has become the important limiting factors threatening the safe production of wheat. However, biological control of wheat and other crops in the early stage can reduce the outbreak of head blight and protect the yield and quality of crops (Li et al., 2007; Wen et al., 2012). In this study, experimental strains were collected from the occurrence area of FHB. And a strain XY-1 which was identified as *Bacillus amyloliquefaciens*, had a highly antagonistic effect on *F. graminearum*.

Bacillus amyloliquefaciens has strong stress resistance, and its secondary metabolites have different degrees of inhibitory effect on all kinds of pathogens. It is one of the main strains in biocontrol research at present. *B. amyloliquefaciens* can induce host defense responses and increase the enzymatic activity associated with disease resistance. The content of growth-promoting hormones such as gibberellin and auxin in plants inoculated with *B. amyloliquefaciens* was higher, and the activities of defense-related enzymes such as peroxidase were also higher (Zhang et al., 2020). *B. amyloliquefaciens* TWC2 can induce the activity of resistance enzymes in sugarcane and enhance the disease resistance of plants (Liang et al., 2018). *B. amyloliquefaciens* can produce volatile substances during the growth process to inhibit the growth and development of pathogenic fungi. The 34 volatile substances produced by *B. amyloliquefaciens* LJ02 have inhibitory effects on various pathogenic fungi such as Black rot fungus (Hao et al., 2016). Among the 36 volatile substances produced by *B. amyloliquefaciens* NJN-6, 11 kinds of gases can completely inhibit the growth of *Fusarium oxysporum* and have a preventive effect on banana Fusarium wilt (Yuan et al., 2012).

Through the determination of physiological and biochemical characteristics of strain XY-1. *B. amyloliquefaciens* XY-1 not only had highly antagonistic effect on FHB, but also had good resistance to four fungal pathogens, *Colletotrichum gloeosporioides*, *Rhizoctonia solani*, *Sclerotium rolfsii*, and *Alternaria alternata*. So XY-1 could be used as a biological control resource in the prevention and control of various diseases. At the same time, XY-1 showed strong resistance to *chloramphenicol* and *ampicillin*, which further highlights the application potential of the strain in biological control.

Winter Wheat Region in the Middle and Lower Reaches of the Yangtze River, China, FHB is one of the main diseases affecting wheat production (Ma and Lu, 2010). For many years, spraying carbendazim has been the main measure to control FHB in

production. But carbendazim can induce drug resistance in fungal pathogens and promote the synthesis of DON toxin, resulting in more serious and wider spread of FHB in China (Li et al., 2006). The key to biological control is to inhibit the occurrence of field diseases, so we will require large-scale and systematic field trials in different pilots and different years to verify the actual biological control effect of the strains. The active ingredients will be screened from the culture supernatant of the antagonist XY-1. The compound with better antifungal effect will be isolated and its antifungal mechanism will be explored. This study will provide materials for the development of bacterial agents for biological control of FHB.

Conclusion

In this study, the strain XY-1 with the best antagonistic effect on FHB was screened out of 7 endophytes isolated from wheat roots using dual culture assays. The 16S rDNA sequence identified that the antagonistic XY-1 was *Bacillus amyloliquefaciens*. Further research found that XY-1 also had antagonistic activity against *Colletotrichum gloeosporioides*, *Rhizoctonia solani*, *Sclerotium rolfsii*, and *Alternaria alternata*. Antibiotics tolerance cultivation showed that XY-1 had strong resistance to *Chloramphenicol* and *Ampicillin*. The strain XY-1 displayed strong antifungal activity against *F. graminearum*. In conclusion, this study provides a novel *B. amyloliquefaciens* strain which is a powerful biocontrol bacterium.

Data availability statement

The original contributions presented in the study are included in the article/supplementary material. Further inquiries can be directed to the corresponding authors.

Author contributions

DM and HS designed this article; XX and YC directed the data analysis and manuscript writing. DM and JY supervised the experiment. ZF confirmed the manuscript. All authors contributed to the article and agreed to submit version of the manuscript.

Funding

This research was supported by "Open Project Program of Engineering Research Center of Ecology and Agricultural Use of Wetland, Ministry of Education (KFT202102)", and "the National Key Research and Development Program of Jiangsu (BE2021335)".

Conflict of interest

The authors declare that the research was conducted in the absence of any commercial or financial relationships that could be construed as a potential conflict of interest.

Publisher's note

All claims expressed in this article are solely those of the authors and do not necessarily represent those of their affiliated organizations, or those of the publisher, the editors and the reviewers. Any product that may be evaluated in this article, or claim that may be made by its manufacturer, is not guaranteed or endorsed by the publisher.

References

Bouanaka, H., Bellil, I., Harrat, W., Boussaha, S., Benbelkacem, A., and Khelifi, D. (2021). On the biocontrol by *trichoderma afroharzianum* against *fusarium* culmorum responsible of *fusarium* head blight and crown rot of wheat in algeria. *Egypt. J. Biol. Pes. Co.* 31, 1–13. doi: 10.1186/S41938-021-00416-3

Crane, J. M., Gibson, D. M., Vaughan, R. H., and Bergstrom, G. C. (2013). Iturin levels on wheat spikes linked to biological control of *Fusarium* head blight by *Bacillus amyloliquefaciens*. *Biol. Control* 103, 146–155. doi: 10.1094/PHYTO-07-12-0154-R

Gong, A. D., Li, H. P., Yuan, Q. S., Song, X. S., Yao, W., He, W. J., et al. (2015). Antagonistic mechanism of iturin a and plipastatin a from *Bacillus amyloliquefaciens* S76-3 from wheat spikes against *Fusarium graminearum*. *PloS One* 11, 269–272. doi: 10.1371/journal.pone.0116871

Gu, Q., Yang, Y., Yuan, Q. M., Shi, G. M., Wu, L. M., Lou, Z. Y., et al. (2017). *Bacillomycin* d produced by is involved in the antagonistic interaction with the plant-pathogenic fungus. *Environ. Microbiol.* 83. doi: 10.1128/AEM.01075-17

Hanif, A., Zhang, F., Li, P. P., Li, C. C., Xu, Y. J., and Zubair, M. (2019). Fengycin produced by *Bacillus amyloliquefaciens* FZB42 inhibits *Fusarium graminearum* growth and mycotoxins biosynthesis. *Toxins* 11, 295–305. doi: 10.3390/toxins11050295

Hao, X. R., Lu, Z. J., Wang, J., Li, J., and Wang, Y. H. (2016). Study on volatile organic compounds inhibition of *bacillus amyloliquefaciens* LJ02. *J. Tianjin Agric. Univ.* 23, 23–26+30. doi: 10.3969/j.issn.1008-5394.2016.03.006

Kim, K., Lee, Y., Ha, A., Kim, J., Park, A. R., Yu, N. H., et al. (2017). Chemosensitization of *Fusarium graminearum* to chemical fungicides using cyclic lipopeptides produced by *Bacillus amyloliquefaciens* strain JCK-12. *Front. Plant Sci.* 8. doi: 10.3389/fpls.2017.02010

Lamichhane, J. R., Dachbrodt-Saaydeh, S., Kudsk, P., and Messéan, A. (2016). Toward a reduced reliance on conventional pesticides in European agriculture. *Plant Dis.* 100, 10–24. doi: 10.1094/PDIS-05-15-0574-FE

Liang, Y. Q., Wu, W. H., Huang, X., Xi, J. G., Li, R., Zheng, J. L., et al. (2018). The induction of defense-related enzymes in sugarcane by *Bacillus amyloliquefaciens* TWC2. *Sugar Crops China* 40, 13–16. doi: 10.13570/j.cnki.scc.2018.03.004

Li, W., Huang, W., Dong, Y., Chen, H., Wang, J., and Shan, J. (2017). Estimation on winter wheat scab based on combination of temperature, humidity and remote sensing vegetation index. *Trans. Chin. Soc. Agric. Engineering* 33, 203–210. doi: 10.11975/j.issn.1002-6819.2017.23.026

Li, Y. T., Liu, X., Xiao, Y. X., Wen, Y., Li, K. K., and Ma, Z. L. (2022). Genome-wide characterization and function analysis uncovered roles of wheat lims LIMs in

responding to adverse stresses and *TaLIM8-4D* function as a susceptible gene. *Plant Genome* 5, e20246. doi: 10.1002/tpg2.20246

Liu, Y. K., Tong, H. W., Zhu, Z. W., Chen, L., Zou, J., Zhang, Y. Q., et al. (2016). Progress in research on mechanism of resistance to *FHB* in wheat. *Sci. Agricult. Sinica* 49, 1476–1488. doi: 10.3864/j.issn.0578-1752.2016.08.005

Liu, H. F., Zhou, J., Liao, J., Yi, J. P., Ma, D. F., and Deng, J. X. (2019). Grafted twig rot on citrus sinensis caused by a member of the *Fusarium solani* species complex. *Can. J. Plant Pathol.* 42, 1–7. doi: 10.1080/07060661.2019.1633412

Li, Z. H., Xiang, J. J., Chen, J. H., Ge, C. F., and Ge, S. R. (2007). Isolation and identification of actinomycete against *Fusarium graminearum*. *J. Triticeae Crops* 27, 149–152. doi: 10.7606/j.issn.1009-1041.2007.01.037

Li, H. K., Zhou, M. G., Wang, J. X., and Ni, Y. P. (2006). Controlling wheat scab with JS399-19 and carbendazim resistance management. *Agrochemicals* 45, 92–94 +103. doi: 10.3969/j.issn.1006-0413.2006.02.005

Ma, X., Du, X. Y., Liu, G. J., Yang, Z. D., Hou, W. Q., Wang, H. W., et al. (2015). Cloning and characterization of a novel UDP-*glycosyltransferase* gene induced by DON from wheat. *J. Integr. Agr.* 14, 830–838. doi: 10.1016/S2095-3119(14)60857-1

Ma, H. X., and Lu, W. Z. (2010). Progress on genetic improvement for resistence to *Fusarium* head blight in wheat. *Jiangsu J. Agric. Sci.* 26, 197–203. doi: 10.3969/j.issn.1000-4440.2010.01.037

Miedaner, T., Schneider, B., and Geiger, H. H. (2003). Deoxynivalenol (don) content and FHB resistance in segregating populations of winter rye and winter wheat. *Crop Sci.* 43, 519–526. doi: 10.2135/cropsci2003.0519

Rahman, S. F. S. A., Singh, E., Pieterse, C. M., and Schenk, P. M. (2018). Emerging microbial biocontrol strategies for plant pathogens. *Plant Sci.* 267, 102–111. doi: 10.1016/j.plantsci.2017.11.012

Redburn, A. C., and Patel, B. K. C. (1993). Phylogenetic analysis of *Desulfotomaculum thermobenzoicum* using polymerase chain reaction-amplified 16S rRNA-specific DNA. *FEMS Microbiol. Lett.* 113, 81–86. doi: 10.1111/j.1574-6968.1993.tb06492.x

Senatore, M. T., Ward, T. J., Cappelletti, E., Beccari, G., and Prodi, A. (2021). Species diversity and mycotoxin production by members of the *fusarium tricinctum* species complex associated with *fusarium* head blight of wheat and barley in italy. *Int. J. Food. Microbiol.* 358, 1–11. doi: 10.1016/j.ijfoodmicro.2021.109298

Su, T., Lu, M., Zhou, Q., Wang, F., Wang, G. F., and Xie, G. L. (2010). Evaluation and identification of antagonistic bacteria against different biovars of ralstonia solanacearum and their active metabolites. *Acta Phytophylacica Sinica* 37, 431–435. doi: 10.3724/SP.J.1142.2010.40521

Sun, L. J., Lu, Z. X., Bie, X. M., Lu, F. X., and Yang, S. Y. (2006). Isolation and characterization of a co-producer of fengycins and surfactins, endophytic *Bacillus amyloliquefaciens* ES-2, from *Scutellaria baicalensis* georgi. *World J. Microb. Biot.* 22, 1259–1266. doi: 10.1007/s11274-006-9170-0

Wen, H. Q., Pei, Z. Y., Zhang, L. S., Cheng, T. L., and Li, X. (2012). Antagonism of wheat endophytic bacteria identification on *fusarium graminearum schw*.in wheat. *J. Shanxi Agric. Sci.* 40, 765–767. doi: 10.3969/j.issn.1002-2481.2012.07.18

William, E., Nganje, D. A., Bangsund, F., Larry., L., William, W. W., and Napoleon, M. T. (2004). Regional economic impacts of *fusarium* head blight in wheat andbarley. *Appl.econ.perspect.pol* 26, 315–425. doi: 10.1111/j.1467-9353.2004.00183.x

Xia, Y. C., Zhu, Y. X., Ma, D. F., Liu, L. C., and Yin, J. L. (2019). Isolation and identification of antagonistic strain of *Fusarium graminearum*. *Acta Agricult. Universitatis Jiangxiensis* 41, 33–42. doi: 10.13836/j.jjau.2019005

Yin, J. L., Gu, B., Huang, G. Y., Tian, Y., Quan, J. L., Lindqvist-Kreuze, H., et al. (2017). Conserved RXLR effector genes of phytophthora infestans expressed at the early stage of potato infection are suppressive to host defense. *Front. Plant Sci.* 8 (2155). doi: 10.3389/fpls.2017.02155

Yuan, J., Raza, W., Shen, Q. R., and Huang, Q. W. (2012). Antifungal activity of *bacillus amyloliquefaciens* njn-6 volatile compounds against *fusarium oxysporum* f. sp. cubense. *Appl. Environ. Microb.* 78, 5942–44. doi: 10.1128/AEM.01357-12

Zhang, X. B., Yang, X. Y., Yang, Y. Z., and Jian, W. (2020). Research progress on the *mechanism* of *Bacillus* sp. promoting plant growth. *Jiangsu Agric. Sci.* 48, 73–80. doi: 10.15889/j.issn.1002-1302.2020.03.012

Zhang, J., Yi, Y. J., Wang, J. S., Chen, S. H., and Li, G. L. (2014). Research progress of control techniques on wheat scab. *China Plant Protection* 34, 24–28. doi: 10.3969/j.issn.1672-6820.2014.01.005

Zhang, P. G., Zhu, Y. X., Ma, D. F., Xu, W. J., Zhou, J. J., Yan, H. W., et al. (2019). Screening, identification, and optimization of fermentation conditions of an antagonistic endophyte to wheat head blight. *Agronomy* 9, 1–10. doi: 10.3390/agronomy9090476

Frontiers in
Plant Science

Cultivates the science of plant biology and its applications

The most cited plant science journal, which advances our understanding of plant biology for sustainable food security, functional ecosystems and human health.

Discover the latest Research Topics

See more →

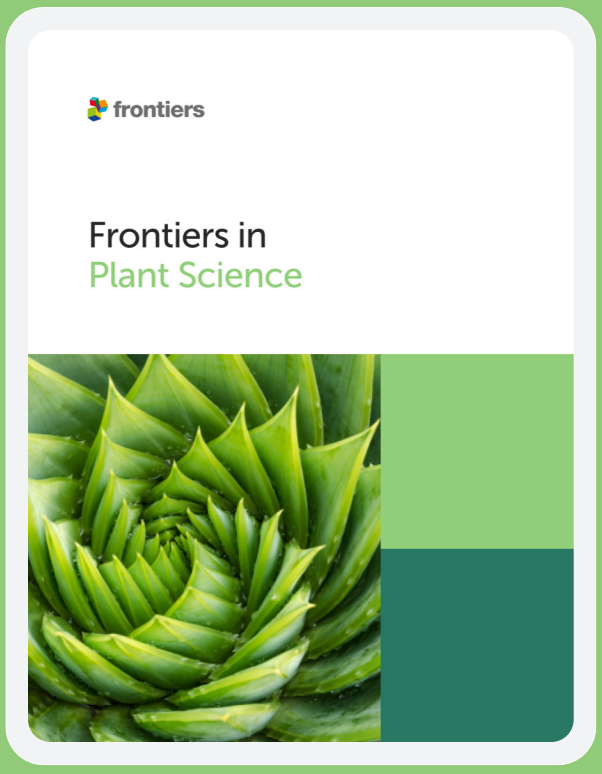

Frontiers

Avenue du Tribunal-Fédéral 34
1005 Lausanne, Switzerland
frontiersin.org

Contact us

+41 (0)21 510 17 00
frontiersin.org/about/contact